Numerical studies on the linear Ising-Heisenberg model.

Bonner, Jill Christine

NUMERICAL STUDIES ON THE LINEAR ISING-HEISENBERG MODEL

A thesis entered in candidature for

the degree of Doctor of Philosophy in the

University of London

by

JILL CHRISTINE BONNER

1968

ABSTRACT

Linear rings and chains of S = 1/2 spins with the anisotropic (Ising-Heisenberg) Hamiltonian

$$\mathcal{H} = -2J\sum_{i=1}^{N}\left\{S_i^z S_{i+1}^z + \gamma\left(S_i^x S_{i+1}^x + S_i^y S_{i+1}^y\right)\right\} - g\beta\sum_{i=1}^{N}\underline{H}\cdot\underline{S}_i$$

have been studied by exact machine calculations for N=2 to 11 (rings) and N=4, 6 and 8 (chains), for γ in the range 0 to 1 and for ferromagnetic and antiferromagnetic coupling. The results reveal the dependence on finite size and anisotropy of the spectrum and dispersion laws. From the eigenvalues and appropriate eigenvectors, the variation with N and γ of the energy, entropy and specific heat, of the magnetisation and parallel and perpendicular static isothermal susceptibilities, and of the pair correlations has been obtained. A non-physical, antiferromagnetic, zero-point entropy which is a characteristic feature of the Ising limit is shown to disappear for the more general model with $\gamma > 0$. The limiting $N \to \infty$ behaviour is accurately indicated, for all γ, in the region $kT/|J| \geq 0.5$ which includes the maxima in the specific heat and susceptibility. The behaviour of thermal and magnetic properties of infinite chains at low temperatures is estimated by extrapolation, in conjunction with inferences concerning the nature of the spectral behaviour which is likely to dominate at low temperatures. For infinite antiferromagnetic chains the ground-state degeneracy, the anisotropy energy gap, and the magnetisation, perpendicular susceptibility, and pair correlations at T=0 are studied in a similar manner. Ferromagnetic infinite chains are generally less interesting in these particular respects. Estimates of the long-range order suggest that it vanishes only at the Heisenberg limit $\gamma=1$.

ACKNOWLEDGEMENTS

This research topic was suggested to the author by Professor Michael E. Fisher to whom the author is deeply indebted for his enthusiastic interest and dynamic guidance during the course of this work.

A tribute is due also to Professor C. Domb, under whose auspices this research was primarily carried out.

Acknowledgement is made to the former Department of Scientific and Industrial Research for the award of a maintenance grant during the years 1959 to 1962.

To Dr. R. L. Orbach and to Dr. R. B. Griffiths the author offers a grateful acknowledgement of their willingness to supply results of their own unpublished calculations and for much helpful correspondence and discussion. It is particularly appreciated that Dr. Griffiths delayed publication of some of his own work to allow this work to come to full fruition.

Finally, the author wishes to thank Dr. John F. Nagle very sincerely for encouragement and advice during the course of preparation of this thesis.

TABLE OF CONTENTS

FIGURES

For easy reference the figures in this thesis are placed near the relevant material in the text. However, please notice that there are two kinds of figures. One kind is denoted by Fig. (n.m) with a capital F; these are full page graphs and figures with captions. The other kind is denoted by fig. (n.m) with a lower case f; these small figures are inserted directly into the text and the numbering sequence is <u>independent</u> of the Fig. (n.m) numbering sequence.

CHAPTER I

INTRODUCTION AND REVIEW OF THE FIELD

Introduction

Experimental and theoretical studies have shown that in many magnetic materials the magnetic part of the Hamiltonian may be quite accurately represented as a set of localised spins $\underline{S}_i$ with bilinear interactions. For certain highly anisotropic systems, the coupling energy can be approximated by the pure Ising form $-2JS_i^zS_j^z$, but for most systems the anisotropy, although important, is not very large and the pure Heisenberg coupling $-2J\underline{S}_i \cdot \underline{S}_j$ is more realistic. Between these extremes is the anisotropic "intermediate" coupling $-2J\left\{\gamma\underline{S}_i \cdot \underline{S}_j + (1-\gamma)\, S_i^zS_j^z\right\}$ which reduces to the Ising case when $\gamma=0$ and the Heisenberg case when $\gamma=1$. Experimental evidence in support of these remarks will be presented in sub-sections (1.1) and (1.3).

The Heisenberg-Ising magnetic model has an important analogue in the quantum lattice gas model of Matsubara and Matsuda (1956, 1957). The range of physical phenomena embraced by Hamiltonians of the Heisenberg-Ising type has thus been extensively broadened to include, for example, superfluid effects in liquid helium (Fisher 1967), a topic of high current interest. (The quantum lattice gas analogue will be discussed in more detail in sub-section (1.2)). In addition, it has recently been found that the linear Heisenberg-Ising model at zero temperature is related to a class of two-dimensional ferroelectric models (Lieb, 1967).

With pure Ising interaction the partition function of a finite or infinite chain of spins in a parallel or perpendicular magnetic field, and thence the thermal and magnetic properties, may be calculated

exactly (Domb, review, 1960, and Katsura, 1962). For simple two-dimensional Ising lattices exact solutions may be obtained in zero field (Onsager, 1944 and Domb, review, 1960). For the Heisenberg, or intermediate γ spin Hamiltonians, however, exact closed formulae for the finite-temperature behaviour have not been found even for the linear chain despite much theoretical effort. The detailed review of sub-section (2.1) will amplify this point. Recently, however, a fully rigorous analytical treatment of the zero-temperature properties of the infinite linear chain has been presented (Yang and Yang, 1966).

Although, naturally, greatest interest attaches to three-dimensional lattices, the properties of linear chains with non-Ising spin coupling are of both experimental and theoretical significance. The experimental background will be reviewed in sub-section (1.3).

Theoretically the linear chain Heisenberg-Ising model is interesting as one of the simplest many-body systems in which quantum effects play a vital part. The quantum effects greatly complicate the theoretical problem, as is illustrated by the calculation of the ground-state energy for the antiferromagnetic linear chain (Bethe, 1931; Hulthén, 1938; Orbach, 1958; Walker, 1959).

Accurate values for other properties are valuable as an aid to judging various approximate theoretical treatments which are also applicable to more complex systems. We shall see in sub-section (2.3) that certain well-established field-theoretic techniques with extensive application in other branches of physics, appear rather unreliable when put to this test. (Katsura and Inawashiro, 1965a).

From the view-point of statistical mechanics, it is also of interest to study how the limiting behaviour for infinite systems is approached by finite systems. (The effect of boundary conditions is also a question of interest.) Such insight is useful since, with the advent of fast digital computers, it is feasible to perform exact or Monte Carlo

calculations on finite models of many types of physical systems (C.P.Yang 1963; Runnels, 1966)

With this motivation we have undertaken a numerical study of finite chains and rings of N spins with the Hamiltonian

$$\mathcal{H} = -2J\sum_{i=1}^{N}\left\{S_i^z S_{i+1}^z + \gamma\left(S_i^x S_{i+1}^x + S_i^y S_{i+1}^y\right)\right\} - g\beta\sum_{i=1}^{N}\underline{H}\cdot\underline{S}_i \qquad (1.1)$$

for spin values of 1/2 only. We have computed the energy levels and certain of the eigenvectors, and thence the thermal and magnetic properties for varying anisotropy γ and varying magnetic field H for rings of size N=2 to 11 and chains for N=4, 6 and 8. Our calculations include both ferromagnetic and antiferromagnetic coupling.

The plan of this thesis is as follows. In the rest of this chapter we present a more detailed version of the important points mentioned in this introduction. In Chapter II we discuss the nature of the quantum-mechanical problem involved in finding eigenvalue spectra (and eigenvectors) for finite spin clusters, and machine computations are outlined. At the beginning of Chapter III we examine the possibilities of extrapolation from finite N to the limit $N \to \infty$, from a study of the antiferromagnetic ground state as a function of γ. In the remainder of Chapter III, details of the energy spectrum are discussed and the ferromagnetic and antiferromagnetic anisotropy gaps and the asymptotic degeneracy of the antiferromagnetic ground state are estimated. The spin-wave (and bound state) dispersion laws for ferro- and antiferromagnetic rings and chains are illustrated and discussed. The thermal properties, particularly the specific heat, and entropy in a magnetic field, are discussed in Chapter IV for antiferromagnetic and ferromagnetic rings and chains. Estimates of limiting ($N = \infty$) behaviour are presented wherever possible. The magnetic properties are described in Chapter V. Attention is given especially to the magnetisation curves at T=0 and

the temperature-dependent parallel and perpendicular susceptibilities. The short-range antiferromagnetic order and further pair correlation functions are described in Chapter VI. The long-range order is estimated by extrapolation and compared with other approximations.

Our results are for the most part presented graphically, but tables of eigenvalues for rings and chains for $\gamma=1$ and $\gamma=0.5$ and tables of the thermal and magnetic properties for N=9, 10 and 11 and $\gamma=1$ and 0.5 are given in Appendices 2 and 3. In Appendix 1 group-theoretical approaches for the Heisenberg limit are outlined and used in connection with estimates for the feasibility of this procedure in two and three dimensions.

1. PHENOMENOLOGICAL SURVEY

1.1) Magnetic Phenomena

A comprehensive description of magnetic phenomena in relation to our model Hamiltonian is presented in a treatise on Magnetism edited by Rado and Suhl (1963, 1965, 1966) and books of Mattis (1965) and Goodenough (1963) and therefore we shall only review briefly certain highlights in this sub-section.

Our Hamiltonian (1.1) is descriptive of an assembly of localised spins characteristic, for example, of the class of magnetic insulators which are compounds of the rare earth metals. The incomplete magnetic electronic shell of the rare earths is the 4f-shell which is surrounded by several diamagnetic completed outer shells. The transition metals, on the other hand, have the outermost 3d-shell as the incomplete, magnetic shell, and thus 3d electrons are relatively free to move throughout the metal crystal as conduction electrons. The transition metals are therefore perhaps better described, at least to a first approximation, by the collective or band model of Slater (1936) and Stoner (1938). The Slater collective model will not be discussed further in this thesis. (Transtion metal salts, however, are again insulators, since the intervening diamagnetic atoms keep the 3d electrons localised at the metal atom site.)

An important parameter in the Hamiltonian (1.1) is the exchange integral, J, relating to electron orbital overlap. The quantum-mechanical foundations of the Heisenberg Hamiltonian and, particularly, the sign of the exchange integral remains a controversial subject. However, very accurate many-electron configuration interaction calculations for a system of six hydrogen atoms arranged in a regular hexagonal array with a variable lattice spacing have been carried out by Mattheiss (1961). The principal result is that the effects of configuration interaction can be represented quite accurately at large inter-nuclear separations in terms of a parameter J_{eff}, analogous to a nearest-neighbour exchange integral.

Perturbation calculations are then presented for a general linear chain of monovalent spin-1/2 atoms which are in good agreement with the accurate 6-hydrogen-atom calculation. These results justify the use of the Heisenberg exchange operator $-2J_{eff}\ (\sum_i \underline{S}_i \cdot \underline{S}_{i+1})$ to describe the magnetic interaction at large interatomic separations.

The effective exchange integral, J_{eff}, is shown to consist of two contributions. A positive definite part results from direct exchange, and this phenomenon always gives rise to ferromagnetic effects. However additional terms enter with the opposite sign resulting from the effects of ionic (i.e. higher excited) configurations. These effects are closely related to the phenomenon of superexchange which is always antiferromagnetic. The sign of J_{eff}, and hence the resultant magnetic behaviour of the system, is determined by the relative magnitudes of the two contributions.

Other exchange effects (Anderson, 1963) which are one or two orders of magnitude smaller than direct exchange and superexchange, are indirect exchange through closed outer shells (ferromagnetic) and double exchange which is a higher-order form of superexchange and also antiferromagnetic. Other forms of spin-coupling, not of interest in this thesis, include long-range dipole-dipole interactions and the Ruderman-Kittel-Yosida mechanism of ferromagnetic indirect interaction via polarised conduction electrons.

Most magnetic substances possess intrinsic anisotropy even when external sources of anisotropy, for example the shape effect, do not operate. The magnetic anisotropy is connected with the crystal structure and macroscopic effects of technical importance (magnetostriction) result. The microscopic origins of magnetic anisotropy (Kanamori, 1963) depend on the electronic spin states (the main source of the spontaneous magnetisation in ferro- and antiferromagnets) and moreover they reflect the symmetry of the atomic arrangements in the crystal. A well-known source

of anisotropy is the inter-ionic magnetic dipolar interaction, which, however, is not large enough to account for the observed magnitude of the anisotropy energy in many cases. An alternative factor is the coupling between the spin and the orbital motion of electrons: the spin can see the lattice through the orbital coupling. Two classes of anisotropy arise from this source a) 'single ion anisotropy' which depends on the spin state of a single ion only and b) various anisotropic interactions among the spins of two or more ions.

In this thesis we consider an anisotropic Hamiltonian which is a special case of a general, bilinear (spin-1/2) interionic spin-spin interaction of the general form

$$\mathcal{H} = -2J^z_{ij}\, S^z_i\, S^z_j - 2J^x_{ij}\, S^x_i\, S^x_j - 2\, J^y_{ij}\, S^y_i\, S^y_i \quad . \tag{1.2}$$

This interaction, though simple, is sufficiently realistic to give rise to a worth-while model to examine theoretically.

The general validity of the concept of a spin Hamiltonian is discussed by Stevens (1963). A spin Hamiltonian has the virtue that a mass of spatial and empirical information is wrapped up neatly in adjustable parameters which may be obtained experimentally.

1.2) Quantal Fluid-Magnet Analogies

There exists a well-known analogy between Ising model magnets and classical lattice gases (Yang and Lee, 1952). A corresponding analogy can be traced between the parameters of a quantum-mechanical Heisenberg-Ising model Hamiltonian and a quantum lattice gas Hamiltonian (Matsubara and Matsuda, 1956). The latter, of course, represents a statistical quantum mechanical model of gas/liquid behaviour. The details of the analogy are well-known (see, for example Table II of paper III of Yang and Yang, 1966), so we shall merely remark, for convenience, that the volume of the fluid corresponds to the magnetisation, and the chemical potential (or, more loosely, the pressure) corresponds to an applied magnetic field. The

analogy correlates quite a richness of behaviour (Fisher, 1966, 1967). For example, the phase diagram for a magnet with general ferromagnetic interactions closely corresponds to the simple liquid/gas phase diagram. Of much greater interest is an analogy between phase diagrams which relates the well-known spin-flop phase of a class of anisotropic antiferromagnets to the superfluid phase of liquid He^4.

The exact analytical solution of Yang and Yang (1966) has revealed that our anisotropic spin-1/2 linear chains show vestigial traces of a spin-flopping effect in the shape of the zero-temperature magnetisation versus magnetic field curves as the magnetisation tends to zero. More promising signs of a spin-flop effect are to be seen in linear systems with spin >1/2 and, we expect, in two- and three-dimensional antiferromagnets.

1.3) Relation to Experiment

Widely different experimental techniques have been used in investigating magnetically ordered materials. Apart from the usual magnetic and thermal measurements, conclusive information on the magnetic structure is obtained for many substances from neutron diffraction, nuclear resonance or electronic resonance. A clear review of the present relation of theory and experiment is available in the review article of Domb and Miedema (1964).

The first fully convincing demonstration of agreement between theory and experiment for linear magnetic compounds was the analysis by Griffiths (1964a) of susceptibility and specific heat measurements on copper tetrammine sulphate, $Cu(NH_3)_4SO_4 \cdot H_2O$. Since this substance is now well-known as the archetypal magnetic linear chain, a brief review of its properties will be presented to illustrate the field. The crystal structure has been determined by an x-ray analysis of Mazzi (1955) to consist of magnetic Cu^{2+} ions arranged in chains in the manner $-Cu^{2+}-O_{H_2}-Co^{2+}-O_{H_2}-Cu^{2+}$, the chains being linked through the weaker interchain interaction

$-Cu^{2+} - NH_3 - Cu^{2+} - NH_3 - Cu^{2+}$. Experimentally, the susceptibility has a low broad maximum at about 3°K with a sharp anomaly at a lower temperature which various authors have estimated at 0.37°K to 0.42°K (Wat anabe and Haseda, 1958; Haseda and Miedema, 1961; Wittekoek, thesis, 1967). The specific heat measurements (Fritz and Pinch, 1959 ; Ukei, unpublished; Haseda and Miedema, 1961) also show broad maxima and an anomaly at corresponding temperatures. Onsager (1944) showed rigorously that an Ising square net with unequal exchange interactions in the two principal directions had a specific heat in general agreement with an Ising linear chain, but with a superimposed logarithmic singularity characteristic of a two-dimensional assembly, at a temperature below the maximum, when the ratio of exchange constants was in the region of $J_1/J_2 \simeq 0.01$. It is very plausible that similar effects will be seen in substances with strong interactions within each chain and rather weak interactions between chains (Haseda and Miedema, 1961). According to Griffiths, the susceptibility and specific heat data are best fitted to the theoretical isotropic antiferromagnetic Heisenberg curves obtained in this thesis (and, independently by Griffiths, 1961, 1963) by considering a value for the intrachain exchange constant $|J| = 3.15 \pm 0.2$°K. The maximum in the specific heat then has the value $C_{max}/Nk \simeq 0.36$ (in comparison with the theoretical Heisenberg value of 0.35 and an Ising value of 0.439). Oguchi (1964) has estimated that the ratio of interchain to intrachain exchange constants is $|J'| / |J| = 0.01$.

Haseda and Kobayashi (1964) independently compared specific heat and susceptibility data to theoretical studies of the author and of Griffiths and also concluded that $|J| /k = 3.15$°K. (Haseda and Kobayashi also compare their experimental measurements on the magnetisation curves versus magnetic field for various temperatures with theory.) However, Griffiths' work has priority in that an unpublished report containing essentially

the same conclusions was available prior to eventual publication. The author of this thesis must apologize for unintentionally delaying publication of the work (the experimental report was earmarked for simultaneous publication with the work of the author (Bonner and Fisher, 1964).)

$Cu(NH_3)_4\ SO_4 \cdot H_2O$, on account of its established linear Heisenberg chain properties, has recently been the subject of theoretical studies on time correlations and magnetic resonance linewidth, which have proved to be in much better agreement with experiment than any of the current approximate theories (Carboni and Richards, 1968; Rogers, Carboni and Richards, 1967).

The spectrum of the Cu^{2+} free ion shows a Kramers doublet well separated from higher levels, and Cu^{2+} is thus well-described as a spin-1/2 ion. It is probable that this character will be maintained in combination with diamagnetic ions, and suggests that copper compounds should form a fruitful source of spin-1/2 magnetic compounds. The dominant magnetic interaction is of the superexchange type and therefore antiferromagnetic.

$CuSO_4 \cdot 5H_2O$ and an isomorphic compound $CuSeO_4 \cdot 5H_2O$ were subsequently discovered to resemble antiferromagnetic linear chains, with exchange integrals $|J|/k \simeq 1.45°K$ (susceptibility measurements) and $1.57°K$ (specific heat measurements) for $CuSO_4 \cdot 5H_2O$; and $|J|/k = 0.80°K$ (susceptibility) and $0.81°K$ (specific heat) respectively for $CuSeO_4 \cdot 5H_2O$, (Wittekoek, Poulis and Miedema, 1964 ; Miedema, van Kempen, Haseda, Huiskamp, 1962; Van Kempen, thesis, 1965; Geballe and Giauque, 1962). Wittekoek (thesis, 1967) suggests the presence of a small amount of anisotropy to account for a small discrepancy in curve fitting below the susceptibility maximum, which lies outside experimental and theoretical errors.

Coordination polymers containing Cu^{2+} magnetic ions are another possible source of spin-1/2 magnetic linear chains. Haseda, Miedema, Kobayashi and Kanda (1962) and Kobayashi, Haseda, Kanda and Kanda (1963)

have reported experimental evidence on various cupric quinone metalorganic substances (Cu-Q-H, Cu-Q-Br and Cu-Q-Cl) which suggests the existence of independent finite chains of 5 to 20 magnetic ions. Recent susceptibility measurements on a rubeanato-copper coordination polymer (Kanda, Ito and Nogaito, 1967) show a good fit to antiferromagnetic isotropic chains of about N = 9 for a value of the exchange integral $|J| \simeq 550°K$ (much larger than the values quoted above for the linear chain inorganic salts).

Other compounds exist which show more complex behaviour in that the interchain interactions are becoming comparable with the intrachain interactions. Examples are anhydrous $CuCl_2$ ($T_{max} = 70°K$, $T_N = 23.91 \pm 0.1°K$) and anhydrous $CrCl_2$ ($T_{max} = 40°K$, $T_N = 16.06°K$) (Stout and Chisholm, 1962); anhydrous $CuBr_2$ ($T_{max} = 226°K$) (Barraclough and Ng, 1964); $CuCl_2 \cdot 2H_2O$ which is well-known to display spin-flopping properties (T_{max} = about 5°K, Gorter et al., 1955; $T_N = 4.33°K$) (Poulis and Hardeman, 1952) and $Cu_2Cs_3Cl_7 \cdot 2H_2O$ ($T_{max} \simeq 3.2°K$, $T_N = 1.625°K$) (Wittekoek, thesis, 1967). Clearly the strong interchain interactions complicate comparison with our nearest-neighbour interaction results. (Note that T_{max} refers to a broad maximum in susceptibility.)

Berger, Friedberg and Schriempf (1963) reported susceptibility measurements on $Cu(NO_3)_2 \cdot (3)H_2O$ which could be interpreted in terms of either isotropic antiferromagnetic linear chain effects or, more probably, an assembly of binary $Cu^{2+} - Cu^{2+}$ clusters similar to the well-known copper acetate dimer structure (Bleaney and Bowers, 1952). Wittekoek (thesis, 1967) favours the binary cluster interpretation as a result of proton magnetic resonance lineshift studies. Recently Friedberg and Raquet (1968) have reported specific heat measurements which strongly support the binary cluster hypothesis.

Recently, the existence has been reported of two magnetic substances which show a strikingly good accordance with theoretical estimates of the author and Griffiths. Rogers and Dempesy (1967) report specific heat measurements on $Cu(NH_3)_4(NO_3)_2$ over the temperature range 16°K down to

1°K which are interpreted as indicating the existence of nearest-neighbour linear antiferromagnetic coupling with $|J|/k = 3.70 \pm 0.04$°K. No traces of an anomaly associated with interchain coupling are seen down to 1°K. According to Kadota, Yamada, Yoneyama and Hirakawa (1967) a simple perovskite compound K Cu F_3 shows antiferromagnetic linear chain behaviour characterised by $|J|/k = 190$°K and a value of N of about 15, (provided the chains are identical.) Neutron diffraction studies show no long-range ordering down to 4.2°K, so again, other interactions in the compound are apparently relatively weak. Both these compounds are interesting in that at present there is no geometrical evidence of linear chain-like ionic arrangements in the compounds (unlike the case of $Cu(NH_3)_4SO_4 \cdot H_2O$, for example).

A linear chain crystal with anisotropic intrachain interactions is $K_3Fe(CN)_6$ ($T_N = 0.129$°K, Duffy, Lubbers, van Kempen, Haseda and Miedema 1962). The exchange constant is believed to be 25% anisotropic (Ohtsuka, 1961). An example of a compound showing linear chain behaviour which is both highly anisotropic (Ising-like) and also ferromagnetic is $CoCl_2 \cdot 2H_2O$. (The Co^{2+} ion is a spin-1/2 ion like Cu^{2+}, but highly anisotropic.) The magnetic structure of this substance, however, is apparently complicated by several additional antiferromagnetic superexchange interactions (Kobayashi and Haseda, 1964; Oguchi and Takano, 1964). In sub-section (2.4), an account of work by Duffy and Barr (1968) is given, who discuss some complex organic free radicals according to an alternating Hamiltonian which varies between isotropic linear chain and binary cluster behaviour. It is not convincingly established that the properties of at least certain of these substances (eg. 2, 2-bis (p-nitrophenyl) - 1 - picrylhydrazil) could not equally well be accounted for by our anisotropic Hamiltonian.

Finally, work has recently been reported (Friedberg, private communication) which establishes reasonably good accordance between experimental

work on an apparently linear manganese compound ($CsMnCl_3 \cdot 2H_2O$) and theoretical studies on spin-5/2 Heisenberg linear antiferromagnetic chains (Weng, private communication).

2. THEORETICAL SURVEY

2.1 Exact Analytic Approaches

Theoretical work on the Hamiltonian (1.1) with $\gamma=1$ dates back to 1930 when Bloch (1930) introduced the concept of a spin wave and gave the exact eigenstates for one overturned spin ($\sum S_i^z = NS - 1$) for ferromagnetic interactions. Using a similar approach, Bethe (1931) formulated sets of coupled integral equations which, in principle, gave the exact eigenstates corresponding to interacting spin waves for an arbitrary number of overturned spins on a linear chain ($\gamma=1$). He showed how the states may be classified as "unbound" (i.e., of a spin-wave nature) or "bound" (localised complexes of two or more spins). Hulthén (1938), as part of a comprehensive paper (thesis), used Bethe's formulation to obtain an integral equation which he was able to solve analytically to obtain an exact value for the antiferromagnetic ground-state energy of an infinite linear chain. The arguments of Bethe and Hulthén were extended by Orbach (1958) to the full anisotropic Hamiltonian (1.1). Orbach obtained an integral equation for the limiting ground-state energy and hence also for the short-range order for antiferromagnetic chains as a function of γ. Whereas Orbach presented numerical solutions of his integral equation, Walker (1959), in an important paper, was able to obtain an analytic solution which revealed that the antiferromagnetic ground state $E_o(\gamma)$ was non-analytic at $\gamma = 1$. (The fact that $\gamma = 1$ is a mathematical singularity of $E_o(\gamma)$ follows immediately from Walker's observation that his formula exhibits a pole in any interval, however small, of the open segments $|\gamma| > 1$.)

Des Cloizeaux and Pearson (1962) computed the lowest antiferromagnetic states for rings of $N = 16, 48, \ldots$ spins as a function of wave-vector k numerically by extending the Bethe-Hulthén formalism. They also derived the limiting dispersion law $\varepsilon(k)/|J| = \pi|\sin k|$ for the corresponding class of states of an infinite chain. Griffiths (1964) also extended the Bethe-Hulthén formalism to calculate numerically the lowest (antiferromagnetic) energies of the levels corresponding to all possible numbers of overturned spins and hence obtained the zero-temperature magnetisation curve as a function of field for an infinite Heisenberg chain. With the aid of very accurate numerical calculations, Griffiths was able to infer that the zero-field susceptibility of an infinite antiferromagnetic Heisenberg chain is finite and given by $|J|\chi(T)/Ng^2\beta^2 = \frac{1}{2\pi^2}$. He also demonstrated that the zero-temperature magnetisation curve M as a function of H is non-analytic at M = 0, since the second derivative diverges to $+\infty$ at this point.

Des Cloizeaux and Gaudin (1966) extended the previous calculations of des Cloizeaux and Pearson (1962) on the Heisenberg antiferromagnetic dispersion relation to take account of anisotropy. They obtained an exact analytic formula representing an energy gap between the ground state and first excited states which has its maximum value at the Ising limit and vanishes exponentially as $\gamma \to 1$. They also presented a rather complicated analytic expression for the dispersion relation for the first excited states as a function of γ which reduces to the simple sin k function at $\gamma = 1$ which we have already quoted. Des Cloizeaux and Gaudin also discuss the lowest antiferromagnetic ground states in the range $\gamma = 1$ to $\gamma = \infty$. They show that the antiferromagnetic ground state energy $E_0(\gamma)$ over this extended range is analytic except at the point $\gamma = 1$ where there is an essential singularity. ($E_0(\gamma)$ is actually represented by two distinct functions for $\gamma < 1$ and for $\gamma > 1$.) However, $E_0(\gamma)$

and all its derivatives remain continuous at the point $\gamma = 1$. We thus have an explanation of our observed result that the Walker singularity at $\gamma = 1$ is not detectable by numerical calculations. The analytic work we have so far described in this sub-section has been non-rigorous on two accounts a) integral equations have been solved numerically rather than analytically and b) the mathematical formulation depends on an assumption due to Bethe (1931) and that the eigenfunctions of the problem have a particular form (Bethe ansatz). Recently Yang and Yang (1966) have at last rigorously justified the use of the Bethe ansatz. In a comprehensive series of papers they have presented an exhaustive, rigorous analytic account of the free energy of the infite linear chain as a function of anisotropy $0 \leq \gamma \leq \infty$ and ferro- and antiferromagnetic coupling at T = 0. Of particular interest is their discussion of singularities $\overset{as}{M \to 0}$ of the zero-temperature magnetisation M versus applied field H curves. For antiferromagnetic magnetisation curves with $0 \leq \gamma < 1$, the MvH curve displays a vertical tangent at M = 0. At $\gamma = 1$ the singularity becomes second order since d^2M/dH^2 diverges to infinity (in confirmation of the work of Griffiths). For $1 < \gamma < \infty$, the curve has a singularity in some derivative at M = 0. For $\infty > \gamma > 1$ and ferromagnetic coupling we again have a singularity in some derivative, the order becoming high as $\gamma \to 1$. Only the curve for the special point $\gamma = \infty$ has no singularity at M = 0.

So far, however, the problem has not been solved for temperatures greater than zero.

2.2) Numerical Work

Hulthén (1938) first found the exact, finite N antiferromagnetic ground state energies for rings of 4, 6, 8 and 10 spin-1/2 atoms to compare with his limiting analytic result (sub-section (2.1)). The energy for N = 12 was subsequently added by Ledinegg and Urban (1952). A numerical study of the complete set of eigenvalues of small finite rings

using analogous matrix techniques to our own was first undertaken by Orbach (1959) in an attempt to determine the small wavevector limit of the dispersion law for linear Heisenberg antiferromagnets. Orbach also performed similar calculations for small linear Heisenberg systems with end spins coupled to the rest of the chain by an Ising interaction such that the two end spins were held either parallel or antiparallel. This study represented a quantum-mechanical formulation of the Bloch wall problem in place of the usual semi-classical treatments (Orbach, 1959).

Independently of the author, and at the same time, Griffiths calculated the energy levels for N = 3, 5, 7, 9 and 10 for the Heisenberg limit only. Griffiths evaluated the energies, entropies, specific heats and susceptibilities in zero field and compared them with the series expansions (Griffiths, 1961, unpublished report). The author of this thesis is considerably indebted to both Dr. R. L. Orbach and Dr. R. B. Griffiths for receipt of their unpublished calculations for checking purposes, and for helpful discussions and correspondence. An acknowledgement is due to Dr. Griffiths who, on learning of the concurrent and more extensive calculations presented in this thesis agreed to forego immediate and independent publication of his own work in order that a more comprehensive approach to the problem might result (Bonner and Fisher, 1964, and Griffiths, 1964a, companion papers).

A striking prediction of the spin-wave theory of antiferromagnets is that the lowest energy states should obey a dispersion law of the $\varepsilon(k) = E - E_o \sim \sin k$. Mattheiss (1961) independently calculated the eigenvalues of the Heisenberg rings N = 6 and N = 8 as a function of wave-vector k and was the first to find an approximately sin k dependence.

Griffiths (1964b) was able to obtain rigorous upper and lowerbounds for the free energy of the antiferromagnetic Heisenberg linear chain which are interesting in connection with extrapolation estimates of the low-temperature thermal behaviour near T = 0.

A different approach to the problem is the method of high-temperature series expansions. Baker, Rushbrooke and Gilbert (1964) successfully exploited a graphological simplication inherent in considering free-ended rather than periodic clusters of up to 10 spins to obtain a long (21 term) series expansion for the partition function in zero field for the infinite linear chain. Numerical curves for the thermal properties obtained with the aid of Padé approximant extrapolation techniques are in very good agreement with the work presented in this thesis for the Heisenberg limit. No series are presented for the case of general anisotropy, however, and the corresponding field-dependent series of Baker, Rushbrooke and Gilbert are much shorter (about 10 terms) and consequently, much less informative.

Richards and his co-workers have recently begun a significant extension of our zero-temperature pair correlation function calculations to include some higher order correlations and, particuarly, time dependent correlations. Their numerical study requires the complete set of eigenvectors for finite spin systems, as well as the eigenvalues, whereas our zero-temperature work required only the antiferromagnetic ground state eigenvector. Their work, to date, (Carboni, thesis, 1966; Carboni and Richards, 1968; Rogers, Carboni and Richards, 1967) has involved periodic systems of 4 to 11 spins and the author understands (Richards, 1967, private communication) that free-ended chains of 4 to 9 spins are now under consideration to improve numerical estimates for the infinite N behaviour. The general time-correlation functions are basic to the study of certain dynamical properties of solids such as magnetic resonance linewidth and neutron scattering.

2.3) Approximate Theoretic Methods

Approximate methods in common use for treating interacting spin problems are spin-wave theories and Green's function theories. (Molecular

(mean) field theory has been considered extensively in attempts to compare theory and experiment because of its mathematical simplicity (Smart, 1963) but its predictions are no longer considered reliable for spin assemblies in the absence of long-range interactions (Fisher, 1965).)

Spin-wave theories contain the premise that spin assemblies can be discussed in terms of wave-like deviations from perfect ferromagnetic or antiferromagnetic spin ordering. The theories run into difficulties when the number of spin deviations becomes large, and are therefore regarded as having maximum validity at low temperatures well away from the critical point (Van Kranendonk and van Vleck, 1958). Green's function theories, on the other hand, are regarded as applicable over the whole temperature range, from low temperatures right up to the critical point. However, Green's function approximate decoupling schemes (Haas and Jarrett, 1964) which are sophisticated enough to give agreement at low temperatures with the best spin-wave treatments (e.g. Dyson, 1956) result in critical point behaviour which is still essentially mean-field-like. In this respect exact series expansions are much more reliable and informative. However, Wortis (1963) has successfully employed Green's function techniques to treat the problem of two overturned spins in the Heisenberg nearest-neighbour model in one, two and three dimensions. His description of the behaviour of bound states of two overturned spins agrees with more exact calculations, where available, to effects of order $(1/\sqrt{N})$ (Katsura, 1965, as reinterpreted in this thesis) which are, of course, in practice neg ligible in the thermodynamic limit. Wortis is also able to disprove a result of Dyson (1956) that bound states of two overturned spins do not exist in three dimensions. Bound states still exist, although they are apparently dominated by lower-lying spin-wave states in the ferromagnetic limit.

The usual procedure adopted by current spin wave theories is to replace the interacting spin operators of the Hamiltonian (spin operators

obey a mixed set of commutation values) by either boson operators (Van Kranendonk and van Vleck, 1958) or fermion operators (Nambu, 1950; Syozi, 1951; Meyer, 1956). The remainder of the Hamiltonian is then ignored or treated as a perturbation. (It is worth noting that the X-Y model Hamiltonian (see sub-section (2.4)) can be expressed exactly as a non-interacting fermion Hamiltonian (Lieb, Schultz and Mattis, 1961; Katsura, 1962). In this way the statistics of the problem are rendered considerably more straightforward. Unfortunately the wide variations in predicted behaviour when the various theories are applied to the same problem, for example the Heisenberg linear chain, illustrate that this is not without considerable cost.

As was first demonstrated by Bloch (1930), the boson theories yield integrals for the magnetisation which diverge in one and two dimensions. Katsura (1965) remarks that this is non-physical behaviour which results from overcounting of magnetic states in the boson approximation. The corresponding divergence of integrals in Green's function theories produces zero spontaneous magnetisation in one and two dimensions. Rigorous proofs have been presented that this is the correct behaviour (Mermin and Wagner, 1967) and therefore in this respect the Green's function theories may be regarded as an improvement upon bose-type spin-wave theories. Fermion spin-wave theories, unfortunately, predict a finite spontaneous magnetisation for all ferromagnets, which deviates from saturation as $T^{1/2}$ for the linear chain and T for planar lattices (Frank, 1956; Mannari, 1958). A more recent antiferromagnetic version of the fermion theory for linear magnetic chains (Falk and Ruijgrok, 1961) shows a sub-lattice magnetisation behaviour equivalent to the ferromagnetic behaviour described above. The susceptibility rises from zero exponentially (whereas we know rigorously from the work of Yang and Yang, 1966, that $\chi(0)$ is finite and non-zero) as also does the specific heat (we believe a power law rise from zero to be the correct situation). Both properties

show divergences at the spurious critical point.

Variational calculations provide a further distinct approach to Heisenberg-Ising linear chain. Hulthén (1938) first employed a constant-coupling variational method; one approximation involved two-spin clusters and a higher approximation used three-spin clusters. The first approximation of Hulthen was generalised by Kasteleijn (1952) to the anisotropic linear chain. The method indicated a critical anisotropy constant $\gamma = 0.483$ beyond which the zerotemperature long-range order (present when $\gamma = 0$) vanished identically. The variational short-range order and energy showed singularities in γ at the same point. Orbach's numerical solutions (1958) indicated that these singularies are spurious. Kasteleijn's work illustrates a fundamental defect of variational calculations: their order parameter predictions — particularly that of the long-range order — are unreliable, essentially because a trial wave-function which gives a good approximation to, say, the ground state energy is still sufficiently unlike the true wave-function. Apparently only the exact answer will do! Successive variational treatments of the antiferromagnetic ground state of the linear chain by Rodriguez (1959) and Ruijgrok and Rodriguez (1960) also illustrate this effect.

Finally let us consider perturbation methods which share with the approach adopted in this thesis the advantage that successively higher orders indicate a trend and perhaps put bounds on the error, in distinction to 'single-shot' approximations such as variational or spin-wave calculations. Walker (1959) presented perturbation series in powers of γ^2 for the short-range and long-range order. His series for the long-range order seems to indicate that it does not vanish for γ less than about 0.9. A further term in the Walker expansion has recently been obtained by Nagle (1968, private communcation) and the series now indicates that the long-range order does not vanish for γ less than about 0.92.

Perturbation calculations equivalent to those of Walker though not including long-range order have been presented by Boon (1961), but to lower order and containing inaccuracies. Boon also considered higher spin and higher dimensional lattices. Walker (1964, private communication) has now extended his method, using a digital computer to perform the tedious algebra, in this direction. Recently Goodman and Arai (1967) have published similar calculations, though to lower order than Walker.

An interesting variant on the perturbation approach for the energy and long-range order is due to Davis (1960) who considered perturbations about a 'free-particle Hamiltonian' rather than about the Ising limit. Davis's results became equivalent to those of Walker in the high-spin, high-coordination number limit

Unfortunately, although the short and long-range order series for the spin-1/2 linear chain give reasonably sensible results despite their short length, the long-range order series for two dimensional lattices do not appear to go to zero at $\gamma = 1$

nor do they make a convincing distinction between two and three dimensional lattices.

Katsura and Inawashiro have considered two rather elaborate perturbation approaches for the thermal and magnetic properties of the antiferromagnetic linear chain in terms of linked-spin-cluster expansions. The first method (Katsura and Inawashiro, 1964) considers a perturbation about the X-Y model (Katsura, 1962). However, the convergence is rather slow and therefore Katsura and Inawashiro (1965) considered an alternative approach, taking as unperturbed Hamiltonian a finite temperature Hartree-Fock calculation of Bulaevskii (1962). The Bulaevskii calculation reproduces the general features of the Heisenberg thermodynamic properties quite well, as may be seen by comparison with the work in this thesis. The Katsura and Inawashiro (1965) improvement on the work of Bulaevskii appears to give very good agreement of the thermal properties

and not quite such good agreement of the magnetic properties in temperature regions where we believe our results to be absolutely reliable. If, however, the Katsura and Inawashiro approach is applied to the ferromagnetic linear chain, a non-physical, finite temperature phase transition results, which has a mean-field character. The original Bulaevskii method shows similar behaviour when applied to ferromagnets (Hunt and Girardeau, 1967).

To summarise the conclusions of this sub-section: we have seen that the standard approximate theories, mean field theories, spin-wave theories, variational calculations or low-order perturbation theories give seriously conflicting and unreliable results when applied to the problem of the Heisenberg-Ising linear chain. An approach of Katsura and Inawashiro which gives the best general agreement with exact results and our own calculations for antiferromagnets fails seriously for ferromagnets. We shall see in the rest of this thesis that our numerical approach, though subject to 10-15% quantitative error in the neighbourhood of a non-analytic point, must be regarded as generally superior in accuracy and relability to all known approximation methods. It is second only to the exact solution.

2.4) Related Models

We will conclude this section with a brief review of both exact analytical and numerical treatments of closely related models.

In 1961, Lieb, Schultz and Mattis pointed out the interesting result that the spin-1/2 model obtained by deleting the parallel or Ising terms $S_i^z S_{i+1}^z$ in equation (1.1) to leave only the transverse Hamiltonian is completely and rigorously soluble. They investigated the spectrum (and zero-temperature pair correlations) in detail (Lieb, Schultz and Mattis, 1961). Katsura (1962) independently derived the same exact solution, although his interest lay in the thermal and magnetic properties including the behaviour in a field. Although the

transverse Hamiltonian is somewhat artificial, the behaviour of this model resembles in many respects the results we have found for the full Hamiltonian (1.1).

It is also possible to calculate by elementary methods the zero-field free energy, correlations and susceptibility for isotropic Heisenberg chains in the limit of infinite spin (Fisher, 1964). The low-temperature behaviour of the thermal properties in this case is somewhat unrealistic since in the classical limit, $S = \infty$, the specific heat necessarily goes to a non-zero value as $T \to 0$. The susceptibility, however, correlates quite closely with the results we find for the S=1/2 Heisenberg chains (except that a non-physical contradiction of the third law is shown again by a non-zero slope for small T).

For spin values intermediate between 1/2 and ∞, an analytic approach (say akin to the Bethe-Hulthén formalism for spin 1/2) is not at present available. Numerical approaches, therefore, seem to be the only feasible possibility. The author understands (Weng and Griffiths, private communication) that numerical calculations very similar to those described in this thesis are in progress on a linear Heisenberg-Ising spin-1 model. Numerical studies for spin > 1/2 are hampered by the increased sizes of Hamiltonian matrices, which vary as $(2S+1)^N$, thus restricting the maximum length of soluble cluster to about 7 to 8 spins for spin-1 and even less for higher spin. A similar restriction exists in applying our numerical techniques to two-dimensional clusters (Weng and Griffiths, private communication, have also investigated spin-1/2 toroidal spin clusters of up to 3x4 spins.)

Let us consider the effect of including further-neighbour interactions in addition to the nearest neighbour interactions we have been concerned with so far. An extreme model of this type is the "equivalent-neighbour" model where all inter-spin interactions are permitted and all are of equal strength. The Heisenberg limit solutions are trivial (they

are essentially the complete set of eigenvalues of the total spin operator for an N-spin system.) This result has been exploited by Kittel and Shore (1965) to obtain numerical thermodynamic properties for ferromagnetic clusters of up to N=20,000 spin-1/2 atoms (which they remark is less difficult than calculating the 10-spin ring for the nearest-neighbour Hamiltonian). In contrast to the spin-1/2 linear case, an expected finite temperature phase transition is shown to develop which is demonstrated to be of the mean-field type.

There is some experimental evidence to suggest that a class of substances exist which are linear in type but have variable interaction strengths between pairs of spins along the chain. Duffy and Barr (1968) have considered the "alternating" Hamiltonian for certain of these substances (Nordio, Soos and McConnell, 1966)

$$\mathcal{H} = 2|J|\sum_{i=1}^{N/2} \left(\underline{S}_{2i} \cdot \underline{S}_{2i-1} + \alpha\, \underline{S}_{2i} \cdot \underline{S}_{2i+1} \right) \qquad (1.3)$$

where, as the parameter α varies from 0 to 1, the corresponding Hamiltonian describes a system which varies between an assembly of antiferromagnetic binary clusters to an isotropic antiferromagnetic linear chain. Duffy and Barr have undertaken a numerical study of this Hamiltonian, which follows the approach of this thesis. Their estimated limiting results, as α varies from 1 to 0 are generally very similar to our results for increasing anisotropy γ. The only distinction is seen between their susceptibility curves, which are always isotropic, and go to zero as $T \to 0$ and our perpendicular susceptibility curves for all γ which remain non-zero as $T \to 0$. Powder susceptibility measurements do not appear to extend to low enough temperatures to distinguish between the two models and therefore the alternating hypothesis of the behaviour of certain substances (e.g. doubly-nitrated DPPH (Duffy and Strandburg, 1967)) appears subject to some doubt.

It is interesting that Duffy and Barr present a comparison of their numerical work with various field-theoretic treatments which echoes our conclusions on the general inadequacy of such treatments.

It is interesting to note that whereas the Heisenberg spin-1/2 linear chain problem is considerably more difficult than the spin-1/2 Ising linear chain, the reverse is true for spin- ∞. An exact analytical solution to the linear chain Ising spin- ∞ model has not yet been obtained. However Joyce (1967) has treated the general anisotropic linear, spin- ∞, model by series expansion techniques and equivalent series results for the Ising spin- ∞ limit have been reported by Thompson (to be published).

CHAPTER II

QUANTUM-MECHANICAL ASPECTS OF THE PROBLEM AND COMPUTATIONAL TECHNIQUES

Introduction

In this chapter we present an account of matrix techniques for evaluating the eigenvalues and eigenvectors of linear spin-1/2 systems with quantum-mechanical coupling. The magnetic and thermodynamic properties of these systems may then be determined. The ultimate interest lies in predicting the properties of an infinitely large spin system by extrapolating the results for a series of small systems of increasing size. Thus it is obviously advantageous to extend the calculations to as large a system as possible.

Since practical limitations exist on the size of matrices which may conveniently be diagonalised, we must look for techniques which simplify the form of the Hamiltonian matrix for larger systems. Symmetry properties of the Hamiltonian can be exploited to this effect. We define a set of symmetry related quantum-mechanical operators which commute with the Hamiltonian. Each of these operators may be used to convert the Hamiltonian matrix to a block diagonal matrix. Further, when a subset of these operators commute among themselves, the operators can be used successively in a stage-by-stage breakdown (repeated block diagonalisation) of the Hamiltonian matrix.

This reduction process can be made very powerful, provided all relevant symmetry properties are defined and exploited. Previous authors have observed and made use of some of these symmetry operators. Here, however, we present for the first time a list of such operators which is complete in the special sense that the resulting reduction of the Hamiltonian matrix is maximal, implying that all energy level degeneracies have been removed.

In section (1) we discuss the quantum-mechanical formulation of the problem, in which the Hamiltonian appears as a finite matrix. A knowledge of

the properties of the relevant one- and two-spin operators makes it possible to set up this matrix.

In section (2) a complete list of the symmetry properties of the Hamiltonian is presented and a corresponding quantum-mechanical operator is defined in each case. In section (3) it is proved that certain of these operators commute with each other. The nature and extent of the matrix reductions which result are considered in both sections (2) and (3).

In section (4) the results of successive matrix reduction are explicitly illustrated for the case of a ring of 11 spins. The effect of placing the spin system in an external magnetic field is also discussed in this section. Reduction schemes used by other authors are briefly mentioned, and in Appendix 1 a detailed account of other work for the special case of the Heisenberg limit is presented. In section (5) the detailed application of these methods is discussed together with the numerical computer techniques required for the final solution of the eigenvalue problem. At the end of the section an inventory of eigenvalues and eigenvectors obtained in this way is given. Tables of eigenvalues are to be found in Appendix 2.

1. MATRIX REPRESENTATION OF THE HAMILTONIAN

1.1) Operator Representation of the Hamiltonian

Let us consider, for simplicity, the basic nearest-neighbour Heisenberg Hamiltonian for an N-particle, spin-1/2 linear system

$$\mathcal{H} = -2J \sum_{i=1}^{N} \underline{S}_i . \underline{S}_{i+1} \qquad (2.1.1)$$

where for ferromagnetic coupling, $J = |J|$

and for antiferromagnetic coupling, $J = -|J|$.

One-Particle Operator $\underline{S}_i$

The spin operator $\underline{S}_i$ corresponding to the i^{th} site along the chain, may be written in terms of the Pauli spin matrices $\underline{S}_i = 1/2\,\hbar\,\underline{\sigma}_i$, where $\underline{\sigma}_i$ has the familiar components

$$\sigma_x = \begin{bmatrix} 0 & 1 \\ 1 & 0 \end{bmatrix} \; ; \; \sigma_y = \begin{bmatrix} 0 & -i \\ i & 0 \end{bmatrix} \; ; \; \sigma_z = \begin{bmatrix} 1 & 0 \\ 0 & 1 \end{bmatrix} \qquad (2.1.2)$$

The Hamiltonian then becomes

$$\mathcal{H} = -\frac{J}{2} \sum_{i=1}^{N} \underline{\sigma}_i . \underline{\sigma}_{i+1} \qquad (2.1.3)$$

$\underline{S}_i^z$ has two eigenvalues, (which may, without loss of generality, be taken as $\pm\, 1/2\hbar$) corresponding to 'spin up' and 'spin down'. The corresponding complete set of eigenvectors, which we may call α and β , are then defined as

$$S_i^z \alpha = \tfrac{1}{2}\hbar\alpha \; ; \quad S_i^z \beta = -\tfrac{1}{2}\hbar\beta \qquad (2.1.4)$$

Two-Particle Operator $\underline{S}_i \cdot \underline{S}_{i+1}$

This operator operates in a four-dimensional manifold which is the product of the two, 2x2, spin spaces of the i^{th} and $(i+1)^{st}$ sites. Hence the four basic wave-functions may be taken as products of one-particle functions namely:- $\alpha_1 \times \alpha_2$, $\beta_1 \times \alpha_2$, $\alpha_1 \times \beta_2$, $\beta_1 \times \beta_2$, or using the symbolic Dirac bracket notation $|\uparrow\uparrow\rangle$; $|\downarrow\uparrow\rangle$; $|\uparrow\downarrow\rangle$; $|\downarrow\downarrow\rangle$. The operator

$$\underline{\sigma}_i . \underline{\sigma}_{i+1} = \sigma_i^z \sigma_{i+1}^z + \sigma_i^x \sigma_{i+1}^x + \sigma_i^y \sigma_{i+1}^y \qquad (2.1.5)$$

may then be expressed as a 4x4 matrix such that

$$\sigma_i^z \sigma_{i+1}^z = \begin{bmatrix} 1 & 0 & 0 & 0 \\ 0 & -1 & 0 & 0 \\ 0 & 0 & -1 & 0 \\ 0 & 0 & 0 & 1 \end{bmatrix} \qquad \sigma_i^x \sigma_{i+1}^x = \begin{bmatrix} 0 & 0 & 0 & 1 \\ 0 & 0 & 1 & 0 \\ 0 & 1 & 0 & 0 \\ 1 & 0 & 0 & 0 \end{bmatrix}$$

$$\sigma_i^y \sigma_{i+1}^y = \begin{bmatrix} 0 & 0 & 0 & -1 \\ 0 & 0 & 1 & 0 \\ 0 & 1 & 0 & 0 \\ -1 & 0 & 0 & 0 \end{bmatrix} \qquad \underline{\sigma}_i \cdot \underline{\sigma}_{i+1} = \begin{bmatrix} 1 & 0 & 0 & 0 \\ 0 & -1 & 2 & 0 \\ 0 & 2 & -1 & 0 \\ 0 & 0 & 0 & 1 \end{bmatrix}$$

and

$$\left\{ \sigma_i^x \sigma_{i+1}^x + \sigma_i^y \sigma_{i+1}^y \right\} := \begin{bmatrix} 0 & 0 & 0 & 0 \\ 0 & 0 & 2 & 0 \\ 0 & 2 & 0 & 0 \\ 0 & 0 & 0 & 0 \end{bmatrix} \qquad (2.1.6)$$

Hence we see that $\sigma_i^z \sigma_{i+1}^z$ is a diagonal operator in this representation, whereas $\sigma_i^x \sigma_{i+1}^x$ and $\sigma_i^y \sigma_{i+1}^y$ contain off-diagonal terms.

Effects of $\underline{\sigma}_i \cdot \underline{\sigma}_{i+1}$ on an N-Spin System.

The quantum theory of many-particle systems implies that when considering an N-particle system we work in a 2N dimensional space and choose as basic states, functions of the type

$$\varphi = \left| \uparrow_1 \cdots \uparrow_{i-1} \uparrow_i \downarrow_{i+1} \uparrow_{i+2} \cdots \downarrow_N \right\rangle$$

$\sigma_i^z \sigma_{i+1}^z$

From our previous explicit matrix representation we see that $\sigma_i^z \sigma_{i+1}^z$ operating on a system with the neighbouring spins on the i^{th} and $(i+1)^{st}$ sites parallel leaves the system unchanged and yields an eigenvalue +1. If $\sigma_i^z \sigma_{i+1}^z$ operates on two neighbouring antiparallel spins it again leaves the system unchanged and gives eigenvalue -1.

Ising Model

The sum of such operators over all spins, denoted by

$$O^z = \sum_{i=1}^{N} \sigma_i^z \sigma_{i+1}^z \qquad (2.1.7)$$

is, in fact, the Ising operator and hence we conclude that the particular set of basic states we have chosen for our representation are those states which diagonalise the Ising Hamiltonian.

$\sigma_i^x \sigma_{i+1}^x + \sigma_i^y \sigma_{i+1}^y$

We see from equation (2.1.6) that this operator operating on a system with a neighbouring parallel spin pair annihilates the whole wave-function. If, however, it operates on a system with a neighbouring antiparallel spin pair it produces a wave-function with the spin pair interchanged:

$$\left\{\sigma_i^x \sigma_{i+1}^x + \sigma_i^y \sigma_{i+1}^y\right\} \left|\uparrow \cdots \underset{i}{\uparrow}\underset{i+1}{\downarrow} \cdots \downarrow\right\rangle = 2 \left|\uparrow \cdots \underset{i}{\downarrow}\underset{i+1}{\uparrow} \cdots \underset{N}{\downarrow}\right\rangle \qquad (2.1.8)$$

Defining $O^{x+y} = \sum_{i=1}^{N} \left\{\sigma_i^x \sigma_{i+1}^x + \sigma_i^y \sigma_{i+1}^y\right\}$, we obtain the following properties of O^z and O^{x+y} operating on a given basic state

$$\varphi = \left|\uparrow \cdots \underset{i-1}{\uparrow}\underset{i}{\uparrow}\underset{i+1}{\downarrow}\underset{i+2}{\uparrow} \cdots \underset{N}{\downarrow}\right\rangle$$

$$O^z \varphi = \left(n_{par} - n_{antipar}\right) \varphi \qquad (2.1.9)$$

where n_{par} = no. of $\uparrow\uparrow$ spin pairs in φ, $n_{antipar}$ = no. of anti-$\uparrow\uparrow$ spin pairs in φ.

$$O^{x+y} \varphi = 2 \sum_{n_{antipar}} \varphi' \qquad (2.1.10)$$

where φ' is a spin function differing from φ by interchange of a pair of neighbouring anti-$\uparrow\uparrow$ spins and the sum goes over all $n_{antipar}$ distinct functions φ'.

1.2) Dirac Permutation Operator

The general, anisotropic, Hamiltonian may be written as the operator

$$\mathcal{H} = -\frac{J}{2} O^{z} - \frac{\gamma J}{2} O^{x+y} \qquad (2.1.11)$$

and the matrix elements evaluated in our representation from the properties of the operators O^{z} and O^{x+y}. There is another approach, useful in the Heisenberg limit, which expresses the Hamiltonian in terms of the permutation operator which is defined in the case of spin-1/2 as

$$P_{ij} = 2\left(\underline{S}i.\underline{S}j + \frac{1}{4}\right) \qquad (2.1.12)$$

which interchanges the i^{th} and j^{th} spins, if different, otherwise giving unity.

Hence

$$\mathcal{H}_{Heis} = J\sum_{i=1}^{N} P_{i,i+1} - \tfrac{1}{2}NJ \quad . \qquad (2.1.13)$$

The rather simpler properties of the operator P_{ij} make this approach somewhat preferable to the preceeding. By writing the general, anisotropic, Hamiltonian in the form

$$\mathcal{H} = 2\gamma J\sum_{i=1}^{N}\left\{\underline{S}i.\underline{S}_{i+1} + \frac{(1-\gamma)}{\gamma} S_i^z S_{i+1}^z\right\} \qquad (2.1.14)$$

this technique can be used to simplify the writing down of matrix elements in the anisotropic case also, since the first term brings in P_{ij} and the second term merely adds in additional, diagonal, Ising factors.

The resulting spin matrix corresponding to an N-spin linear system has dimensionality 2^N (for spin-1/2) since the spin at each site may be either 'up' or 'down'. However, the symmetry properties of the Hamiltonian and a special choice of boundary conditions enable

the size of the matrices to be reduced sufficiently for the problem to become numerically soluble on digital computers to a chain length of about 11 spins.

1.3) Boundary Conditions

It is commonly accepted that the use of periodic boundary conditions leads to the most mathematically tractable formulation of the problem. In the case of a linear chain, this means that the spins form a ring and every spin on the ring is equivalent. It happens that not only does this approach drastically simplify the matrix diagonalization problem but the results are, on the whole, better behaved from the point of view of estimating the properties of an infinitely long chain, than those obtained by other choices of boundary conditions. However, in so far as this model has a relation to experimentally investigated substances, ring boundary conditions for small systems ($N \leq 15$) are rather artificial and 'free end' boundary conditions are indicated. Spin systems with 'ring' and 'free end' boundary effects will henceforth be termed 'rings' and 'chains' respectively.

1.4) Properties of the Spin Operators

Single Spin Systems

The single-spin vector operator $\underline{S}_i = \frac{1}{2} \hbar \underline{\sigma}_i$ is well-known to obey the following commutation relations

$$\underline{S}_i \times \underline{S}_j = i \underline{S}_i \delta_{ij} \qquad (2.1.15)$$

(from now on we work in units of $\hbar$) or in terms of cartesian components

$$\begin{aligned} S_i^x S_i^y &= \tfrac{1}{2} i S_i^z = -S_i^y S_i^x \\ S_i^y S_i^z &= \tfrac{1}{2} i S_i^x = -S_i^z S_i^y \\ S_i^z S_i^x &= \tfrac{1}{2} i S_i^y = -S_i^z S_i^x \end{aligned} \qquad \left[S_i^{xyz}, S_j^{xyz} \right] = 0 \qquad (2.1.16)$$

In the literature the use of spin flip operators is common.

They are defined as:

$$S_i^+ = S_i^x + iS_i^y \quad ; \quad S_i^- = S_i^x - iS_i^y \qquad (2.1.17)$$

In the matrix representation of section (1.1) they would appear as

$$S_i^+ = \begin{bmatrix} 0 & 1 \\ 0 & 0 \end{bmatrix} \quad ; \quad S_i^- = \begin{bmatrix} 0 & 0 \\ 1 & 0 \end{bmatrix} \qquad (2.1.18)$$

Representing the state α ($|\uparrow\rangle$) as the coordinate vector $\begin{bmatrix} 1 \\ 0 \end{bmatrix}$ and β ($|\downarrow\rangle$) as $\begin{bmatrix} 0 \\ 1 \end{bmatrix}$, it is easy to verify that

$$\begin{aligned} S_i^+ |\uparrow\rangle &= 0 \quad ; \quad S_i^+ |\downarrow\rangle = |\uparrow\rangle \\ S_i^- |\uparrow\rangle &= |\downarrow\rangle \quad ; \quad S_i^- |\downarrow\rangle = 0 \end{aligned} \qquad (2.1.19)$$

Hence S_i^+ is an operator tending to turn up the i^{th} spin, and S_i^- an operator trying to turn down the i^{th} spin, The off-diagonal terms in the Hamiltonian may be expressed in terms of S_i^+ and S_i^-. Since

$$\left(S_i^x S_j^x + S_i^y S_j^y\right) = \frac{1}{2}\left(S_i^+ S_j^- + S_i^- S_j^+\right)$$

the operator $0^{x+y} = 2\gamma J \sum_{i=1}^{N} \left(S_i^+ S_{i+1}^- + S_i^- S_{i+1}^+ \right) \qquad (2.1.20)$

N-Spin Operators

Consider the total spin operator $\underline{S} = \sum_{i=1}^{N} \underline{S}_i$ whose square is

$$S^2 = \left(\sum S_i\right)^2 = \left(S^x\right)^2 + \left(S^y\right)^2 + \left(S^z\right)^2 \qquad (2.1.21)$$

(cf, the corresponding single-spin relation $S_i^2 = \left(S_i^x\right)^2 + \left(S_i^y\right)^2 + \left(S_i^z\right)^2$).

The Hamiltonian corresponding to the basic nearest-neighbour ring system (equation 2.1.1) now situated in an applied magnetic field $\underline{H}$ is

$$\begin{aligned} \mathcal{H} &= -2J \sum_{i=1}^{N} \underline{S}_i \cdot \underline{S}_{i+1} + g\beta \underline{H} \cdot \left(\sum_{i=1}^{N} \underline{S}_i\right) \\ &= -2J \sum \underline{S}_i \cdot \underline{S}_{i+1} + g\beta \underline{H} \cdot \underline{S} \end{aligned} \qquad (2.1.22)$$

where m is the magnetic moment per spin, and $m\underline{H}\cdot\underline{S}$ is a Zeeman-type term representing the energy of interaction of the spin system with a field in an arbitrary direction. ($\underline{H}\cdot\underline{S}$ has components $H_z S^z$

parallel to the z-direction and $H_x S^x$ and $H_y S^y$ in a perpendicular direction).

The operator S^2 may also be expressed as

$$S^2 = \sum_{i=1}^{N} S_i^2 + 2 \sum_{1 \le i < j}^{N} \underline{S}_i \cdot \underline{S}_j \qquad (2.1.23)$$

(A two parameter double sum as in the second term will henceforth be denoted $\sum_{(i,j)}$). The general theory of angular momentum tells us that the total spin operators obey the same kind of relations as the single spin operators. In particular, we have the total spin analogue of equations (2.1.15)

$$\underline{S} \times \underline{S} = i \underline{S} \qquad (2.1.24)$$

Expanded in terms of the cartesian components of $\underline{S}$, equation (2.1.24) becomes

$$\begin{aligned} [S^x, S^y] &= i S^z \\ [S^y, S^z] &= i S^x \\ [S^z, S^x] &= i S^y \end{aligned} \qquad (2.1.25)$$

(Notice that the special simplification $S_i^x S_i^y = \frac{1}{2} i S_i^z$, etc., applies only to spin-1/2 operators.)

2. SYMMETRY PROPERTIES OF THE HAMILTONIAN.

2.1) Conservation Properties

In this sub-section we shall introduce a set of quantum-mechanical operators which all have the property of commuting with the Hamiltonian. The investigation of the eigenvalues of the Hamiltonian may simplify considerably when the eigenvalues and eigenfunctions of such operators are known. This result depends on a fundamental theorem concerning commuting operators in quantum mechanics.

Suppose $\underline{B}$ is an operator which commutes with $\underline{H}$ and we represent by $\varphi_{k,p}$ $(p = 1, 2, \ldots, p_k)$ the eigenfunctions of $\underline{B}$ corresponding

to an eigenvalue B_k, which may be degenerate. Then the linear combinations $\sum_p C_p \varphi_{k,p}$, with suitably chosen C_p are eigenfunctions of $\underline{\mathcal{H}}$. Therefore our eigenvalue problem of degree 2^N can be reduced to other eigenvalue problems of lower degree (equal in each case to p_k, the degeneracy of the k^{th} eigenvalue of $\underline{B}$).

In matrix terms, this means that if we represent the Hamiltonian in the basis $\varphi^B_{k,p}$, the matrix will appear in block diagonal form, each block corresponding to a particular B_k, and of size $p_k \times p_k$. From now on, we shall speak of this process as 'reducing the Hamiltonian'. The problem of diagonalisation of $\underline{\mathcal{H}}$ then becomes the problem of choosing the coefficients C_p; in other words, diagonalising the blocks.

2.2) Spin Inversion Symmetry

The Hamiltonian is invariant under the operation of replacing all 'up' spins by 'down' spins and vice-versa. This has been occasionally termed in the literature 'rotational invariance', apparently since it corresponds to rotating all spins through 180° (Orbach, 1959). This property holds for the general anisotropic Hamiltonian as well as for the Ising and Heisenberg special limits. Its validity is independent of the boundary conditions. The spin-inversion operator, in fact, has the significance of the 'time reversal' operator for spin systems.

We may define a spin inversion operator $\underline{I}$

$$\text{eg. } \underline{I} \,|\uparrow\uparrow\uparrow\downarrow\downarrow\rangle = |\downarrow\downarrow\downarrow\uparrow\uparrow\rangle \qquad (2.2.1)$$

It follows that $I^2 = 1$, and hence the eigenvalues of $\underline{I}$ are $I = \pm 1$.

At this point we will briefly discuss the fact that if the Hamiltonian is invariant under a given operator $\underline{P}$, then $\underline{P}$ commutes with the Hamiltonian. Suppose the eigenvalue equation is

$$\mathcal{H}\,\psi_\lambda = E_\lambda\,\psi_\lambda \tag{2.2.2}$$

where, of course, the E_λ are the complete set of eigenvalues and ψ_λ the complete set of eigenfunctions of $\underline{\mathcal{H}}$. The invariance of $\underline{\mathcal{H}}$ with respect to $\underline{P}$ implies the relation

$$\underline{\mathcal{H}}\ (\underline{P}\,\psi_\lambda) = E_\lambda\,(\underline{P}\,\psi_\lambda) \tag{2.2.3}$$

operating on(2.2.2) with P gives

$$\underline{P}\,\underline{\mathcal{H}}\,\psi_\lambda = E_\lambda\,\underline{P}\,\psi_\lambda \tag{2.2.4}$$

which together with(2.2.3) implies $[\,\underline{\mathcal{H}},\ \underline{P}\,]\,\psi_\lambda = 0$ for all λ, and therefore $\underline{\mathcal{H}}$ commutes with $\underline{P}$.

Effect on the Hamiltonian Matrix

In any representation of the Hamiltonian, half the states will be spin inverses of the other half. Therefore, in a representation in terms of symmetric and antisymmetric combinations of states with their inverses, the Hamiltonian matrix will split into two equal blocks corresponding to I = +1 and I = -1.

2.3) Conservation of Z-Component of Total Spin

$S^z = \sum_{i=1}^{N} S_i^{\,z}$ is the z-component of the total spin. It can easily be shown that this quantity commutes with the Hamiltonian

$$\mathcal{H} = -2J\sum^{N}\left\{ S_i^{\,z}S_j^{\,z} + \gamma\left(S_i^{\,x}S_j^{\,x} + S_i^{\,y}S_j^{\,y}\right)\right\} \tag{2.2.6}$$

Since S^z obviously commutes with itself and with all products of the form $S_i^{\,z}\,S_j^{\,z}$ it only remains to show that S^z commutes with the term $(S_i^{\,x}\,S_j^{\,x} + S_i^{\,y}\,S_j^{\,y})$. The general term of this commutator is

$$\left[S_i^{\,z},\ \left(S_j^{\,x}S_k^{\,x} + S_j^{\,y}S_k^{\,y}\right)\right] = \left[S_i^{\,z},\ S_j^{\,x}S_k^{\,x}\right] + \left[S_i^{\,z},\ S_j^{\,y}S_k^{\,y}\right] \tag{2.2.7}$$

The two commutators on the right obviously vanish for $i \neq j \neq k$.

We now consider other cases:

a) Put i = j. $\left[S_j^z, S_j^x S_k^x\right] = S_j^z S_j^x S_k^x - S_j^x S_k^x S_j^z$

$= i S_j^y S_k^x$ (using equations (2.1.15))

and

$$\left[S_j^z, S_j^y S_k^y\right] = -i S_j^x S_k^y \qquad (2.2.8)$$

b) Put i = k.

$$\left[S_k^z, S_j^x S_k^x\right] = i S_k^y S_j^x; \quad \left[S_k^z, S_j^y S_k^y\right] = -i S_k^x S_j^y$$

Hence $\left[\sum S_i^z, (S_j^x S_k^x + S_j^y S_k^y)\right] = 0$ since the term with i = j cancels with the term i = k. (2.2.9)

Hence $\left[\sum S_i^z, \sum_{j<k} (S_j^x S_k^x + S_j^y S_k^y)\right] = 0$ for all j and k. (2.2.10)

Hence we see that S^z commutes with $\mathcal{H}$ for all γ, including the limits $\gamma=1$ and $\gamma=0$.

Effect on Matrix

From considerations advanced in section (1.1), it is easy to show that the effect of $S^z = \sum_i S_i^z$ operating on a given, basic, Ising wave-function is to give the same function multiplied by a factor $1/2\hbar \times$(number of 'up' spins - number of 'down' spins). In other words S^z is diagonal in the basis which diagonalises the Ising operator, and the basic states are therefore eigenfunctions of S^z. The eigenvalue of S^z corresponding to a given basic function is determined only by the number of over-turned spins (with reference to the state with all spins aligned) and not on their arrangement. Therefore the basic states break up into groups, the states within each group being degenerate with respect to the operator S^z, corresponding to each of its eigenvalues $N/2, N/2-1, \cdots\cdots, -N/2$.

(Thus there are (N+1) distinct eigenvalues in all.)

It follows that the size of a particular S^z group of states, which by virtue of the theorem of sub-section (2.1), is also the size of the corresponding block of the reduced Hamiltonian, is given by the simple binomial expression $\binom{N}{r}$; where $r = N/2 - S^z$, (2.2.11)

and corresponds physically to the number of overturned spins.

Size of the Blocks.

It follows that the size of a particular S^z group of states, which, by virtue of the theorem of sub-section (2.1) is also the size of the corresponding block of the reduced Hamiltonian, is given by the simple binomial expression

$$\binom{N}{r} \qquad (2.2.11)$$

where $r = N/2 - S^z$ and corresponds physically to the number of overturned spins.

The largest S^z block will arise when $r \sim N/2$. N odd, i.e. $N = 2n+1$. There are two equal blocks of maximum size. of order

$$\binom{2n-1}{n-1} = \binom{2n-1}{n} \qquad (2.2.12)$$

The corresponding S^z eigenvalues are $\pm 1/2$. N even, i.e. $N = 2n$.

The largest block will now be an $S^z = 0$ block of order

$$\binom{2n}{n} = \frac{(2n)!}{(n!)^2} \qquad (2.2.13)$$

However we shall see in sub-section (3.2) of this chapter that the spin inversion symmetry cuts down this particular block by a factor of $\frac{1}{2}$, and hence the effective largest blocks are the $|S^z| = 1$ blocks of order $\frac{(2n)!}{(n-1)!\ (n+1)!}$. (2.2.14)

2.4) Conservation of the Square of the Total Spin.

The square of the total spin operator is $S^2 = \sum_{i=1}^{N} S_i^2 + 2 \sum_{(i,j)} \underline{S}_i . \underline{S}_j$.

Let us investigate the commutator $[S^2, \mathcal{H}]$.

Heisenberg Hamiltonian

Consider the Hamiltonian $\mathcal{H} = 2J \sum_{(i,j)} \underline{S}_i \cdot S_j$. This corresponds to an "equivalent neighbour model" applicable to close-packed clusters, since all interactions are permitted, and all are of equal strength. Since $\mathcal{H}$ obviously commutes with itself, we need to prove the commutation relation $[\sum_{i=1}^{N} S_i^2, \mathcal{H}] = 0$ to show that S is conserved for this

for this model. Now $[S_i^2, \underline{S}_j \cdot \underline{S}_k] = 0$ for all i, j, k, since S_i^2 is a scalar. But $[S_i^2, \underline{S}_j \cdot \underline{S}_k]$ is the general term in the sum $[\Sigma\, S_i^2, \sum_{(j,k)} \underline{S}_j \cdot \underline{S}_k]$ and hence $\sum_i S_i^2$ always commutes with $\mathcal{H}$ and with all sub-Hamiltonians with various restrictions on the sum over k, e.g. the ring and chain Hamiltonians.

To extend the commutation proof to all sub-Hamiltonians, we must now show that the operator $\sum_{(i,j)} \underline{S}_i \cdot \underline{S}_j$ also commutes with them. Consider the commutator $C = [\underline{S}_i \cdot \underline{S}_j, \underline{S}_\ell \cdot \underline{S}_m]$ which is the general term of the sum commutator $[\sum_{(i,j)} \underline{S}_i \cdot \underline{S}_j, \sum_{\{\ell,m\}} \underline{S}_\ell \cdot \underline{S}_m]$ where $\{\ell,m\}$ denotes the sum over ℓ and m, which may be subject to restrictions on m, e.g. $m = \ell + 1$ for nearest-neighbour models, and generally $\ell \neq m$. C contains terms of two basic types

a) $\underline{S}_i \cdot \underline{S}_j \cdot \underline{S}_\ell \cdot \underline{S}_m - \underline{S}_\ell \cdot \underline{S}_m \cdot \underline{S}_i \cdot \underline{S}_j = 0$ for all $i \neq j \neq \ell, \neq m$

b) $\underline{S}_i \cdot \underline{S}_j \cdot \underline{S}_j \cdot \underline{S}_m - \underline{S}_j \cdot \underline{S}_m \cdot \underline{S}_i \cdot \underline{S}_j = S_j^2 (\underline{S}_i \cdot \underline{S}_m - \underline{S}_m \cdot \underline{S}_i)$

$= 0$, all i, m. (2.2.16)

Hence we have proved that the total spin is conserved for all Hamiltonians of the Heisenberg type. This result leads to a powerful reduction of the Hamiltonion matrix which will not be discussed further here, but will be referred to in sub-section (3.2) of this chapter, and treated in detail in Appendix 1.

Anisotropic Hamiltonian

The anisotropic Hamiltonian with, in general, a restricted summation $\{\}$,

$$\mathcal{H}_\gamma = 2J \sum_{\{i,j\}} \left\{ S_i^z S_j^z + \gamma \left(S_i^x S_j^x + S_i^y S_j^y \right) \right\} \qquad (2.2.17)$$

may be written

$$\mathcal{H}_\gamma = 2\gamma J \sum_{\{i,j\}} \underline{S}_i \cdot \underline{S}_j + 2J(1-\gamma) \sum_{\{i,j\}} S_i^z S_j^z \qquad (2.2.18)$$

Since we have proved that S^2 always commutes with the first term, we must now investigate the possibility of commutation with the second term.

Consider

$$\left[S^z, S_\ell^z S_m^z\right] = \left[\sum S_i^z, S_\ell^z S_m^z\right] + 2J\left[\sum_{(i,j)} \underline{S}_i . \underline{S}_j, S_\ell^z S_m^z\right] \quad (2.2.19)$$

It follows from equation (2.2.15) above that $[S_i^z, S_\ell^z S_m^z]=0$ (2.2.20)

for all i, ℓ, m, and hence we need only consider the second term on the right. The terms in the commutator sum are of the basic types:-

$$\text{I)} \quad \left[\underline{S}_i . \underline{S}_j, S_\ell^z S_m^z\right] = 0 \; ; \qquad i,j \neq \ell, m \quad (2.2.21)$$

$$\text{II)} \quad \underbrace{\left[\underline{S}_i . \underline{S}_j, S_i^z S_m^z\right]}_{(1)}; \underbrace{\left[\underline{S}_i . \underline{S}_j, S_\ell^z S_i^z\right]}_{(2)}; \underbrace{\left[\underline{S}_i . \underline{S}_j, S_j^z S_m^z\right]}_{(3)}; \underbrace{\left[\underline{S}_i . \underline{S}_j, S_\ell^z S_j^z\right]}_{(4)} \quad (2.2.22)$$

Types (2) and (4) are equivalent to types (1) and (3). Hence consider

$$\text{a)} \quad \left[\underline{S}_i . \underline{S}_j, S_i^z S_m^z\right] = \left[\left(S_i^x S_j^x + S_i^y S_j^y + S_i^z S_j^z\right), S_i^z S_m^z\right]$$

The terms in z commute. Now $\left[S_i^x S_j^x, S_i^z S_m^z\right] = -i S_m^z S_i^y S_j^x$

$$\left[S_i^y S_j^y, S_i^z S_m^z\right] = +i S_m^z S_i^x S_j^y \quad (2.2.23)$$

$$\text{b)} \quad \left[\underline{S}_i . \underline{S}_j, S_j^z S_m^z\right] = \left[\left(S_i^x S_j^x + S_i^y S_j^y + S_i^z S_j^z\right), S_j^z S_m^z\right]$$

Now

$$\left[S_i^x S_j^x, S_j^z S_m^z\right] = -i S_m^z S_i^x S_j^y$$

$$\left[S_i^y S_j^y, S_j^z S_m^z\right] = i S_m^z S_i^y S_j^x \quad (2.2.24)$$

Hence

$$\left[\underline{S}_i . S_j, S_i^z S_m^z\right] = i S_m^z \left(S_i^x S_j^y - S_i^y S_j^x\right) = -\left[\underline{S}_i . \underline{S}_j, S_j^z S_m^z\right] \quad (2.2.25)$$

$$\text{c)} \quad \left[\underline{S}_i . \underline{S}_j, S_i^z S_j^z\right]$$

Now

$$\left[S_i^x S_j^x, S_i^z S_j^z\right] = -\tfrac{1}{4}\left(S_i^y S_j^y\right) - \left(-\tfrac{1}{4} S_i^y S_j^y\right) = 0 \quad (2.2.26)$$

and similarly

$$\left[S_i^y S_j^y, S_i^z S_j^z\right] = 0 \quad (2.2.27)$$

Hence type c) vanishes for any Hamiltonian. (Results (2.2.26) and (2.2.27) hold only for spin 1/2. For higher spin, using the complete computation relations (2.1.25), type C still vanishes owing

to cancellations of terms.) However it is interesting to notice that for the equivalent neighbour close-packed model, and only for this model, every term of type 11)(1) is paired off with a corresponding term of type 11)(3).

Hence S is a good quantum number only for the special Hamiltonian

$$\mathcal{H} = 2J\sum_{(i,j)} \left\{ S_i^z S_j^z + \gamma\left(S_i^x S_j^x + S_i^y S_j^y\right)\right\} \qquad (2.2.28)$$

for all γ, including the Ising limit. This is because the situation $0<\gamma<1$ does not correspond to the presence of realistic anisotropy for this equivalent neighbour model, since the anisotropic term commutes with the isotropic term in the Hamiltonian and hence does not influence the antiferromagnetic ground state. This was pointed out by Kasteleijn (1960, private communication) for the simplest system of two coupled spins.

2.5) Reflection Symmetry

The Hamiltonian of a cluster having at least one symmetry axis, as shown, for example, in fig. (2.1), is invariant under the appropriate re-labelling of corresponding spins. In this example re-labelling implies ($1 \rightleftharpoons 2$, 3, $4 \rightleftharpoons 5$, $6 \rightleftharpoons 7$). In the case of a chain of N spins, the single symmetry axis passes through the mid-point of the chain and the corresponding re-labelling is ($1 \rightleftharpoons N$, $2 \rightleftharpoons (N-1)$, etc.). For rings, several symmetry axes are available, whose type depends on whether N is even or odd. Reflection symmetry is a property of the anisotropic Hamiltonian, as well as the special limits. From fig. (2.2) we see that for even rings there are two types of reflection axis which we denote as A and B. For odd rings there is only one, called Θ. We may therefore define corresponding reflection operators R_A, R_B and R_Θ such that

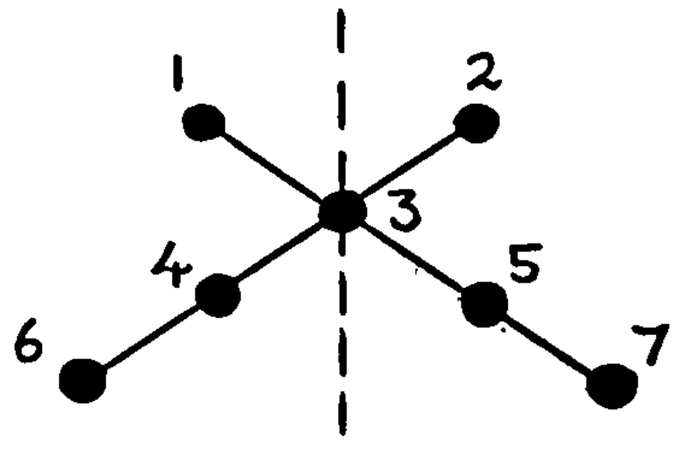

fig. (2.1)

$$R_A \quad |\uparrow\uparrow\uparrow\uparrow\downarrow\downarrow\rangle = |\downarrow\downarrow\uparrow\uparrow\uparrow\uparrow\rangle$$

$$R_B \quad |\uparrow\uparrow\uparrow\uparrow\downarrow\downarrow\rangle = |\uparrow\downarrow\downarrow\uparrow\uparrow\uparrow\rangle \qquad (2.2.24)$$

$$R_\theta \quad |\uparrow\uparrow\uparrow\downarrow\downarrow\rangle = |\downarrow\downarrow\uparrow\uparrow\uparrow\rangle$$

It is trivial to verify that all reflection operators R have eigenvalues ± 1. If we are considering even-spin chains, the only appropriate axis is the A- type (we may assume the 'broken bond' is the 1 - 6 bond) and for odd-spin chains we have, of course, R_θ.

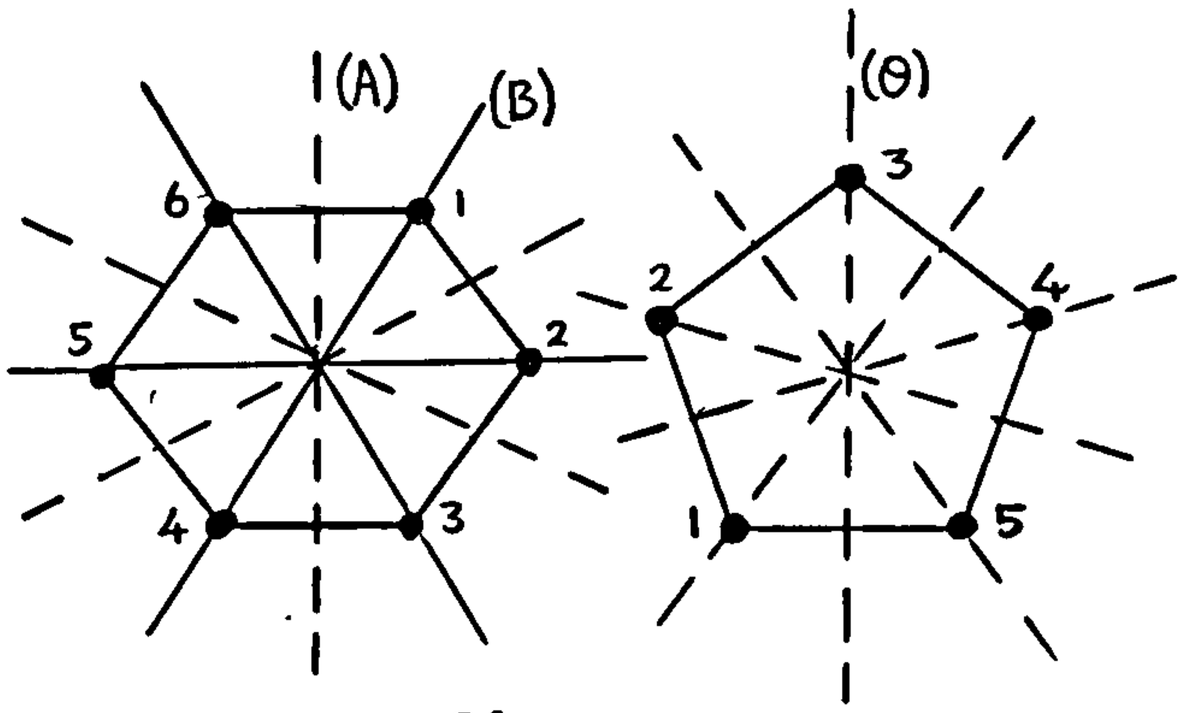

fig. (2.2)

Any representation of the Hamiltonian will be in terms of states, some of which reflect into themselves (corresponding, of course, to R = +1). The remaining states can be split into two unequal groups corresponding to symmetric and anti-symmetric combinations of states with their 'reflection twins', i.e. belonging to eigenvalues R = +1 and R = -1 respectively. The total R = +1 sub-block will therefore always be larger than the R = -1 sub-block since it includes the 'self-reflecting' states. The dimensions of each block depend on the type of operator, and are given in Table (2.1).

Operator	Number of Self-Reflecting States	Dimension of R = +1 Block	Dimension of R = -1 Block
R_A	$2^{N/2}$	$\frac{1}{2}(2^N + 2^{N/2})$	$\frac{1}{2}(2^N - 2^{N/2})$
R_B	$2^{N/2} + 1$	$\frac{1}{2}(2^N + 2^{N/2+1})$	$\frac{1}{2}(2^N - 2^{N/2+1})$
R_θ	$2^{(\frac{N+1}{2})}$	$\frac{1}{2}(2^N + 2^{\frac{N+1}{2}})$	$\frac{1}{2}(2^N - 2^{\frac{N+1}{2}})$

Table (2.1)

Block Diagonalisation by the Reflection Operators.

It will be observed, from Table (2.1), that there are twice as many self-reflecting states under the operation of R_B than R_A. This is because only basic states with an even number of reversed spins can reflect into themselves under A- type reflection, while B- type self-reflection applies to both odd and even reversed spin states. Hence type-A reflection is on the whole preferable, for rings, since there are fewer self-reflecting states which make the matrix approach a little more complicated to consider.

2.6) Translational Symmetry

It is obvious that if the spins are cyclically permuted round the ring, the physical situation remains unchanged. Let us denote by $\underline{T}$ the operator which rotates the spins so that each of the particles moves to the next highest site number, the N^{th} particle moving to the first site. First of all one sees that this operator is only defined in the case of periodic boundary conditions (rings). The effect of the operator $\underline{T}$ must be, at most, to change the phase of the wave-function. This introduces another characteristic of a given eigenstate of the system, ψ_n, namely its wave-vector $\underline{k}'$ defined through the relation

$$\underline{T}\,\psi_n = e^{i\underline{k}'.\underline{a}}\,\psi_n \qquad (2.2.30)$$

where a is the lattice spacing.

Properties of the Operator T

Consider the case N = 7, and a particular basic wave-function

$$|\uparrow\ \uparrow\ \uparrow\ \downarrow\ \uparrow\ \downarrow\ \downarrow\rangle$$

$$T\ |\uparrow\ \uparrow\ \uparrow\ \downarrow\ \uparrow\ \downarrow\ \downarrow\rangle = |\downarrow\ \uparrow\ \uparrow\ \uparrow\ \downarrow\ \uparrow\ \downarrow\rangle \qquad (2.2.31)$$

$$\text{Since } T^7\ |\uparrow\ \uparrow\ \uparrow\ \downarrow\ \uparrow\ \downarrow\ \downarrow\rangle = |\uparrow\ \uparrow\ \uparrow\ \downarrow\ \uparrow\ \downarrow\ \downarrow\rangle \qquad (2.2.32)$$

ie. $T^7 = 1$ for all such wavefunctions, the eigenvalues of T are the seven

7^{th} primitive roots of unity $1, \omega, \omega^2, \omega^3, \omega^4, \omega^5, \omega^6$ distributed round the unit circle, i.e.

$$\omega^q = \exp\left(2\pi i q/N\right), \qquad q = 0, 1, 2, \cdots, N-1.$$

The corresponding wave-number k' is given by

$$k'a = 2\pi q/N \quad \text{i.e.} \quad k' = 2\pi q/Na \tag{2.2.33}$$

Consider the Hermitian projection operator

$$F(\omega) = [1 + \omega^6 T + \omega^5 T^2 + \ldots + \omega T^6] \tag{2.2.34}$$

Now $$T\,F(\omega) = F(\omega)\,T = \omega\,F(\omega) \tag{2.2.35}$$

and hence, when applied to any wave-function, generates an eigenfunction of $\underline{T}$ with eigenvalue ω.

3) Mutual Commutation Properties and Matrix Reduction

3.1) Mutual Commutation Relations

In the previous sub-section we have studied the operators I, S^z, S, R and T, and shown that since each commutes with the fundamental $2^N \times 2^N$ Hamiltonian, a block diagonalisation is possible in each case. We shall now investigate the commutation properties of these operators with each other to see if further substantial reductions can be made.

This would arise by virtue of the argument introducing sub-section (2.1). Suppose we have a set of operators $\underline{A}$, $\underline{B}$, $\underline{C}$, ... etc. We have seen that if $\underline{A}$ commutes with $\underline{B}$, $\underline{A}$ is, in general, block diagonal in a representation diagonalising $\underline{B}$. Suppose, further, $\underline{C}$ commutes with both $\underline{B}$ and $\underline{A}$. Then, in a representation which diagonalises $\underline{C}$, $\underline{B}$ remains diagonal and each block of $\underline{A}$ is broken down yet again into a sequence of sub-blocks corresponding to the degeneracies of the eigenvalues of $\underline{C}$. Clearly, this process can be repeated, provided we have a set of operators all of which commute among themselves. The result of the process is that of successive matrix reduction. The process breaks down if two operators along the line fail to commute

with each other. When considering the maximum degree of matrix reduction, the interesting question still remains as to whether we have assembled an exhaustive list of effective operators. It is our belief, though we have no definite proof, that we have, in fact, achieved this, and the careful and detailed examination of commutation properties in the following sub-section has been undertaken to support this claim. The question will be discussed in more detail at the end of this section.

Let us now therefore examine the mutual commutation properties of our set of operators S^z, S^2, T, R and I, with these ideas in mind. We notice at the start there are limitations: T cannot be used for chains, and S is a good quantum number only in the Heisenberg limit, $\gamma = 1$.

3.2) Effects of the Mutual Commutations $[S^2, S^z]$:

$$[S^2, S^z] = [\{(S^x)^2 + (S^y)^2 + (S^z)^2\}, S^z] \qquad (2.3.1)$$

Now $[(S^z)^2, S^z] = 0$, hence consider $[(S^x)^2, S^z] + [(S^y)^2, S^z]$.

The total spin components obey the commutation relations

$$\therefore [(S^x)^2, S^z] = S^x S^x S^z - S^z S^x S^x = S^x [S^x, S^z] + [S^x, S^z]S^x$$

$$= -i(S^xS^y + S^yS^x) \qquad (2.3.2)$$

Now, by similar arguments we may show $[(S^y)^2, S^z] = +i(S^xS^y + S^yS^x)$. (2.3.3)

These two commutators, therefore, always cancel, and hence

$$[S^2, S^x] = 0 \qquad (2.3.4)$$

Matrix Reduction

In the scheme of reduction by S^z, described in sub-section (2.3), each S^z block contains states of total spin S in the range $N/2 \geq S \geq |S^z|$, with corresponding multiplicities $(N + 1)$ down to $(2|S^z| + 1)$. Hence we see, for example, that only the $S^z = 0$ block contains the singlet states (N even). A breakdown of the states

for N = 11 in terms of both S^z and S, which makes this point clear, is discussed in sub-section (4.2) of this chapter.

From the work of (Bloch 1929) the number of eigenfunctions of S^2 which belong to a given spin quantum number S and to a specified total spin component S^z, is independent of S^z and is given by the expression

$$A(S) = \binom{N}{\frac{N}{2}+S} \frac{2S+1}{N/2+S+1} \qquad (2.3.5)$$

This expression is easily obtained from relation (2.2.11) which implies that the number of states of total spin S (=| S^z|)

$$A(S) = \binom{N}{\frac{N}{2}+|S^z|} - \binom{N}{\frac{N}{2}+|S^z|+1} = \binom{N}{\frac{N}{2}+|S^z|} \frac{2S+1}{\frac{N}{2}+|S^z|+1} \qquad (2.3.6)$$

Reduction by S will be discussed in much greater detail in Appendix 1.

Translation Operator

Let us now consider the translation operator $\underline{T}$

$$[T, S^z]: \quad S^z \,|\uparrow\downarrow\uparrow\downarrow\downarrow\rangle = -\tfrac{1}{2}\,|\uparrow\downarrow\uparrow\downarrow\downarrow\rangle$$

$$\therefore T\,S^z \,|\uparrow\downarrow\uparrow\downarrow\downarrow\rangle = -\tfrac{1}{2}\,|\downarrow\uparrow\downarrow\uparrow\downarrow\rangle$$

$$= S^z\,T\,|\uparrow\downarrow\uparrow\downarrow\downarrow\rangle \qquad (2.3.7)$$

for all such basic, Ising states. Hence $\underline{T}$ and S^z commute, and therefore $\underline{T}$ may be used to reduce the S^z blocks of the Hamiltonian by a factor of $\simeq$ N corresponding to the N eigenvalues of $\underline{T}$.

Effect on Matrix

Suppose we are interested in the states (for N=7) for which $S^z = 3/2$. The three types of states

$$\mathcal{G}_1 = |\downarrow\downarrow\uparrow\uparrow\uparrow\uparrow\uparrow\rangle$$

$$\mathcal{G}_2 = |\downarrow\uparrow\downarrow\uparrow\uparrow\uparrow\uparrow\rangle \qquad (2.3.8)$$

$$\mathcal{G}_3 = |\downarrow\uparrow\uparrow\downarrow\uparrow\uparrow\uparrow\rangle$$

together with the states obtained from these by translation (21 states in all) form a basis for representing the $S^z = 3/2$ block of the Hamiltonian. It may easily be verified that

$$\begin{aligned} \mathcal{H} g_1 &= 5 g_1 + (1 + T^{-1}) g_2 \\ \mathcal{H} g_2 &= (1+T) g_1 + 3 g_2 + (1 + T^{-1}) g_3 \\ \mathcal{H} g_3 &= (1+T) g_2 + (3 + T^3 + T^{-3}) g_3 \end{aligned} \qquad (2.3.9)$$

If the states $F(\omega) g_1$, $F(\omega) g_2$, $F(\omega) g_3$ are used instead of $g_1, g_2 + g_3$ we replace T by the eigenvalue ω, e.g.

$$\mathcal{H} \left[F(\omega) g_1\right] = 5 \left[F(\omega) g_1\right] + (1+\omega^6) \left[F(\omega) g_2\right] \qquad (2.3.10)$$

The Hamiltonian matrix then has the form

$$\mathcal{H} = \begin{bmatrix} 5 & 1+\omega^6 & 0 \\ 1+\omega & 3 & 1+\omega^6 \\ 0 & 1+\omega & 3+\omega^3+\omega^4 \end{bmatrix} \qquad (2.3.11)$$

In this way the size of the matrix to be diagonalised has been reduced by a factor of N, i.e. instead of diagonalising a 21 x 21 matrix, it is only necessary to consider seven 3 x 3 matrices of the above form, one matrix for each eigenvalue of $\underline{T}$. Hence, starting from matrix (2.3.11) the other six are easily obtained by substituting successive powers of ω, e.g. the second matrix of the set is

$$\begin{bmatrix} 5 & 1+(\omega^6)^2 & 0 \\ 1+(\omega)^2 & 3 & 1+(\omega^6)^2 \\ 0 & 1+(\omega)^2 & 3+(\omega^3)^2+(\omega^4)^2 \end{bmatrix} = \begin{bmatrix} 5 & 1+\omega^5 & 0 \\ 1+\omega^2 & 3 & 1+\omega^5 \\ 0 & 1+\omega^2 & 3+\omega+\omega^6 \end{bmatrix} \qquad (2.3.12)$$

This is convenient for machine computation. Since $\omega^6 = \omega^*$; $\omega^5 = (\omega^2)^*$; $\omega^4 = (\omega^3)^*$, and the matrices are Hermitian, the eigenvalues for a given ω are the same as those for ω^* and hence it is only necessary to diagonalise four matrices.

[T, S^2]:

This is essentially equivalent to $[T, \sum_{i<j\leq 1}^{N} \underline{S}_i \cdot \underline{S}_j]$. Now T is

equivalent to the permutation (1,2....N-1, N). The operator $\sum_{(i,j)}^{N} \underline{S}_i . \underline{S}_j$ is invariant under this permutation and hence S^2 and T must commute.

We therefore have four mutually commuting operators $\underline{H}$, S^z, $\underline{T}$ and S. The Hamiltonian may thus be successively reduced by S^z, T and S, as is demonstrated by the example N=6 in sub-section (4.1) of this chapter.

Reflection Operator

The three types of reflection operator have similar commutation properties and we may therefore, with *no* loss of generality, consider R_θ.

$[R_\theta, S^z]$:

$$S^z \mid \uparrow \downarrow \uparrow \downarrow \downarrow \rangle = + \frac{1}{2} \mid \uparrow \downarrow \uparrow \downarrow \downarrow \rangle$$

$$R_\theta S^z \mid \uparrow \downarrow \uparrow \downarrow \downarrow \rangle = \frac{1}{2} \mid \downarrow \downarrow \uparrow \downarrow \uparrow \rangle$$

$$= S^z R_\theta \mid \uparrow \downarrow \uparrow \downarrow \downarrow \rangle . \qquad (2.3.13)$$

for all such basic Ising states. Hence, generally R and S^z commute, and the S^z blocks of the Hamiltonian are further reduced.

Effect on Matrix

To illustrate this reduction process consider Fig. (2.1). This figure refers to the $S^z = 1$ block for N = 6. Matrix 1 shows the matrix representation of this Hamiltonian block for chains: the modifications introduced by the ring Hamiltonian are shown in brackets. The 15 basic states are numbered off in fig. (2.3) as follows:

ℓ_{j_1}		ℓ_{j_2}		ℓ_{j_3}	
1.1	$\mid \downarrow \downarrow \uparrow \uparrow \uparrow \downarrow \rangle$	2.1	$\mid \downarrow \uparrow \downarrow \uparrow \uparrow \uparrow \rangle$	3.1	$\mid \downarrow \uparrow \uparrow \downarrow \uparrow \uparrow \rangle$
1.2	$\mid \uparrow \downarrow \downarrow \uparrow \uparrow \uparrow \rangle$	2.2	$\mid \uparrow \downarrow \uparrow \downarrow \uparrow \uparrow \rangle$	3.2	$\mid \uparrow \downarrow \uparrow \uparrow \downarrow \uparrow \rangle$
1.3	$\mid \uparrow \uparrow \downarrow \downarrow \uparrow \uparrow \rangle$	2.3	$\mid \uparrow \uparrow \downarrow \uparrow \downarrow \uparrow \rangle$	3.3	$\mid \uparrow \uparrow \downarrow \uparrow \uparrow \downarrow \rangle$
1.4	$\mid \uparrow \uparrow \uparrow \downarrow \downarrow \uparrow \rangle$	2.4	$\mid \uparrow \uparrow \uparrow \downarrow \uparrow \downarrow \rangle$		
1.5	$\mid \uparrow \uparrow \uparrow \uparrow \downarrow \downarrow \rangle$	2.5	$\mid \downarrow \uparrow \uparrow \uparrow \downarrow \uparrow \rangle$		
1.6	$\mid \downarrow \uparrow \uparrow \uparrow \uparrow \downarrow \rangle$	2.6	$\mid \uparrow \downarrow \uparrow \uparrow \uparrow \downarrow \rangle$		

fig. (2.3)

Matrix 2 corresponds to the chain Hamiltonian alone. We see that the states are grouped in pairs, each pair corresponding to a state and its reflections 'twin', under the reflection operator R_A.

e.g. $R_A \; |\downarrow\downarrow\uparrow\uparrow\uparrow\uparrow\rangle = |\uparrow\uparrow\uparrow\uparrow\downarrow\downarrow\rangle$ and $R_A \; |\uparrow\uparrow\uparrow\uparrow\downarrow\downarrow\rangle = |\downarrow\downarrow\uparrow\uparrow\uparrow\uparrow\rangle$ (2.3.14)

i.e. $R_A \; |1.1\rangle = |1.5\rangle$ and vice versa.

Hence state 1.5 is the reflection twin of 1.1 under R_A.

Matrix 3 corresponds to the ring Hamiltonian. Here we have paired up states with their reflection twins under the reflection operator R_B. (R_B is not suitable for chains.) (For definitions of R_A and R_B, see sub-section (2.5) under the heading 'Reflection Symmetry'. The operator R_A is equivalent to the permutation {(16) (25) (34)} and R_B to {(1) (26) (35) (4)}.)

Matrix 4 is the transform matrix appropriate to reflection symmetry which corresponds to taking (suitably normalised) symmetric and anti-symmetric combinations of states and their twins. The effect of the complete transformation on both matrices 2 and 3 is shown by the elements in brackets in these matrices. Notice that only self-reflecting states are affected. Finally, in matrices 5 and 6, the transferred states are grouped according to whether they correspond to eigenvalues +1 or -1 of the appropriate reflection operators. In both cases the +1 blocks are 9x9, and the -1 blocks 6x6, in size. Hence the original 15x15 S^z block has been broken up into two sub-blocks of these dimensions.

<u>$[R, S^z]$</u>:

This is essentially equivalent to $[R, \sum_{(i,j)} \underline{S}_i \cdot \underline{S}_j]$. Now R is equivalent to the permutation $\{(1,N) \; (2,N-1) \; \ldots\ldots \; (N,1)\}$. The operator $\sum_{(i,j)} \underline{S}_i \cdot \underline{S}_j$ is invariant under this permutation and hence S^2 and R must commute.

FIGURE (2:1)

Hamiltonian Matrices For Rings and chains

(1)

	1·1	1·2	1·3	1·4	1·5	1·6	2·1	2·2	2·3	2·4	2·5	2·6	3·1	3·2	3·3
1	·1	−1 (−2)					γ					(γ)			
	·2		−2				γ	γ							
	·3			−2				γ	γ						
	·4				−2				γ	γ					
	·5					−1 (−2)				γ	(γ)				
	·6						−2				γ	γ			
2	·1	γ	γ				−3 (−4)						γ	(γ)	
	·2		γ	γ				−4					γ	γ	
	·3			γ	γ				−4				γ	γ	
	·4				γ	γ				−3 (−4)			(γ)	γ	
	·5					(γ)	γ				−3 (−4)		γ	γ	
	·6	(γ)					γ					−3 (−4)		γ	γ
3	·1							γ	γ	(γ)	γ		−3 (−4)		
	·2								γ	γ	γ	γ		−4	
	·3							(γ)		γ	γ	γ			−3 (−4)

(4)

	1·1	1·2	2·1	2·2	2·5	3·1	1·3	1·6	3·2	1·5	1·4	2·4	2·3	2·6	3·3
	1/√2 1/√2 / 1/√2 −1/√2														
		1/√2 1/√2 / 1/√2 −1/√2													
			1/√2 1/√2 / 1/√2 −1/√2												
				1/√2 1/√2 / 1/√2 −1/√2												
					1/√2 1/√2 / 1/√2 −1/√2											
						1/√2 1/√2 / 1/√2 −1/√2									
							1								
								1							
									1						

(2)

	1·1	1·6	1·2	1·5	1·3	1·4	2·1	2·5	2·2	2·4	3·2	3·3	2·3	2·6	3·1
	−1 / −1				γ / γ										
		−2 / −2			γ / γ		γ / γ								
	γ / γ		γ / γ		−3 / −3						γ / γ				
		γ / γ		γ / γ			−4 / −4				γ / γ		(γ/√2γ) γ / (0)		(γ/√2γ) γ / (0)
					γ / γ				−3 / −3		γ / γ			(γ/√2γ) γ / (0)	(γ/√2γ) γ / (0)
			γ / γ		γ / γ		γ / γ		γ / γ		−3 / −3				
							γ / γ (γ/√2γ)	γ / γ (0)	γ / γ (γ/√2γ)	γ / γ (0)			−2		
							γ / γ (γ/√2γ)	γ / γ (0)	γ / γ (γ/√2γ)	γ / γ (0)				−2	
							γ / γ (γ/√2γ)	γ / γ (0)	γ / γ (γ/√2γ)	γ / γ (0)					−4

(5)

	1·1	1·2	1·3	2·1	2·2	3·2	2·3	2·6	3·1	1·6	1·5	1·4	2·5	2·4	3·3
	−1			γ											
		−2		γ	γ										
			−3			γ									
	γ	γ		−4		γ	√2γ		√2γ						
	γ				−3	γ		√2γ	√2γ						
		γ	γ	γ	γ	−3									
							−2								
				√2γ				−2							
					√2γ	√2γ			−4						
										−1	γ				
											−2	γ	γ		
										γ	γ	−3			γ
											γ		−4		γ
														−3	γ
												γ	γ	γ	−3

(3)

	1·1	1·6	1·2	1·5	1·3	1·4	2·1	2·5	2·2	2·4	3·2	3·3	2·3	2·6	3·1
	−2 / −2						γ / γ							(γ/√2γ) γ / (0)	
			−2 / −2				γ / γ		γ / γ						
					−2 / −2				γ / γ				(γ/√2γ) γ / (0)		
	γ / γ		γ / γ				−4 / −4				(γ) γ / γ (−γ)				(√2γ) γ / (0)
			γ / γ						−4 / −4		γ / γ				(√2γ) γ / (0)
							(γ) γ / γ (−γ)		γ / γ		−4 / −4		(√2γ) γ / (0)	(√2γ) γ / (0)	
					γ / γ								−4 / −4		
	γ / γ						γ / γ		γ / γ					−4 / −4	
							γ / γ		γ / γ						−4 / −4

(6)

	1·1	1·2	1·3	2·1	2·2	3·2	2·3	2·6	3·1	1·6	1·5	1·4	2·5	2·4	3·3
	−2			γ				√2γ							
		−2		γ	γ										
			−2		γ		√2γ								
	γ	γ		−4		γ			√2γ						
	γ	γ	γ		−4	γ			√2γ						
			γ	γ	−4	√2γ	√2γ								
		√2γ			√2γ	−4									
	√2γ				√2γ		−4								
				√2γ	√2γ			−4							
										−2	γ				
										γ	−2	γ			
											γ	−4	γ		
												γ	−4	γ	
													γ	−4	

S^z	3	2						1															
k	0	0	1	2	3	4	5	0	0	0	1	1	2	2	2	3	3	4	4	4	5	5	
S	3	3	2	2	2	2	2	3	1	1	2	1	2	1	1	2	1	2	1	1	2	1	
																						I	

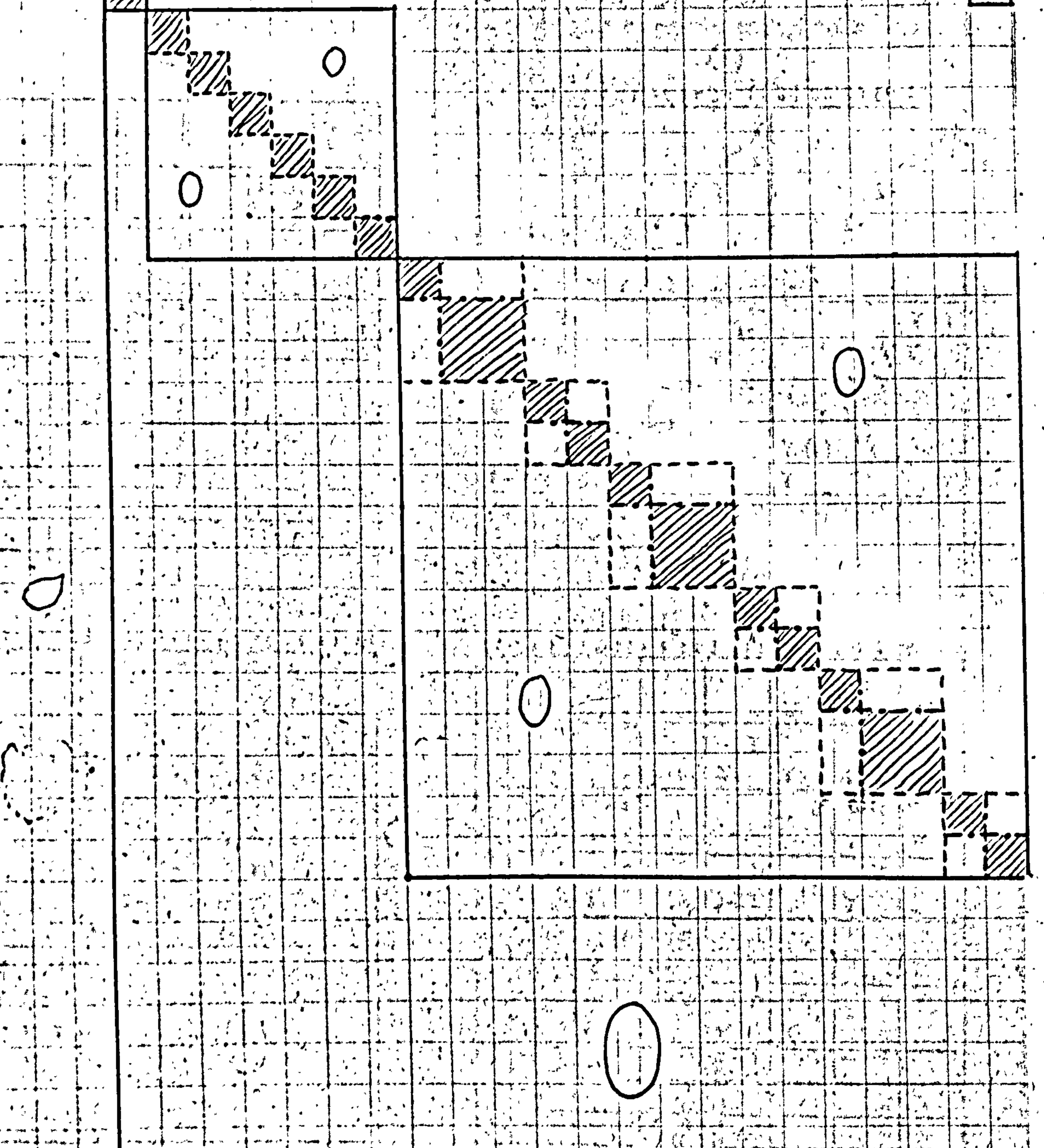

Successive Hamiltonian Matrix

Reduction for the $S^z = 0$ Block

of N = 6 (Ring).

FIG. (2.2)

O										O									
0	0	0	1	2	2	3	4	4	5	0	1	1	2	3	3	3	4	5	5
3	1	1	1	1	1	1	1	1	1	0	2	0	2	2	0	0	2	2	0
+1										-1									

———	breakdown by S^z
- - - - -	breakdown by k in addition to S^z
—·—·—·—	breakdown by S, k and S^z
+++++	application of spin inversion symmetry.

FIG. (2.2) (cont.)

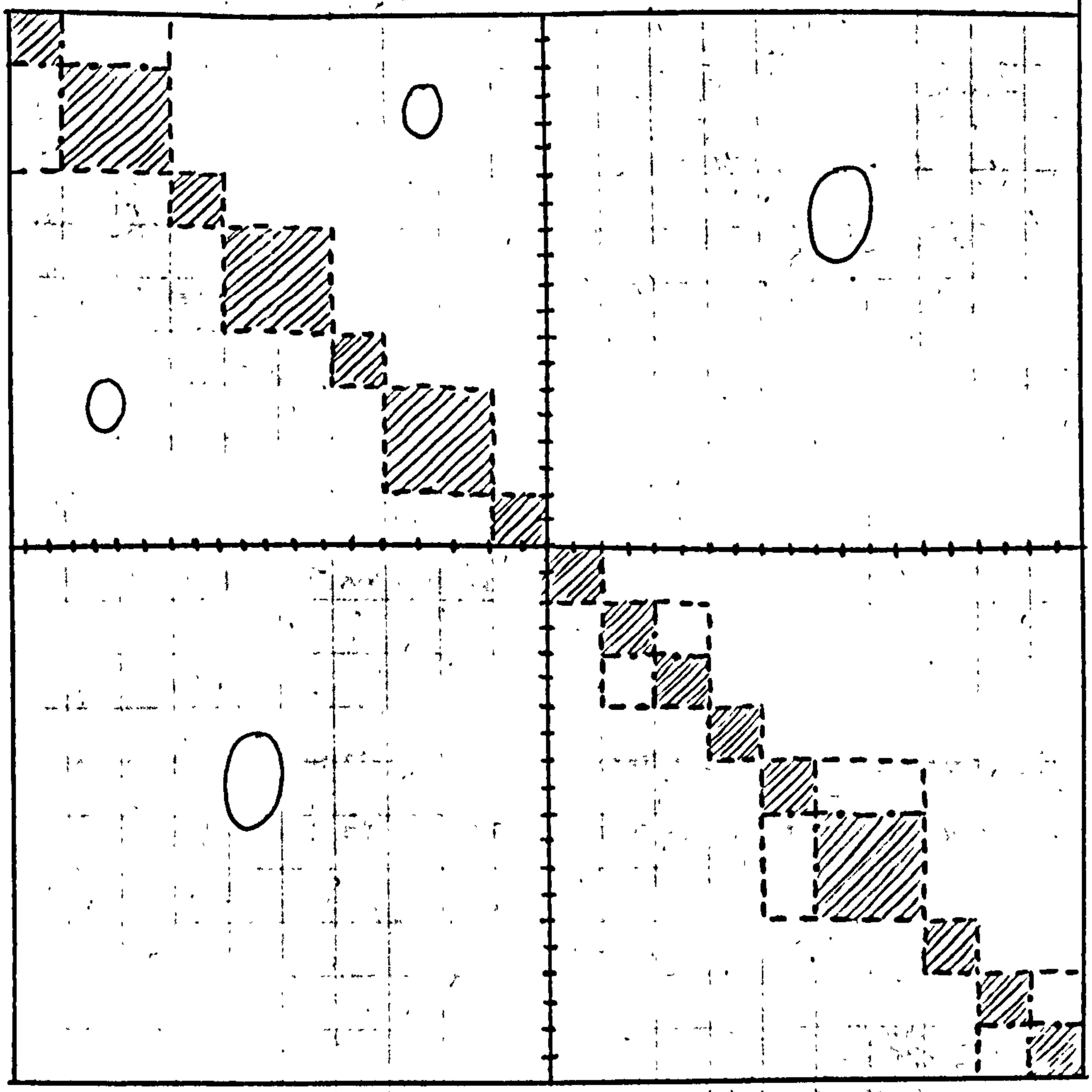

Hence we have another set of four mutually commuting operators $\underline{\mathcal{H}}$, S^z, R and S, which are suitable for the successive reduction of chains. We might, perhaps, hope that R could be used in addition to the set $\underline{\mathcal{H}}$, S^z, T and S to secure further reduction of the ring Hamiltonian.

Unfortunately R does not, in general, commute with T. It may easily be verified that

$$RT \neq TR = T^{-1}R = (RT)^{-1} \qquad (2.3.15)$$

Hence $(RT)^2=1$ and RT is a reflexive operator like R.

[R, T]:

$$R\,|\uparrow\downarrow\uparrow\downarrow\downarrow\rangle = |\downarrow\downarrow\uparrow\downarrow\uparrow\rangle;\quad T|\uparrow\downarrow\uparrow\downarrow\downarrow\rangle = |\downarrow\uparrow\downarrow\uparrow\downarrow\rangle$$

$$\therefore TR\,|\uparrow\downarrow\uparrow\downarrow\downarrow\rangle = |\uparrow\downarrow\downarrow\uparrow\downarrow\rangle;\quad RT|\uparrow\downarrow\uparrow\downarrow\downarrow\rangle = |\downarrow\uparrow\downarrow\uparrow\downarrow\rangle$$

$$T^{-1}R\,|\uparrow\downarrow\uparrow\downarrow\downarrow\rangle = |\downarrow\uparrow\downarrow\uparrow\downarrow\rangle = RT|\uparrow\downarrow\uparrow\downarrow\downarrow\rangle \qquad (2.3.16)$$

Thus, for rings, one may simultaneously diagonalise the mutually commuting sets of operators $\mathcal{H}$, S^z, T, S or $\mathcal{H}$, S^z, R, S; but not $\mathcal{H}$, S^z, T, R, S. Since reflection symmetry (see sub-section 2.5) yields a reduction factor of ~ 2, whereas T gives N/2, it is obviously more advantageous to use translation symmetry for rings. However, R obviously commutes with T^N (identity) and with $T^{N/2}$ for the case of N even. Now, for even-spin rings, the blocks of wave-number q = 0 or q = N/2 (where q is related to the wave-vector k' through equation (2.2.23)) contain states of special physical interest (see Chapter III), e.g. the ferromagnetic and antiferromagnetic ground states. For these special blocks, reflection symmetry may be used in addition to translation symmetry.

Combined Operators

It is perhaps worth verifying that combined operators of the form $R^p\,T^q$ do not yield a reduction factor > N. In fact, when not trivial,

they are equal, or equivalent, to R alone. Now $R^2=1$ and therefore we only consider P odd. Without loss of generality we may assume

$p = q$ (q odd) or $p = q + 1$ (q even)

q odd : Consider $R^q T^q$. Now $[RT]^{q-1} = 1$ since $[RT]^2 = 1$.

Hence $R^q T^q = RT$. (2.3.17)

q even: Consider $R^{q+1} T^q$. $[RT]^q = 1$ and hence $R^{q+1} T^q = R$. (2.3.18)

Spin Inversion Operator

The spin inversion operator commutes with S^z only for the case $S^z = 0$. Hence, in a representation in terms of the eigenvectors of S^z, the states do not generally possess inversion symmetry.

[I, S^z] $S^z \mid \downarrow \uparrow \downarrow \uparrow \uparrow > = +\frac{1}{2} \mid \downarrow \uparrow \downarrow \uparrow \uparrow >$; $I \mid \downarrow \uparrow \downarrow \uparrow \uparrow > = \mid \uparrow \downarrow \uparrow \downarrow \downarrow$

Proof $I S^z \mid \downarrow \uparrow \downarrow \uparrow \uparrow > = +\frac{1}{2} \mid \uparrow \downarrow \uparrow \downarrow \downarrow >$; $S^z I \mid \downarrow \uparrow \downarrow \uparrow \uparrow > = -\frac{1}{2} \mid \uparrow \downarrow \uparrow \downarrow \downarrow$ (2.3.19)

Hence I and S^z anticommute. This means that the states for a given negative S^z are the spin inverses of the states for a given positive S^z and hence if the states are appropriately ordered, the corresponding block matrices are identical. The eigenvalues are therefore the same.

For the $S^z = 0$ (N even) block, half the states are spin inverses of the other half and hence if symmetric and antisymmetric groupings of states and their inverses are taken, the block size is reduced by a half. This reduction is illustrated in Fig. (2.2) for the $S^z = 0$ block for N=6. We may observe that the symmetric sub-block contains S = 1 and S = 3 states, while the antisymmetric block contains S = 0, and S = 2 states. For N = 8, however, the symmetric block contains S = 0, S = 2 and S = 4 states, and the antisymmetric block S = 1 and S = 3 states. There is only one state of S = N/2 in any S^z block and this state is, in fact, a component of the ferromagnetic ground state (see Table(2.3), sub-section (4.2)). We see therefore that the ferro ground state component is always to be found in the symmetric sub-block of the

$S^z = 0$ block. The antiferromagnetic ground state is, as we have mentioned in chapter I, always a singlet and hence is to be found in the symmetric sub-block for N = 2n, n even, and in the antisymmetric sub-block for N = 2n, n odd., i.e. it is a state with spin inversion eigenvalue I = +1 and -1 respectively.

[I, S⁻], [I, R] and [I, T]

It is obvious that I and S^2 commute. Hence the eigenstates corresponding to a given total S may always be expressed as eigenvectors of I. It is easy to show that I commutes with both R and T. This result is not helpful except for the $S^z = 0$ block, N even, where application of spin inversion symmetry does not upset the S^z, T reduction scheme. Reflection symmetry does not give any additional reduction after the application of spin inversion symmetry for $S^z = 0$ blocks for N ≤ 10, since the reflection operator, operating on linear combinations of states and their spin inverses, yields either the same (combined) state, or the same state rotated around the ring. Since we must consider only q= 0 and q = N/2 sub-blocks, a rotated state is equivalent to the parent state or its negative. For N = 10, there are 26 basic parent states for the $S^z = 0$ block, generating 252 states in all, when states generated from the parent states by operation of T (translation) are taken into account. When linear combinations of these parent states and their spin inverses are taken, we have 15 combination parent states corresponding to I = +1 and an equal number corresponding to I = -1.

Let us consider the four parent states from this block:-

|↓↓↓↓↑↑↓↑↑↑>; |↓↓↓↑↑↑↑↓↓↑>; |↓↓↓↓↑↑↑↓↑↑>; |↓↓↓↑↓↓↑↑↑↑>,
(a) (b) (c) (d)

It is easy to show that a and b are related to each other by spin inversion symmetry and likewise c and d; and all four a, b, c and d are brought into association by a combination of reflection and inversion

symmetry. There is another set of four states in the N = 10, $S^z = 0$ block with this property, namely:-

$$|\downarrow\downarrow\downarrow\uparrow\downarrow\uparrow\uparrow\downarrow\uparrow\uparrow\rangle;\quad |\downarrow\downarrow\downarrow\uparrow\uparrow\downarrow\uparrow\uparrow\downarrow\uparrow\rangle;\quad |\downarrow\downarrow\uparrow\downarrow\downarrow\uparrow\downarrow\uparrow\uparrow\uparrow\rangle;\quad |\downarrow\downarrow\uparrow\downarrow\downarrow\uparrow\uparrow\uparrow\downarrow\uparrow\rangle$$

In this way it is possible to reduce the maximum matrices belonging to the k = 0 and k = 5 blocks from 15 x 15 to 13 x 13.

Where spin inversion symmetry is not applicable, spin reflection symmetry may be helpful in reducing the matrix for lower N. Examples are the $|S^z|$ = 1 blocks of N = 8 for chains, or the $|S^z|$ = 1, k = 0 or 4 blocks for N = 8 rings.

3.3) Summary of Commutation Properties

In sections 2 and 3, we have introduced the six quantum mechanical operators $\underline{\mathcal{H}}$, S^z, S^2, T, R and I, and discussed their mutual commutation properties in the light of matrix reduction. An insight may be obtained into the behaviour of these operators by noting that $\underline{\mathcal{H}}$ and S^2 are closely related since they are two-particle operators; the effect of both T and R is to shift spins around to different sites; and finally S^z and I are single-particle operators. In general, therefore, we see why it is that commutation is assured between pairs of operators such that each member is selected from one of these three different types,

e.g. $[\mathcal{H}, T]$; $[\mathcal{H}, R]$; $[\mathcal{H}, S^z]$; $[\mathcal{H}, I]$;
$[S^2, T]$; $[S^2, R]$; $[S^2, S^z]$; $[S^2, I]$;
$[T, S^z]$; $[T, I]$; $[R, S^z]$; $[R, I]$;

All these commutators must vanish. The possibility of non-commutation, as one would expect, arises only when we consider two operators of the same type, eg. $[\mathcal{H}, S^2]$; [R, T]; $[S^z, I]$ are non-vanishing.

3.4) Possibility of Additional Commuting Operators

Another useful division of our quantum-mechanical operators is into 'spin-type' operators; namely $\mathcal{H}$, S^2, S^z and I; and operators T and R which have a purely geometrical significance. The geometry of the linear rings is clearly very simple and our choice of the operators T and R is in accordance with the work of Carson (1952) (see Appendix 1) who points out that the group representation corresponding to a ring of N spins is the dihedral group of order N. There are clearly a very large number of spin operators containing various sums or products over the individual spins (spin identities exist to reduce multiple to single powers of spin combinations). Any uncertainty as to the exhaustive nature of our list of operators reduces to the possibility of constructing additional 'spin-type' operators independent of the four we have already. For example, in sub-section (3.3) of Chapter III, we discuss an interesting operator which rotates the individual x and y components of the spins on one sub-lattice. But this operator does not commute with the Hamiltonian and therefore cannot be used for reduction purposes.

However the set of operators we have discussed can be used to effect completely the removal of all degeneracy in the Hamiltonian for N up to and including 11, and hence no additional spin operators are required for these small clusters. We are unable to prove that for higher N additional degeneracies which are not removable through the techniques discussed in subsections 2 and 3 will not appear, but we feel, intuitively that this is unlikely. The work of Kawasaki (1966) supports these conclusions.

4. OVERALL MATRIX REDUCTION

4.1) Sets of Commuting Operators

Maximal reduction of the Hamiltonian matrix is achieved by successive block diagonalisation processes, utilizing as many of the operators S^z, S, I, T and R as commute among themselves (as described in section (3)). There is the further restriction that T cannot be used for chains and S^2 cannot be used for anisotropic $\mathcal{H}$. The appropriate operators for a given situation are summarised in the table below.(Table (2.2)).

Table (2.2)

Cluster Type	Heisenberg Limit ($\gamma=1$)	General γ (ie. $\gamma \neq 0,1$)
Rings	S^2, S, T, I when $S^2=0$.	S^2, T, I when $S^2=0$.
(cont.)	R when $T = T^N$ or $T^{N/2}$	R when $T = T^N$ or $T^{N/2}$
Chains	S^2, S, R, I when $S^2=0$.	S^2, R, I when $S^2=0$
Others	S^2, S, T? R?	S^2, T? R?
(Cont.)	I when $S^2=0$	I when $S^2=0$

(We should comment that the symbols ? mean that the associated operator is defined only if the cluster contains the appropriate reflection or rotation axes.)

The effect of successive employment of S^z, T, S, and I (for $S^z = 0$) conservation to the original $2^6 \times 2^6$ matrix for the ring N=6 in the Heisenberg limit is illustrated in Fig.(2.2). As each successive symmetry is utilised, the matrix becomes more nearly diagonal, the final, irreducible, block sizes being, at maximum 2x2. (If the operators are applied in this order, I does not yield any further reduction. See the discussion of Appendix 1, section (A.1.2). When anisotropy is present, S is no longer conserved and the maximum block size increases to 3x3.) We see therefore that each eigenstate

of the Hamiltonian, $\mathcal{H}$, when it is finally diagonal, can be classified in terms of the eigenvalue of S^2, S^z, and T. Equivalently, it is possible to obtain a complete set of orthonormal eigenfunctions such that all four operators are diagonal in this basis, i.e.

$$\begin{aligned} \mathcal{H}\psi_n &= E_n \psi_n \\ S^2\psi_n &= S_n(S_n+1)\psi_n \\ S^z\psi_n &= S^z_n \psi_n \\ T\psi_n &= \exp(ik_n)\psi_n . \end{aligned} \qquad (2.4.1)$$

N = 6 is too small a ring for R to become operative (see discussion in sub-section (3.2). However, additional reductions may be effected by use of reflection symmetry for special blocks for the case of N = 8 ($S^z \neq 0$), N = 10 and higher N rings.

4.2 Application to N = 11

The largest system that has been solved in the sense that all the eigenvalues and certain of the eigenvectors have been found numerically, is the 11-spin ring in the Heisenberg limit. It is therefore instructive to discuss the reduction effects in the light of this system.

The conservation of total S^z means that the initial $2^{11} \times 2^{11}$ matrix breaks up into 12 blocks whose order and corresponding S^z values are listed below in fig. (2.4).

fig. (2.4)

Size	1	11	55	165	330	462	462	330	165	55	11	1
S^z	$\frac{11}{2}$	$\frac{9}{2}$	$\frac{7}{2}$	$\frac{5}{2}$	$\frac{3}{2}$	$\frac{1}{2}$	$-\frac{1}{2}$	$-\frac{3}{2}$	$-\frac{5}{2}$	$-\frac{7}{2}$	$-\frac{9}{2}$	$-\frac{11}{2}$

Spin inversion symmetry means we need only consider the first six blocks. The translational invariance reduces the maximum matrix to be diagonalised for each of the first six blocks to

(1), 1, 5, 15, 30, 42.

However, as we shall see in sub-section (5.2), the complex nature of

some of the matrices puts up the effective order by a factor of two.

In sub-section (3.2) we have remarked that any S^z block contains states of total spin equal to, or greater than S^z. This is illustrated in Table (2.3) for N = 11. In the column farthest to the right are listed the total number of states in a given S^z block.

S^2 \ S	$\frac{11}{2}$	$\frac{9}{2}$	$\frac{7}{2}$	$\frac{5}{2}$	$\frac{3}{2}$	$\frac{1}{2}$	Total
$\frac{11}{2}$	1						1
$\frac{9}{2}$	1	10					11
$\frac{7}{2}$	1	10	44				55
$\frac{5}{2}$	1	10	44	110			165
$\frac{3}{2}$	1	10	44	110	165		330
$\frac{1}{2}$	1	10	44	110	165	132	462
Mult. M	12	10	8	6	4	2	

Table (2.3)

In the corresponding horizontal rows we have a breakdown of these states according to their total spin quantum number S. Hence we see, for example, that the 462 states of the $S^z = \frac{1}{2}$ (largest) block comprise 132 doublets, 165 quartets, 110 sextets, 44 octets and so on. A method of obtaining the eigenfunctions of S^2 belonging to a given spin quantum number S, and to a specified S^z is described in Appendix 1. The basis of the method is due to Hulthén (1938), who used it to calculate certain of the singlet states for N = 4, 6, 8 and 10 spin rings. It has been extended by the author to take account of translation symmetry, and higher S^z and S. Since N is prime, in this example, translation symmetry gives an extra reduction factor of 11, and the largest matrix to be diagonalised is a sub-block of the 165 quartets of order 15.

4.3) Effect of a Magnetic Field

We have remarked in sub-section (1.4) of this chapter that the Hamiltonian for a spin system placed in an external magnetic field

has the form

$$\mathcal{H} = -2J\sum_{(i,j)} \left\{ S_i^z S_j^z + \gamma\left(S_i^x S_j^x + S_i^y S_j^y\right)\right\} - g\beta\, \underline{H}\cdot\underline{S} \qquad (2.4.2)$$

where the Zeeman term may be expanded as $g\beta H^z S^z + g\beta H^x S^x + g\beta H^y S^y$

The total angular momentum operators $S^z = \sum S_i^z$; $S^x = \sum S_i^x$; $S^y = \sum S_i^y$; obey the general rules governing angular momentum operators; in particular, although each operator commutes separately with both the Hamiltonian and the square of the total spin S^2, the operators do not commute with each other. It is therefore interesting to consider the matrix form of the Hamiltonian (2.4.2) in the representation in which S^z is diagonal, i.e. the Ising representation. Obviously the parallel Zeeman interaction $\sim H^z S^z$ (the Z-axis is taken as the preferred axis of quantisation) merely adds in diagonal terms corresponding to an appropriate eigenvalue of S^z multiplied by the coefficient $g\beta H^z$ (see sub-section (2.3)). This clearly does not affect the techniques required for the subsequent complete diagonalisation of the Hamiltonian, and is independent of amount of anisotropy $(1-\gamma)$.

Let us now examine the effect of the transverse Zeeman terms on the matrix Hamiltonian in the same basic representation. Since S^x and S^y are essentially equivalent, let us, for simplicity, consider only S^x. From the Pauli matrices of sub-section (1.1) we see that

$$S_i^x|\uparrow\rangle = \tfrac{1}{2}|\downarrow\rangle \;;\; S_i^x|\downarrow\rangle = |\uparrow\rangle \quad (\text{in units of } \hbar) \qquad (2.4.3)$$

Hence the effect of $S^x = \sum_{i=1}^{N} S_i^x$ operating on an N-spin product wave-function is to generate from it N wave-functions, each with a different flipped-over spin.

eg. $S^x|\uparrow\uparrow\uparrow\uparrow\downarrow\downarrow\rangle = \frac{1}{2}|\downarrow\uparrow\uparrow\uparrow\downarrow\downarrow\rangle + \frac{1}{2}|\uparrow\downarrow\uparrow\uparrow\downarrow\downarrow\rangle + \frac{1}{2}|\uparrow\uparrow\downarrow\uparrow\downarrow\downarrow\rangle + \frac{1}{2}|\uparrow\uparrow\uparrow\downarrow\uparrow\downarrow\rangle + \frac{1}{2}|\uparrow\uparrow\uparrow\downarrow\downarrow\uparrow\rangle$

$(S^z = \frac{1}{2})$ (-1/2) (-1/2) (-1/2) (+3/2) (+3/2)

(2.4.4)

The S^z value of each of these states clearly differs by ± 1 from the original state (except where the original state has maximum $|S^z|$).

The pattern of the resulting matrix is demonstrated by the following sketch (fig. 2.5). The unshaded blocks along the diagonal represent the form of the Hamiltonian (2.4.2) without transverse Zeeman terms: the effect of the latter is to introduce non-zero matrix elements in the shaded blocks adjoining the diagonal blocks, as indicated in the sketch (fig. 2.5). The loss of

fig. (2.5)

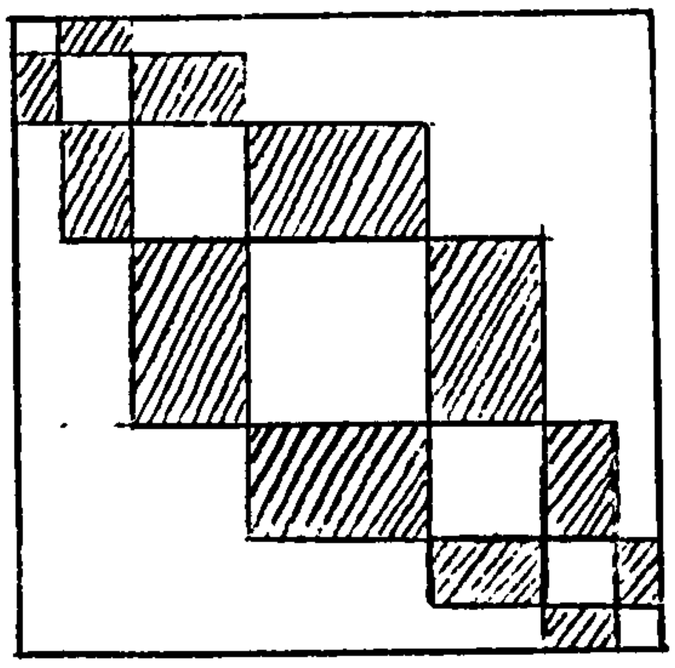

block diagonal form results in severely increased difficulty of finding the eigenvalues of this matrix. These eigenvalues could be used to determine a set of thermodynamic properties in a transverse field, analogous to the corresponding set in a parallel field. However the property of experimental interest is the susceptibility measured in the limit of a zero transverse field, commonly called the zero-field perpendicular susceptibility and denoted by $\chi_\perp$. Fortunately, as will be shown in Chapter V, the perpendicular susceptibility may be obtained exactly from a second order perturbation theory calculation, thus avoiding the difficulty of complete diagonalisation. The transverse Zeeman term is regarded as a perturbation linking states of S^z differing by ± 1.

The procedure of determining the second order changes in the eigenvalues may be facilitated by studying the properties of the operator S^x, in particular commutation with the translation operator T.

$[S^x, T]$

$$S^x\ |\uparrow\uparrow\uparrow\downarrow\downarrow\rangle = \tfrac{1}{2}|\downarrow\uparrow\uparrow\downarrow\downarrow\rangle + \tfrac{1}{2}|\uparrow\downarrow\uparrow\downarrow\downarrow\rangle + \tfrac{1}{2}|\uparrow\uparrow\downarrow\downarrow\downarrow\rangle + \tfrac{1}{2}|\uparrow\uparrow\uparrow\downarrow\downarrow\rangle + \tfrac{1}{2}|\uparrow\uparrow\uparrow\downarrow\uparrow\rangle$$

$$\therefore T\ S^x\ |\uparrow\uparrow\uparrow\downarrow\downarrow\rangle = \tfrac{1}{2}|\downarrow\downarrow\uparrow\uparrow\downarrow\rangle + \tfrac{1}{2}|\downarrow\uparrow\downarrow\uparrow\downarrow\rangle + \tfrac{1}{2}|\downarrow\uparrow\uparrow\downarrow\downarrow\rangle + \tfrac{1}{2}|\downarrow\uparrow\uparrow\uparrow\downarrow\rangle + \tfrac{1}{2}|\uparrow\uparrow\uparrow\uparrow\downarrow\rangle$$

also

$$T\ |\uparrow\uparrow\uparrow\downarrow\downarrow\rangle = |\downarrow\uparrow\uparrow\uparrow\downarrow\downarrow\rangle$$

$$\therefore S^x T\ |\uparrow\uparrow\uparrow\downarrow\downarrow\rangle = \tfrac{1}{2}|\uparrow\uparrow\uparrow\uparrow\downarrow\rangle + \tfrac{1}{2}|\downarrow\downarrow\uparrow\uparrow\downarrow\rangle + \tfrac{1}{2}|\downarrow\uparrow\downarrow\uparrow\downarrow\rangle + \tfrac{1}{2}|\downarrow\uparrow\uparrow\downarrow\downarrow\rangle + \tfrac{1}{2}|\downarrow\uparrow\uparrow\uparrow\uparrow\rangle$$

Hence $[S^x, T] = 0$ (2.4.5)

We thus have the important simplifying feature that the perturbation only links states of the unperturbed Hamiltonian which have the same q wave-number. For example, in the case of N=6, the antiferromagnetic ground state is a state with $S^z = 0$ and q = 3. The perturbation will, in general, link this state with those states having $S^z = \pm 1$ and q=3, which by inspection of Fig. (2.2) we see are two in number for each S^z block (cf. the total number of states in the $|S^z| = 1$ blocks = 15.) However, for the Heisenberg limit only, S^x commutes with S^2, and hence the transverse perturbation will link states having the same q number and the same multiplicity. The antiferromagnetic ground state for all finite N is a singlet, and since no states exist with S=0 and $S^z = \pm 1$, the transverse perturbation can have no effect on the antiferromagnetic ground state, and hence the perpendicular antiferromagnetic susceptibility (in zero field) must vanish at T=0 for all finite even N. This result is perhaps more obvious in the parallel case where, since the antiferromagnetic ground state is always an $S^z = 0$ state (N even) the parallel perturbation also has no effect on the ground state and the parallel susceptibility $\chi_{\parallel}$ must also go to zero as $T \to 0$.

4.4) Other Matrix Work

The first worker in the field to consider the spin matrices appropriate to a series of spin clusters (rings) was (Hulthén 1938). Hulthén, however, was only interested in obtaining the lowest (antiferromagnetic) energy state for rings of spins of size 2,4,6,8 and 10. He pioneered the classification by total spin S(method of irreducible representations of the symmetric group) which will be discussed in detail in Appendix 1. Ledinegg and Urban (1951) extended the Hulthén approach to the case N=12, but again only solved for the antiferromagnetic ground state.

Orbach (1959) was the first to find the complete set of eigenvalues and eigenvectors of spin rings for N > 5, for the Heisenberg

limit and other values of the anisotropy parameter, numerically, using matrix methods. He used the S^z breakdown, but not the translation symmetry as described in sub-sections (2.6) and (3.2) of this chapter. He solved rings of 6, 8 and 10 spins in the Heisenberg limit, and N = 8 for the 10 values of γ, 0.05 by increments of 0.1 through 0.95 (thesis 1959). For the larger clusters he employed spin inversion symmetry to reduce the $S^z = 0$ block by $\frac{1}{2}$; for blocks of higher $|S^z|$ he used a kind of translation symmetry to reduce these blocks also by $\frac{1}{2}$ (rather than N). This technique corresponds to taking symmetric and antisymmetric combinations of states, and others of the same family obtained by rotating the first state half-way round the ring, e.g. for N = 8 and S^z = 1, combination states of the type

$$\frac{1}{\sqrt{2}} \{ |\downarrow\downarrow\downarrow\uparrow, \uparrow\uparrow\uparrow\uparrow\rangle \pm |\uparrow\uparrow\uparrow\uparrow, \downarrow\downarrow\downarrow\uparrow\rangle \}$$

However Orbach's failure to take account of the properties of T led him into error when he attempted to consider dispersion relations (Orbach, 1959).

Griffiths, (1961) obtained eigenvalues for rings of 5, 7, 9 and 10 spins in the Heisenberg limit only. He considered N = 10 because the Orbach results (thesis, 1959) appear to be incomplete, pertaining only to the $S^z = 0$ and $S^z = 1$ sub-blocks of the Hamiltonian. Griffiths used classification by S^z and translation symmetry, but not conservation of S. This work was contemporaneous with, but independent of, the work of the present author, the results of which will be described in detail in sub-section (5.5) of this chapter.

Lieb, Schultz and Mattis (1961) solved the 6-spin free-ended chain using classificiation by S and S^z and reflection symmetry in order to obtain the antiferromagnetic ground state and its eigenfunction.

Recently, Baker, Rushbrooke and Gilbert (1964) have considered the matrix representation of Heisenberg clusters of general structure using the technique of irreducible representations of the symmetric (permutation) group. This approach is equivalent to classification by S and S^z (reflection and translation symmetries are, of course, absent in the general case.) However, they were not interested in obtaining the eigenvalues of the matrices but in traces of powers of matrices as part of a high-temperature series expansion.

4.5) Comparison with Present Work

The results of the author are more extensive than those quoted in sub-section (4.4) in the following general respects: (a) the complete spectrum for N=11, γ=1 has been obtained; (b) results have been obtained for a range of values of the anisotropy parameter γ; (c) results are available for free-ended chains as well as rings; (d) a greater range of eigenvectors has been calculated. (To comment more fully on the last point:- Griffiths has not attempted to calculate eigenvectors. Orbach has published a complete set of eigenvectors for γ=1 for the rings N=4, 6 and 8 (Orbach, 1958) and additional results are available in his unpublished thesis, (1959).)

4.6) Limitations on Solvable Cluster-Size.

Since the matrix solutions on which this thesis is based were performed there has been a substantial improvement in the capacity and performance of digital computers. On present day (1968) large computers a reasonable limit on matrix order for finding eigenvalues and eigenvectors numerically is about 150. In general, for anisotropic clusters, this would allow us to obtain one or perhaps two longer clusters.

In Appendix 1 arguments are presented which allow the estimation of upper limits on solvable size of spin clusters of various types

for the special case of the Heisenberg limit. In view of their importance, the conclusions implicit in this work will be summarised here. For spin rings, we estimate that the largest cluster for which it should now be possible to find both eigenvalues and a complete set of eigenvectors is N = 14: in the case of open-ended chains about N = 12. If only eigenvalues and perhaps a few selected eigenvectors are required, the estimates increase to 15 and 13 respectively. For the interesting case of two-dimensional spin clusters, the solution of a 4x4 cluster appears to be just on the bounds of possibility. In general, for periodic clusters of one, two and three dimensions, the upper limit will remain a cluster of about 16 spins. It thus appears that the matrix techniques discussed in this chapter can be applied to a reasonable range of one-dimensional clusters, a very limited range of two-dimensional clusters, and are not very useful in three dimensions.

The estimates for linear clusters for $\gamma = 1$ represent a substantial advance on the limits obtained when this work was first performed. However the results obtained then have been found to be reasonably adequate for the purposes described in this thesis and it has been felt that the difficulties of solving longer clusters (see sub-section (5.1)) would result in a policy of "diminishing returns".

5. COMPUTATIONAL TECHNIQUES

5.1) Choice of Technique

From the foregoing account it is clear that maximal reduction in matrix size arises from the simultaneous application of all mutually commuting symmetry properties. For the Heisenberg limit this would imply the use of conservation of total spin, S, in addition to S^z and T. However, since a great part of the interest of this work lies in the anisotropic region where S is no longer a good quantum number, the

method finally adopted consisted in utilising only S^z and T for both the Heisenberg and anisotropic cases. This technique has appreciable computational advantages.

The fact that all the energy eigenvalues for a given positive S^z and a given **k** (or q) must also be in the spectrum for all smaller positive values of S^z and the same k, means that we have a very valuable check on the calculations at each stage. We also obtain an indication of the degree of 'rounding' which increases as the number of machine operations increases (roughly as n^x, with $2<x<3$, where n is the order of the matrix) and limits the final accuracy of the results. In addition, the eigenvectors are easily obtainable by this method in a form convenient for subsequent calculation of, for example, spin-pair correlation functions and zero-field perpendicular susceptibilities.

In Appendix 1 methods are presented, applicable only in the Heisenberg limit, which use conservation of S in addition. Although it would be possible to make somewhat more extensive calculations using these methods, it would appear that they are computationally less convenient. They have not been significantly exploited, since the first method described in this sub-section has proved satisfactory in elucidating the results of greatest interest. In the following sub-section (5.2) we consider in detail the problems which arise in the use of this particular reduction scheme.

5.2) 'Sub-Standard' Block Problem

When N is prime each S^z block of the Hamiltonian splits up exactly into N equal sub-blocks under the influence of translation symmetry. It may easily be proved that this is possible, i.e. that the size of each S^z block is a multiple of N, if N is prime. When N is not prime, however, complications arise.

Proof:

The size of the r^{th} S^z block of the Hamiltonian is given by

$$\binom{N}{r} = \frac{N!}{(N-r)!r!} = \frac{N(N-1)!}{(N-r)!r!} = p, \text{ say } (p \text{ integral})$$

We need to show that $p/N = (N-1)!/(N-r)!r!$ is an integer.

Now (N-1)! is integral and equal to $\frac{p}{N}(N-r)!\,r!$. Since N is prime, and r< N, by definition, N is not divisible by any factors of (N-r)! or r! Hence, since (N-r)! r! is integral, p/N must also be integral.

The procedure described in sub-section (3.2) under the heading Translation Operator, may be regarded equivalently, and perhaps more directly, as a matrix transformation in which the transform matrix is a block diagonal matrix of p/N identical NxN blocks. Each block is composed of N normalized vectors of the form $\frac{1}{\sqrt{N}}\left[1, \omega, \omega^2, \cdots, \omega^{N-1}\right]^t$ (t denotes transpose) where ω successively takes on the values of the N^{th} roots of unity. Each block, in fact, constitutes the well-known transformation which diagonalises a cyclic matrix. The whole transformation is a simple generalisation which diagonalises a block cyclic matrix, the structure of the Hamiltonian under periodic boundary conditions (see, for example, Muir (1960)).

When N is not prime, some of the set of S^z blocks contain sub-blocks which are no longer square and of order N, i.e. blocks either or both of whose dimensions are factors of N. However, since such blocks still retain the essential cyclic structure, a block-cyclic transformation is still possible. The blocks of the block-diagonal transform matrix corresponding to the 'sub-standard' blocks of the S^z matrix are those appropriate to diagonalising a cyclic matrix whose dimensions are factors of N. The normalisation also corresponds to matrices of reduced dimensions.

To illustrate this transform explicitly we have chosen in Fig. (2.3) a simple example, corresponding to the $S^z = 1$ block of the N=6

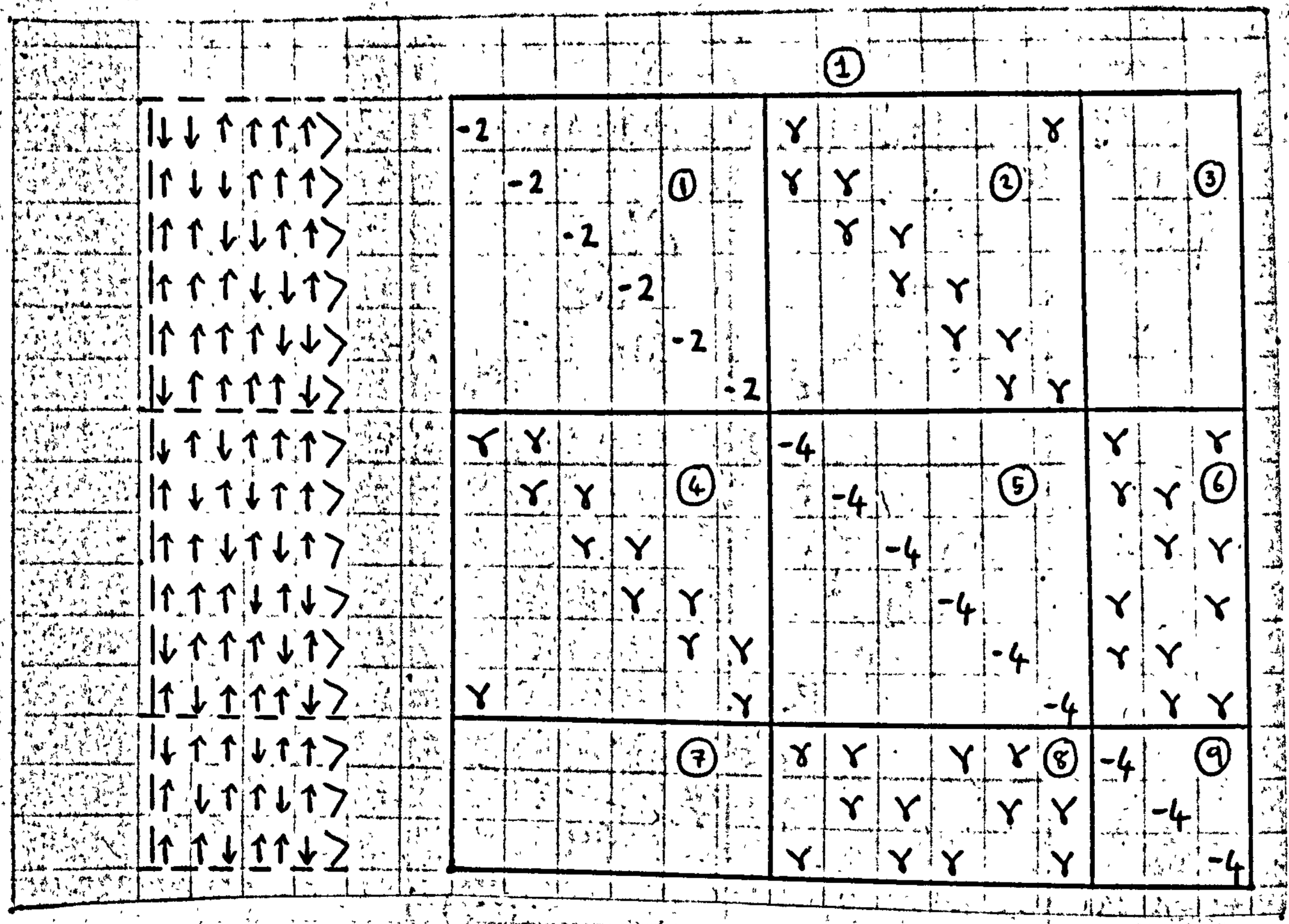

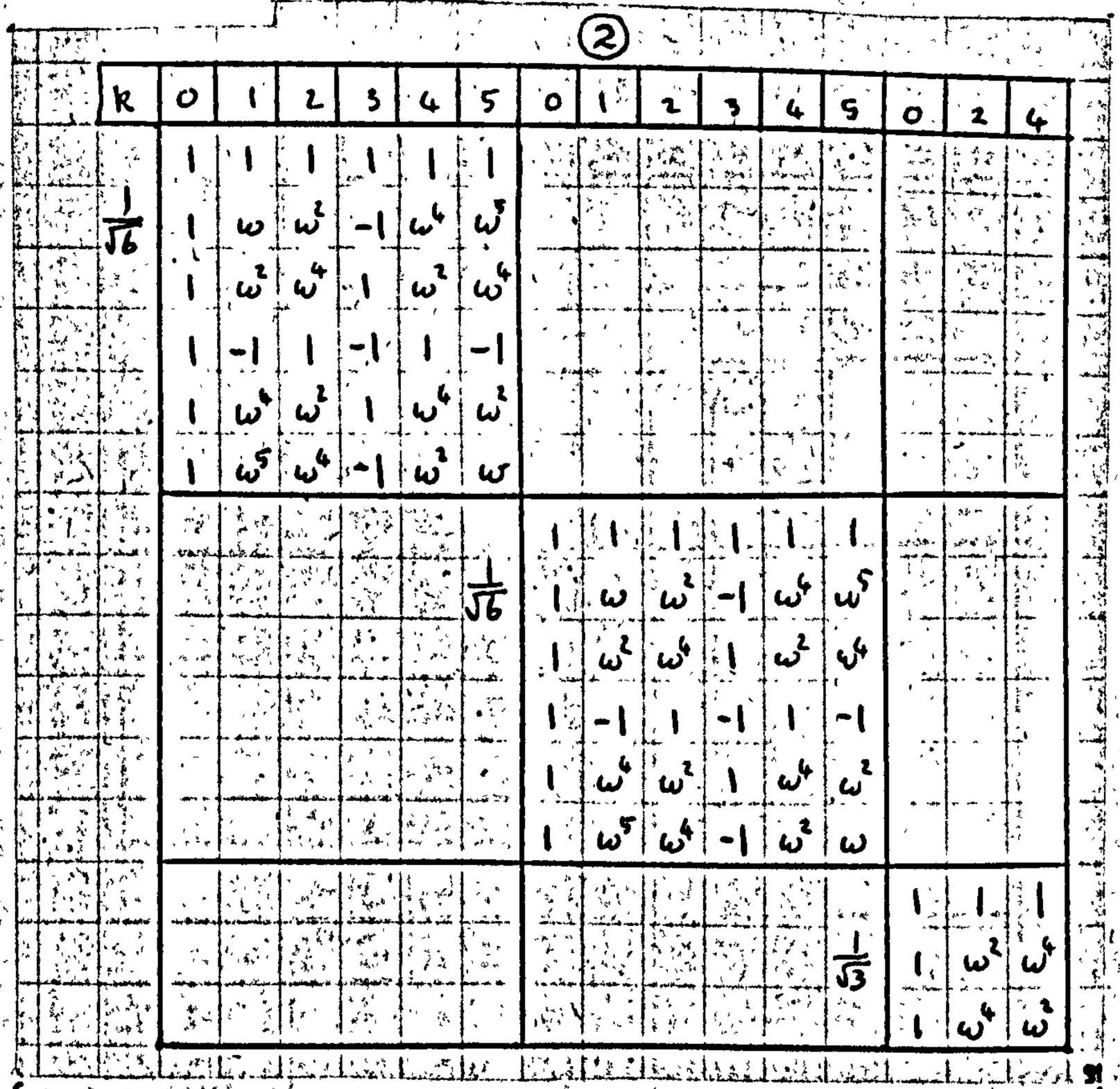

FIG. (2.3)

Unitary and Orthoganal Transformations

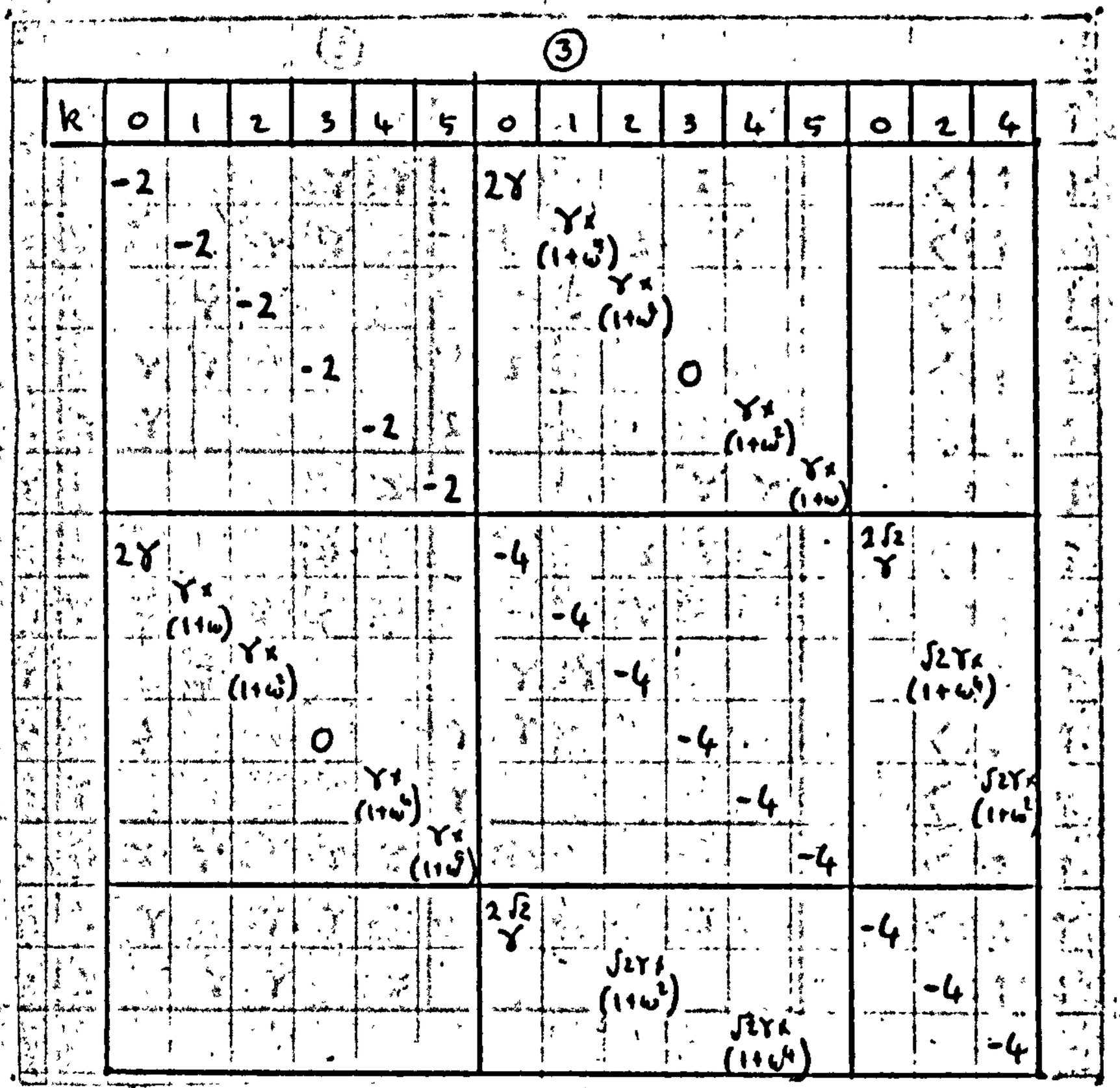

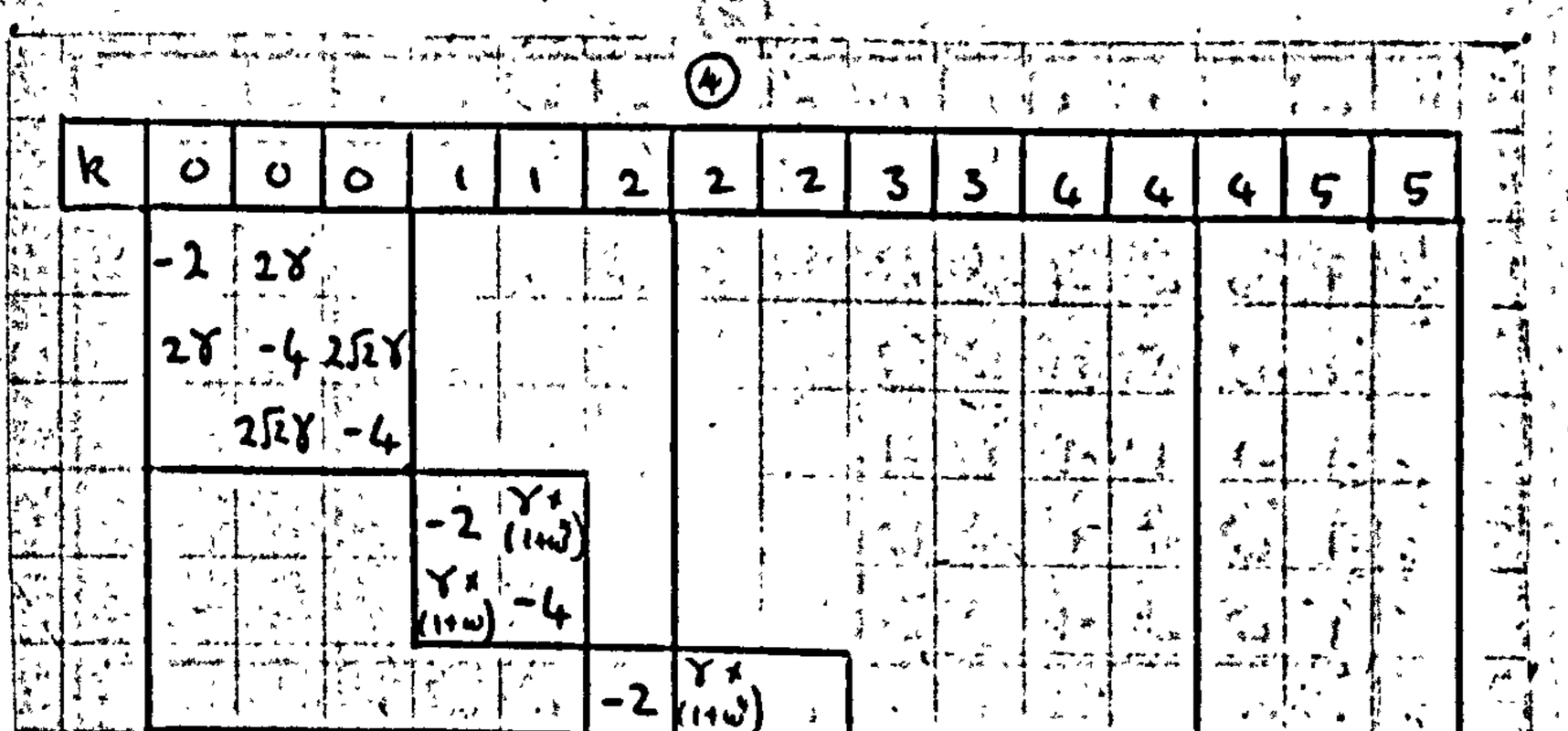

FIG. (2.3) (cont.)

For Reducing the Hamiltonian Matrix

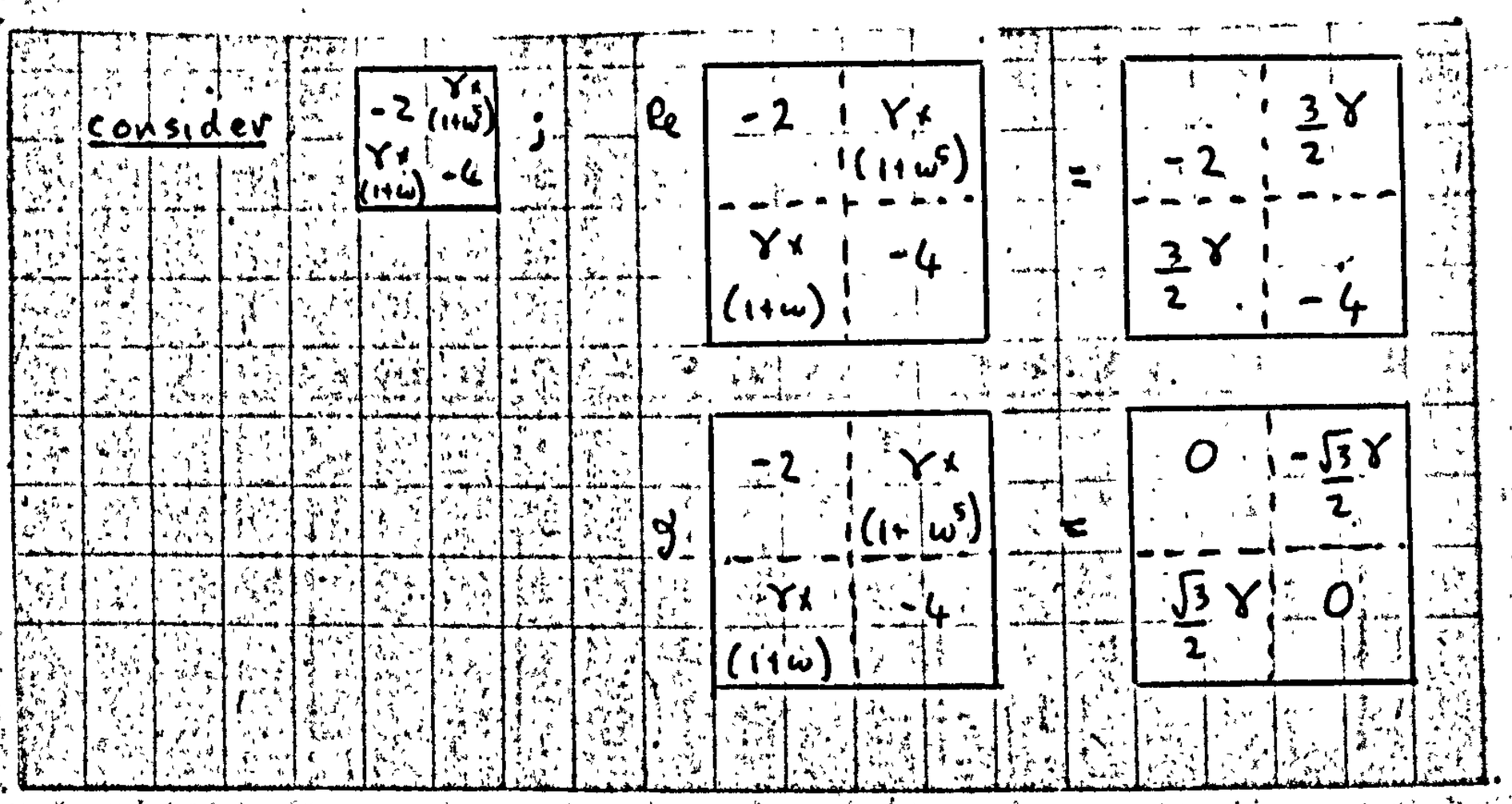
consider
-2 Y√6/(1+ω²)
Y√6/(1+ω) -6
j
Re
-2 | Y√6/(1+ω²)
Y√6/(1+ω) | -4
=
-2 | 3/2 Y
3/2 Y | -4
g
-2 | Y√2/(1+ω²)
Y√2/(1+ω) | -4
=
0 | -√3/2 Y
√3/2 Y | 0

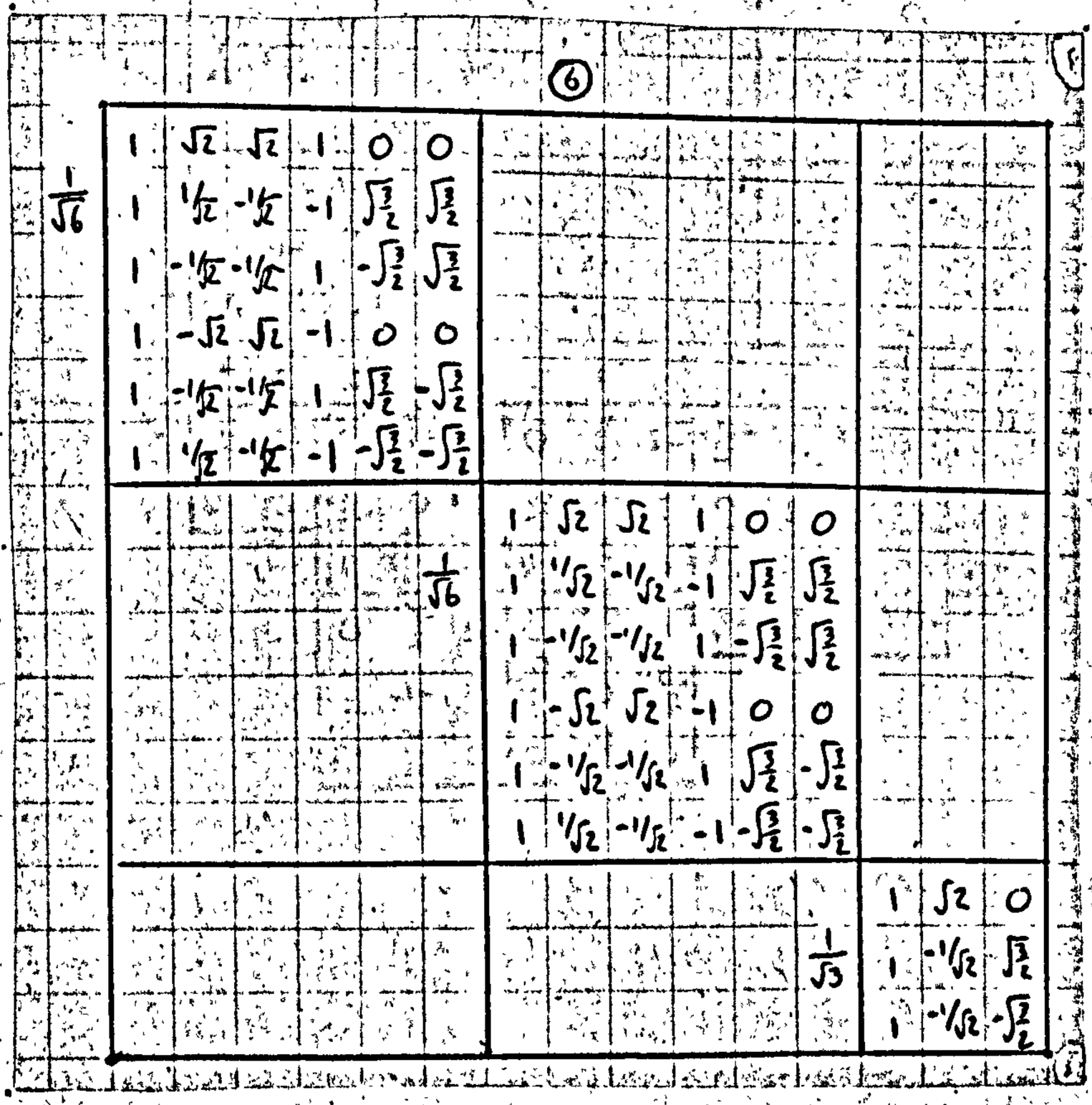
⑥
1/√6
1 √2 √2 1 0 0
1 1/√2 -1/√2 -1 √3/2 √3/2
1 -1/√2 -1/√2 1 -√3/2 √3/2
1 -√2 √2 -1 0 0
1 -1/√2 -1/√2 1 √3/2 -√3/2
1 1/√2 -1/√2 -1 -√3/2 -√3/2
1/√6
1 √2 √2 1 0 0
1 1/√2 -1/√2 -1 √3/2 √3/2
1 -1/√2 -1/√2 1 -√3/2 √3/2
1 -√2 √2 -1 0 0
1 -1/√2 -1/√2 1 √3/2 -√3/2
1 1/√2 -1/√2 -1 -√3/2 -√3/2
1/√3
1 √2 0
1 -1/√2 √3/2
1 -1/√2 -√3/2

FIG.: (2.3) (cont.)

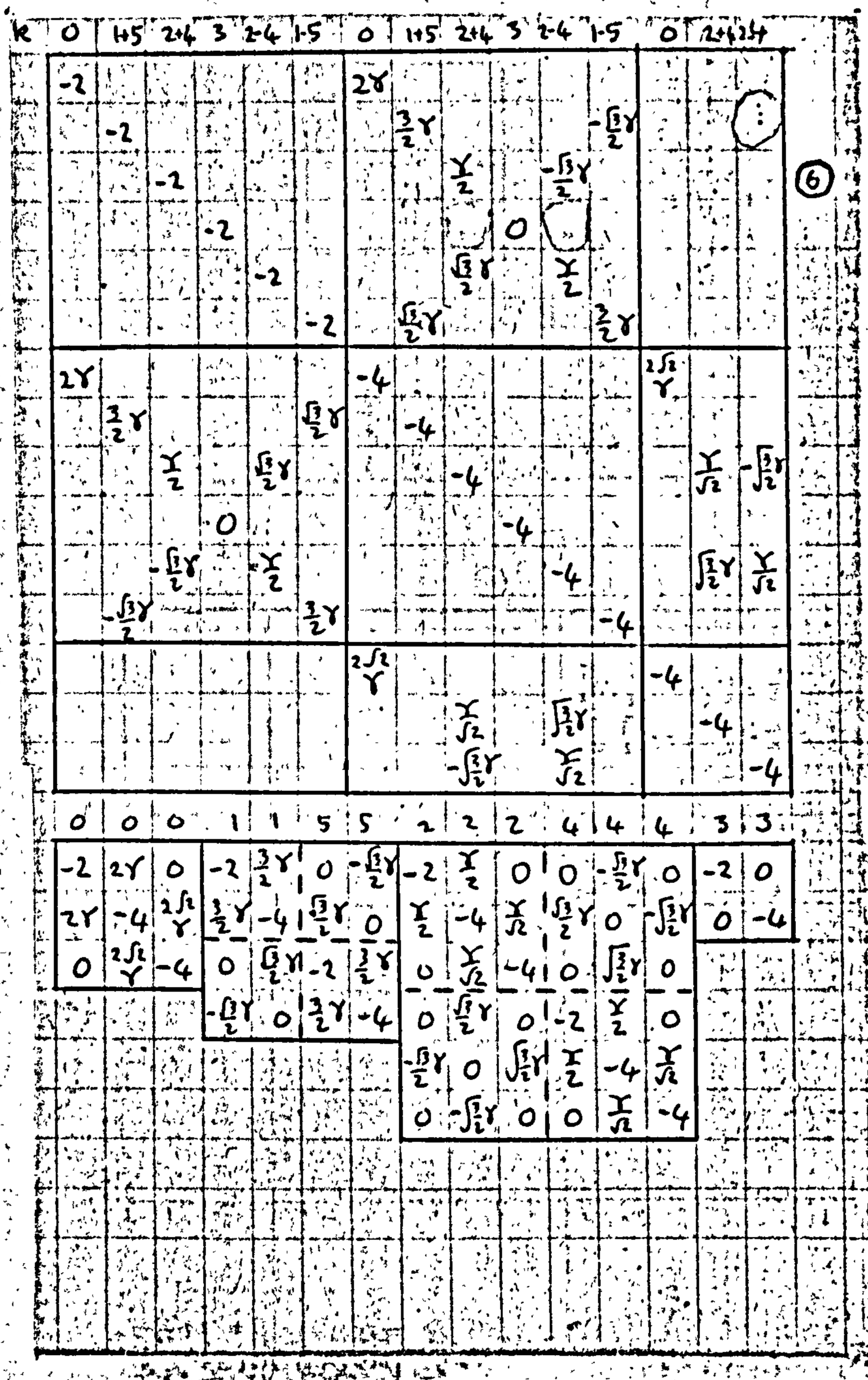

FIG. (2.3) (cont.)

ring. The matrix representatives are the matrix elements between the 15 basic states which derive from three 'families'

$$\mathcal{G}_1 = |\downarrow\downarrow\uparrow\uparrow\uparrow\uparrow\rangle \; ; \; \mathcal{G}_2 = |\downarrow\uparrow\downarrow\uparrow\uparrow\uparrow\rangle ; \quad \mathcal{G}_3 = |\downarrow\uparrow\uparrow\downarrow\uparrow\uparrow\rangle$$

The complete set of states generated from these is listed beside matrix 1, (The Hamiltonian has been normalised by subtraction of a factor JN/2 from each diagonal element, corresponding to a Hamiltonian

$$\mathcal{H} = 2J\sum_{i=1}^{N}\left\{S_i^z S_{i+1}^z - \frac{1}{4} + \gamma\left(S_i^x S_{i+1}^x + S_i^y S_{i+1}^y\right)\right\} \qquad (2.5.1)$$

With this normalisation the largest eigenvalue of the system equals zero for all N.) Notice that the family, $\mathcal{G}_3$, on account of symmetry, has only three members. Hence the corresponding matrix 1 displays the phenomenon of 'sub-standard' blocks. In this particular example we see that the rectangular sub-standard block ⑥ is obtained from the full NxN block ② by 'cutting' down the dotted axis and superposing, as illustrated in fig. (2.6).

fig. (2.6)

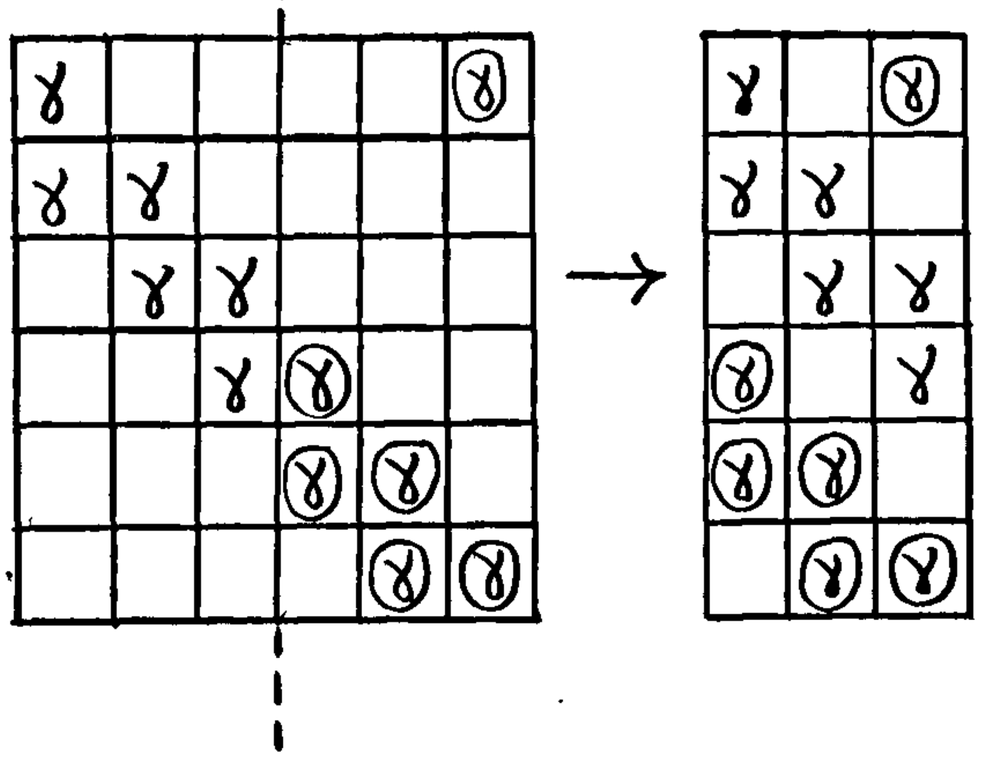

In general, the rectangular sub-standard blocks are obtained from full size blocks reduced in this way. Matrix 2, illustrates the right hand block diagonal transforming matrix which reduces 1 in accordance with translation symmetry. The numerical factors adjacent to each diagonal block are the appropriate normalising factors for the complete vectors. The whole transformation is a unimodular, unitary (similarity) transformation and its effect on matrix 1 is shown in matrix 3. The transform has rendered each sub-block of 1 diagonal (or the equivalent of diagonal). Each vector

of 2 is an eigenvector of $\underline{T}$ corresponding to a particular eigenvalue

$\omega = e^{ik}$ where $k = 2\pi q/N$, $q = 0, \pm 1, \pm 2, \cdots$

The appropriate wavenumbers, q, are shown at the top of each vector. In matrix 4 we have grouped together all states with the same q values and the matrix is now in block diagonal form. The q=0 blocks and and the q = N/2 block (N even) are always real symmetric; all other blocks are Hermitian. This presents a problem from the point of view of machine diagonalisation, since routines designed to handle real symmetric matrices can only be adapted to handle complex matrices with a substantial increase in running time.

The actual technique adopted was to convert the Hermitian blocks into real symmetric blocks according to the following scheme. A complex matrix may be represented in terms of its individual elements as [a + ib]. Then the eigenvalues, (each of which is doubly degenerate) of the matrix $\begin{bmatrix} [a] & [b] \\ -[b] & [a] \end{bmatrix}$ where [a] denotes the block matrix formed of the real parts of the original matrix elements and [b] denotes the block of imaginary parts, are equal to the eigenvalues of the original matrix [a + ib]. Also the eigenvectors are simply related to the original eigenvectors. Hence a real matrix has been generated, twice as large as the original complex one.

An approach which is exactly equivalent, but rather more physical, is to employ an orthogonal transformation derived from the original unitary transformation by a simple, linear combination of vectors. The transformation is represented by the basic matrix block (N even) shown in fig. (2.7). The vectors of this transformation correspond to standing wave rather than running-wave states.

fig. (2.7)

$$\begin{vmatrix} 1 & \varphi_0 & \varphi_0 & \cdots & 1 & \cdots & \psi_0 & \psi_0 \\ 1 & \varphi_1 & \varphi_2 & \cdots & 1 & \cdots & \psi_2 & \psi_1 \\ 1 & \varphi_2 & \varphi_4 & \cdots & 1 & \cdots & \psi_4 & \psi_2 \\ \vdots & \vdots & \vdots & & \vdots & & \vdots & \vdots \\ 1 & \varphi_{N-1} & \varphi_{N-2} & \cdots & 1 & \cdots & \psi_{N-2} & \psi_{N-1} \end{vmatrix}_{N \times N}$$

where $\varphi_r = \frac{1}{\sqrt{2}}(\omega^r + \omega^{*r})$

$= \frac{1}{\sqrt{2}}(\omega^r + \omega^{N-r})$

$= \frac{1}{\sqrt{2}}(\omega^r + \bar{\omega}^r)$

$$\psi_r = \frac{1}{\sqrt{2}i}(\omega^r - \omega^{N-r})$$

hence $\varphi_0 = \sqrt{2}$; $\psi_0 = 0$

The orthogonal transformation appropriate to N = 6 is shown as matrix 5 of fig. (2.3) and the effect on matrix 1 is shown as matrix 6. The effect of re-arranging 6 to block-diagonal form is shown immediately below. Two blocks, (1) and (4), are the same as before (the q=0 and q = N/2 blocks, as one would expect). It may easily be verified (see foot of matrix 4 for an example) that the remaining, larger, blocks (2) and (3) are related to, say, the q=1 and q=2 blocks of the running wave transform by the relationship described above. Effectively we have linked up the q=1 block and its conjugate q=5 and the q=2 with q=4. This result is general.

However, for the special case of two overturned spins ($S^z = N/2 - 2$), of which this is an example, the Hermitian matrices may be converted into real symmetric matrices without increasing the order, by simply replacing the off-diagonal elements by their absolute values. This property results directly from the Hermitian and continuant nature of the matrices for 2 overturned spins, i.e. all elements are zero except those in the main diagonal and in the two adjacent parallel super- and sub- diagonals on each side.) Unfortunately this is no longer the case for three or more overturned spins.

5.3) Basic States

The process of writing down the types of Ising wave-functions for a given S_z becomes rather lengthy for $N > 10$. In Fig. (2.4), we show the matrix corresponding to $N = 11$, $|S^z| = \frac{1}{2}$. The basic (parent) states are listed at the side and serve to illustrate this point. A counting theorem of Pólya serves as a useful check on the correctness of this process. (Pólya, 1937; Uhlenbeck and Ford, 1962). In this sub-section we shall describe the theorem and show how this comes about.

The Pólya theorem, as applied to this problem, introduces a polynomial $F(x,y)$ in two variables x and y which correspond to the two spin configurations $\uparrow$ and $\downarrow$, say. $F(x,y)$ may be expanded as a series of homogeneous products $x^r y^s$, where $r+s = N$, each of which represents an Ising wavefunction consisting of r 'up' spins and s 'down' spins. The coefficient of the term $x^r y^s$ tells us how many distinct configurations of r 'up' spins and s 'down' spins occur for a given N. More explicitly, the generating polynomial $F_{(x,y)}$ is given as

$$F_{(x,y)} = \frac{1}{g} \sum_{(P)} f_1^{k_1}(x,y) f_2^{k_2}(x,y) \cdots f_p^{k_p}(x,y) \quad (2.5.2)$$

where the sum goes over all permutations P of the cyclic group on N spins, and g is the number of elements in the group, written in cycle form (g is equal to N, in this case). Suppose P consists of k_1 cycles of length 1, k_2 cycles of length 2, etc. The polynomials f_i correspond to cycles of length i and are defined as $f_i = (x^i + y^i)$

We have also $1 \cdot k_1 + 2 \cdot k_2 + \cdots + p k_p = N \quad (2.5.3)$

Consider, as a simple example, the cyclic group on 6 spins corresponding to the 6-spin ring. Table (2.5) lists the elements of the corresponding permutation group and their contributions to F(x,y). The coefficients of the configurations x^6, x^5y, x^4y, x^3y^3,

corresponding to zero, one, two and three overturned spins, respectively, are evaluated.

Table (2.5)

Cycle Type	Number of Elements	Term in $F(x,y)$	Coeff. of x^6	x^5y	x^4y^2	x^3y^3
(123456)	2	$2(x^6+y^6)$	2	0	0	0
(135)(246)	2	$2(x^3+y^3)^2$	2	0	0	4
(14)(25)(36)	1	$(x^2+y^2)^3$	1	0	3	0
(1)(2)(3)(4)(5)(6)	1	$(x+y)^6$	1	6	15	20
Total Number of Elements g	6	Coefficient of x^ry^s in $F(x,y)$	1	1	3	4

From the third column from the left of Table (2.4) we have

$$F(x,y) = \frac{1}{6}\left\{(x+y)^6 + (x^2+y^2)^3 + 2(x^3+y^3)^2 + 2(x^6+y^6)\right\} \quad (2.5.4)$$

From the bottom row we have the numbers 1, 1, 3 and 4 for the coefficients of x^6; x^5y; x^4y^2 and x^3y^3 respectively. Hence there is one type of Ising basic function with no overturned spins; one with one overturned spin; three with two overturned spins and four with three overturned spins. The comparison with the case of N = 11 is interesting. Table (2.5) gives the corresponding results for this example, in which N is prime. The Pólya polynomial for N = 11 is

$$F(x,y) = \frac{1}{11}\left\{(x+y)^{11} + 10(x^{11}+y^{11})\right\} \quad (2.5.5)$$

Table (2.6)

Cycle Type	No. of Elements	Term in $F(x,y)$	Coeff. of x^{11}	$x^{10}y$	x^9y^2	x^8y^3	x^7y^4	x^6y^5
(1234567891011)	10	$10(x^{11}+y^{11})$	10	0	0	0	0	0
(1)(2)(3)(4)(5)(6)(7)(8)(9)(10)(11)	1	$(x+y)^{11}$	1	11	55	165	330	462
Total Number of Elements g	11	Coeff. of x^ry^s in $F(x,y)$	1	1	5	15	30	42

We see from Table (2.6) that the identity permutation generates all the basic types except for the trivial case of no overturned spins. From Table (2.5) we see that corrections to this simple

FIGURE (2.4)a

- ✱ -

Basic Parent States and

N = 11 (Ring) Basis Vectors for $|S^z| = 1/2$.

ψ_{12} $|\downarrow\downarrow\uparrow\downarrow\downarrow\uparrow\downarrow\uparrow\uparrow\uparrow\uparrow\rangle$

ψ_1 $|\downarrow\downarrow\downarrow\downarrow\downarrow\uparrow\uparrow\uparrow\uparrow\uparrow\uparrow\rangle$

ψ_2 $|\downarrow\downarrow\downarrow\downarrow\uparrow\downarrow\uparrow\uparrow\uparrow\uparrow\uparrow\rangle$

ψ_3 $|\downarrow\downarrow\downarrow\downarrow\uparrow\uparrow\downarrow\uparrow\uparrow\uparrow\uparrow\rangle$

ψ_4 $|\downarrow\downarrow\downarrow\downarrow\uparrow\uparrow\uparrow\downarrow\uparrow\uparrow\uparrow\rangle$

ψ_5 $|\downarrow\downarrow\downarrow\downarrow\uparrow\uparrow\uparrow\uparrow\downarrow\uparrow\uparrow\rangle$

ψ_6 $|\downarrow\downarrow\downarrow\downarrow\uparrow\uparrow\uparrow\uparrow\uparrow\downarrow\uparrow\rangle$

ψ_7 $|\downarrow\downarrow\downarrow\uparrow\downarrow\downarrow\uparrow\uparrow\uparrow\uparrow\uparrow\rangle$

ψ_8 $|\downarrow\downarrow\downarrow\uparrow\uparrow\downarrow\downarrow\uparrow\uparrow\uparrow\uparrow\rangle$

ψ_9 $|\downarrow\downarrow\downarrow\uparrow\uparrow\uparrow\downarrow\downarrow\uparrow\uparrow\uparrow\rangle$

ψ_{10} $|\downarrow\downarrow\downarrow\uparrow\uparrow\uparrow\uparrow\downarrow\downarrow\uparrow\uparrow\rangle$

ψ_{11} $|\downarrow\downarrow\downarrow\uparrow\uparrow\uparrow\uparrow\uparrow\downarrow\downarrow\uparrow\rangle$

ψ_{13} $|\downarrow\downarrow\uparrow\downarrow\downarrow\uparrow\uparrow\downarrow\uparrow\uparrow\uparrow\rangle$

ψ_{14} $|\downarrow\downarrow\uparrow\downarrow\downarrow\uparrow\uparrow\uparrow\downarrow\uparrow\uparrow\rangle$

ψ_{15} $|\downarrow\downarrow\uparrow\downarrow\downarrow\uparrow\uparrow\uparrow\uparrow\downarrow\uparrow\rangle$

ψ_{16} $|\downarrow\downarrow\uparrow\uparrow\downarrow\downarrow\uparrow\downarrow\uparrow\uparrow\uparrow\rangle$

ψ_{17} $|\downarrow\downarrow\uparrow\uparrow\downarrow\downarrow\uparrow\uparrow\downarrow\uparrow\uparrow\rangle$

ψ_{18} $|\downarrow\downarrow\uparrow\uparrow\downarrow\downarrow\uparrow\uparrow\uparrow\downarrow\uparrow\rangle$

ψ_{19} $|\downarrow\downarrow\uparrow\uparrow\uparrow\downarrow\downarrow\uparrow\downarrow\uparrow\uparrow\rangle$

ψ_{20} $|\downarrow\downarrow\uparrow\uparrow\uparrow\downarrow\uparrow\uparrow\downarrow\uparrow\uparrow\rangle$

ψ_{21} $|\downarrow\downarrow\uparrow\uparrow\uparrow\downarrow\uparrow\downarrow\uparrow\downarrow\uparrow\rangle$

ψ_{22} $|\downarrow\downarrow\uparrow\downarrow\uparrow\downarrow\uparrow\downarrow\uparrow\uparrow\uparrow\rangle$

ψ_{23} $|\downarrow\downarrow\uparrow\downarrow\downarrow\uparrow\uparrow\downarrow\uparrow\uparrow\uparrow\rangle$

ψ_{24} $|\downarrow\downarrow\uparrow\downarrow\downarrow\uparrow\uparrow\uparrow\downarrow\uparrow\uparrow\rangle$

ψ_{25} $|\downarrow\downarrow\uparrow\downarrow\downarrow\uparrow\uparrow\uparrow\uparrow\downarrow\uparrow\rangle$

ψ_{26} $|\downarrow\downarrow\uparrow\uparrow\downarrow\downarrow\uparrow\downarrow\uparrow\uparrow\uparrow\rangle$

ψ_{27} $|\downarrow\downarrow\uparrow\uparrow\downarrow\downarrow\uparrow\uparrow\downarrow\uparrow\uparrow\rangle$

ψ_{28} $|\downarrow\downarrow\uparrow\uparrow\downarrow\downarrow\uparrow\uparrow\uparrow\downarrow\uparrow\rangle$

ψ_{29} $|\downarrow\downarrow\uparrow\uparrow\uparrow\downarrow\downarrow\uparrow\downarrow\uparrow\uparrow\rangle$

ψ_{30} $|\downarrow\downarrow\uparrow\uparrow\uparrow\downarrow\downarrow\uparrow\uparrow\downarrow\uparrow\rangle$

ψ_{31} $|\downarrow\downarrow\uparrow\uparrow\uparrow\uparrow\downarrow\downarrow\uparrow\downarrow\uparrow\rangle$

ψ_{32} $|\downarrow\downarrow\uparrow\downarrow\uparrow\downarrow\uparrow\downarrow\uparrow\uparrow\uparrow\rangle$

ψ_{33} $|\downarrow\downarrow\uparrow\downarrow\uparrow\downarrow\uparrow\uparrow\downarrow\uparrow\uparrow\rangle$

ψ_{34} $|\downarrow\downarrow\uparrow\downarrow\uparrow\downarrow\uparrow\uparrow\uparrow\downarrow\uparrow\rangle$

ψ_{35} $|\downarrow\downarrow\uparrow\downarrow\uparrow\uparrow\downarrow\uparrow\downarrow\uparrow\uparrow\rangle$

ψ_{36} $|\downarrow\downarrow\uparrow\downarrow\uparrow\uparrow\downarrow\uparrow\uparrow\downarrow\uparrow\rangle$

ψ_{37} $|\downarrow\downarrow\uparrow\downarrow\uparrow\uparrow\uparrow\downarrow\uparrow\downarrow\uparrow\rangle$

ψ_{38} $|\downarrow\downarrow\uparrow\uparrow\downarrow\uparrow\downarrow\uparrow\downarrow\uparrow\uparrow\rangle$

ψ_{39} $|\downarrow\downarrow\uparrow\uparrow\downarrow\uparrow\downarrow\uparrow\uparrow\downarrow\uparrow\rangle$

ψ_{40} $|\downarrow\downarrow\uparrow\uparrow\downarrow\uparrow\uparrow\downarrow\uparrow\downarrow\uparrow\rangle$

ψ_{41} $|\downarrow\downarrow\uparrow\uparrow\uparrow\downarrow\uparrow\downarrow\uparrow\downarrow\uparrow\rangle$

ψ_{42} $|\downarrow\uparrow\downarrow\uparrow\downarrow\uparrow\downarrow\uparrow\downarrow\uparrow\uparrow\rangle$

FIGURE (2.4)b

Reduced Hamiltonian Matrix for N = 11

MATRIX CORRESPONDING TO $|S^z| = 1/2$.

(Anisotropic, normalised Hamiltonian)

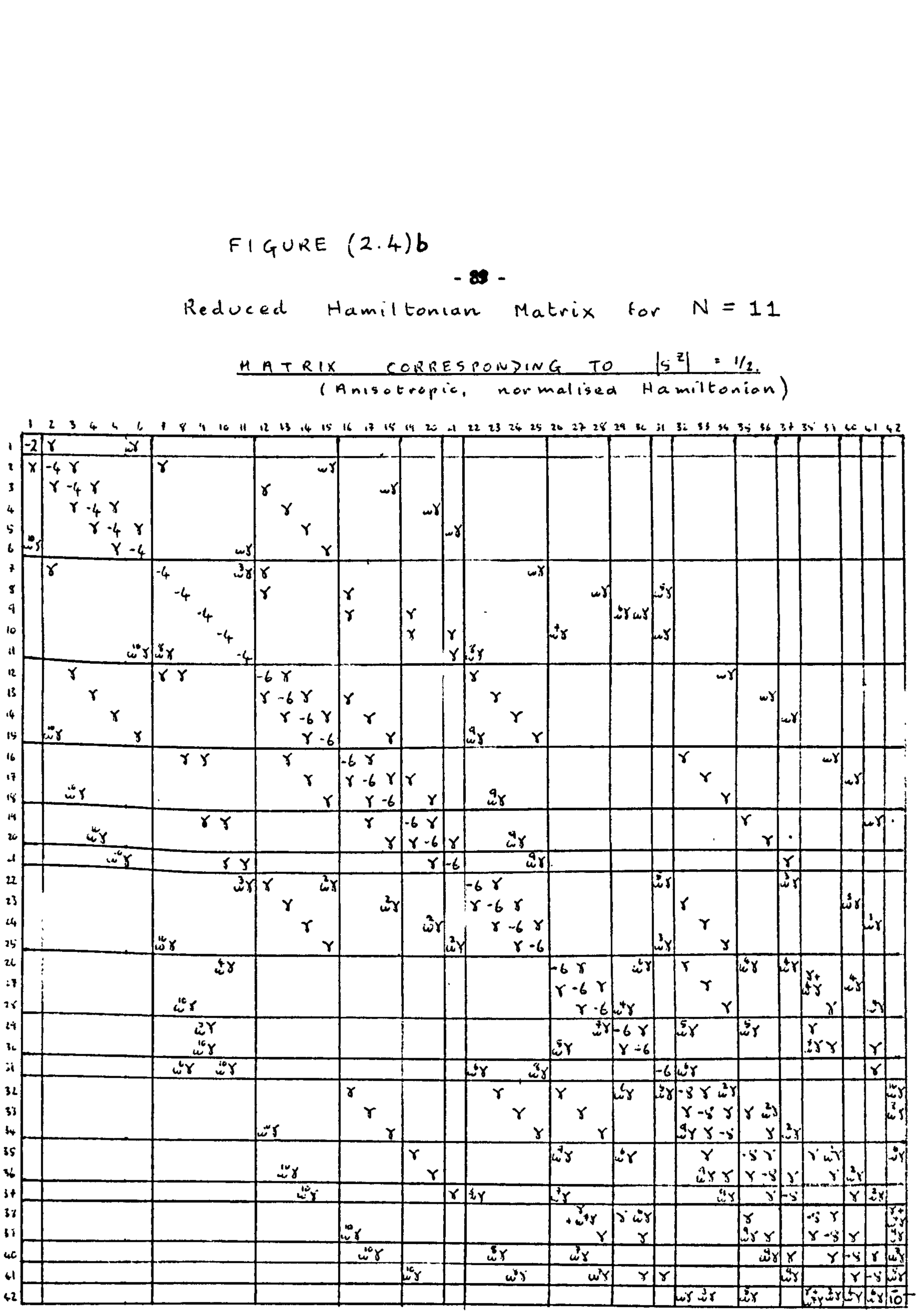

scheme arise from terms containing cycles intermediate in length between 1 and N. These cycle types appear when there exist symmetry axes in the cluster; and the corresponding wave-functions, which are, of course, the wave-functions belonging to the sub-standard blocks discussed at length in the previous section, have the same symmetry properties. They may easily be written down for a given number of overturned spins by distributing spins in accordance with the symmetries. For $N = 12$, there are four symmetry axes, as illustrated in fig. (2.8). (The arrows denote equivalent spin positions).

fig. (2.8)

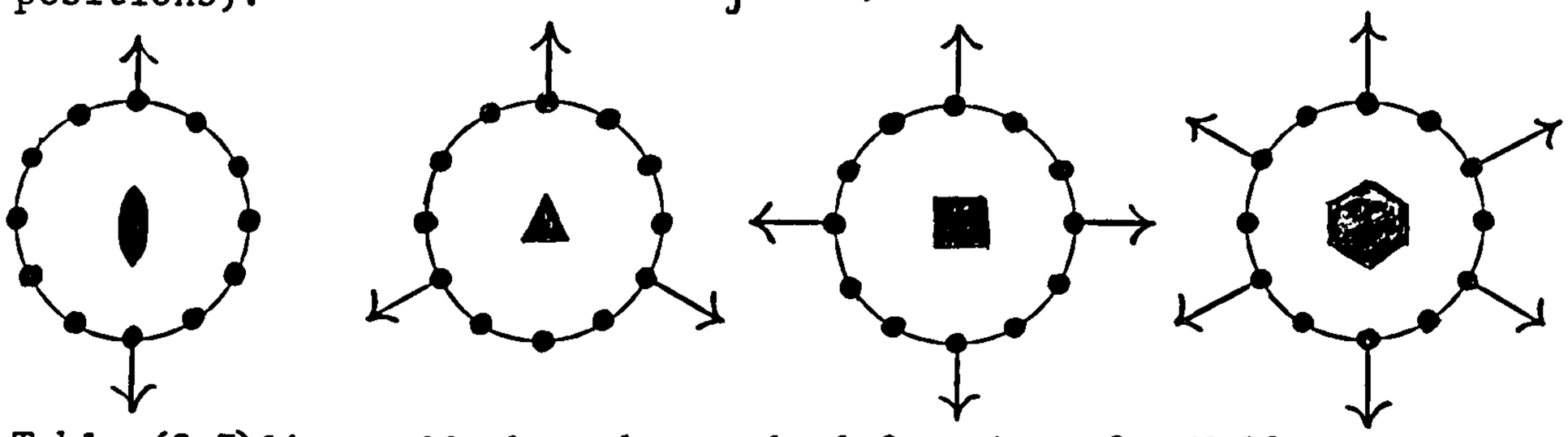

Table (2.7) lists all the sub-standard functions for N=12.

Table (2.7)

No. of Over. Spins	2	3	4	5	6
Basic	$\|\downarrow\uparrow\uparrow\uparrow\uparrow\downarrow\uparrow\uparrow\uparrow\uparrow\uparrow\uparrow\rangle$ (6)	$\|\downarrow\uparrow\uparrow\uparrow\downarrow\uparrow\uparrow\downarrow\uparrow\uparrow\uparrow\rangle$ (4)	$\|\downarrow\downarrow\uparrow\uparrow\uparrow\downarrow\downarrow\uparrow\uparrow\uparrow\uparrow\rangle$ (6)		$\|\downarrow\downarrow\downarrow\uparrow\uparrow\uparrow\downarrow\downarrow\uparrow\uparrow\uparrow\rangle$ (6)
"Sub-			$\|\downarrow\uparrow\downarrow\uparrow\uparrow\uparrow\downarrow\uparrow\downarrow\uparrow\uparrow\rangle$ (6)		$\|\downarrow\downarrow\uparrow\downarrow\uparrow\uparrow\downarrow\downarrow\uparrow\downarrow\uparrow\uparrow\rangle$ (6)
Standard"			$\|\downarrow\uparrow\uparrow\downarrow\uparrow\uparrow\downarrow\uparrow\uparrow\downarrow\uparrow\uparrow\rangle$ (3)		$\|\downarrow\downarrow\uparrow\uparrow\downarrow\uparrow\downarrow\downarrow\uparrow\uparrow\downarrow\uparrow\rangle$ (6)
Types					$\|\downarrow\downarrow\uparrow\uparrow\downarrow\uparrow\uparrow\downarrow\downarrow\uparrow\uparrow\rangle$ (4)
					$\|\downarrow\uparrow\downarrow\uparrow\downarrow\uparrow\downarrow\uparrow\downarrow\uparrow\downarrow\uparrow\rangle$ (2)

The numbers in parentheses give the size of the family in each case.

5.4) Computing Details

The original computations were performed for the rings N = 6 to 11 inclusive on the Ferranti 'Mercury' Computer at the University of London Computer Unit (now the Institute of Computer Science). (The cases N=2 to 5, and N=6 for the limit $\gamma = 1$, are trivial enough to be done easily by hand.) The matrices were first set up by hand as shown in Fig. (2.4). This procedure was not too laborious, since the set of matrices for the same number of overturned spins shows a characteristic

pattern, which means that most of the elements may be filled in by inspection. This part could have done by machine, but the programming would have been complicated by the presence of the 'sub-standard' blocks.

The actual diagonalisation process was carried out using a library programme (programme-517) based on Given's process for real, symmetric matrices (Givens, 1954). The program design was such that it was possible to obtain some or all of the eigenvalues and some, all or none of the eigenvectors. The program arranged the roots in descending algebraic order, and it was possible to set a parameter to specify a particular root which could then be calculated together with its eigenvector.

The time taken on the machine appeared to rise rather more rapidly than quadratically with the order of the matrix. The largest matrices solved, for eigenvalues only, were the 42 x 42 set of complex matrices for N = 11, $S^z = \frac{1}{2}$. The procedure used, described in sub-section (5.2) of this chapter, resulted in an effective order of 84. Each such matrix took 47 minutes on the Mercury computer, and the time would have been appreciably longer had the eigenvectors been required as well. The upper limit on the size of matrices to be solved depends on three main factors:-

a) the efficiency of the program, as implemented on the particular machine, b) the storage capacity, and c) the speed and mean free time between faults of the computer. Using programme-517 on Mercury, the estimated upper limit was order 90, which prevented the extension of the complete calculations to N>11, though isolated results were obtained for higher N, as described in Chapter V.

The total time required to complete the calculation of the eigenvalues of the 11-spin ring was about 6 hours and for the 10-spin ring a little over two hours. Very recently equivalent calculations for

chains have been carried out on the Science Research Council Atlas Computer at Chilton, Berkshire. The technique adopted was to expand the ring matrices in the machine, to represent the loss of translation symmetry, and then make adjustments to cover the change of boundary conditions. Chains of 6 and 8 spins were solved and partial results were obtained for N = 10. Additional use of reflection symmetry was required to complete the solution of N = 10, and to obtain higher N values. The author was unable to complete this project before leaving the country.

The programming language used was E.M.A. (Extended Mercury Autocode) and the matrix diagonalisation routines were the I.C.S. routines 922, 923, 924 and 925. Routine 922 reduces a real, symmetric matrix, where only the upper triangle is stored, to a symmetric tridiagonal matrix by Householder's transformation (Wilkinson, Computer Journal, 1960) and routine 923 then goes on to calculate the eigenvalues of the tridiagonal matrix by the Q. D. method. Routine 924 finds the eigenvector of a symmetric tridiagonal matrix corresponding to a given eigenvalue (Wilkinson, Computer Journal, 1958). Routine 925 combines routines 922, 923 and 924 so as to calculate all the eigenvalues and a specified number of eigenvectors of the original real symmetric matrix.

5.5) List of Results

Complete sets of eigenvalues of the Hamiltonian with periodic boundary conditions are available for the following values of cluster size N and anisotropy parameter γ, conveniently presented in Table. (2.8). In the case of eigenvectors, however, only limited results have been obtained. For the calculation of spin-pair correlation functions described in Chapter VI, it was necessary to obtain the antiferromagnetic ground state eigenvector(s) corresponding to

Table (2.8)

N \ γ	0	0.1	0.2	0.3	0.4	0.5	0.6	0.7	0.8	0.9	1.0
2	✓	✓	✓	✓	✓	✓	✓	✓	✓	✓	✓
3	✓	✓	✓	✓	✓	✓	✓	✓	✓	✓	✓
4	✓	✓	✓	✓	✓	✓	✓	✓	✓	✓	✓
5	✓	✓	✓	✓	✓	✓	✓	✓	✓	✓	✓
6	✓	✓	✓	✓	✓	✓	✓	✓	✓	✓	✓
7	✓	✓	✓	✓	✓	✓	✓	✓	✓	✓	✓
8	✓	✓	✓	✓	✓	✓	✓	✓	✓	✓	✓
9	✓					✓					✓
10	✓					✓					✓
11	✓										✓

N = 2 to 11, inclusive, for the values of γ of Table (2.8). In the case of eigenvectors, however, only limited results have been obtained. For the calculation of spin-pair correlation functions described in Chapter VI, it was necessary to obtain the antiferromagnetic ground state eigenvector(s) corresponding to N = 2 to 11, inclusive, for the values of γ of Table (2.8). Additional eigenvectors are required for the perpendicular susceptibility calculations of Chapter V. The eigenvectors corresponding to the lowest-lying antiferromagnetic states of both sub-blocks $k=0$ and $k=\pi$ for the $S^z = 0$ blocks of the even rings N = 4, 6, 8 and 10 have been obtained (the antiferromagnetic ground state eigenvectors are included in this set, of course). In addition <u>all</u> the eigenvectors of the $S^z = 1$, k = 0 and $k = \pi$ sub-blocks are required.

In the case of chains, the complete set of eigenvalues for all the values of γ of Table (2.8) has been obtained for N = (2) 4, 6 and 8. No eigenvectors have been calculated.

In Appendix 2, we present, in Table I, the eigenvalues for γ =1 of the <u>rings</u> N = 2 to 11 inclusive and in Table II the eigenvalues for γ = 0.5 of the <u>rings</u> N = 2 to 10 inclusive. In Table III we show the eigenvalues for γ =1 of the <u>chains</u> N = 2, 4, 6 and 8 and in Table IV the eigenvalues for γ = 0.5 of the <u>chains</u> N = 2, 4, 6 and 8.

5.6) Accuracy of the Eigenvalues

The general correctness of the eigenvalue spectra obtained for both rings and chains for the Heisenberg limit has been checked by

comparing the appropriate sums of roots and powers of roots against, for example, the exact trace relations $\mathrm{Tr}\,\mathcal{H} = 0$; $\mathrm{Tr}\,\mathcal{H}^2 = 3/4\ N\ 2^N J^2$; and $\mathrm{Tr}\,\mathcal{H}(S^z)^2 = -1/4\ N2^N J$ for rings and $\mathrm{Tr}\,\mathcal{H} = 0$; $\mathrm{Tr}\,\mathcal{H}^2 = 3/4(N-1)2^N J^2$; and $\mathrm{Tr}\,\mathcal{H}(S^z)^2 = -1/4(N-1)2^N J$ for chains. Also, a particularly sensitive test is the feature that all eigenvalues of a given S^z block appear in all blocks of lower S^z (See sub-section (5.1)).

It has been verified that an error in a single off-diagonal matrix element for clusters up to $N = 11$ produces an appreciable disturbance of this scheme. Finally the results of our calculations have been checked against the available calculations of Orbach (thesis, 1959) and Griffiths (1961). For $\gamma = 0.5$, similar trace relations hold, but we can no longer employ the conservation of total spin check. Regarding the degree of accuracy of the numerical results, the ring eigenvalues appear accurate to at least six significant figures for all values of N and γ. In the case of chains, the accuracy is more dependent on the magnitude of N. For N = 6 we have six figure accuracy but the eigenvalues for N=8 may be in error by $\pm$ 0.00005 (corresponding to a maximum error of 0.1%).

CHAPTER III

THE SPECTRUM IN ZERO MAGNETIC FIELD

Introduction

The bulk of this chapter is devoted to a descriptive account of the spectrum of energy levels of anisotropic and Heisenberg linear magnetic rings and chains. The spectrum is of interest in its own right. However, underlying and unifying our description are three important theoretical contentions. First, it will be seen that we can reasonably hope to learn some of the properties of infinitely large systems by extrapolation from the appropriate properties of small finite systems. Secondly, it appears very plausible that the thermal behaviour at low temperatures can be predicted from a knowledge of the energy gap between the ground state and first excited states. Thirdly, it turns out that the thermal behaviour for temperature greater than zero is determined not so much by the unbound states, appropriately described by spin-wave theory, as by bound spin-complexes which are harder to treat theoretically.

The first point supports the use of extrapolation techniques in later chapters. The second point provides us with a valuable supplement to the direct thermal property extrapolations, which are more successful at high temperatures. The third point suggests that any satisfactory theory must take into account the bound states of the spectrum, especially when considering the case of anisotropy.

1. ANTIFERROMAGNETIC GROUND STATE

1.1) Heisenberg Limit: Test of Extrapolation Procedures

First of all we will perform a fundamental test to investigate the possibility of extrapolating results obtained for the eigenvalue spectra of small finite rings and chains (see Chapter II and Appendix 1) to the limit of large N. Let us consider the Hamiltonian

$$\mathcal{H} = -2J\sum_{i=1}^{N} S_i . S_{i+1} \qquad (3.1.1)$$

with a negative value of the exchange integral J i.e. $J = -|J|$. This situation is conventionally held to correspond to antiferromagnetic coupling and hence the eigenvalue of lowest energy will be the antiferromagnetic ground state. The Heisenberg antiferromagnetic ground state energy is equal to

$$E_o = -2N|J|\,\ell n 2 + 0.5\,N\,|J| \qquad (3.1.2)$$

in the limit $N \to \infty$, as was first shown explicitly by Hulthén (1938).

It is convenient to define normalised ground state energies for finite N:

$$\mathcal{E}_o(N) = \frac{-E_o(N)}{N\,|J|} \qquad (3.1.3)$$

and these energies are tabulated numerically in the first column ($\gamma = 1.0$) of Table (I) in Appendix 3. (Note that the values for N=4, 6, 8 and 10 (rings) were given exactly by Hulthén (1938), and that for N=12 by Ledinegg and Urban (1953).) In Fig. (3.1) the ring energies are plotted versus 1/N (circles) and also versus $1/N^2$ (squares) and the chain energies are plotted versus 1/N (diamonds). First of all we observe that the ring energies comprise two distinct sequences for odd and even N. Also the $1/N^2$ (but not the 1/N) plots are linear down to N=4 or 5. Hence, for rings, we suggest the ground states obey a relation of the form

$$\mathcal{E}_o(N) \simeq \mathcal{E}_o(\infty) + a/N^2 \qquad (3.1.4)$$

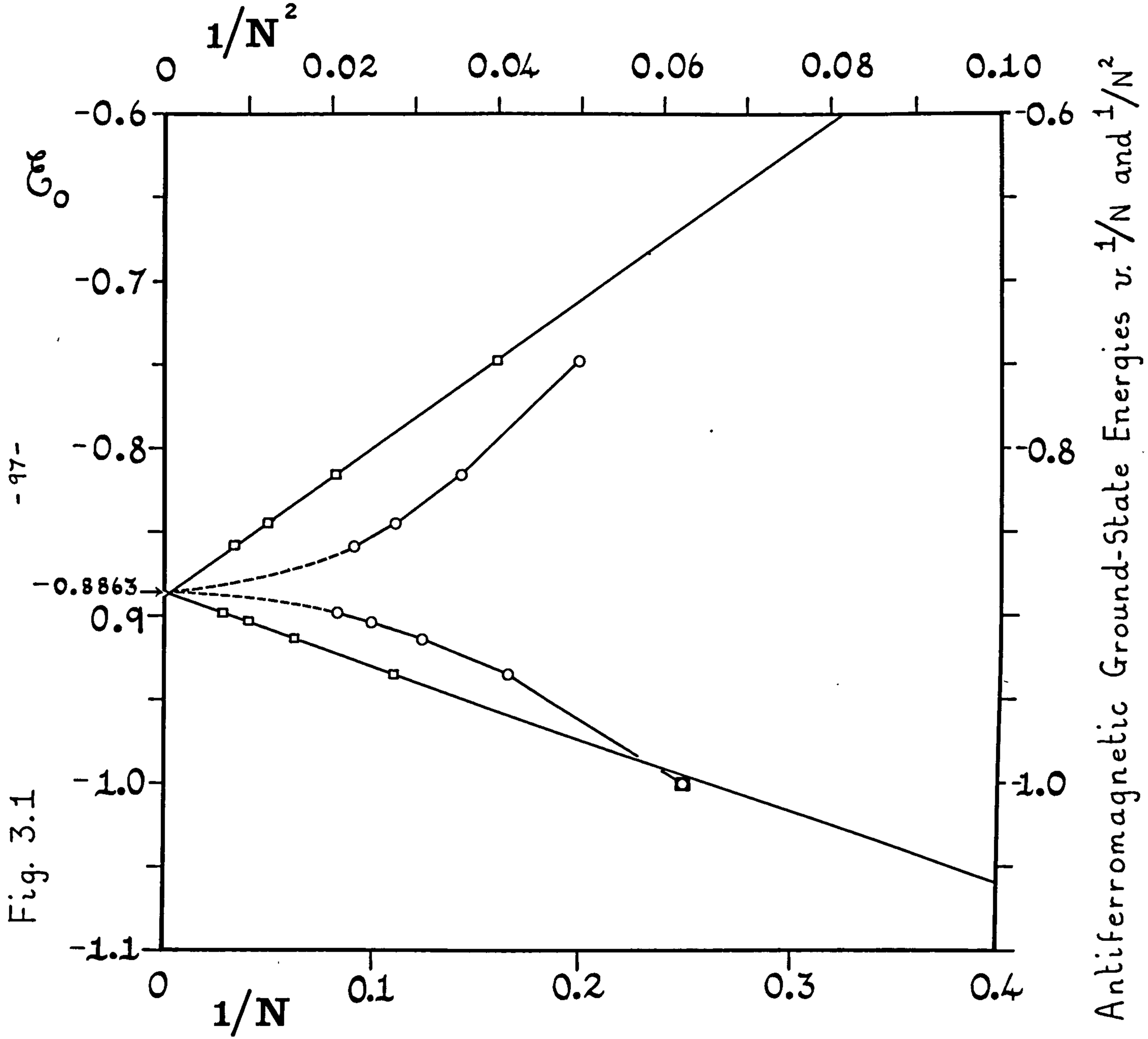
1/N²
0
0.02
0.04
0.06
0.08
0.10
-0.6
-0.7
-0.8
-0.8863
0.9
-1.0
-1.1
ε₀
0
0.1
0.2
0.3
0.4
1/N
Antiferromagnetic Ground-State Energies v. 1/N and 1/N²

Fig. 3.1

where $a_{odd} \simeq -2a_{even}$, quite accurately down to N=4 or 5. (Recently Griffiths and Weng (private communication), from a study of the antiferromagnetic ground states for small finite rings of spin-1, have conjectured a general approximate relation of the form

$$\mathcal{E}_o(N,S) \simeq \mathcal{E}_o(\infty,S) + a/N^{2S+1} \qquad (3.1.5)$$

where S is the total spin of the homogeneous linear system.) In the case of chains we have a slower convergence and the 1/N plot is linear, the linearity extending down to N=2 (not shown on the figure). In the case of chains, therefore, we have the approximate relation

$$\mathcal{E}_o(N) \simeq \mathcal{E}_o(\infty) + b/N \qquad (3.1.6)$$

The constants a_{odd}, a_{even} and b may be roughly estimated numerically to be 3.5, -1.75 and 0.28, respectively. If we did not know the limiting value, we could estimate it to about 0.1% accuracy by linear extrapolation of ring energies with $1/N^2$ and to about 0.3% by linear extrapolation of chain energies with 1/N.

1.2) General Anisotropy

Let us also consider convergence of anisotropic antiferromagnetic ground state energies to the known limit, illustrated in Figs.(3.2) and (3.3). In Fig. (3.2) we show the antiferromagnetic ground state energy as a function of γ for finite and infinite rings. The exact limiting curve is taken from a numerical solution due to Orbach (1958), and appears as the dashed curve. The analytic form of the anisotropic solution was first found by Walker (1959) and again by des Cloizeaux and Gaudin (1966) who gave the infinite series expression

$$\frac{E_o(\gamma)}{N|J|} = -\sinh\varphi\left[0.5 + \sum_{n=1}^{\infty}(1-\tanh n\varphi)\right] \qquad (3.1.7)$$

where γ (anisotropy parameter) = $\operatorname{sech}\varphi$, and the same result is implicit in the work of Yang and Yang (1966).

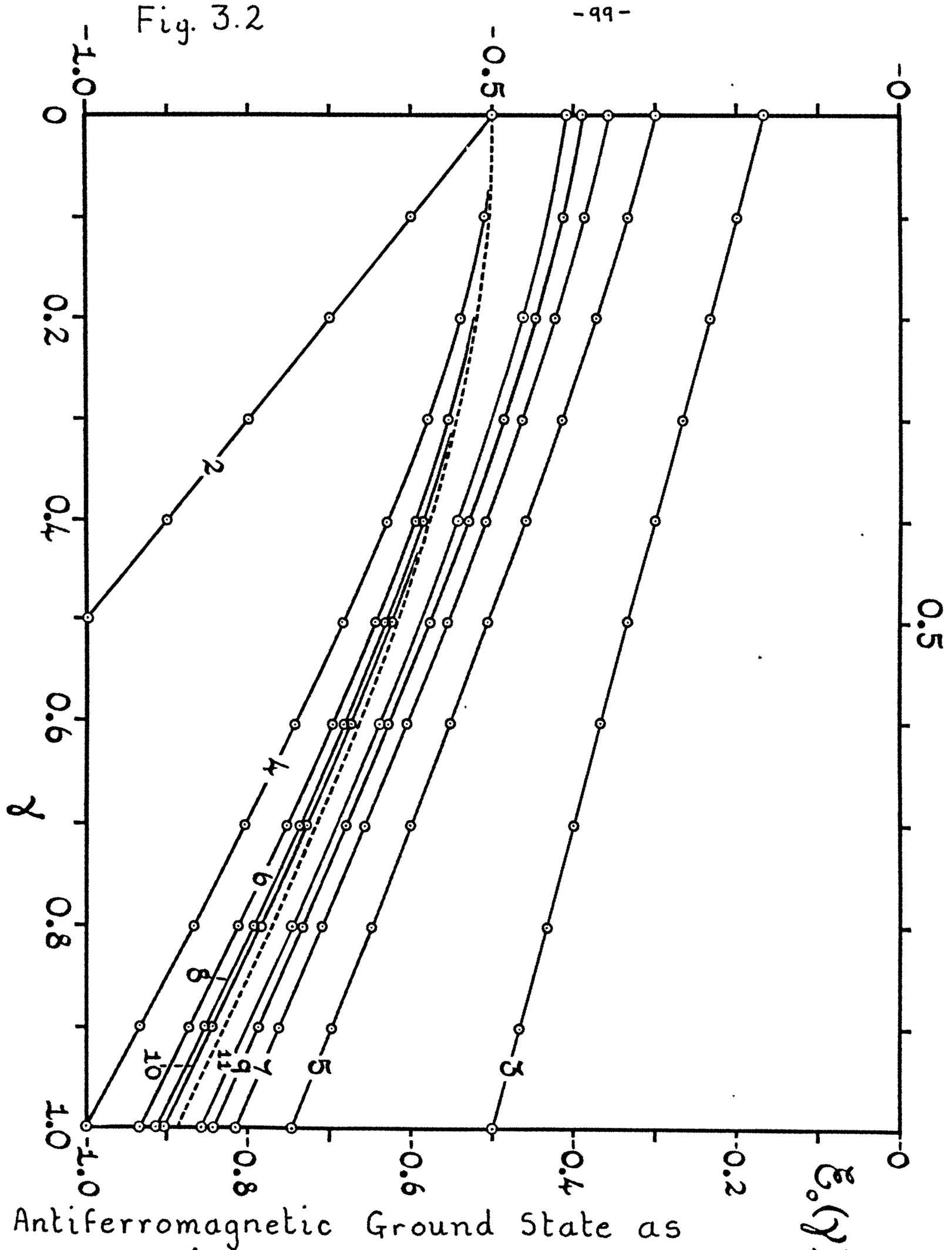

Fig. 3.2 Antiferromagnetic Ground State as Function of γ for Finite and Infinite $\mathcal{L}$ Rings

Again we observe, in Fig. (3.2), that odd and even rings form two distinct converging sequences which bracket the limiting result. Over the whole range of γ we observe that the Orbach curve is rather well defined by these small finite N results.

For pure Ising rings ($\gamma = 0$), for N even, the ground state Ising eigenfunctions are the doubly degenerate $S^z = 0$ pair, corresponding to alternate up and down spins, typified in the case of N=6 by $|\uparrow\downarrow\uparrow\downarrow\uparrow\downarrow\rangle$ and $|\downarrow\uparrow\downarrow\uparrow\downarrow\uparrow\rangle$. Using the methods of Chapter I, section (1), it is easy to verify that the finite (and infinite) N ground state energy is given by

$$\mathcal{E}_o(N_{even}) = -0.5 \tag{3.1.8}$$

For odd N Ising rings the ground state energies are given by

$$\mathcal{E}_o(N_{odd}) = -0.5\left(1 - 2/N\right) \tag{3.1.9}$$

In this case the ground state is 2N-fold degenerate, being composed of N states with $S^z = 1/2$ and N states with $S^z = -1/2$. Hence the ground state energy approaches the limit as 1/N, a result which may be regarded as an effect of the 'misfit seam' for N odd, i.e. we can only turn over exactly half the spins to obtain perfect alternating antiferromagnetic ordering when N is even.

In the case of Fig. (3.3) we have a very similar plot, again with good convergence to the Orbach curve. Here we have substituted a set of even chains for N=2, 4, 6 and 8 for the previous set of odd rings (even chains and odd rings both converge to the limit from above: so also do odd chains). We are thus comparing the convergence of even rings and even chains over the complete range of γ . For chains, the Ising limit energies may again be calculated directly as

$$\mathcal{E}_o(N) = -0.5\left(1 - 1/N\right) \tag{3.1.10}$$

Thus the energies approach the limit as 1/2N for all N, whereas the even ring energies are exact. This, of course, is an effect of the changed boundary conditions, i.e. 'end effects'. The energy values for the values

Fig. 3.3

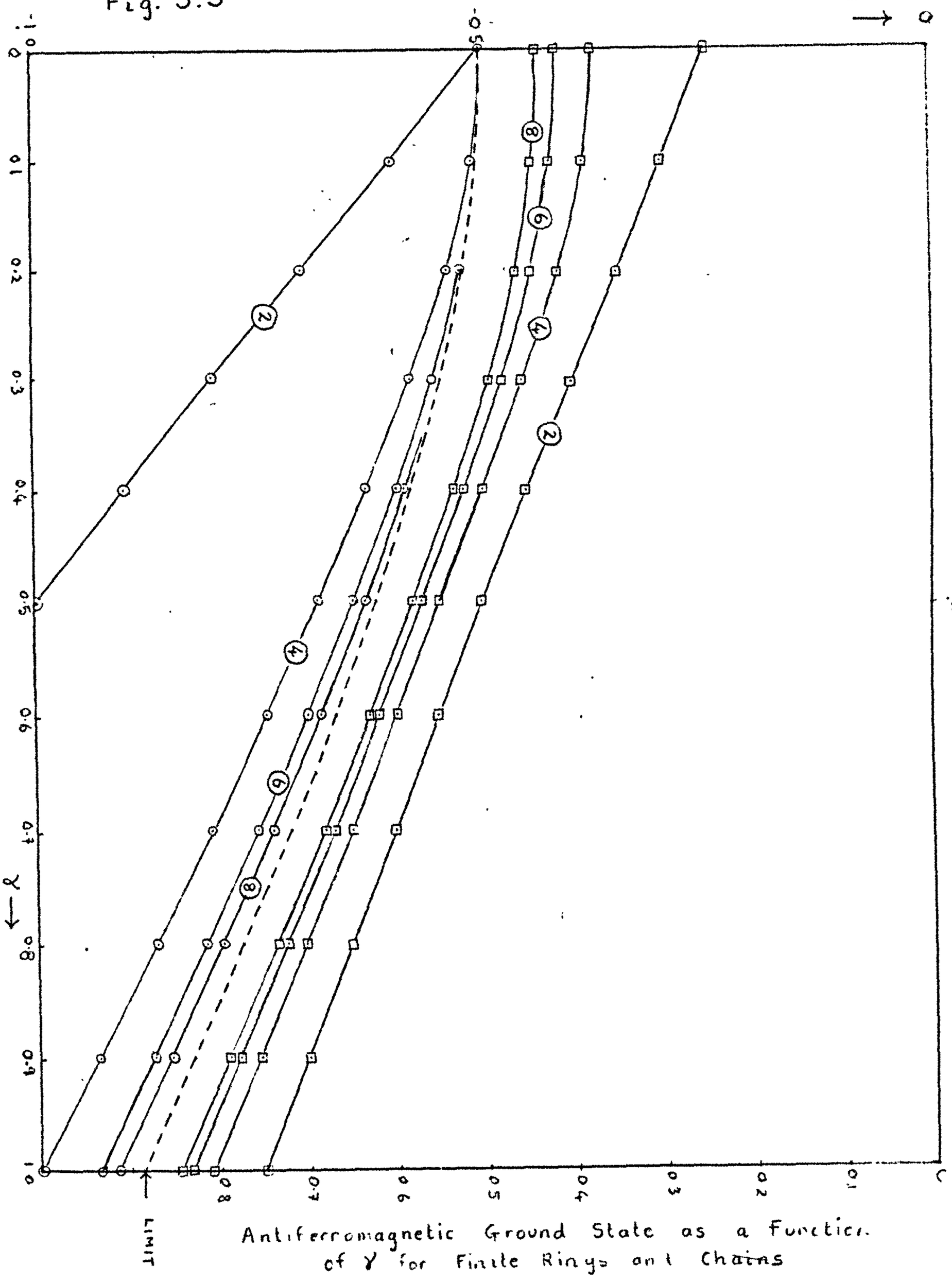

Antiferromagnetic Ground State as a Function of γ for Finite Rings and Chains

Fig. 3.4

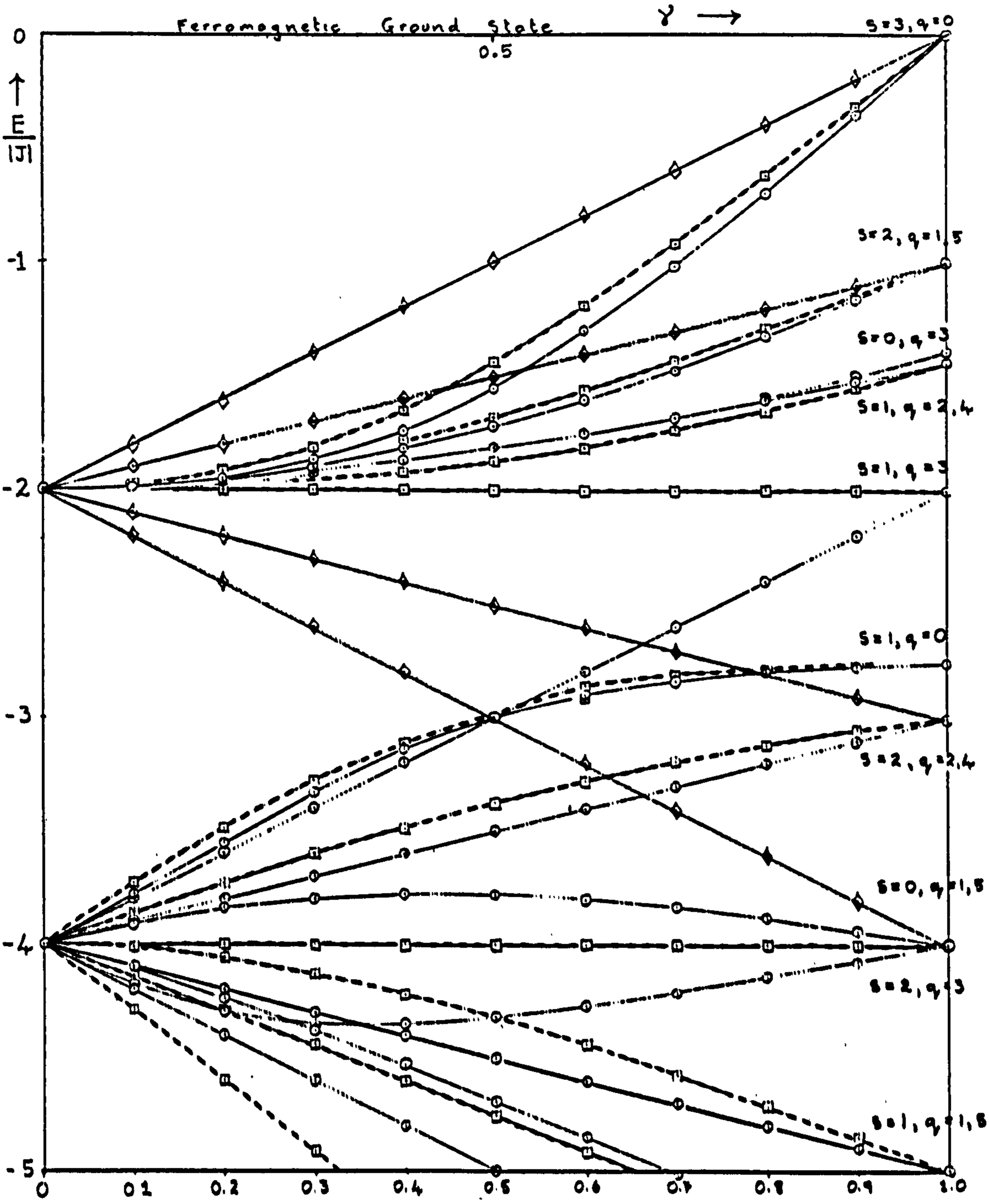

Ferromagnetic Ring Spectrum as Function of γ

Fig. 3.5

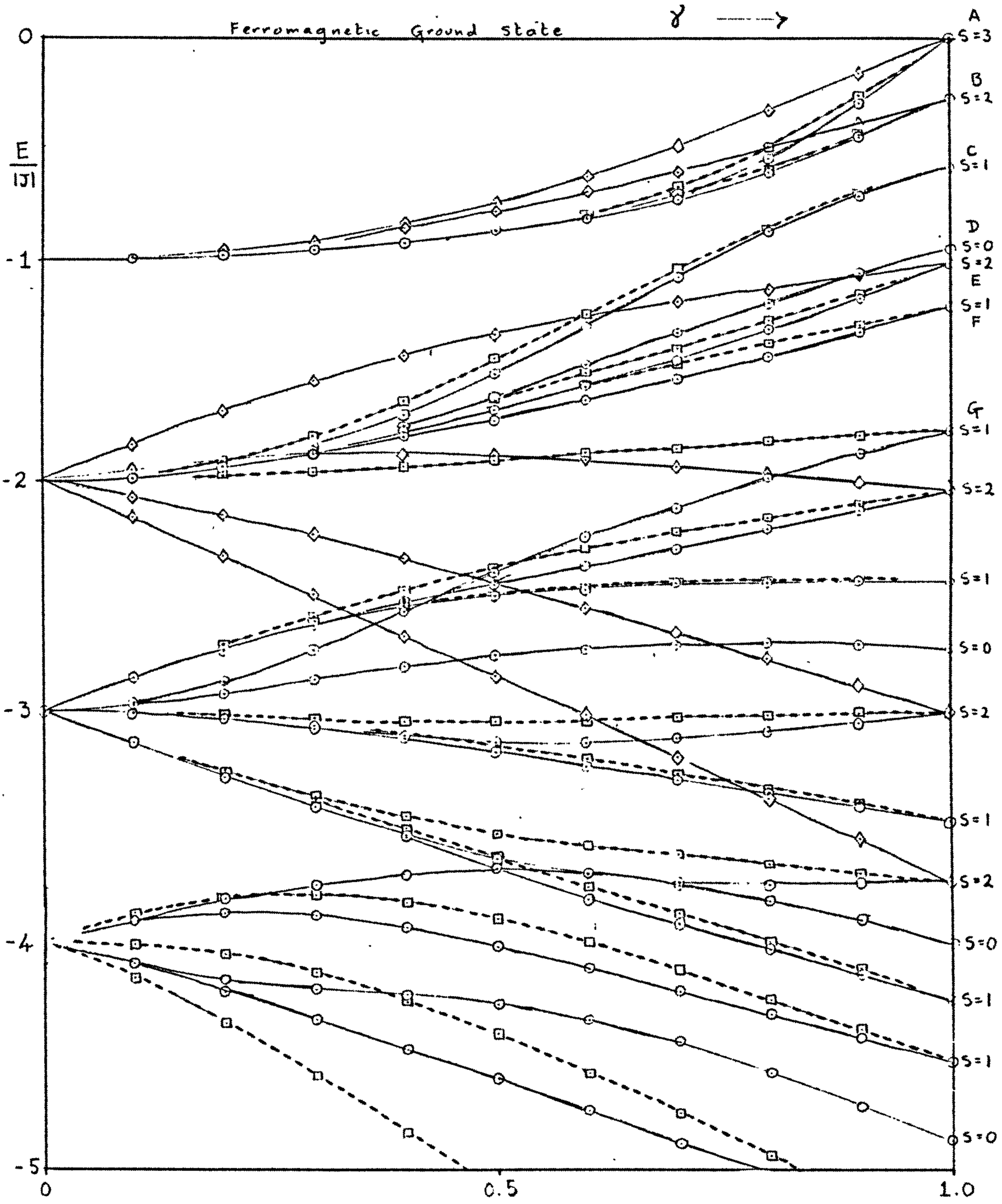

Ferromagnetic Chain Spectrum as Function of γ

of γ shown in Fig. (3.2) and Fig. (3.3) are contained in Table (I) of Appendix 3.

Encouraged by the relatively simple and regular behaviour of the finite N results we have found so far, we may go on to examine properties for which the exact $N = \infty$ results are unknown with the reasonable expectation that careful extrapolation to large N will not be misleading.

2. GENERAL FEATURES OF THE EIGENVALUE SPECTRUM: LOW-LYING FERROMAGNETIC STATES.

Let us now proceed to survey the spectrum of eigenvalues and their behaviour as functions of γ . In Fig. (3.4) we plot the energy levels near the ferromagnetic ground state for N=6 (the number of levels for higher N would be so large as to cause confusion). Rings are discussed primarily: chains are introduced when they differ in some significant aspect. For example, an important difference in the Ising spectrum is carefully discussed in relation to the low-temperature thermal properties.

2.1) Ferromagnetic Ground State

If we consider the ferromagnetic Hamiltonian

$$\mathcal{H} = -2|J| \sum_{i=1}^{N} \left\{ S_i^z S_{i+1}^z + \gamma \left(S_i^x S_{i+1}^x + S_i^y S_{i+1}^y \right) \right\} \qquad (3.2.1)$$

it is well-known that the ferromagnetic ground state for all $\gamma < 1$ is doubly degenerate and is given by

$$E_o = -\ 0{\cdot}5\, N|J| \qquad (3.2.2)$$

corresponding to $S^z = N/2$ (all spins aligned). For N=6, for example, the ferromagnetic ground state eigenfunctions are $|\uparrow\uparrow\uparrow\uparrow\uparrow\uparrow\rangle$ and $|\downarrow\downarrow\downarrow\downarrow\downarrow\downarrow\rangle$. In the Heisenberg limit the ground state energy is still $E_o = -0.5\,N|J|$, but the state is now (N+1)-fold degenerate corresponding to the (N+1) distinct, orthogonal, completely symmetric linear combinations of all Ising basis functions of a given S^z, which constitute the eigenfunctions. For example, for N=4, the normalised ground state eigenfunctions are explicitly

$$
\begin{aligned}
&a) \quad |\uparrow\uparrow\uparrow\uparrow\rangle && (S^z = 2)\\
&b) \quad 1/2\,[\,|\downarrow\uparrow\uparrow\uparrow\rangle + |\uparrow\downarrow\uparrow\uparrow\rangle + |\uparrow\uparrow\downarrow\uparrow\rangle + |\uparrow\uparrow\uparrow\downarrow\rangle\,] && (S^z = 1)\\
&c) \quad \frac{1}{\sqrt{6}}\,[\,|\downarrow\downarrow\uparrow\uparrow\rangle + |\uparrow\downarrow\downarrow\uparrow\rangle + |\uparrow\uparrow\downarrow\downarrow\rangle + |\downarrow\uparrow\uparrow\downarrow\rangle + |\downarrow\uparrow\downarrow\uparrow\rangle + |\uparrow\downarrow\uparrow\downarrow\rangle\,] && (S^z = 0)\\
&d) \quad 1/2\,[\,|\uparrow\downarrow\downarrow\downarrow\rangle + |\downarrow\uparrow\downarrow\downarrow\rangle + |\downarrow\downarrow\uparrow\downarrow\rangle + |\downarrow\downarrow\downarrow\uparrow\rangle\,] && (S^z = -1)\\
&e) \quad |\downarrow\downarrow\downarrow\downarrow\rangle && (S^z = -2)
\end{aligned}
\qquad (3.2.3)
$$

If, therefore, we consider the normalised Hamiltonian

$$
\mathcal{H} = 2|J| \sum_{i=1}^{N} \left\{ \left(S_i^z S_{i+1}^z - 1/2 \right) + \gamma \left(S_i^x S_{i+1}^x + S_i^y S_{i+1}^y \right) \right\} \qquad (3.2.4)
$$

the ground state will lie at $E_o = 0$ for all γ. In Fig. (3.4), since we are actually considering an antiferromagnetic Hamiltonian, the ferromagnetic ground state at $E_o = 0$ will be the highest-lying state shown on the figure. (We display the levels in this manner for the sake of continuity when going on to discuss the antiferromagnetic limit.)

2.2) Excited States

First of all we observe, from Fig. (3.4), that in the Ising limit the eigenvalues are very highly degenerate. The first excited state lies at energy $-2|J|$ below the ground state and comprises all Ising states with one, two, three, up to (N-1) adjacent overturned spins (hence has degeneracy N(N-1)). In fact, all the Ising level energies are given by the sequence $0, -2|J|, -4|J|, \ldots\ldots\ldots, -N|J|$, and all are degenerate. The off-diagonal terms in the Hamiltonian are then seen to split the Ising degeneracy, the levels fanning out but eventually showing some degeneracy again in the Heisenberg limit. However, there is less degeneracy in the Heisenberg limit, i.e. the degeneracy is of order N rather than N^2.

2.3) Energy Levels for One Overturned Spin

Let us investigate in some detail the levels emanating from the first excited Ising level at $-2|J|$. A sub-class of these levels of order

2N corresponding to one and (N-1) overturned spins may easily be investigated exactly. The Hamiltonian block matrix corresponding to $S^z = N/2 - 1$ is of order N and has the very simple cyclic form shown in fig. (3.1). In terms of the N^{th} roots of unity, ω^q, where $0 \leq q \leq (N-1)$, the eigenvalues, in descending order of energy, are $(-2+2\gamma)|J|$; $(-2+\gamma(\omega+\omega^{N-1}))|J|$;.... $(-2+\gamma(\omega^q+\omega^{N-q}))|J|$. These levels are shown on Fig. (3.4) by solid straight lines, with diamonds indicating the individual values for $\gamma = 0$ by increments of 0.1 through 1.0.

fig. (3.1)

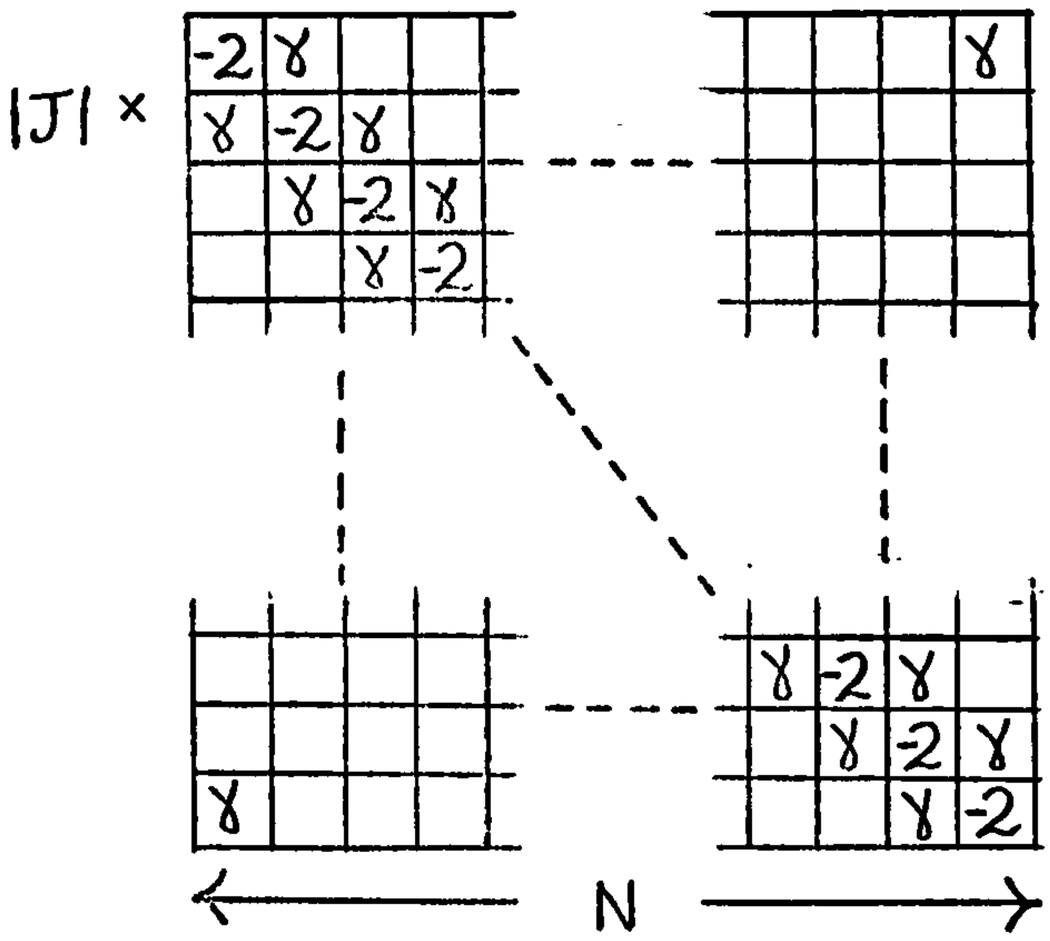

We observe that the level (actually two-fold degenerate) $-2(1-\gamma)|J|$ is the first excited ferromagnetic level for $0<\gamma<1$, for rings. As N increases more of these levels appear between the two limiting levels $(-2 \pm 2\gamma)|J|$ and in the limit $N \to \infty$ we obtain a continuum of levels, the energy difference between adjacent levels being $O(N^{-1})$.

We may easily obtain the dispersion curve (energy versus wave-vector k) for these levels for all γ. Replacing ω^q by e^{ik} where $k = \frac{2\pi q}{N}$, $q = 0, \pm 1, \pm 2, \cdots$ we have

$$E - E_0 = \left[-2 + (e^{ik} + e^{-ik})\gamma\right]|J| \qquad (3.2.5)$$

$$= -2|J|(1 - \gamma \cos k)$$

(In the limit, of course, k becomes a continuous variable.) This dispersion curve is sinusoidal and may be described as a 'spin wave' corresponding to a single overturned spin. Equation (3.2.5) is identical with that obtained by analytic treatment of the Bethe-Hulthén equations, and was first derived by Bloch (1930).

2.4) Energy States for Two Overturned Spins

We may also distinguish a second set of excitations (dashed curves with squares) corresponding to two overturned spins. The (translationally reduced) Hamiltonian block matrix corresponding to two overturned spins has the general form shown in fig. (3.2), where $\varphi = (1 + \omega^{N-q})$ and $\varphi^* = (1 + \omega^{q})$. A11

fig. (3.2)

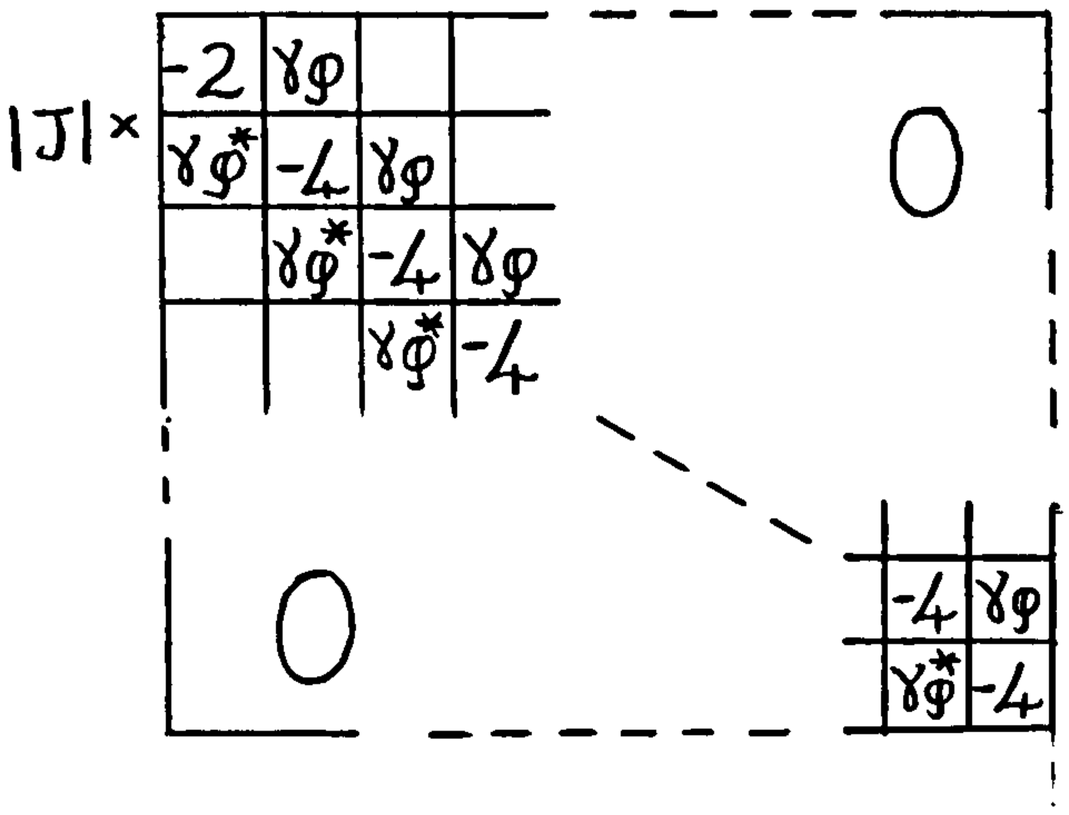

diagonal elements are equal to -4 except the first, equal to -2, which corresponds to the set of N states which have the two reversed spins as neighbours. Second order perturbation theory yields the formula for this special set

$$|J|^{-1}(E-E_0) = -2 + 0.5\gamma^2\varphi\varphi^* = -2 + 0.5\gamma^2(2 + \omega^{q} + \omega^{N-q}) \qquad (3.2.6)$$

$$= -2 + \gamma^2(1 + \cos k)$$

defining k as previously. This formula is also obtained as an exact result in the limit of large N by means of the Bethe-Hulthén formalism (Orbach 1958). We thus observe that the levels for two neighbouring overturned spins are split more slowly with γ, i.e. as γ^2, than the corresponding levels for one overturned spin which go as γ.

2.5) Heisenberg Limit

Let us now discuss the Heisenberg limit where, as we have already noted, appreciable degeneracy reappears. From Chapter II and Appendix 1, we know this degeneracy is associated with conservation of the square of the total spin $S^2 = (\sum_i \mathbf{S}\, i)^2$ for this limit. The levels now appear as multiplets corresponding to the various eigenvalues of S, namely N/2, N/2-1, ..., 0 (N even). (For N=6 we see that at γ=1 the ferromagnetic ground state becomes a septet corresponding to S=3.) We observe that the

lowest-lying levels are, in order of decreasing excitation energy, S=2 (quintet), S=0 (singlet), S=1 (triplet), S=1 (triplet) etc. For a periodic system we have seen in Chapter II that the levels may also be classified in terms of wave-numbers q, related to eigenvalues of the translation operator T. The appropriate value of q is marked beside a given multiplet of levels (the q classification is the same for all members of the multiplet and continues to hold as the levels split with decreasing γ.) We now compare the low-lying ferromagnetic levels of rings in Fig. (3.4) with a similar set of levels for chains shown in Fig. (3.5). First of all we can regard the chain Hamiltonian as a perturbed form of the ring Hamiltonian, and accordingly we would expect the level scheme to be generally similar but relatively distorted. On inspection of Fig. (3.5) this appears to be the case; however we apparently have more levels. This is because we have lost the ring classification by wave-vector q which introduces a two-fold degeneracy for $q \neq o, N/2$. (The matrices for ω^q and ω^{N-q} for $q \neq o, N/2$ have identical eigenvalues.) The possibility of a wave-vector classification for chain eigenstates is discussed in a later sub-section of this chapter. With this in mind we may identify chain levels with ring levels as follows: - the chain spin-3 level A correlates with the ring spin-3, q=0 level (Heisenberg ferromagnetic ground state in both cases); the chain spin-2 levels B and E correlate with the ring spin-2 level for q=1 and q=5; the chain spin-1 levels C and F correlate with the ring spin-1 level for q=2 and q=4; the chain spin-0 level D correlates with the ring spin-0 level for q=3; the chain spin-1 level G correlates with the ring spin-1, q=3 level, etc.. In this way a complete correlation of ring and chain levels may be made over the whole Heisenberg spectrum.

2.6) Ising Limit Energy Gaps: Rings and Chains

At the Ising limit the chain levels form a significantly different pattern from the rings, i.e. we have levels at E=0, $-|J|$, $-2|J|$, $-3|J|$, ... $-(N-1)|J|$ rather than just for E=0, $-2|J|$, $-4|J|$, ... as

is the case for rings. The first excited ferromagnetic Ising level for chains at $-|J|$ contains $\simeq 4(\frac{N}{2} - 1) + 2 \simeq 2N - 2$ states which can be regarded as having split off the ring level at $-2|J|$ under the influence of a perturbation. The degeneracy of the second excited chain level at $-2|J|$ is then $N(N-1) - 2(N-1) = (N-1)(N-2)$ and is still of order N^2. Since this dissimilarity persists to the limit $N = \infty$, it appears that finite rings and chains predict different limiting behaviour for the spectrum; in particular for the excitation energy gap $\Delta E_F(o)$ between the ground and first excited states.

From the study of many examples in elementary statistical mechanics one learns that the specific heat at low temperatures behaves as exp $[-\Delta E_{F(O)}/kT]$. Since $\Delta E_F(O)$ is different for rings and chains one might be led to expect that the specific heat at low T is different for rings and chains. However, this is wrong as one can easily see by examining the exact solution, for rings

$$Z = (2e^{-J/2kT})^N \left[\cosh^N(J/2kT) + \sinh^N(J/2kT)\right] \quad (3.2.7)$$

and for chains

$$Z = (2e^{-J/2kT})^N \cosh^N(J/2kT) \quad (3.2.8)$$

One can also see from a series expansion of (3.2.7) that there is an "accidental" cancelling of the odd powers of exp (-J/kT) in accordance with the description of the spectrum of rings. This cancelling is due to the effect of the $\sinh^N(J/2kT)$ term which, however, is completely negligible in determining the thermodynamic properties in the limit $N \to \infty$. This means that the low temperature behaviour is not determined just by the low-lying states but may be governed by all the energy levels, especially when the level degeneracies go as high powers of N.

Thus, one must exercise some discretion in interpreting low temperature thermodynamic behaviour from energy gaps. The preceding Ising example suggests some rules of thumb which, of course, are not rigorous. If the degeneracy of the first excited level is of O(N), then it seems plausible that the primary excitation gap is the same gap that determines the initial behaviour of the thermal properties in the limit. If the levels are of $O(N^2)$, as we have for the Ising rings, the effective gap is half the finite N primary gap; (in general, if the levels are of $O(N^r)$ we may presume that the effective gap=r^{-1} x primary gap). If the levels are of O(1), the apparent primary gap has no relation to the effective limiting gap.

Finally, it seems that quite often the chains exhibit the true energy gap whereas the rings exhibit the double gap. Since it is sometimes difficult to find the required degeneracies, the chains are seen to play a useful independent role.

3. GENERAL FEATURES OF THE EIGENVALUE SPECTRUM:

LOW-LYING ANTIFERROMAGNETIC STATES

In this section we continue our general survey, this time examining the spectrum near the antiferromagnetic limit. Interesting questions of the degeneracy of the antiferromagnetic ground state and the existence of an antiferromagnetic anisotropy energy gap between the ground state and the first excited states in the limit are examined with the help of extrapolation methods. A unitary transformation of the Hamiltonian is presented which, in affecting the wave-vector classification of the antiferromagnetic ground sub-states, regularises the transition from a ferromagnetic to an antiferromagnetic Hamiltonian.

3.1) Degeneracy of the Antiferromagnetic Ground State

We have already considered the question of the energy of the antiferromagnetic ground state in detail in section (1). With the aid of Fig. (3.6), a lower energy continuation of Fig. (3.5), for N=6, we now go

Fig. 3.6

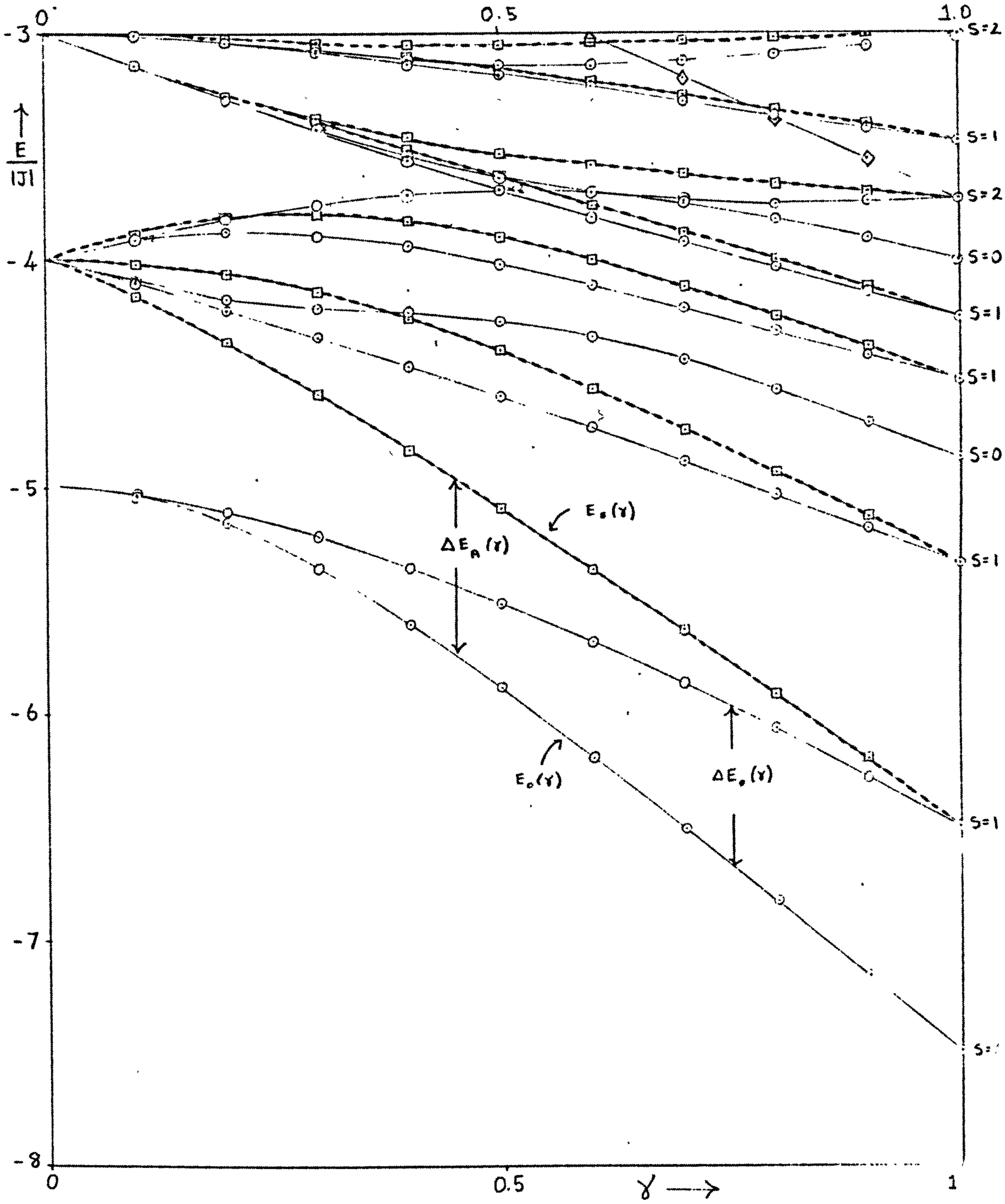

Antiferromagnetic Chain Spectrum as Function of γ

on to consider the degeneracy of the ground state. We observe that the two-fold degeneracy (for both rings and chains) of the antiferromagnetic ground state at the Ising limit is split by the transverse terms in the Hamiltonian, the upper level becoming degenerate with a (two-fold degenerate) $|S^z|=1$ level (the second excited state for finite rings and chains) to form a spin-1 triplet in the Heisenberg limit. It may easily be verified that the ground state splitting occurs only in high order, in fact N^{th} order. We therefore suspect that in the limit $N \to \infty$, the ground state should again become degenerate, at least in some sense. To investigate this point we shall examine the ground-state splitting $\Delta E_o(N,\gamma)$ as a function of N and γ. If ΔE_o varies as 1/N for N large, the levels close up, but only at a rate characteristic of a continuum of levels (as, for example, the one-overturned spin continuum) in the limit of $N = \infty$. If, however, ΔE_o vanishes more rapidly than 1/N, e.g. as $1/N^2$, then we may consider the levels as asymptotically degenerate even if they lie within a continuum. In Fig. (3.7) the product $N\Delta E_o(N)/|J|$ has been plotted versus 1/N for N=4, 6, 8 and 10, and for values of γ in the range 0 to 1. We should mention here that the lowest-lying region of the antiferromagnetic spectrum, consisting of the split ground state and the first excited state $E_S(N,\gamma)$, is similar for both rings and chains, hence we do not present a companion figure to Fig. (3.6) for the N=6 ring. However, for an Ising ring the first excited states lie at an energy $\Delta E_A(o) = 2|J|$ above the ground state whereas the corresponding energy gap for chains is $\Delta E_A(o) = |J|$. (We have already implicitly expressed the fact that the ground state for chains is $E_o(o) = -(N-1)|J|$ whereas it is $E_A(o) = -N|J|$ for rings.) This does not affect Fig. (3.6) where we are concerned only with the ground state.

We observe that for $\gamma \leq 0.5$, $N\Delta E_o$ is rapidly decreasing and there seems little doubt that the limit is zero. For $\gamma = 0.6$, 0.7 and 0.8 the decrease is slower but the rate of decrease appears to increase for larger N. It

Fig. 3.7

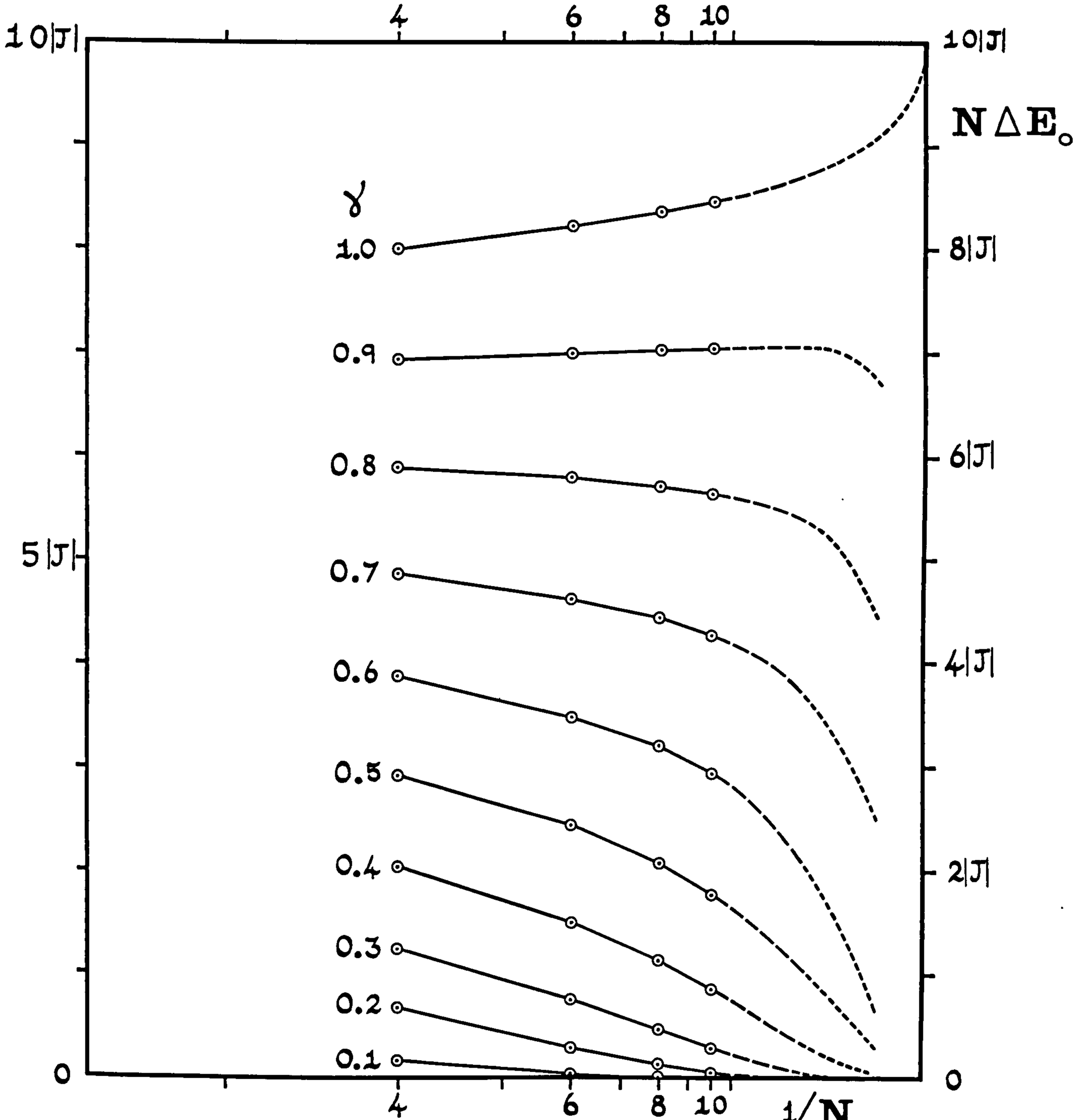

Dependence of Antiferromagnetic Ground-State Splitting on γ and N.

thus seems probable that the limit is again zero. The probable behaviour of $N\Delta E_o$ for N>10 is suggested by the broken lines. (These broken lines do not, of course, correspond to numerical extrapolations in these cases.) At $\gamma = 0.9$, for rings, the values of $N\Delta E_o$ at first increase slightly with N, but for N=8 and 10 they are almost equal, and we believe that larger values of N would again yield a product decreasing at first slowly, but eventually rapidly. Extrapolation plots for chains show very similar features, and hence we do not present a separate figure.

At the limit $\gamma=1$, on the other hand, $N\Delta E_o$ seems to be rising steadily and approaching a definite limit at 1/N=0, consistent with a state lying in a continuum bounded by the ground state. For rings, a direct extrapolation of the values for N=4, 6, 8 and 10 indicates a limiting value of $N\Delta E_o \simeq 9|J|$. (For odd rings we have a limiting value of $N\Delta E_o \simeq 18|J|$. See sub-section (3.2) of this chapter.) For chains, a linear extrapolation of the values for N=4, 6 and 8 yields $N\Delta E_o \simeq 8|J|$. In sub-section (5.2) we shall discuss the analytic work of des Cloizeaux and Pearson (1962) which has a bearing on these results.

In summary, we feel that the evidence of Fig. (3.7) definitely suggests that for all $\gamma < 1$ (anisotropic coupling) ΔE_o decreases more rapidly than 1/N (i.e. $N\Delta E_o \to 0$), so that the limiting ground state may be said to be (two-fold) degenerate. In the isotropic limit, however, ΔE_o decreases only as 1/N and the antiferromagnetic ground state should be regarded as non-degenerate. Prior to the work of des Cloizeaux and Pearson, Marshall (1955) proved that there existed a singlet ground state, but did not exclude the possibility of there being several degenerate ground states, some of which may not be singlets. Lieb, Schultz and Mattis (1961) were able to prove a stronger theorem; namely that for a linear chain of spin-1/2 atoms with nearest-neighbour antiferromagnetic Heisenberg interactions, the ground state is also non-degenerate. By a second theorem they were able to prove in addition that there exists an excited state (E_S) for the

cyclic linear chain with nearest-neighbour Heisenberg interactions, with excitation energy of order 1/N. More precisely, they obtained the result

$$E_s \leq E_o + (2\pi^2/N) \tag{3.3.1}$$

The conclusion is that there is no energy gap in the limit $N \to \infty$ for $\gamma=1$, and the ground state is the limit of a continuum.

3.2) Anisotropy Energy Gap

Let us now investigate the existence of an anisotropy energy gap $\Delta E_A(\gamma)$ for intermediate values of γ . We shall study a) the difference $\Delta E_a(\gamma,N)$ between the 'lowest excited state' $E_S(\gamma,N)$ and the finite N ground state $E_o(\gamma,N)$ (see Fig. (3.8)), and b) the gap $\Delta E_A'(\gamma,N)$ between $E_S(\gamma,N)$ and the limiting ground state $N|J|\,\mathcal{E}_o(\gamma,\infty)$ for rings. We should expect the two sets of values to form two distinct sequences but ultimately tend to the same limiting value. Let us investigate this point for $\gamma=1$. Since $\Delta E_A = E_S(N) - E_o(N)$ and $\Delta E_A' = E_S(N) - N|J|\mathcal{E}_o(\infty)$ we have that

$$\Delta E_A' - \Delta E_A = E_o(N) - N|J|\mathcal{E}_o(\infty) = N|J|\left[\mathcal{E}_o(N) - \mathcal{E}_o(\infty)\right] \tag{3.3.2}$$

But from Fig. (3.1) and the discussion of sub-section (1.1) we have (for rings) $\mathcal{E}_o(N) - \mathcal{E}_o(\infty) \approx a/N^2$. Hence

$$|J|^{-1}\left(\Delta E_A' - \Delta E_A\right) \simeq a/N \longrightarrow 0 \tag{3.3.3a}$$

in the limit. For other values of γ we have the result that $\mathcal{E}_o(\gamma,N) - \mathcal{E}_o(\gamma,\infty)$ vanishes also as $1/N^2$ or more rapidly, and hence more generally we have

$$\Delta E_A'(\gamma) - \Delta E_A(\gamma) \longrightarrow 0 \tag{3.3.3b}$$

At the Heisenberg limit the conjecture that $\Delta E_A(1,N)$ and $\Delta E_A'(1,N)$ fall to zero like 1/N may be checked fromthe values for small finite N. For $\gamma=1$, the first excited state E_S is degenerate with the upper component of the split ground state and hence $N\Delta E_A(1,N) = N\Delta E_o$ and therefore both

tend to the same limit. However we should expect $N\Delta E'_A(1, N)$ to tend to a different limit, since from equation (3.3.3a) we have

$$N|J|^{-1}\left[\Delta E'_A - \Delta E_A\right] \simeq a \qquad (3.3.4)$$

where $a_{even} = -1.75$ and $a_{odd} = 3.5$ from sub-section (1.1). (Since for chains $\mathcal{E}_o(N) - \mathcal{E}_o(\infty) = -\frac{b}{N}$, we have that

$$|J|^{-1}(\Delta E'_A - \Delta E_A) \to -b \text{ and } N|J|^{-1}(\Delta E'_A - \Delta E_A) \to \infty \qquad (3.3.5)$$

Hence, for chains, values of $\Delta E'_A(N)$ cannot be used in addition to values for $\Delta E_A(N)$ to estimate the limiting anisotropy gap.)

For other values of γ also, linear extrapolation with 1/N seems to be appropriate in estimating the limiting gap. In Fig. (3.8) we show our estimate for the limit $\Delta E_A(\gamma)$ of the antiferromagnetic anisotropy gap $\Delta E_A(\gamma,N)$. As we have already noted, at the Ising limit the anisotropy gap for rings is exactly $2|J|$. Our extrapolations indicate, in fact, that $\Delta E_A(\gamma)$ is non-zero for all $\gamma < 1$, though we observe a very slow increase in the gap as $(1-\gamma)$ increases from zero to 0.3 or 0.4. Since this work was performed , analytic work has appeared (des Cloizeaux and Gaudin (1966) and Yang and Yang (1966)) which on the whole substantiates our conclusions. Des Cloizeaux and Gaudin present the following analytic formula for the anisotropy gap

$$G(\rho) = \sinh\varphi \sum_{n=-\infty}^{\infty} \frac{(-1)^n}{\cosh n\varphi} = \frac{\pi \sinh\varphi}{\varphi} \sum_{n=-\infty}^{\infty} \frac{1}{\cosh\left(\frac{2n+1}{2}\frac{\pi^2}{\varphi}\right)} \qquad (3.3.6)$$

where $\rho = \cosh\varphi$ (=1/ γ in the present notation). This formula corresponds to an energy gap appearing at $\rho = \gamma = 1$, just as we have found by numerical extrapolation. Using formula (3.3.6) it may be verified that near the Heisenberg limit

$$G(\rho) \simeq 4\pi \exp\left[-\pi^2/2\sqrt{2(\rho-1)}\right] \qquad (3.3.7)$$

Hence our observed very slow increase in the gap as $(1-\gamma)$ increases from zero is confirmed by the exponentially slow increase of the analytic solution. Near the Ising limit, $\rho \to \infty$, $\gamma \to 0$, formula (3.3.6), on conversion to our notation, yields the approximate expression

(3.3.8)

This result is identical with that obtained by second order perturbation theory applied to the appropriate Hamiltonian matrices. On Fig.(3.8) we have plotted the finite N anisotropy gap $\Delta E_A(\gamma,N)$ for N=4, 6, 8, 10, 7, 9 and 11. Again even and odd curves form two distinct sequences, the even N curves converging more rapidly in this case. For each of these finite N curves the limiting form near the Ising limit is found to be linear and is also given by perturbation theory. On Fig.(3.9) we plot the alternative set of finite N anisotropy gap curves for N=4, 6, 8 and 10 for comparison purposes. This set appears to converge rather more rapidly. The finite N perturbation theory linear approximations to the curves near $\gamma=0$ are the same for both $\Delta E_A(\gamma,N)$ and $\Delta E'_A(\gamma,N)$ and are shown on this graph.

Returning to Fig. (3.8), we compare the extrapolated limiting curve (a) with the des Cloizeaux and Gaudin curve (shown dashed as curve (b)). We see that our curve (a), though very similar in shape to the exact result (b), is not in as close agreement as we would have expected. The discrepancy rises to more than 15% in the region of $\gamma=0.5$, where the extrapolation uncertainties suggest only about 5%. We expect that the series of finite N extrapolation points for small N will presumably tend linearly to the limiting values we have estimated, but for larger values of N (say $N \gtrsim 30$) will begin to turn up to indicate a rather higher value. This point will receive further discussion in Chapter V, sub-section (3.6).

On Fig. (3.9) we plot also values of $\Delta E_A(\gamma,N)$ for chains of N=4, 6 and 8. When extrapolated in a similar manner to the ring points, these points indicate a limiting anisotropy energy gap (curve (c)) which is roughly half the ring gap. We strongly suspect that, by analogy with the Ising limit, the chain energy gaps for $0 < \gamma < 1$ constitute, in fact, the effective anisotropy gap for general γ which determines the low-temperature behaviour of the thermal properties.

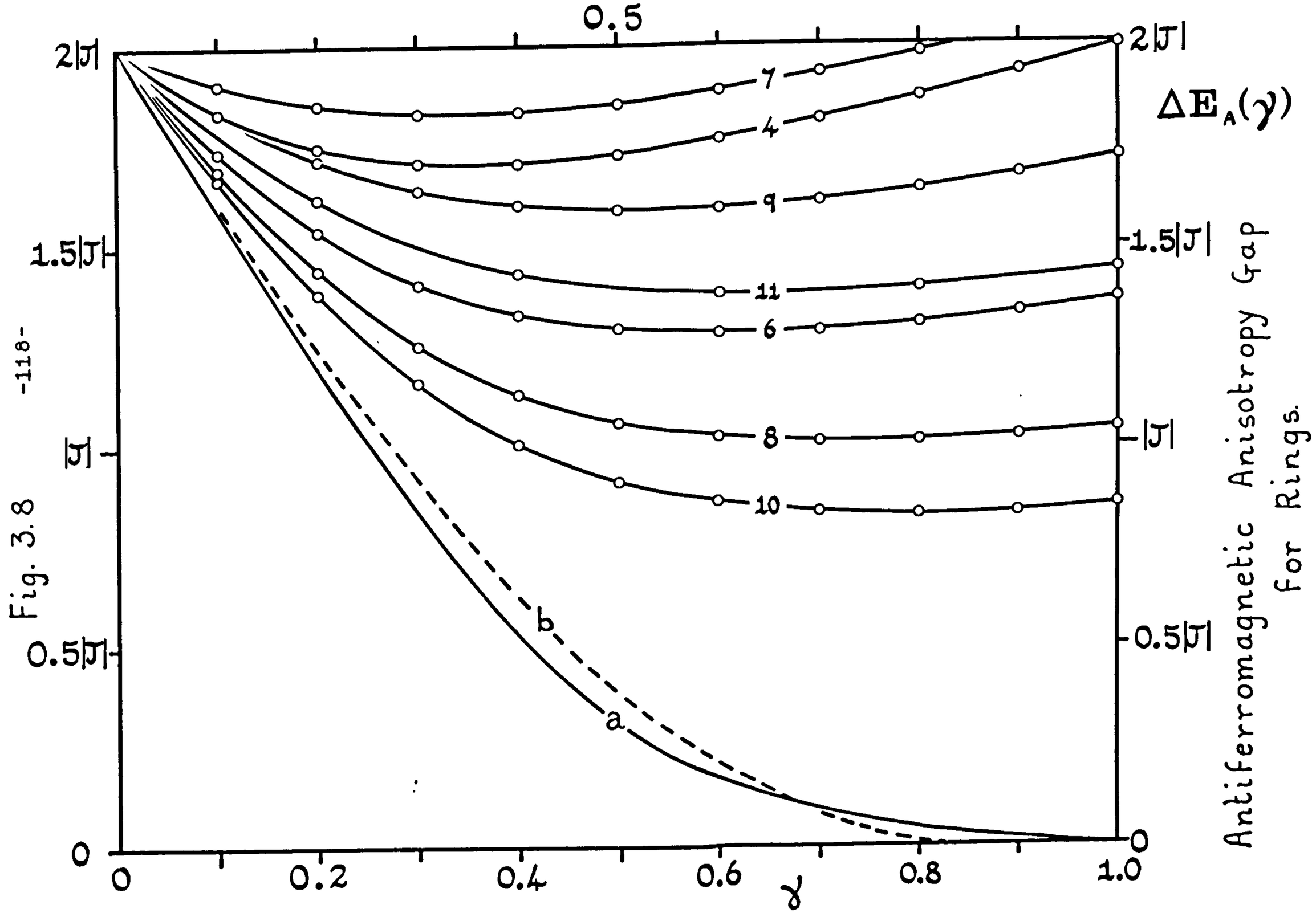
0.5
2|J|
1.5|J|
|J|
0.5|J|
0
7
4
9
11
6
8
10
b
a
0
0.2
0.4
0.6
γ
0.8
1.0
2|J|
1.5|J|
|J|
0.5|J|
0
ΔE_A(γ)
Antiferromagnetic Anisotropy Gap
For Rings.

Fig. 3.8

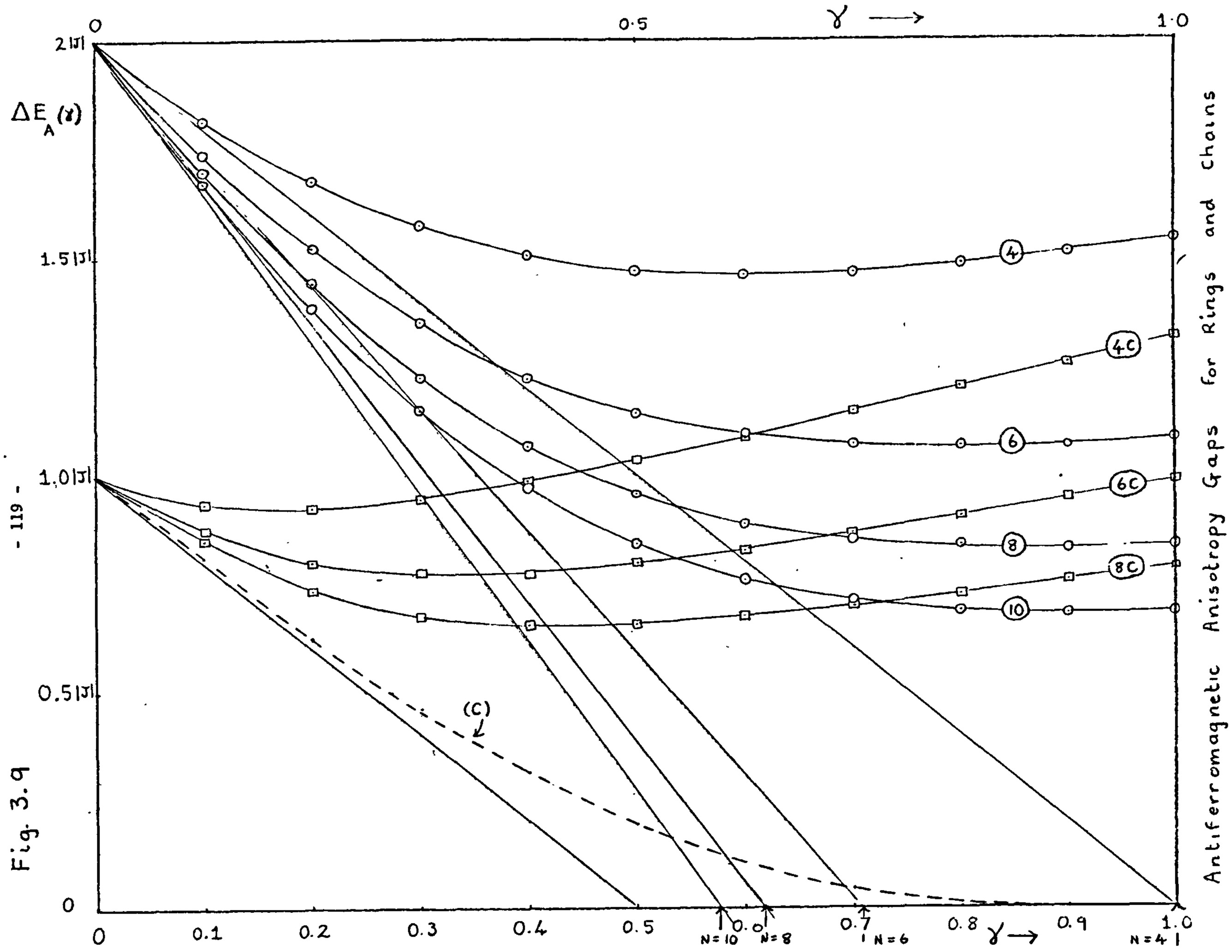
0
0·5
γ ⟶
1·0
2|J|
ΔE_A(γ)
1.5|J|
1.0|J|
0.5|J|
0
4
4C
6
6C
8
8C
10
(C)
0
0.1
0.2
0.3
0.4
0.5
0.6
0.7
0.8
0.9
1.0
N=10
N=8
N=6
N=4
γ ⟶
Antiferromagnetic Anisotropy Gaps for Rings and Chains

Fig. 3.9

3.3) Antiferromagnetic Ground Sub-states

So far we have confined our attention to the levels in the region of the ferromagnetic and antiferromagnetic limits. We shall now comment on the spectrum as a whole. A particular class of levels which are important in studying the zero-temperature magnetic properties of the linear chain are the lowest-lying levels in each S^z block of the Hamiltonian matrix. We shall term these levels the antiferromagnetic ground sub-states. In the case of $S^z = S^z_{max} = N/2$ we have only a single level in the block (a component of the ferromagnetic ground state); for the blocks corresponding to $S^z = S^z_{min} = 0$ (even N) or 1/2 (odd N) the lowest-lying level is (of course) the antiferromagnetic ground state. It is interesting to investigate each ground sub-state as a function of wave-vector q. For $S^z = N/2$ we have q = 0; for $S^z = N/2-1$, q=N/2; for $S^z = N/2-2$, q = 0; etc. Hence the ground sub-state alternates between q = 0 and q = N/2 as S^z is successively decreased by unity. This result is, in fact, a generalisation of that, previously quoted in sub-section (3.2) of Chapter II and sub-section (A.1.2) of Appendix 1, that the antiferromagnetic ground state lies in the $q \neq 0$ and $S^z = 0$ sub-block for N/2 even and the q = N/2, $S^z = 0$ sub-block for N/2 odd. This result was first pointed out by Mattheiss (1961) who gave a plot of all the energy levels versus k for N=6 and N=8. For odd N = 2m+1 we have found that the two degenerate ground states are at $k = \pi m/N$ for m even and $k = \pm \pi(m+1)/N$ for m odd. Also the state at k = 0 or $k \simeq \pi$ is the higher according as m is odd or even.

Recently des Cloizeaux and Gaudin (1966) and Yang and Yang (1966) have considered a rather more general Hamiltonian which is essentially

$$\mathcal{H}_c = J' \sum_{i=1}^{N} \left\{ \rho S_i^z S_{i+1}^z + \left(S_i^x S_{i+1}^x + S_i^y S_{i+1}^y \right) \right\} \qquad (3.3.9)$$

If we make the transformation $J = \frac{J'\rho}{2}$ and $\gamma = \rho^{-1}$ we have

$$\mathcal{H} = 2J \sum_{i=1}^{N} \left\{ S_i^z S_{i+1}^z + \gamma \left(S_i^x S_{i+1}^x + S_i^y S_{i+1}^y \right) \right\} \qquad (3.3.10)$$

which is our anisotropic Hamiltonian. Des Cloizeaux and Gaudin observe that $H_c(\rho)$ and $H_c(-\rho)$ are related by a canonical transformation

$$U = \exp\left[i\pi \sum_{j=1}^{N} j S_j^z\right] \tag{3.3.11}$$

in such a way that

$$U \mathcal{H}_c(\rho) U^{-1} = -\mathcal{H}_c(-\rho) \tag{3.3.12}$$

and

$$U \mathcal{H}(\gamma) U^{-1} = +\mathcal{H}(-\gamma) \tag{3.3.13}$$

The transformation U may be interpreted physically as a rotation of π in the x-y plane for the x and y components of the spins on odd numbered sites i.e. on one sub-lattice. The transformation is therefore equivalent to the replacement of

$$\begin{aligned} S_i^z \quad & \text{by} \quad S_i^z \ ; \\ S_i^x \quad & \text{by} - S_i^x \\ \text{and} \quad S_i^y \quad & \text{by} - S_i^y \end{aligned} \qquad \text{for one sub-lattice.} \tag{3.3.14}$$

Yang and Yang (1966) introduce a very closely related operator $A = \Pi' \sigma_i^z$, where $\sigma_i^z = 2S_i^z$, such that the product runs through sites on one sub-lattice. This transforms our anisotropic Hamiltonian in the same way, namely

$$A \mathcal{H}(\gamma) A^{-1} = \mathcal{H}(-\gamma) \tag{3.3.15}$$

The two operators have identical effects on the Ising wave-functions when N/2 is even, but differ slightly when N/2 is odd (we are assuming N even). The operator U commutes with S^z and conserves the cyclic boundary conditions. In respect to the translation operator, however, its effects are interesting. By expanding the operator we have

$$U\psi = e^{i\pi\left(S_1^z + 2S_2^z + 3S_3^z + \cdots\cdots + NS_N^z\right)}\psi \tag{3.3.16}$$

and also

$$UT\psi = e^{i\pi\left(S_2^z + 2S_3^z + 3S_4^z + \cdots + (N-1)S_N^z + NS_1^z\right)}T\psi \tag{3.3.17}$$

Hence
$$\frac{UT\psi}{TU\psi} = e^{i\pi\left(S_1^z + S_2^z + \cdots + S_N^z\right) - N i\pi S_1^z}$$

$$= e^{i\pi\left(S^z - NS_1^z\right)} \tag{3.3.18}$$

Now $S^z = N/2, N/2-1, \ldots\ldots, -N/2$; and $S_1^z = \pm 1/2$.

Consider the following cases for N even:-

$$
\begin{aligned}
S^z = N/2: \quad & \mathcal{U}T\psi / T\mathcal{U}\psi = e^{i\pi\left(\frac{N}{2} \mp \frac{N}{2}\right)} \equiv 1 \\
S^z = N/2-1: \quad & \text{"} = e^{i\pi\left(\frac{N}{2} \mp \frac{N}{2} - 1\right)} = e^{-i\pi} = -1 \\
S^z = N/2-2: \quad & \text{"} = e^{i\pi\left(\begin{smallmatrix}0\\N\end{smallmatrix} - 2\right)} = 1 \\
& \vdots \qquad\qquad \vdots \\
S^z = 1: \quad & \text{"} = e^{i\pi\left(1 \mp \frac{N}{2}\right)} = -1 \quad (N/2 \text{ even}) \\
& \qquad\qquad\qquad\quad = +1 \quad (N/2 \text{ odd}) \\
S^z = 0: \quad & \text{"} = e^{\mp i\pi\frac{N}{2}} = +1 \ (N/2 \text{ even}) \\
& \qquad\qquad\quad = -1 \ (N/2 \text{ odd}) \qquad (3.3.19)
\end{aligned}
$$

Equivalent results hold for negative S^z.

We see, therefore, that U either commutes or anticommutes with T, for N even, depending on the S^z block of the Hamiltonian under consideration and also on the parity of N/2. Alternatively we may say that the effect of U on a given function of the Hamiltonian is either to leave the k-vector of the state unchanged or rotate it through π. More specifically, let us consider the states near the ferromagnetic end of the spectrum. The ferromagnetic ground state is a $k = 0$ state and is unaffected by the operation of U. The (antiferromagnetic) ground sub-state of the $S^z = N/2-1$ block of the Hamiltonian, however, is a $k = \pi$ state and is converted into a $k = 0$ state by the transformation U. Considering the states near the antiferromagnetic end of the spectrum, let us assume N/2 is even. The antiferromagnetic ground state is a $k = 0$ state and is not affected. However, the ground sub-state of the $S^z = 1$ block is a $k = \pi$ state, which is converted to a $k = 0$ state. These results, in the case of N/2 odd, are reversed. We see, therefore, that the effect of the transformation U is to convert all the antiferromagnetic ground sub-states (lowest states of each S^z block for negative J) into $k = 0$ states. As Mattheiss remarked, the previous alternation of wavevectors between $k = 0$ and $k = \pi$ for these states appeared to have no physical interpretation. We therefore conclude that the physically reasonable

way to make a transformation of the Hamiltonian from ferromagnetic to antiferromagnetic is not only to change the sign of J, the exchange integral, but also to perform the transformation

$$\mathcal{H}_A = \mathcal{U}\left(-\mathcal{H}_F\right)\mathcal{U}^{-1} \qquad (3.3.20)$$

For odd N, the appropriate transformation is similar in character, but a little more complicated. It may easily be verified that if N = 2m+1, the transforming operator for m even is

$$\mathcal{U} = e^{\frac{2mi\pi}{N}\left(\sum_{j=1}^{N} j S_j^z\right)} \qquad (3.3.21)$$

and if m is odd, we have

$$\mathcal{U} = e^{\frac{2(m+1)i\pi}{N}\left(\sum_{j=1}^{N} j S_j^z\right)} \qquad (3.3.22)$$

This transformation converts the antiferromagnetic ground state from a $k = \pm m\pi/N$ state for m even and a $k = \pm(m+1)\pi/N$ for m odd to a k = 0 state in both cases.

4. FERROMAGNETIC DISPERSION CURVES

Section 4 can be regarded as a continuation of section 2, which in a sense forms an introduction to it. Classes of ferromagnetic levels are examined in detail as a function of wave-vector k for N=10 and N=11, and the resulting dispersion curves are relevant to a classification of energy states into bound and spin-wave categories. The relative importance of these categories in determining the low-temperature thermodynamic properties in the large N limit is discussed for the Heisenberg and anisotropic cases. A careful study reveals that the low-lying ferromagnetic spectrum also can be described in terms of an anisotropy energy gap, analogous to the antiferromagnetic gap.

4.1) Pictorial Representation of Interacting Spin-Waves

We have so far been primarily concerned with the energy eigenvalues as functions of anisotropy γ. We shall now turn our attention to studying the levels as functions of wave-vector k for a given value of anisotropy.

For the ferromagnetic limit we have already derived a (single) spin-wave dispersion relation which has the form

$$J^{-1}(E_1 - E_0) = \varepsilon_1(k) = 2(1 - \cos k) \qquad (3.4.1)$$

where $k = 2\pi q/N$, $q = 0, \pm1, \pm2, \ldots\ldots$ With two overturned spins, the simple spin-wave approximation predicts

$$J^{-1}(E_2 - E_0) = \varepsilon_2(k_1 + k_2) = \varepsilon_1(k_1) + \varepsilon_2(k_2) \qquad (3.4.2)$$

but this is not exact owing to the spin-wave 'interactions'. For anisotropic linear chains the problem of (one and) two overturned spins has been discussed by Orbach (1958) who followed Bethe's analysis for $\gamma = 1$ (Bethe 1931). The interaction of two spin waves is illustrated for the Heisenberg limit in Fig. (3.10) which shows energy levels for a ring of N=11 spins for $\gamma = 1$. The solid curve through the dark circles is the single spin-wave dispersion law (equation 3.4.1). The other solid curves represent the superimpositions (equation 3.4.2) and their intersections are thus the simple spin-wave approximations to the levels for two overturned spins. The arrows indicate the energy due to the interactions, the exact energy levels lying at the points of the arrowheads. (The open circles at the foot of the dispersion curves represent 'missing states' i.e. levels predicted by equation (3.4.2) which do not occur for the true Hamiltonian.) For most combinations of k_1 and k_2 the interactions are evidently repulsive and the spin-waves 'scatter' and remain 'unbound'. However, for $k_1 \simeq k_2 \simeq (1/2)k$, the interactions are strongly attractive and the spin waves condense into 'bound states' whose dispersion law is

$$\varepsilon_{II}(k) = 2\left(1 - \tfrac{1}{2}\gamma^2[1 - \cos k]\right) \qquad (3.4.3)$$

as we have already derived in sub-section (2.4) of this chapter. This curve is indicated by the dotted line (b) in Fig. (3.10). The corresponding eigenfunction relates to two closely associated overturned spins travelling around the ring together (Orbach 1958).

Fig. 3.10

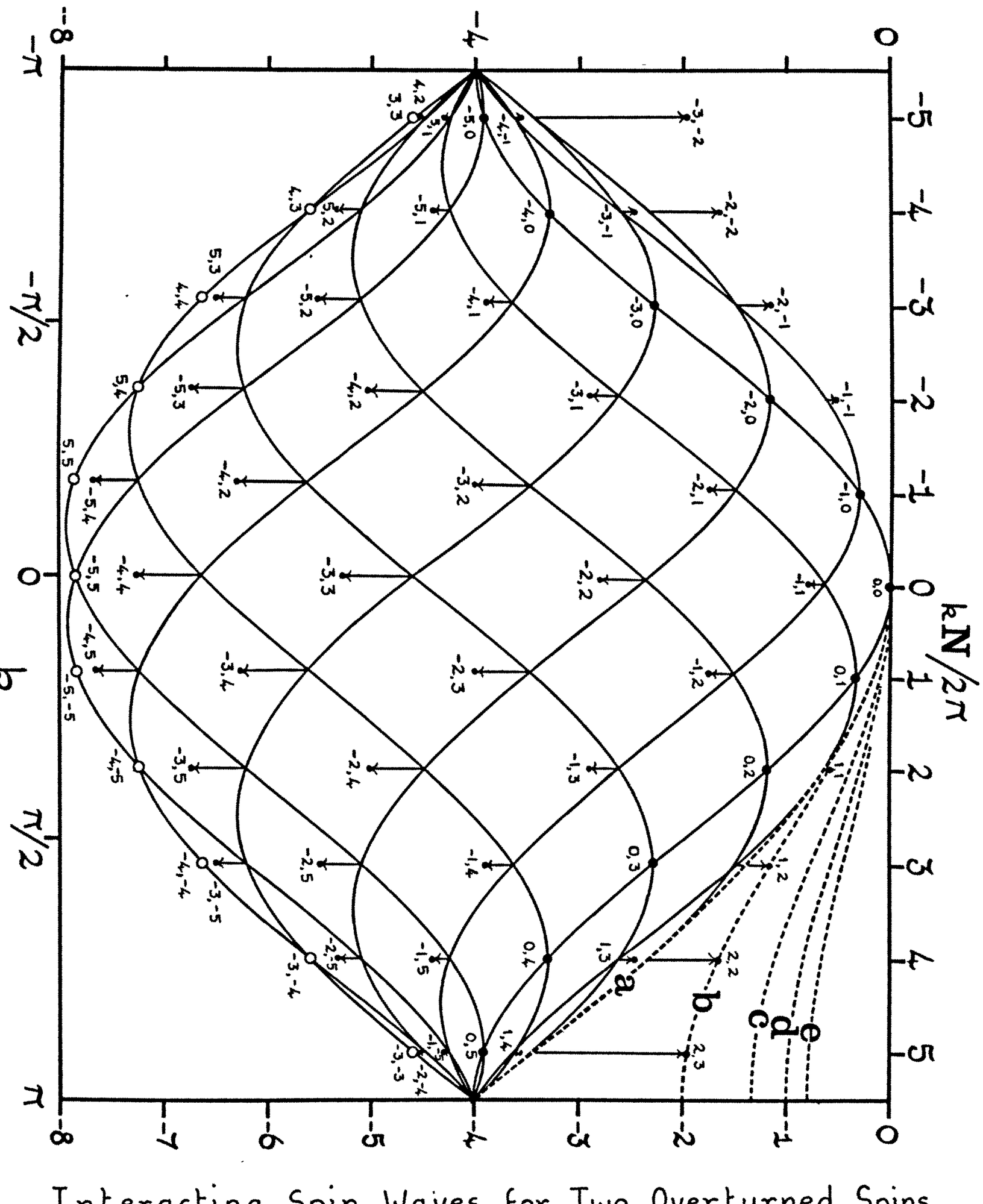

Interacting Spin Waves for Two Overturned Spins.

4.2) Bound States of Two Overturned Spins

Recently there has been some interest in the existence and properties of bound states. Wortis (1963) using an approximate Green's function method has studied bound states of two spin waves of general spin S in one, two and three dimensions for a simple nearest-neighbour Heisenberg model. For a linear chain lattice with spin-1/2, Wortis states that in the limit as the lattice becomes large there exists a unique bound state for each value $k_1 + k_2 = k$ of the total momentum of the pair. However, our finite chain results suggest that the conclusions of Wortis may not be quite correct. To see this, let us consider Fig. (3.11) which is essentially equivalent to Fig. (3.10) except that we are considering states of two overturned spins for N=10, not N=11, and k runs from 0 to 2π rather than $-\pi$ to π . The extent of the two-spin-wave continuum, indicated by curve (a) in Fig. (3.10) is shown shaded. The continuum limits are given by the equation

$$\varepsilon_1^{LIM}(k) = 4\left(1 - \gamma \cos \tfrac{1}{2}k\right) \qquad (3.4.4)$$

which is the envelope of the curves (3.4.2). We notice that the single spin-wave dispersion curve (solid curve through open circles) lies within the continuum for all k. The two-spin bound-state dispersion curve (curve (b) in Fig. (3.10)) is shown as a solid curve through dark circles which are the bound states. We see from Fig. (3.11) that there are no bound states for q = 0 and q = 1, in disagreement with Wortis. This result is, a priori, of some importance since the missing bound states are those of lowest energy in a ferromagnetic representation.

4.3) Katsura's Exact Solution

Katsura (1965) has been able to simplify the analytic treatment of the Bethe-Hulthén equations for two overturned spins by introducing a transformation which decouples them. (This transformation, unfortunately, does not apply to more than two overturned spins.) His conclusions (in which an important error has been corrected by the author) are valid for

finite and infinite rings, and confirm our finite ring results. Katsura places the lowest-lying ferromagnetic states (excluding the ground state) in categories he calls III, IV, V, VI, VII, VIII and X. Categories IV, VI and VIII are quite equivalent to the categories III, V and VII, respectively, except that they have wave-vectors $k' = \pi - k$. Category X includes a single state that is really a category V state which clearly does not exist when N is odd. Katsura shows that categories III and V include only bound states but that category VII states are always of a spin-wave type. Category III (and IV) states always number

$$\begin{cases} N/2 - 1 \text{ for } N \text{ even}, N/2 \text{ odd} \\ N/2 - 2 \text{ for } N \text{ even}, N/2 \text{ even}. \end{cases} \qquad (3.4.5)$$

However, and this is important in a discussion of the low-temperature thermodynamic properties, it follows from Katsura's arguments that in the limit of large N there are of the order of $\sqrt{N}$ category VII states distributed along the bound state dispersion curve, and that there are altogether as many states in the combined categories VII and V as in category III. Hence the lowest ferromagnetic states fall into two classes:-

Class A: category III only:

even k vectors 2,4,6, ..., N-4, N-2. (3.4.6)

Class B: category VII (VIII):

odd k vectors 1,3,5, ..., n+2,n and N-n,N-n+2, ...,N-3,N-1

category V (VI): odd k vectors n+2, n+4, ..., N-n-2 (3.4.7)

where $n \sim \frac{2}{\pi}\sqrt{N}$ for large N.

More precisely, the number of category VII (and VIII) spin-wave solutions is $2N_1$ (=n+1), where N_1 is the largest number which satisfies

$$\cos \frac{\pi(2N_1 - 1)}{N} \geq 1 - \frac{2}{N} \qquad (3.4.8)$$

This implies that, for N=10, N_1 =1: for N_1 =2 i.e., for the second category VII state to appear at q = 3, N must be greater than about 25, and for N_1 =3, N must be greater than about 60, etc..

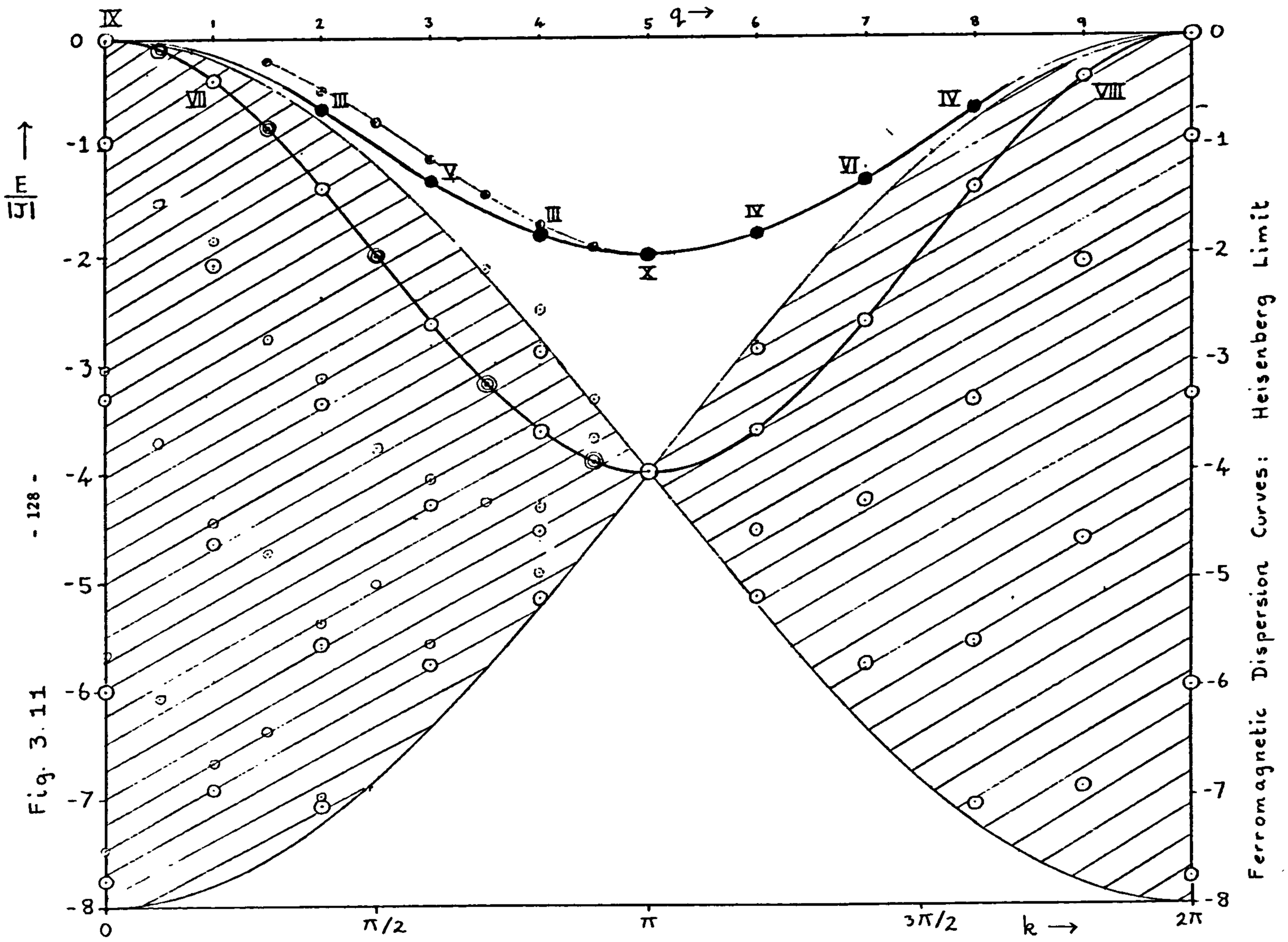
IX
q →
0
1
2
3
4
5
6
7
8
9
E/|J|
-1
-2
-3
-4
-5
-6
-7
-8
VII
III
V
III
X
IV
VI
IV
VIII
0
π/2
π
3π/2
k →
2π
Ferromagnetic Dispersion Curves: Heisenberg Limit

Fig. 3.11

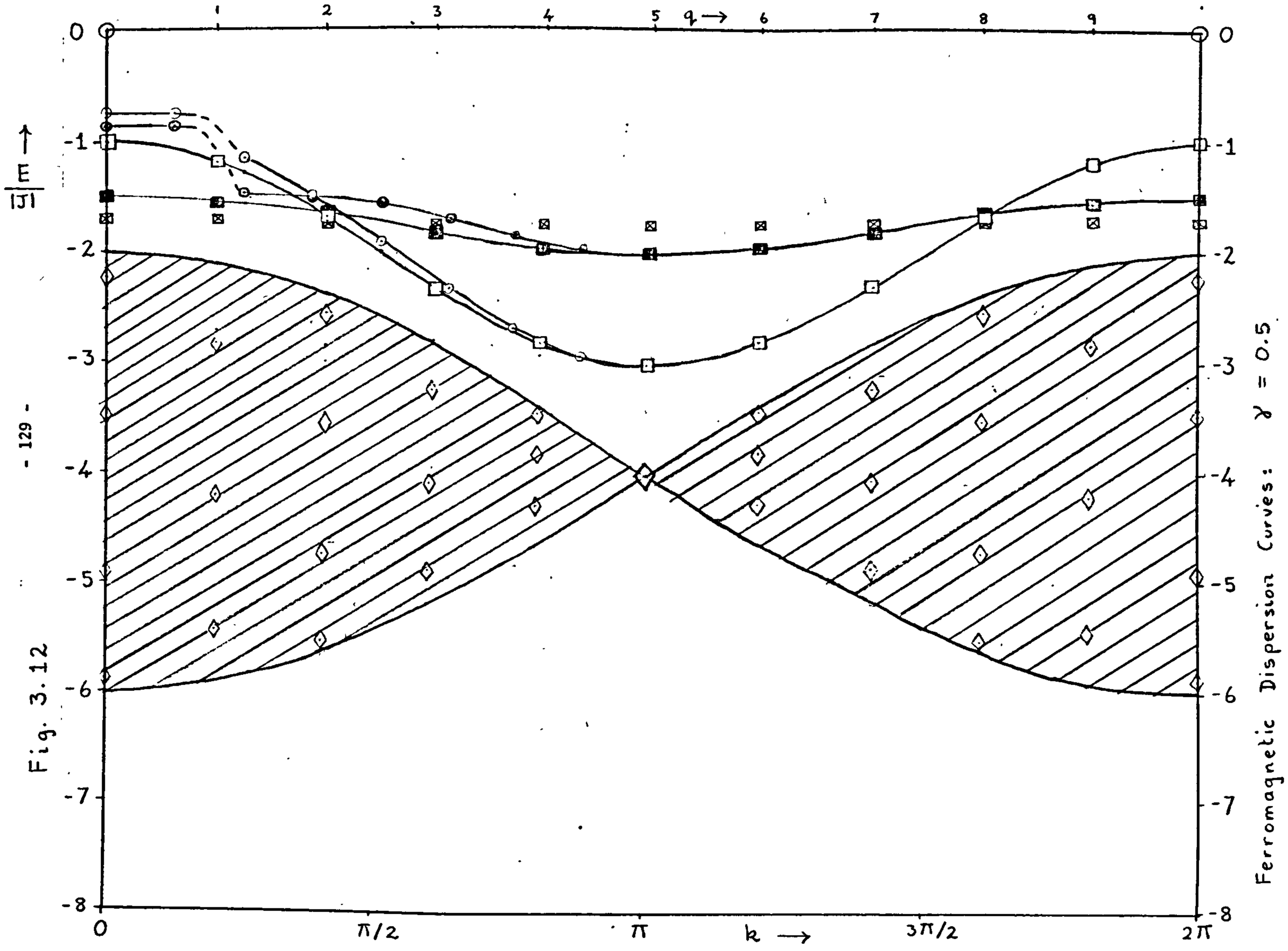

Fig. 3.12 Ferromagnetic Dispersion Curves:

The work of Bethe (1931) (for $\gamma = 1$) and Orbach (1958) is, of course, closely related to the work of Katsura. Bethe and Orbach actually obtained the same condition as Katsura (equation 3.4.8), for the Heisenberg limit, which Orbach quoted in the form

$$\cos k/2 \geq 1 - 2/N \qquad (3.4.9)$$

This equation was then erroneously taken to imply that no spin-wave (Category VII) states can exist in the limit of an infinite chain.

4.4) Anisotropic Dispersion Curves for Rings

Let us now consider the effects of anisotropy on the number and distribution of bound states for our small finite rings. Fig. (3.12) is a companion figure to Fig. (3.11), showing the distribution of one- and two-overturned-spin states for $\gamma = 0.5$. Both figures are on the same scale and we notice that for $\gamma = 0.5$ the area covered by the two-spin-wave continuum (the individual two-spin-wave states for N=10 are shown as diamonds) has shrunk appreciably, according to equation (3.4.4.). In fact, the single spin-wave dispersion curve (open squares) now lies completely outside the two-spin-wave continuum (i.e. completely below the continuum in a ferromagnetic representation). For this value of anisotropy we see also that a bound state exists for all q, including $q = 0$ and $q = 1$, and that the bound state dispersion curve (solid curve through dark squares) also lies outside the continuum. (Note that the individual states give a very close fit to the solid curve representing equation (3.4.3) for $\gamma = 0.5$). Since the bound state dispersion curve differs significantly from that at $\gamma=1$, it is interesting to investigate how this change comes about as a function of anisotropy. The single spin-wave curve of Fig. (3.11) is degenerate with a set of states of two overturned spins. When $\gamma < 1$, this degeneracy is broken and the one-overturned-spin component follows equation (3.4.1). The component for two overturned spins shows a discontinuity, the states for $q = 0$ and $q = 1$ apparently tending to join the bound state dispersion curve for two overturned spins. When $(1-\gamma)$ is sufficiently large, the

two-spin states at $q = 0$ and $q = 1$ lie outside the two-spin-wave continuum limits and are more properly regarded as bound states. Our finite ring studies suggest that in the limit of large N, bound states of two overturned spins will exist for all values of q, for all $\gamma < 1$.

We can re-interpret the work of Orbach for the case of two overturned spins in the presence of anisotropy. The number of spin-wave (category VII) solutions is given by the condition

$$\cos \frac{\pi (2N_1 - 1)}{N} \geq \gamma^{-1} (1 - 2/N) \qquad (3.4.10)$$

Hence for $\gamma < (1-2/N)$ there are no spin-wave (cat. VII) solutions for either finite or infinite N. Thus in the limit $N = \infty$, no such solutions exist for $\gamma < 1$, and the two-spin bound state dispersion curve contains bound states for all values of k (q), in agreement with our finite N study predictions.

It is perhaps worth noting that Orbach expects the number of cat. VII-type states to increase significantly as γ becomes greater than unity, a situation we have not been concerned with.

4.5) Anisotropic Dispersion Curves for Chains

A discussion of the properties of the ferromagnetic spectrum for one- and two-overturned spins will not be complete without a consideration of free-ended chains. An exact solution will first be attempted.

Let us consider the case of one overturned spin. First of all, we shall consider rings of 2N spins and show that half of the energy levels are identical with the energy levels for a chain of length N, in the Heisenberg limit only. Consider the appropriate matrix for a ring of 8 spins, shown in fig. (3.4a) as having eight-fold cyclic structure.

Fig. (3.4a)

1	2	3	4	5	6	7	8
-2	1						1
1	-2	1					
	1	-2	1				
		1	-2	1			
			1	-2	1		
				1	-2	1	
					1	-2	1
1						1	-2

Fig. (3.4b):

1	2	3	4	8	7	6	5
-2	1		(A)	1			(B)
1	-2	1					
	1	-2	1				
		1	-2	1			
			1	-2	1		
				1	-2	1	
					1	-2	1
1			(B)	-2	1		(A)
				1	-2	1	
					1	-2	1
			1			1	-2

The rows and columns of the matrix may be rearranged as in fig. (3.4b) to display 4x4 block cyclic structure, and the 4x4 matrix which results from adding blocks (A) and (B) is shown in fig. (3.4c). This matrix is identical with the matrix for the chain of 4 spins. (The remaining solutions of the 8-ring arise from the 4x4 matrix corresponding to (A)-(B).) The result may be generalised, and hence the chain solutions are always a subset of the ring solutions for $\gamma = 1$. Let us now consider the general chain matrix for one overturned spin operating on a trial eigenvector, illustrated in fig. (3.5a) and fig. (3.5b) respectively.

-1	1		
1	-2	1	
	1	-2	1
		1	-1

Fig. (3.4c)

fig. (3.5 a)

$$\begin{bmatrix} -1 & 1 & 1 & & & \\ 1 & -2 & & \cdots & & 0 \\ & 1 & -2 & & & \\ \vdots & & & \ddots & & \vdots \\ & & & & -2 & 1 \\ 0 & \cdots & & & 1 & -2 & 1 \\ & & & & & 1 & -1 \end{bmatrix}$$

fig. (3.5 b)

$$\begin{bmatrix} \cos\theta/2 \\ \cos 3\theta/2 \\ \vdots \\ \cos\left(r-\frac{1}{2}\right)\theta \\ \vdots \\ \cos\left(N-\frac{1}{2}\right)\theta \end{bmatrix}$$

Consider the effect of operating on the eigenvector with level (α) of matrix (3.5a):

level (α): $$(-1-\lambda)\cos\frac{\theta}{2} + \cos\frac{3\theta}{2} = 0 \qquad (3.4.11)$$

from which $$\lambda = -2 + 2\cos\Theta \qquad (3.4.12)$$

In general, for all levels ≠ (α) or (β)

$$\cos\left(r - \tfrac{3}{2}\Theta\right) + (-2-\lambda)\cos\left(r - \tfrac{1}{2}\Theta\right) + \cos\left(r + \tfrac{1}{2}\Theta\right) = 0 \qquad (3.4.13)$$

hence $$\lambda + 2 = \frac{\cos\left[\left(r - \tfrac{1}{2}\Theta\right) - \Theta\right] + \cos\left[\left(r - \tfrac{1}{2}\Theta\right) + \Theta\right]}{\cos\left(r - \tfrac{1}{2}\Theta\right)}$$

and finally $$\lambda = -2 + 2\cos\Theta \qquad (3.4.14)$$

<u>level (β)</u>: $$\cos\left(N - \tfrac{3}{2}\right)\Theta + (-1-\lambda)\cos\left(N - \tfrac{1}{2}\right)\Theta = 0 \qquad (3.4.15)$$

from which $$\lambda + 1 = \cos\Theta + \frac{\sin\left(N - \tfrac{1}{2}\right)\Theta \sin\Theta}{\cos\left(N - \tfrac{1}{2}\right)\Theta} \qquad (3.4.16)$$

In order for level (β) to yield an eigenvalue -2 +2 cos θ we must have the condition (boundary condition)

$$\frac{\sin\left(N - \tfrac{1}{2}\right)\Theta \sin\Theta}{\cos\left(N - \tfrac{1}{2}\right)\Theta} = -1 + \cos\Theta \qquad (3.4.17)$$

From equation (3.4.17) we obtain the trivial solution

$$\sin\Theta/2 = 0 \qquad \text{i.e. } \Theta = 2r\pi, \quad r = 0, 1, 2, \ldots$$

and the non-trivial solution

$$\sin N\Theta = 0 \qquad \text{i.e. } \Theta = \frac{r\pi}{N}, \quad r = 0, 1, 2, \ldots \qquad (3.4.18)$$

Hence the chain states may also be classified in terms of a wave-vector $k_c = \frac{r\pi}{N}$, which has twice as many allowed frequencies with half the frequency interval as the corresponding wave-vector for rings $k_R = \frac{2r\pi}{N}$. The situation is similar to the case of dynamical vibrating linear systems with fixed and periodic end-conditions.

We thus conclude that the energy levels for chains lie on the same dispersion curve as the states for rings, but occur at half-integral wave-number spacings. For example, in the case of N=10, the ring distribution of states may be equivalently regarded as follows:- a single state at k=0, two (degenerate) states at k=1, 2, 3 and 4 and a single state at k=5. The chain distribution is single states at k=0, 1/2, 1, 3/2, 2, 5/2, 3, 7/2, 4 and 9/2, comprising, of course, the same number of states in all. This result is displayed in Fig. (3.11), where the chain states for half-integral k are shown by the concentric circles on the left-hand portion of the single

spin-wave dispersion curve. In a sense, therefore, a chain of N spins is equivalent to a ring of 2N spins, which again shows the value of considering free-ended systems for elucidating ferromagnetic thermodynamic properties.

Let us now examine the solution for one overturned spin for the general case of anisotropy. The corresponding matrix and trial eigenvector are shown in fig. (3.6a) and fig.(3.6b) respectively.

fig. (3.6 a)

$$(\alpha)\begin{bmatrix} -1\gamma & & & \\ \gamma & -2\gamma & \cdots & 0 \\ & \gamma-2 & & \\ \vdots & & \ddots & \vdots \\ 0 & \cdots & & -2\gamma \\ & & & \gamma-2\gamma \\ & & & \gamma-1 \end{bmatrix}(\beta)$$

fig. (3.6b)

$$\begin{bmatrix} \cos\theta/2 \\ \cos 3\theta/2 \\ \vdots \\ \cos(r-\frac{1}{2})\theta \\ \vdots \\ \cos(N-\frac{1}{2})\theta \end{bmatrix}$$

Proceding as before we have:-

In general, for levels ≠ (α) or (β):

$$\gamma\cos\left(r-\tfrac{3}{2}\right)\theta + (-2-\lambda)\cos\left(r-\tfrac{1}{2}\right)\theta + \cos\left(r+\tfrac{1}{2}\right)\theta = 0 \qquad (3.4.19)$$

from which $$\lambda = -2 + 2\gamma\cos\theta \qquad (3.4.20)$$

<u>level (α):</u> $$(-1-\lambda)\cos\theta/2 + \gamma\cos 3\theta/2 = 0 \qquad (3.4.21)$$

from which $$\lambda = -1-\gamma+2\gamma\cos\theta \qquad (3.4.22)$$

<u>level (β):</u> $$\gamma\cos\left(N-\tfrac{3}{2}\right)\theta + (-1-\lambda)\cos\left(N-\tfrac{1}{2}\right)\theta = 0 \qquad (3.4.23)$$

from which $$\lambda = \cos\theta + \frac{\gamma\sin(N-\frac{1}{2})\theta\sin\theta}{\cos(N-\frac{1}{2})\theta} \qquad (3.4.24)$$

First of all we observe that the eigenvector of fig. (3.6b) cannot represent the true eigenvector of the system, since equations (3.4.20) and (3.4.22) cannot be simultaneously satisfied except in the limit $\gamma = 1$. We can, however, as an approximate solution, choose θ so that the end levels (α) and (β) have the same form. The condition reduces to that in the Heisenberg case, namely

$\theta = \frac{r\pi}{N}$, $r = 0, 1, 2, \ldots$ Hence our approximate solution has the following characteristics:-

a) The eigenstates have the same k values as for $\gamma = 1$.

b) In general, the levels obey the same dispersion law as do rings, namely $\varepsilon(k) = 2(1-\gamma \cos k)$ (3.4.25)

c) The end levels obey a different dispersion law, namely

$$\varepsilon_c(k) = 1 + \gamma - 2\gamma \cos k \quad (3.4.26)$$

Although we do not expect conditions (a), (b) and (c) to hold exactly for small, finite N, we believe the solution has increasing validity as $N \to \infty$.

In the light of our approximate solution, we have plotted the finite N (actually N = 8) chain states obtained numerically, at exact integral and half-integral q values, as at the Heisenberg limit. The result is shown as the curve through the open circles in Fig. (3.12). The approximate character of our anisotropic solution is revealed by the fact that the numerical states, under these conditions, actually lie on a smooth dispersion curve which is slightly displaced from the corresponding ring curve. However, in the limit $N \to \infty$, we can expect this discrepancy to disappear. Our approximate analytic solution implies that the two end-level states correspond to wave-vector values k = 0 and $k = \frac{\pi}{N}$ and will be split off the rest of the dispersion curve in the direction of the ground state. This behaviour is to be observed in the numerical solutions of Fig. (3.12).

We are unable to obtain an exact solution even in the Heisenberg limit for the case of more than one overturned spin. Hence, as an approximation, we have chosen to plot the energy levels obtained numerically in such a way that the half-integral character of the distribution is maintained in the case of two or more overturned spins. In Fig. (3.11) the resulting two-spin bound-state dispersion curve is shown as the curve through the dark circles, slightly displaced from the corresponding curve for rings. Again we see that no bound states exist for $q < 1$. In Fig. (3.12), the chain curve for two-spin bound-states is again similar to the ring curve except that the q=0 and q=1/2 bound states have suffered an upward displacement

like the corresponding states for one overturned spin.

4.6) Anisotropic Levels for Many Overturned Spins

Our detailed investigations of the dispersion curves for S^z blocks near the maximum have been of interest in their own right; particularly the division into spin-wave and bound states. If, however, we hope to obtain sufficient information on the nature of the ferromagnetic spectrum to make a reasonable conjecture about the low-temperature thermodynamic properties, we must investigate states of more overturned spins, particularly $S^z = 0$ states. In view of the difficulty of obtaining analytic results in these cases, we are forced to rely mainly on our finite ring and chain numerical studies. We are encouraged by the very close correspondence between predictions derived from numerical studies and analytic limiting results that we have seen so far for the ferromagnetic limit. We shall consider, first of all, the case of general anisotropy, where we feel that reasonable conclusions may be drawn. Later, we shall see that the Heisenberg limit is rather pathological.

Let us return to Fig. (3.12) to review the situation with respect to the low-lying levels as a function of wave-vector q, for $\gamma=0.5$. In the region $q < 1$, near $E/|J| = 0$, we see the chain end-levels as the two (two-fold degenerate) open circles corresponding to $S^z = N/2-1$, and the two dark circles just below them which represent not only states of two overturned spins but also states of three, four, etc., up to N/2 overturned spins which all appear degenerate on the scale of our figure. Consider next the set of N (or N-2 for chains) bound levels for two overturned spins (dark squares and circles) whose energies lie on dispersion curves in the region just above $-2|J|$. Examining the lowest-lying levels for rings for other values of S^z down to $S^z = 0$ we obtain a set of limiting dispersion curves apparently similar in form to the curve for two overturned spins but with successively reduced dispersion amplitudes. The entire set of curves lies within the limits of the two-overturned-spin curve, and the N individual

states for $S^z = 0$ are shown by the set of crosses within squares in Fig.(3.12). Clearly the variation in energy with q is very small, and we presume that in the limit $N \to \infty$, the N states for $S^z = 0$ will be degenerate in energy (the dispersion curve amplitudes appear to decrease as γ^r, where r is the number of overturned spins). Altogether, therefore, we shall have of the order of N^2 such states for two or more overturned spins in a fairly narrow energy band - (the situation for chains is quite analogous). The average excitation energy of these N^2 levels is very close to twice the energy of the N chain end-levels. This is suggestively similar to the situation in the Ising limit discussed in sub-section (2.6) where the lowest-lying excited states are N-fold degenerate, the next excited states are N^2-fold degenerate and the effective energy gap is given by the difference of the ground state energy and the first excited energy levels. Notice that the lowest one-overturned-spin levels are of O(1) in number and do not affect energy gap considerations. The remaining one-overturned-spin levels, although of order (N) in number, do not affect the energy gap because they are higher in energy (ferromagnetically) than the N end-levels for two and more overturned spins. We conclude, therefore, that the situation for chains in the case of anisotropy $\gamma \leq 0.5$, and probably for all $\gamma < 1$, closely resembles the Ising limit. Also for rings, we see that for general anisotropy the situation is again equivalent to the case of the Ising limit, since there are no levels at the top of the energy gap and N^2 levels at twice the energy gap. Having made plausible the idea of anisotropic energy gaps for rings and chains at the ferromagnetic end of the spectrum with the aid of the dispersion curves of Fig. (3.12), we shall now attempt to study these gaps as functions of γ. We shall start by performing preliminary studies on the appropriate chain Hamiltonian matrices with the aid of perturbation theory. All Hamiltonian matrices for two and more overturned spins have the simplified form shown in fig. (3.7). Second order perturbation theory for the end-levels of block (α), which form the lowest-lying ferromagnetic levels of the problem,

fig. (3.7)

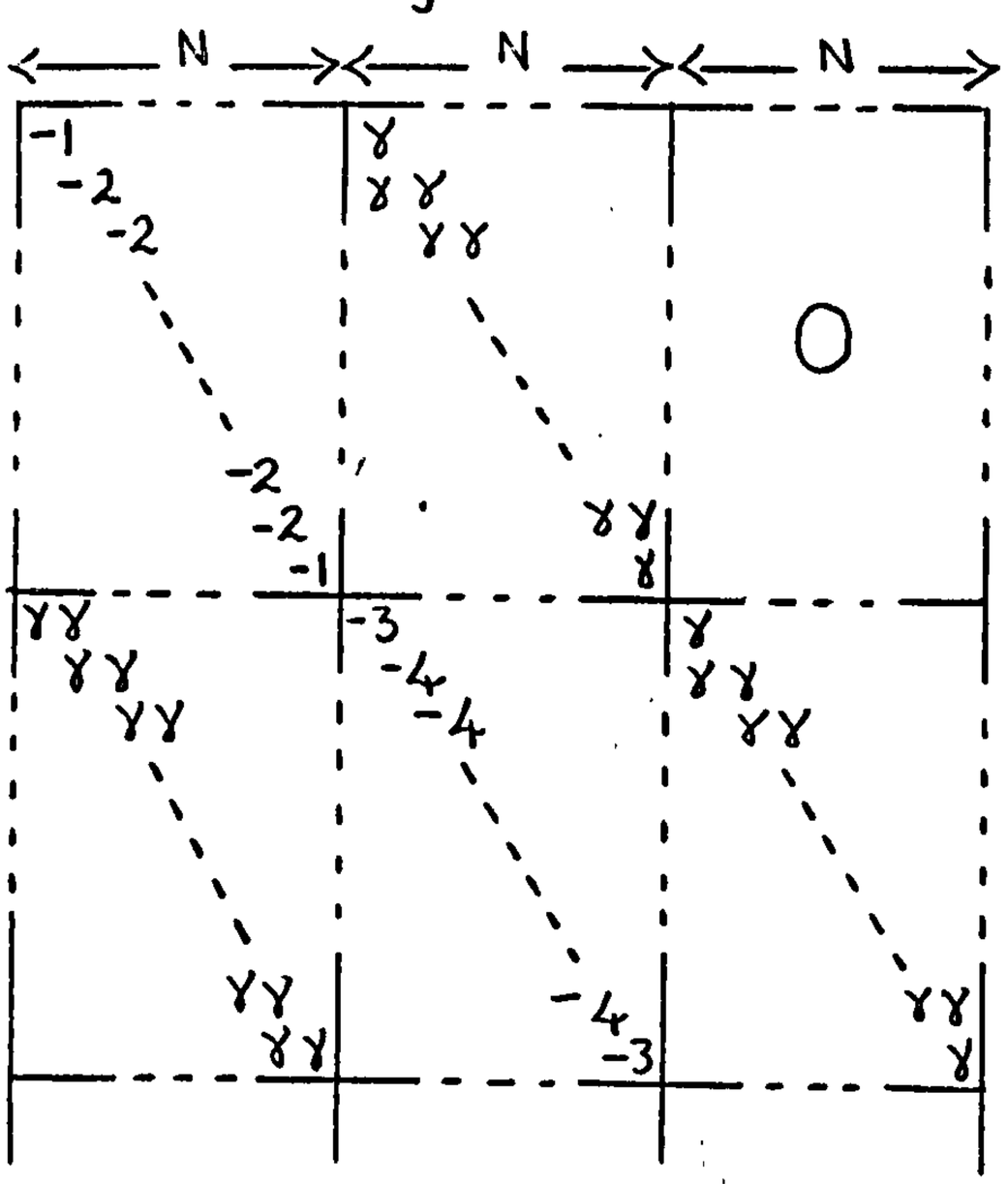

gives

$$\lambda = -1 + \frac{\gamma^2}{3-1} = -1 + 1/2\ \gamma^2 \qquad (3.4.27)$$

(The actual matrices are rather more complicated than is suggested here, but give identical results as far as perturbations of the two lowest-lying end-levels are concerned.) Since we must consider states of positive and negative S^z, we have, in the Ising limit, altogether 2(N-1) such lowest-lying levels (as we have mentioned previously). Of these, the four states for one overturned spin deviate from -J as $1-\gamma^2$, according to second order perturbation theory. These four states are not thermodynamically significant in comparison with the remaining 2(N-3) states. These 2(N-3) states, which appear to remain degenerate according to second order perturbation theory, deviate more slowly from -J as $1-1/2\gamma^2$. For γ near 1 and for finite N, the levels must separate in higher order perturbation theory in order to agree with exact numerical calculations.

Comparing these predictions with our numerical results for chains of 4, 6 and 8 spins, we see that the perturbation equations

$$E_1 = -|J|\,(1-\gamma^2) \qquad (3.4.28)$$

and

$$E_{>1} = -|J|\,(1-\tfrac{1}{2}\gamma^2) \qquad (3/4/29)$$

appear to give a very plausible account of the probable limiting behaviour of the relevant chain energy levels, at least for $\gamma \leq 0.6$. For $\gamma > 0.8$, the $2(N-3)$ levels, instead of following equation (3.4.29) to a finite value as $\gamma \to 1$, turn fairly sharply upwards, and in the limit may be expected to go to zero (for the normalised Hamiltonian we are considering) for $\gamma \to 1$. The

development of these 2(N-1) levels as functions of anisotropy may be seen, in the case of N=6, by reference back to Fig. (3.5). These are the levels which comprise the multiplets A and B in the Heisenberg limit.

For finite N, the levels divide into two equal groups, one of which joins the upper component of the end-levels for one overturned spin to form a total-spin-N/2 multiplet: in fact, these are the levels which join the two degenerate levels of the ferromagnetic ground state for $\gamma < 1$, to form the (N+1)-fold degenerate levels of the ferromagnetic ground state in the Heisenberg limit. The other set joins the lower component of the end-levels for the one overturned spin to form a total-spin-(N/2-1) multiplet which lies on the dispersion curve corresponding to one overturned spin for $S^z = N/2-1$. We shall see in the following sub-section that this multiplet is the first excited state for finite N, differing in energy by terms of order $(1/N^2)$ from the ground state. Hence, at $\gamma = 1$, the latter multiplet is the special spin-wave state replacing the 'missing bound state' for $q \lesssim 2\pi/N$. At $\gamma = 1$, therefore, these low-lying chain levels change their character and become 'spin-wave-like' rather than 'bound'. The fact that they are degenerate at $\gamma = 0$ and again at $\gamma = 1$, and the intermediate splitting is slight, suggests that in the limit $N \to \infty$ the levels will remain degenerate for all γ. (The levels for one overturned spin will remain split off, but they do not interest us since they will not affect the thermal properties.)

In Fig. (3.13) we present an estimate of the limiting behaviour of these levels as a function of γ obtained by extrapolation of the chain results for N=4, 6 and 8 (dashed curve (a)), shown with the appropriate chain levels. Also on this figure (dashed curve (b)) we show the perturbation estimate (equation (3.4.28)) for the four levels for one overturned spin, with a level for N=8 for comparison. Finally (dashed curve (c)) we have estimated, with the aid of results for finite rings and chains, the continuum limit of the next excited set of levels emanating from the Ising level

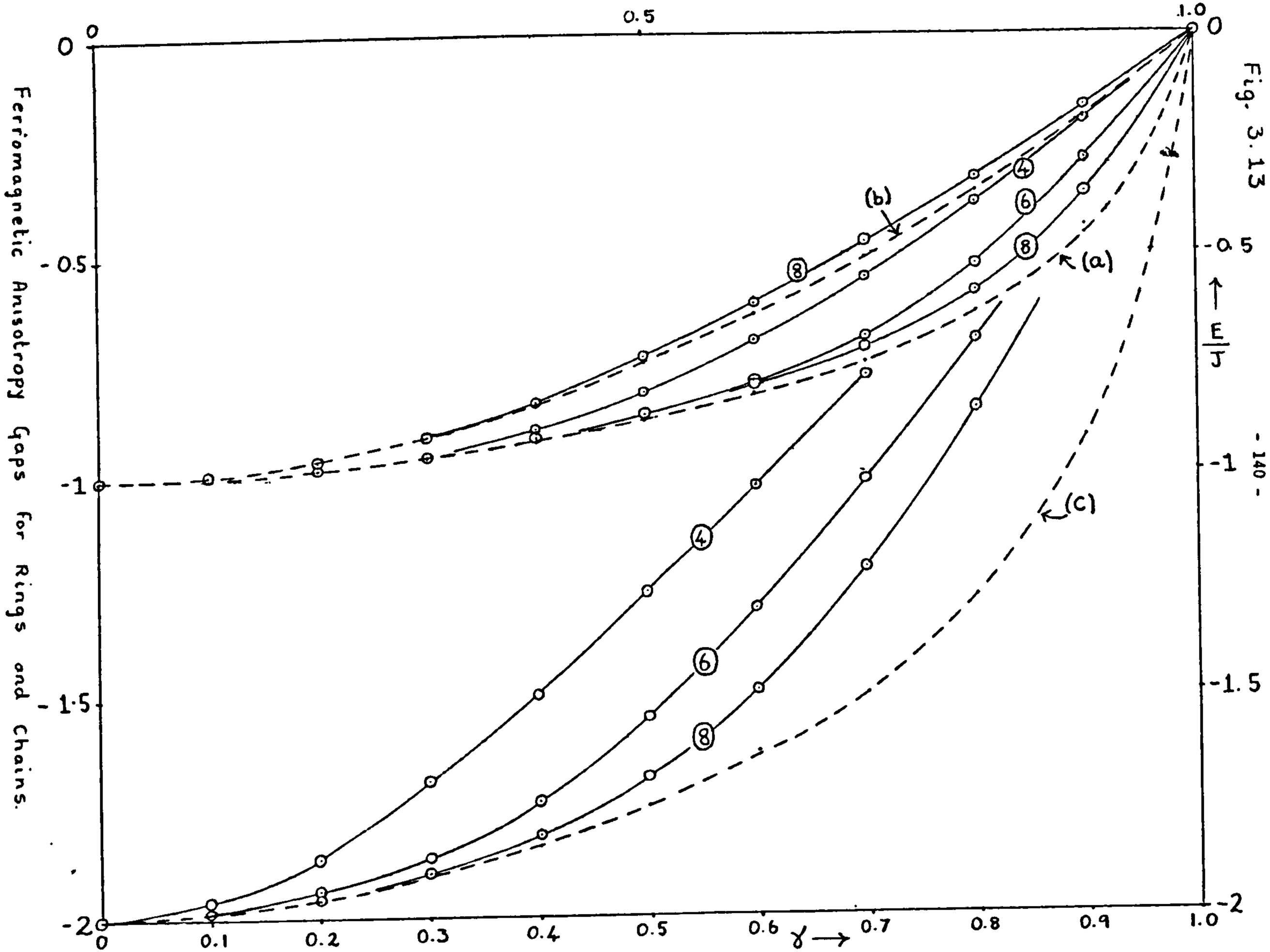
Ferromagnetic Anisotropy Gaps for Rings and Chains.
E/J
γ
(a)
(b)
(c)
4
6
8
0
0.5
1.0
-0.5
-1
-1.5
-2
0.1
0.2
0.3
0.4
0.5
0.6
0.7
0.8
0.9

Fig. 3.13

$-2|J|$, or $N \to \infty$. The ring levels for N=4, 6 and 8 are shown also. We conjecture that the energy gap between the ferromagnetic ground state and curve (a) in Fig. (3.13) can be regarded as the effective anisotropy energy gap $\Delta E_F(\gamma)$ (or energy gap for chains) for ferromagnets, analogous to curve (C) of Fig. (3.9) for antiferromagnets. Also that curve (c) of Fig. (3.13) is the energy gap for ferromagnetic rings (i.e. twice the effective energy gap) analogous to curve (a) (or more exactly to curve (b) of des Cloizeaux and Gaudin) of Fig. (3.8) for antiferromagnets. However, the ferromagnetic gaps do not have the same form as the corresponding antiferromagnetic gaps, vanishing rather rapidly as $\gamma \to 1$ instead of exponentially slowly, and varying quadratically with γ near the Ising limit, rather than linearly.

4.7) States of More Than Two Overturned Spins:

Heisenberg Limit

At $\gamma = 1.0$ the spectral distribution is rather complicated. For example, the two-spin-wave continuum comes down to join the single-spin-wave continuum, and bound states of two overturned spins also lie just above the ferromagnetic ground state. In Fig. (3.14) are shown the lowest-lying ferromagnetic states for rings, for different numbers of overturned spins, for N=10 (open circles) and N=11 (dark circles). Curve (a) corresponds to one overturned spin, curve (b) to two overturned spins, curve (c) to three, curve (d) to four and curve (e) to five overturned spins, the maximum for N=10 and N=11. We recognise curve (b) as the two-spin bound state dispersion curve and hence conclude that curves (c), (d) and (e) must also be bound state dispersion curves of three, four and five overturned spins respectively. The curves may also be characterised by their total spin quantum numbers; for example, curve (a) contains spin-(N/2-1) states, curve (b) spin-(N/2-2) states, curve (c) spin-(N/2-3) states, down to curve (e), spin-0 states for N=10 and spin-1/2 states for N=11. In general there will be ~ N/2 of these curves, arranged so that the curves of minimum total

Fig. 3.14

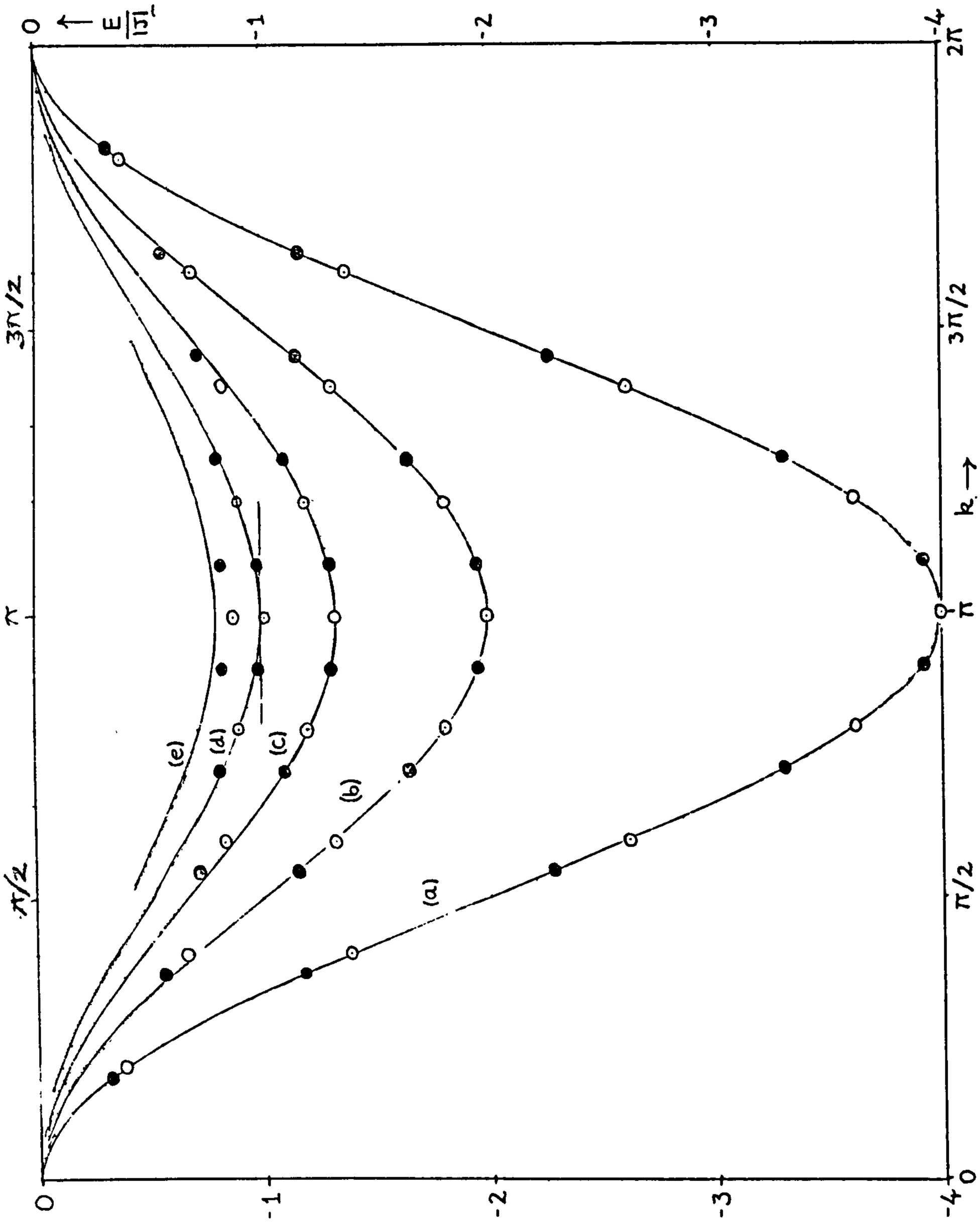

Bound States of Several Overturned Spins: $\gamma = 1$. Ferromagnets.

spin lie nearest to the ferromagnetic ground state. It may be observed that the individual states lie very close to the solid curves which represent the formulae

$$\varepsilon^{(r)}(k) = (2J/r)(1 - \cos k) \qquad (3.4.30)$$

where r is the number of overturned spins. This is in accordance with Bethe's analytic result (Bethe 1931) for the dispersion curves of the lowest-lying bound states. However, Bethe's results imply that bound states are uniformly distributed along the dispersion curves in the limit. If this were the case, these bound states would undoubtedly form the lowest-lying states of the ferromagnetic linear chain. But we have already observed that for our small values of N, the q=1 two-spin bound state is missing. We see from Fig. (3.14) that the rest of the curves also have missing states, and relatively more of them. For curve (c) bound states are missing up to and including q=2, for curve (d) states are missing as far as q=3 and so on. Thus, in general, for small finite even N, the bound state curve for spin S=0 will contain only a single state. In the light of the Katsura solution, it seems most reasonable to infer that these bound states will still be absent in the large N limit, and that probably others also will be missing in this limit. Since the two-spin-wave continuum states of total spin S=N/2-2 and the bound states of total spin zero up to N/2-2 are found to be roughly comparable in total number, mean spin degeneracy and position in the spectrum it is likely that both will contribute to the thermal behaviour for T > 0.

However, we ought to examine the higher excited states for more than two overturned spins. Some of these are shown in Fig. (3.15) (which, incidentally, has a scale half as large as Fig. (3.14)). One interesting conclusion is that there do not seem to be any additional spin-wave continua of total spin less than N/2-2, at least as far up the ferromagnetic energy scale as the states shown in Fig. (3.15). (The number of states becomes rather large for higher ferromagnetic energies and interpretation becomes increasingly difficult.) The states of total spin less than N/2-2

Fig. 3.15

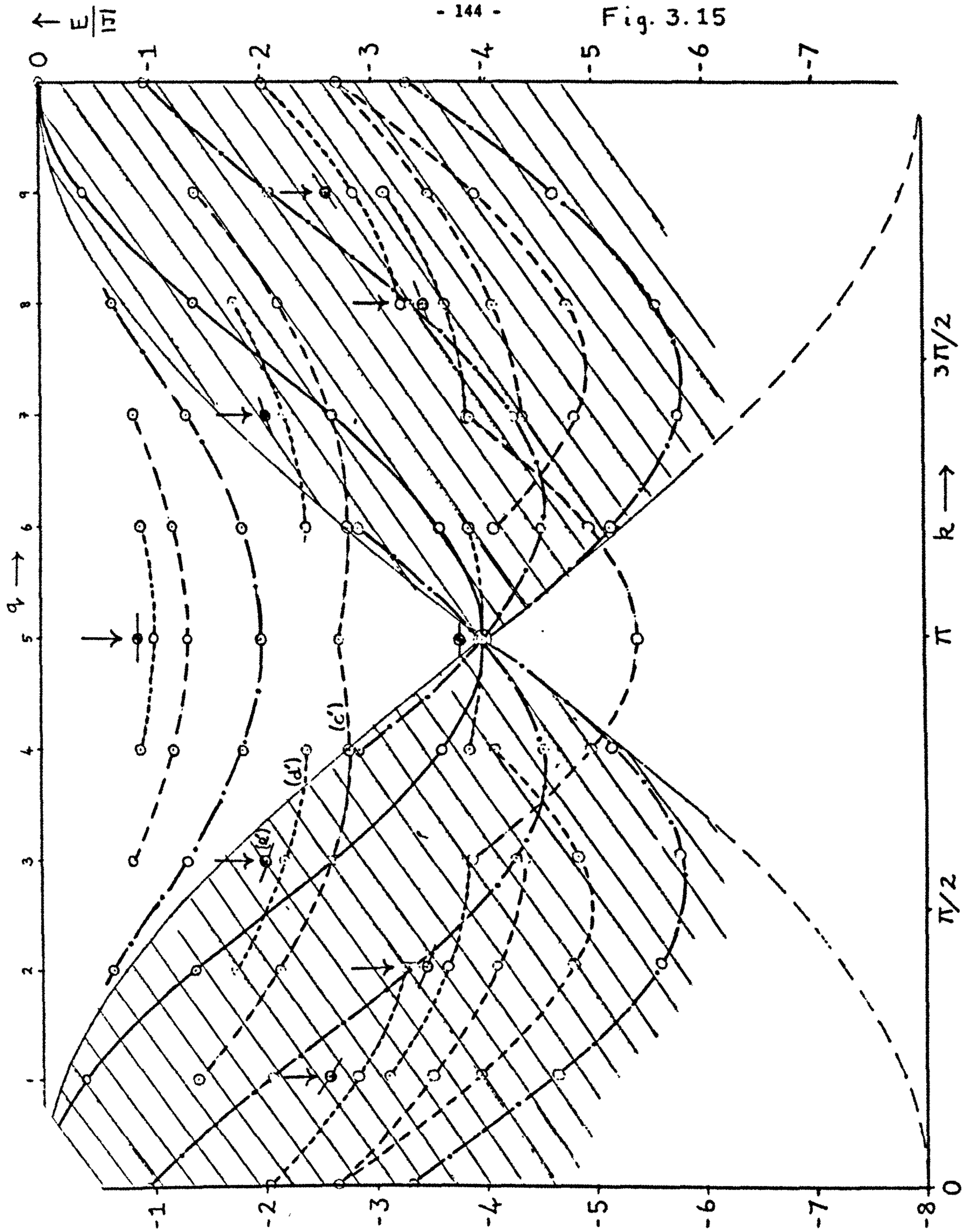

Higher Bound State Dispersion Curves: $\gamma = 1.0$: Ferromagnets.

in this region appear to be bound states lying in families of dispersion curves very similar to those of Fig. (3.14). Six such families are shown in Fig. (3.15), corresponding to N=10, the leading singlet dispersion curves (dark circles) being indicated by the arrows. Let us study the family of dispersion curves at q=3. Curve (e′) is a singlet dispersion curve, curve (d′) a triplet and curve (c′) a quintet. The shapes of these curves are obviously closely similar to the corresponding curves of the lowest-lying bound state family (with some understandable distortion), and unlike the spin-wave dispersion curves. We are thus led to conjecture they are bound states.

As a final comment, it appears that the first excited state for large N will be the (N-1)-fold degenerate first excited state on the single spin-wave dispersion curve. The missing states along the lowest-lying bound-state dispersion curves prevent states of this type from beating it; and a survey of numerical results for small rings indicates that the higher bound state families do not lie low enough to affect it.

5. ANTIFERROMAGNETIC DISPERSION CURVES

In this section the finite N antiferromagnetic dispersion curves for rings and chains are identified and compared with analytic results where available, for the Heisenberg limit and for general anisotropy. The apparent existence is noted of a low-lying set of antiferromagnetic dispersion curves which do not accord with the usual prescription for spin-wave curves, but which nevertheless show a dispersion pattern essentially similar to that of the spin-wave states.

5.1) Heisenberg Primary Dispersion Curves

Let us now study the energy states at the bottom of the antiferromagnetic spectrum as a function of wave-vector k in a like manner to the low energy ferromagnetic states. We shall consider first of all the Heisenberg limit.

Plotting the lowest energy states for a given value of k we obtain a dispersion curve (primary dispersion curve) for small finite N of approximately sinusoidal form. The curves show an interesting double periodicity over a range in k of 0 to 2π, consistent with an approximate $|\sin k|$ behaviour. Des Cloizeaux and Pearson (1962) have conducted an analytic investigation of the antiferromagnetic dispersion properties. They conjectured that these lowest states of a given k were included in the spin-wave category; that is that the wave-vectors of the individual spins of the state are all real. They devised a prescription for obtaining these states for finite and infinite N, in terms of quantities related to the individual wave-vectors. Feeding this prescription into the Bethe-Hulthén coupled equations, they were able to obtain the correct energies for these low-lying antiferromagnetic states for rings of 6 and 8 spins, i.e. the energies obtained by analytic calculations agreed with the results of matrix diagonalisation. (Note that they also obtained these states for rings of 16 and 48 spins.) They then went on to obtain the following expression for the dispersion curve in the limit of large N:-

$$\varepsilon(k) = E^{(1)}(k) - E_o = \pi \left| \sin k \right| \qquad (3.5.1)$$

These points are illustrated in Fig. (3.16) which shows the low-lying states of the antiferromagnet N=10 for $\gamma = 1$. The character of the states is signified as follows:- singlet states are dark circles; total-spin-1 states are open circles; spin-2 states are open squares and spin-3 states are circles with crosses. (States of spin-4 (spin-N/2-1) do not extend sufficiently far down the spectrum to appear on Fig. (3.16).) The N lowest-lying states of Fig. (3.16) comprise the antiferromagnetic ground state (singlet) situated here at $q = \pm 5$, together with 9 (in general (N-1)) triplet states. We have already established that the lowest triplet state, here situated at q=0, becomes degenerate with the singlet ground state in the large N limit. We show for comparison the des Cloizeaux and Pearson limiting spectrum superimposed on the finite N ground state as the continuous curve

Fig. 3.16

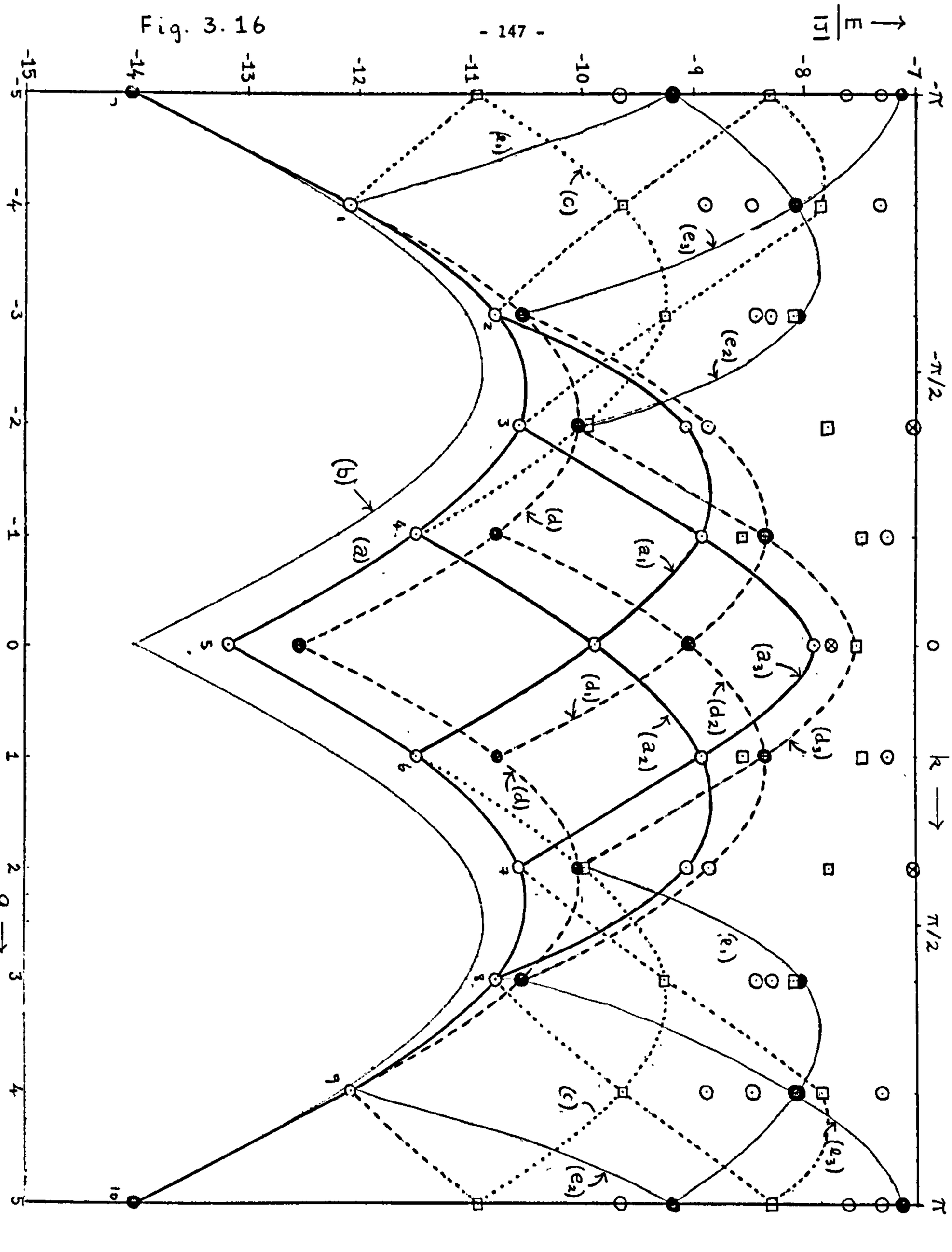

Antiferromagnetic Dispersion Curves: Heisenberg Limit

lying below the N=10 triplets (curve (b)). In this limiting curve there is complete symmetry between the two branches of the curve, which is not the case for finite N. However, numerical extrapolation of the appropriate energy differences versus 1/N for a sequence of finite clusters up to N=11 indicates a limiting value in good agreement (i.e. to within 5 to 10%) with the des Cloizeaux and Pearson value of $|J|\ \pi$ for the amplitude. The des Cloizeaux and Pearson curve may be compared with the result of Anderson (1952), which also gives $|\sin k|$ dependence but with a modified amplitude of 2 instead of π. The Anderson dispersion curve is actually the same as the dispersion curve for the X-Y model solved independently by Lieb, Schultz and Mattis (1961) and Katsura (1962).

5.2) Inferences From the des Cloizeaux and Pearson Analytic Result

We may use the des Cloizeaux and Pearson result to infer an analytic result for the way in which the anisotropy energy gap vanishes at $\gamma = 1$ as $N \to \infty$. Let us consider the finite N dispersion curve for an odd ring e.g. for N = 11, which is sketched in fig. (3.8).

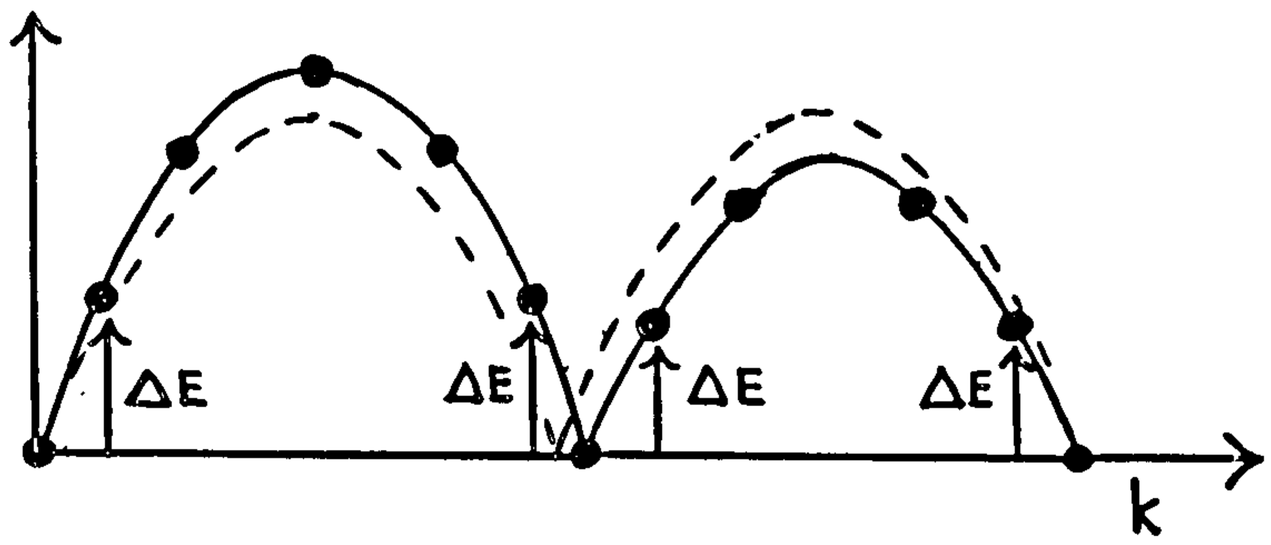

fig. (3.8)

We observe that the dispersion relation for odd rings differs slightly from that for even rings in that a) the energy states at $k = 0$ and $k \simeq \pi$ are always degenerate but b) the two portions of the dispersion curve are not symmetrical, the lower branch converging to the limiting curve (shown dashed in fig. (3.8)) from above and the smaller branch from below. The states at $k = 0$ and $k \sim \pi$ are total-spin-1/2 doublet states constituting an antiferromagnetic ground state which is fourfold degenerate for all finite N. The remaining states are quartet states of total-spin-3/2. Hence, as we observe from the sketch, the finite N anisotropy gap is governed by the

energy difference ΔE between a doublet ground state and a quartet state of neighbouring k. In the limit this energy gap will correspond to the energy difference between states of $k = 0$ and $k = \frac{2\pi}{N}$ along the des Cloizeaux and Pearson dispersion curve; namely $\frac{\Delta E}{|J|} = \pi \sin \frac{2\pi}{N} \sim 2\pi^2/N$. The value $2\pi^2$ for $\frac{N\Delta E}{|J|}$ compares reasonably well with the extrapolated value of 18 mentioned in sub-section (3.1).

However, we see from Fig. (3.16) that the ground state and the first excited state are separated by a wave-vector difference of π, for even rings, and it is not obvious how to determine the limiting behaviour of the energy gap, ΔE, from the des Cloizeaux and Pearson relation in this case. In sub-section (3.1) of this chapter, however, we have noticed that

$$\mathrm{Lim}\left(N\Delta E/|J|\right)_{even} = \tfrac{1}{2}\,\mathrm{Lim}\left(N\Delta E/|J|\right)_{odd} \qquad (3.5.2)$$

according to our numerical extrapolations. This result suggests that

$$\mathrm{Lim}\left(N\Delta E/|J|\right)_{even} = \pi^2 \qquad (3.5.3)$$

(This conclusion is supported by the discussion in sub-section (3.3) of Chapter V that the zero-temperature magnetisation curve as a function of applied field should have the same limiting, low-field, slope for both odd and even rings.)

5.3) Higher Excited Heisenberg Dispersion Curves

We have seen that at the ferromagnetic end of the spectrum the states can be divided into two categories. The spin-wave states lie close to the intersections of like curves arising from the primary spin-wave dispersion curve: the bound states lie on different dispersion curves. It is interesting to study the antiferromagnetic end of the spectrum to see if similar phenomena can be observed. The triplet states (open circles) on curve (a) (Fig. 3.16) are numbered 1 to 9 inclusive. We observe that three curves (a1), (a3) and (a2) may be drawn originating from states 6, 7 and 8 (or 2, 3 and 6), respectively, having a very similar form of dispersion curve to curve (a). Situated on these curves we have 6 states which are also spin-1

triplets. By analogy with our discussions of the ferromagnetic limit, we expect this family of states to be spin-wave states. This conclusion is in accordance with analytic work by Hulthén (1938), des Cloizeaux and Pearson (1962) and Griffiths (1963, unpublished).

In Bethe's formalism, an eigenstate of the Hamiltonian (3.3.9) with total spin S and wave-number k is associated with a set of N/2-S integers λi satisfying

$$0 \leq \lambda_i \leq (N-1) \tag{3.5.2}$$

and
$$k = 2\pi/N \times \sum_i \lambda_i \pmod N \tag{3.5.3}$$

'Spin-wave' states are characterised by sets of λi, no two of which differ by less than 2. This scheme is easily verified in the ferromagnetic limit for the case of two overturned spins. The bound states of the problem are shown to be specified by sets of λi, such that some of the λi are (a) equal or (b) differ by 1. Actually the latter category does contain some spin-wave states, but Katsura's (1965) solution shows that the number of these is small. Let us consider, as an example, the antiferromagnetic region of the spectrum for N=10. Hulthén (1938) points out that the number of spin-wave states with a given total spin S is given by

$$n(s) = \binom{N/2 + S}{2S} \tag{3.5.4}$$

(Each of these n(s) states is, of course, (2S+1)-fold degenerate.)

We see straightaway that only a single state out of the class of singlets is a spin-wave state: this state is, in fact, the antiferromagnetic ground state. For N=10, formula (3.5.4) predicts the existence of 15 spin-wave triplets, which we shall proceed to identify on Fig. (3.16). We have two possible choices for the set of λi for the antiferromagnetic ground state:-

(a) $0, 2, 4, \cdots, (N-2)$ such that $k = 0, \frac{N}{2}$ odd; $= \frac{N}{2}, \frac{N}{2}$ even (3.5.5)

(b) $1, 3, 5, \cdots, (N-1)$ such that $k = \frac{N}{2}, \frac{N}{2}$ odd; $= 0, \frac{N}{2}$ even (3.5.6)

From Fig. (3.16) we observe that the lowest state is a $q = N/2$ state, and, in general, we discover that the finite N antiferromagnetic ground state is always given by the set $\lambda i = 1, 3, 5, \ldots\ldots, (N-1)$. (3.5.6)

We further observe that the alternative λ distribution gives rise to the $S^z = 0$ component of the first excited state, which is a triplet. Orbach (1958) gives a brief consideration of the two distributions, pointing out that the integral equations derived from these distributions differ only by terms of $0(1/N)$. This result is in accordance with our conclusions concerning the behaviour of the Heisenberg energy gap when $N \to \infty$. Des Cloizeaux and Pearson first obtained the sets of λi corresponding to the set of triplet states along the lowest-lying dispersion curve, curve (a). This prescription is conveniently illustrated in Table (3.1) for the set of $S^z=0$

Table (3.1)

State \ λi	0	1	2	3	4	5	6	7	8	9	k	S^z
5	X		X	X	X		X		X		0	0
6	X		X		X		X			X	1	0
7	X		X		X			X		X	2	0
8	X		X			X		X		X	3	0
9	X			X		X		X		X	4	0
10 (A.G.S)		X		X		X		X		X	5	0

components, which shows the particular set of λi for a given excited state and its corresponding k-value.

The series of states is obtained from the starting state, state 5, by displacing the largest λ ($\lambda = 8$) one place to the right and following this by a systematic similar displacement of the smaller λ's. This scheme has been discussed by Griffiths (1963, unpublished) who points out that a series of displacements of this type constitutes a single-spin-wave excitation. In Table (3.2) we see the corresponding series of $|S^z| = 1$ states which also, of course, lie on curve (a). These states are associated with only 4 λi, and

Table (3.2)

State \ λ_i	0	1	2	3	4	5	6	7	8	9	k	S^z
5			X		X		X		X		0	1
6			X		X		X			X	1	1
7			X		X			X		X	2	1
8			X			X		X		X	3	1
9				X		X		X		X	4	1

differ from their $S^z = 0$ counterparts by omission of $\lambda i = 0$, according to the rule for obtaining the different components of a multiplet given by des Cloizeaux and Pearson. It is interesting to observe how this scheme predicts the absence of an $S^z = 1$ component for the antiferromagnetic ground state - the series becomes complete at state 9, since any further displacement of λ's would produce either a state of higher S^z or a state which does not fulfil the spin-wave specification. In accordance with the conclusions of Griffiths (1963, unpublished) that the states of negative k do not form an independent set, we have considered only states for which $k \geq 0$.

With these ideas in mind, we now turn to the problem of identifying dispersion curves containing higher numbers of spin-waves. In Table (3.3) we consider the various spin-wave excitation possibilities arising from state 6.

1	2	3	4	5	6	7	8	9	k	S^z	Type
	X		X		X			X	1	1	single spin-wave
	X		X		X				2	2	double spin-wave
X			X		X			X	0	1	two single spin-waves

Table (3.3)

There are, in fact, only two possibilities within the spin-wave framework. Recalling that state 6 was obtained from state 5 by displacing $\lambda i = 8$ one place to the right, we see that if we displace the same λ to the right again we have a state with $k = 3$ and only 3 remaining λ's. This state is therefore an $S^z = 2$ state. Since the same λ has been doubly shifted, this state is a double-spin-wave state, i.e. two spin-waves have been excited at the same site. (Griffiths (1963) unpublished). The series of $S^z = 2$ states lying on this double-spin-wave dispersion curve, the dotted curve (c), we then obtained in a like manner to the states of curve (a). We observe other low-lying S = 2 states in Fig. (3.16) which can also be shown to lie on approximate sin k dispersion waves arising from states 7, 8, and 9.

Returning to state 6, we can distinguish another set of excitations, the curve (a1) we have mentioned previously, which arise from state 6 by displacing the <u>first</u> λ one place to the left. This set comprises a set of $S^z = 1$ states of decreasing k. Since two separate λ's have suffered a single displacement, we have a dispersion curve corresponding to two single-spin-wave excitations. Curves (a2) and (a3) are obtained in a like manner from states 8 and 7 respectively. This result confirms our earlier expectations that the 15 states lying on curves (a), (a1), (a2) and (a3) comprise all the 15 triplet spin-wave states.

We observe that there are still a large number of low-lying singlet and triplet states which cannot be obtained from the spin-wave prescription for the λi. We are interested to observe a set of singlet states lying just above the fundamental dispersion curve (a) on the dashed curve (d) which has a very similar form to curve (a). In fact, numerical studies in a sequence of values of N suggests that in the limit $N \to \infty$, curve (d) becomes degenerate (to order 1/N) with curve (a) and hence has the identical dispersion formula

$$\varepsilon(k) = \pi \left| \sin k \right| \qquad (3.5.7)$$

Further we observe that associated with curve (d) are sets of dispersion curves, presumably corresponding to higher order excitations, namely curves (d1), (d2) and (d3) (shown dashed) and (e1), (e2) and (e3) (shown as faint solid lines), which are really very similar to the sets of spin-wave curves (ai) and (ci). If it were possible to discover a λi prescription which simply and unambiguously reproduced the states of curve (d) and the apparent excitations, this prescription could then be fed into the Bethe-Hulthén formalism and the analytic properties deduced. Unfortunately, it has not been found possible to discover a satisfactory prescription.

Griffiths (1963, unpublished) attempted a spin-wave calculation of the thermodynamic properties of the antiferromagnetic linear chain using the spin-wave states we have just described. Although his calculations were in good agreement with the numerical results for finite rings, he presented arguments demonstrating that the class of spin-wave states, as determined by the λ prescription described above, form too small a sub-set of the levels for an infinite chain to have <u>any</u> influence on the thermodynamic properties at a finite temperature. It appears from Fig. (3.16) that we have been able to distinguish a second class of levels whose λ prescription is unknown but is certainly not the spin-wave prescription, whose dispersion properties seem to be remarkably similar to those of the spin-wave states we have just discussed. It may happen that this second class of states is sufficiently numerous to influence (or even dominate) the limiting partition function. Since the low-temperature thermal properties of these states will resemble those due to the spin-wave states, we have a possible explanation of Griffiths' result that the low-temperature thermal behaviour obtained from numerical extrapolations appears to be 'spin-wave-like'.

5.4) <u>Isotropic Dispersion Curves for Chains: Brillouin Zones</u>

It is implicit in Griffiths' (1963, unpublished) spin-wave analysis that in the limit of infinite N the approximate double periodicity of the antiferromagnetic dispersion curves becomes exact (as was first pointed

out by des Cloizeaux and Pearson (1962)) and the Brillouin Zone reduces from 0 to 2π, say, to 0 to π . The des Cloizeaux and Pearson spin-wave dispersion law is more properly

$$\varepsilon(k) = \pi \sin k \quad , \qquad 0 \leq k < \pi \qquad (3.5.8)$$

According to Griffiths, therefore, the first antiferromagnetic Brillouin Zone contains N/2 states with wave-vectors in the range $0 \leq k < \pi$ spaced at intervals of $\Delta k = 2\pi/N$. This conclusion is supported by our results for chains, where, in Fig. (3.17), we compare the Heisenberg dispersion curves for N = 8 for both rings and chains. The state notation is as in Fig.(3.16). Hence singlet states are denoted by black circles, triplet states by light circles and spin-2 quintets by light squares. The ring dispersion curves are shown by dark solid lines, and we see at a glance that the dispersion pattern is essentially the same as for N = 10. In the case of the chain of 8 spins, we appear to have a one-to-one correspondence near the antiferromagnetic end of the spectrum between chain states of a particular spin and their ring counterparts in the region 0 to π . The chain states are plotted at the same k values as the corresponding ring states, involving an assumption which presumably becomes more valid as N increases. As we see, the chain dispersion curves, shown dotted, are closely similar to the corresponding ring dispersion curves, with some additional distortion which is probably partly due to the fact that the chain k values are approximate only. In the ferromagnetic case we have already implicitly observed that the first Brillouin Zone for chains is defined by $0 \leq k < \pi$ and the state separation is given by $\Delta k = \pi/N$. For rings, therefore, it is probably better to define the first Brillouin Zone also as $0 \leq k \leq \pi$, with a state separation given by $\Delta k = 2\pi/N$. Then all states except the states at k = 0 and $k = \pi$ are two-fold degenerate. However, it has been found convenient throughout this chapter to consider an enlarged Brillouin Zone, given by $0 \leq k < 2\pi$, since characteristic dispersion patterns are then more easy to perceive.

Fig. 3.17

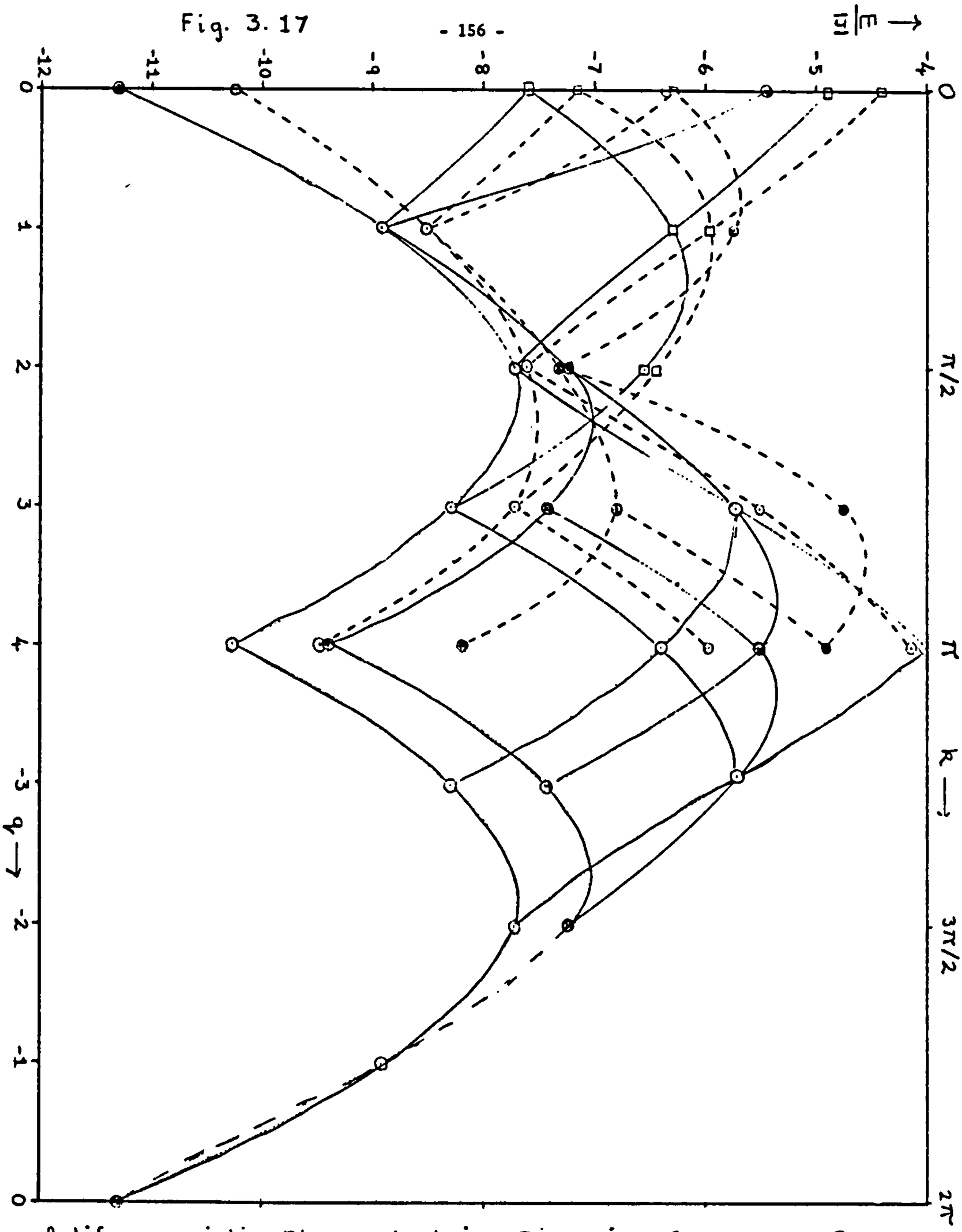

Antiferromagnetic Ring and Chain Dispersion Curves : N = 8.

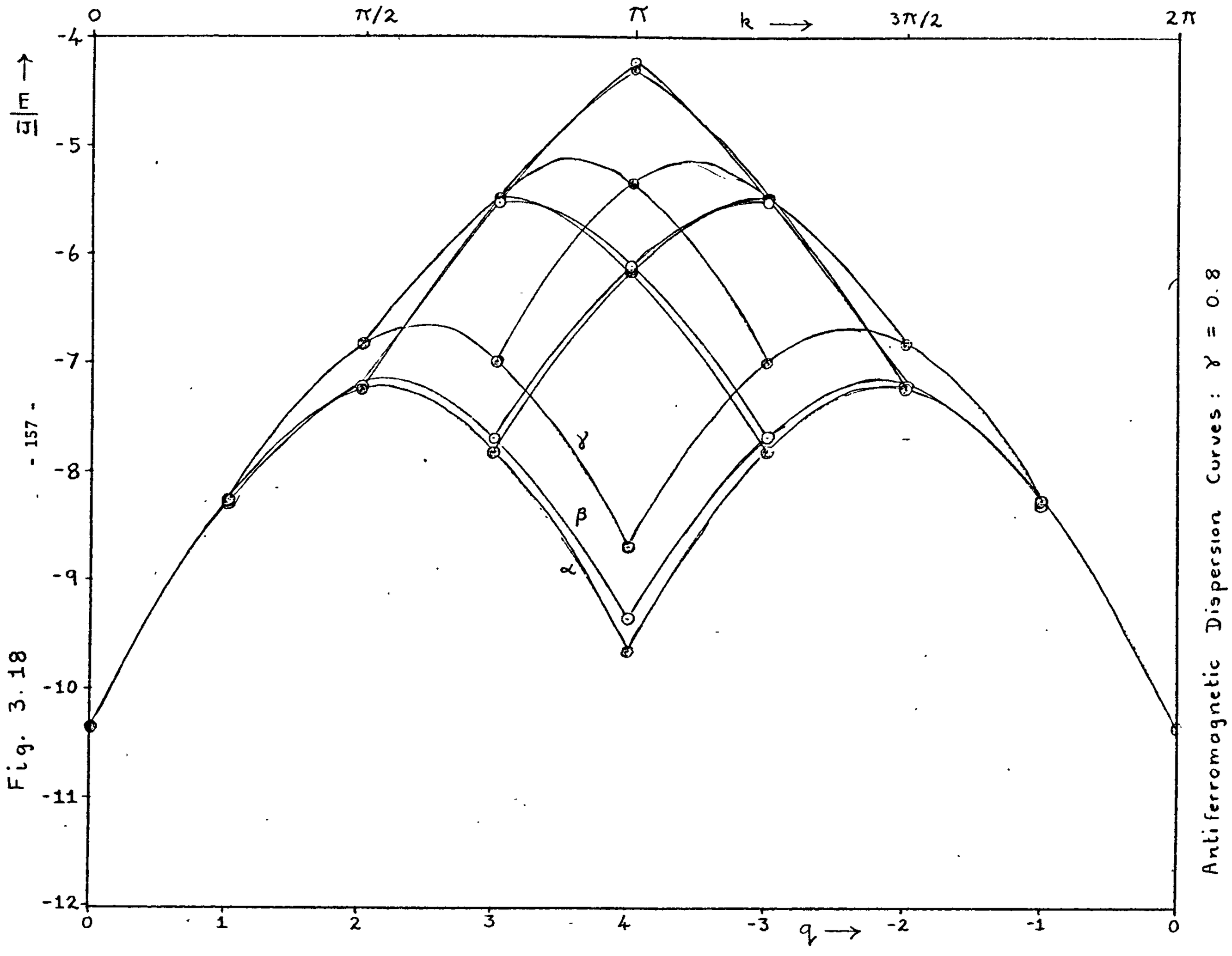
0
π/2
π
k ⟶
3π/2
2π
-4
-5
-6
-7
-8
-9
-10
-11
-12
E/|J|
γ
β
α
0
1
2
3
4
-3
-2
-1
0
q ⟶
Curves : γ = 0.8
Antiferromagnetic Dispersion Curves

Fig. 3.18

5.5) Anisotropic Dispersion Curves

The effect of a small amount of anisotropy on the ring dispersion curves of Fig. (3.17) is shown in Fig. (3.18) which applies to $\gamma = 0.8$. The triplet states are seen to be split into $|S^z| = 1$ and $S^z = 0$ components, but this splitting is relatively slight and the same splitting for $\gamma = 0.5$ (not shown) is hardly more appreciable. As $\gamma \to 0$, the two $S^z = 0$ states at $k = 0$ and $k = \pi$ detach themselves from the rest of the dispersion spectrum (i.e. the α branch) and become degenerate in the limit $\gamma = 0$ for finite N (for infinite N we have concluded in subsection (3.1) of this chapter that these two states are degenerate for all γ). The remaining three branches of the low-lying antiferromagnetic spectrum, two $S^z = 0$ and *one* (degenerate) $S^z = 1$ branches, for convenience labelled α, γ and β, respectively in Fig. (3.18), become degenerate and flatten into a 'horizontal' line lying at an energy gap of $\Delta E/|J| = 2$ above the two-fold degenerate antiferromagnetic ground state for rings. For the branches α and β, des Cloizeaux and Gaudin (1966) have recently obtained analytic expressions which do not both seem to be wholly correct. For the α branch, corresponding to $S^z = 0$, they obtain an analytic expression which cannot be expressed in very simple form except at the Heisenberg limit where, of course, we obtain the familiar dispersion curve

$$\varepsilon(k) = \pi \sin k \qquad (3.5.9)$$

and at the Ising limit where des Cloizeaux and Gaudin find that

$$\varepsilon(k) = 2(1 - \cos 2k) \qquad (3.5.10)$$

In our notation, equations (3.5.9) and (3.5.10) must be multiplied by the appropriate value of γ, which leaves (3.5.9) unaffected but which 'flattens' equation (3.5.10) into a 'horizontal' line given by

$$\varepsilon(k) = 0, \quad \text{all } k \qquad (3.5.11)$$

But this equation implies that we have a total of (N/2-1) states all degenerate with the antiferromagnetic ground state. We know this is not the case for either finite or infinite N. Equation (3.5.10) must therefore be

regarded as spurious. Des Cloizeaux and Gaudin discuss their spurious states for $0 < k < \pi$ and conclude they must be collective states. A more plausible explanation is that these states do not occur! In the case of the β branch, corresponding to $|S^z| = 1$, des Cloizeaux and Gaudin obtain a dispersion curve which is the same dispersion curve as they obtained for $S^z = 0$ superimposed on an energy gap given by equation (3.3.6), subsection (3.2) of this chapter. When compared with the finite ring results, this excitation pattern seems perfectly plausible. Although we have not been able to follow through the des Cloizeaux and Gaudin analysis to show that the evident error for the α branch is not matched by an error in the β branch, we believe that the β branch results (and the anisotropy energy gap calculation) are, in fact, correct. Our finite ring results suggest that the α branch dispersion curve is identical with the β branch dispersion curve in the limit of infinite N for all γ, not just at the Heisenberg limit, $\gamma = 1$, where the two branches combine to give a set of total-spin-1 triplets. We conclude that the $S^z = 0$ γ branch also is degenerate with the α and β branches in the limit for all anisotropy.

CHAPTER IV

THERMAL PROPERTIES

Introduction

Our fundamental aim in this chapter will be to estimate the general limiting thermal properties. We shall see that the convergence of the finite ring curves is sufficient to indicate the limiting behaviour for all γ quite accurately at temperatures above $kT/|J| \simeq 0.5$ This temperature region includes the maxima in the antiferromagnetic specific heat (and susceptibility) and also in the Heisenberg ferromagnetic specific heat (the ferromagnetic specific heat for $\gamma=0.5$ appears to show a maximum at a rather lower temperature). These maxima, despite their experimental importance, had not previously been estimated with any accuracy prior to our beginning this study.

At lower temperatures, extrapolation procedures are supplemented by low-temperature theoretical studies based upon our detailed discussion of the properties of the spectrum in the preceding Chapter III. The combination of techniques enables us to carry the limiting estimate of the thermal (and magnetic) properties right down to T=0.

Extensive comparison is made of our limiting results with the other more successful approximate theories in the field. The Baker, Rushbrooke and Gilbert Padé approximant evaluations of high-temperature, zero-field series for $\gamma=1$ are in excellent agreement with our own work for temperatures above $kT/|J| \simeq 0.5$ for antiferromagnets and $kT/|J| = 0.3$ for ferromagnets. This gives us confidence in pointing out the relative unreliability of the other methods which are in agreement only at much higher temperatures.

Field-dependent effects on the thermal properties are considered also in this chapter. An anomalous zero-point entropy peak in Ising

antiferromagnets at a critical value of the applied magnetic field is shown to disappear for the more physically realistic anisotropic and Heisenberg models. "Pseudo-phase" boundaries, i.e. the limiting loci of the entropy maxima as a function of field and temperature are estimated for various values of γ. The rather short length of our chains does not enable us to study very critically the high-field, low-temperature region to investigate the possibility of additional phase boundaries related to an incipient spin-flop transition.

The actual calculation of the thermodynamic properties was performed by direct evaluation of the appropriately weighted partition sums on a computer, using sets of numerical eigenvalues obtained as described in Chapter II.

As background both to this chapter and the following Chapter V, we present at the outset a brief review of the properties of the Ising spin-1/2 linear chain. While the limiting, $N \to \infty$, behaviour is, of course, well-known, the way in which the finite N properties approach the limit is interesting, and not available in published form. In fact, finite N Ising studies have afforded valuable clues concerning the nature of the convergence of the corresponding anisotropic and Heisenberg properties where, of course, the <u>exact</u> limiting values are not at present available.

1. THE ISING LINEAR CHAIN

Let us consider the problem of a chain of N Ising-coupled spins of magnitude 1/2 (Ising, 1925). The problem is very simple, but serves as a useful introduction to the bulk of this thesis and gives valuable clues as to how one should approach the problem of the linear chain with a more physically realistic coupling, which does not, at present, admit of general exact solutions. A feature of particular interest, not previously investigated, is how the behaviour of finite chains systematically approaches the limiting case of $N = \infty$.

1.1) Limiting Partition Function

The Ising Hamiltonian for nearest-neighbour coupled spins in the presence of a magnetic field H applied parallel to the z-axis is

$$\mathcal{H} = -2J\sum_{i=1}^{N} S_i^z S_{i+1}^z - g\beta H\sum_{i=1}^{N} S_i^z \qquad (4.1.1)$$

(where $g\beta$ is the magnetic moment per spin). It is well-known that the special simplicity of the Ising model (see, for example, (Domb , 1960)) allows the partition function for an N-spin system with periodic boundary conditions to be written in the matrix form

$$Z_N = \mathrm{Tr}\,\underline{P}^N \quad ; \quad \text{where } \underline{P} = \begin{bmatrix} e^{K/2+MK/2} & e^{-K/2} \\ e^{-K/2} & e^{K/2-MK/2} \end{bmatrix} \qquad (4.1.2)$$

where $K = J/kT$ and $MK = g\beta H/kT$. The roots of $\underline{P}$ are

$$\lambda_{\frac{1}{2}} = e^{\frac{K}{2}}\cosh MK/2 \pm \left[e^{K}\sinh^2 MK/2 + e^{-K}\right]^{1/2} \qquad (4.1.3)$$

In the limit, $N \to \infty$, we have that $Z_N \sim \lambda_1^N$ and hence

$$\ln Z = \ln (Z_N)^{1/N} \sim \lambda_1 \qquad (4.1.4)$$

where λ_1 is the largest root of the interaction matrix $\underline{P}$. Hence the partition function for an infinite linear chain is

$$Z = e^{K/2}\cosh MK/2 + \left[e^{K}\sinh^2 MK/2 + e^{-K}\right]^{1/2} \qquad (4.1.5)$$

Note that for H = 0,

$$Z = 2 \cosh K/2 \qquad (4.1.6)$$

and for K = 0 (i.e. non-interacting particles)

$$Z = 2 \cosh g\beta H/kT \qquad (4.1.7)$$

Thus the properties of, say, an assembly of spins in a magnetic field at high temperatures are similar to those of an assembly of interacting particles in zero field.

The transformation from a ferromagnet to an antiferromagnet is given by replacing J by $-J$ and hence K by $-K$. It may be seen from Table (4.1) that the zero-field partition function and hence the zero-field thermal (but not magnetic) properties are invariant with respect to this transformation. This ferro-antiferro symmetry is shown by other models, e.g. the X-Y model of Lieb, Schultz and Mattis (1961) and Katsura (1962) and the infinite spin linear Heisenberg model of Fisher (1964), but does not occur for the Heisenberg (and anisotropic) linear chains with S = 1/2.

1.2) Critical Behaviour

From equation (4.1.5) we observe that the partition function Z is analytic in T for $0 < T \leq \infty$ (since it is analytic in K for $0 \leq K < \infty$), and hence there is no transition at a finite temperature. By writing the partition function in the alternative notation (Domb , 1960)

$$Z = A\left\{(1+\mu) + \left[(1-\mu)^2 + 4\mu z^2\right]^{1/2}\right\} \qquad (4.1.8)$$

where $z = e^{-J/kT} = e^{-K}$; $\mu = e^{-g\beta H/kT} = e^{-MK}$; $A = \frac{1}{2}\mu^{-1/2} z^{-1/2}$,

we see that a power series expansion in μ and z is possible about any point for which $\mu \neq 1$, $z \neq 0$. No expansion however is possible about the point $\mu = 1$, $z = 0$, hence we may describe the Ising linear chain as a ferromagnet whose Curie point has gone to zero.

Table (4.1)

Property	Ferromagnets	Antiferromagnets
Partition Fctn. Z	$e^{K/2} + e^{-K/2} = 2\cosh K/2$	$2\cosh K/2$
Free Energy $F/NIJI$	$-K^{-1}\ln(2\cosh K/2)$	$-K^{-1}\ln(2\cosh K/2)$
Int. Energy $U/NIJI$	$-\frac{1}{2}\tanh K/2$	$-\frac{1}{2}\tanh K/2$
Entropy S/Nk	$KU/NIJI + \ln(2\cosh\frac{K}{2})$	$KU/NIJI + \ln(2\cosh\frac{K}{2})$
Specific Ht. C/Nk	$\frac{1}{4}K^2\,\mathrm{sech}^2 K/2$	$\frac{1}{4}K^2\,\mathrm{sech}^2 K/2$
Magnetisation $\frac{M}{g\beta N}$	zero	zero
Susceptibility $\frac{IJI\chi}{Ng^2\beta^2}$	$K/4\ \exp(K)$	$K/4\ \exp(-K)$

Thermodynamic Properties in Zero Field

Table (4.2)

	Arbitrary H, T	$H = H_c, T = 0$
Z	$0.5\, e^{-K/2}\,\alpha$	$0.5\, e^{-K/2}(1+\sqrt{5})$
F/NJ	$K^{-1}\ln 2 + 0.5 - K^{-1}\ln\alpha$	$-0.5 - K^{-1}\ln\frac{1}{2}(1+\sqrt{5})$
U/NJ	$0.5 - 0.5(M\varphi+\delta)/\alpha$	-0.5
S/Nk	$-\ln 2 + \ln\alpha - 0.5K(M\varphi+\delta)/\alpha$	$\ln\frac{1}{2}(1+\sqrt{5}) = 0.4812$
C/Nk	$\frac{K^2}{4}\left\{\frac{M^2\Theta}{\alpha} + \frac{M^2(\Theta^2+\varphi^2)}{\alpha\beta} + \frac{32\,e^{2K}}{\alpha\beta} - \frac{\gamma^2}{\alpha\beta} - \frac{(M\varphi+\delta)^2}{\alpha^2}\right.$	0
$M/Ng\beta$	$-0.5\,\varphi(1+\Theta/\beta)/\alpha$	$\sqrt{5}/10 = 0.2236$
$IJI\chi/Ng^2\beta^2$	$\frac{K}{4}\left\{-\frac{\Theta}{\alpha} - \frac{(\Theta^2+\varphi^2)}{\alpha\beta} + \frac{\Theta^2\varphi^2}{\alpha\beta^3} + \frac{\varphi^2}{\alpha^2} + \frac{\varphi^2\Theta}{\alpha^2\beta} + \frac{\varphi^2\Theta^2}{\alpha^2\beta^2}\right\}$	$K/5\sqrt{5} = 0.895\,K$

where we define $\Theta = e^{\frac{MK}{2}} + e^{-\frac{MK}{2}}$; $\varphi = e^{\frac{MK}{2}} - e^{-\frac{MK}{2}}$;

$\alpha = \left(\Theta + [\varphi^2 + 4e^{2K}]^{1/2}\right)$; $\beta = [\varphi^2 + 4e^{2K}]^{1/2}$; $\delta = (M\Theta\varphi + 8e^{2K})/\beta$

Antiferromagnetic Properties of the Ising Linear Chain

The magnetisation (per spin) is

$$\mathcal{M}/N = g\beta \sinh MK\left[\sinh^2 MK + e^{-2K}\right]^{\frac{1}{2}} \quad . . (4.1.9)$$

and hence there is no spontaneous magnetisation since $M \rightarrow 0$ as $H \rightarrow 0$. The ferromagnetic susceptibility, however, diverges at $T = 0$, as one might suspect, whereas the antiferromagnetic susceptibility vanishes at $T = 0$ and $T = \infty$, and shows a typical rounded maximum

$$|J|\chi / Ng^2\beta^2 = 0.0920 \quad \text{at } kT/|J| = 0{\cdot}5 \quad (4.1.10)$$

The behaviour of the antiferromagnet at $T = 0$ is no longer peculiar in zero field but in a critical field $g\beta H_c = 2|J|$. Table (4.2) gives expressions for antiferromagnetic properties in arbitrary field and temperature (the corresponding ferromagnetic properties may be simply obtained by the transformation of sub-section (1.1)) and also in the critical field at absolute zero. The entropy, magnetism and susceptibility show anomalies in the critical field, the non-zero entropy contradicting the third law of thermodynamics and the susceptibility diverging as T^{-1}.

1.3) Finite N Partition Function: Rings and Chains

For finite N, the second root, λ_2, of the interaction matrix is no longer negligible compared with the first, and must be included. Hence, for example, the zero-field partition function is

$$Z_N = 2^N \cosh^N K/2 + 2^N \sinh^N K/2 \qquad (4.1.11)$$

First of all, we notice that when N is even, the partition function (4.1.11) is invariant between ferromagnets and antiferromagnets (as is the limiting zero-field partition function) but this is not the case for the odd rings. This is the effect of the 'misfit-spin' in antiferromagnetic odd rings. The effect becomes increasingly less important at higher N values, becoming significant only in the region

of absolute zero for very large N, and disappearing in the limit $N \to \infty$. In an applied magnetic field the partition function is

$$Z_N = \left[e^{K/2} \cosh \frac{MK}{2} + \left(e^{-K} + e^{K} \sinh^2 \frac{MK}{2} \right)^{\frac{1}{2}} \right]^N + \left[e^{K/2} \cosh \frac{MK}{2} - \left(e^{-K} + e^{K} \sinh^2 \frac{MK}{2} \right)^{\frac{1}{2}} \right]^N \quad (4.1.12)$$

Again, for free-ended chains, we may derive the partition function by the standard transfer matrix method. The results are:

$$Z_N = 2^N \left(\cosh K/2 \right)^{N-1} \quad \text{For } H = 0, \quad (4.1.13)$$

and, more generally, in a magnetic field

$$Z_N = \left[e^{K/2} \cosh \frac{MK}{2} + \left(e^{-K} + e^{K} \sinh^2 \frac{MK}{2} \right)^{\frac{1}{2}} \right]^{N-1} \left[\frac{e^{-K/2} \cosh \frac{MK}{2} + \left(e^{-K} + e^{K} \sinh^2 \frac{MK}{2} \right)^{\frac{1}{2}}}{\left(e^{-K} + e^{K} \sinh^2 \frac{MK}{2} \right)^{1/2}} \right]$$

$$+ \left[e^{K/2} \cosh \frac{MK}{2} - \left(e^{-K} + e^{K} \sinh^2 \frac{MK}{2} \right)^{\frac{1}{2}} \right]^{N-1} \left[\frac{-e^{-K/2} \cosh \frac{MK}{2} + \left(e^{-K} + e^{K} \sinh^2 \frac{MK}{2} \right)^{\frac{1}{2}}}{\left(e^{-K} + e^{K} \sinh^2 \frac{MK}{2} \right)^{1/2}} \right] \quad (4.1.14)$$

It is easy to verify, by taking logarithms of equations (4.1.11) and (4.1.13), that the ring and chain partition functions give rise to the same free energy in the limit. (Also see the discussion of sub-section (2.6), Chapter III). The equivalent result holds in the presence of a magnetic field.

1.4) Thermodynamic Properties; Convergence to the Limit

From the invariance of the zero-field partition function for rings for N even, we conclude that the thermal properties, i.e. the energy, entropy and specific heat will be independent of the sign of K. This point is explicitly illustrated by the following expressions (also derived by Griffiths in an unpublished report (1961)):

$$\frac{U}{NJ} = \left(\frac{U}{NJ} \right)_{Lim} - \left[\frac{\operatorname{cosech} K}{(\coth K/2)^N + 1} \right] \quad (4.1.15)$$

$$\frac{S}{Nk} = \left(\frac{S}{Nk} \right)_{Lim} + \frac{1}{N} \ln \left[1 + (\tanh K/2)^N \right] \quad (4.1.16)$$

$$\frac{C}{Nk} = \left(\frac{C}{Nk}\right)_{Lim} \times \left\{1 + \frac{2}{(\cosh K - 1)} \times \frac{1}{\left(1 + (\coth K/2)^N\right)} \times \left[\frac{N}{\left(1 + (\tanh K/2)^N\right)} - \cosh K\right]\right\} \tag{4.1.17}$$

The limiting values are, of course, those given in Table (4.1). For the magnetic thermodynamic properties we must consider the partition function in an applied field (equation (4.1.12)). Hence we may derive the following well-known expression for the susceptibility of finite rings in the limit of zero magnetic field

$$\frac{J\chi}{N g^2 \beta^2} = \frac{K e^K}{4} \left\{ \frac{1 - (\tanh K/2)^N}{1 + (\tanh K/2)^N} \right\} \tag{4.1.18}$$

In the case of chains, the analogues of equations (4.1.15), (4.1.16) and (4.1.17) for the thermal properties are

$$\frac{U}{NJ} = -\frac{1}{2}\left(1 - \frac{1}{N}\right)\tanh\frac{K}{2} = \left(\frac{U}{NJ}\right)_{Lim} \times \left(1 - \frac{1}{N}\right) \tag{4.1.19}$$

$$\frac{S}{Nk} = K\left(\frac{U}{NJ}\right)_{Lim} \times \left(1 - \frac{1}{N}\right) + \ln 2 \cosh\frac{K}{2} - \frac{1}{N}\ln\cosh\frac{K}{2} \tag{4.1.20}$$

$$\frac{C}{Nk} = \left(1 - \frac{1}{N}\right)\frac{K^2}{4}\operatorname{sech}^2\frac{K}{2} = \left(\frac{C}{Nk}\right)_{Lim} \times \left(1 - \frac{1}{N}\right) \tag{4.1.21}$$

We observe the simple convergence properties of chains: the thermal properties clearly differ from their limiting values by terms in 1/N. By contrast, we see that in the case of rings the finite N correction terms have not nearly such a simple form.

Specific Heat

The convergence to the limit $N \to \infty$ for the specific heat function is shown in Fig. (4.1) for ferromagnetic and antiferromagnetic rings and chains. The curves are labelled with the number of spins in each case, with subscripts R and C to denote rings and chains respectively, and prefixes F or A to denote ferro- or antiferromagnets respectively.

(an unmarked curve is invariant). The dashed curve is the limiting $N = \infty$ curve given in Table (4.1). First let us consider the chains for N = 4, 6, 8 and 10. They form a well-behaved set converging monotonically from below, as equation (4.1.21) would lead us to expect. At low temperatures they are in much better agreement with the limit curve than are the corresponding rings. At higher temperatures, kT/J > 0.5, on the other hand, the agreement is not as good, but if points for N = 4, 6, 8 and 10 are extrapolated with 1/N at a fixed temperature, the extrapolations are in excellent agreement with the limit. The chains for odd N values (not shown) form part of the same sequence, i.e. they also converge monotonically from below, the curve for N (odd) lying between the curves for (N-1) (even). For all chains, odd and even, the partition function and hence thermal properties are invariant under the ferro/antiferro transformation. In the case of rings the convergence is much more complicated. Rings give good agreement with the limit at higher temperatures (at sufficiently high temperatures, finite and infinite rings and chains behave asymptotically as $K^2/4$). For example, the 10-ring curve is in 1 % agreement with the limit above kT/J~1.0, the 20-ring curve agrees down to lower temperatures, kT/J~0.6, and the 30-ring down to kT/J~0.45. Since, however, the specific heat maximum, $C_{max}/Nk = 0.439$ occurs at $kT_{max}/J = 0.417$, we must go out to a ring size of about 50 spins before the specific heat maximum is well defined. Let us consider the convergence of the sequence of rings N even, which are invariant under the ferro/antiferro transformation. For N = 10, the maximum is greater than the limiting maximum and occurs at a slightly higher temperature. As N increases, the peak falls in height and moves to slightly lower temperatures. At N = 30, a <u>double</u> maximum begins to develop; and the higher temperature peak eventually, as N further

Fig. 4.1

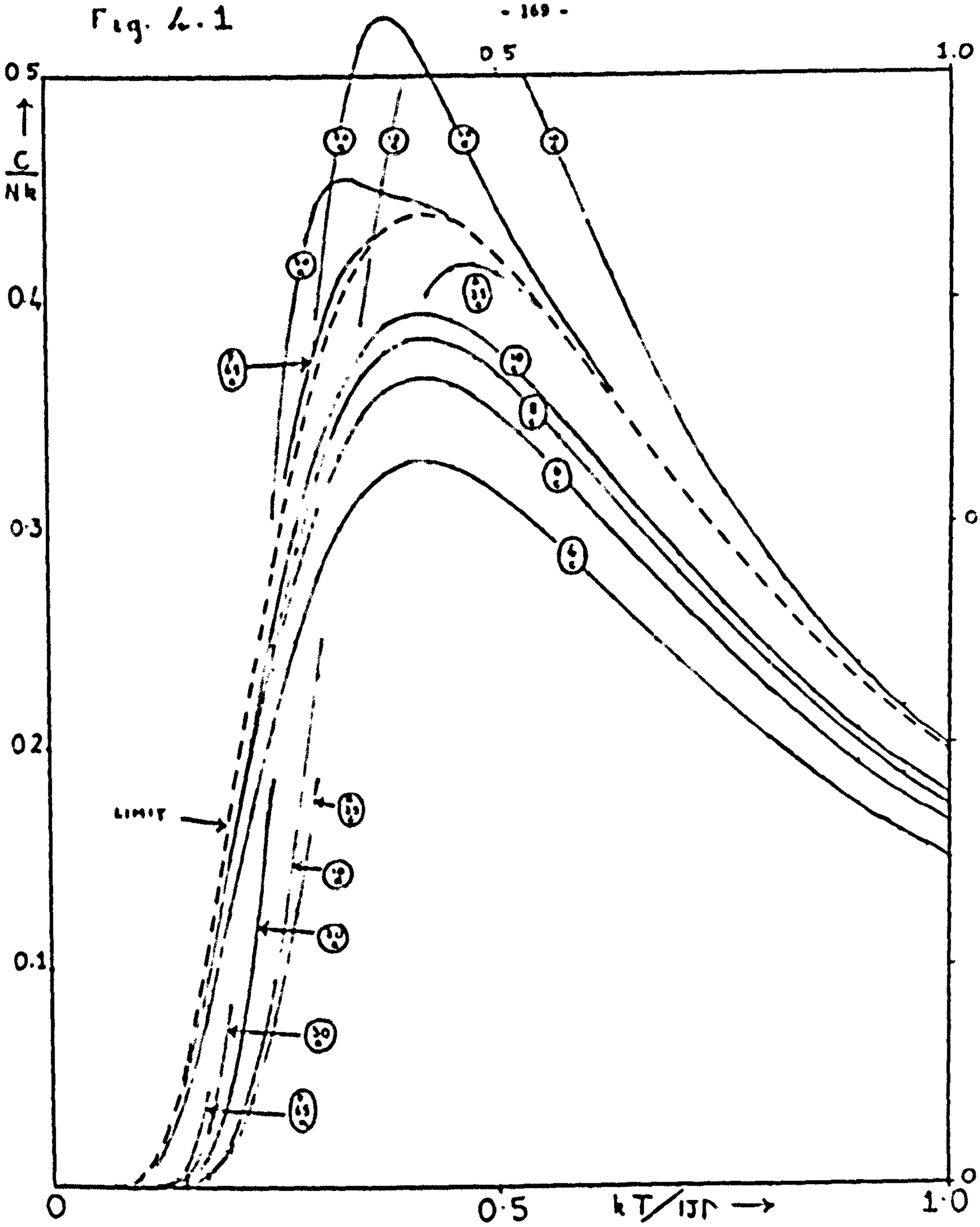

Ising Limit Specific Heat Convergence : Rings and Chains

increases, defines the limiting maximum. Studies of rings up to $N \sim 500$ show that the second, spurious, local maximum appears at consecutively lower temperatures, and is less and less pronounced as N increases. At very low temperatures, the rings appear to tend to a different limit from the chains (and the limit curve itself!). However, we recall the discussion of Chapter III, subsection (2.6) where the energy gaps between the ground and first excited states (and also between the first and second set of excited states) for both ferromagnetic and antiferromagnetic rings is shown to be 2J instead of J as in the case of chains. In this sense the chains are more realistic than rings, since the effective limiting energy gap is also J. The 'artificially large' energy gaps for rings cause the curves to 'take off' from zero at $kT/J \sim 0.125$ instead of $kT/J \sim 0.075$ and also cause the spurious second peak which ultimately disappears as $N \to \infty$. The odd N rings fall into two distinct converging sets for the ferromagnetic and antiferromagnetic limits. The ferromagnetic rings follow the same convergence scheme as the even N rings which we have just described in detail, the curve for N (odd) lying between the curves for $(N \pm 1)$ (even). In the antiferromagnetic case, the even rings converge from above and the odd rings converge monotonically from below, somewhat similarly to the chains. For illustration we compare, in Fig. (4.1), the antiferromagnetic N=25 curve and the ferromagnetic N=65 curve.

For these Ising systems, the monotonicity properties of the chains are obvious from equation (4.1.21) and those of the antiferromagnetic rings may be deduced rigorously, e.g. by differentiating equation (4.1.17) with respect to N. (In addition, it may also be proved rigorously that the internal energy at a given temperature increases monotonically with N in the ferromagnetic case. For the antiferromagnetic

case the energy for even N is monotone increasing in N at a fixed temperature, and for odd N monotone decreasing. Also the antiferromagnetic entropy at a fixed temperature is monotone decreasing in N for N odd.). Our justification for discussing the convergence properties in such detail is that the convergence for anisotropic and Heisenberg coupling appears to be qualitatively similar. We thus have valuable information to help us in investigating the probable form of the limiting curves in these cases.

Antiferromagnetic Susceptibility

In Fig. (4.2) we have plotted as a function of temperature the antiferromagnetic parallel susceptibility in the limit of vanishingly small applied field, i.e. the zero-field response to a magnetic field applied along the z-axis, for rings and chains. Again, the number of spins is shown by a label on the curve together with a suffix R for rings or C for chains. The low temperature region of the limiting curve (see Table (4.1)) is shown dashed; the rest of the curve is well defined by the appropriate odd and even rings. First of all we observe that the even rings for N = 4, 6, 8 and 10 form a well-behaved sequence converging monotonically from below. The 10-spin ring is in 1% agreement with the limiting curve above kT/J ~ 0.7, and is a large enough system to define the maximum of the curve (see equation (4.1.10). The limiting curve at rather lower temperatures is defined by the rings for N = 20 and N = 30. Again we see that the even rings appear to tend to a different low temperature limit from the limit curve, but this is again the effect of the abnormally large energy gap between the antiferromagnetic ground state with $S^z = 0$ and the lowest state with $S^z = 1$, i.e. the first magnetic excitation. It is therefore a feature of the particular choice of boundary conditions.

An interesting feature of the odd N ring susceptibilities is that they ultimately diverge in a positive sense as $T \rightarrow 0$. The smaller the ring, the higher is the temperature at which this paramagnetic behaviour sets in. However the 11-ring is large enough to define the maximum of the limiting susceptibility curve and show a minimum before divergence occurs. As we proceed through a sequence of odd N values to the 29-ring, we see this minimum moving to lower temperatures and expect that in the limit the divergence will no longer occur. The antiferromagnetic ground state for rings is a $|S^z| = 1/2$ state which is 2N-fold degenerate. The corresponding Ising wavefunctions have antiparallel ordering, giving rise to a zero magnetic moment, except for a single pair of parallel 'misfit seam' spins which cause this residual paramagnetism. In the case of general spin S the antiferromagnetic ground state is (2S + 1)N-fold degenerate. The wavefunctions consist of antiparallel ordered spins corresponding to the maximum value of $|S_i^z| = S$ for each spin, together with an extra 'misfit' spin. States with all allowed values of the misfit spin $S_i^z = S, S-1, \ldots -S$ are degenerate in energy. The zero-temperature susceptibility may be calculated from the relation $\frac{\chi J}{N g^2 \beta^2} = \langle (S^z)^2 \rangle - \langle S^z \rangle^2$ where the brackets $\langle\ \rangle$ denote thermal average. Hence we have the general result

$$\frac{|J| \chi_0}{N g^2 \beta^2} = \frac{K \times \left(\sum_{r=-S}^{S} r^2 \right)}{(2S+1)N} \qquad (4.1.22)$$

We see, therefore, that the parallel zero-field susceptibility of antiferromagnetic odd N rings for general S also diverges as $T \rightarrow 0$. [For spin-1/2 the result becomes $|J| \chi / N g^2 \beta^2 \simeq K/4N$ at low temperatures. Hence $\lim_{T \to 0} \lim_{N \to \infty} \left(\frac{K}{4N} \right) \to 0$ and this divergence disappears in the limit.] It is easy to show that relation (4.1.22) also holds for odd N chains. Hence the odd N chains will converge in a

Fig. 4.2

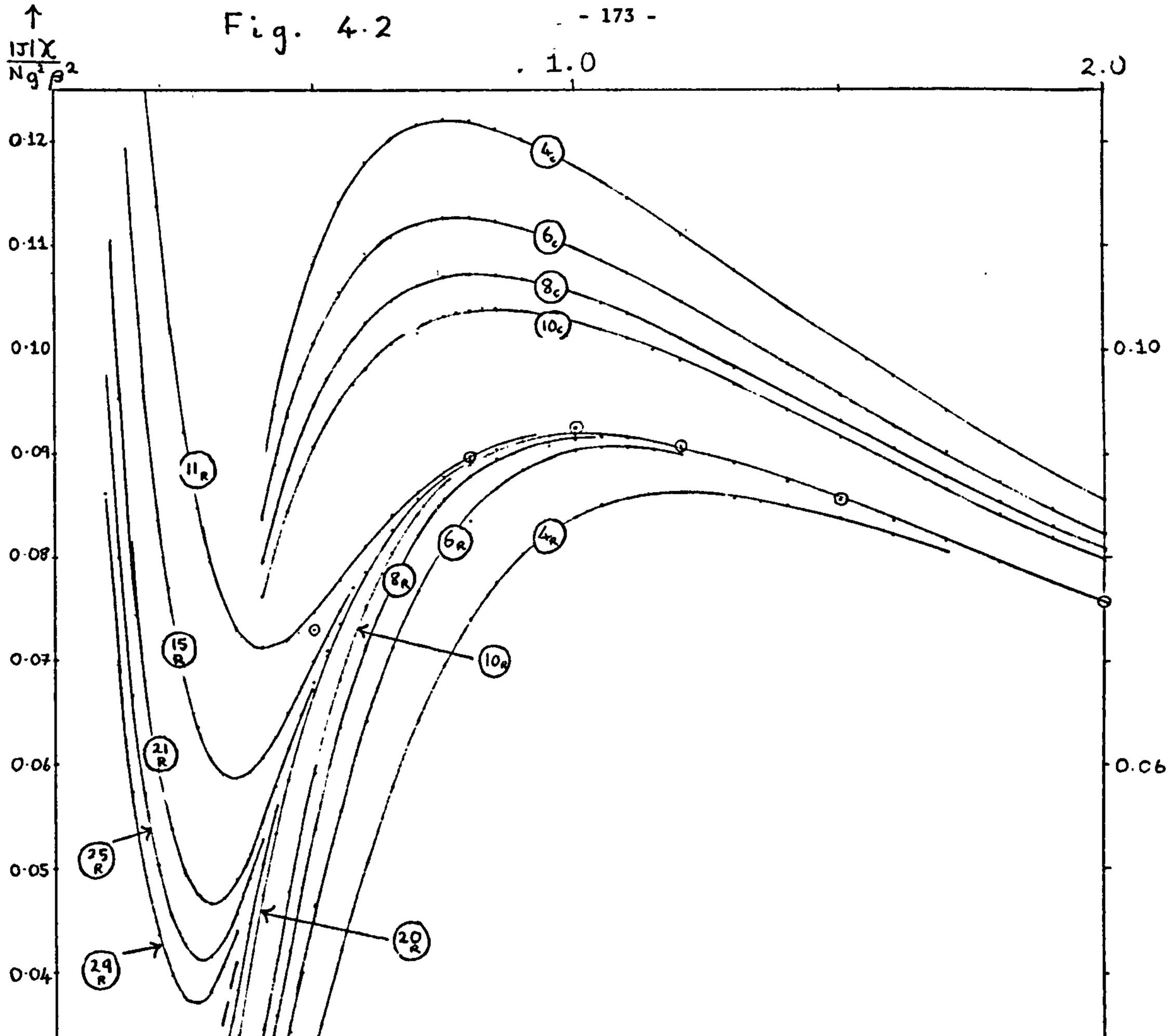

Ising Limit Susceptibility Convergence : Rings and Chains

similar manner to the odd N rings. The even chains, N = 4, 6, 8 and 10, on the other hand, form a well-behaved set converging mononically from above to the limit. At the lowest temperatures the convergence is very good. At higher temperatures, i.e. in the region of or just above the maximum the convergence appears to be slow. If however points for N = 4, 6, 8 and 10 are extrapolated with 1/N at a fixed temperature, the extrapolated points (shown encircled at $kT/|J| = 2.0, 1.5, 1.2, 1.0$ and 0.8) are in excellent agreement with the limiting curve. Below the maximum, at $kT/|J| = 0.5$, the extrapolations are not so good (about 10% agreement with the limit). We thus see the usefulness of taking sequences of chains into account, as well as sequences of rings, in estimating the limit. In the case of short linear systems of about 10 spins, we observe that there is a 12% difference in the height of the maximum and a 15% difference in the location of the maximum between free-ended and periodically bounded systems. This may need taking into account when comparison is made with experimental measurements on linear chain substances.

2. THERMAL PROPERTIES IN THE HEISENBERG LIMIT: ANTIFERROMAGNETS

2.1) Thermal Properties of Rings. Internal Energy

In Fig. (4.3) we show the internal energy per spin in zero field as a function of temperature for antiferromagnetic pure Ising and Heisenberg rings of N = 2 - 11 spins. The values of the energy functions at zero temperature are just the antiferromagnetic ground state energies for $\gamma = 0$ and $\gamma = 1$ discussed in Chapter III, subsections (1.1) and (1.2). We have already observed that odd and even rings form two distinct sequences at T = 0 and we see that this behaviour persists as a function of temperature for both Ising and Heisenberg curves. We have already discussed the monotonicity properties of

g. 4.3

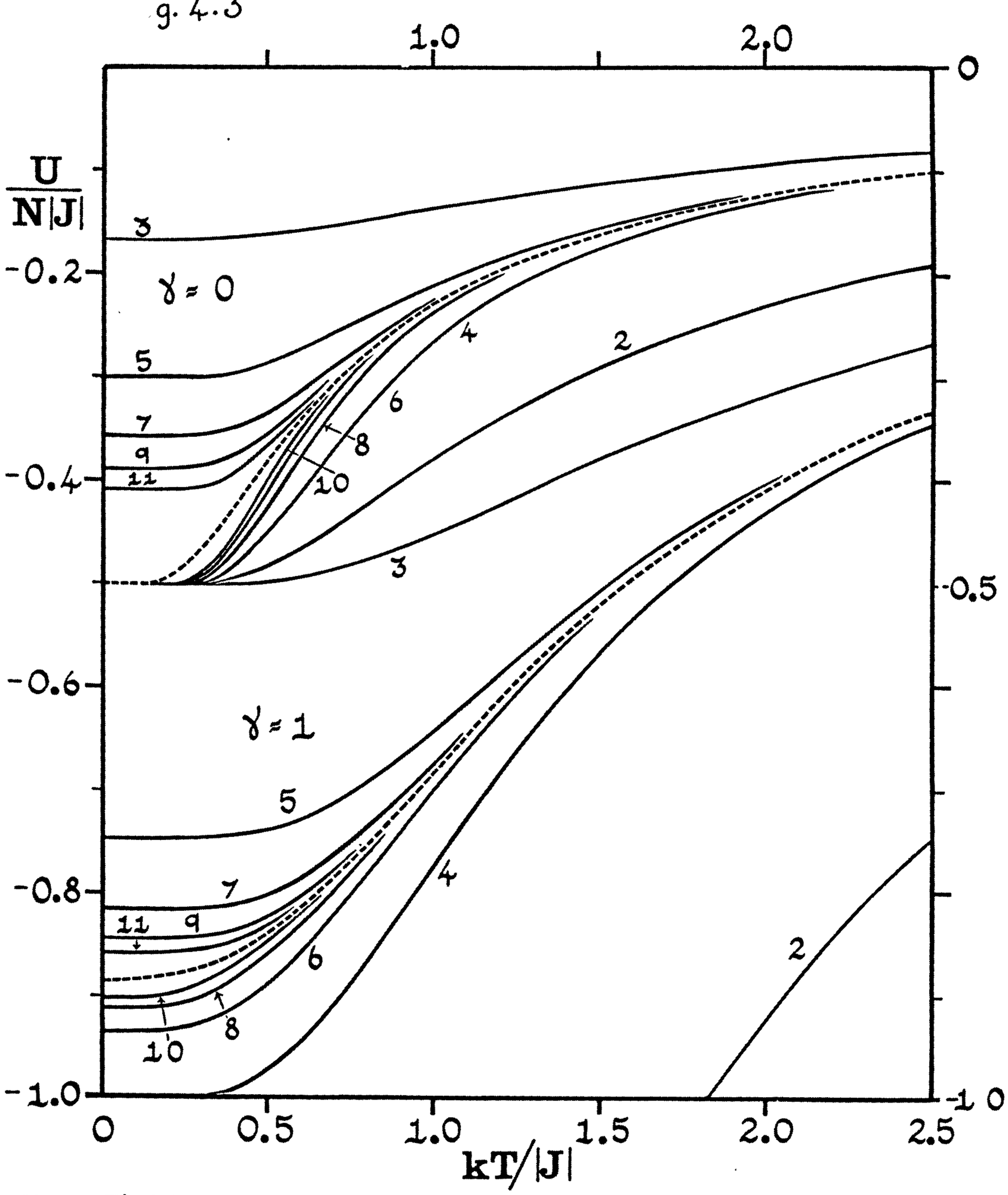

Zero-Field Energy v. Temperature for $\gamma=0$ and $\gamma=1$ (Rings).

the Ising curves (essentially that antiferromagnetic even N curves approach the limit monotonically from one side and odd N curves approach monotonically from the other side), in subsection (1.4) of this chapter. There seems no reason to doubt that the same situation will prevail at $\gamma = 1$. The energy of an infinite Heisenberg chain is thus defined to an accuracy of better than $\pm 0.5\%$ down to temperatures of $kT/J = 0.5$ by the mean of the curves for N = 10 and N = 11. Tabulated values for these two curves and for the estimated limiting curve are given in Appendix 3, Table (VI), together with corresponding values for the entropy and specific heat. Further, since the value at T = 0 is known exactly, even a roughly estimated limiting curve for the intermediate temperature region would be accurate to $\pm 1\%$. We shall shortly discuss in some detail various extrapolation methods for the low temperature portions of the limiting curves for the thermal properties.

Entropy

The entropy for antiferromagnetic Heisenberg rings is shown in Fig. (4.4). The convergence appears to be similar to that for the energy and the limit seems well determined down to $kT/|J| = 0.5$ by interpolation between the curves for odd N and even N. For odd N at T = 0 the ground state is fourfold degenerate and the entropy per spin thus goes to zero only as $2k \ell n\, 2/N$ [For the Ising limit, for odd N, the ground state is 2N-fold degenerate and the entropy per spin goes to zero as $k \ell n\, 2N/N$. For even N, where the ground state is two-fold degenerate the entropy per spin goes to zero as $k \ell n\, 2/N$, whereas in the Heisenberg case the ground state is a singlet for all even N and the corresponding entropy vanishes].

Fig. 4.4

Entropy v. Temperature for Antiferromagnetic Rings at $\gamma=1$

Specific Heat

The specific heats for antiferromagnetic Heisenberg rings are shown in Fig. (4.5). Again the convergence appears to be very similar to the corresponding Ising case. For temperatures above $kT/|J| = 0.5$ for $N > 4$, the convergence appears to be monotonic from above for even N rings and monotonic from below for odd N rings. For lower temperatures the odd N rings continue to converge regularly but the even N rings show a more complicated convergence, with vestiges of the 'spurious bump' or 'second maximum' effect we have discussed in connection with Ising rings in subsection (1.4) of this chapter. At low temperatures, however, we expect the convergence to be rather complex, since, for finite N, the specific heat always vanishes exponentially fast as $T \to 0$, owing to the finite energy gap between the ground and first excited states. As $N \to \infty$, however, the states close up (as 1/N) and merge into a continuum which runs from the ground state (see Chapter III) subsection (3.2)). Hence we would expect a power law behaviour for antiferromagnetic thermal properties at low temperatures.

In the Heisenberg limit, the convergence in the region of the maximum is more rapid than in the Ising case, and the limiting curve (shown dashed) can be estimated quite accurately through the maximum of height

$$C_{max}/Nk \simeq 0.350 \quad (\gamma = 1) \tag{4.2.1}$$

at

$$kT_{max}/|J| \simeq 0.962 \quad (\gamma = 1) \tag{4.2.2}$$

2.2) Weighted Means

The property of monotonic convergence by odd and even N sequences, which is a feature of antiferromagnetic thermal properties, suggests that convergence may be rendered considerably more rapid by taking means of pairs of odd and even N curves. We consider three types of weighted

Fig. 4.5

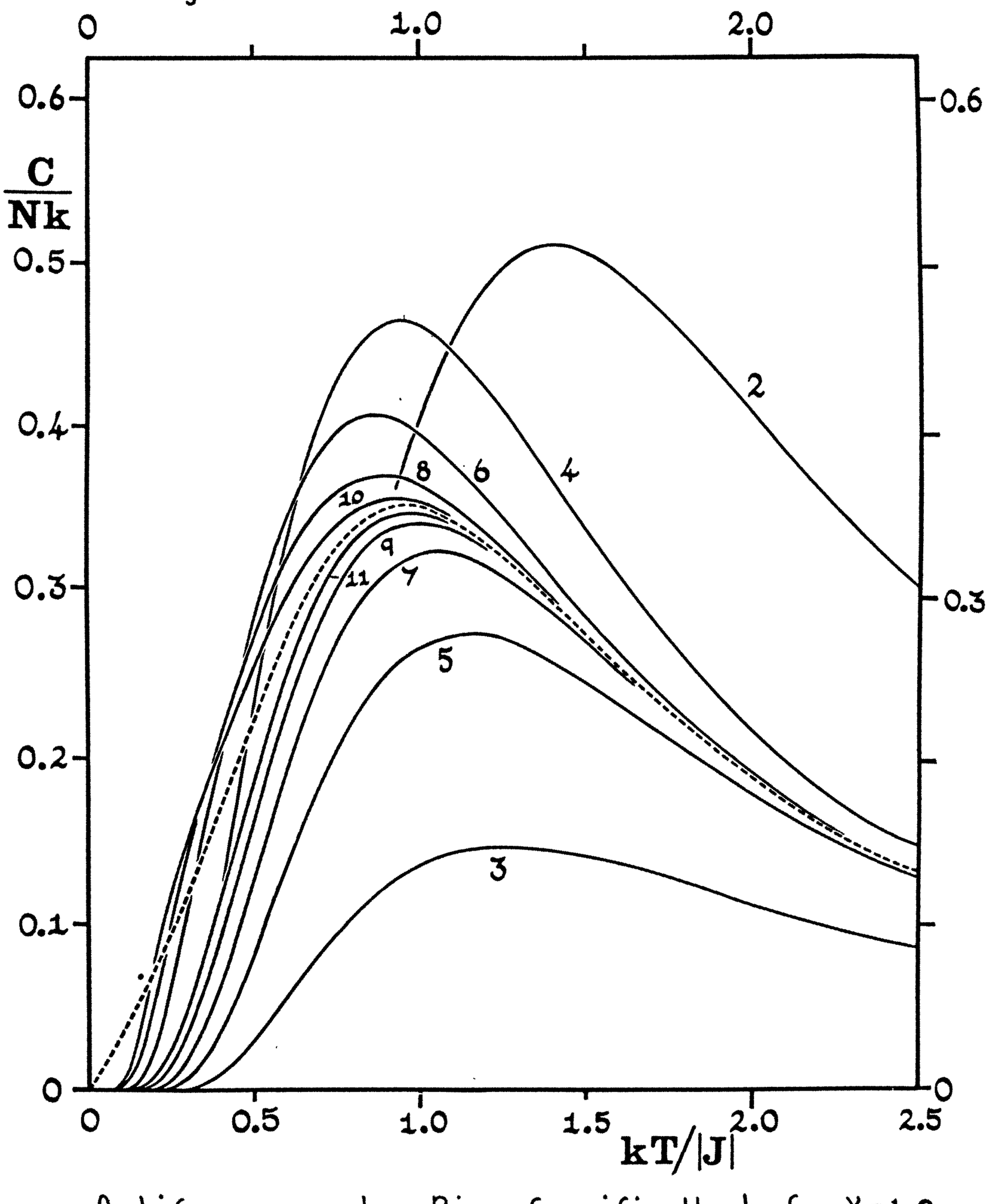

Antiferromagnetic Ring Specific Heats for $\gamma = 1.0$.

means

$$\text{a)}\quad \frac{N P_N + (N-1) P_{N-1}}{(2N-1)} \quad ; \qquad \text{b)}\quad \tfrac{1}{2} P_N + \tfrac{1}{2} P_{N-1}$$

$$\text{c)}\quad \frac{(N-1) P_N + N P_{N-1}}{(2N-1)} \qquad (4.2.3)$$

where P is the thermodynamic property in question. An example of the improved convergence is Fig. (4.6) which shows the specific heat means weighted as in a) for N even and c) for N odd, and which is to be compared with the preceding Fig. (4.5) (actually Fig. (4.6) is drawn to a slightly larger scale — the effect would be even more marked on the same scale as Fig. (4.5)). At temperatures in the region of the maximum and above we still have two monotonic converging sequences, the odd/even and the even/odd sequences. The 11/10 mean and the 10/9 mean appear to bracket the limiting curve very closely, e.g. the discrepancy is only a little over 1% in the region of the maximum.

2.3 Low Temperature Estimates

In connection with the specific heat we have already discussed the reasons for expecting power law behaviour (rather than exponential behaviour as in the case of the Ising model) at low temperatures for antiferromagnetic Heisenberg thermal properties. Suppose we have the following functional form for the limiting internal energy

$$U(T) - U(0) = A N |J| \left(kT / |J| \right)^{\alpha} \qquad (4.2.4)$$

where A and α are fixed (as $T \to 0$) [The corresponding expression for the free energy would be $F = - \frac{A N |J|}{(\alpha - 1)} \left(kT / |J| \right)^{\alpha}$]. Then, for the entropy we have

$$S(T) / Nk = A \alpha (\alpha - 1)^{-1} \left(kT / |J| \right)^{\alpha - 1} \qquad (4.2.5)$$

and for the specific heat we obtain

Fig. 4.6

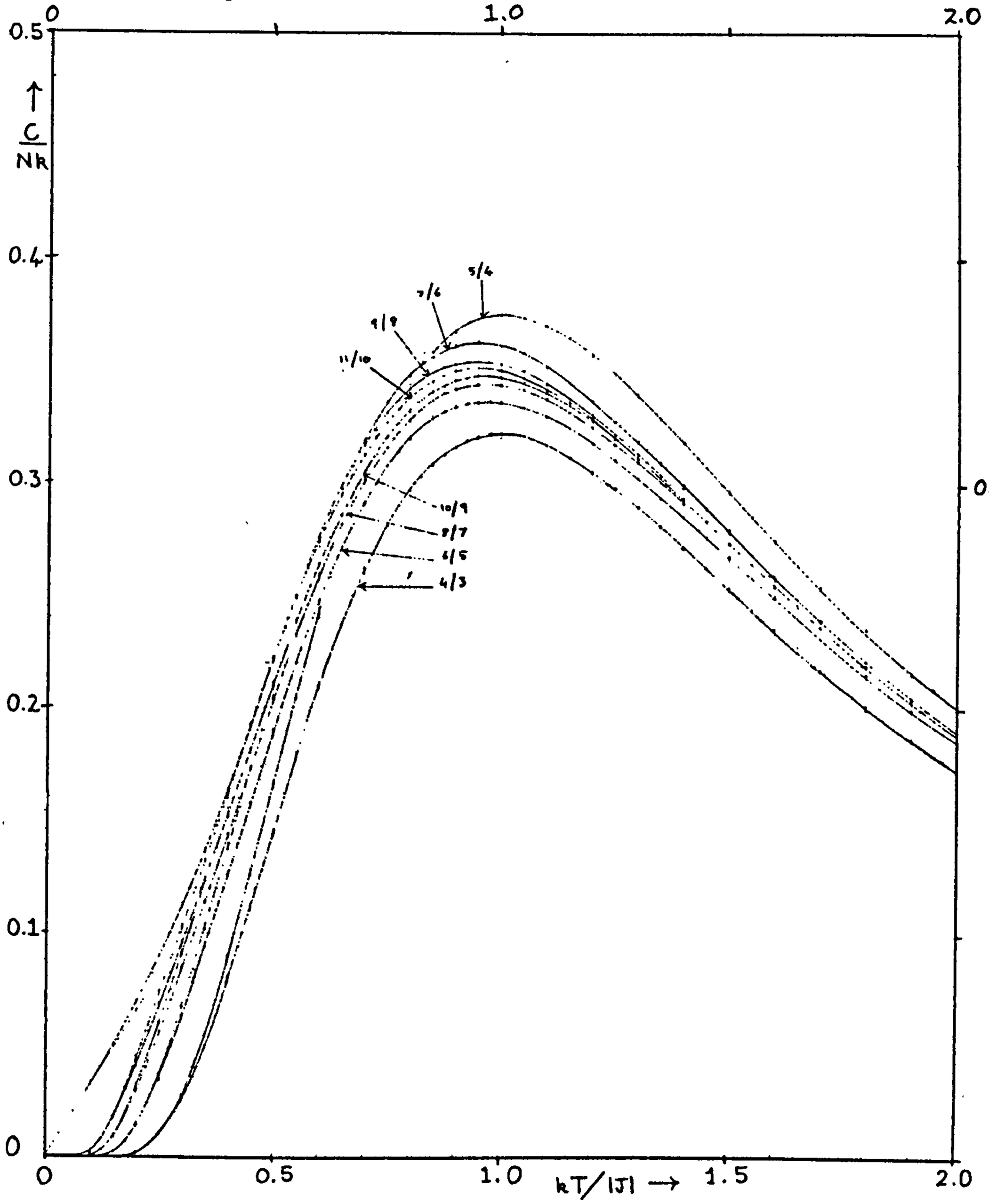

Improved Convergence of Antiferromagnetic Weighted Specific Heat Means: $\gamma = 1.0$.

$$C/Nk = A\alpha\,(kT/|J|)^{\alpha-1} \qquad (4.2.6)$$

By combining equations (4.2.4) and (4.2.5) we obtain

$$U(T) - U(0) = (1-\alpha^{-1})\,TS(T) \qquad (4.2.7)$$

Hence a plot of energy $U/N|J|$ versus $TS/N|J|$ for $N\to\infty$ should be linear, with slope determined by the index α. In Fig. (4.7) this plot is shown for N = 10 and N = 11 and supports the view that the limiting curve would indeed be linear. The solid line which is drawn from the exact ($N\to\infty$) ground state with slope 0.515 should be close to any reasonable 'best fit'. This line corresponds to an estimate $\alpha \simeq 2.06 \pm 0.03$. This value is largely determined by interpolation between data for temperatures in the range $kT/|J| =$ 0.30 - 0.60. The dashed line, on the other hand, is of slope 1/2 and corresponds to $\alpha = 2$ exactly. It seems likely that this is the true limiting value which would be obtained by fitting data for larger N at lower temperatures. These conclusions closely parallel work of Griffiths in an unpublished report (1963). Griffiths plotted $U(T)$ versus $S(T)$ and estimated the index α by fitting B and β in the power law $U(T) - U(0) = B\,S_{(T)}^{\beta}$. By this means Griffiths estimated $\alpha = 2.1$ but also suggested $\alpha = 2$ was probably the exact value. If we assume $\alpha = 2$, the equations (4.2.4) to (4.2.6) become

$$\frac{U(T) - U(0)}{N|J|} = A\left(\frac{kT}{|J|}\right)^2 \qquad (4.2.8)$$

$$\frac{S(T)}{Nk} = 2A\left(\frac{kT}{|J|}\right) \qquad (4.2.9)$$

and

$$\frac{C}{Nk} = 2A\left(\frac{kT}{|J|}\right) \qquad (4.2.10)$$

Fig. 4.7

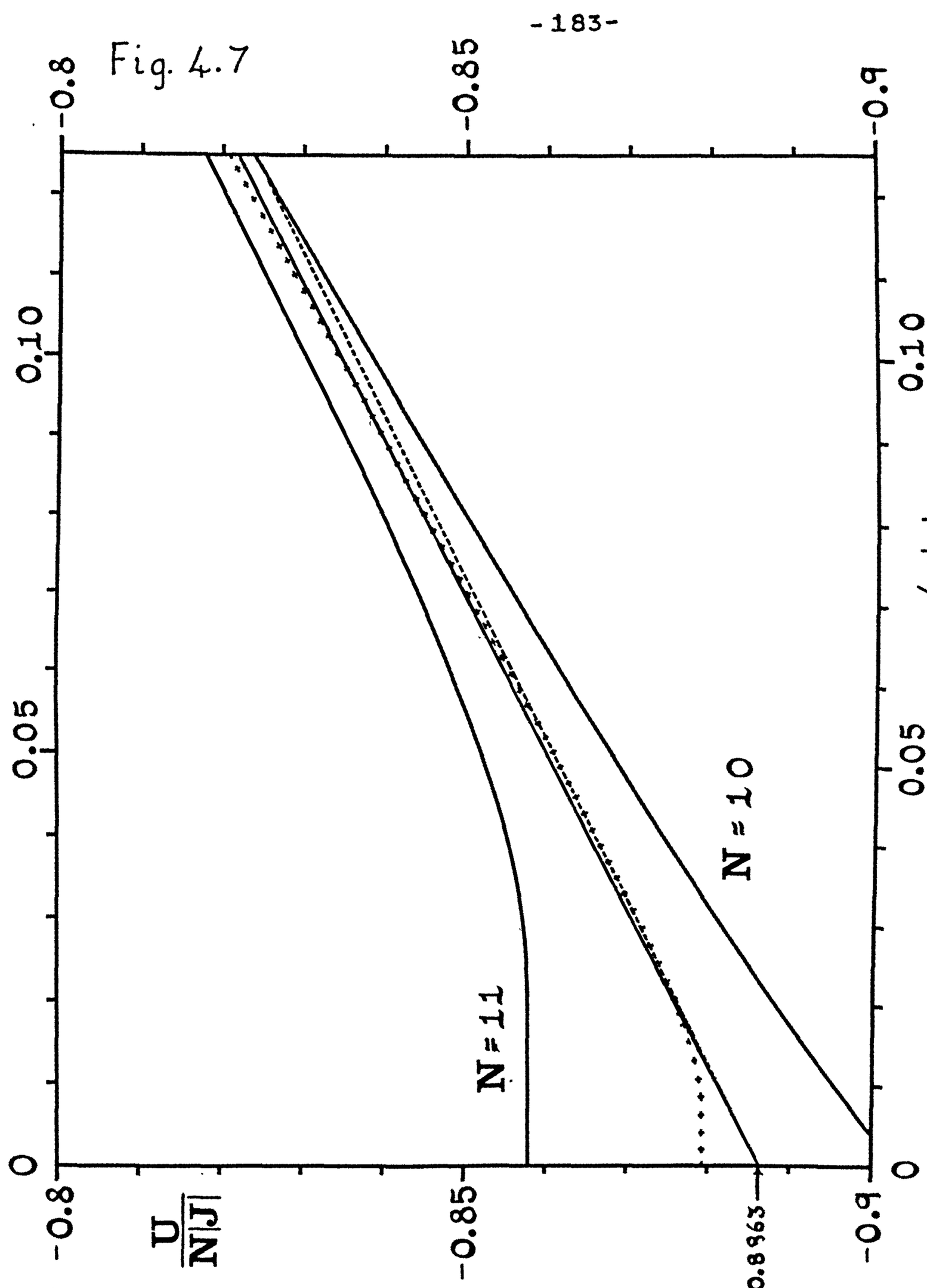

ıtiferromagnetic Energy v. Temperaturex
Entropy for $\gamma = 1.0$.

The amplitude A may now be estimated in a variety of ways a) by curve-fitting for the temperature variation of $\frac{U(T)}{N|J|}$ and $\frac{TS}{N|J|}(T)$; b) from plots of $U/N|J|$ versus $(S/Nk)^2$ using the weighted means; and c) from the slope of the weighted entropy means at low temperatures.

To give some idea of the reliability of the procedure we show in Fig. (4.8), the entropy means weighted as in b), 5/4, 7/6, 9/8, and 11/10. We assume that in the limit these means will come into T = 0 as T, and hence we draw tangents from the origin to the curves, obtaining a regular sequence of values for the slopes (2A) of 0.363, 0.355, 0.349 and 0.345. If this trend were to continue, we would expect a limiting slope of $\alpha \simeq 0.34$. However, other procedures suggest a slightly higher value, and we finally conclude that $2A = 0.35 \pm 0.01$. Hence we have the estimated asymptotic results

$$U(T) \simeq U(0) + 0.175\, N|J| \left(kT/|J|\right)^2 \qquad (4.2.11)$$

$$S(T) \simeq 0.35\, Nk \left(kT/|J|\right) \qquad (4.2.12)$$

and

$$C(T) \simeq 0.35\, Nk \left(kT/|J|\right) . \qquad (4.2.13)$$

These results have been used to estimate the limiting curves (shown dashed) on Figs. (4.3), (4.4) and (4.5) respectively, and are in close agreement with Griffiths' unpublished estimates (1963).

2.4) Spin-Wave Theory Predictions

Let us compare the low-temperature numerical estimations for the thermal properties with the predictions of a simple form of spin-wave theory; namely a bose-type harmonic oscillator approximation based on the des Cloizeaux and Pearson (1962) fundamental dispersion relation.

Fig. 4.8

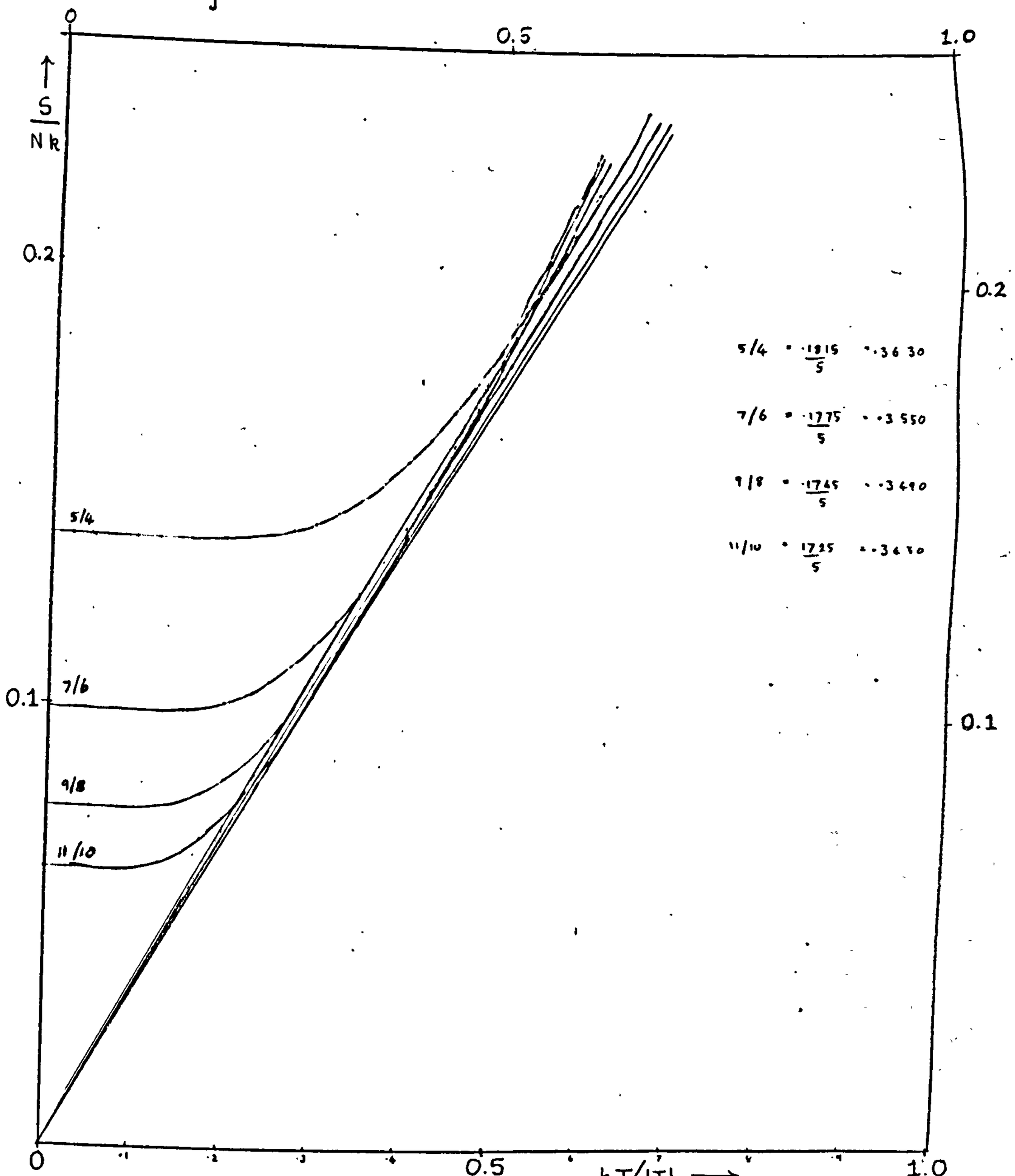

Limiting Low Temperature Thermal Behaviour: Weighted Entropy Mean Estimates

It is easy to show that the harmonic oscillator approximation in conjunction with a general dispersion relation $\varepsilon(k)$ yields the following expressions for the free energy and internal energy respectively:

$$-F/kT = \frac{N}{2\pi}\int_0^{\pi} \ln\left[1 - \exp\left(-\beta\varepsilon(k)\right)\right] dk \qquad (4.2.14)$$

and
$$u - u_o = \frac{N}{\pi}\int_0^{\pi/2} \frac{\varepsilon(k)}{e^{\beta\varepsilon(k)} - 1}\, dk \qquad (4.2.15)$$

where $\beta = (kT)^{-1}$.

These formulae assume a basic Brillouin zone from 0 to π containing N/2 energy states spaced at a frequency interval of $\Delta k = 2\pi/N$ (see Chapter III, subsection (5.4)). Substituting the des Cloizeaux and Pearson formula
$$\varepsilon(k) = \pi |J| \sin k \qquad (4.2.16)$$
we have for the internal energy

$$u - u_o = N|J| \int_0^{\frac{\pi}{2}} \frac{\sin k \; dk}{e^{\pi\beta|J|\sin k} - 1} \qquad (4.2.17)$$

The low temperature assumption allows us to consider only states near the antiferromagnetic ground state, i.e. k is small and $\sin k \simeq k$. With a convenient change of variables, equation (4.2.17) becomes

$$\frac{u - u_o}{N|J|} \simeq \frac{1}{(\pi\beta|J|)^2}\int_0^{\alpha} \frac{x}{e^x - 1}\, dx \qquad (4.2.18)$$

the upper limit, α, may be replaced by $+\infty$, and the integral evaluated in terms of Riemann-Zeta functions as

$$\frac{u - u_o}{N|J|} \simeq \frac{1}{(\pi\beta|J|)^2}\zeta(2) \simeq \frac{1}{6}\left(\frac{kT}{|J|}\right)^2 \qquad (4.2.19)$$

We observe with interest that spin-wave theory predicts the same power of T as we find numerically, namely T^2, for the internal energy (and also for the free energy). Also the value of the coefficient, 0.167, in equation (4.2.19) is very close to the approximate value 0.175

obtained numerically (see equation (4.2.11)). This feature was first discussed by Griffiths (unpublished report, 1963) who felt the agreement was spurious since he was able to demonstrate that the spin-wave states make a negligible contribution to the partition function for finite temperatures. However we have been able to identify additional states, which are not in accordance with the spin-wave prescription, in the spectrum of the finite N systems (see Chapter III, sub-section (5.3)) which appear to have very similar dispersion behaviour to the spin-wave states. If this second class of states is sufficiently numerous in the limit, $N \to \infty$, equation (4.2.19) may still be a valid and reasonable low temperature approximation to the limiting thermal properties of the antiferromagnetic linear chain.

Finally, we remark that a higher-order form of spin-wave theory due to Kubo (1952) also predicts a T^2-like dependence for the antiferromagnetic energy at low temperatures, but the corresponding constant, $\pi/6$, is appreciably larger.

2.5) Thermal Properties of Chains

We have seen in our previous discussion of the Ising model that free-ended chains form an alternative sequence, with different convergence properties, for estimating the limiting thermal properties. Unfortunately, it appears that in the antiferromagnetic limit, for the Heisenberg model, chain convergence is irregular and rather poor. As an example, in Fig. (4.9) we display the low temperature entropy curves for chains, hoping for further evidence in confirmation of our low temperature entropy limiting behaviour. However, the entropy curves cross each other in the temperature region $kT/|J| = 0.4$ to 0.8. The antiferromagnetic specific heat curves in Fig. (4.10) are also irregular. However the maximum for N = 6 is only slightly higher

(less than 0.5%) than that of the estimated limiting curve, while the height of the N=8 chain curve is actually the same as for the estimated limit! Further for temperatures between kT/|J| = 0.4 to 2.0 these two curves are very similar in shape to the limit. (For lower temperatures the chains slow the Ising-like 'spurious-peak' convergence.) However the positions of their maxima are 10-12% away from the limit, and it is not clear what the pattern of convergence for N> 8 will be. The 3-chain is included as a sample of the odd N behavior.

2.6) High-Temperature Series Expansions

In subsection (2.2) of Chapter (I) we have outlined the method of high-temperature series expansions, the most successful method to date for treating the Heisenberg and anisotropic models with general (in practice rather small) spin values and nearest- and further-neighbour interactions. A particular case of a more general theorem tells us that a power series expansion in K = J/kT of the logarithm of the partition function in a) zero and b) a finite magnetic field of a ring-cluster of N spins agrees through the first (N-1) coefficients (or through the power K^{N-1}) with the corresponding expansion of the infinite linear lattice. Hence it was possible to obtain the coefficients through K^{10} in the expansion of the zero-field free energy and also the coefficients through K^{10} of the susceptibility high-temperature expansions for the linear chain. [With the aid of auxiliary theorems one or two additional terms in each expansion may be obtained from the same cluster. However there is appreciable loss of accuracy in the higher terms, essentially as a result of the limited accuracy of the cluster eigenvalues themselves.] When the series for the thermodynamic properties were analytically continued with the aid of Padé approximant techniques, reasonable agreement was obtained with the direct extrapolations of, for example, the specific heat and

Fig. 4.9

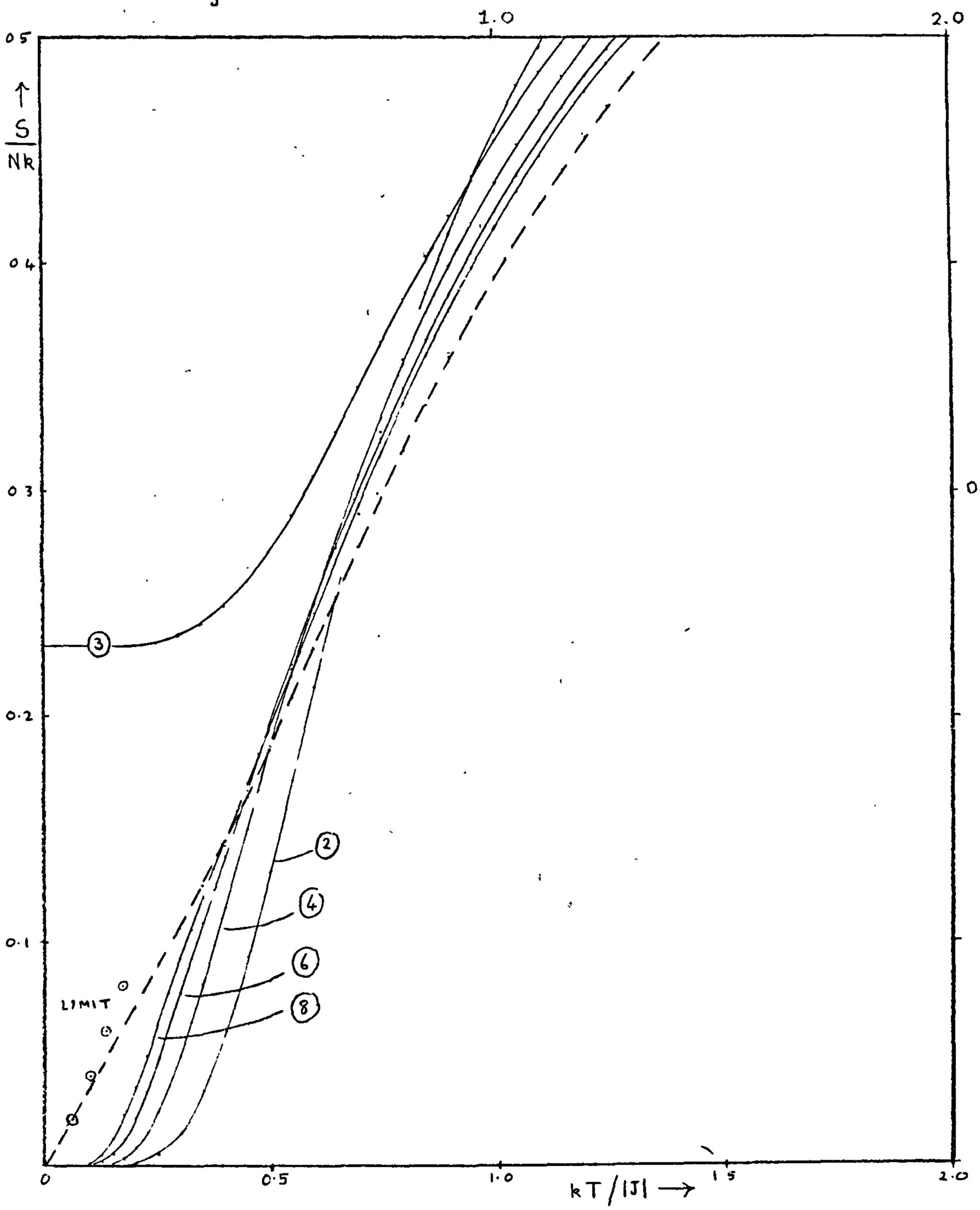

Entropy versus Temperature for Antiferromagnetic Heisenberg Chains

susceptibility in a temperature range extending upwards from just below the maximum in each case. At lower temperatures the various extrapolation techniques on finite clusters just described yielded much more information on probable low-temperature limiting behaviour. Recently, however, Baker, Rushbrooke and Gilbert (1964) have considered high-temperature series expansions for general spin-1/2 clusters of up to and including 10 spins. As a by-product of this undertaking they observed that the sub-set of clusters corresponding to free-ended linear chains gave essentially twice as many terms in the zero-field free energy expansion as did the corresponding ring clusters (polygons). This breakthrough enabled them to obtain a free-energy expansion with coefficients correct up to 21 terms by considering the 10-spin chain. (In the case of a magnetic field, however, their technique breaks down and they were able to obtain only the first 10 terms in the susceptibility expansion). It was therefore of great interest to independently apply Padé approximant techniques to the B.R.G. published series. As was to be expected, the longer series gave more information at low temperatures than our ring series. Since we expect the specific heat to vanish as T, the Padé sequence of prime interest is the [N+1, N] sequence. [The Padé approximant notation used in this thesis is [Denom, Num.] where the first term in the square bracket denotes the number of terms in the denominator and the second term denotes the number of terms in the numerator.] Bearing in mind that the high-temperature series is a series in reciprocal temperature, it is easy to see that such Padé's behave asymptotically as T at low temperatures. In addition, and as a possible check on the correctness of our T conjecture, we have examined sequences of [N, N] and [N + 2, N] Padé's, vanishing as a constant and as T^2 respectively. Baker, Rushbrooke and Gilbert performed their own Padé

Fig. 4.10

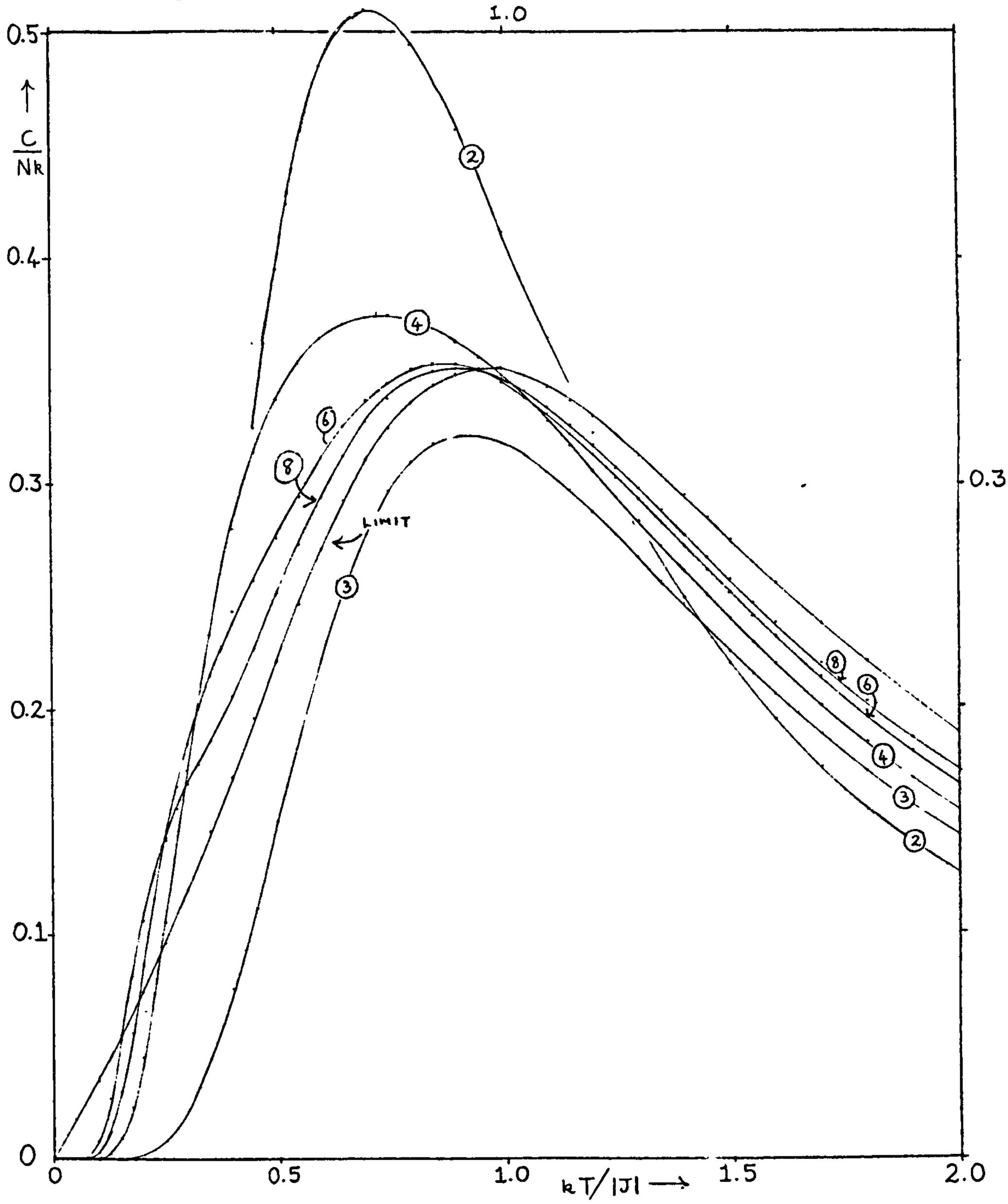

Variation of Specific Heat with Temperature for Antiferromagnetic Heisenberg Chains

analyses on this series and concluded that a branch cut crossing the negative real axis at about $kT/|J| = -2$ was spoiling the convergence of the Padé sequences below about $kT/|J| = 0.6$. We do appear to see evidence of such a branch cut, roughly an arc of a circle in form, behaving as described. Certainly it appears that the [N+1, N] and the [N+2, N] Padé sequences are affected by rather strong poles in this low temperature region. In Fig. (4.11) we display the [11,10] and [9.8] Padé's, for which the corresponding evaluations are identical as far as we have plotted them. They appear to behave well down to a temperature of about $kT/|J| = 0.5$ or perhaps 0.4, and are in excellent agreement with our extrapolations over this range. At lower temperatures, however, they encounter a pole at $kT/|J| = 0.054$ and consequently their behaviour is unreliable. The [10,9] Padé runs rapidly into trouble with a pole at $KT/|J| = 0.588$ and is not useful. It is interesting that the [10,10] and [9,9] Padés, which show perfect convergence but which go in to T=0 as a rather small positive constant (0.077) do not show these troublesome poles. However, since they do not show the expected asymptotic low temperature behaviour we are not inclined to rely on them below $T = 0.5$ or perhaps 0.4. Finally we observe that the [11,9] Padé finds a pole at $kT/|J| = 0.361$. We conclude, therefore, that the antiferromagnetic Padé approximants are likely to be reliable down to about $kT/|J| = 0.5$, and are in excellent agreement with our extrapolations. The evidence of the [10,10] and [11,10] Pade's in the region 0.4 to 0.5 suggests that the limiting curve may lie about 2% lower than our extrapolations in the region 0.2 to 0.5, but this is very tentative. The agreement with each other of the [11,10] and [9,8] Padé series and the [10,10] and [9,9] series, shows that the 21 term series is long enough to show about four figure convergence right down to T=0.

Fig. 4.11

Antiferromagnetic Specific Heat: BRG Pade' Approximants for $\gamma = 1.0$

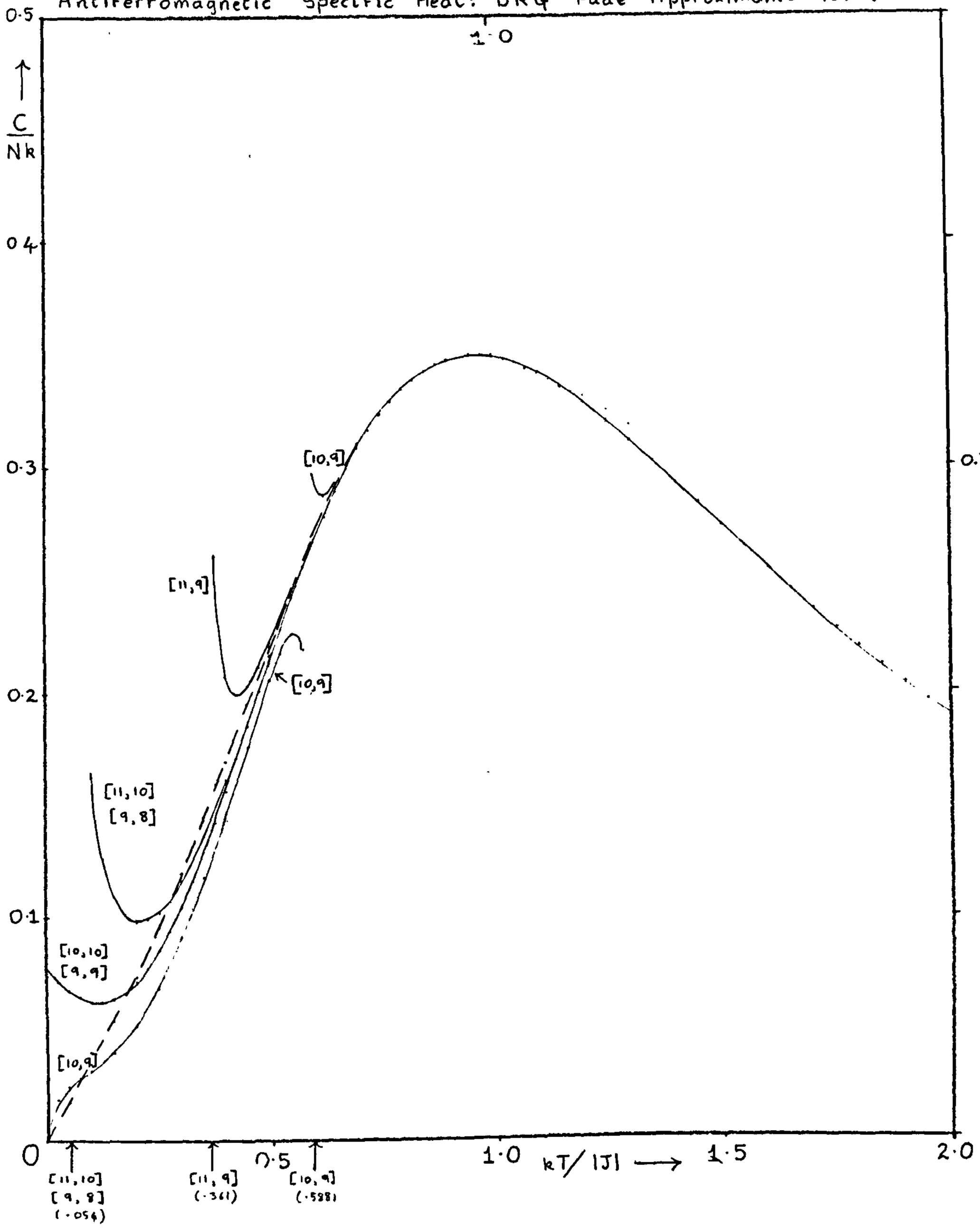

Unfortunately, the occurrence of the poles causes convergence to the wrong values. As Baker suggests, these poles are probably related to the existence of the branch cut crossing the negative real axis. There is, we feel, also a possibility, though not a strong one, that these divergences are the result of incorrect asymptotic behaviour near T=0. Perhaps it might be worth investigating the $T^{1/2}$ Padé sequence as a check on this, although these Pade's are much less straightforward to perform.

Finally, the excellent agreement of the Pade's with our extrapolation in the region of a maximum suggests that we use the more precise Padé evaluations to obtain the position and height of the peak to higher accuracy. We conclude that

$$C_{max}/Nk = 0.3497 \pm 0.0001 \qquad (4.2.14)$$

$$\text{at} \quad kT_{max}/|J| = 0.961 \pm 0.001 \qquad (4.2.15)$$

(cf. equations (4.2.1) and (4.2.2)).

We have also examined the Padé approximants for the internal energy and the entropy. However, again we run into trouble with poles below about $kT/|J| = 0.5$, just as in the case of the specific heat. Since the energy and extropy are less sensitive functions than the specific heat, we believe our own extrapolations should really be quite reliable down to T = 0, and, in these two cases, clearly superior to the B.R.G. Pade's. In the case of the specific heat, extrapolations and Pade's are comparable.

2.9) Comparison with Other Models and Approximations.

Let us now compare our numerically estimated limiting curves with the predictions of some closed form approximations (the more successful in the field), and the X-Y model of magnetism. The appropriate

curves are shown in Fig. (4,12). Curve (C) is the specific heat curve for the spin-1/2 X-Y model which has the Hamiltonian (for linear n.n chains)

$$\mathcal{H}^{X-Y} = 2J\sum_{i=1}^{N}\left(S_i^x S_{i+1}^x + S_i^y S_{i+1}^y\right) \qquad (4.2.16)$$

Katsura (1962) solved the model exactly for the thermodynamic properties. The analytic expression for the specific heat is

$$\frac{C}{Nk} = \frac{4k^2}{\pi}\int_0^{\pi}\frac{\cos^2 k\ dk}{\cosh^2(2K\cos k)} \qquad (4.2.17)$$

where $K = |J|/kT$ and curve (C) was obtained by numerical integration. The curve has a maximum

$$C_{max}/Nk \simeq 0.3260 \pm 0.0001 \qquad (4.2.18)$$

at $KT_{max}/|J| = 0.635 \pm 0.005$. (4.2.19)

The low-temperature expansion is

$$C/Nk \simeq \frac{\pi}{6K} + \frac{7}{240}\frac{\pi^3}{K^3} + \cdots\cdots \qquad (4.2.20)$$

and the high-temperature expansion is

$$C/Nk \simeq K^2/2 - 3K^4/8 + \cdots\cdots \qquad (4.2.21)$$

The overall shape of the curve is rather similar to that of our limiting curve (a): in particular, the specific heat varies as T $(C/Nk \simeq 0.5236(kT/|J|))$ at low temperature. A rather successful approach to the linear Heisenberg antiferromagnetic model is the Hartree-Fock approximation of Bulaevskii (1963). The specific heat is given by the for mulae:

$$1 - p = \frac{2}{\pi}\int_0^{\pi}\frac{\cos k\ dk}{1 + \exp\left(\frac{2p}{T}\cos k\right)} \qquad (4.2.22)$$

where

$$C/Nk = -0.5\,p\,\frac{dp}{dT} \qquad (4.2.23)$$

The quantity p was obtained, self-consistently, by repeated numerical integration of equation (4.2.22), and the resulting curve for the specific heat is shown as curve (d) in Fig. (4.12). The maximum is given by

$$C_{max}/Nk \simeq 0.382 \pm 0.001 \qquad (4.2.24)$$

$$\text{at} \quad kT_{max}/|J| \simeq 1.02 \pm 0.01 \qquad (4.2.25)$$

The low-temperature expansion is given by Bulaevskii as

$$C/Nk \simeq \frac{\pi T}{6(1+2/\pi)} + O(T^3) \simeq 0.3200\,T + \cdots \qquad (4.2.27)$$

and the high-temperature expansion is $C/Nk \simeq$ (4.2.28)

Katsura and Inawashiro (1964) attempted an approximation method which treated the X-Y model as the unperturbed Hamiltonian with the additional terms (components in the z direction) of the full Heisenberg Hamiltonian as a perturbation. The resulting approximation to the antiferromagnetic specific heat is curve (e) in Fig. (4.12). Clearly the convergence of this method is distinctly poor.

Accordingly, Katsura and Inawashiro have recently (1965) employed a similar perturbation method which, however, treats the approximate Hamiltonian of Bulaevskii as the unperturbed Hamiltonian. Curve (f) in Fig. (4.12) (shown dashed) is the resulting specific heat curve (read off Fig. (11) of Katsura and Inawshiro (1965).) The agreement with our limiting curve appears to be rather good (i.e. to within a few percent) over the whole range of temperature.

3) THERMAL PROPERTIES IN THE HEISENBERG LIMIT: FERROMAGNETS

3.1) Thermal Properties of Rings

Internal Energy. Let us, first of all, plot the energy per spin as a function of temperature for N = 3, 4, ... 11 spins in Fig. (4.13).

Fig. 4.12

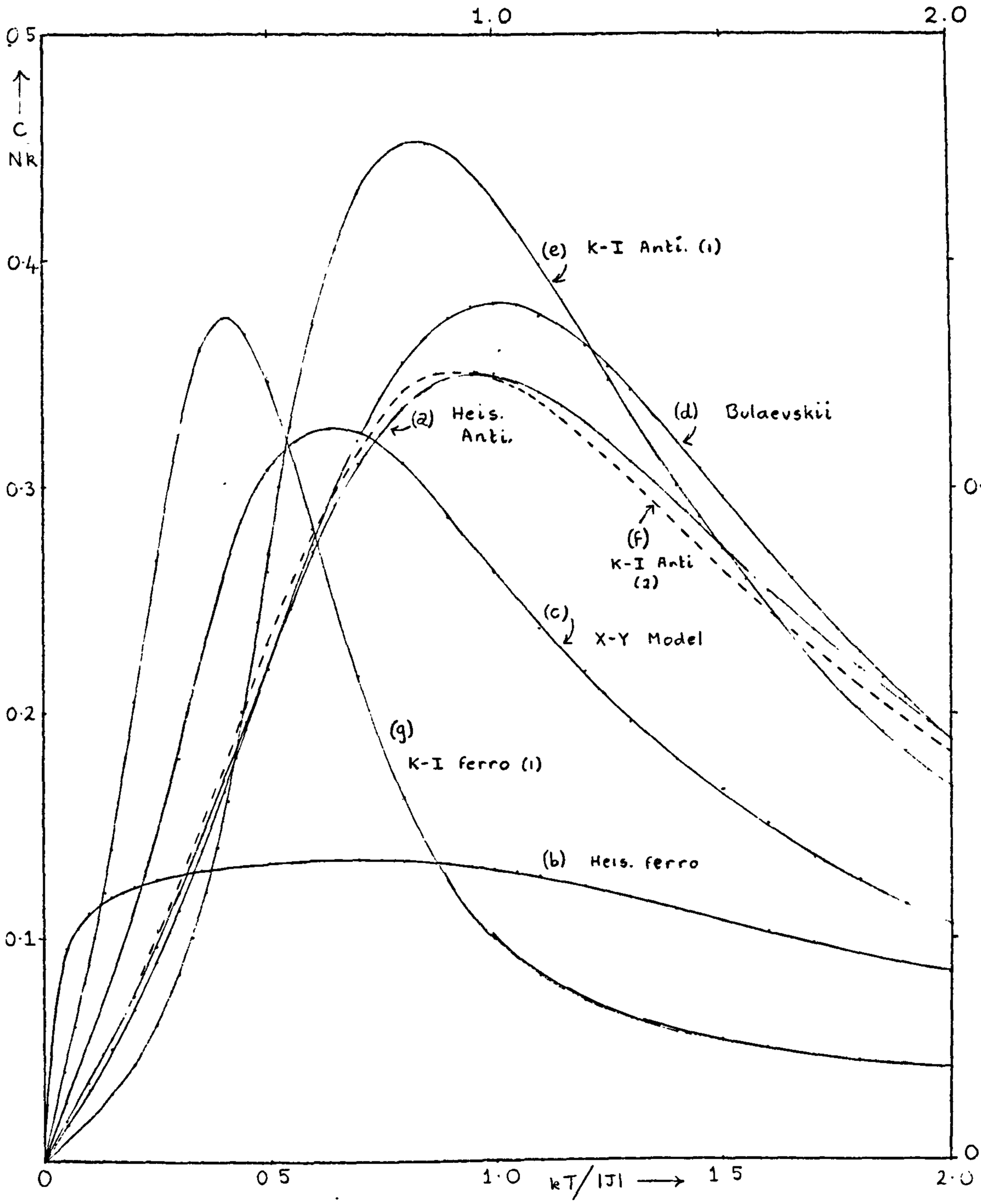

Heisenberg Specific Heats : Comparison of Various Models and Approximations

In contrast to the antiferromagnetic case, the curves for finite N do not appear to bracket the limiting curve but rather increase monotonically towards it. Their behaviour is very similar to their counterparts in the Ising limit. (See inset in Fig. (4.13) on a smaller scale.) We see at once that low temperature extrapolations will be much more difficult than in the antiferromagnetic case. However, above KT/J = 0.5 the convergence is rapid, and the limit seems quite accurately defined. Note that, as in the Ising case, all curves approach the exact limiting ground state $\mathcal{E}_o = -0.5$. In Table (VII) of Appendix 3 we present tabulated values of the curves for N=10 and N=11 together with the estimated limiting curve, for the energy, entropy and specific heat.

In Fig. (4.14) we show a selection of curves, rings and chains, for the entropy per spin. The ring curves show a complicated convergence, successive curves crossing at low temperatures, similar to the antiferromagnetic Ising even N rings and the ferromagnetic Ising rings (see inset graph on same scale for the latter). The chains, on the other hand, for N = 4, 6 and 8 are well-behaved, apparently converging monotonically to the limit. Although, as is usual with chains, they do not converge very rapidly at higher temperatures, the shape of the N=8 chain is clearly very similar to the estimated limiting curve, for which we expect it to provide an upper bound. We know that the ferromagnetic ground state is (N+1)-fold degenerate for both rings and chains. Hence the zero-point entropy is

$$S_o / Nk = \ln (N+1) / N \quad , \qquad (4.3.1)$$

which approaches zero rather slowly.

The specific heats of Heisenberg rings for N = 4 to 11, inclusive, are shown in Fig. (4.15). Again there is no bracketing effect, and the

Fig. 4.13

Ferromagnetic Ring Energies for $\gamma = 1.0$ and also $\gamma = 0$ (Inset)

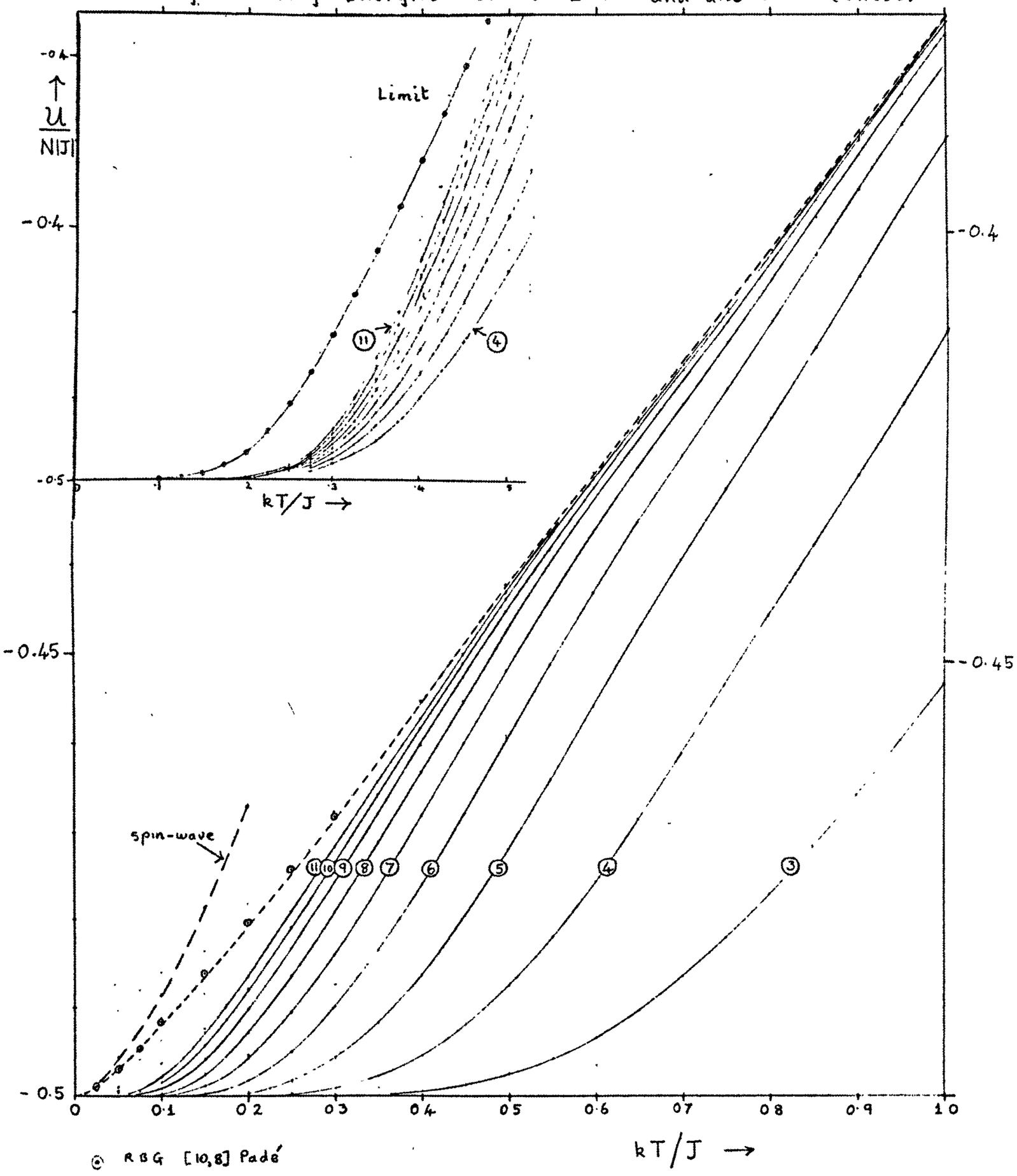

Fig. 4.14

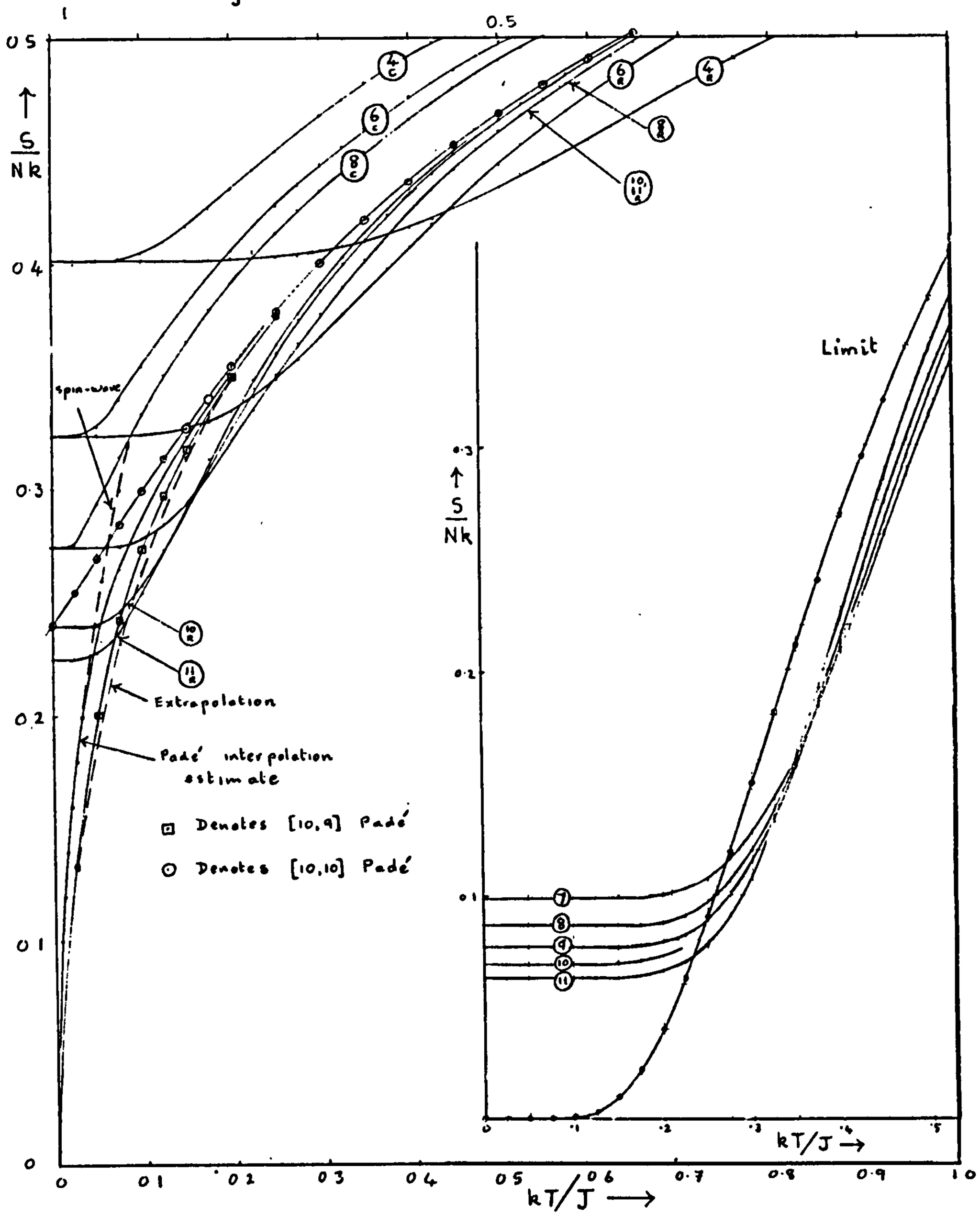

Ferromagnetic Entropies : Rings and Chains for $\gamma = 1.0$: ' Rings for $\gamma = 0$ (Inset)

Fig. 4.15

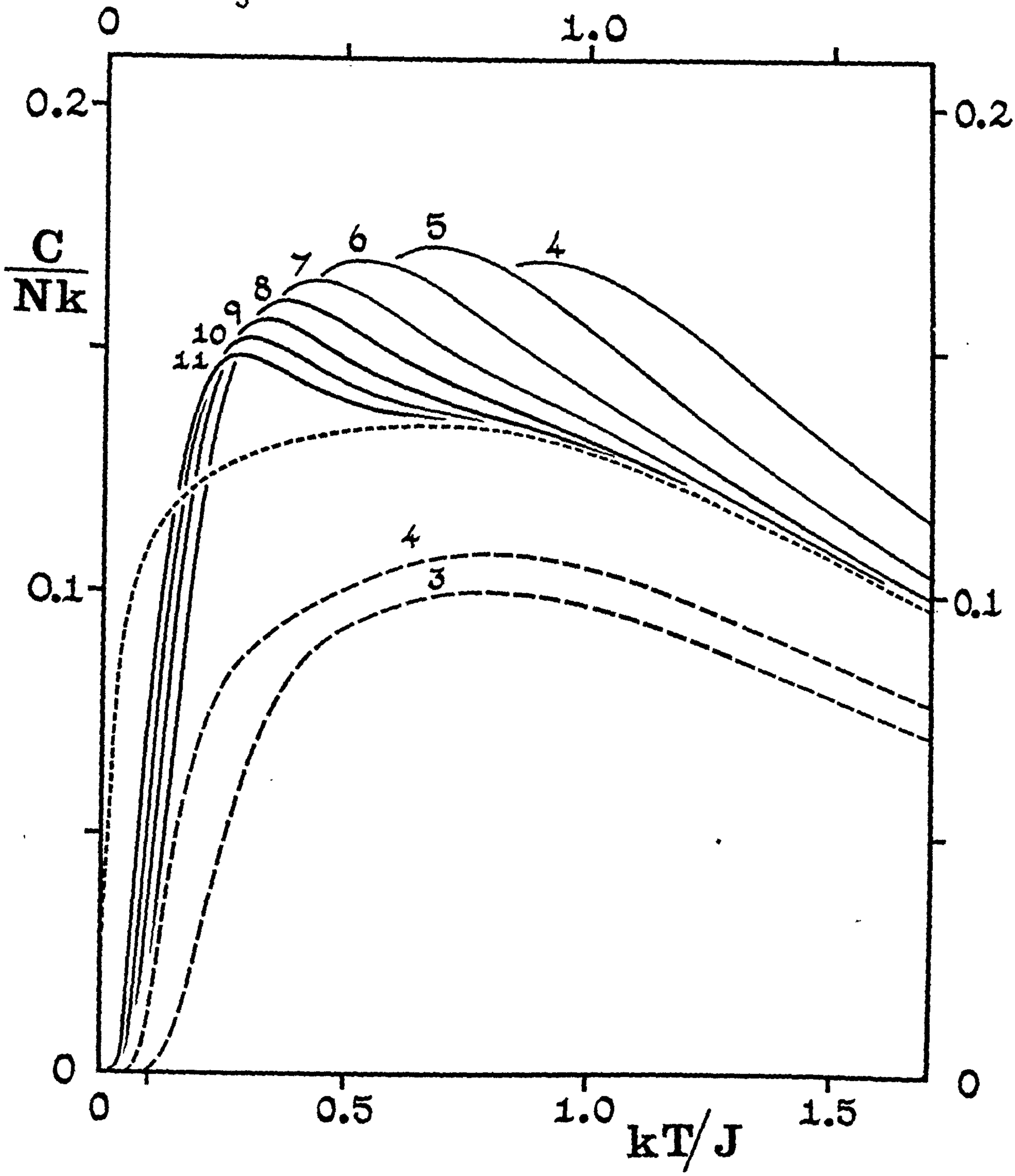

Ferromagnetic Specific Heats for Heisenberg Rings.

convergence appears to be monotonic decreasing at temperatures above $kT/J = 0.3$ for $N \geq 8$. We observe that the convergence is going to be very similar to the case of ferromagnetic Ising rings. It appears that a double maximum will develop when N = 13 or 14 and that the maximum of the limiting curve will not derive from the maxima in the curves for $N \leq 11$. Clearly, the limiting behaviour for $kT/J < 0.5$ will be quite difficult to estimate.

In Fig. (4.16) we study the convergence of the chains N = 4, 6 and 8. Although they do not converge very fast, they appear to converge regularly and their general shape is much more suggestive of the limiting curve than that of the corresponding rings. In particular, they indicate unmistakably an extensive flat top with a rather poorly defined maximum for the limiting curve in the temperature region kT/J = 0.3 to 1.2. At temperatures below kT/J = 0.2 the chain convergence indicates that the limiting curve is likely to rise rather rapidly from zero. The rather peculiar behaviour of the limit curve in the region 0-0.4 comes as no surprise in view of our earlier studies in Chapter III, subsection (4.7) of the spectrum of Heisenberg rings and chains near the ferromagnetic limit. We have seen that lying below the single spin-wave dispersion curve whose dispersion law is given by $\varepsilon(k) = 2J(1-\cos k)$ there are a whole family of bound states with dispersion curves $\varepsilon(k) = \frac{2J}{r}(1-\cos k)$ where r = 2, 3, ... N/2. The effect of this family of states will be experienced in the temperature region below $kT/J \simeq 0.3$.

3.2) Estimation of Limiting Behaviour

The convergence of the rings is adequate to determine the specific heat limit for temperatures above $kT/J \doteq 0.8$. In the region 0.3 - 0.8 the following procedure was employed. Plots of the quantity T/C were made for N = 9, 10 and 11. Then limiting points in the region

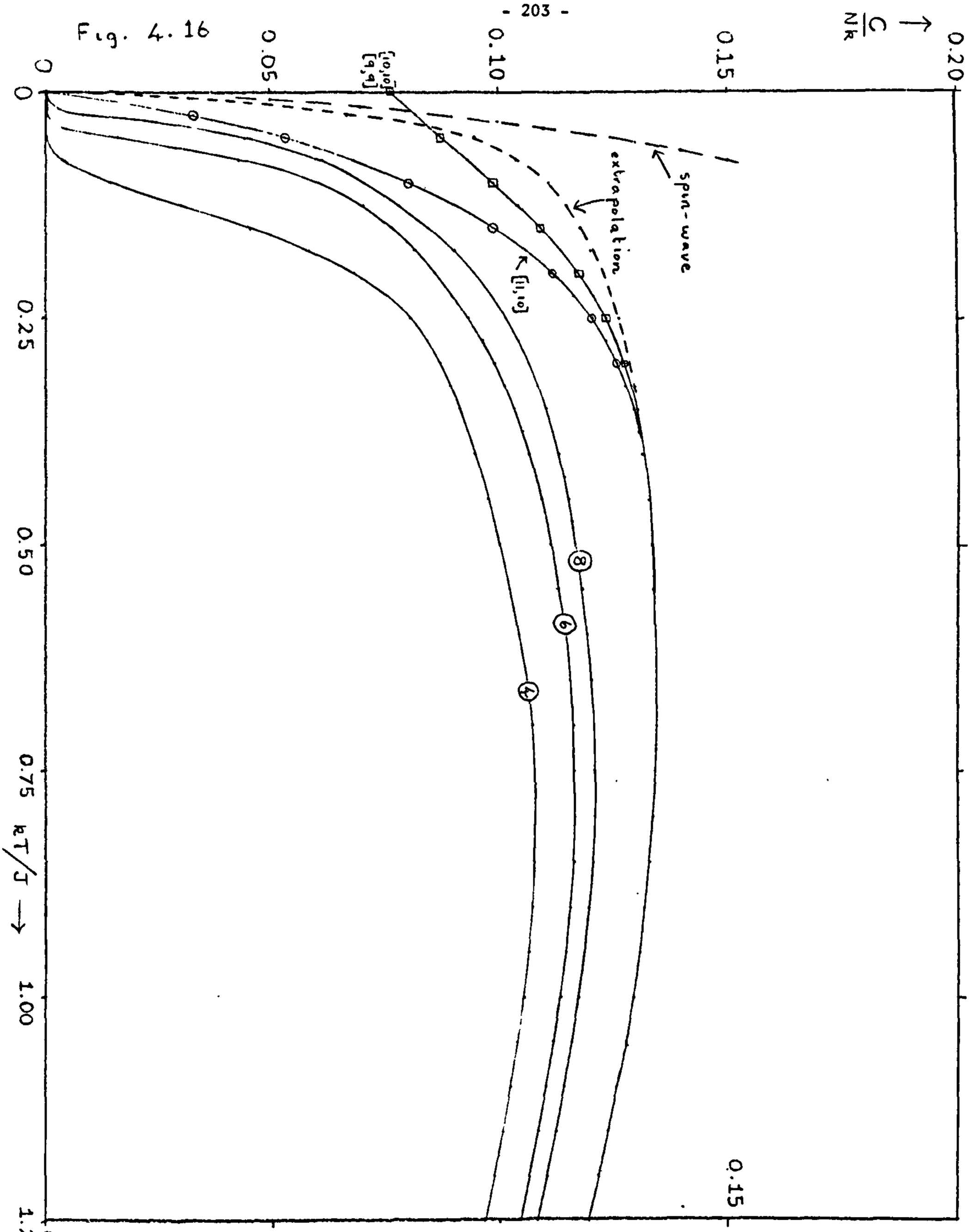

Fig. 4.16 Ferromagnetic Heisenberg Specific Heats: Finite Chains; Spin-Wave and BRG Padé Approximant Theories.

0.8 to 1.2 were put on the graph, and the rest of the limiting curve down to kT/J = 0.3 was estimated. This extrapolation was almost linear, showing that the limit curve is approximately flat-topped in this region. The corresponding entropy values were then determined from an inverse plot of this extrapolation, i.e. from the thermodynamic relation

$$S_2 - S_1 = \int_{T_1}^{T_2} \frac{C}{T}\, dT \qquad (4.3.2)$$

The limiting entropy points were plotted on Fig. (4.14) and examined for consistency. This process was repeated a few times until self-consistency resulted. The process appeared to be fairly sensitive. For example, if trial specific heat points were taken a few percent higher than the optimum limit curve, the corresponding entropy points were reduced a few percent. However, we see from Fig. (4.14) that the limiting entropy is well defined by finite N results to lower temperatures than is the specific heat, i.e. to about kT/J = 0.35 instead of 0.8. Hence these fluctuations were easy to discard. A further check on the correctness of the result was the fact that the integrated area under the specific heat curve must check with the energy. The flat-topped curve made the position of the maximum rather difficult to estimate. Our conclusion was

$$C_{max}/Nk \simeq 0.134 \qquad (4.3.3)$$

$$\text{at} \quad kT_{max}/J \simeq 0.70 \qquad (4.3.4)$$

We attempted to estimate the low-temperature behaviour by the power law analysis presented in subsection (2.3). The corresponding $U(T)$ versus TS(T) plots are shown in Fig. (4.17), which covers a temperature range of kT/J = 0 to 0.3, and considers the largest rings N = 9, 10 and 11. Over this range, the plots are fairly straight, except for very small values of TS/NJ (below 0.04) or temperatures

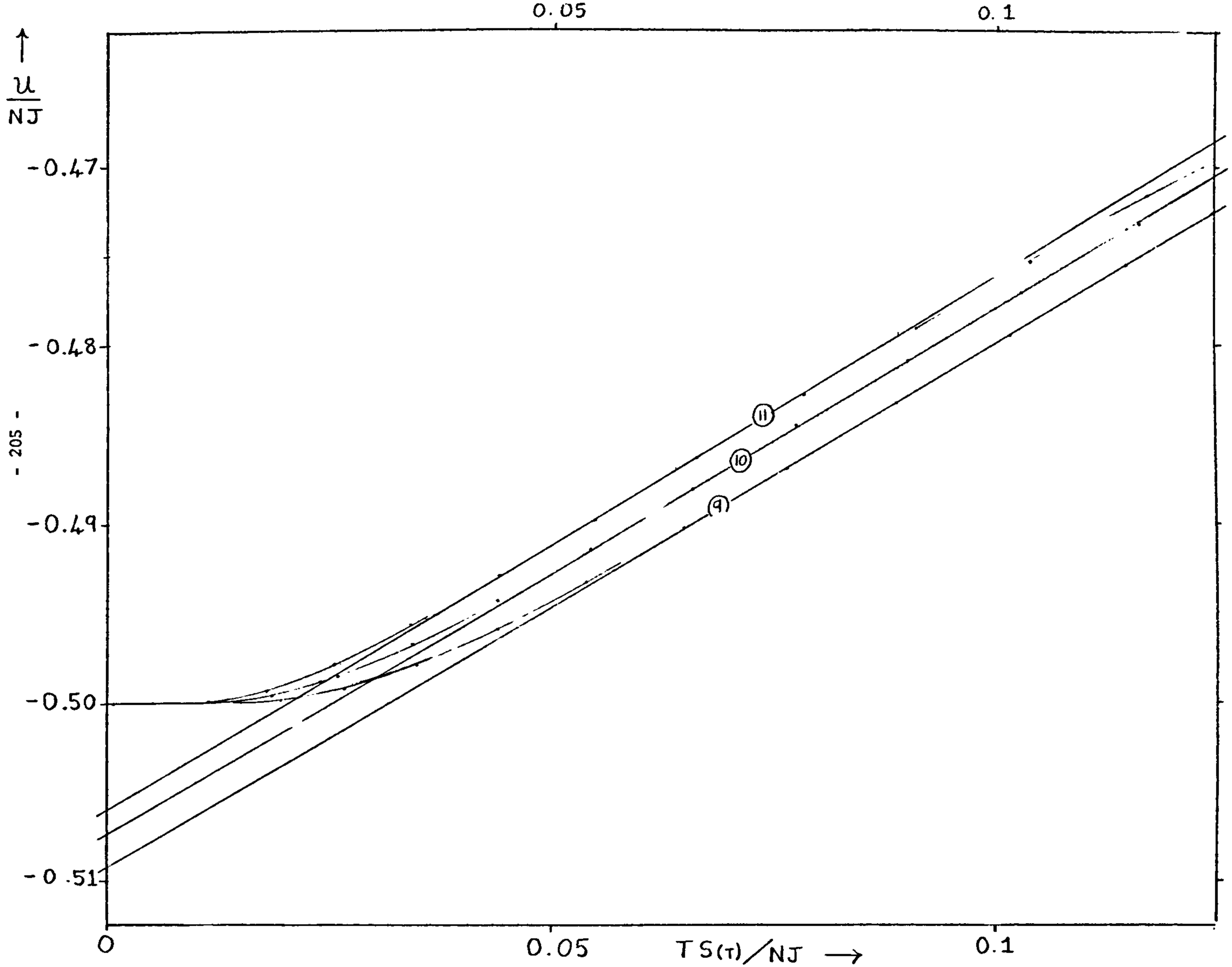

Fig. 4.17 Energy versus the Product of Temperature and Entropy for Heisenberg Ferromagnetic Rings.

below kT/J = 0.025, where an exponential decay sets in. At higher temperatures, the curves deviate from straight lines, becoming concave downwards. The onset of curvature is observed for the N = 11 curve on Fig. (4.17). The maximum slopes appear to increase monotonically with N, ~~and the slopes appear to increase monotonically with N~~, and the slopes shown on the graph for N = 9, 10 and 11 correspond to values of the index α of 1.415, 1.419 and 1.427 respectively. Rough extrapolation linearly in 1/N suggests that the true index might lie in the neighbourhood of α = 1.45 to 1.5, but the corresponding pure power laws would only be closely followed below temperatures of kT/J $\simeq$ 0.25.

Accepting the value α = 3/2, we may go on to estimate the constant A (see equations (4.2.4) to (4.2.6)) numerically, choosing the value which best appears to fit the low temperature energy, entropy and specific heat simultaneously. We thus obtained:

$$U_{(T)} - U_{(0)} \simeq 0.28\, NJ \left(\frac{kT}{J}\right)^{3/2} \qquad (4.3.5)$$

$$S_{(T)} \simeq 0.85\, Nk \left(\frac{kT}{J}\right)^{1/2} \qquad (4.3.6)$$

$$C_{(T)} \simeq 0.42\, Nk \left(\frac{kT}{J}\right)^{1/2} \qquad (4.3.7)$$

These results were then used to complete the estimates of the extrapolated limiting curves (shown dashed) on Figs. (4.13), (4.14) and (4.15).

3.3) Spin-Wave Theory Predictions

Let us apply the harmonic oscillator approximation of sub-section (2.4) to the ferromagnetic Heisenberg limit. For ferromagnets, it is convenient to consider a basic Brillouin zone of 0 to π containing N states spaced at a frequency interval $\Delta k = \pi/N$ (see Chapter III, sub-section (5.4)). The ferromagnetic analogue of equation (4.2.15) is therefore

$$U - U_o = \frac{N}{\pi} \int_0^{\pi} \frac{\varepsilon(k)\, dk}{e^{\beta\varepsilon(k)} - 1} \qquad (4.3.8)$$

substituting the ferromagnetic dispersion relation

$$\mathcal{E}(k) = 2J(1-\cos k) \tag{4.3.9}$$

and the small k approximation $\mathcal{E}(k) \sim J k^2$ (4.3.10)

we have

$$u - u_o = \frac{NJ}{\pi} \int_0^{\pi} \frac{k^2\, dk}{e^{\beta J k^2} - 1} \tag{4.3.11}$$

with the aid of a suitable change of variables the integral (4.3.8) may be evaluated as

$$u - u_o \simeq \frac{1}{2\pi(\beta J)^{\frac{3}{2}}} \int_0^{\infty} \frac{x^{1/2}\, dx}{e^x - 1} \simeq \frac{1}{2\pi(\beta J)^{\frac{3}{2}}} \Gamma\left(\tfrac{3}{2}\right) \zeta\left(\tfrac{3}{2}\right) \tag{4.3.12}$$

$$\frac{u - u_o}{NJ} \simeq \frac{\zeta(\frac{3}{2})}{4\sqrt{\pi}\,(\beta J)^{3/2}} \simeq 0.3685 \left(\frac{kT}{J}\right)^{\frac{3}{2}} \tag{4.3.13}$$

As in the antiferromagnetic case, we observe that this approximation predicts the same low-temperature dependence of the internal energy, namely $T^{3/2}$, as we found numerically. However, the constant, 0.37, in equation (4.3.13) is about 1.3 times larger than the constant 0.28 of equation (4.3.5). The spin-wave approximation for the energy may be compared with the estimated limit curve in Fig. (4.13). The spin-wave constant does appear to be rather too large. For the entropy and specific heat, our spin-wave theory predicts

$$S_{(T)} = 1.106\, Nk \left(\frac{kT}{J}\right)^{\frac{1}{2}} \tag{4.3.14}$$

and

$$C_{(T)} = 0.553\, Nk \left(\frac{kT}{J}\right)^{\frac{1}{2}} \tag{4.3.15}$$

In addition to the spin-wave states, we have observed the presence of low-lying families of bound states having the dispersion formulae (see Chapter III, sub-section 4.7)

$$\mathcal{E}^{(r)}(k) = \frac{2J}{r}(1-\cos k)\ ;\ r = 2, 3, \cdots, \frac{N}{2}. \tag{4.3.16}$$

It is of interest to examine the thermal behaviour predicted by states of this type in conjunction with the harmonic oscillator approximation. Equation (4.3.13) becomes

$$\frac{U - U_o}{NJ} \simeq \frac{\sqrt{\pi}}{4\sqrt{\pi}} \frac{\zeta(3/2)}{(\beta J)^{3/2}} \simeq \sqrt{\pi} \times 0.37 \left(\frac{kT}{J}\right)^{3/2} \qquad (4.3.17)$$

Again we have a $T^{3/2}$ temperature dependence, though with a modified constant that appears to be even less in agreement with our numerical estimates than the spin-wave constant.

3.4) High Temperature Series Expansions

The 21 term high-temperature series in K = kT/J due to Baker, Rushbrooke and Gilbert (1964) can be examined by Padé approximants also in the ferromagnetic case simply by changing the sign of J and hence K. On the whole, the ferromagnetic Pade's are much better behaved than their antiferromagnetic counterparts. The [10,10] and [9,9] Pade's show perfect self-convergence right down to T = 0, with no troublesome low-temperature poles, going into zero at C/Nk = 0.077, (the same value as for the antiferromagnetic [10,10] Pade). The [11,10] Padé also has no poles to spoil its behaviour near T = 0. These Pade's are shown in Fig. (4.16). Since we believe that the low-temperature asymptotic behaviour goes as $T^{1/2}$, probably neither of these Pade's is correct. Assuming that the $T^{1/2}$ Padé lies between the [10,10] and [11,10] evaluations, a set of points has been interpolated between these two curves, and perhaps these points may be taken as indicating the most probable behaviour of the limiting curve below kT/J = 0.3. However this is somewhat speculative since we are not completely assured of the $T^{1/2}$ behaviour or that the $T^{1/2}$ Pade definitely lies between the constant and T Pade's.

Effects of the asymptotic behaviour of the various Padé evaluations only set in below kT/J $\simeq$ 0.3, i.e. all Pade's converge above this temperature. We therefore conclude that the BRG Padé series for the ferromagnetic specific heat is reliable down to kT/J = 0.3. It is most encouraging to observe that the Padé evaluations above 0.3 are in excellent agreement with our own extrapolations. Below $\frac{kT}{J}$ = 0.3 however, our extrapolations do seem to be significantly higher than the [10,10] and [11,10] Pade's and the $T^{1/2}$

interpolations, although our quoted probable error allows discrepancies of this order. The behaviour at very low temperatures of the ferromagnetic specific heat limit is clearly quite subtle and nothing less than the complete analytic solution is really satisfactory.

As in the antiferromagnetic case, we may now use the Padé evaluations to reestimate the height and position of the maximum. We obtain

$$C_{max}/Nk = 0.13425 \pm 0.00002 \qquad (4.3.18)$$

$$\text{at} \quad kT_{max}/J = 0.665 \pm 0.005 \qquad (4.3.19)$$

(cf. equations (4.3.3) and (4.3.4). It does appear that our extrapolation estimate for the position of the maximum is about 5% in error, since the Pade's are likely to be completely reliable at these temperatures. This is really not at all bad in view of the nature of the limiting curve.

¶ Let us now return to Fig. (4.14) for the entropy. In addition to the finite N curves already listed, we show our extrapolated curve (dashed) and the [10,10] and [10,9] Pade's for comparison. (The [11,10] Padé has a pole near T = 0 and is therefore omitted.) Since the extrapolated specific heat curve lies above the Padé s, we expect the corresponding entropy extrapolation also to lie above. The dashed, extrapolated curve does, in fact, lie slightly <u>below</u> the [10,9] Padé in the temperature region kT/J = 0.05 to 0.25, arguing against the thermodynamic consistency of the low-temperature Pade's. The [10,9] Padé in turn lies below the [10,10] Padé. Above kT/J = 0.3, of course, the assorted Pade's and our extrapolations are in excellent agreement. Finally, in Fig. (4.13) we compare the [10,8] Padé with our extrapolations. (The [10,9] and [9,8] Pade's converge but their low-temperature asymptotic behaviour is quite unrealistic. This may be verified by direct extrapolation of the low-temperature energy curves.)

3.5 Comparison with Other Models and Approximations

In sub-section (2.7) we compared our antiferromagnetic specific heat curve (curve (a) in Fig. (4.12)) with the X-Y model specific heat and two perturbation approaches of Katsura and Inawashiro. The X-Y model curve (curve (c) in Fig. (4.12)) is invariant under the transformation from antiferromagnet to ferromagnet. The earlier perturbation method of Katsura and Inawashiro (1964) treats the X-Y curve as the zeroth approximation, and the first order approximation to the ferromagnetic specific heat is shown as curve (g). The agreement with our numerically estimated curve (b) is even worse than in the antiferromagnetic case. However, the (Bulaevskii, 1963) Hartree-Fock approach applied to the ferromagnetic case recently by Hunt and Girardeau (1967), breaks down, since it predicts a mean-field-type phase transition at a finite temperature for ferromagnets. A similar, mean-field-type, spurious transition occurs also for the Katsura and Inawashiro (1965) approximation which is based on the Bulaevskii Hamiltonian as zeroth order.

It appears that there is no approximate closed-form treatment extant which is even moderately successful in predicting the form of the ferromagnetic thermal properties of the Heisenberg linear chain.

To round off our studies of the thermal properties of the Heisenberg linear chain we compare, on the same scale, in Fig. (4.18) the exact and estimated specific heats for infinite chains with (a) S = 1/2 Ising coupling, ferro- or antiferromagnetic ; (b) S = 1/2 ferro- or antiferromagnetic X-Y coupling; (c) S = 1/2 Heisenberg antiferromagnetic coupling; (d) S = 1/2 Heisenberg ferromagnetic coupling; (e) $S = \infty$ (classical) Heisenberg ferro- or antiferromagnetic coupling (Fisher, 1964). The large difference between the relatively sharp-peaked antiferromagnetic S = 1/2 Heisenberg specific heat and the low broad ferromagnetic specific heat is striking testimony to the lower stability of the isotropic ferromagnetic coupling. Curve (e) for $S = \infty$ continues to rise monotonically to a maximum at T = 0 of height C/Nk = 1.0.

Fig. 4.18

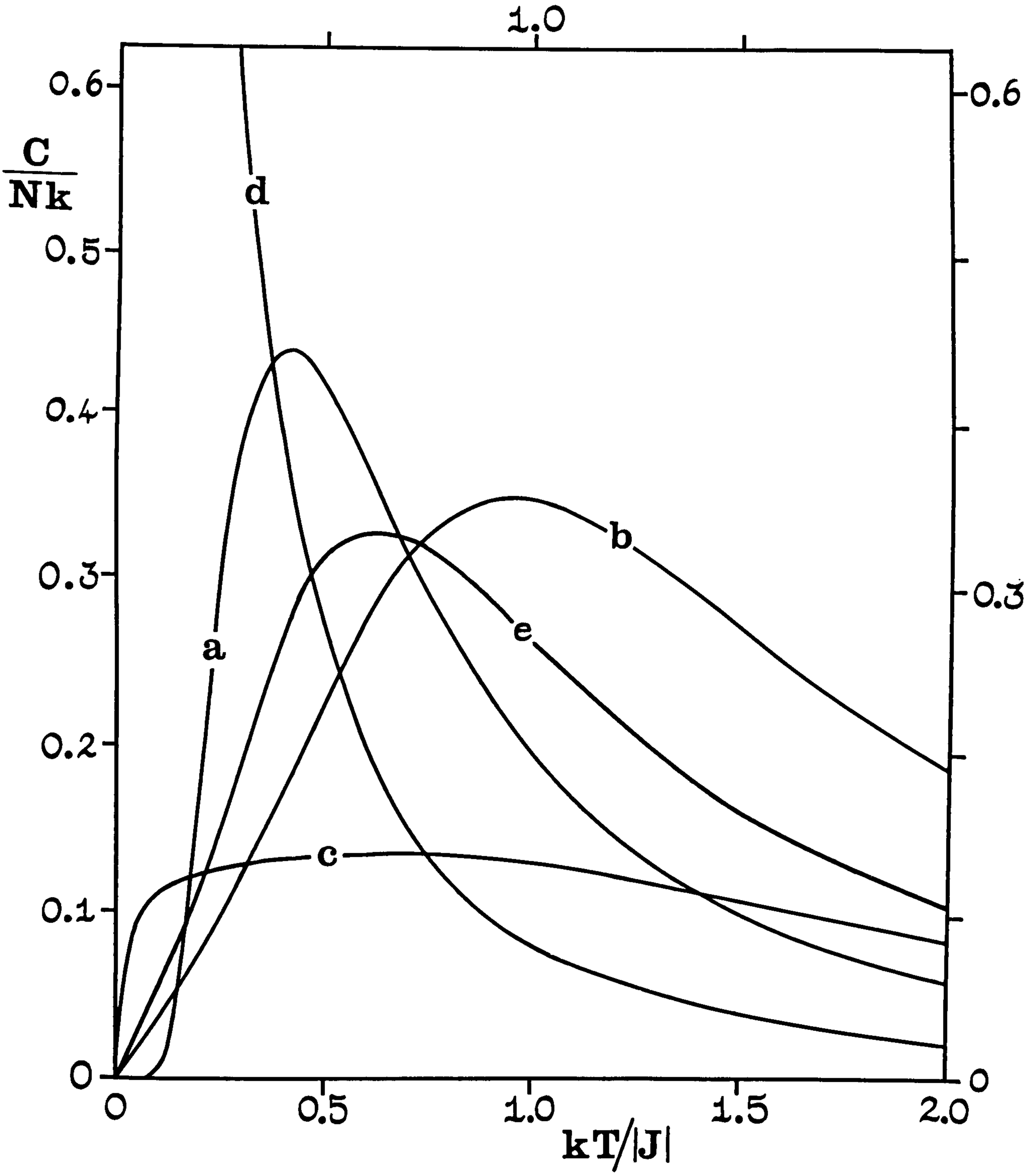

Comparison of Specific Heats for Various Models

4. ANISOTROPIC THERMAL PROPERTIES

4.1) Antiferromagnets: General Anisotropy

Let us first of all study the behaviour of the specific heat as a general function of anisotropy. In Fig. (4.19) we see the specific heats for rings of N=8 spins. The exact limiting curve for $\gamma = 0$ and the estimated limit for $\gamma = 1$ are plotted as dashed lines to indicate the degree to which the results for N = 8 approach the limit. The effect of increasing γ from the Ising value $\gamma = 0$ is to shift the specific heat maximum to higher temperatures, to reduce its height and to broaden the peak. At low temperatures ($kT/|J| \simeq 0.1$) the curves for finite N (even) and γ in the range 0.1 to 0.6 display anomalous small peaks and points of inflection. These are "small number effects" due to the finite splitting of the degenerate Ising ground state by the transverse terms in the Hamiltonian. For fixed γ and increasing N, the splitting diminishes and eventually goes to zero as $N \to \infty$ (see Chapter III, sub-section (3.1)). Correspondingly the anomalies move to lower temperature and are reduced in magnitude, finally disappearing in the limit $N = \infty$.

For $\gamma \neq 1$ and large, finite N, the specific heat curves of the rings at low temperatures (but above the anomalies) vanish exponentially fast, roughly as $\exp [- \Delta E_A(\gamma) / kT]$, where $\Delta E_A(\gamma)$ is the limiting anisotropy gap between the ground state and the first excited states for rings. The value of this gap was estimated in Chapter III, sub-section (3. 2): it approaches zero as $\gamma \to 1$ and the Ising value $2|J|$ as $\gamma \to 0$. However, in Chapter III, sub-sections (2.6) and (3.2) we have discussed reasons for believing that in the limit $N \to \infty$, the "effective gap" $\Delta E_A(\gamma)$ is about half the anisotropy gap for rings. $\Delta E_A^*(\gamma)$ is obtained by extrapolating energy gaps for small finite free-ended chains, and the situation parallels that in the Ising limit, $\gamma = 0$.

Fig. 4.19

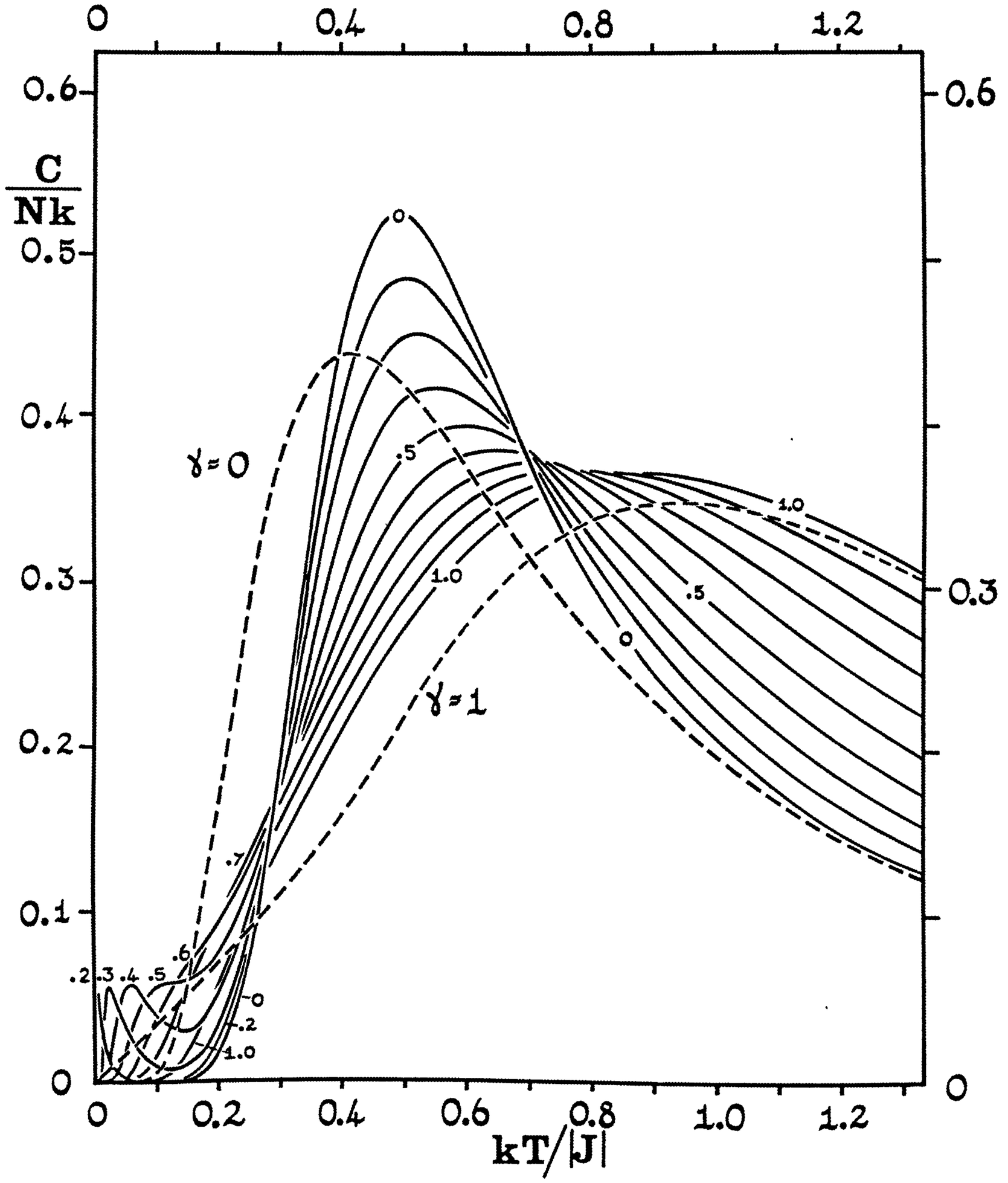

Variation of Antiferromagnetic Specific Heat with γ

4.2) Antiferromagnets: Thermal Properties at $\gamma = 0.5$

Let us now examine the internal energy, entropy and specific heat curves at $\gamma = 0.5$ with a view to predicting the limiting curve as $N \to \infty$ in each case. The techniques employed will be similar to those for the Heisenberg limit. In Figs. (4.20) and (4.21) we see, primarily, the ring curves for N = 3 through 10, for the energy and entropy respectively. The situation is clearly qualitatively similar to the Ising and Heisenberg limits in both cases, although at low temperatures traces of the anomalies remarked on in sub-section (4.1) in the case of the specific heat are evident. Again we see that odd and even rings appear to form two distinct, essentially monotonically converging, sequences bracketing the limiting result. The energy of an infinite chain is defined to an accuracy of better than $\pm$ 0.7% down to temperatures of $kT/|J| = 0.5$ by the means of the curves for N =9 and N = 10. The entropy is also well defined down to $kT/|J| = 0.5$ by interpolation between the rings for odd and even N. In Fig. (4.22) we have corresponding bracketing behaviour for the specific heat rings. The specific heat is very well defined by direct interpolation and fairly well defined down to 0.5. down to $kT/|J| \simeq 0.9$, The convergence behaviour in the region of the maximum suggests that we employ various sets of weighted means to determine the maximum more precisely. Two such sets are shown in the inset to Fig. (4.22) on an enlarged scale. The solid curves are the set of means 10/9, 8/7, and 6/5 weighted towards the even rings, and the dashed curves are the set of means 9/8, 7/6 and 5/4 weighted towards the odd rings. Both sets are reasonably consistent in predicting the limiting curve which we determine by extrapolation. For the position and height of the maximum we obtain

$$C_{max}/Nk \simeq 0.358 \pm 0.003 \qquad (4.2.1)$$

at $$kT_{max}/|J| \simeq 0.635 \pm 0.025 \qquad (4.2.2)$$

We do not feel we can determine the maximum as precisely as in the Heisenberg limit since we have one less ring, and the convergence is rather less

Fig. 4.20

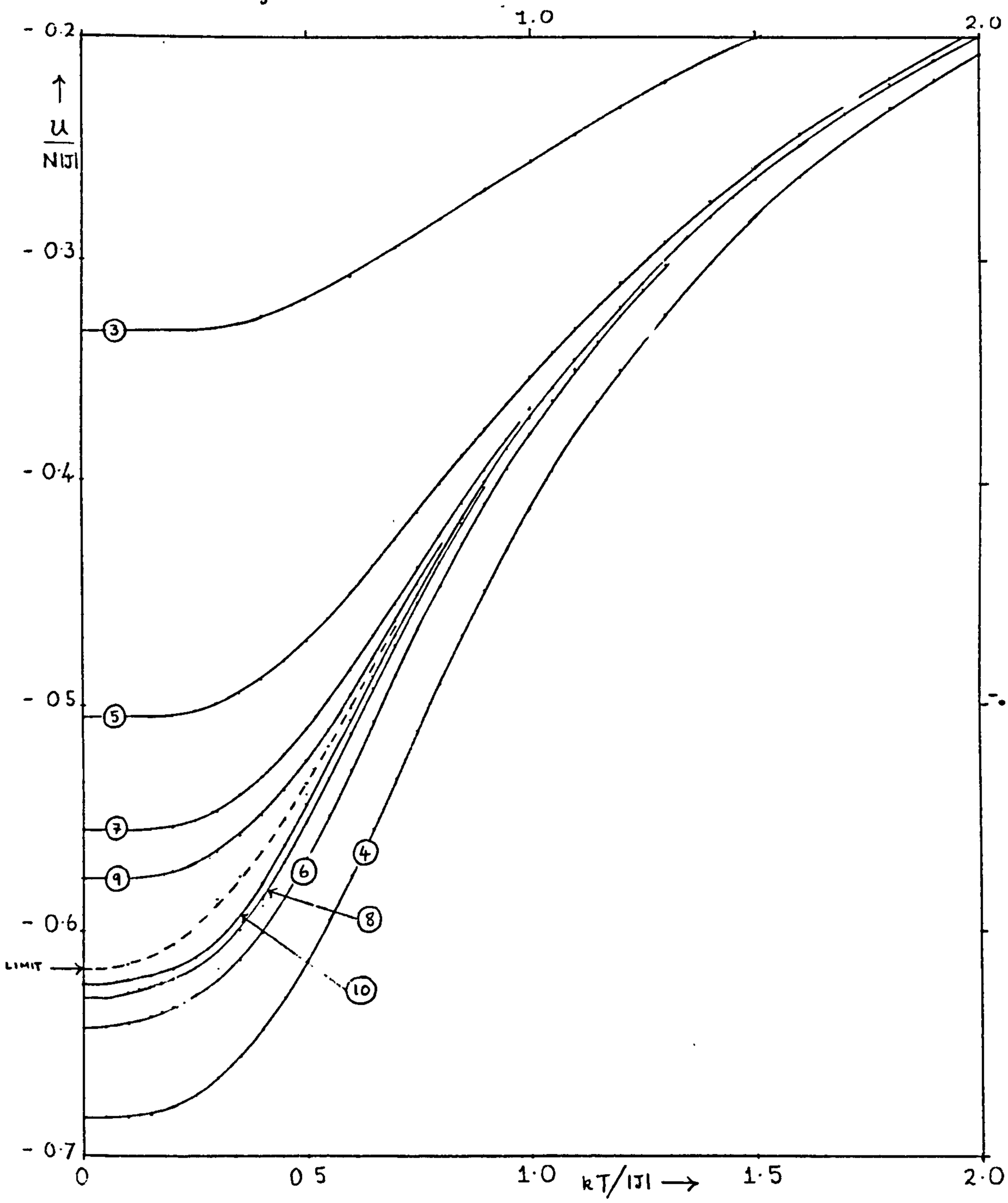

Antiferromagnetic Ring Energies for $\gamma = 0.5$

Fig. 4.22

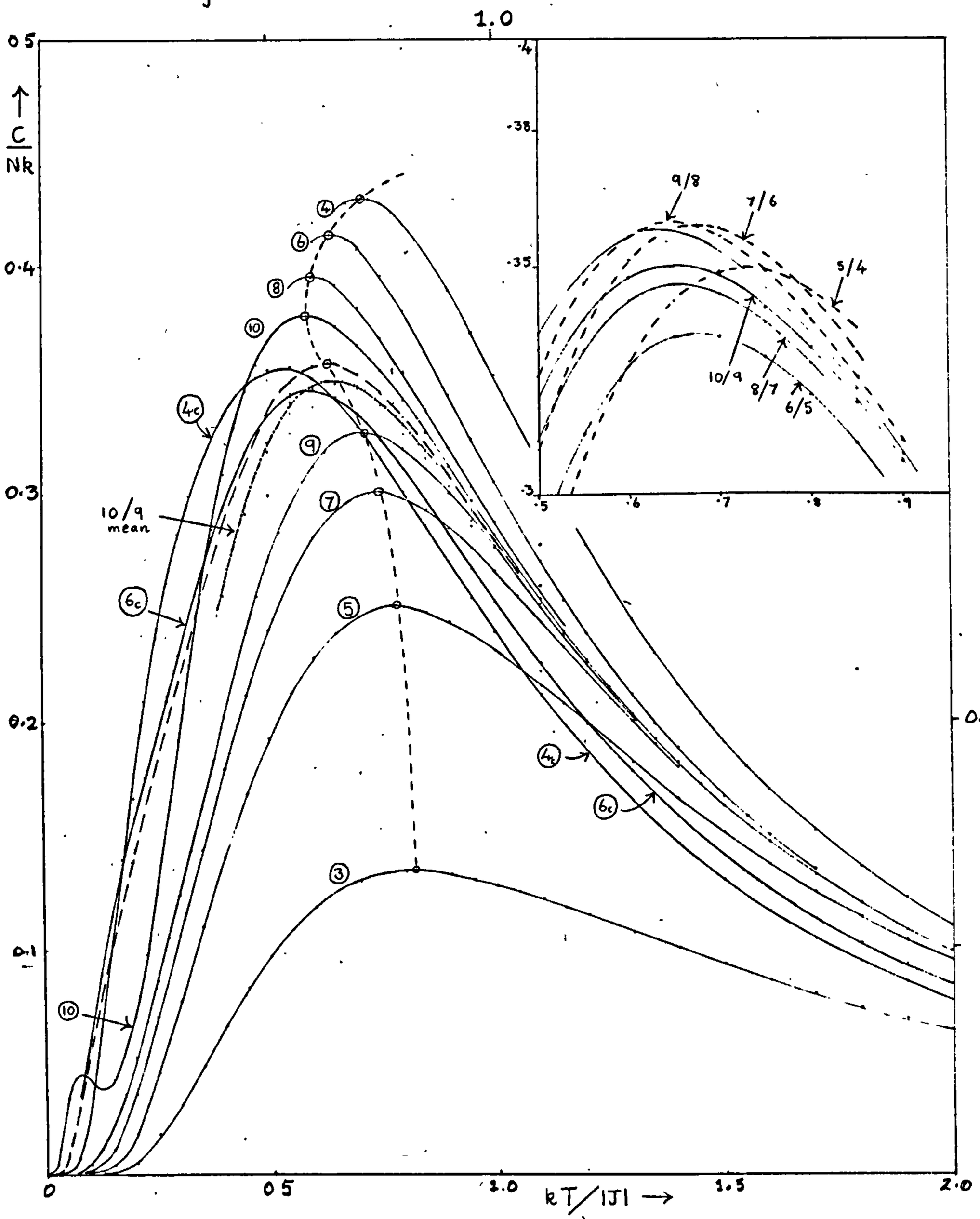

Antiferromagnetic Specific Heats for $\gamma = 0.5$: Estimation of Maximum from Weighted Means (Inset)

Fig. 4.21

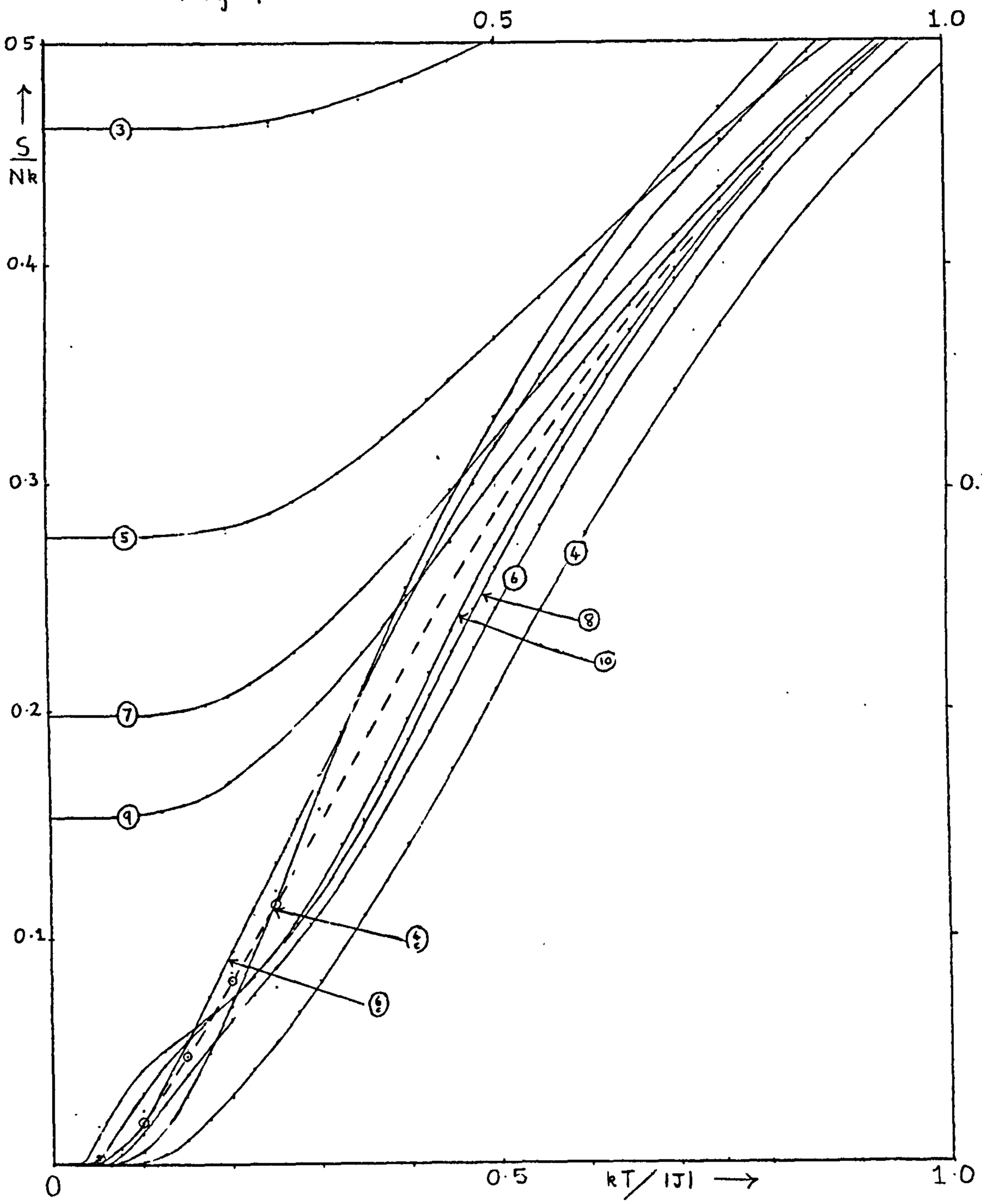

Antiferromagnetic Ring and Chain Entropies for $\gamma = 0.5$

regular. Chains are included in Fig. (4.22) for comparison purposes, and seem reasonably consistent with our estimated limiting curve in the region of the maximum. However the apparently rather irregular convergence of the chains for $\gamma = 0.5$, similar to the chain convergence for $\gamma = 1$, discourages us from using the chains for extrapolation purposes.

4.3) Low-Temperature Approximation

At temperatures below $kT/|J| \simeq 0.5$, convergence of rings and chains is sufficiently irregular to rule out direct extrapolation for estimating the limit. However, in Chapter III, sections (3) and (5), we have discussed the nature of the anisotropic antiferromagnetic low-lying energy level spectrum with some care and detail. We shall now employ this knowledge to construct a low-temperature extrapolation which gives a plausible, though, of course, entirely non-rigorous, account of the thermal behaviour below about $kT/|J| \simeq 0.25$.

A careful reinterpretation of the work of des Cloizeaux and Gaudin (1966) suggests that the anisotropic spectrum, in the limit, consists of an energy gap from the antiferromagnetic ground state (which we believe to be two-fold degenerate) to a continuum of excited states whose density varies in a general sinusoidal fashion with wave-vector k. The dispersion curve for the excited states is sin k—like at $\gamma = 1$ and cos k—like near $\gamma = 0$, and for intermediate γ may be expanded as a power series in k. Examination of Fig. (2) in the paper of des Cloizeaux and Gaudin (1966) suggests that at $\gamma = 0.5$, the dispersion curve is still predominantly sine-like and accordingly we shall use the following approximate expression for the excitation energy from the ground state

$$\varepsilon(k) \simeq \Delta E_A^*(\gamma) + bk \simeq \alpha + bk \qquad (4.3.1)$$

where $\Delta E_A^*(\gamma)$ is the effective anisotropy gap, or limiting energy gap for chains (des Cloizeaux and Pearson use the energy gap for rings) and b is perhaps best regarded as an adjustable parameter. In conjunction with the harmonic oscillator approximation of sub-sections (2.4) and (3.3) of this chapter, our choice of $\varepsilon(k)$ yields the following expression for the internal energy

$$\frac{U-U_0}{N|J|} = \frac{1}{2\pi}\int_0^{\pi} (\alpha + bk)\, e^{-\alpha\beta|J| - b\beta|J|k}\, dk \qquad (4.3.2)$$

$$\simeq \frac{\alpha K^{-1} e^{-\alpha K}}{\pi b} + \frac{K^{-2} e^{-\alpha K}}{\pi b} \quad \text{for } b \neq 0 \text{ and } K \to \infty \qquad (4.3.3)$$

where $K = |J|/kT = \beta|J|$. The corresponding expression for the free energy is

$$F/N|J| \simeq -K^{-2} e^{-\alpha K}/\pi b \qquad (4.3.4)$$

It is encouraging to observe that the functional form of the internal energy and free energy agree with our expectations in going to the Heisenberg limit; $\gamma = 1$, where the anisotropy gap $\alpha \to 0$ (U and $F \sim T^2$). For the specific heat we have

$$C/Nk \simeq \frac{\alpha^2}{\pi b} K e^{-\alpha K} + \frac{2\alpha}{\pi b} e^{-\alpha K} + \frac{2}{\pi b} K^{-1} e^{-\alpha K} \qquad (4.3.5)$$

and this is the function we shall attempt to fit first, taking a value of the chain anisotropy gap read from Fig. (3.9) as $\alpha = 0.194\,|J|$. The function (4.3.5) turns out to have a plausible shape, starting out with an exponential tail from $kT/|J| = 0$ to 0.15, then becoming rather straight for a short range and ultimately starting to curve downwards at 0.3 to 0.4. The best choice of parameter b to fit this low temperature approximation to the extrapolated values in the region of the maximum is $2b = 1.69\,|J|$, and the completed curve is shown dashed in Fig. (4.22). The energy and entropy at low temperatures can be obtained from the appropriate integrations of the specific heat function (and the results checked against the analytic expressions such as equation (4.3.3), of course) and the resulting estimated limiting curves are shown dashed on Figs. (4.20) and (4.21). The limiting curves for the thermal properties, together with some finite N results, are tabulated in Appendix 3, Table (VIII).

4.4) Ferromagnets: General Anisotropy

The behaviour of the ferromagnetic specific heat for a ring of 8 spins as a function of γ is shown in Fig. (4.23) at intervals of $\Delta\gamma = 0.1$. The exact limiting Ising curve and the estimated limiting curve for $\gamma = 1$ are shown dashed, for comparison. We observe that the finite ring curves for both $\gamma = 0$ and $\gamma = 1$, and thus presumably for all γ, lie above the corresponding limiting curves. Let us compare Fig. (4.23) with Fig. (4.24), the corresponding plot for free-ended chains (but on a different scale). The general trend with varying γ is observed to be very similar to the case of the rings, except that the finite N curves for $\gamma = 0$ and $\gamma = 1$, and hence again presumably for all γ, now lie <u>below</u> the corresponding limiting curves.

4.5) Ferromagnets: Thermal Properties at $\gamma = 0.5$

In Figs. (4.25) and (4.26) we see the ferromagnetic energy and entropy curves for finite rings and chains at $\gamma = 0.5$. We observe at once that the convergence pattern (all rings, odd and even N, converging systematically to the limit from one side and chains converging monotonically from the other) appears to be the same as in the Heisenberg and Ising limits. This feature suggests at once that we consider various means not of odd and even rings as in the antiferromagnetic case, but of rings and chains of the same N. This procedure has resulted in the estimate for the limiting specific heat in the region of the maximum shown dashed on Fig. (4.27). Our estimate for the position and height of the maximum itself is

$$C_{max} / Nk \simeq 0.393 \pm 0.005 \qquad (4.5.1)$$

$$\text{at} \quad kT_{max}/J \simeq 0.34 \pm 0.02 \quad , \qquad (4.5.2)$$

The limiting curve is well-defined by the rapidly converging rings in the temperature range above $kT/J = 0.9$, and reasonably well indicated down to 0.5.

4.6) Low-Temperature Approximation

Our studies of the low-lying levels of the ferromagnetic spectrum in Chapter III, sections (2) and (4), suggest that for general anisotropy, the

Fig. 4.23

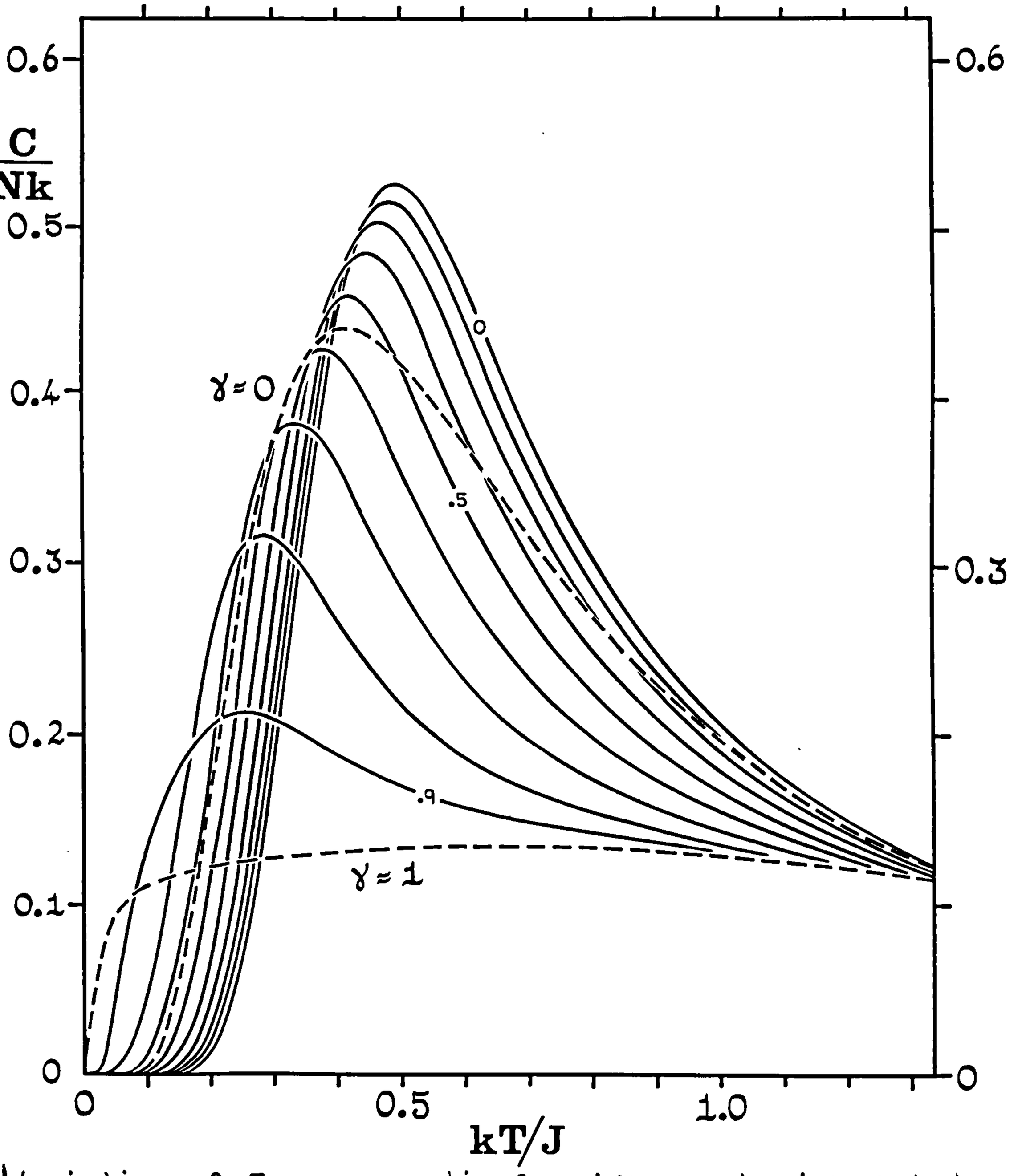

Variation of Ferromagnetic Specific Heat with Anisotropy.

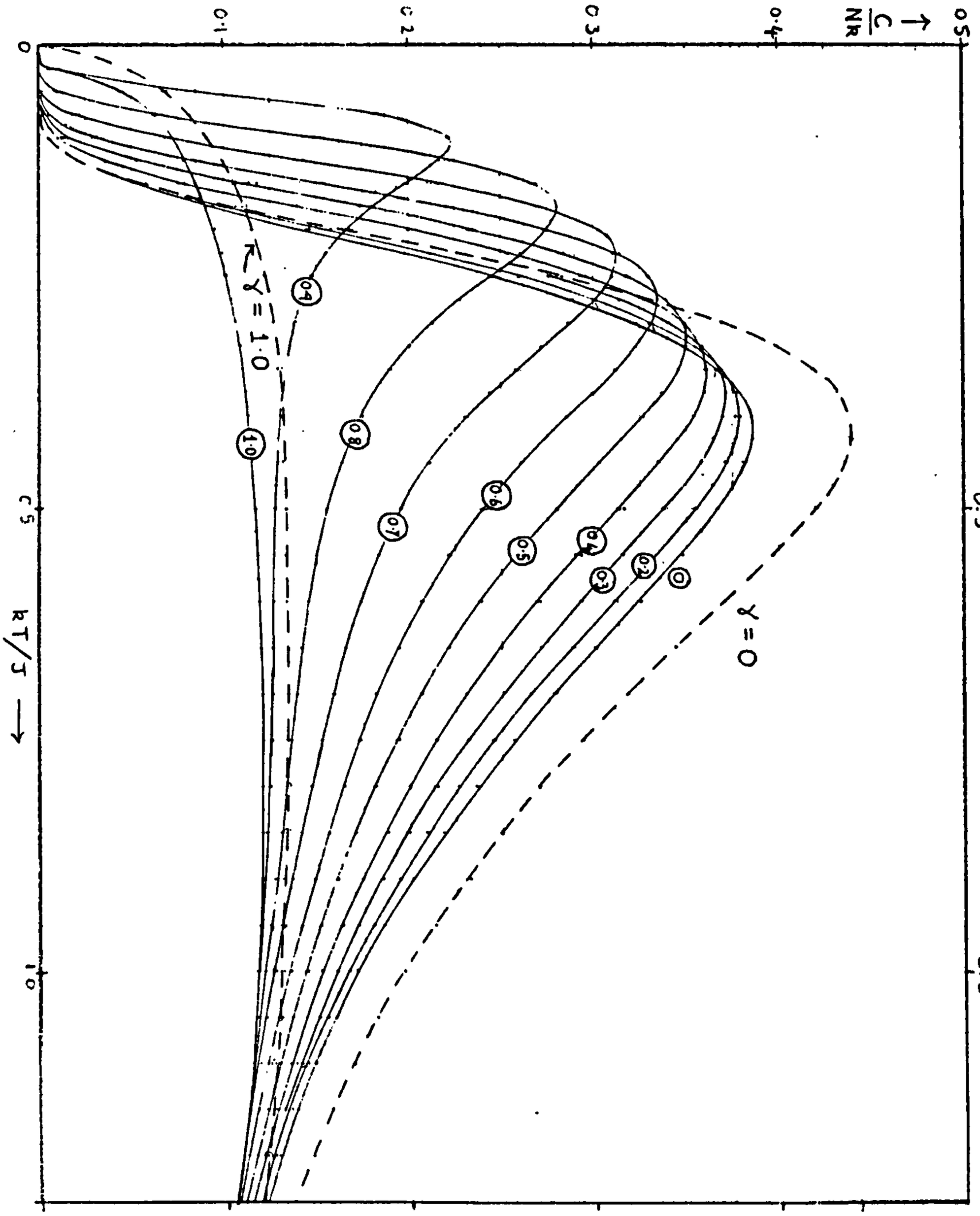

Variation of Ferromagnetic Specific Heats with Anisotropy for Chains of N = 8.

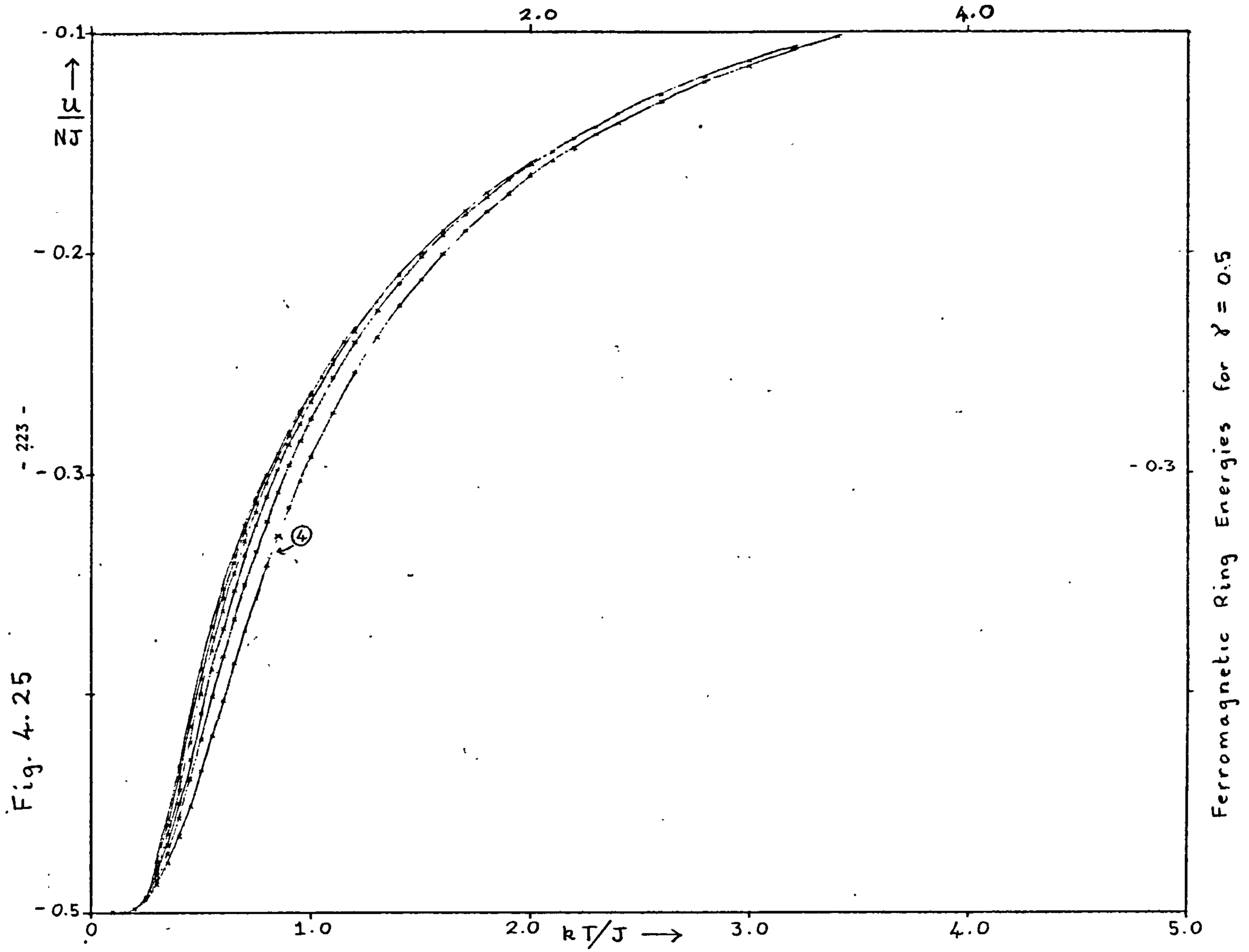
2.0
4.0
- 0.1
$\frac{u}{NJ}$
- 0.2
- 0.3
- 0.5
0
1.0
2.0
kT/J
3.0
4.0
5.0
④
Ferromagnetic Ring Energies for γ = 0.5

Fig. 4.25

Fig. 4.26

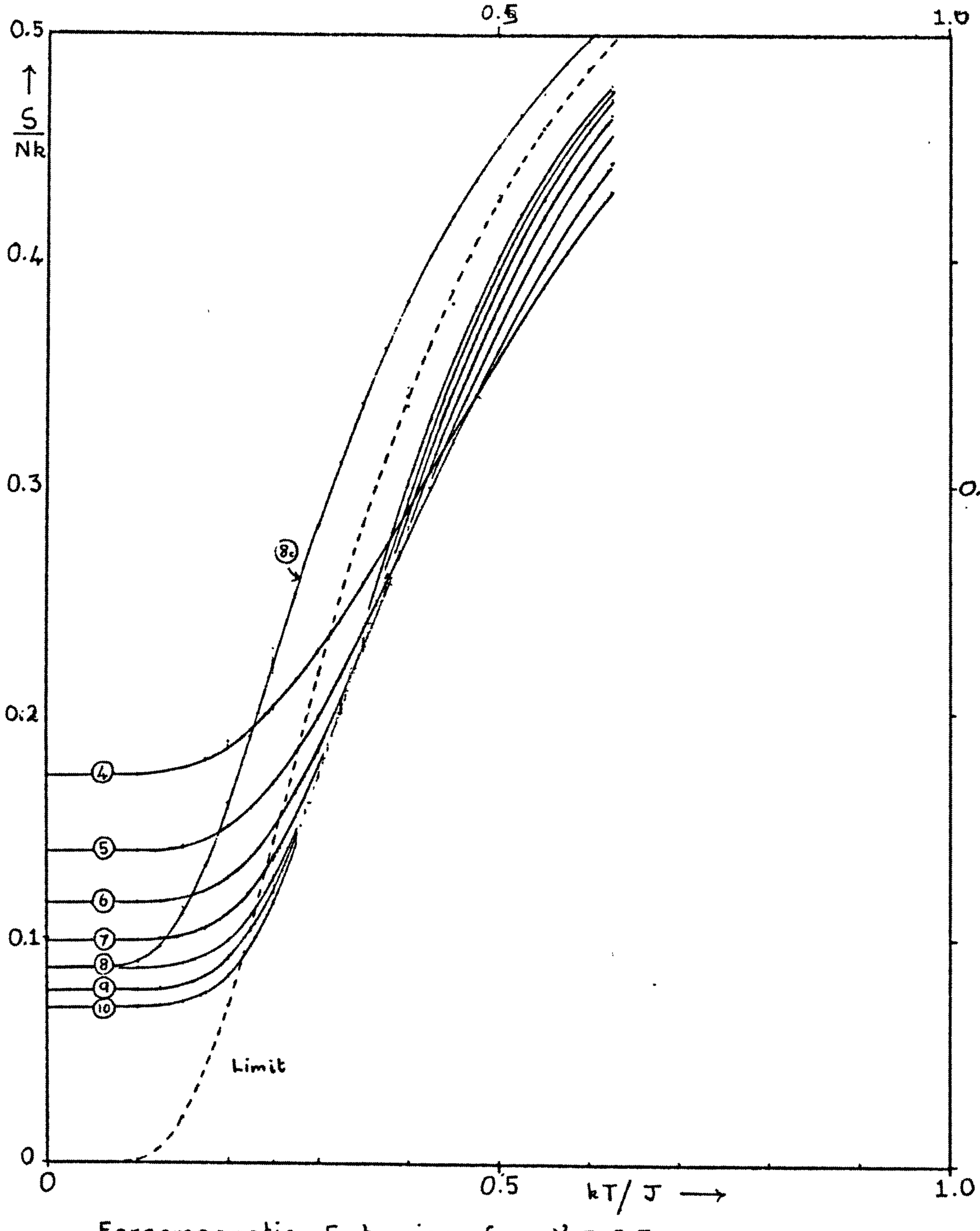

Ferromagnetic Entropies for $\gamma = 0.5$

thermal properties at low temperatures are governed by an effective energy gap (as in the case of antiferromagnets). Except near $\gamma = 1$, we believe that this energy gap is quite accurately given by the expression

$$\Delta E_F^*(\gamma) \sim (1 - \tfrac{1}{2}\gamma^2)J \qquad (4.6.1)$$

Whereas in the case of antiferromagnets, the excited levels above the gap show a sinusoidal distribution with respect to wave-vector k, our ferromagnetic studies show that the dominant levels (the $S^z = 0$ states) are completely degenerate in energy, i.e. the levels are independent of wave-vector k. In this situation it is easy to show that we obtain an approximate free energy of form

$$F/NJ \simeq K \exp\left(-\Delta_F^*(\gamma)\, K\right)$$
$$\simeq K \exp\left\{-(1 - \tfrac{1}{2}\gamma^2)K\right\} \qquad (4.6.2)$$

and internal energy

$$\frac{u - u_o}{NJ} = (1 - \tfrac{1}{2}\gamma^2) \exp\left\{-(1 - \tfrac{1}{2}\gamma^2)K\right\} . \qquad (4.6.3)$$

The corresponding expression for the specific heat gives rise to the dashed limiting curve below $kT/J \sim 0.25$ in Fig. (4.27). This curve closely follows the low-temperature chain specific heats in this region. Similarly, we have completed the limiting curves for the energy and entropy in the same temperature region. (The higher temperature portions of these curves have been obtained from the appropriate integration of the limiting specific heat and from the convergence of the sequence of rings). The limiting results for the thermal properties, together with some finite N results, are tabulated in Appendix 3 (Table (IX)).

5. THERMAL PROPERTIES IN AN APPLIED MAGNETIC FIELD

5.1) Entropy

Third Law of Thermodynamics. It is well known that the Ising model of an antiferromagnet exhibits an anomalous entropy peak at a critical magnetic

field which remains even at the absolute zero of temperature, in violation of the third law of thermodynamics. More precisely, the third law implies that for a macroscopic system in equilibrium consisting of N interacting spins, the entropy per spin should vanish in the limits $N \to \infty$ and $T \to 0$. A magnetic material in thermodynamic equilibrium which does not obey the third law could be used in an adiabatic demagnetisation process to reach the absolute zero in a finite number of steps (Wilks, 1961).

Anomalous Entropy Peaks. It was noted by Brooks and Domb that the plane square Ising model of an antiferromagnet is anomalous in this respect since the entropy displays a maximum as a function of magnetic field which persists down to absolute zero. The point has been discussed more recently by Fisher, and Domb (1960).
(1960)$_A$ The anomalous entropy of an antiferromagnetic linear chain has already been reviewed briefly in Chapter IV, subsection (1.2). It is now convenient to discuss the matter in more detail.

In an antiferromagnetically ordered system at low temperatures a small magnetic field tends to reduce the order (by reversing spins aligned against the field) so that the entropy rises as the field is increased. In a strong field, on the other hand, all the spins become ferromagnetically aligned and the entropy falls to zero. Consequently at an intermediate field (and low enough temperature) the entropy displays a maximum. See, for example, Fig. (4.28). It is a characteristic feature of the Ising model, however, that this entropy maximum persists as a sharp peak right down to T = 0, where it occurs at a field $H = H_c$ (see Fig. (4.28)). The critical field H_c is simply the field at which the gain in magnetic energy on reversing a single spin coupled antiferromagnetically to q neighboring spins is balanced by the loss of coupling energy due to the change over to ferromagnetic alignment. Explicitly, for the Hamiltonian

$$\mathcal{H} = 2|J| \sum_{(ij)} S_i^z S_j^z - g\beta H \sum_i S_i^z \qquad (5.1.1)$$

Fig. 4.27

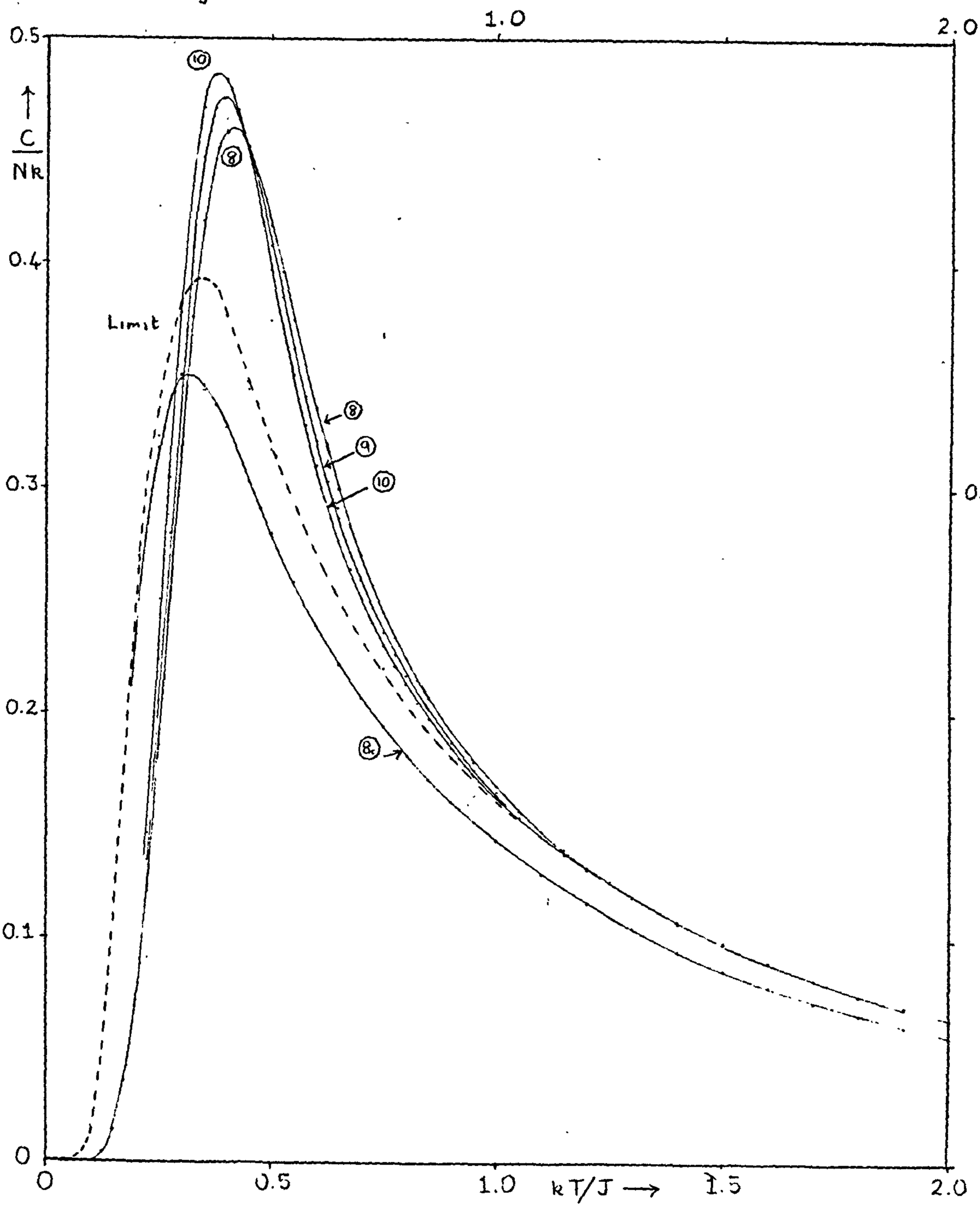

Ferromagnetic Specific Heats for $\gamma = 0.5$

the critical field is $H_c = \frac{q|J|}{g\beta}$ (5.1.2)

The height of the anomalous peak is found to be an appreciable fraction of the maximum possible entropy change ($k\ln 2$ per spin). Thus for the Ising linear chain (Domb, 1960)

$$\frac{S}{S_{max}} = \frac{\ln \frac{1}{2}(1+\sqrt{5})}{\ln 2} = 0.69424 \qquad (5.1.3)$$

while for the plane square "superexchange" model (Fisher, 1960)

$$\frac{S}{S_{max}} = 0.51481 \qquad (5.1.4)$$

For the standard two-dimensional Ising lattices the anomalous entropy is not known exactly, but is approximately 50% of the maximum (Domb, 1960). It was hoped (see Fisher, 1960) that this non-physical feature was a direct consequence of the simplicity of the Ising form of coupling, which would not arise in the case of a more realistic form of interaction. A detailed investigation of the anisotropic Hamiltonian

$$\mathcal{H} = 2|J| \sum_{(ij)} \left\{ S_i^z S_j^z + \gamma \left(S_i^x S_j^x + S_i^y S_j^y \right) \right\} \qquad (5.1.5)$$

was undertaken to clarify this point.

Ising Entropy Peaks. In Fig. (4.28) we have plotted the entropy per spin for an Ising ring of eight spins ($\gamma = 0$) as a function of field for various temperatures. The anomalous entropy peak is evident. Its height is given by $\frac{S}{Nk} = \frac{1}{8}\ln 47 = 0.4813$ which differs from the limiting ($N = \infty$) result 0.4812 by less than 0.03%. For fields less than H_c, however, the entropy does not fall to zero as might be expected, but to the value $(k/N)\ln 2 = 0.0866k$ ($N = 8$). This is a 'small number' effect arising from the twofold degeneracy (N even) of the antiferromagnetic ground state of the Ising model. In the limit $N \to \infty$, of course, this contribution vanishes.

Examination of the spectrum of eigenvalues of the Ising ring as a function of magnetic field (see Fig. (4.29)) reveals that the anomalous entropy peak is due to a confluence of a large fraction of the energy levels at the

Fig. 4.28

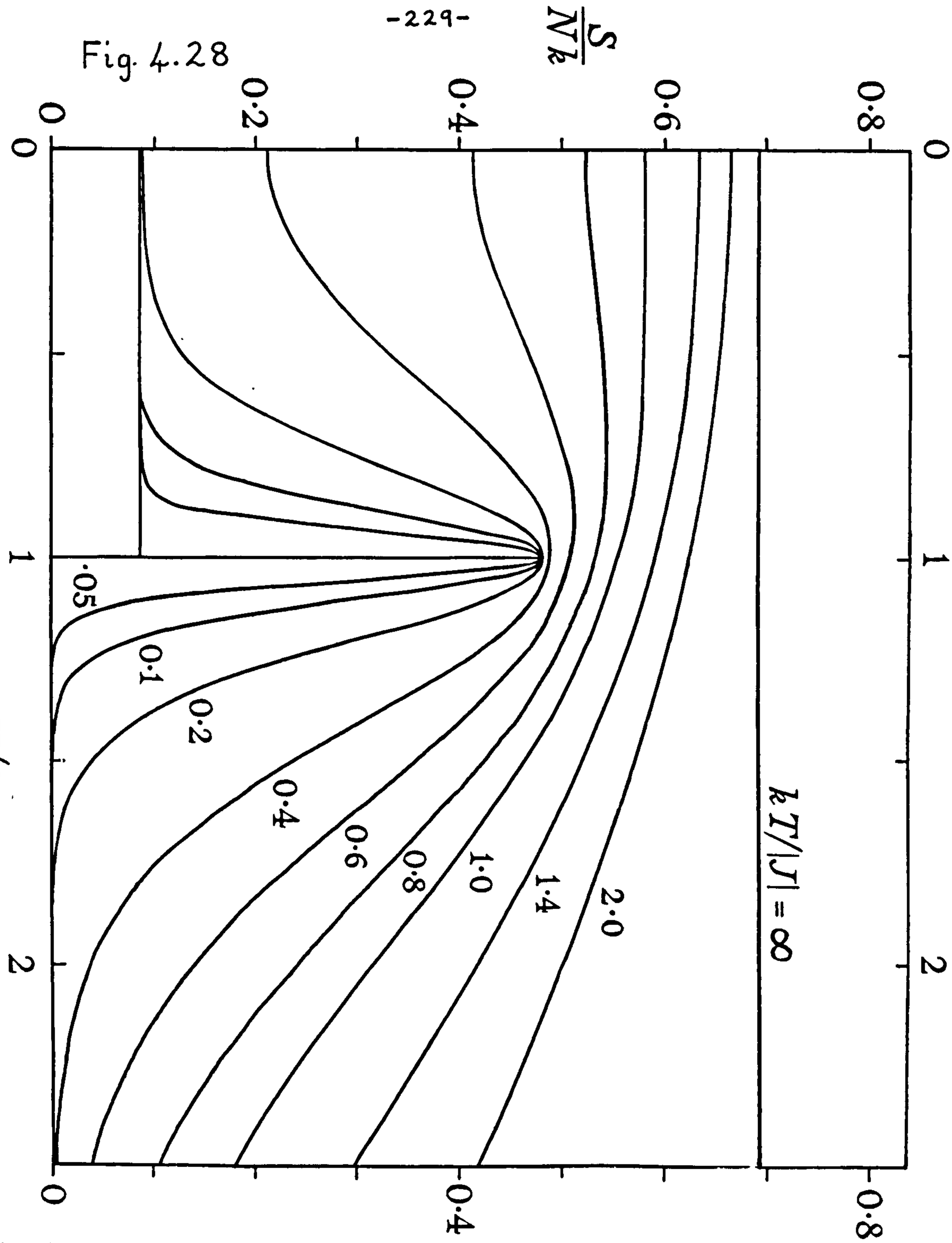

Variation of Entropy with Field and Temperature for $\gamma = 0$

critical field $H = H_c$. The multiplicity of this degeneracy for rings of $N = 2, 3, 4...$ spins is given by the Fibonacci series 3, 4, 7, 11, 18, 29, 47,...., the N^{th} term of which varies as $(\frac{1}{2} + \frac{1}{2}\sqrt{5})^N$ for large N. From this, the limiting result follows immediately. It is clear that any perturbation which splits this high degeneracy should result in the disappearance of the anomalous entropy at sufficiently low temperatures.

Effect of Boundary Conditions. Let us briefly consider the effect of a change in boundary conditions at this point. In the case of the Ising 8-spin free-ended chain, the zero-point entropy shows a different pattern. There are two anomalous peaks which persist down to T = 0. The first occurs at $H = \frac{1}{2} H_c$ and has magnitude $S/Nk = \frac{1}{8} \ln 6 = 0.2240$. The second occurs at $H = H_c$ and has magnitude $S/Nk = \frac{1}{8} \ln 21 = 0.3806$, appreciably lower than the peak for rings. However, it is easy to show that the first peak disappears in the limit $N \to \infty$ as $\frac{1}{N} \ln (N/2 + 2)$. For $N = 2, 3, 4, ...$ the peak at H_c has degeneracy 1, 2, 3, 5, 8, 13, 21,.... which again is a Fibonacci series. For sufficiently large N, this series has the same asymptotic behaviour as the series for rings, and therefore, as we would expect on general physical grounds, the change of boundary conditions makes no difference in the limit.

Effect of Transverse Terms of the Hamiltonian. A more effective way to split the high Ising degeneracy is by introducing, as a perturbation, the transverse part of the Hamiltonian (5.1.5) when $\gamma > 0$. Calculation shows that the degeneracy is indeed appreciably split. Fig. (4.30) shows the relevant part of the spectrum when $\gamma = 0.1$, which still corresponds to a rather anisotropic antiferromagnet. Although the multiple degeneracy is split there is still a considerable density of low-lying level crossings near the critical field. The doubly degenerate zero-field antiferromagnetic ground state is actually split, but by such a small amount (0.024%) that the two levels cannot be distinguished on the scale of the figure.

The situation is quite different at the Heisenberg limit, $\gamma = 1$, as shown

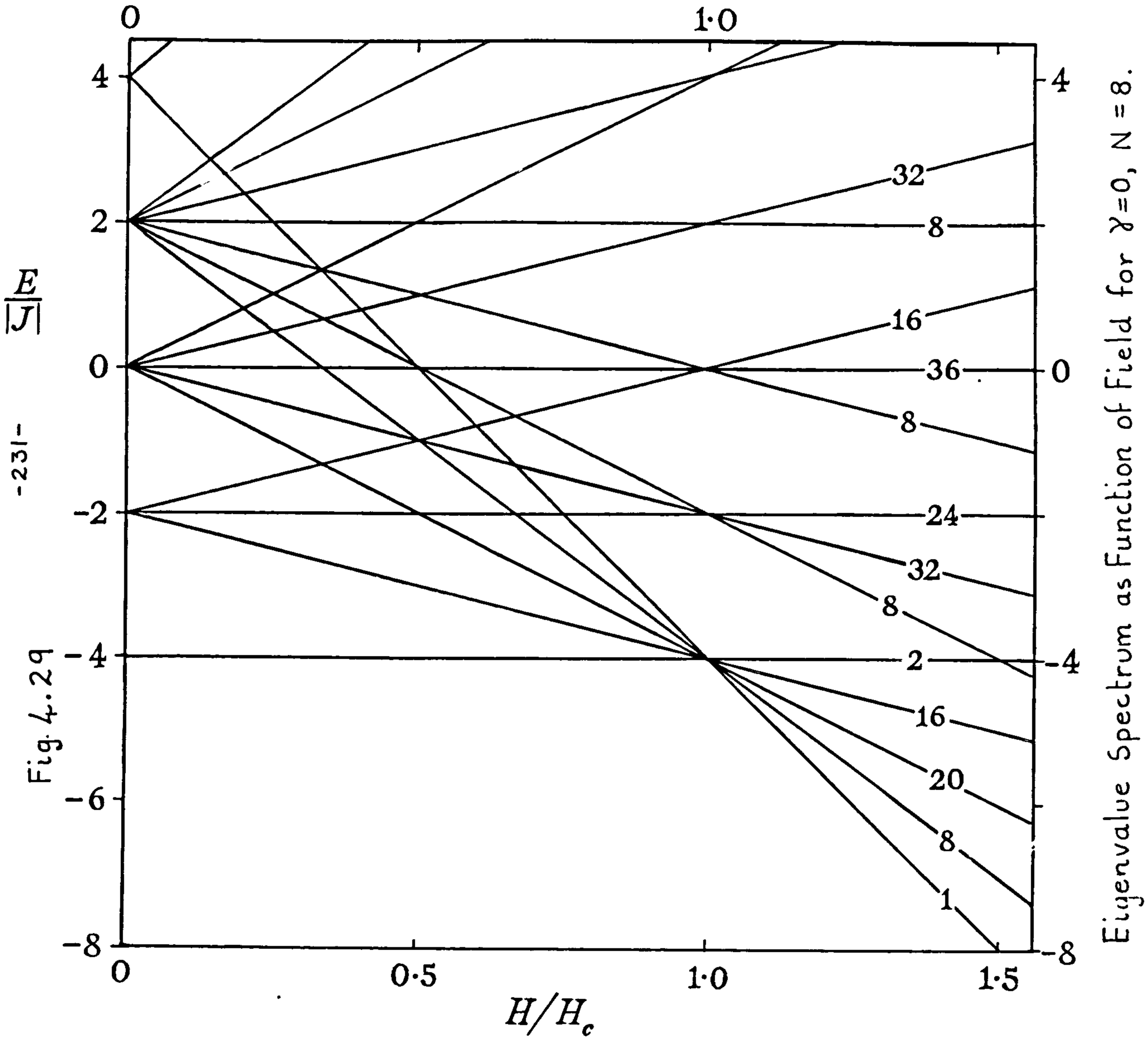
0
1·0
4
2
0
-2
-4
-6
-8
0·5
1·5
$\frac{E}{|J|}$
H/H_c
32
8
16
36
8
24
32
8
2
16
20
8
1
Eigenvalue Spectrum as Function of Field for γ=0, N = 8.

Fig. 4.29

Fig. 4.30

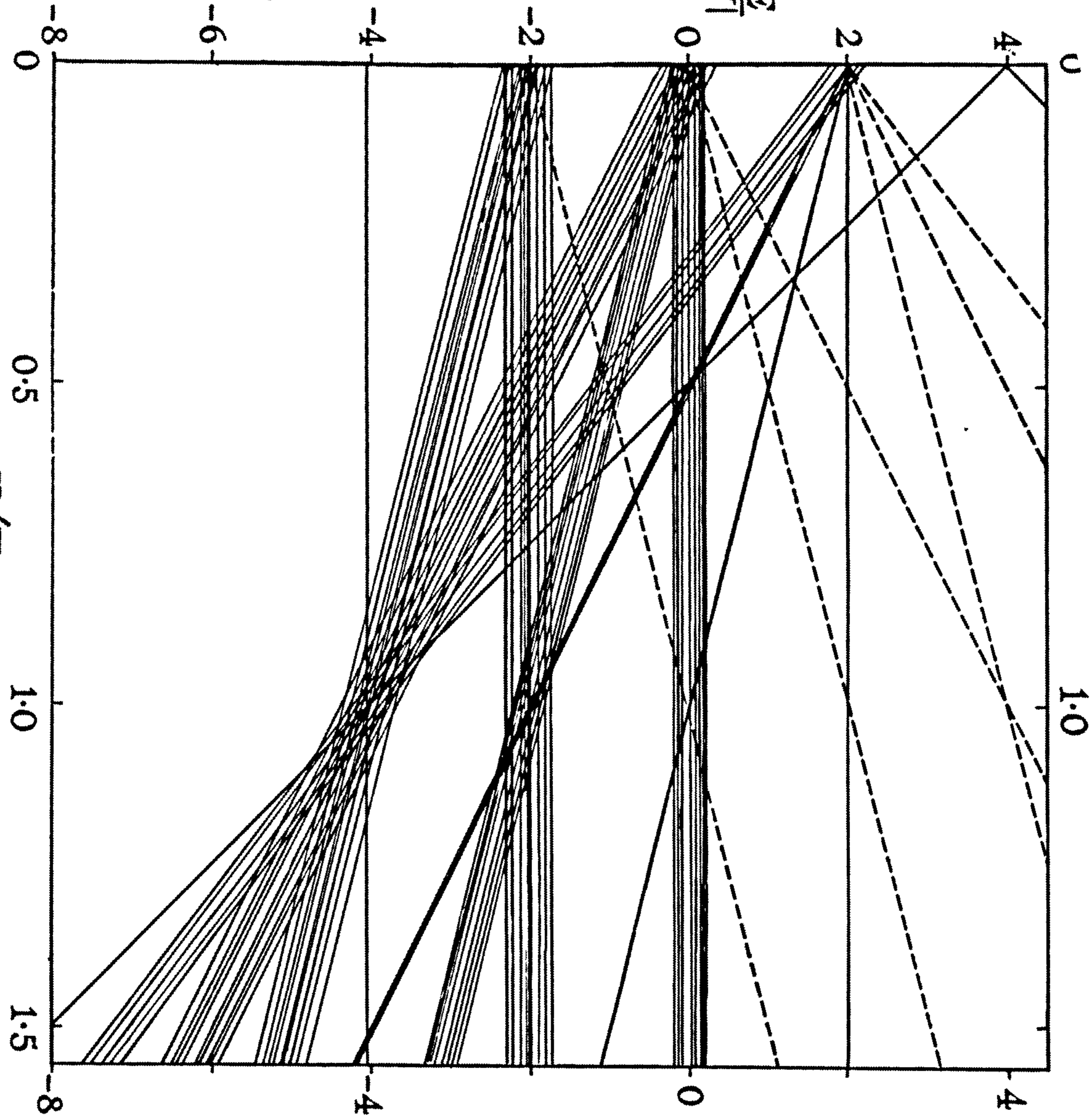

Spectrum of Eigenvalues for $\gamma = 0.1$

Fig. 4.31

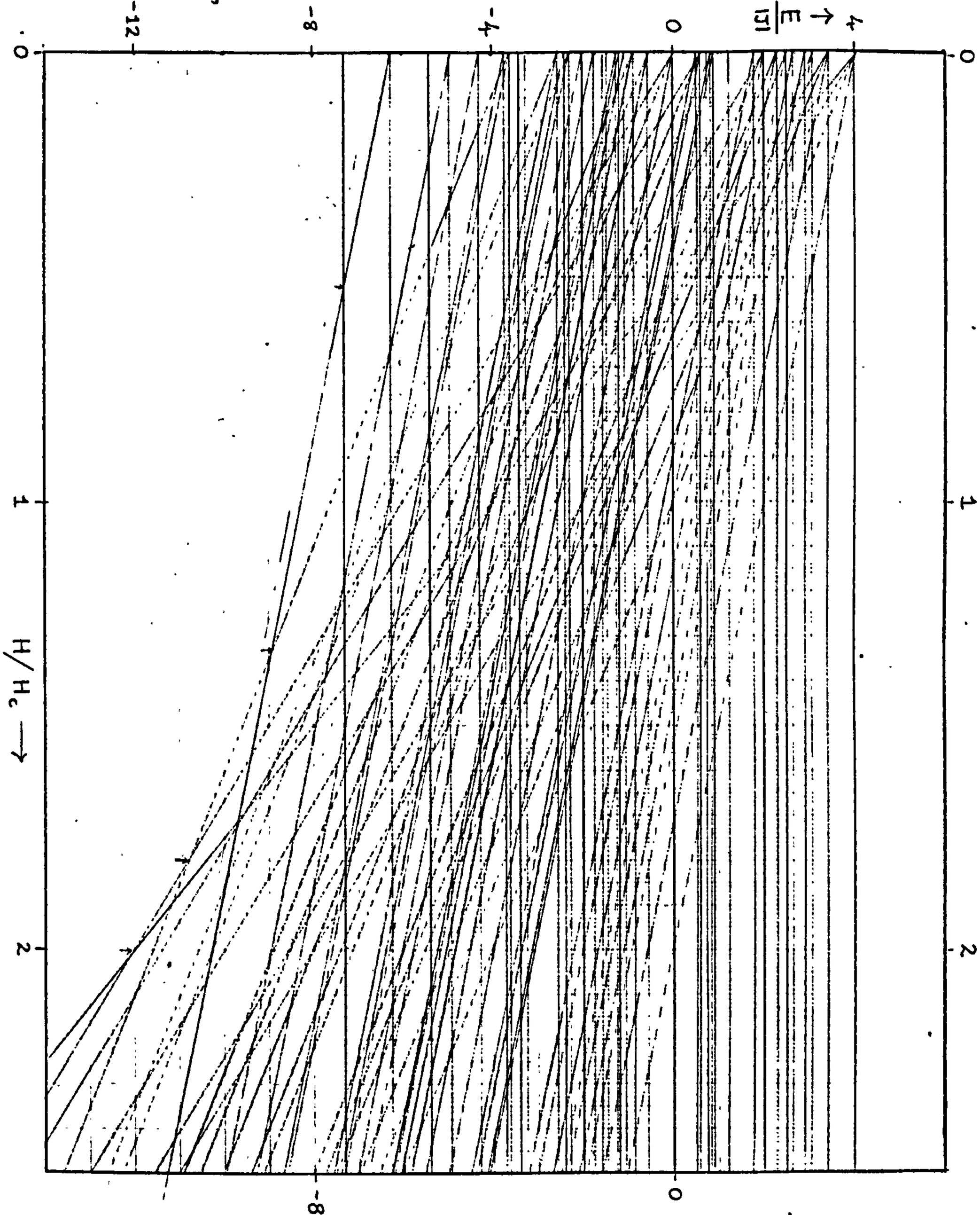

Eigenvalue Spectrum for Heisenberg Ring of 8 Spins.

in Fig. (4.31). The level density is rather uniform and only slowly changing. The only degeneracies in the antiferromagnetic ground state as a function of field, are twofold, and arise from the crossing of one level by a level of higher total S^z. In the general case there will be N/2 of these intersections ($H > 0$). It will be noticed that they spread out between $H=0$ and $H=2H_c$, although they tend to cluster more closely towards $H = 2H_c$. This diagram of crossing energy levels is fundamental to the understanding of other field-dependent thermodynamic properties. For example, each level crossing corresponds to a discontinuous jump in the curve of zero-temperature magnetisation as a function of applied field. The zero-temperature susceptibility curve shows N/2 infinite spikes at these field values. As the temperature is increased from zero, these infinities become finite broadened peaks. As T further increases, a single, rather broad susceptibility peak becomes dominant and the position of this peak moves to lower H values as T increases, reaching H=0 at a temperature equal to the temperature of the maximum in the zero-field susceptibility.

In Figs. (4.32), (4.33) and (4.34) we have plotted the entropies as derived from the calculated spectra for the cases $\gamma = 0.1$, 0.5 and 1 respectively. In Fig. (4.32) with $\gamma = 0.1$ we are still close to the pure Ising model (Fig. (4.28)) and the entropy isotherms are almost unchanged down to temperatures for which $kT/|J| = 0.2$. Below this temperature, however, the height of the entropy peak begins to fall rapidly and eventually the peak splits into separated compoents. This again is a small number effect and we must presume that in the limit $N \to \infty$ the peak will fall smoothly to zero. (Owing to the very small splitting of the zero-field antiferromagnetic ground state, noted above, the entropy below H_c still appears to fall to the value $(k\ln 2/N)$ rather than to zero. At very low temperatures, however, it will eventually fall to zero.) In the case of moderate anisotropy ($\gamma = 0.5$), shown in Fig. (4.33), the entropy maximum is much broader and has shifted to a higher value of the field. It also falls more rapidly at higher temperatures.

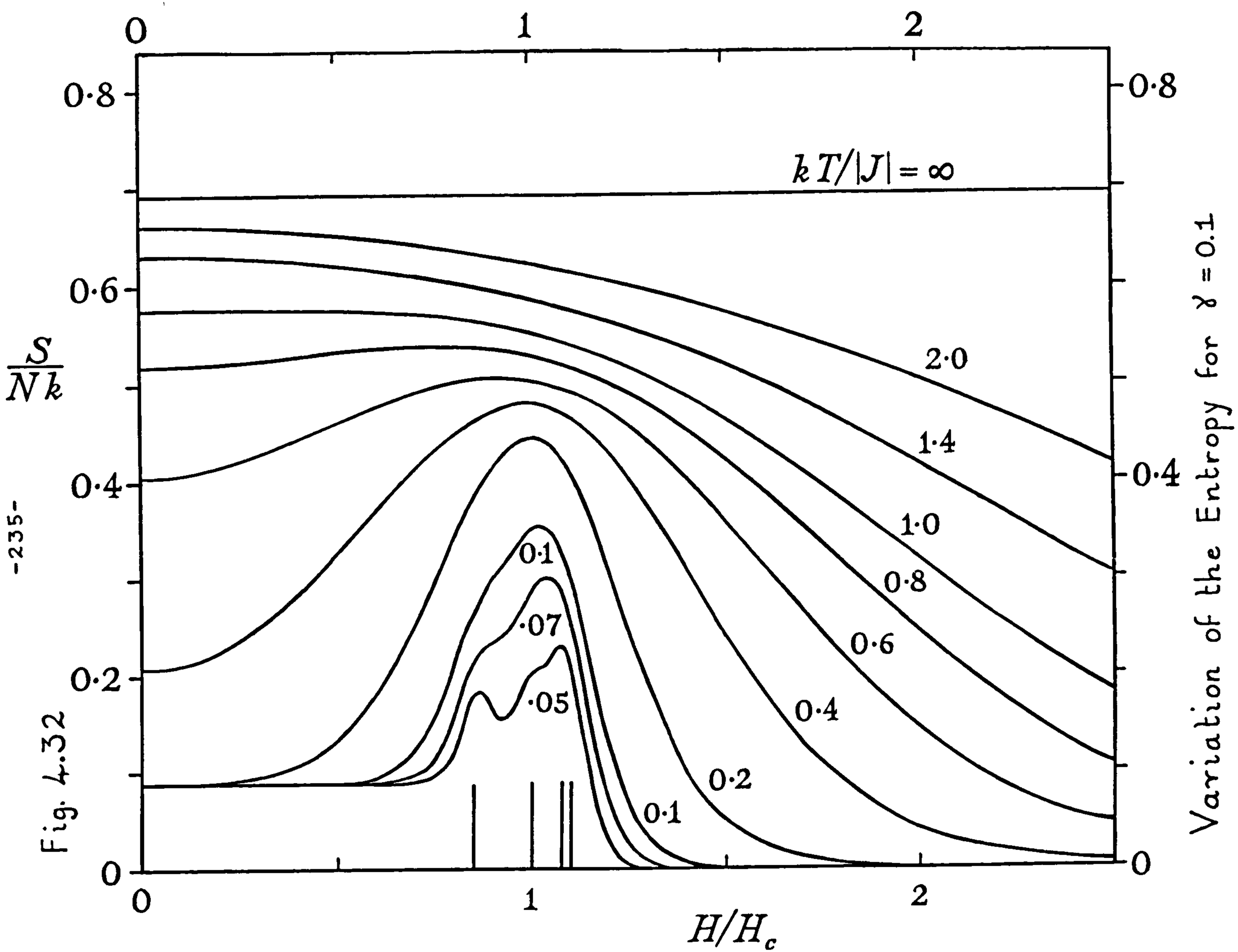

Fig. 4.32 Variation of the Entropy for $\gamma = 0.1$

Fig. 4.33

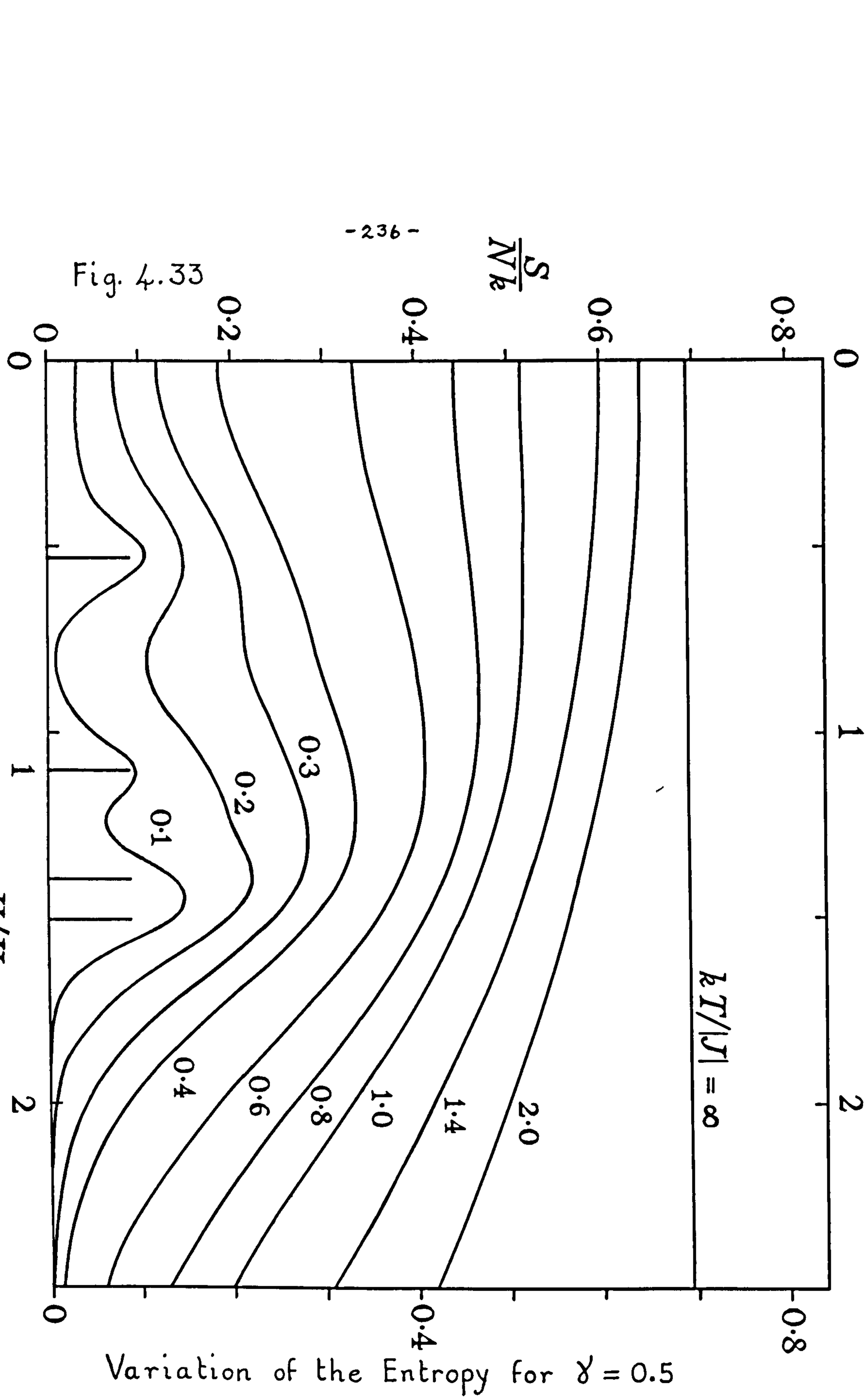

Variation of the Entropy for $\gamma = 0.5$

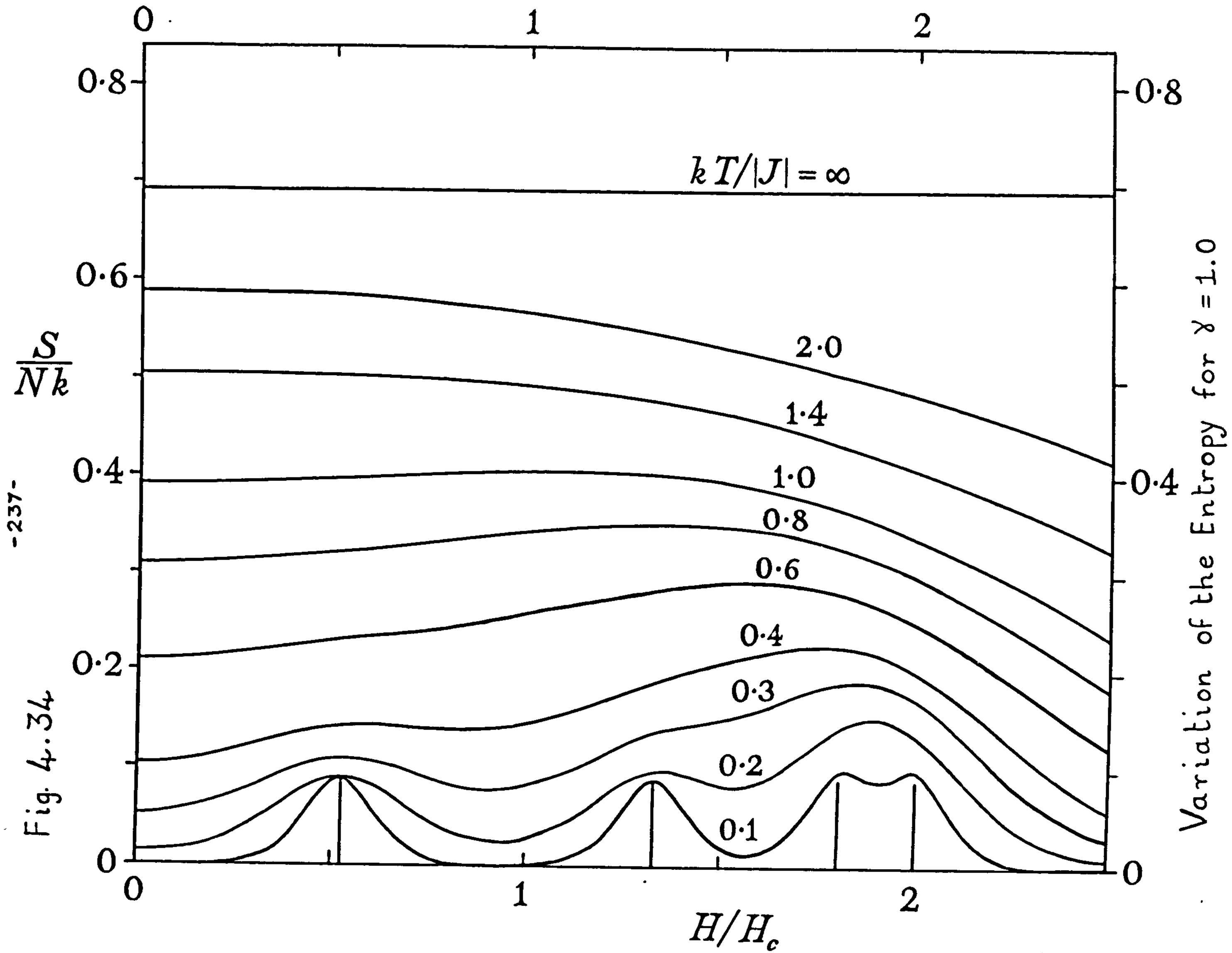

Fig. 4.34

Variation of the Entropy for $\gamma = 1.0$

At a temperature below kT/ |J| = 0.3 the maximum again splits into a series of smaller separated peaks. The same phenomenon occurs in the pure Heisenberg case (Fig. (4.34)) where the maximum is so spread out and so low in height as to be scarcely identified as a feature of interest. The small peaks in all these cases are of height $k\ln 2/N$ and correspond simply to the two-fold degeneracy that occurs when levels of adjacent S^z cross in a field. In the limit $N \to \infty$ these peaks will be absent, and the entropy must fall smoothly to zero in all fields.

Summary and Comparison with Other Models and Approximations. In Figs. (4.35) and (4.36) we summarise the main features of the dependence on anisotropy. In Fig. (4.35) the solid curves show the variation in height of the entropy maximum with temperature for different values of γ. We see that the anomalous zero-point entropy occurs only at the Ising limit, although, if there is sufficient anisotropy, an appreciable entropy peak remains to quite low temperatures, even when $\gamma > 0$. These curves are plotted for N=8 but except at the lowest temperatures, where the curves are shown by broken lines, they are likely to differ by no more than a few percent from the limiting results for $N = \infty$. We also observe, in Fig. (4.35), a set of dotted curves which represent the behaviour, as a function of temperature and anisotropy, of the zero-field entropy minima.

After this study was completed, the X-Y model for a spin-1/2 linear magnetic chain was solved exactly for the thermodynamic properties by Katsura (1962). In particular, Katsura was able to demonstrate that the X-Y model of an infinite chain displays no anomalous entropy peak.

A linear chain of coupled spins does not of course show a phase transition, although we may distinguish a predominantly antiferromagnetic region from a predominantly paramagnetic region, at high fields and temperature. In Fig. (4.36) we show the loci of the entropy maxima for γ =0, 0.5 and 1.0 in the (H, T) plane, the region inside the loci being the region of predominantly antiferromagnetic

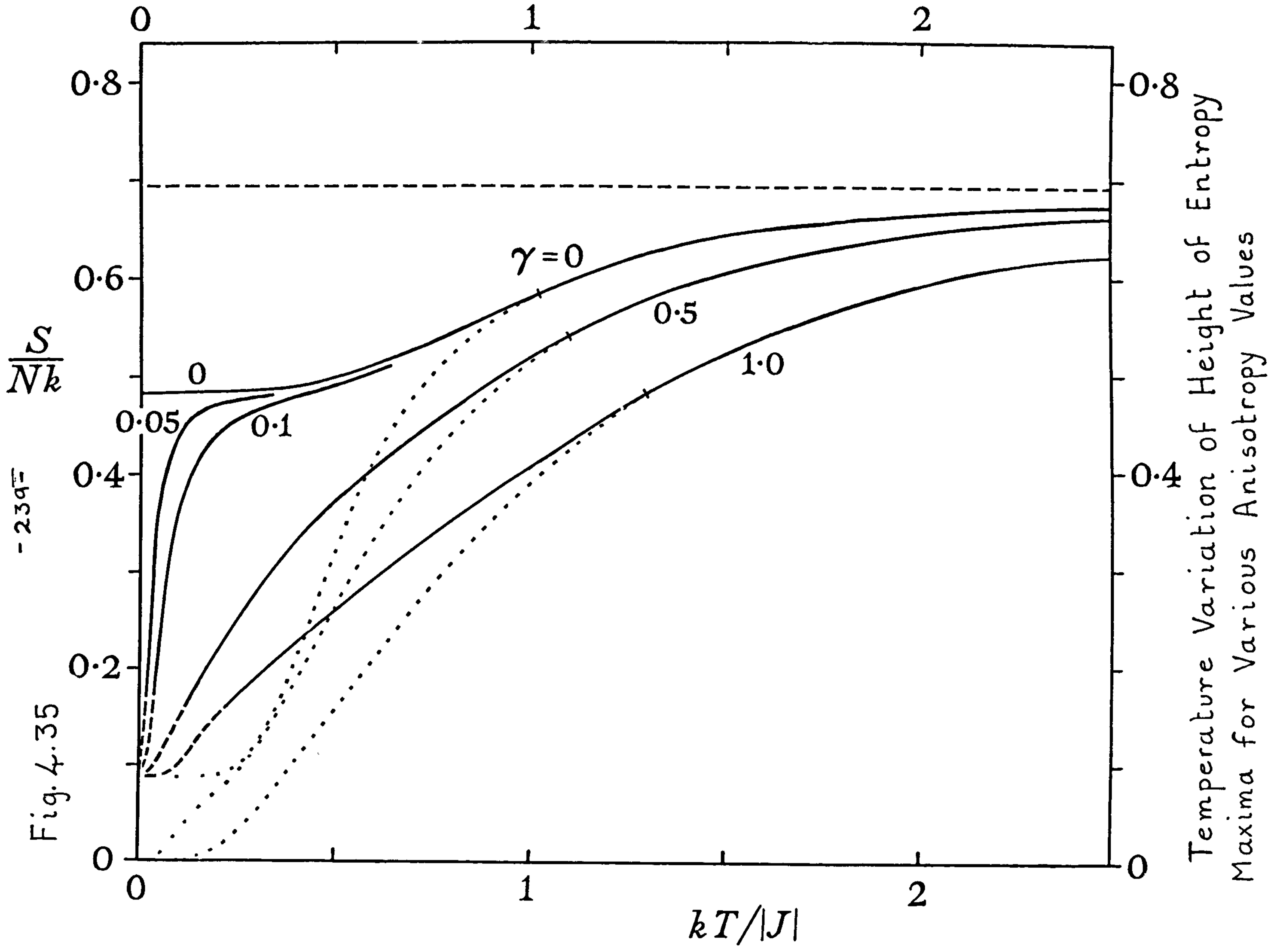
0
1
2
0·8
0·6
0·4
0·2
0
$\frac{S}{Nk}$
$\gamma = 0$
0·5
1·0
0
0·05
0·1
$kT/|J|$
Temperature Variation of Height of Entropy Maxima for Various Anisotropy Values

Fig. 4.35

ordering. (Falk, 1965) refers to this maximum entropy locus as a pseudo-phase boundary, since there is no discontinuity in the thermodynamic quantities as the boundary is crossed, for $T > 0$. Two- and three- dimensional models (except for the Heisenberg limit in two dimensions) must be expected to show a proper transition, with an associated specific heat anomaly, as do real antiferromagnets. The effect of a transition on the entropy variation, however, should not be very marked. According to the exactly soluble two-dimensional super-exchange Ising model (Fisher, 1960), the main change will be merely a steepening up of the rate of increase of entropy with field on the low field side of the entropy maximum. Consequently the general features of the entropy variation and its dependence on anisotropy for linear systems should be valid for two- and three- dimensional Heisenberg-type models and for real antiferromagnets of simple structure.

In Fig. (4.36), the curve for $\gamma = 1.0$ is actually the curve for N = 10. For values of $g\beta H/|J| < 2.0$, the rapid convergence of the curves for N=6 and 8 (not shown) and N=10 suggest that in the region the curve for N=10 should be extremely close to the limiting $N = \infty$ curve. The curve meets the T-axis at $kT/|J| = 1.28$, which is our estimated position of the zero field susceptibility maximum for $\gamma = 1.0$. In the region where $T \rightarrow 0$, we know that the limiting loci must cut the H axis at points given by $g\beta H/|J| = 2(1+\gamma)$. The finite N curves for $\gamma = 1.0$ show a complicated convergence in the low-T region, meeting the H-axis at points 3.618, 3.802, and 3.880 for N = 6, 8 and 10, respectively. The solid curve through the encircled points which meets the H-axis at $g\beta H/|J| = 4$ is a curve obtained by Falk and Ruijgrok (1965) and (Falk, 1965) based on the work of Bulaevskii (1963). We shall observe in Chapter V, subsection (3.7) that the Bulaevskii approximation predicts a behaviour for the curve of zero-temperature magnetisation as a function of field, near the saturation field $g\beta H/|J| = 4.0$, which is equivalent to the exact Heisenberg result. It therefore seems plausible that the Bulaevskii-Falk entropy locus will be very similar to the correct limiting

Fig. 4.36

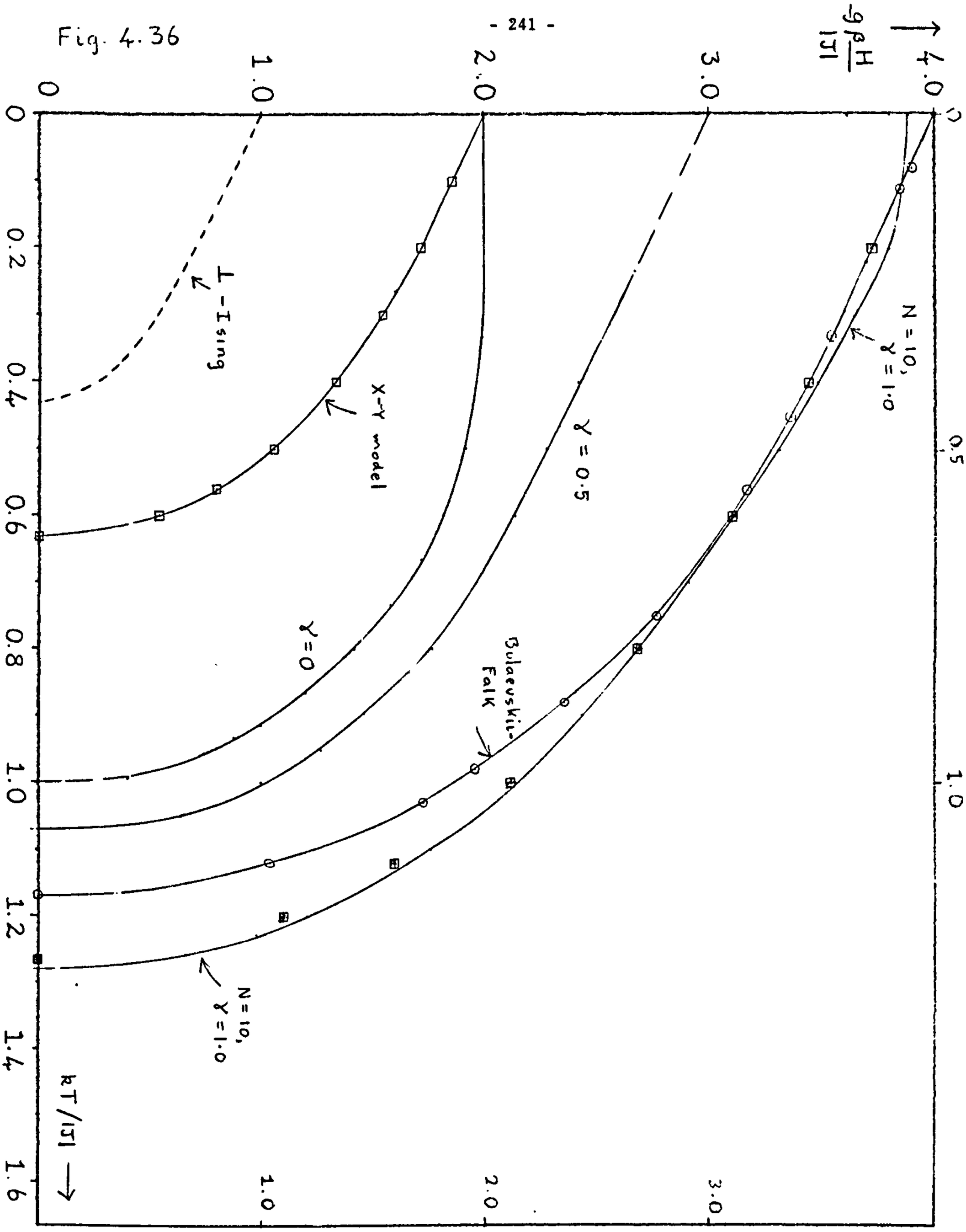

Comparison of Linear Chain 'Pseudo-phase' Boundaries for Various Models and Approximations.

behaviour of the $\gamma = 1.0$ curve in the region $T \to 0$ and $g\beta H/|J| \to 4$. It is consistent, in fact, with the convergence of the finite N curves, that the limiting Heisenberg curve should follow the Bulaevskii-Falk curve for $kT/|J| < 0.7$ and $3.0 < g\beta H/|J| \leq 4.0$. At lower field values, however, the Bulaevskii-Falk curve deviates from the limiting Heisenberg curve, as shown in Fig. (4.36).

The curve for $\gamma = 0.5$ is a similar estimate of the limiting curve, based closely on the N=10 curve for $\gamma = 0.5$, which cuts the T-axis at $kT/|J| = 1.07$ and goes linearly in to the H-axis at $g\beta H/|J| = 3.0$. The slope of our $\gamma = 0.5$ curve near T=0 appears closely similar to slope of the $\gamma = 1.0$ slope, and we have estimated both to be $g\beta\Delta H/kT = 1.20 \pm 0.10$.

Falk quotes a slope of $\frac{g\beta\Delta H}{kT} = 1.25 \pm 0.10$ for the Bulaevskii-Falk curve.

The behaviour of the $\gamma = 1.0$ and $\gamma = 0.5$ curves in this region is to be contrasted with the Ising curve, $\gamma = 0$, which goes in to the H-axis at $g\beta H/|J| = 2$ with zero-slope. The variation at the opposite end of these curves, near H=0, appears to be quadratic in H. Falk was able to demonstrate a similar quadratic behaviour for the Falk-Bulaevskii curve by means of a perturbation analysis. We also show, on Fig. (4.36), the X-Y model curve computed numerically by Falk and Ruijgrok (1965) and (Falk, 1965). In the region near T=0 the curve is linear, with a finite slope which is very similar to the slopes of the Heisenberg curve, the Bulaevskii-Falk curve and the curve for $\gamma = 0.5$. Falk estimates that $\frac{g\beta\Delta H}{kT} = 1.31 \pm 0.10$ for the X-Y model. Near H=0, the curve has again a quadratic variation with H, meeting the T axis at $kT/|J| \simeq 0.632$. It is obvious at once that the X-Y curve and the estimated limiting curve show a striking resemblance of shape, and if we plot the points for X-Y curve on a scale expanded by two for both the H and T axes, we obtain the series of points denoted by dark squares in the neighbourhood of our $\gamma = 1$ curve. It is very suggestive that the curve for N=10 in the region for $H < 2.0$ on which our $\gamma = 1$ limiting curve is based, has not quite converged to the limit, and if we further assume that the X-Y points calculated by Falk have

a small numerical uncertainty (as would appear from a graph due to Falk, 1965 private communication), we would strongly suspect that the X-Y curve and Heisenberg curve are represented by the same function of H and T, i.e. $f_{X-Y}(H,T)$ $= f_{Heis}(H',T')$ where H' = 2H and T' = 2T.

The observed difference in shape between the Heisenberg and Ising curves suggests that the finite non-zero slope of the Heisenberg and X-Y curves near T=0 results from the effect of a field in the z-direction on spin components in the perpendicular directions, x or y. Since the effect of a perpendicular field will be identical for spins aligned either parallel or antiparallel, the X-Y curve applies to both ferromagnets and antiferromagnets. Another curve which will be identical for both ferro- and antiferromagnets is the dotted curve marked '⊥ar-Ising' which may be taken to represent the effect of a magnetic field in the x-direction on a linear chain of coupled Ising spins, i.e. spins ordered either parallel or antiparallel in the z-direction. The '⊥ar-Ising' model, unlike the Ising model, does not show an anomalous entropy peak at absolute zero temperature. For this curve, however, only the points where the curve meets the H- and T-axes are known exactly (Fisher, 1963) and (Katsura, 1962). The curve as a whole must be regarded as a sketch showing a finite slope near T=0 and a quadratic variation with H near T=0.

5.2 Antiferromagnetic Specific Heats

The variation of antiferromagnetic specific heat with magnetic field may be studied just as for zero field. In particular, we shall consider the variation of specific heat with temperature for various fields both below and above the critical field, for a particular γ. We find that in general, in the presence of a field, convergence is improved. In fact, the convergence above $kT/|J| \simeq 0.3$ is quite rapid, especially if consecutive means for N = 2n and N = 2n+1 are considered. At lower temperatures the behaviour of the finite rings is rather erratic because of the rather artificially large variations in low-lying level densities caused by the crossings of levels of various S^z discussed at length in the previous sub-section. In Fig. (4.37) we have

plotted for the pure Heisenberg case the mean specific heats for N=10 and N=9 at various fields (except at H=0 where the estimated limit is shown.) These means should represent the true limiting curves to within 1 or 2% down to temperatures of $kT/|J| \simeq 0.5$. We compare this Fig. (4.37) with Fig. (4.38) which contains the exact, limiting Ising specific heat curves for various fields. The general pattern of convergence is essentially similar. In the Ising case, as the field increases from zero, the maximum at first falls in height and goes to lower temperatures. Eventually (see the curve for H = 1.5) a double peak develops, and the lower peak tends to T = 0 and vanishes altogether at the field $g\beta H/|J| = 2.0$, which is the critical field for Ising antiferromagnets. The general trend is the same in the Heisenberg limit, although the double peak effect does not appear so prominent. The critical field in this case is $g\beta H/|J| = 4.0$. At the critical field magnetic saturation occurs and the peak is relatively low and broad. Above the critical field in the Ising case, the pattern of convergence is similar, only reversed, as H increases. For example, the curve for H=3 is similar to the curve for H = 1.5. At higher fields, the maximum continues to increase in height and pass to higher temperatures. In the Heisenberg case, however, it seems that for higher fields the curve stays rather similar in form to the critical curve, except that the height of the maximum, and the position as a function of temperature, slowly start to increase again. For $\gamma = 0.5$ (see Fig. (4.39)) the situation is generally similar to the Heisenberg limit. For fields greater than H_c, the convergence of the finite N curves is very good indeed. Clearly the energy levels even for small rings have been spread out by the magnetic field in such a way that they have an ordering which is essentially similar to the limiting ordering. The initial rise of the curves is governed by the energy gap

$$\Delta E_H(\gamma) = H - J\beta - 2(1+\gamma)|J| . \qquad (5.2.1)$$

5.3 Ferromagnetic Specific Heats

In Fig. (4.40) we show the variation of the ferromagnetic specific heat

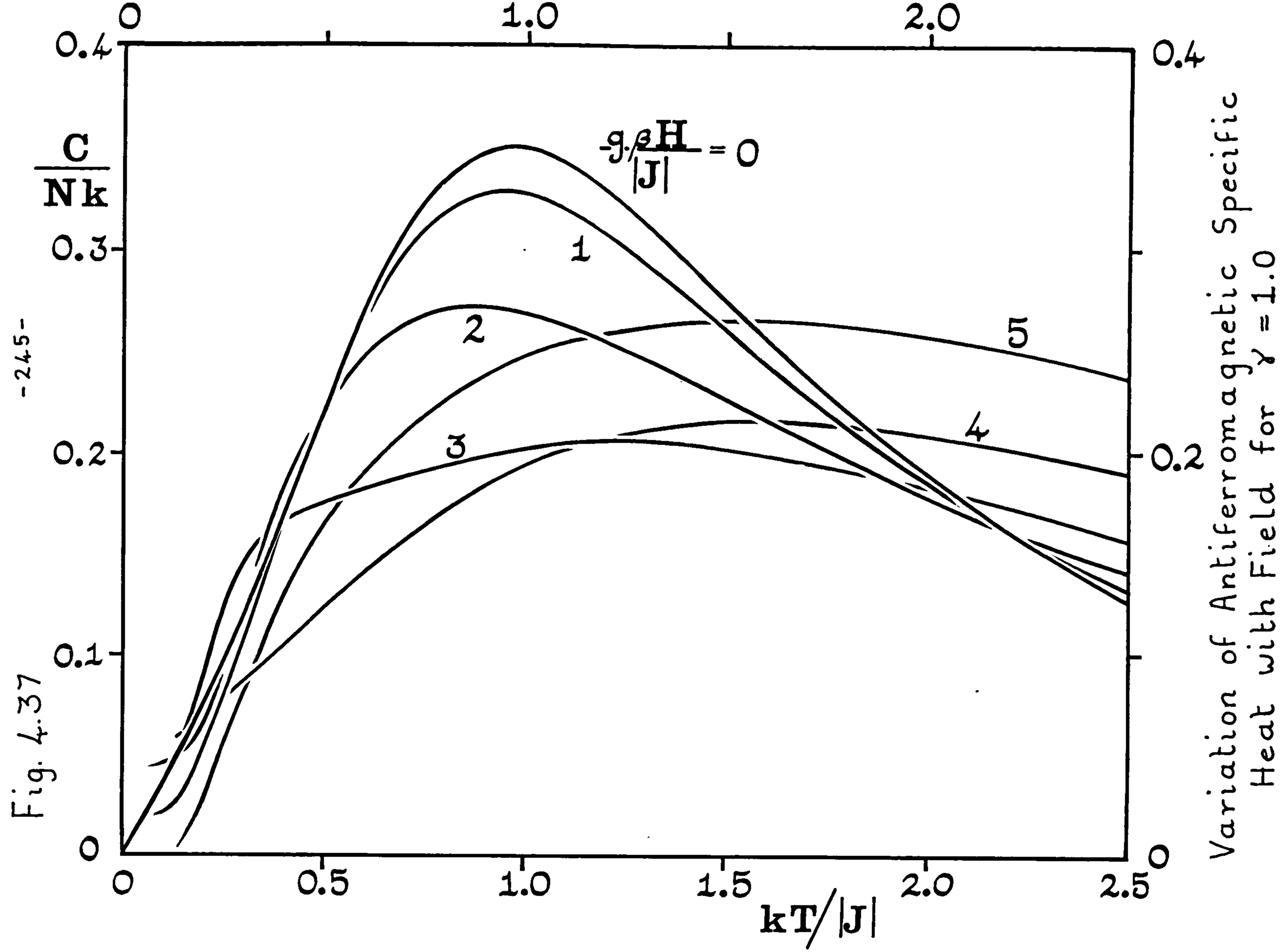

Fig. 4.37 Variation of Antiferromagnetic Specific Heat with Field for $\gamma = 1.0$

Fig. 4.38

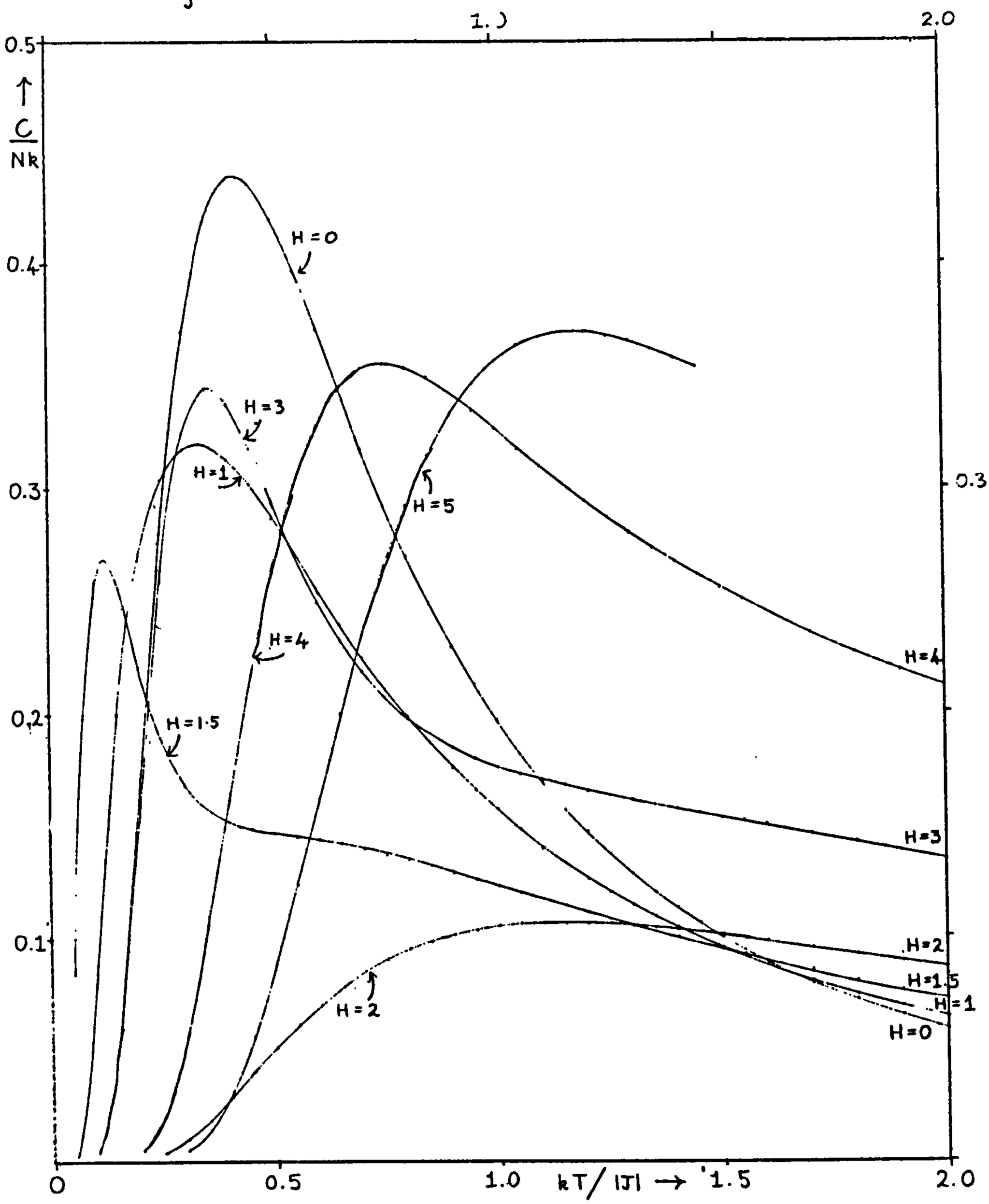

Variation of Antiferromagnetic Specific Heat with Magnetic Field for $\gamma = 0$.

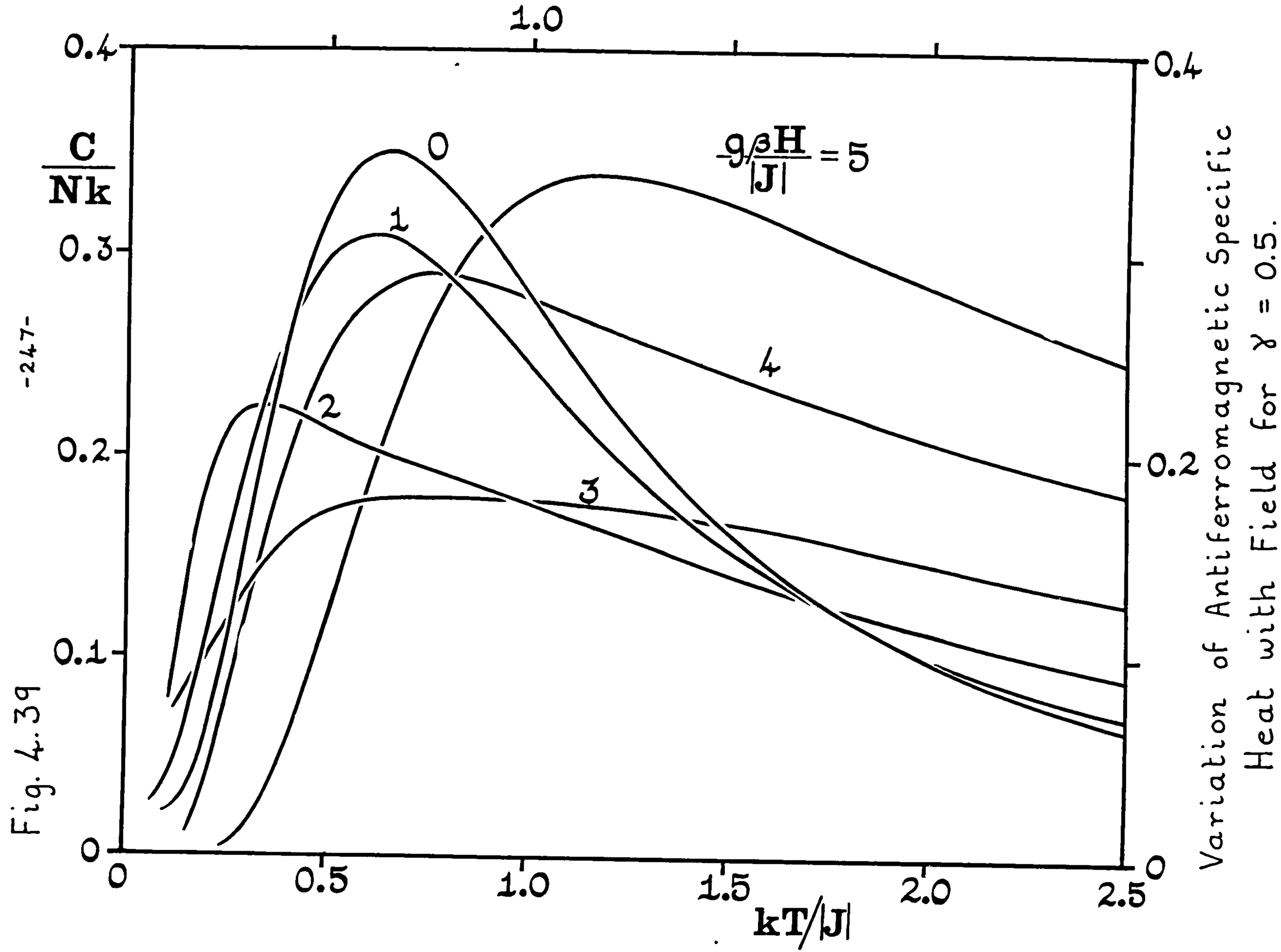

Fig. 4.39 Variation of Antiferromagnetic Specific Heat with Field for $\gamma = 0.5$.

with magnetic field for $\gamma = 1$. The curves are those for N=8 (except for H=0, where the estimated limiting curve is plotted) but should not differ significantly from the corresponding limiting curves since convergence is much faster for $H > 0$. For example, for $\frac{g\beta H}{J} = 2$, the curves for N=6 and N=7 are indistinguishable from N=8 over the whole range of temperature shown on the graph. When $H > 0$, there is an abrupt change in the character of the spectrum, since the degeneracy for $H = 0, \gamma = 1$ due to conservation of total spin is broken for all $H > 0$. In particular, the (N + 1)-fold degeneracy of the ferromagnetic ground state is split, and the ground state becomes non-degenerate and separated from the first excited state by a finite energy gap, even in the limit $N = \infty$. The splitting of degeneracy manifests itself as a sharp increase in the specific heat maximum for $g\beta H/J = 0.5$. The relatively high, narrow maximum shows that the ferromagnetic system in a magnetic field, even a small field, is much more stable than in zero-field. The variation in the height and position of the specific heat maximum are shown in Table (4.1). It may be noted that the effect of increasing magnetic field on the ferromagnetic specific heat is very similar to the effect of increasing anisotropy.

Table (4.1)

$g\beta H/J$	C_{max}/Nk	kT_{max}/J
0	0.134	0.70
0.5	0.368	0.61
1.0	0.419	0.94
1.5	0.443	1.22
2.0	0.454	1.47

Fig. 4.40

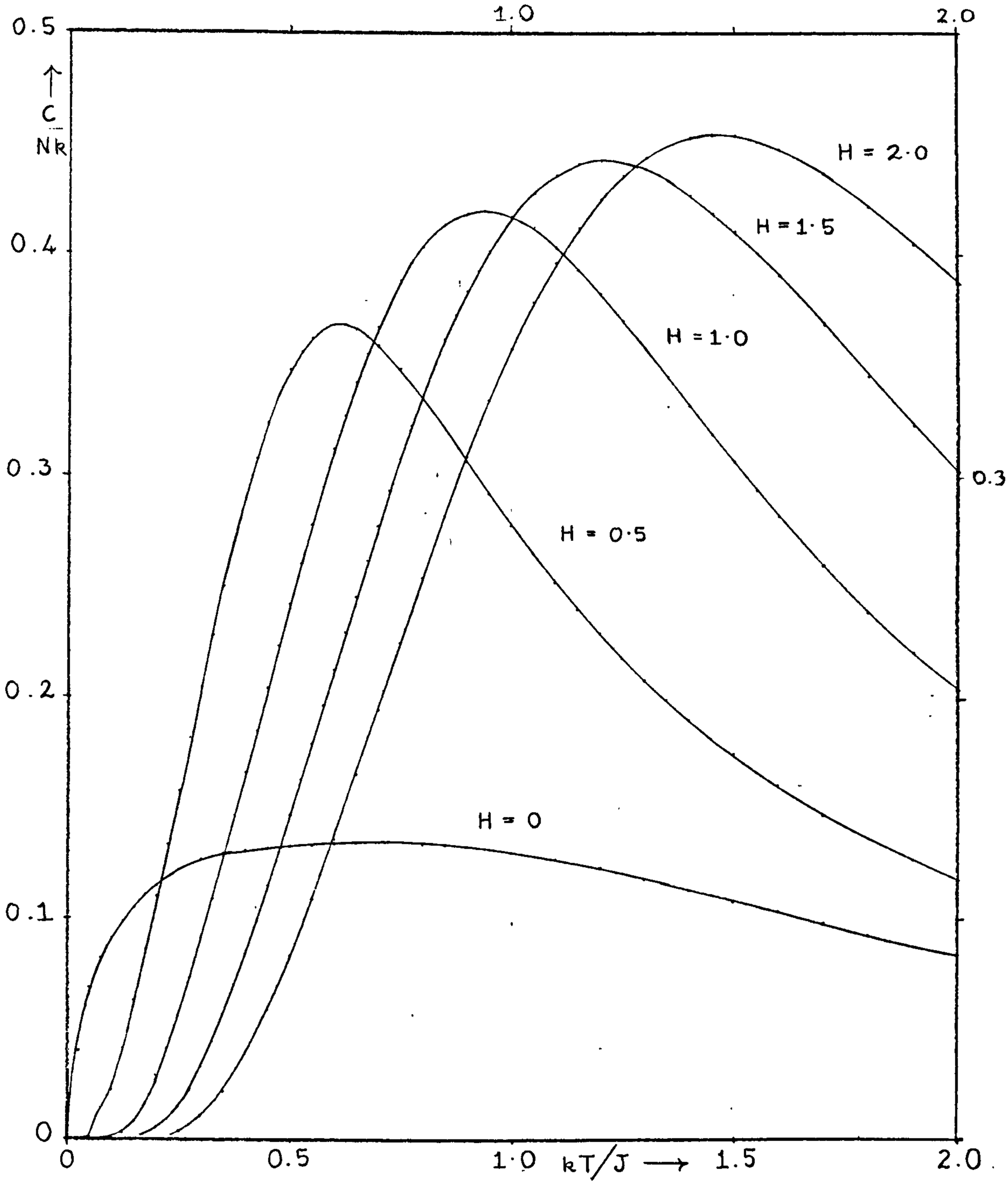

Variation of Ferromagnetic Specific Heat with Magnetic Field for $\gamma = 1.0$

CHAPTER V

MAGNETIC PROPERTIES

Introduction

Our primary aim in this chapter will be to estimate the limiting magnetic properties, especially the magnetisation versus magnetic field isotherms and the various temperature dependent magnetic susceptibilities (parallel and perpendicular, isotropic and anisotropic, ferromagnetic and antiferromagnetic, in zero field and in an applied field.) We shall see, as we remarked in Chapter IV, that the convergence of the finite ring curves is adequate to indicate the limiting behaviour for all γ at temperatures above $kT/|J| \simeq 0.5$.

In the Heisenberg limit, the Baker, Rushbrooke and Gilbert two-point Padé approximation is in fairly good agreement with our results, and other approximate methods are in much poorer agreement.

As in the case of the thermal properties we have attempted to extend our estimates right down to T=0 with the aid of extrapolation techniques and a detailed study of the magnetic energy levels of the spectrum. For example, the zero field, zero temperature susceptibility for $\gamma = 1$ is shown to be finite, in contrast to the predictions of many previous theories. However, our estimate for the limiting value, χ_o, disagrees by 10% with the analytic work of Griffiths (1964) subsequently confirmed rigorously by Yang and Yang (1966). This discrepancy is appreciably larger than our estimated limits of extrapolation uncertainty and the reason for this is apparently related to the fact that the limit T=0, H=0 is a weak non-analytic point for the Heisenberg (γ =1) model. This weak non-analyticity is not evident from our sequence of rather short rings and chains.

A rather similar disagreement arises in the zero temperature M versus H curves near M=0 for $0 < \gamma < 1$. The exact work of Yang and Yang (1966) indicates that the M versus H curves come into the M=0 axis with infinite slope, which our extrapolation procedures were not sufficiently sensitive to detect. However, it should be pointed out that our extrapolation methods are generally quite accurate for the form of, for example, the zero temperature magnetisation curve at $\gamma = 1$, and we have been able to deduce the correct analytic form of the T=0 magnetisation curves near the point of saturation.

1. PARALLEL SUSCEPTIBILITY

1.1) Antiferromagnetic Coupling

In Fig. (5.1) we plot the antiferromagnetic susceptibilities for isotropic Heisenberg coupling ($\gamma = 1$) in zero field for finite rings of $N = 3, 4, 5, \ldots\ldots, 11$ spins. The limiting curve is apparently bracketed by the curves for odd N, which approach monotonically from above, and those for even N, which approach monotonically from below. The convergence is clearly very similar to the corresponding case with Ising coupling (as discussed in Chapter IV, subsection (1.3)) where all the finite odd N curves diverge as T^{-1} as $T \to 0$, although in the limit they converge to a finite value (zero) at $T = 0$. The convergence is rather rapid above $kT/|J| = 0.6$, at which temperature the values for $N = 10$ and 11 differ by only 5%, and their mean probably differs from the true limiting curve by less than 1%. As in the Ising case, at lower temperatures the convergence is more complicated. For N even, the antiferromagnetic ground state for $\gamma = 1$ and also general γ, has $S^z = 0$, and there is an energy gap to the first excited state of non-zero S^z. Consequently, for all finite rings, the susceptibility parallel to the z-axis approaches zero exponentially fast as $T \to 0$, at a rate governed by the energy gap. For finite odd N and $\gamma \neq 0$, the ground state is a $|S^z| = 1/2$ state which is just twofold degenerate. The susceptibilities go as $\frac{|J|\chi}{Ng^2\beta^2} \simeq \frac{K}{4N}$, for all γ. [Note that this formula is the same as we derived for the Ising limit in Chapter IV, subsection (1.3)]. However, for the isotropic pure Heisenberg case, we expect the behaviour as $T \to 0$ to be different from the Ising case. We know that in the limit $N \to \infty$, the energy gap vanishes as 1/N. This implies that the limiting susceptibility for $\gamma = 1$ can approach a finite <u>non-zero</u> value χ_o at $T = 0$. The detailed mechanism by which this behaviour comes about will be discussed in detail in subsection (3.1) of this chapter. A non-zero χ_o for isotropic coupling occurs in the limiting case of infinite spin, where its existence can be demonstrated rigorously (Fisher, 1964). The X-Y model of

Fig. 5.1

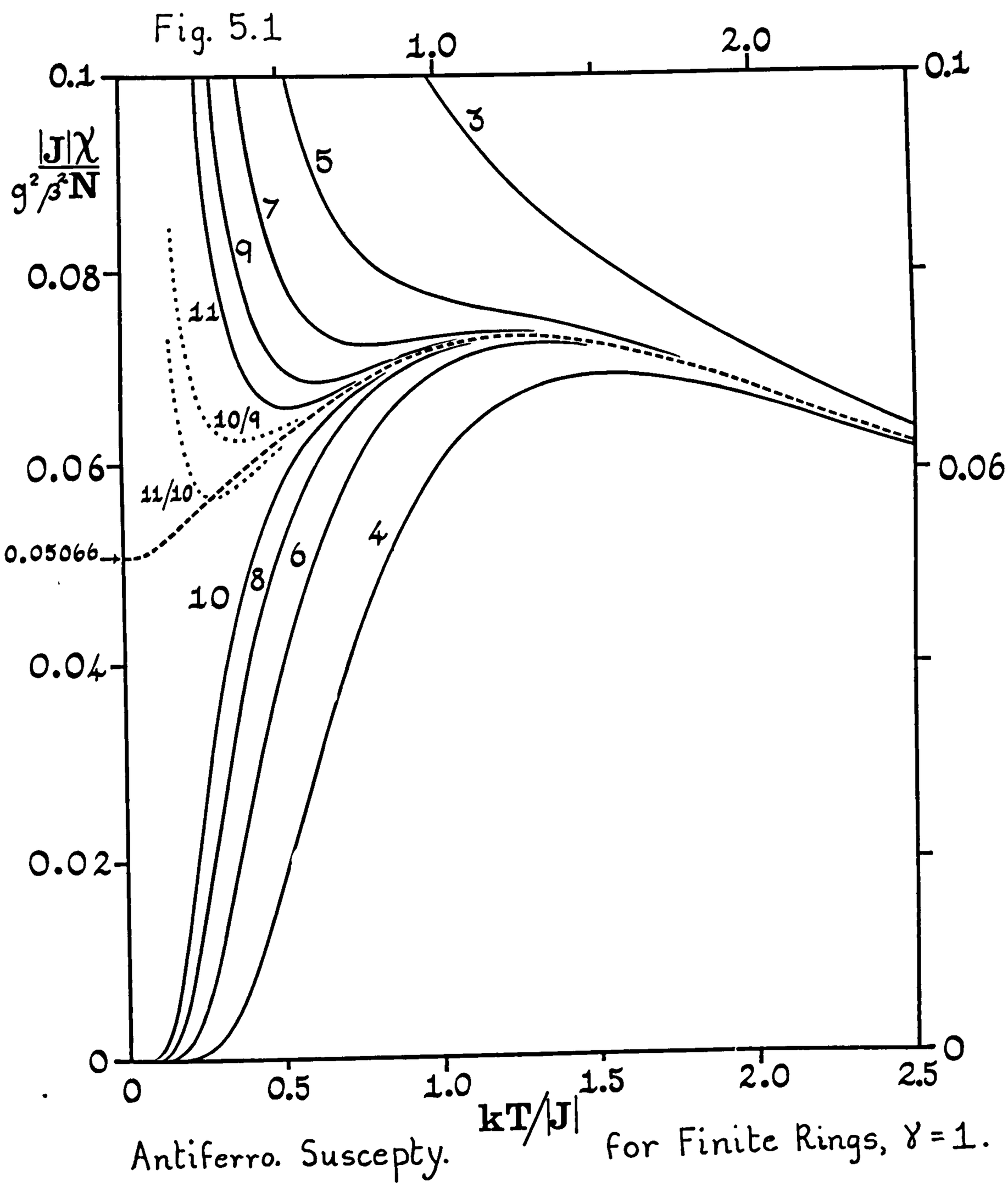

Antiferro. Suscepty. for Finite Rings, $\gamma = 1$.

Fig. 5.2

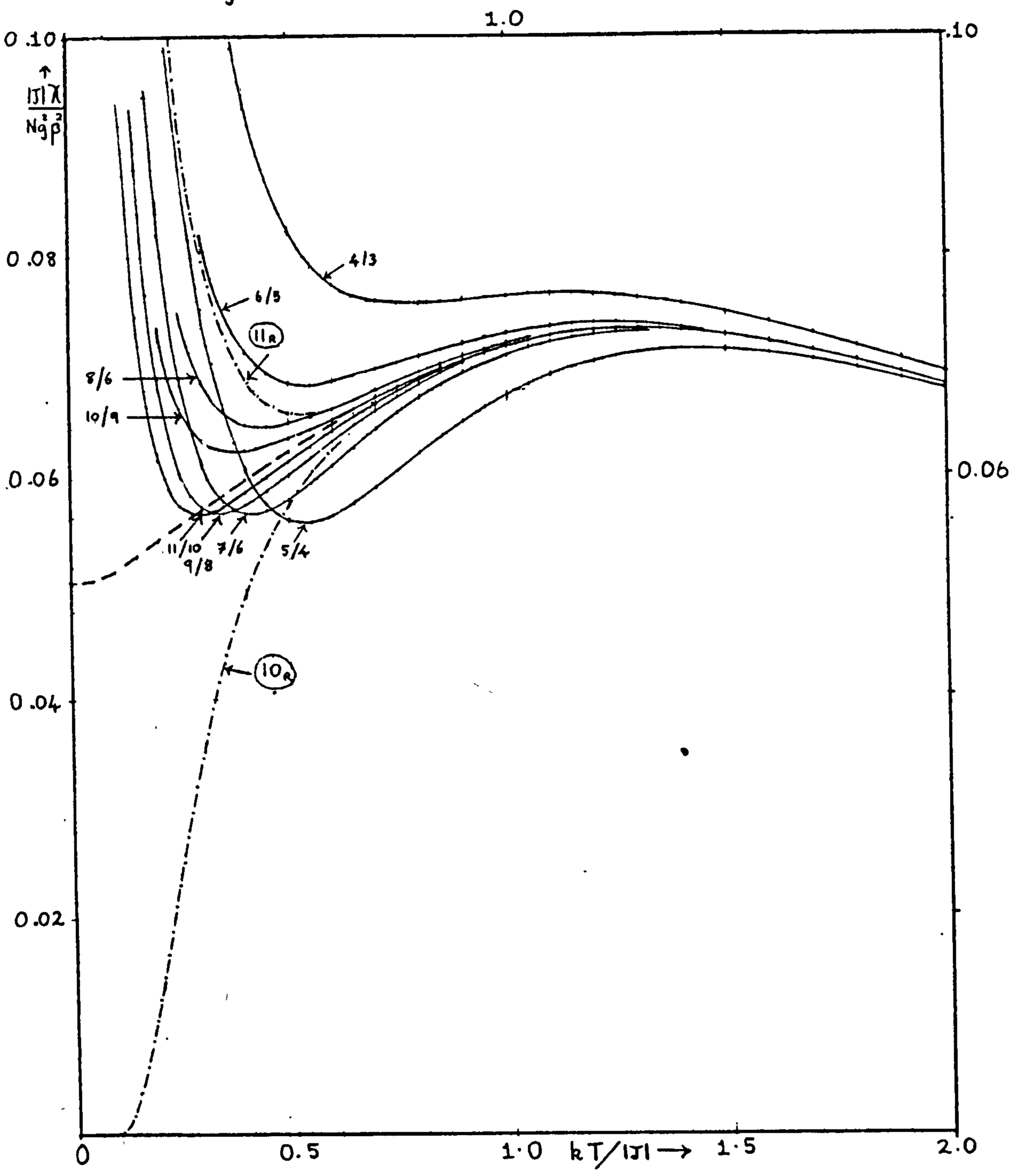

Antiferromagnetic Susceptibility versus Temperature for $\gamma = 1.0$: Weighted Mean Convergence

Lieb, Schultz and Mattis (1961) and Katsura (1962) also shows this behaviour.

To estimate roughly the value of the limiting zero-point susceptibility χ_o for S = 1/2, we may examine the trend of the weighted means, shown on Fig. (5.2), in the range kT/|J| = 0.4 to 0.8. These curves suggest that $\frac{|J|\chi_o}{Ng^2\beta^2}$ lies between 0.048 and 0.056.

The parallel susceptibility, quite generally, may be written in the form

$$\chi_N(T) = \left[g^2\beta^2 N/4kT \right] \xi_N(T) \qquad (5.1.1)$$

where

$$\xi_N(T) = 4/N \left\langle \left(\sum_{i=1}^{N} S_i^z \right)^2 \right\rangle \qquad (5.1.2)$$

the angular brackets denoting the canonical average. In Fig. (5.3) we show the function $\xi_N(T)$ for rings of N = 2 to 11. We see that this function closely resembles Fig. (4.3) for the antiferromagnetic internal energy. The curves for odd and even N clearly bracket the limiting result. From arguments advanced earlier in this section, we infer that $\xi(o)$ for odd N will be given by 1/N and $\xi(o)$ for even N will always be zero. Hence the limiting $\xi(T)$ will rise from zero at T = 0, approaching unity as 1/T. This may be seen from Fig. (5.3). At high temperatures, the individual spins on the ring will become uncoupled, and then $\left(\sum_i S_i^z\right)^2 = N \times (S_i^z)^2$ $= N \times 1/4$. These general features of the ξ function will hold good for all values of γ, including the Ising limit. In Chapter VI, section (1) we will discuss the behaviour of the pair correlation functions, with reference to U and ξ. In the Heisenberg limit as $T \to 0$, we expect ξ to rise from zero proportional to T, since we believe that χ_o is a positive constant. In this respect, for $\gamma = 1$, $\xi(T)$ differs from the internal energy $U(T) \sim T^2$. We see from Fig. (5.3) that linear behaviour in T appears plausible from the general form of the $\xi_N(T)$ near T = 0. Since $\xi(T) \sim 4T\chi(T)$, the limiting slope will give us a value for χ_o. To improve

our estimates of χ_o, therefore, we adopt a method analogous to that described in Chapter IV, subsection (2.3) for finding the low temperature behaviour of the antiferromagnetic specific heat, and consider the slope of tangents from the origin to a suitable set of weighted mean ξ curves. The results are shown in Fig. (5.4) where we display the means 5/4, 7/6, 9/8 and 11/10, weighted as in b) (see Chapter IV, subsection (2.2)). We obtain the set of values for χ_o of 0.0598, 0.0589, 0.0580 and 0.0578 respectively. Extrapolation of these values, and corresponding values for other sets of weighted means, suggests that $\chi_o \simeq 0.0559$ with an apparent uncertainty in the region of 1%.

1.2) Parallel Susceptibilities of Chains

In Fig. (5.5) we compare the parallel susceptibilities of rings and chains for N = 2 to N = 10 spins (N even). (The plotted values for the N = 10 chain actually are extrapolated from the values for 2, 4, 6 and 8 spins. They were obtained in a preliminary study on a magnetic substance which appeared to resemble an antiferromagnetic Heisenberg 8 or 10 spin free-ended chain). We see at once that the chain convergence is rather slow. For example, the apparent locus of the chain maxima does not approach the limiting maximum in a very regular manner. The 8-ring adequately defines the position and height of the limiting maximum given by

$$\chi_{max} / (g^2\beta^2/|J|) \simeq 0.07346 \qquad (5.1.3)$$

at

$$kT_{max}/|J| \simeq 1.282 \qquad (5.1.4) .$$

[These values were actually obtained by careful numerical studies on the weighted means.] The peak for the 8-chain differs by 12.5% in height and about 22% in position from this limit. It was, in fact, this large discrepancy which motivated the calculation of the chain eigenvalues in the hope of securing better agreement with some experimental susceptibility data on a possible linear chain substance.

Fig. 5.3

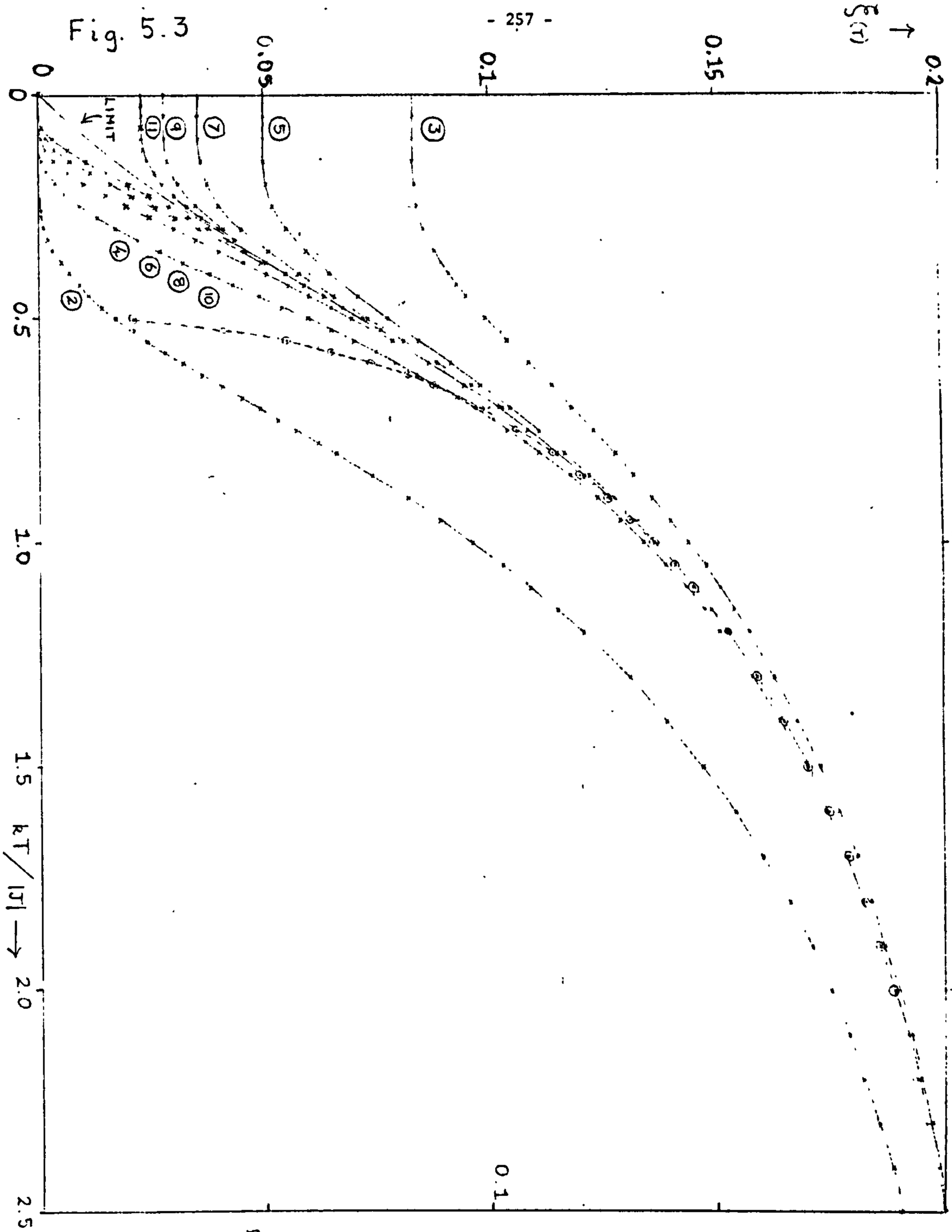

Variation of $\xi(T)$ with Temperature for Antiferromagnetic Heisenberg Rings.

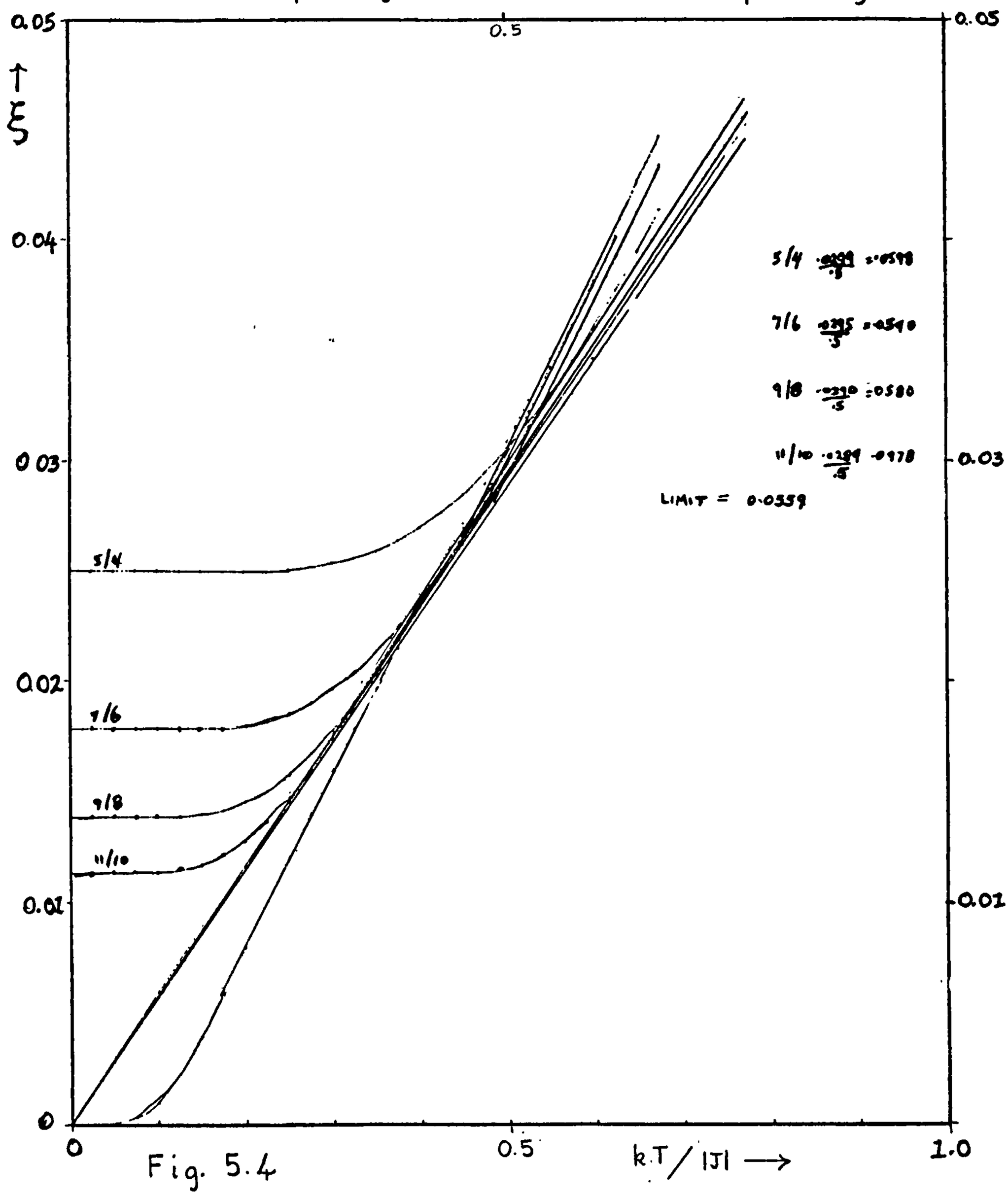
Zero-Point Susceptibility Estimation from Low Temperature ξ Means.
0.05
0.5
0.05
ξ
0.04
0.03
0.03
5/4 .0598
7/6 .0540
9/8 .0580
11/10 .0578
LIMIT = 0.0559
5/4
7/6
9/8
11/10
0.02
0.01
0.01
0
0
0.5
1.0
k.T / |J| ⟶

Fig. 5.4

Fig. 5.5

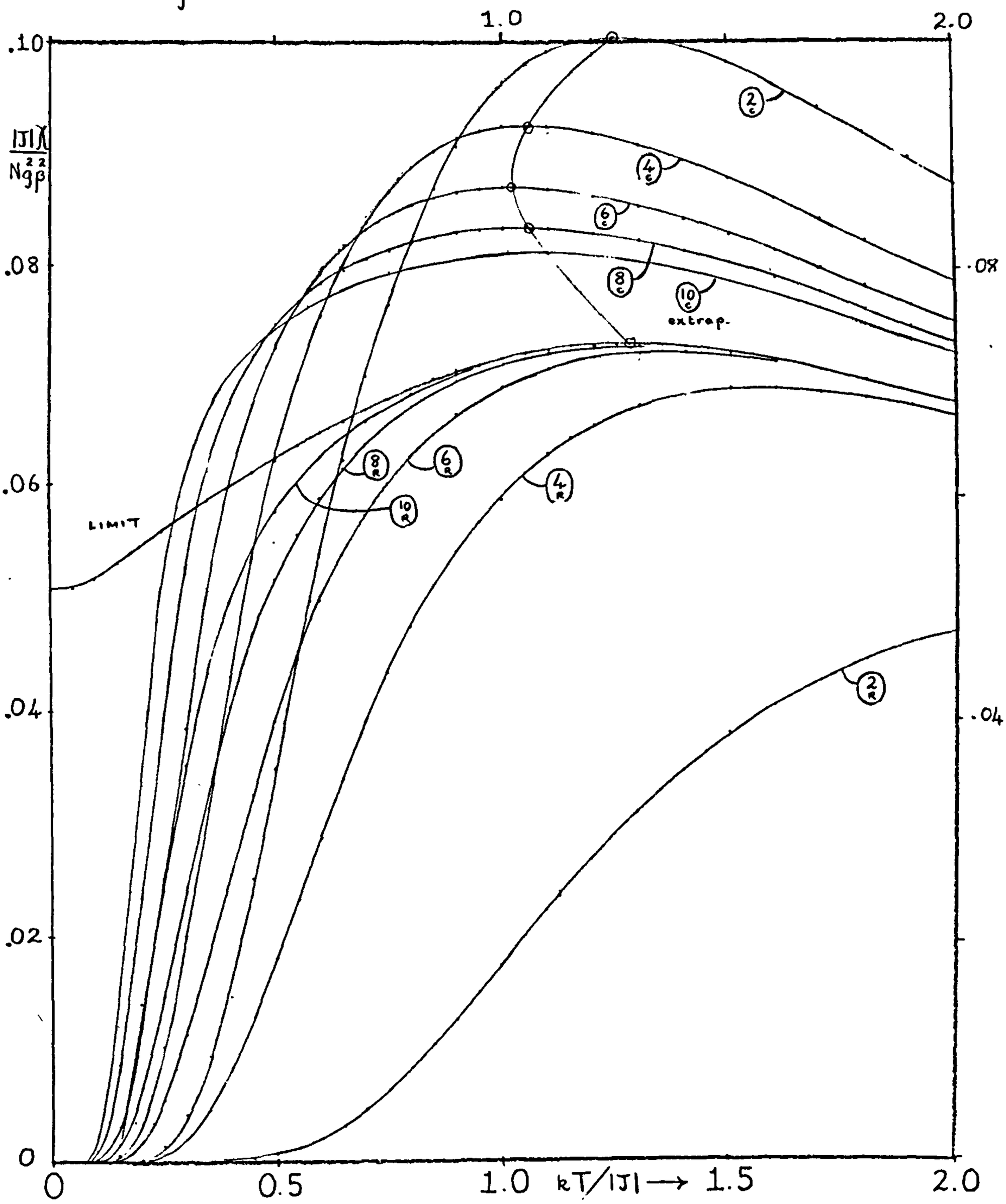

Antiferromagnetic Susceptibility for Finite Heisenberg Rings and Chains

Fig. 5.6

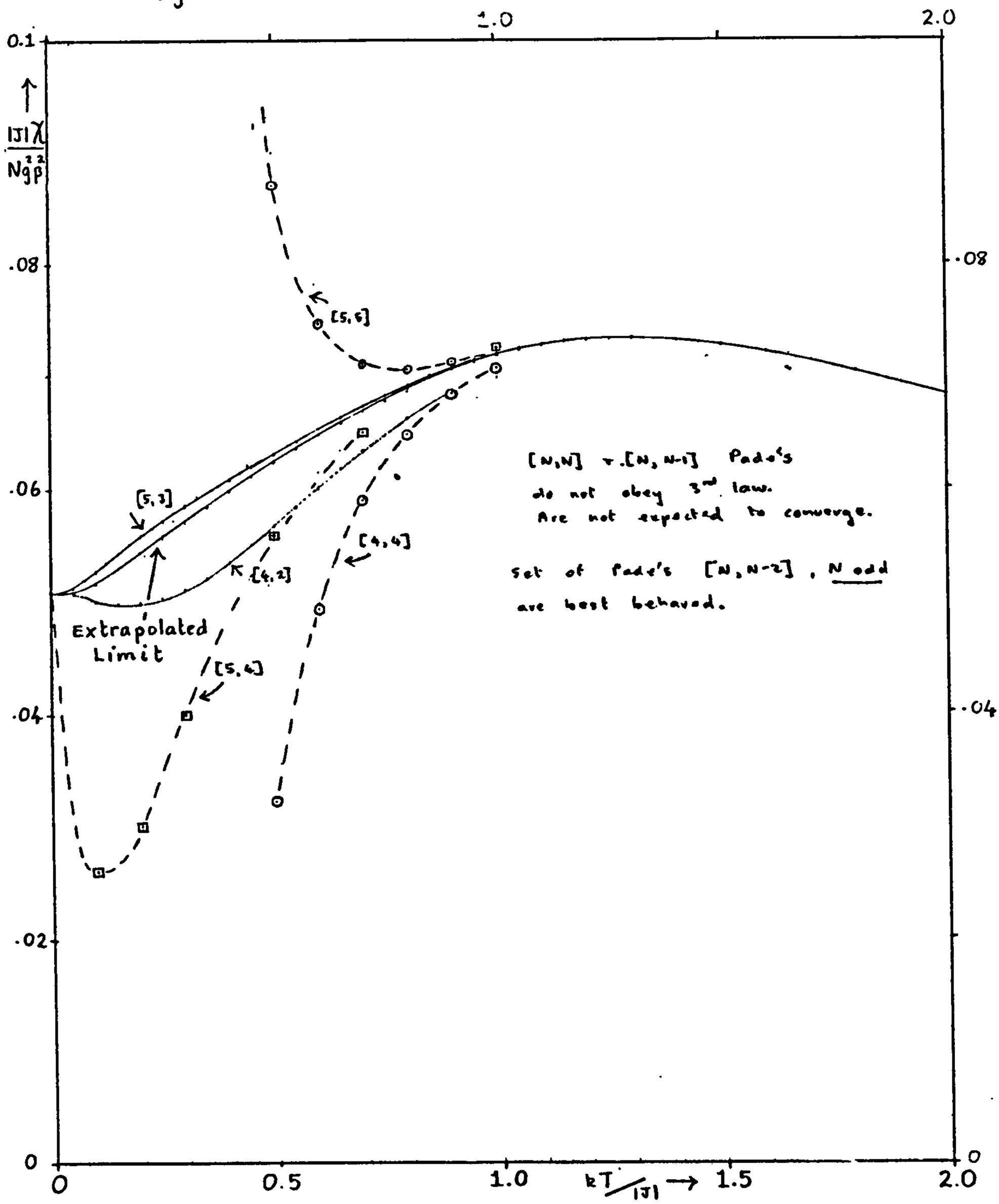

Comparison of BRG Padé Approximant Evaluations with Estimated Susceptibility Limit

1.3) High-Temperature Series Expansions

We have already, in Chapter IV, subsections (2.6) and (3.4) discussed in some detail the Baker, Rushbrooke and Gilbert (1964) high-temperature series expansions for the linear chain. Whereas the series for the thermal properties are quite long (~ 20 terms) the susceptibility series contains only 10 terms. However, it is interesting to apply Padé techniques to this series to compare with our extrapolations. BRG do not present a figure for the antiferromagnetic susceptibility in their paper. The author understands (Rushbrooke, private communication) that BRG encountered difficulties in this direction which they attributed to a branch cut on the negative real axis. (see previous discussion in Chapter IV, subsection (2.6)). The author adopted the same technique, namely that of the "two-point" Padé and considered the Padé sequences [N, N], [N, N-1] and [N, N-2]. The "two-point Padé" introduced by BRG, feeds the value of the series at infinity, if known, into the Padé approximants. In this way, extra information about the series is utilised. Since the high-temperature series are in powers of the reciprocal temperatures, the point at infinity corresponds to the point T = 0. This point was fixed at the Griffiths analytical result of $1/2\pi^2 = 0.050661 \ldots .$. The resulting Padé evaluations are shown in Fig. (5.6). We observe at once that the [5.5] and [4.4] and the [5.4] Padés show very poor convergence. However, these Padés correspond to an asymptotic low-temperature behaviour a) of a constant and b) proportional to T. Effectively, in the case of the [N,N] Padés, we are losing the value of the second point in the two-point Padé, and would therefore not expect good convergence. In the case of the [N, N-1] Padés, we are expecting the function to show asymptotic behaviour which contradicts the third law of thermodynamics, which implies that $\left(\frac{\partial \chi}{\partial T}\right)_{H=0} \to 0$ as $T \to 0$. [The proof follows from elementary thermodynamics.] This non-physical behaviour actually occurs in the case of the infinite spin Heisenberg chain (Fisher, 1964), where the low-temperature behaviour

is given by

$$\chi_{(T)} \simeq \chi_o + \text{const.} \times T + \cdots \qquad (5.1.5)$$

This system displays other features which contradict the third law. The specific heat goes in to a finite constant as $T \to 0$ and the entropy diverges to $-\infty$ as $T \to 0$. Since the infinite spin Heisenberg model is, in fact, a classical system, such features are to be expected in the region of absolute zero. The quantum-mechanical spin-1/2 Heisenberg model does not show such features in the case of the entropy and specific heat, and we do not expect non-physical behaviour in the case of the susceptibility. Hence we feel that the poor convergence of the [N, N-1] Padés is more probably due to their contradiction of the third law than to the effects of the branch-cut. Let us now consider the [N, N-2] Padés which vanish asymptotically as T^2. Their behaviour seems to be quite smooth, and the [5,3] Padé is in reasonably close agreement (i.e. to within 3%) with our extrapolations in the temperature range $kT/|J| < 0.6$ and in very good agreement (better than 1%) at higher temperatures. An estimation of the height and position of the maximum from this Padé evaluation is

$$\chi_{max} / (Ng^2\beta^2/|J|) \simeq 0.07352 \qquad (5.1.6)$$

at

$$kT_{max}/|J| \simeq 1.275 \qquad (5.1.7)$$

However, these Padés are too short for more than three-figure convergence near the maximum. Hence the slight discrepancies between this estimate and our previous extrapolation estimate (equations (5.1.3) and (5.1.4)) cannot be regarded as significant. The numerator of the Padé approximants appears to show a regular alternation of signs, while the coefficients in the denominator are all positive, at least for these short Padés. Hence the [N, N-2] Padés, where N is even, are likely to have the wrong sign for their asymptotic behaviour. The best-behaved Padé sequence appears to be the [N, N-2] sequence, where N is odd. Therefore, the next best Padé after the [5,3] will be the [7,5] Padé, requiring two extra terms in the

high-temperature series. Of course, our choice of T^2-type asymptotic behavior has been rather arbitrary. Other power law behavior consistent with the third law cannot be ruled out. However, the low-temperature susceptibility behaviour given by the X-Y model (Katsura, 1962) and also predicted by the Bulaevskii (1963) Hartree-Fock approximation to the Heisenberg model goes as

$$\chi_{(T)} = \chi_0 + \text{const.}\, T^2 + \cdots\cdots \qquad (5.1.8)$$

which makes our choice seem not unreasonable.

1.4 Anisotropic Parallel Susceptibilities

For γ non-zero, but less than unity, we have seen , in Chapter III, subsection (3.2) that the anisotropy gap between the ground state(s) and first excited states persists even in the limit $N \to \infty$. Consequently, the limiting behaviour of the antiferromagnetic parallel susceptibility should be similar to the Ising case (see Chapter IV, subsection (1.4)) where $\chi_{\parallel}(T)$ tends to zero exponentially as $T \to 0$. Fig. (5.7) shows the parallel susceptibilities for rings of N=8 spins for γ = 0.3, 0.5 and 0.7 (solid lines) and the approximate limiting curves, roughly estimated on the basis of the limiting anisotropy gap. These curves should be accurate to within 5 or 10% down to $kT/|J| = 0.3$. The height of the maxima for various values of anisotropy are given in Table (5.1) . Clearly, the effect of increasing γ is to shift the susceptibility peak to a higher temperature, to reduce its height and to increase its width. (Note that, for small γ , the variation appears to be quadratic in γ).

Table (5.1)

γ	$kT_{max} / \lvert J \rvert$
0	1.00
0.3	~ 1.03
0.5	~ 1.07
0.7	~ 1.14
1.0	1.28

In Fig. (5.8) we study, for comparison, the variation of $\chi_{\parallel}(T)$ with various values of anisotropy for free-ended chains with N=6. We see

Fig. 5.7

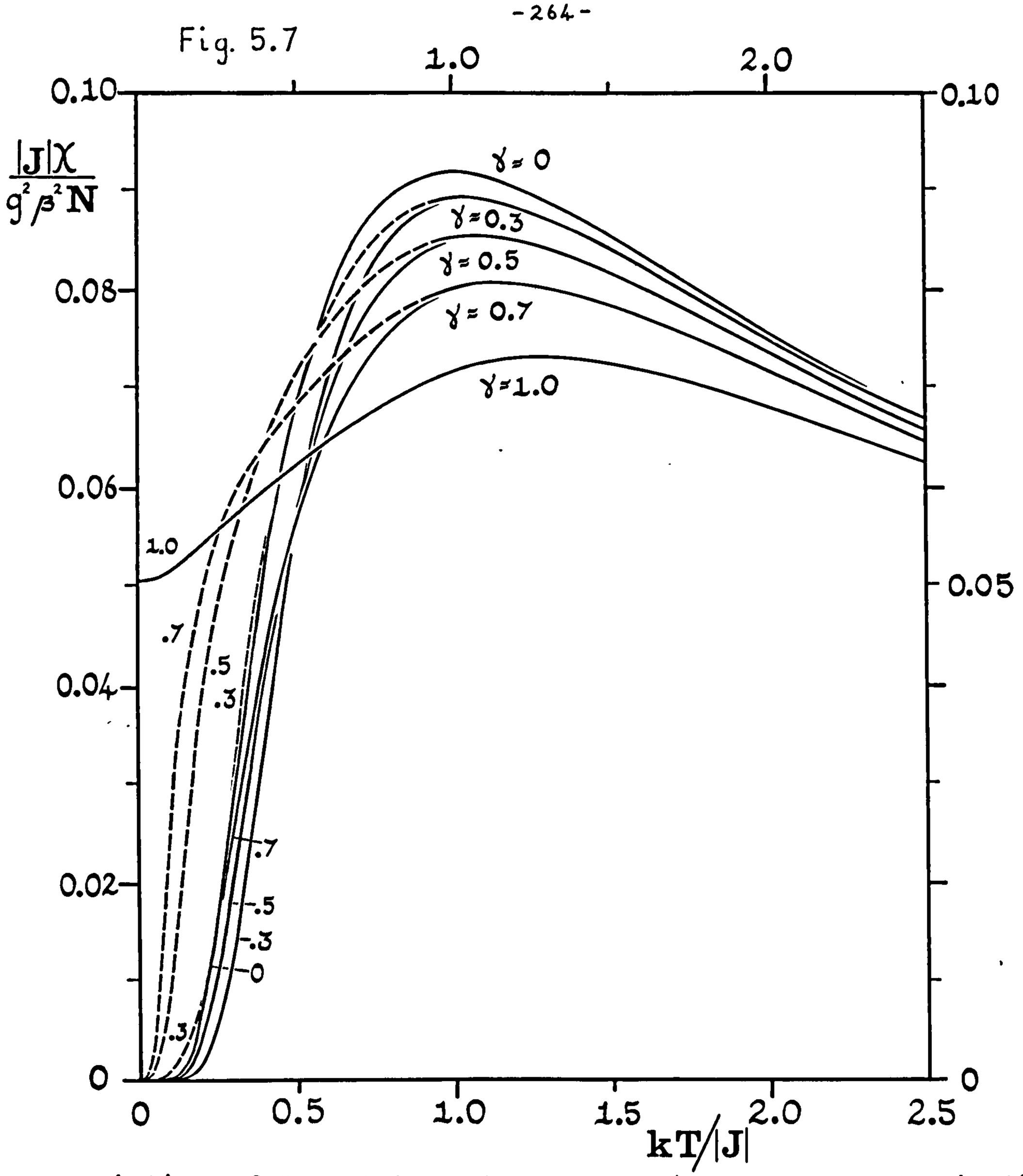

Variation of Parallel Antiferromagnetic Susceptibility with γ.

Fig. 5.8

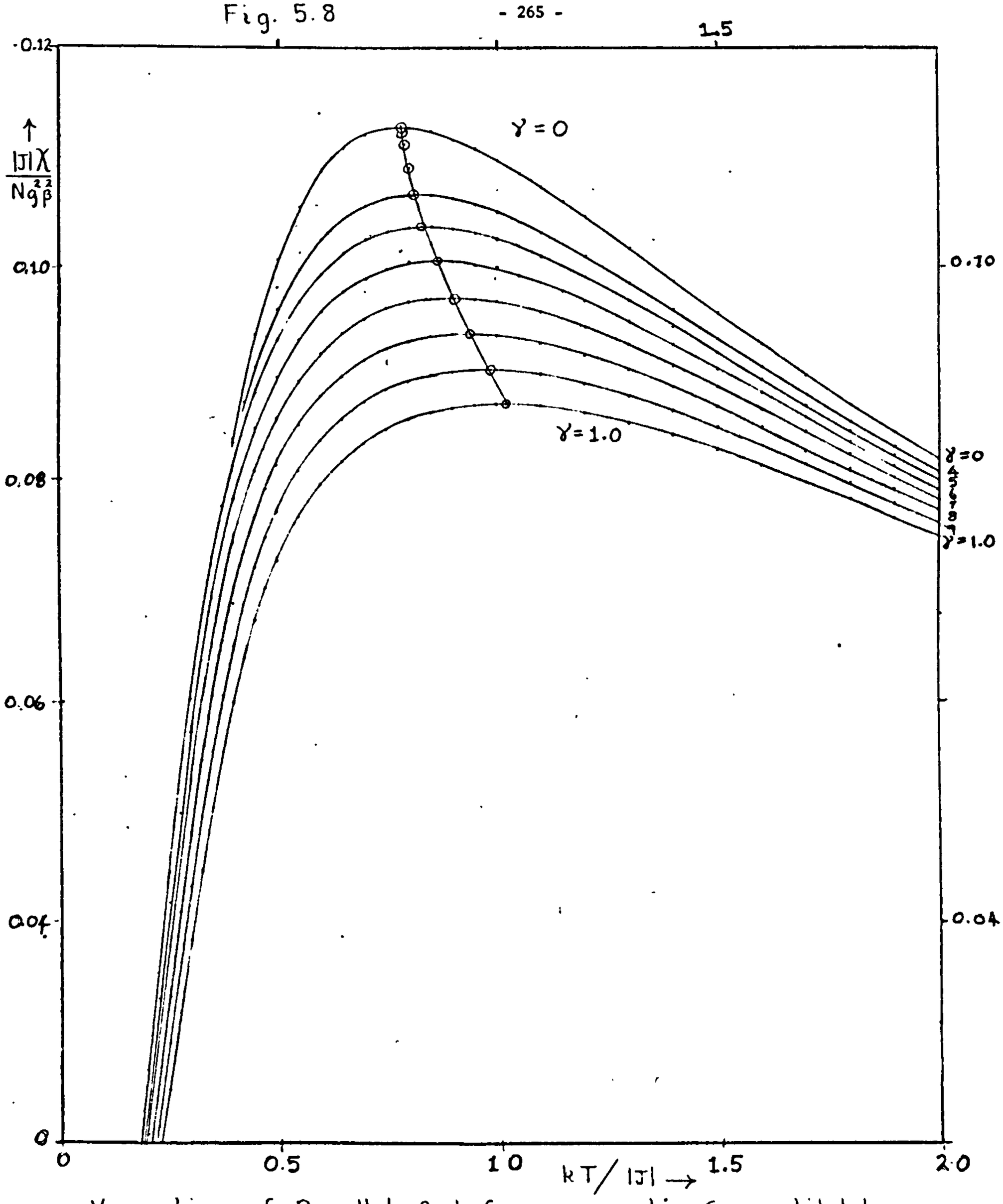

Variation of Parallel Antiferromagnetic Susceptibility
for the Chain N = 6

Fig. 5.9

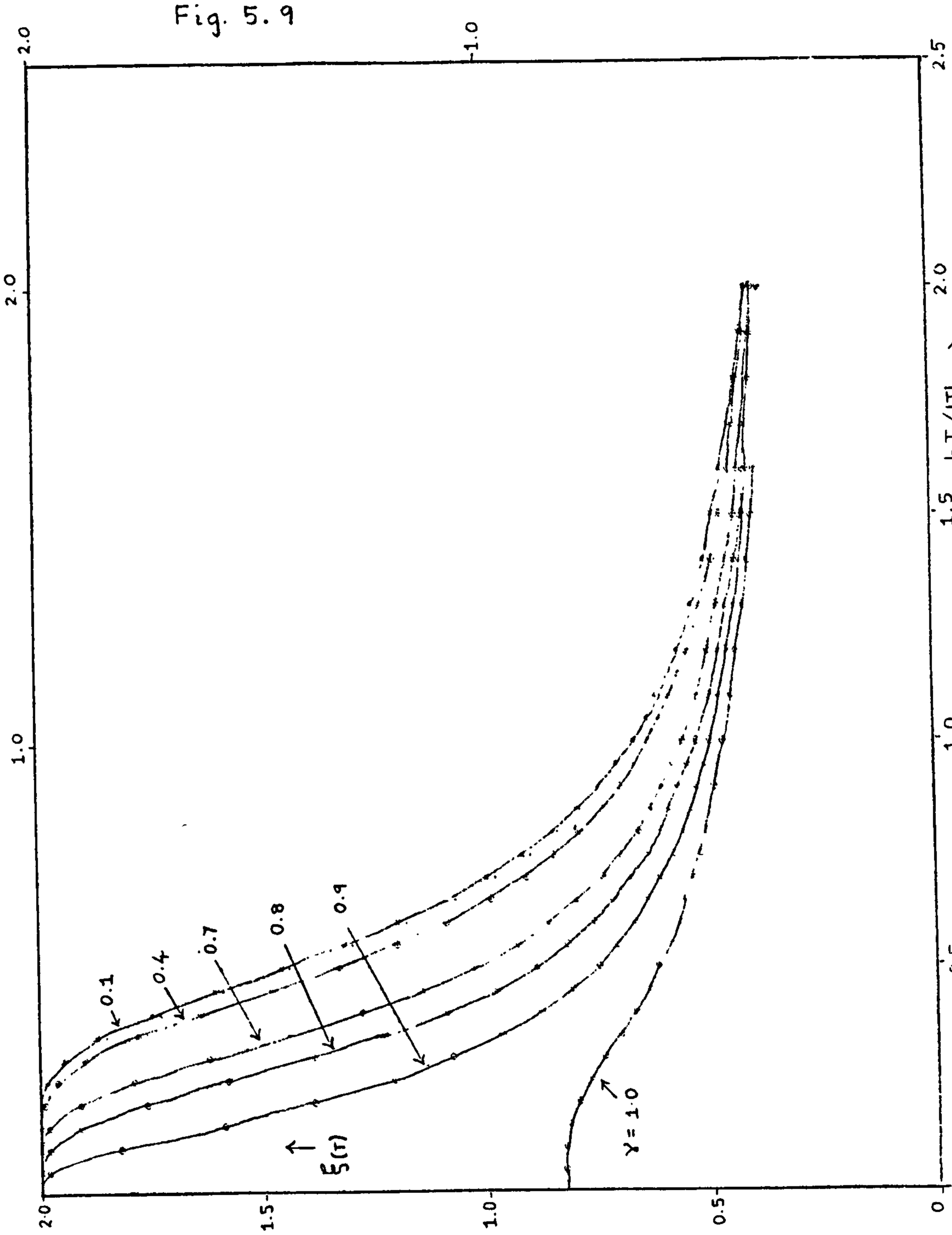

Variation of $\xi(T)$ with γ for N = 8 Ring: Ferromagnets.

that the general trend of the locus of the maxima is very similar to the case of the estimated locus for the limiting curves.

1.5) Ferromagnetic Coupling

Heisenberg Limit

The susceptibility for ferromagnetic chains is conveniently discussed in terms of the function $\xi(T)$ introduced in subsection (5.1) of this chapter. As in the case of antiferromagnets, at high temperatures $\xi_N(T)$ approaches unity as 1/T. As the temperature falls, $\xi_N(T)$ rises monotonically in the ferromagnetic limit and, for finite N, levels off at a value determined by the properties of the ground state. For anisotropic chains ($\gamma < 1$) the ferromagnetic ground state is two-fold degenerate with $\sum_i S_i^{'z} = \pm \frac{1}{2} N$ so that $\xi_N(o) = N$. Since $\xi_N(o)$ is already normalised per spin, this result implies divergence as N as $N \to \infty$. In the isotropic ($\gamma = 1$) case, on the other hand, we know that the ground state has total spin N/2 and is (N+1)-fold degenerate. For finite pure Heisenberg rings, therefore, $\xi_N(T)$ rises to a maximum value

$$\xi_N(o) = \frac{4\sum_{r=o}^{N/2} 2r^2}{N(N+1)} = \frac{1}{3} \cdot \frac{N(N+1)(N+2)}{N(N+1)} = \frac{1}{3}(N+2) \qquad (5.1.9)$$

Similar results obtain for free-ended chains for all γ, since the ferromagnetic ground states have the same properties. The behaviour of $\xi_8(T)$ for various anisotropy values is shown in Fig. (5.9).

Therefore, in the limit $N \to \infty$, we see that for all γ, $\xi(T)$ diverges as $T \to 0$. For infinite Ising chains ($\gamma = 0$) this divergence is exponentially fast since we have, rigorously,

$$\xi(T) = \exp[J/kT] \qquad (5.1.10)$$

This rapid divergence finds its origin in the anisotropy gap which ensures that all the pair correlation functions $\langle S_i^z S_j^z \rangle$ (where the angular products denote canonical average) approach their zero-point values exponentially fast. (The properties of the pair correlation functions will be discussed in detail in Chapter VI). For this reason

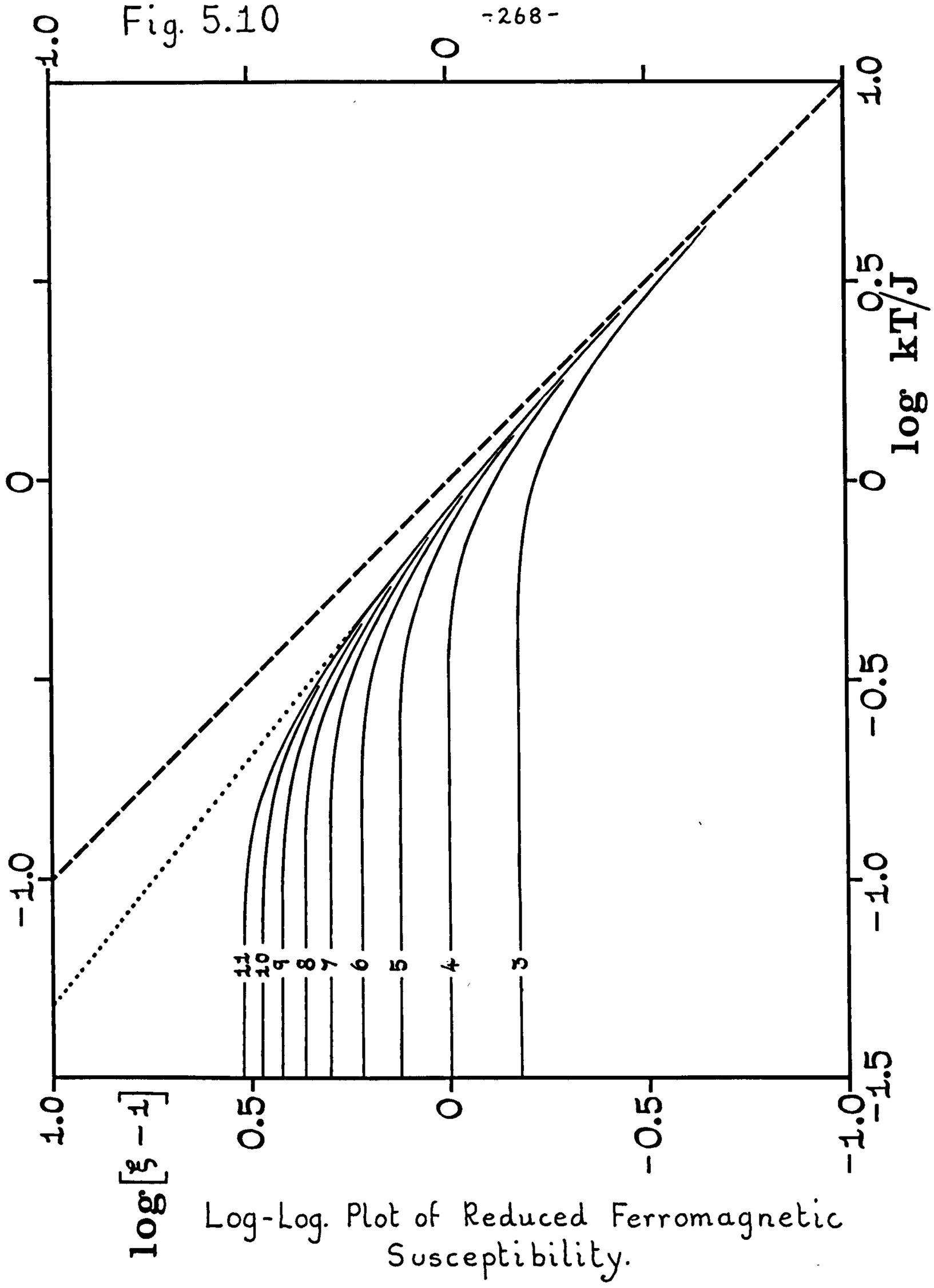

Fig. 5.10 Log-Log. Plot of Reduced Ferromagnetic Susceptibility.

we expect the limiting divergence for other values of $\gamma < 1$ will also be of the form exp [$\alpha J/kT$] with α depending on the limiting anisotropy gap.

For pure Heisenberg coupling, however, a power law might be expected (since, for example, the initial terms in the low-temperature expansion are likely to be of the form exp [$\alpha J/kT$] (see Chapter IV, subsection (4.1)) which reduce to unity in the Heisenberg limit). Indeed, in the limit $S = \infty$ ($\gamma = 1$) the susceptibility diverges as $1/T^2$ so that $\xi(T) \sim 1/T$ as $T \to 0$. Fig. (5.10) is a log-log plot of $[\xi_N(T) - 1]$, a quantity which conveniently measures deviations from Curie's law, versus the temperature for finite isotropic rings of N=3 to 11 spins. The curves evidently approach the limit from below. The convergence is quite rapid, and for $kT/J > 0.3$ the limiting curve is indicated quite accurately. At high temperatures the log-log plot becomes linear with slope unity as shown by the broken line in Fig. (5.10). This simply confirms the 1/T deviations from Curie's law.

[From the paper of Baker, Rushbrooke and Gilbert (1964), we infer that the high-temperature series expansion of $[\xi(T) - 1]$ starts out as

$$\left[\xi(T) - 1\right] \simeq 2K - 16K^3/3! + 80K^4/4! + 672K^5/5! + O(K^6). \quad (5.1.11)$$

At lower temperatures in the range $kT/J = 0.25$ to 1.0, the limiting curve is again almost linear but with slope close to 4/5 (see dotted line in Fig. (5.10). If the curves for larger N continued this trend it would imply a divergence of $\xi(T)$ like $1/T^{4/5}$ and of $\chi(T)$ like $1/T^{9/5}$ as $T \to 0$. It is quite possible, however, that the true asymptotic behaviour sets in only below $kT/J = 0.2$. Nevertheless, the qualitative behaviour is clearly rather similar to that for $S = \infty$. [The high-temperature series expansion for the infinite spin linear Heisenberg model, ferromagnetic limit, is given by

$$\left[\xi_{(T)} - 1/3\right] \simeq K/6 + K^2/24 + \cdots \quad (5.1.12)$$

The factor 1/3 is the appropriate Curie law limit factor for $S = \infty$. For general spin, the limit factor is given by $1/3(1 + 1/S)$]. We may remark that Baker, Rushbrooke and Gilbert (1964) estimated a rather lower value of $0.67 \pm 0.1 (\simeq 2/3)$ for the index of divergence of $\xi(T)$, and further suggested that

$$\xi(T) \simeq \frac{\pi}{4} \left(\frac{J}{kT}\right)^{2/3} \qquad (5.1.13)$$

but with an estimated error in the coefficient of about 10%. These results were obtained by a Padé approximant analysis of their high-temperature susceptibility series (see sub-section (1.3) of this chapter).

2. PERPENDICULAR SUSCEPTIBILITY

2.1) Effect of Anisotropy

When anisotropy is present in a magnetic system, the measured susceptibility depends on the direction, relative to the anisotropy axes, in which the measurement is made. It is convenient to distinguish the z-axis as the axis of anisotropy, as we have done by our particular choice of anisotropic Hamiltonian, and talk about a parallel susceptibility, the response to a field applied in the z-direction (see section (1) of this chapter) and a perpendicular susceptibility which is the response to a field applied perpendicular to the z-axis. For the Ising linear chain, the exact limiting result for the perpendicular susceptibility as a function of temperature has been worked out by Fisher (1963) and also by Katsura (1962), who obtained an exact solution for an infinite linear chain in an arbitrary perpendicular field. Katsura verified that the thermal properties of an Ising linear chain are independent of anisotropy, but not the magnetic properties.

The formula for $\chi_\perp(T)$ is

$$\frac{|J|\chi_\perp(T)}{N g^2 \beta^2} = \frac{1}{4}\left[\tanh K/2 + K/2 \operatorname{sech}^2 K/2\right], \qquad (5.2.1)$$

where $K = |J|/kT$.

and the curve is illustrated in Fig. (5.11). Firstly, we observe that the formula is independent of the transformation $J \to -J$ and $K \to -K$, and is therefore the same for ferromagnets and antiferromagnets in contrast to the parallel susceptibility. We see also that $\chi_\perp(o)$ for $\gamma = 0$ is non-zero. In the limit $N \to \infty$ this will remain true for all γ and in fact as $\gamma \to 1$, $\chi_\perp(o,\gamma) \to \chi_o(\gamma)$. For this reason the susceptibility in the isotropic case is perhaps better regarded as a perpendicular susceptibility. The question of the behaviour of $\chi_\perp(o,\gamma)$ for finite N and the convergence to the limiting curve is an interesting one which has formed a topic of private correspondence (Fisher and Kasteleijn, 1960). Also, since the curves for $\chi_\perp(o,\gamma)$ for finite N, as $\gamma \to 1$ are expected to converge to the limiting χ_o, their calculation provides another independent approach to the estimation of χ_o.

2.2) Perturbation Calculations of $\chi_{\perp N}$ in Zero Field

The quantum-mechanical problems of calculating $\chi_{\perp N}(T)$, since the applied perpendicular field, H^x say, results in a term in the Hamiltonian which does not commute with the field independent terms, are discussed in detail in Chapter II, subsection (4.3).

In a transverse field, H^x, the partition function may be written

$$Z_N = \sum_i \exp\left[-E_i(H^x)/kT\right] \qquad (5.2.2)$$

where the energy levels E_i are field-dependent. The perpendicular susceptibility is given by (5.2.3)

$$\chi_\perp(T) = -\left\langle \partial^2 E_i / \partial H_x^2 \right\rangle + \left(\frac{1}{kT}\right)\left\langle (\partial E_i/\partial H_x)^2 \right\rangle - \left(\frac{1}{kT}\right)\left\langle \partial E_i/\partial H_x \right\rangle^2$$

In zero-field, the first and second derivatives of E_i with respect to H^x are given by the standard first and second order perturbation formulae, respectively. The actual perturbation matrices contain off-diagonal elements involving H^x in a representation which diagonalises

Fig. 5.11

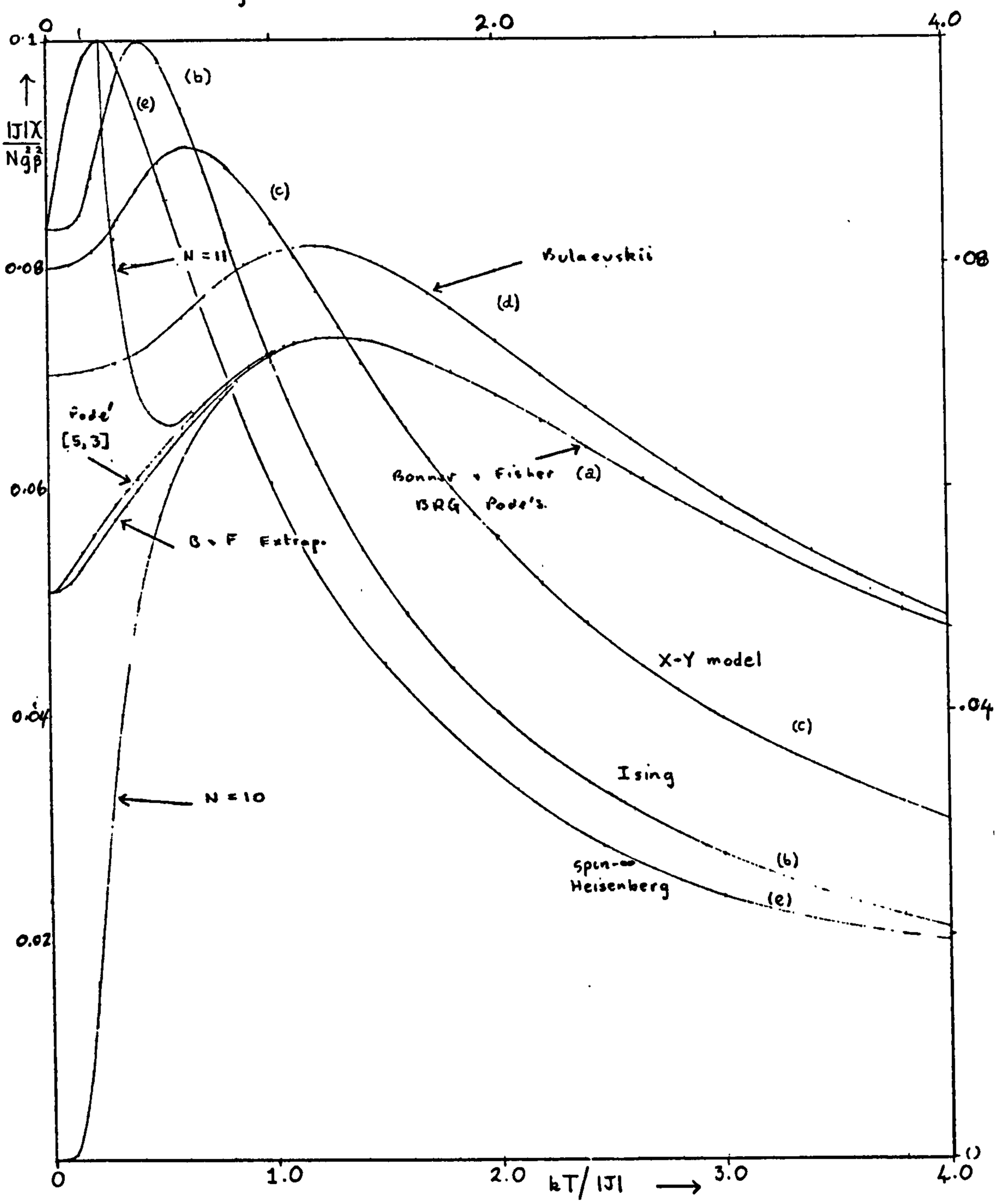

Perpendicular Susceptibility : Comparison of Various Models and Approximations

the zero-field Hamiltonian. The transverse Zeeman perturbation is such that it a) links only states whose S^z values differ by ± 1, b) links only states having the same k wave-vector and c) acting on states which are reflection inverses produces states which remain the reflection inverses of their counterparts. These properties considerably simplify the calculation of $\chi_\perp(T)$. In particular, if there is no degeneracy between states of different S^z, it follows that the first derivatives $\partial Ei/\partial Hx$ vanish identically, and only the first term of equation (5.2.3) need be retained. This is the case for $0 < \gamma < 1$. In general, for the Ising and Heisenberg limits, degeneracy must be taken into account. However, the antiferromagnetic ground state is non-degenerate for $\gamma > 0$ for all finite N and hence the zero-temperature zero-field perpendicular susceptibility may be obtained <u>exactly</u> by application of second order perturbation theory.

In the Heisenberg limit we already know that $\chi_{\parallel}^{N}(o)\left(= \chi_{\perp}^{N}(o)\right)$ for even N vanishes for all finite N, whereas $\chi_{\perp}^{N}(o)$ for odd N diverges as $K/4N$. (The same as $\chi_{\parallel}^{N}(o)$.). In the Ising limit perturbation theory shows that for N even ,

$$\frac{|J|\,\chi_{\perp}^{N}(o)}{N g^2 \beta^2} \longrightarrow \frac{1}{4} \quad , \quad \text{all} \quad N \, , \qquad (5.2.4)$$

the same value as in the limit. (See Fisher (1963), equation (3.7)). This result may easily be verified by direct calculation for the simplest system, N=2.

The two-spin ring is, however, anomalous in that if the Hamiltonian is written in terms of isotropic and anisotropic terms, the anisotropic terms commute with the isotropic terms, and this system is not a realistic model of an anisotropic system. It is a particular case of the general class of close-packed clusters discussed in Chapter II, sub-section (2.4) which all have this property. Hence $\chi_\perp(o)$ for all $\gamma > 0$ is zero. For a realistic model of anisotropy, it is convenient

Fig. 5.12

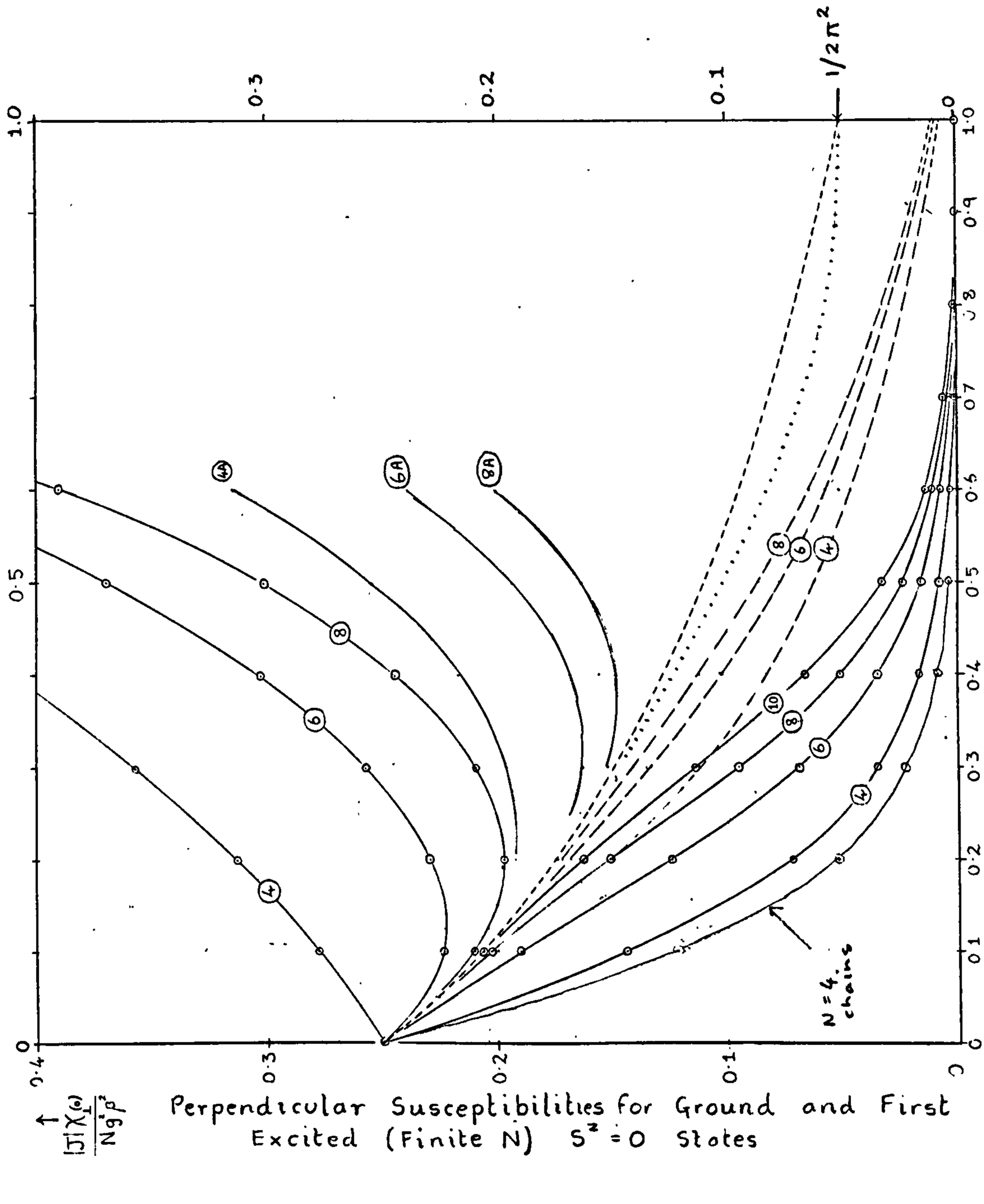

Perpendicular Susceptibilities for Ground and First Excited (Finite N) $S^z = 0$ States

to proceed to the next simplest even N example, a ring of four spins, which is still exactly soluble. Let us calculate the susceptibility at T = 0 (a calculation which involves only perturbation of the ground state) in a direction at an angle Θ with the axis of anisotropy (z-axis.). The result is

$$\frac{|J|\chi(o,\gamma)}{Ng^2\beta^2} = \frac{1}{4}\frac{\left[(1+8\gamma^2)^{1/2}-(4\gamma-1)\right]^2 \sin^2\Theta}{\left[1+2\gamma+(1+8\gamma^2)^{1/2}\right]\left[1+8\gamma^2+(1+8\gamma^2)^{1/2}\right]} \quad (5.2.5)$$

The formula (5.2.5) has a maximum for $\theta = \pi/2$ corresponding to $\chi_\perp(o)$ and a minimum for $\theta = 0$ corresponding to $\chi_{||}(o)$. The behaviour as a function of γ is shown in Fig. (5.12) as the curve for N=4.

An equivalent calculation may be performed for the four-spin free-ended chain. For general γ, the formula is not so simply expressible as equation (5.2.5) since solution of algebraic cubic equations is required, but it has been numerically evaluated and is also shown in Fig. (5.12). The curve is clearly very similar to that of the 4-ring, though it lies somewhat lower. This suggests that a set of finite N curves for chains will converge more slowly than the set of corresponding curves for rings, and hence chain calculations have not been pursued further.

2.3) Convergence to the Limit

The remainder of the lowest set of solid curves in Fig. (5.12) shows $\chi_\perp(o,\gamma)$ for rings of 6, 8 and 10 spins, obtained numerically on a computer. We see that as $\gamma \to 1$, for N even and finite, $\chi_\perp(o,\gamma)$ approaches zero in accordance with previous arguments. Furthermore, for $\gamma > 0.2$, the convergence for N increasing is evidently very slow.

In an attempt to improve the convergence, we calculated also the contribution to $\chi_{\perp}(o,\gamma)$ of the first excited state. These curves are the upper solid curves in Fig. (5.12). Since we have shown that in the limit the first excited state for finite N becomes degenerate with the ground state (see Chapter III, sub-section (3.1)), we expect that in the limit $N \to \infty$, the first excited state curves will approach the ground state results. For finite N, the curves for the ground state and first excited state appear to bracket the limiting curve, although the bracketing is only useful for $\gamma < 0.2$. In the low γ range a perturbation formula due to Fisher (1960a) which for ferromagnets is

$$\frac{J\chi_{\perp}(o)}{Ng^2\beta^2} = \frac{1}{2q(1-\gamma)} \qquad (5.2.6)$$

and for antiferromagnets

$$\frac{|J|\chi_{\perp}(o)}{Ng^2\beta^2} = \frac{1}{2q}\left\{1 - \gamma q/(q-1) + O(\gamma^2)\right\} \qquad (5.2.7)$$

where q is the coordination number of the lattice, may be expected to hold. For the linear chain, q=2 and equation (5.2.7) becomes

$$\frac{|J|\chi_{\perp}(o)}{Ng^2\beta^2} = \frac{1}{4}\left\{1 - 2\gamma + O(\gamma^2)\right\} \qquad (5.2.8)$$

This result is in accordance with the finite N results shown in Fig. (5.12).

The broken curves in Fig. (5.12) are the geometric means of the ground state and excited curves, and they seem to be converging somewhat more rapidly, at least for $\gamma < 0.5$. Near $\gamma = 1$, however, the convergence is very slow, and though a non-zero value for χ_o is indicated, the curves for these small N values cannot be expected to give any reliable estimate of its magnitude. Curves for the arithmetic means, marked (A) are also shown, which appear to converge from above, in contrast to the geometric means.

After our extrapolation estimates for χ_o had been performed, Griffiths (1964), as a result of an accurate numerical calculation based on the Bethe-Hulthén formalism, inferred that

$$\chi_o \simeq \frac{1}{2\pi^2} = 0.050661 \cdots\cdots \qquad (5.2.9)$$

This result has recently been shown to hold rigorously (Yang and Yang, 1966). Hence, using the value of $\chi_o = 1/2\pi^2$, we estimate the limiting zero-point perpendicular susceptibility $\chi_\perp(o,\gamma)$ as the dotted curve marked LIMIT of Fig. (5.12). However, the uncertainty in the intermediate γ range $0.5 < \gamma < 0.9$ could be as much as 10%. An idea of the uncertainty is given by the lower dotted curve, which is an alternative estimate, assuming that the limiting curve departs from its $\gamma = 1$ value very slowly as $(1 - \gamma)$ increases, rather than linearly, as shown by the upper dotted curve.

2.4) Analytic Results for Small Rings and Chains

Since the perturbation of even the ground state alone becomes a rather tricky computational problem when N gets as large as 10 (the 'substandard blocks' discussed in Chapter II, sub-section (5.2) complicate the problem) the calculation of the complete $\chi_\perp(T)$, which involves perturbation of all the eigenstates, has not been attempted except in a few cases for very small N. The following systems are sufficiently trivial for the calculations to be done by hand :- the two-, three- and four-spin rings and the three-spin open-ended chain. The results are displayed in Table (5.2).

Table (5.2a) applies to the Ising limit. The formulae for the 2-ring, 4-ring and 3-chain are independent of the sign of J and hence K, i.e. they apply to both ferromagnets and antiferromagnets, as does the limiting result, equation (5.2.1). The 3-ring is an exception: formulae are quoted in Table (5.2a) for both antiferromagnets and ferromagnets.

In the Heisenberg limit, (Table (5.2b)), $\chi_\perp$ and $\chi_{||}$ will be identical for both finite and infinite N. Hence we can check the results for $\chi_\perp(T)$ obtained by our perturbation method against corresponding

Table (5.2 a)

N = 2 Ring.	$\frac{\lvert J\rvert \gamma_1(K)}{N g^2 \beta^2}$	$= \frac{1}{4} \tanh K$
N = 3 Ring	〃 ANTI	$= \frac{1}{12} \frac{6K + 3 - 3e^{-2K}}{3 + e^{-2K}}$
N = 3 Ring	〃 FERRO	$= \frac{1}{12} \frac{3 + 6Ke^{-2K} - 3e^{-2K}}{1 + 3e^{-2K}}$
N = 4 Ring	〃	$= \frac{1}{4} \frac{8K + 2e^{2K} - 2e^{-2K}}{2e^{2K} + 12 + 2e^{-2K}}$
N = 3 Chain	〃	$= \frac{1}{12} \frac{5 + 2Ke^{-K} - 5e^{-2K}}{1 + 2e^{-K} + e^{-2K}}$

Ising Perpendicular Susceptibilities for Small Spin Clusters

Table (5.2b)

N = 2 Ring	$\frac{\|J\|\chi_\perp(K)}{N g^2 \beta^2}$ ANTI	$= \frac{K e^{-4K}}{1 + 3 e^{-4K}}$
"	" FERRO	$\frac{K}{3 + e^{-4K}}$
N = 3 Ring	" ANTI	$\frac{K}{12} \quad \frac{1 + 5 e^{-3K}}{1 + e^{-3K}}$
"	" FERRO	$\frac{K}{12} \quad \frac{5 + e^{-3K}}{1 + e^{-3K}}$
N = 4 Ring	" ANTI	$\frac{K}{2} \quad \frac{e^{-2K} + 2e^{-4K} + 5e^{-6K}}{1 + 3e^{-2K} + 7e^{-4K} + 5e^{-6K}}$
"	" FERRO	$\frac{K}{2} \quad \frac{5 + 2e^{-2K} + e^{-4K}}{5 + 7e^{-2K} + 3e^{-4K} + e^{-6K}}$
N = 3 Chain	" ANTI	$\frac{K}{12} \quad \frac{1 + e^{-2K} + 10e^{-3K}}{1 + e^{-2K} + 2e^{-3K}}$
"	" FERRO	$\frac{K}{12} \quad \frac{10 + e^{-K} + e^{-3K}}{2 + e^{-K} + e^{-3K}}$

Heisenberg Perpendicular Susceptibilities

For Small Spin Clusters

Fig. 5.13

Variation of Antiferromagnetic Perpendicular Susceptibility with γ

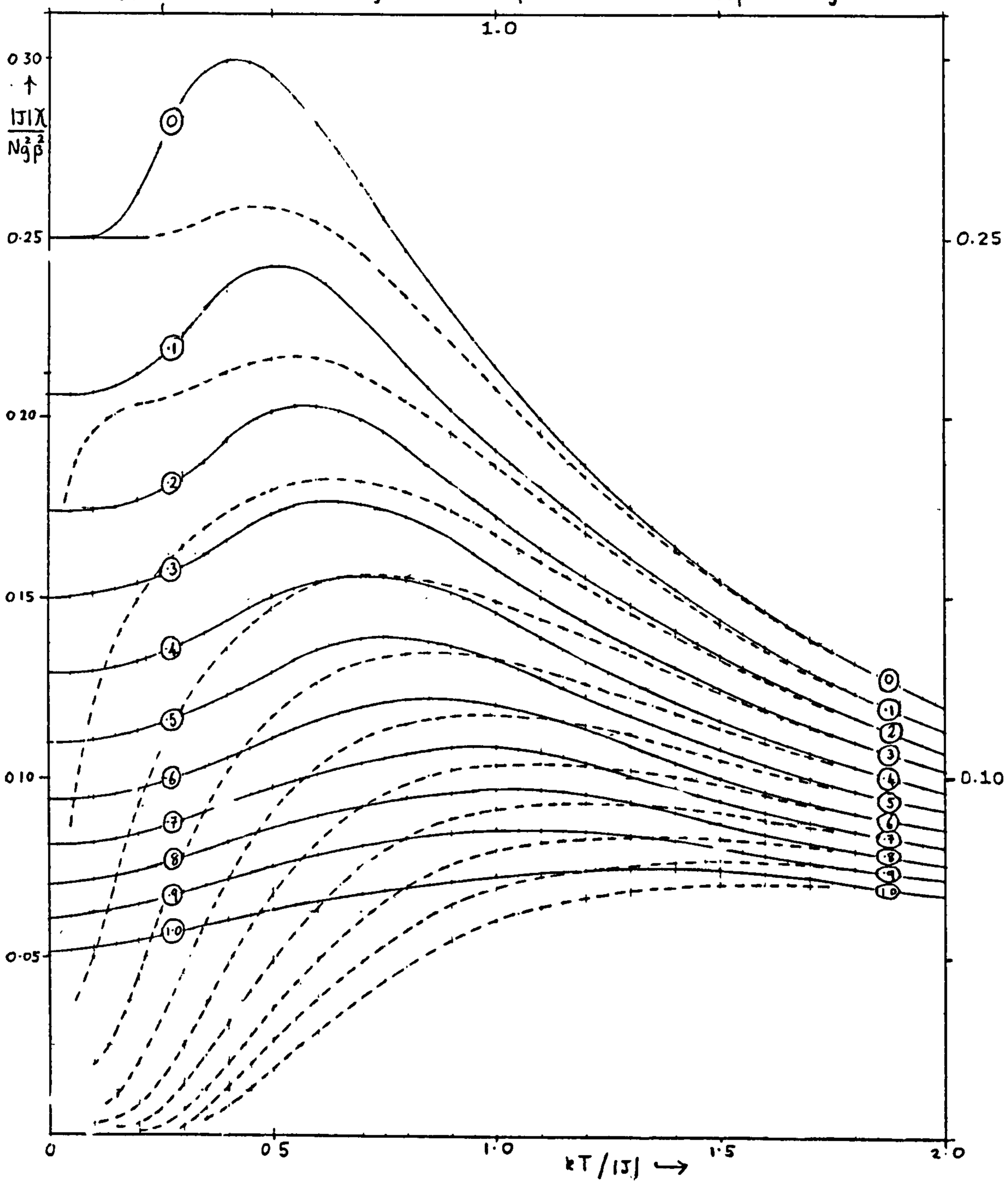

formulae for $\chi_{\parallel}(T)$, which can be obtained more simply and directly. Ferromagnetic and the corresponding antiferromagnetic formulae are distinct in this limit.

For general γ, the corresponding expressions are rather more complicated. We can, however, write down expressions for the 2-ring and 3-ring as follows:

General Anisotropy: Antiferromagnets

$$N = 2: \quad \text{Ring.} \qquad \frac{|J|\chi_{\perp}(K,\gamma)}{Ng^2\beta^2} = \frac{1}{2(1-\gamma)} \frac{\left(e^{-4\gamma K} - e^{-2K-2\gamma K}\right)}{\left(1 + e^{-4\gamma K} + 2e^{-2K-2\gamma K}\right)} \qquad (5.2.10)$$

$$N = 3: \quad \text{Ring} \qquad \frac{|J|\chi_{\perp}(K,\gamma)}{Ng^2\beta^2} = \frac{1}{12(1-\gamma)} \frac{\left(2(1-\gamma)K + 4(1-\gamma)Ke^{-3\gamma K} + 3e^{-3\gamma K} - 3e^{-2K-\gamma K}\right)}{\left(2 + e^{-3\gamma K} + e^{-2K-\gamma K}\right)} \qquad (5.2.11)$$

It is clear that equations (5.2.10) and (5.2.11) pass smoothly into the corresponding Ising limits as $\gamma \to 0$. In the Heisenberg case we have a similar result, which may be verified by expanding the numerator exponentials term by term.

2.5) Estimation of the Limiting $\chi_{\perp}(T,\gamma)$

In the case of the 3-chain and the 4-ring, the corresponding expressions cannot be written down in a very simple form. However, the result for a 4-ring has been evaluated numerically, and is shown in Fig. (5.13) for values of γ of 0, 0.1, 0.2, ... 1.0. (the dashed curves). The low temperature limits of these curves (not shown in the Figure) are as shown for the lower 4-ring curve in Fig. (5.12). We see that the dashed curves progress fairly smoothly as a function of γ from the Heisenberg limit to the Ising limit. The solid curve for $\gamma = 0$ is the $N \to \infty$ limiting curve of equation (5.2.1). The maximum of the N=4 curve for $\gamma = 0$ is clearly very close to the limiting maximum in position, though not in height. (The N=2 system is too trivial to consider in the sense that its maximum occurs at $T = 0$ instead of a finite value of T). At the Heisenberg end, the solid curve marked $\gamma = 1.0$ is

the estimated N = ∞ limit. It seems worthwhile to attempt to estimate the limiting behaviour for intermediate γ from the finite N results. The T = 0 limits of the extrapolated curves will, of course, be the dotted limiting curve of Fig. (5.12). A smooth curve was plotted giving the locus of the maxima of the set of N=4 curves. Then a curve closely similar in shape was drawn between the known maxima of the γ = 0 and γ = 1 limiting curves, which was assumed to approximate closely the locus of the maxima of the limiting curves. Then to locate the actual position of the limiting maxima on this curve a second smooth curve was drawn between points for γ = 0 and γ= 1 identified as follows: the γ = 0 point had ordinate equal to $\underline{\chi_\perp(o)}$ (limiting) for γ = 0 and abscissa equal to kTmax/|J| for the γ = 0 limiting curve: the γ = 1 point was located similarly. The intersection of this curve with the values of $\chi_\perp(o)$ for intermediate γ located the positions of the limiting maxima: the vertical distance between points on this curve and curve (b) having the limiting positions of the maxima as abscissae gave the height of the limiting maxima above the corresponding zero-point values. It was then fairly simple to complete the limiting curve extrapolations, and the results are shown as the set of solid curves in Fig. (5.13), with the N=4 curves (dashed) for comparison.

2.6) Low and High Temperature Series Expansions

Fisher (1963), in addition to obtaining the exact result, equation (5.2.1), for the limiting Ising perpendicular susceptibility, also obtained general expressions for the finite N susceptibilities which he pointed out as having a different form from the infinite limit. We have performed a low-temperature expansion of the equations contained in Table (5.2a) to compare with equation (5.16) in the paper of Fisher (1963). The results are shown in Table (5.3).

Table (5.3).

N	$J\chi_\perp(K)/Ng^2\beta^2 \simeq$
2-Ring	$1/4\{1-2e^{-2K}+2e^{-4K}\cdots\}$
4-Ring	$\frac{1}{4}\{1-6e^{-2K}+34e^{-4K}\cdots\}+Ke^{-2K}\{1-6e^{-2K}+35e^{-4K}\cdots\}$
3-Chain	$\frac{5}{12}\{1-2e^{-K}+2e^{-2K}\cdots\}+\frac{1}{6}Ke^{-K}\{1-2e^{-K}+3e^{-2K}\cdots\}$
3-Ring ANTI	$\frac{1}{12}\{1-\frac{4}{3}e^{-2K}+\frac{4}{9}e^{-4K}\cdots\}+\frac{K}{6}\{1-\frac{1}{3}e^{-2K}+\frac{1}{9}e^{-4K}\cdots\}$
" FERRO	$\frac{1}{4}\{1-4e^{-2K}+12e^{-4K}\cdots\}+\frac{1}{2}Ke^{-2K}\{1-3e^{-2K}+9e^{-4K}\cdots\}$

The Fisher formula for ferromagnets, both even and odd N rings, is

$$\frac{J\chi_\perp(K)}{Ng^2\beta^2} \simeq \frac{1}{4}\{1-2(N-1)e^{-2K}+O(N^2e^{-4K})\} + \frac{K}{4}(N-2)e^{-2K}\{1+O(Ne^{-2K})\} \qquad (5.2.12)$$

and for odd N antiferromagnets

$$\frac{|J|\chi_\perp(K)}{Ng^2\beta^2} \simeq \frac{1}{4}\{1-\frac{2}{3}(N-1)e^{-2K}+O(N^2e^{-4K})\} + \frac{K}{6}(N-2)e^{-2K}\{1+O(Ne^{-2K})\} \qquad (5.2.13)$$

Equation (5.2.12) is in accordance with our results for the 2-ring, 4-ring and ferromagnetic 3-ring. Equation (5.2.13), however, appears to be in error in the following respects: a) it predicts the wrong constant outside the first bracket; b) the second bracket is multiplied by a term in K rather then Ke^{-2K}, and c) the second term inside the second bracket appears to be of $O(N^{-1}e^{-2K})$ rather than $O(Ne^{-2K})$. The antiferromagnetic 3-ring has, in fact, radically different behaviour at low temperatures from that predicted by equation (5.2.13). Instead of approaching the finite value $\chi_\perp(o) \sim 0.25$ as $T \to 0$, the 3-ring perpendicular susceptibility (per spin) diverges as K/6. In fact, as we shall shortly see, the 3-ring continues to diverge as K/6 for all $\gamma < 1$ and diverges as K/12 in the limit $\gamma = 1$. We expected similar

behaviour to hold for all finite odd N antiferromagnetic rings and therefore did not consider N odd for investigating $\chi_{\perp}(0,\gamma)$. The limiting answer, equation (5.2.1) has the low-temperature expansion

$$\frac{J\chi_{\perp}(K)}{Ng^2\beta^2} \simeq \frac{1}{4}\left\{1-2e^{-K}+2e^{-2K}\cdots\right\} + \frac{Ke^{-K}}{2}\left\{1-2e^{-K}\cdots\right\} \qquad (5.2.14)$$

which may be compared with the finite N expansion for rings. The expansion for the 3-chain appears to have a different value for the constants outside the two products, but is otherwise in agreement, at least as far as the leading terms are concerned. Here again we observe that small finite chains are more characteristic of the infinite N limit than the corresponding rings. The high-temperature expansion for the limiting curve, equation (5.2.1), is

$$J\chi_{\perp}(K)/Ng^2\beta^2 \simeq K/4 - K^3/24 \cdots\cdots \qquad (5.2.15)$$

All the small finite systems agree on the formula

$$J\chi_{\perp}(K)/Ng^2\beta^2 \simeq K/4 + O(K^3) \qquad (5.2.16)$$

but the coefficient of K^3 varies among the different systems. This formula may be compared with the high-temperature expansion of the Ising parallel susceptibility, which is

$$\frac{J\chi_{\parallel}(K)}{Ng^2\beta^2} = \frac{Ke^{-K}}{4} \doteq K/4 - K^2/4 + K^3/8 - O(K^4) \qquad (5.2.17)$$

2.7) Susceptibility Comparisons With Other Models and Approximations

Mean Field and Spin-Wave Theory Predictions

For an anisotropic Hamiltonian of the type considered in this thesis, both mean field theory and simple spin-wave theory agree with the exact result for the Ising limit

$$\frac{|J|\chi_{\perp}(0)}{Ng^2\beta^2} = \frac{1}{4} \quad \text{for the linear chain.} \qquad (5.2.18)$$

However, they differ significantly in their predictions for $\chi_{\perp}(T)$ for general lattices. Mean field theory predicts that $\chi_{\perp}(T)$ should remain constant, equal to $\chi_{\perp}(0)$ for $T \leq T_c$ and then decrease for higher T.

Spin-wave theory for the linear chain predicts that $\chi_\perp(T)$ should decrease with T at low temperatures, in contrast to the exact result (see Fig.(5.11)). For general anisotropy both mean field theory and simple spin-wave theory predict that (Kasteleijn, 1960, private communication)

$$\frac{J\,\chi_\perp(0)}{N g^2 \beta^2} = \frac{1}{2q(1-\gamma)} \qquad \text{for ferromagnets} \quad (5.2.19)$$

and

$$\frac{|J|\,\chi_\perp(0)}{N g^2 \beta^2} = \frac{1}{2q(1+\gamma)} \qquad \text{for antiferromagnets} \quad (5.2.20)$$

Equation (5.2.19) agrees with the expression (5.2.4) derived by perturbation theory. However, equation (5.2.20), expanded in terms of γ, disagrees with the corresponding perturbation expression of Fisher, equation (5.2.6). The Kasteleijn expression predicts that $\chi_\perp(0,\gamma)$ should decrease linearly between the Ising and Heisenberg limits, reaching a finite value at the Heisenberg limit of half the Ising value. We now know that the correct value at $\gamma=1$ is close to 1/5 of the Ising limit. However, it seems plausible that a behaviour of $\chi_\perp(0,\gamma)$ proportional to $(1+\gamma)^{-1}$ should be approximately correct near $\gamma=1$, and hence our final limiting curve for $\chi_\perp(0, \gamma)$ in Fig. (5.12) has been drawn to approach $\gamma=1$ linearly.

Other Models and Approximations

In Fig. (5.11) we compare, on the same graph, the exact result for $\chi_\perp(T)$ for Ising linear chains (curve (b)), and the antiferromagnetic susceptibility for the X-Y model which has the form of a perpendicular susceptibility (curve (c)). These two curves, reduced by factors of 3 and 2 respectively, are compared with the estimated limit (curve (a)) for the Heisenberg chain. The reduction factors take account of the fact that the first two susceptibilities are anomalously large owing to the absence of antiferromagnetic spin-coupling between a) spins perpendicular to the z-axis, and b) spins in the z direction, respectively.

The Ising $\chi_\perp(T)$ curve has a maximum (unreduced) of

$$\frac{|J|\,\chi_{max}}{N g^2 \beta^2} \simeq 0.2999 \quad \text{at} \quad \frac{kT}{|J|}_{max} = 0.41677 \qquad (5.2.21)$$

The X-Y curve has a maximum (unreduced) of

$$\frac{J\chi_{max}}{Ng^2\beta^2} \simeq 0.181 \quad \text{at} \quad \frac{kT_{max}}{J} \simeq 0.632 \qquad (5.2.22)$$

We may compare these results with the estimated limiting curve for the Heisenberg model, for which

$$\frac{|J|\chi_{max}}{Ng^2\beta^2} \simeq 0.07346 \quad \text{at} \quad \frac{kT_{max}}{|J|} \simeq 1.28 \qquad (5.2.23)$$

Clearly the effect of increasing the number of independent spin-spin components in the model is to increase the position of the maximum in respect of temperature. We also include on Fig. (5.11) the susceptibility for the antiferromagnetic Heisenberg linear chain with infinite spin (curve (d)) having the normalised Hamiltonian

$$\mathcal{H} = -\frac{J}{2S^2}\sum_{i=1}^{N} \underline{S}_i \cdot \underline{S}_{i+1} - \frac{g\beta}{2S}\sum_{i=1}^{N} (\underline{H} \cdot \underline{S}_i) \qquad (5.2.24)$$

The analytic formula for this curve (Fisher, 1964) is

$$\frac{|J|\chi(K)}{Ng^2\beta^2} = \frac{K}{12}\frac{(1 - u(K/2))}{(1 + u(K/2))}$$

where $$u(K/2) = \coth K/2 - 2/K \qquad (5.2.25)$$

and $K = |J|/kT$.

The corresponding ferromagnetic formula is, of course,

$$\frac{J\chi(K)}{Ng^2\beta^2} = \frac{K}{12}\frac{(1 + u(K/2))}{(1 - u(K/2))} \qquad (5.2.26)$$

which diverges as T^2 as $T \to 0$. For the antiferromagnetic curve we have at zero temperature

$$|J|\chi_0 / Ng^2\beta^2 = 1/12 . \qquad (5.2.27)$$

The curve has a maximum of

$$\frac{|J|\chi_{max}}{Ng^2\beta^2} = 0.100 \quad \text{or} \quad \frac{\chi_{max}}{\chi_0} = 1.2045$$
$$\text{at} \quad kT_{max}/|J| = 0.2382 \qquad (5.2.28)$$

Hence the effect of increasing the value of spin appears to be to decrease the position of the maximum in temperature, (provided, of course, that

normalised Hamiltonians are employed). We also show on Fig. (5.11) the Heisenberg susceptibility curve (curve (e)) resulting from the Bulaevskii method (Bulaevskii, 1963). This curve results from the analytic expressions

$$\frac{|J|\,\chi(K)}{N g^2 \beta^2} = \frac{1}{4(1+J_o^{-1})} \quad ; \quad \text{where } J_o = \frac{8}{\pi T}\int_0^{\frac{\pi}{2}} \frac{dk \exp\left(\frac{2p}{T}\cos k\right)}{\left[1+\exp\left(\frac{2p}{T}\cos k\right)\right]} \tag{5.2.29}$$

and

$$1-p = \frac{2}{\pi}\int_0^{\pi} \frac{\cos k\ dk}{\left[1+\exp\left(\frac{2p}{T}\cos k\right)\right]} \tag{5.2.30}$$

We may determine p self-consistently by repeated numerical integration of equation (5.2.30) and hence find J_o and $\chi(T)$ for successive values of T. The Bulaevskii formula has the low-temperature expansion (as corrected by Katsura and Inawashiro (1965))

$$\frac{|J|\,\chi(T)}{N g^2 \beta^2} \simeq \frac{1}{2(\pi+4)}\left\{1+\frac{\pi}{12}\left(\frac{5}{4}+\frac{\pi}{8}\right)\left(1+\frac{2}{\pi}\right)^{-3}K^{-2}+O(K^{-3})\right\} \tag{5.2.31}$$

i.e.

$$\frac{|J|\,\chi(T)}{N g^2 \beta^2} \simeq 0.0700 + \text{const.}\left(\frac{kT}{|J|}\right)^2 + \cdots\cdots \tag{5.2.32}$$

and at high temperatures goes as $\dfrac{|J|\,\chi}{N g^2 \beta^2} = K/4$.

The zero-point limit is therefore

$$\frac{|J|\,\chi_o}{N g^2 \beta^2} = \frac{1}{2(\pi+4)} \simeq 0.0700 \tag{5.2.33}$$

which differs from the exact value of $1/2\pi^2 \simeq 0.050661....$ by about 20%.

The maximum of the Bulaevskii curve is given by

$$\frac{|J|\,\chi_{max}}{N g^2 \beta^2} \simeq 0.0816 \quad \text{at } kT_{max}/|J| = 1.168. \tag{5.2.34}$$

The height of the maximum differs by about 13% and the position by about 9% from our numerical estimates.

The X-Y model has the analytic expression

$$\frac{|J|\,\chi(K)}{Ng^2\beta^2} = \frac{K}{4}\left(1 - A(K)\right) \qquad (5.2.35)$$

where

$$A(K) = \frac{1}{\pi}\int_0^{\pi} \left[\tanh\left(2K\cos k\right)\right]^2 dk$$

To obtain the points for this curve for Fig. (5.11), the integral equation for A(K) was solved numerically on a computer. The low-temperature expansion of equation (5.2.35) is

$$\frac{|J|\,\chi(K)}{Ng^2\beta^2} \simeq \frac{1}{2\pi} + \frac{\pi}{48}\times\frac{1}{K^2} + \frac{7\pi^3}{1280}\times\frac{1}{K^4} + \cdots \qquad (5.2.36)$$

and the high-temperature expansion is

$$\frac{|J|\,\chi(K)}{Ng^2\beta^2} \simeq \frac{K}{4} - \frac{K^3}{8} \cdots \qquad (5.2.37)$$

Let us compare the low-temperature expansions of the Bulaevskii curve (equation (5.2.29)) and the X-Y model curve (equation (5.2.35)) with the low-temperature expansion of the Ising spin-1/2 perpendicular susceptibility for the linear chain

$$\frac{|J|\,\chi_{\perp}(K)}{Ng^2\beta^2} \simeq 0.25\left(1 - 2e^{-K} + 2e^{-2K} \cdots\right) + 0.5Ke^{-K}\left(1 - 2e^{-K} \cdots\right)$$

(which is also equation (5.2.14)), and the low-temperature expansion of the antiferromagnetic Heisenberg spin-∞ linear chain

$$\frac{|J|\,\chi_{anti}}{Ng^2\beta^2} \simeq \frac{1}{12}\left(1 + K^{-1} + K^{-2} \cdots\right) \qquad (5.2.38)$$

We see that both the Bulaevskii Heisenberg and the X-Y model susceptibilities depart from their constant $\chi_{(o)}$ values as T^2, whereas the Ising curve departs exponentially and the γ=1, spin-∞ curve actually goes as T, which contradicts the third law of thermodynamics. (See the discussion in sub-section (1.3) of this chapter). Let us also compare the high-temperature series expansions of the antiferromagnetic Heisenberg linear chain

$$\frac{|J|\,\chi(K)}{N g^2 \beta^2} \simeq \frac{K}{4}\left(1 + 2K - \frac{8}{3}K^3 + O(K^4)\right) \qquad (5.2.39)$$

(which is based on equation (5.1.11)) with the (unreduced) X-Y model expansion (equation (5.2.37)) and the unreduced Ising, spin-1/2, expansion

$$\frac{|J|\,\chi_\perp(K)}{N g^2 \beta^2} \simeq K/4 - K^3/24 \cdots \qquad (5.2.40)$$

For comparison we show the Ising, spin-1/2, parallel susceptibility expansion for antiferromagnets

$$\frac{|J|\,\chi_{\parallel}(K)}{N g^2 \beta^2} \simeq K/4 - K^2/4 + K^3/8 \qquad (5.2.41)$$

and the Heisenberg spin-∞ expansion for antiferromagnets

$$\frac{|J|\,\chi(K)}{N g^2 \beta^2} \simeq \frac{K}{12}\left(1 - K/2 + K^2/8 \cdots\right) \qquad (5.2.42)$$

Comparison of χ_o Values for Various Approximate Methods

Katsura and Inawashiro have attempted to treat the Heisenberg limit by using perturbation methods based on a) the Katsura X-Y model and b) the Bulaevskii Hartree-Fock approximation as unperturbed Hamiltonians (Katsura and Inawashiro, 1964, 1965). The first method shows very poor convergence and the value for χ_o predicted by the second method is still 30% away from the exact answer. Table (5.4) (based on Table I of Katsura and Inawashiro (1965)) gives a comparison of values of χ_o obtained from various approximate methods with the exact value of

Author	Year	π_o Num.	Theor.
Katsura and Inawashiro	1964	0.1592	$1/2\pi$
Bulaevskii	1963	0.0700	$1/2(\pi+4)$
Katsura and Inawashiro	1965	0.06475	See equation (4.8) of K-I.
Hulthén	1938	0.0591	$\frac{1}{8}\times\frac{27}{28+11\sqrt{7}}$
Ginzburg and Fain	1962	0.05555	$1/18$
Bonner and Fisher	1964	0.055(5)	Extrapolation
Griffiths	1964	0.050661…	$1/2\pi^2$

Table (5.4)

Fig. 5.14

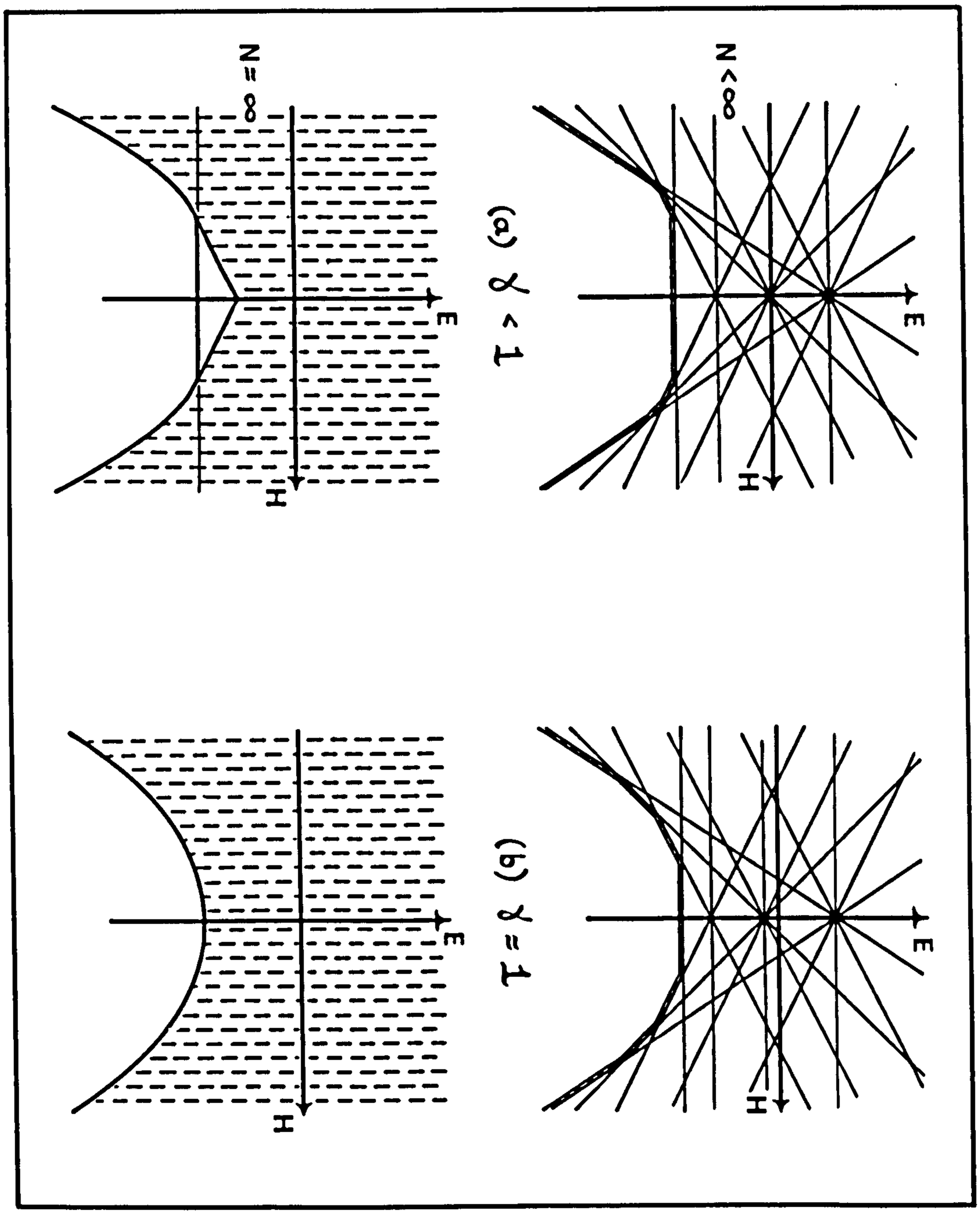

Sketch of Energy Levels v. Magnetic Field for Finite and Infinite Systems.

Griffiths (1964). Although our extrapolated estimate is 10% high, it shares with the method of Ginzburg and Fain (1962) the distinction of being the best approximate value. We might remark, however, that the curve $\chi(T)$ of Ginzburg and Fain (1962) does not display a physically realistic form (since $d\chi/dT < 0$ as $T \to 0$) in the region between T=0 and the maximum.

3. MAGNETIC BEHAVIOUR IN AN APPLIED MAGNETIC FIELD

3.1) Energy Levels in a Magnetic Field

The quantum-mechanical effect of an applied magnetic field H on the Heisenberg linear spin system, described through the Hamiltonian

$$\mathcal{H} = -2J\sum_{i=1}^{N} \underline{S}_i \cdot \underline{S}_{i+1} - g\beta \underline{H} \cdot \sum_{i=1}^{N} (S_i^z) \qquad (5.3.1)$$

is discussed in detail in Chapter II, sub-section (4.3). An examination of the behaviour of the eigenvalues as a function of H shows us how, in the absence of an anisotropy energy gap, the limiting susceptibility for $\gamma=1$ can approach a finite, non-zero value χ_o at T=0. In Fig. (5.14), we have sketched the relevant energy levels for a) $\gamma < 1$ and b) $\gamma=1$ for finite systems (for accurate graphs of all the energy levels as a function of field, see Chapter IV, sub-section (5.1)) and for the corresponding infinite systems as a function of magnetic field. The susceptibility at T=0 is essentially the curvature of the ground state $E_o(H)$ since

$$\chi_{(H)} = \partial^2 E_o(H) / \partial H^2 \qquad (5.3.2)$$

[Similarly the magnetisation is just the slope of $E_o(H)$]. For finite N, the ground state (marked by a bold curve) consists of a series of straight lines and consequently (for N even) the curvature for small H is always zero, so that $\chi_N(o) \equiv 0$ for all γ. In the limit $N \to \infty$, however, the ground-state curve for $\gamma=1$ is smooth, with definite (in general non-zero) curvature. When $\gamma < 1$, on the other hand, the limiting curve consists of a horizontal straight line out to a finite field strength H_a at which

Fig. 5.15

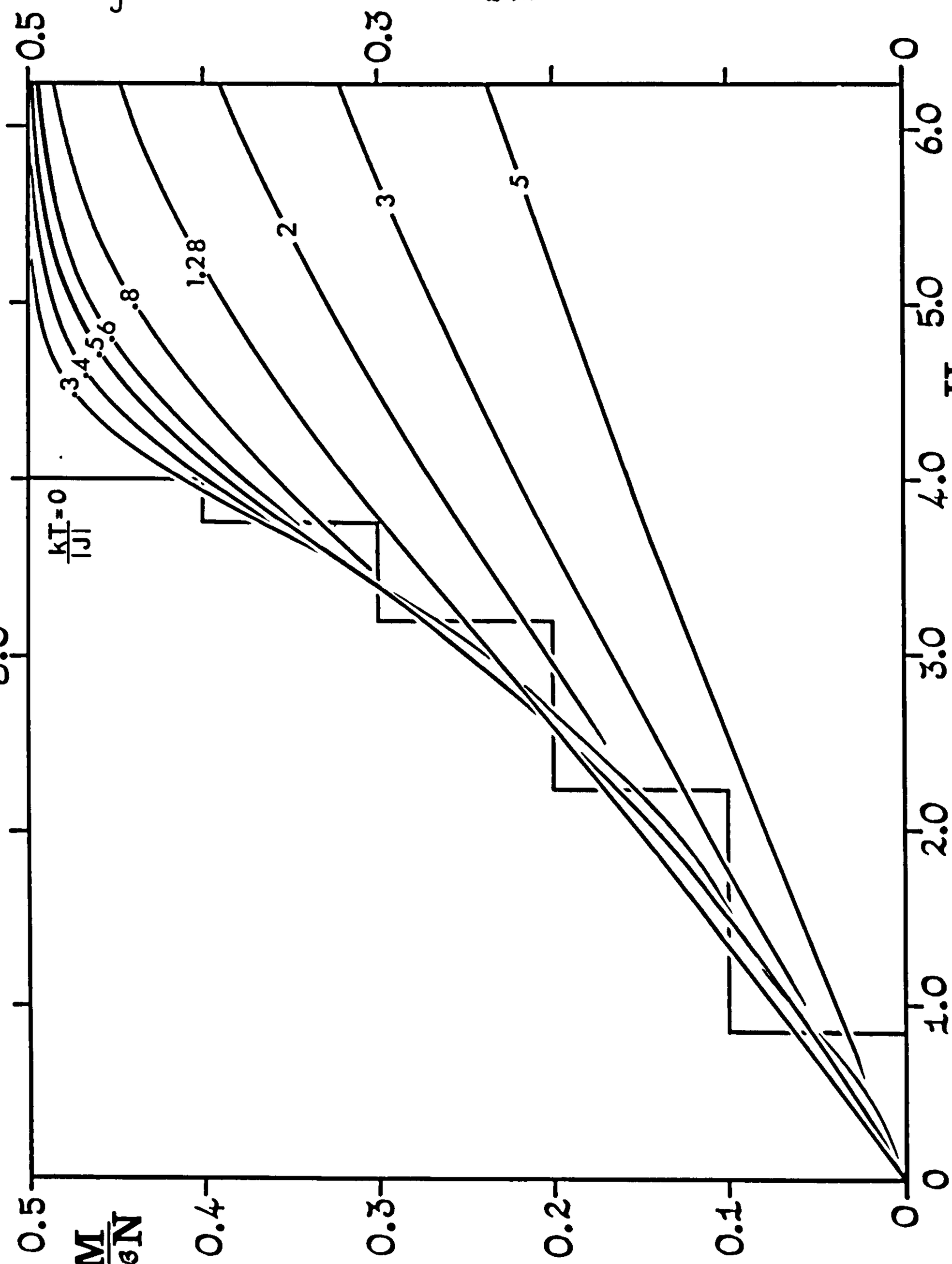

Antiferromagnetic Magnetisation
Curves for $\gamma = 1.0$, $N = 10$.

the anisotropy gap vanishes. The curvature, and hence the magnetisation and susceptibility near H=0 remain zero. [In the case of odd N, the ground state in the presence of a field H is a state of $S^z = + 1/2$. Hence the corresponding energy level on a Fig. (5.14)-type plot has slope -1/2 and corresponding magnetisation per spin, $M/g\beta N = 1/2N$.] These remarks apply to free-ended chains as well as rings.

3.2) Antiferromagnetic Heisenberg Magnetisation Curves

An interesting feature of finite rings and chains is therefore the magnetisation as a function of field. Fig. (5.15) shows the magnetisation for a ring of 10 spins for $\gamma=1$ as a function of field for different temperatures. For temperatures above $kT/|J| = 0.3$ the curves are smooth, and investigation of the convergence with N suggests that the limiting curves are well approximated. For lower temperatures the magnetisation displays oscillations and approaches a staircase function at T=0, the discontinuities being $\Delta M/M_{max} = 2/N$. (For spin-1/2 systems, the magnetisation reaches a maximum when all spins are aligned. The magnetisation is then given by

$$M_{max} = g\beta \times \left(\sum_{i=1}^{N} S_i^z\right) = g\beta \times N \times \tfrac{1}{2}$$

$$\text{ie} \quad \frac{M_{max}}{g\beta N} = 0.5 \qquad (5.3.3)$$

The quantity $\sum_i S_i^z$ is, in fact, evaluated for the component of the ferromagnetic ground state which has maximum $S^z = +N/2$, since this is the antiferromagnetic ground state in the presence of a sufficiently large field. The magnetisation increases discontinuously when two energy levels of adjacent S^z 'cross' as in Fig. (5.14).)

Despite the discontinuities, we notice that the mid-points of the vertical and horizontal parts of the steps lie near a smooth curve which presumably approximates the limiting (N=∞) zero-temperature magnetisation curve. This is confirmed by Fig. (5.16), where the mid-points for a number of the longer rings are plotted. The circles denote points for N even and the squares N odd. The zero-point step functions corresponding to

Fig. 5.16

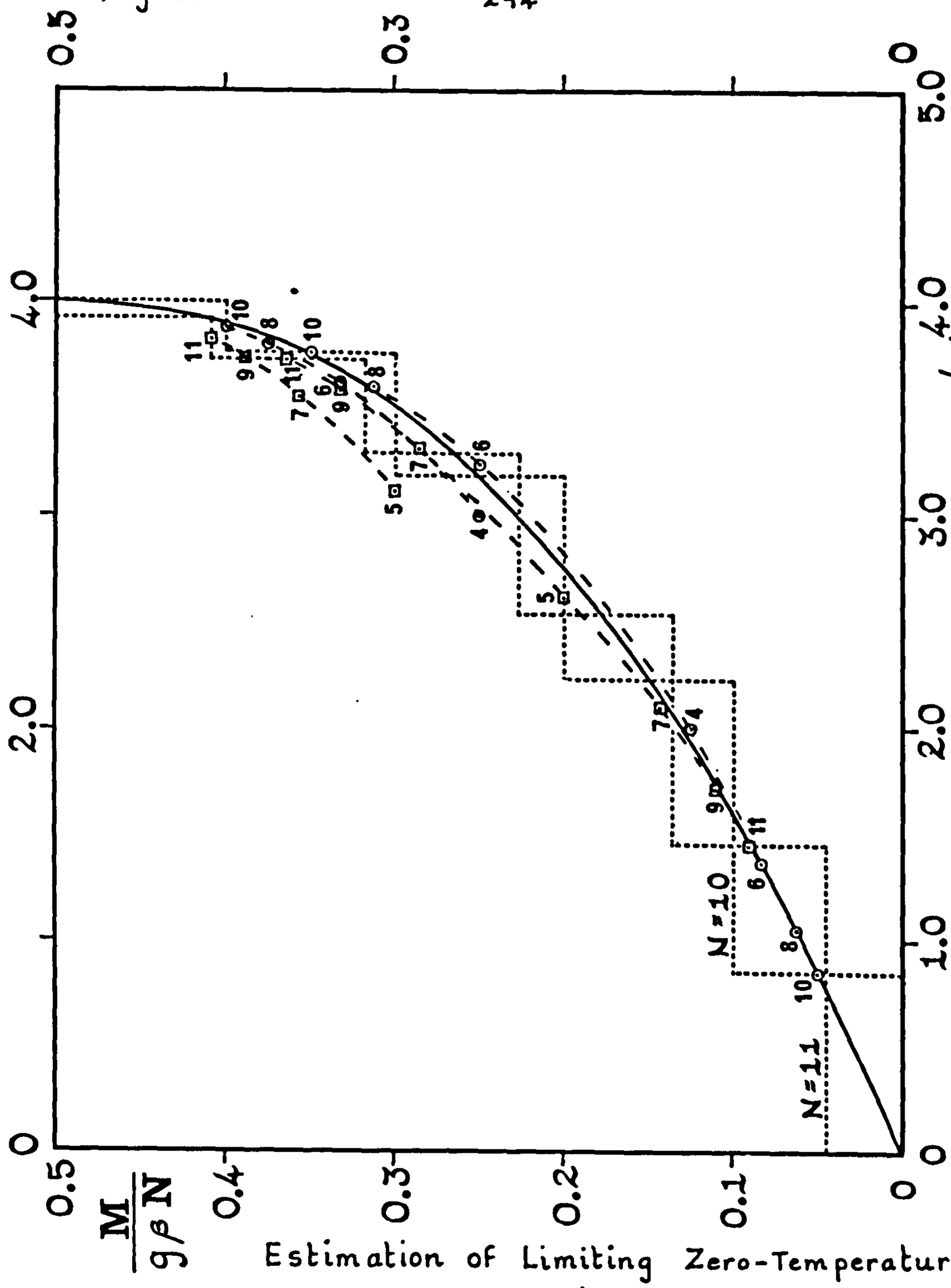

Estimation of Limiting Zero-Temperature Magnetisation Curve

Fig. 5.17

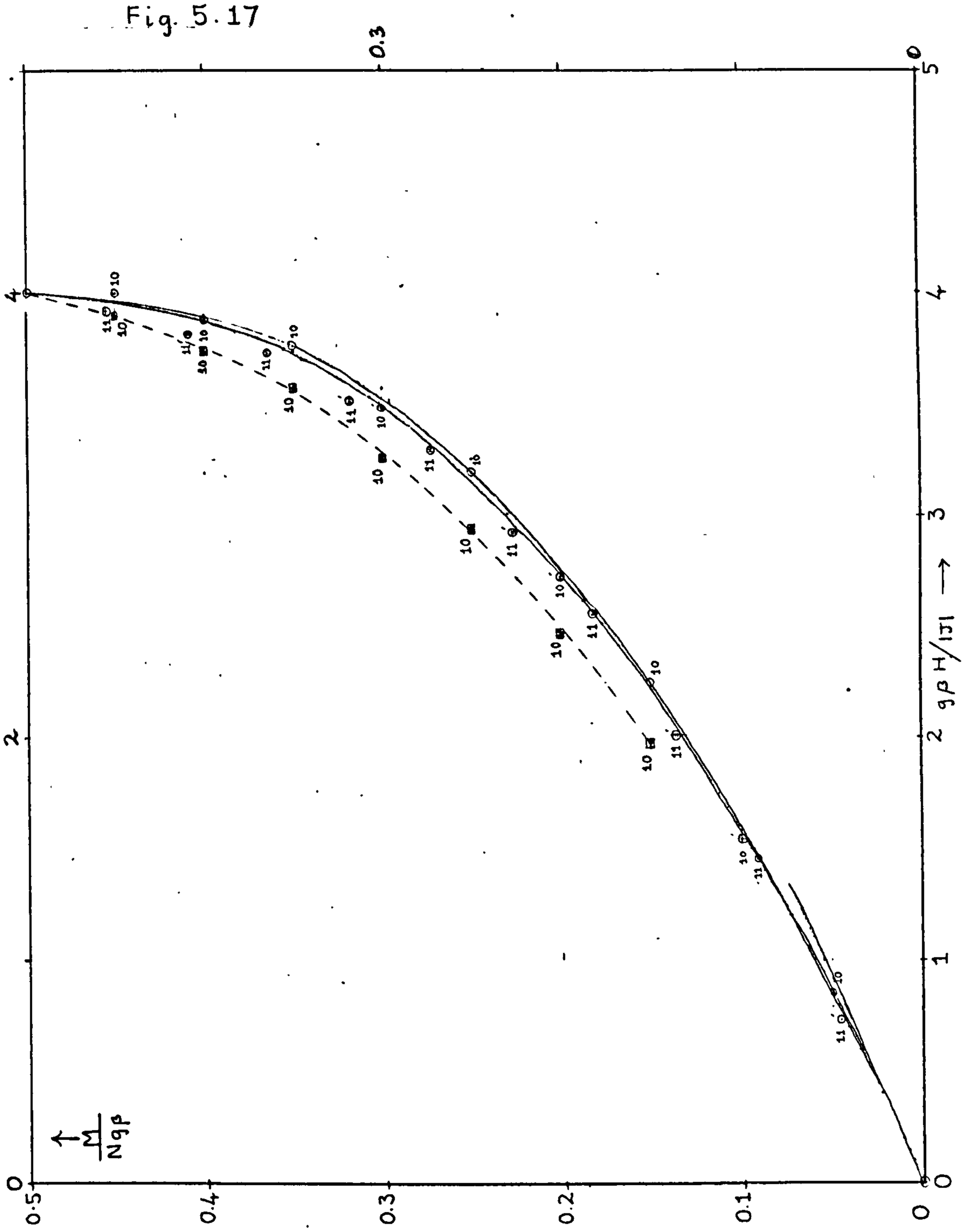

Estimation of Limiting Zero-Temperature Antiferromagnetic $\gamma=1$ Magnetisation Curve from N=10 and 11 (Rings) and 10 (chain)

N=10 and 11 are shown dotted. These points bracket and define a limiting curve (the solid line) rather well. In Fig. (5.17) we show the consistency of this process by considering points only for N=10 and N=11, to avoid confusion. The white circles marked 10 are the midpoints of the vertical parts of the step function for N=10, whereas the dark circles marked 10' correspond to the midpoints of the horizontal portions of the steps. These two sets of points are found to bracket the limiting curve, the dark circles lying to the left. Both sets of points for N=11, on the other hand, lie to the left of the limit (dark circles). We have drawn the two extreme lines through this set of points, indicating the probable uncertainty of the extrapolations, which does not exceed 2-1/2%. We conclude, therefore, that the estimated limiting curve, which lies between these two lines, should be accurate to better than 1% over most of the range. However, the two regions near H=0 and also near saturation (H=4) need special consideration.

Since this work was performed, Griffiths (1964) solved numerically the Bethe-Hulthén coupled integral equations required to find the minimum energy (for antiferromagnetic coupling) of states in each S^z block. From the resulting curve of $\eta = E/N$ versus $\sigma = S^z/N$ a curve of magnetisation as a function of field was obtained by numerical differentiation. [Energy levels from blocks of S^z differing by unity cross at a value of H given by $H \propto E_{S^z} - E_{S^z+1}$ and hence give a point on the magnetisation curve. But $\Delta E = E_{S^z} - E_{S^z+1} = N \frac{d\eta}{d\sigma} \Delta\sigma$ where $\Delta\sigma = 1/N$. Hence $H \propto \frac{d\eta}{d\sigma}$.] The results, presented in Griffiths' Table I are in excellent agreement (i.e. to better than 1%) with our estimated limiting curve.

Also shown on Fig. (5.17) are the midpoints of the vertical and horizontal steps of the zero-temperature magnetisation curve corresponding to the free-ended 10-spin chain (as far as we have points available). The points indicated by dark squares lie very close to a smooth curve (shown dashed) which, however, differs appreciably (i.e. by about 8%)

from the (limiting) curve obtained from the 10-spin ring. If comparison is made with the 8-spin and 6-spin chains, it is obvious that the chains converge to the limit much more slowly than the rings over the region shown.

Magnetisation Curve Near Saturation

The magnetisation at T=0 attains its saturation value in a critical field $H_s = 4|J|/g\beta$. Below this critical field the magnetisation appears to follow a square root law

$$M / M_{max} = 1 - A\left[1 - (H/H_s)\right]^{1/2} \qquad (5.3.4)$$

The plausibility of this conjecture may be demonstrated, and an approximate value for A obtained, by comparing numerical plottings of the form (5.3.4) with the estimated limiting curve near saturation. We obtain $A \simeq 1.2$ and 1.3. Further investigation, which we shall discuss in the next subsection, yields the analytic value

$$A = 4/\pi = 1.2732 \qquad (5.3.5)$$

3.3) Energy Gap Extrapolations

The slope of the limiting magnetisation curve near H=0 is the zero-point susceptibility χ_o. It seems likely that the midpoints of the finite N magnetisation steps approach the limiting curve as fast as 1/N. Consequently, if the limiting magnetisation M(H) has a Taylor series expansion in H about H=0, one would expect the gradients

$g_{1,N} = \frac{1}{2}\,\Delta M_{1,N} / \Delta H_{1,N}$ of the lines from the origin to the midpoints of the first steps (for N even), and similar gradients to other steps, to approach the limiting slope χ_o as fast as 1/N. Examination of the gradients $g_{j,N}$ for small j and N = 4 to 11 results in roughly linear plots versus 1/N. If extrapolations are made, they suggest that

$\chi_o/(g^2\beta^2 N/|J|)$ lies in the range 0.0555 ± 0.0010 (5.3.6)

Let us study these extrapolations more closely. First of all we shall see what information the magnetic step gradients are capable of yielding.

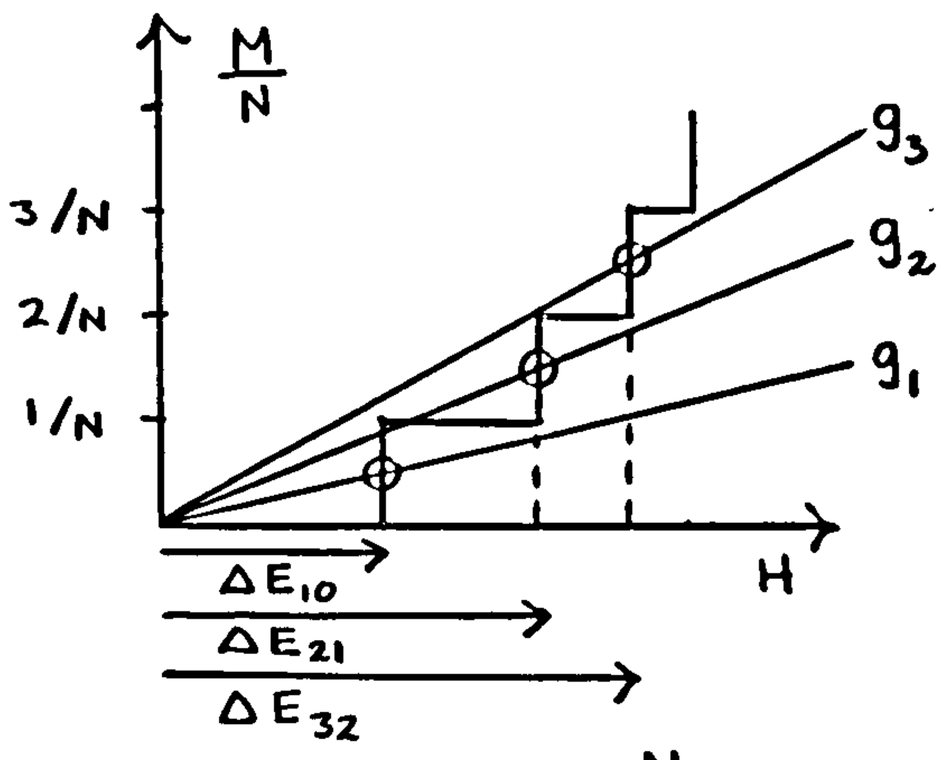

Neven

fig. (5.1 a)

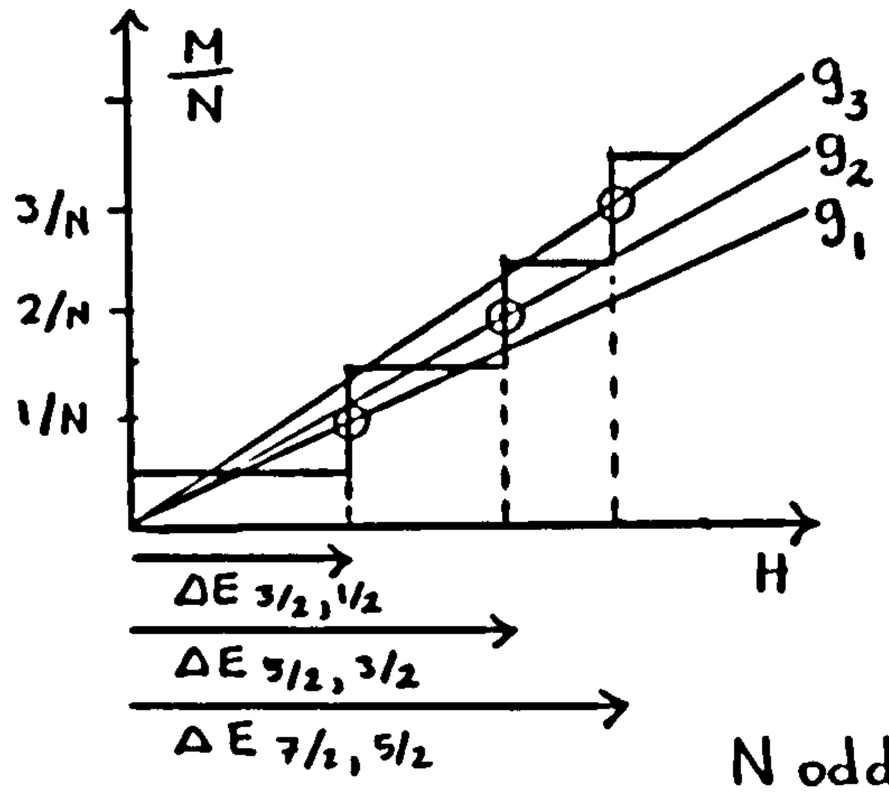

N odd

fig. (5.1 b)

In fig. (5.1a), applicable to the case of N even, we examine the first three gradients g_{1N}, g_{2N} and g_{3N} to the vertical midpoints of the magnetisation steps. Explicitly,

$$g_{1,N} = \frac{1}{2N} \times \frac{1}{\Delta E_{1,0}} \qquad \text{(ignoring units of g, } \beta\text{, J)} \tag{5.3.7}$$

where $\Delta E_{1,0}$ is the energy difference between the lowest zero-field eigenvalue corresponding to the block $|S^z| = 1$ and the lowest eigenvalue of the block $S^z = 0$. Similarly

$$g_{2N} = \frac{3}{2N} \times \frac{1}{\Delta E_{2,1}} \tag{5.3.8}$$

and

$$g_{3N} = \frac{5}{2N} \times \frac{1}{\Delta E_{3,2}} \tag{5.3.9}$$

If we make the plausible assumption that for small j (i.e. j less than 0(N)) we expect the gradients g_{jN} to approach the <u>same</u> limiting value, we have the following limiting relations:

$$\Delta E_{2,1} = 3\Delta E_{1,0} \quad ; \quad \Delta E_{3,2} = 5\Delta E_{1,0} \tag{5.3.10}$$

Let us now consider fig. (5.1b), applicable to N odd. Again, considering vertical midpoints, we have the following limiting relations:

$$\Delta E_{5/2,3/2} = 2\Delta E_{3/2,1/2} \quad ; \quad \Delta E_{7/2,5/2} = 6\Delta E_{3/2,1/2} \tag{5.3.11}$$

Further, if we assume, very plausibly, that gradients for both odd and even N must tend to the same limiting value, we have the important

limiting relation:

$$\Delta E_{3/2,1/2} = 2\Delta E_{1,0} \quad \text{i.e.} \quad \Delta E_{odd} = 2\Delta E_{even} \tag{5.3.12}$$

We can thus draw up a table (Table (5.5)) of limiting energy gaps in terms of the basic, minimum gap $\varepsilon = \Delta E_{1,0}$.

Table (5.5)

A	$\Delta E_{1,0}$	$\Delta E_{3/2,1/2}$	$\Delta E_{2,1}$	$\Delta E_{5/2,3/2}$	$\Delta E_{3,2}$	$\Delta E_{7/2,5/2}$
	ε	2ε	3ε	4ε	5ε	6ε
B	$\Delta E_{1,0}$	$\Delta E_{3/2,1/2}$	$\Delta E_{2,0}$	$\Delta E_{5/2,1/2}$	$\Delta E_{3,0}$	$\Delta E_{7/2,1/2}$
	ε	2ε	4ε	6ε	9ε	12ε

This table may easily be continued to higher order gaps. It may be observed that this table is consistent with a quadratic limiting relation

$$\frac{E - E_o}{N} \propto \left(\frac{S^z}{N}\right)^2 \tag{5.3.13}$$

Hence, at least for longer rings and chains, we have a variety of energy gaps available for extrapolation. In Table (5.6) we list a sample of energy gaps, together with a value for χ_{oN} predicted by each gap for a given N.

Table (5.6)

ΔE \ N	4	6	8	10
$\Delta E_{1,0}$	0.0625	0.0609	0.0598	0.0591
$\Delta E_{2,0}$	0.1000	0.0724	0.0676	0.0650
$\Delta E_{3,0}$	—	0.0872	0.0770	0.0717
ΔE \ N	5	7	9	11
$\Delta E_{3/2,1/2}$	0.0764	0.0681	0.0645	0.0625
$\Delta E_{5/2,1/2}$	0.0962	0.0792	0.0721	0.0682
$\Delta E_{7/2,1/2}$	—	0.0931	0.0812	0.0748

Extrapolations of the χ_{oN} with 1/N are shown in Fig. (5.18) for $\Delta E_{1,0}$, $\Delta E_{3/2,1/2}$, $\Delta E_{2,0}$ and $\Delta E_{5/2,1/2}$. These plots are not straight, since the points corresponding to smaller N especially, deviate

Fig. 5 18

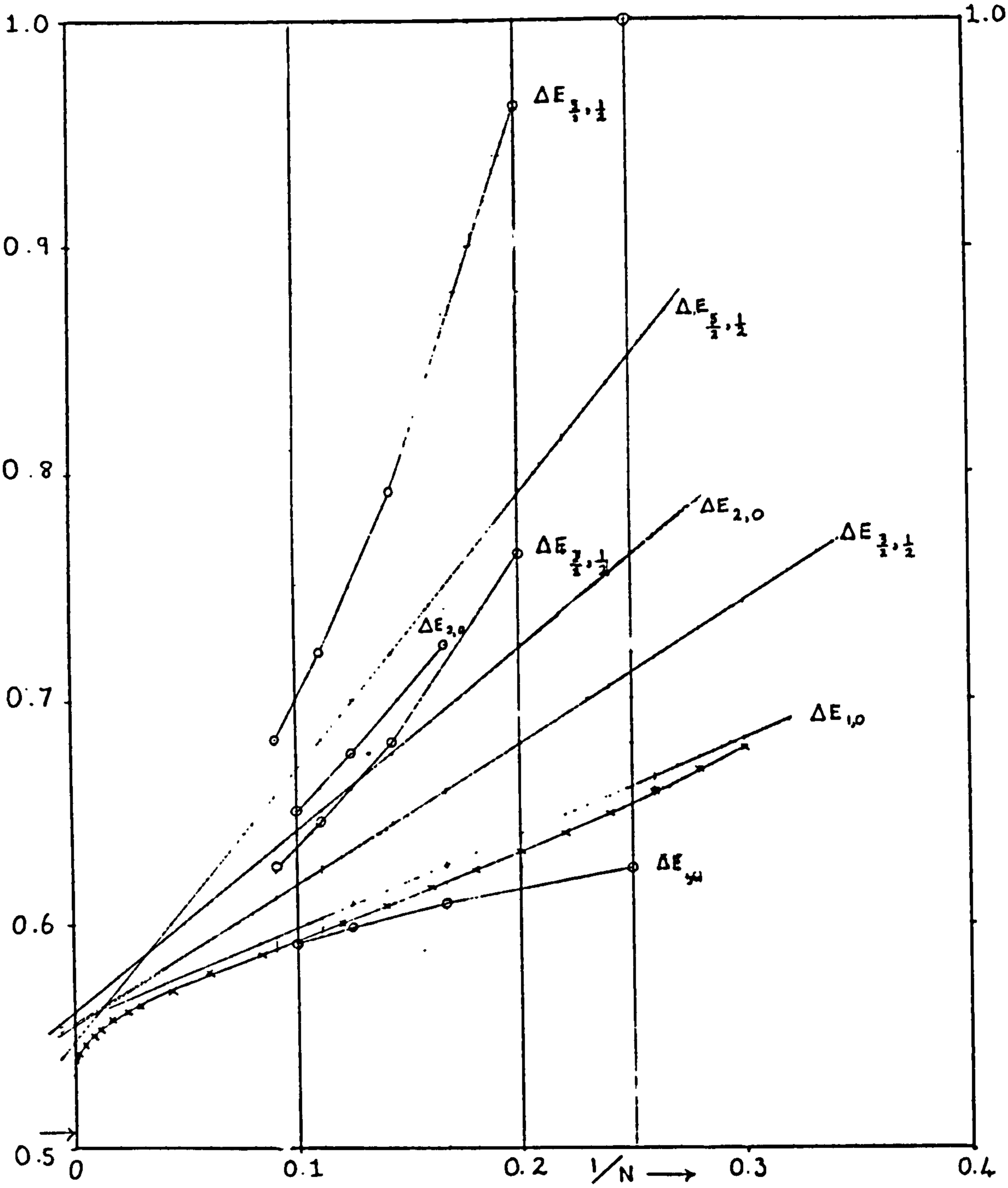

Antiferromagnetic Heisenberg Energy Gap Extrapolations for $\chi(0)$

significantly from the limiting behaviour. If, however, the set of points for a given ΔE are plotted versus $1/(N+j)$ where j is a suitably chosen small integer, these small finite N deviations are 'ironed out' and a straight line extrapolation (as shown on the graph) is obtained, which we hope is a good approximation to the limiting behaviour. The 'best straight lines' corresponding to the ΔE values listed above give rise to limiting estimates for χ_o of 0.0556, 0.0555, 0.0560 and 0.0548 respectively. Hence we have the final estimate (0.0555) quoted above in equation (5.3.6). (This value agrees closely with our earlier value of $\chi_o \sim 0.0559$ obtained from extrapolations on the low-temperature $\xi_N(T)$ curves).

3.4 Comparison With Work of Griffiths

This estimate rests on the assumption that M(H) does not vary too rapidly near H=0. However, it does not agree very closely with the subsequent result due to Griffiths of $\chi_o = 1/2\pi^2 = 0.050661$ .....(equation (5.2.9). Let us show here that Griffiths' value is consistent with a plausible though non-rigorous argument based on the spin wave spectrum of des Cloizeaux and Pearson (1962) (See Chapter III, sub-section (5.2)). By considering the structure of the odd N dispersion spectrum as $N \to \infty$, we were able to deduce that

$$\Delta E_{odd} / |J| \to 2\pi^2 / N \qquad (5.3.14)$$

where ΔE_{odd} is the first magnetic excitation for N odd. The corresponding value for χ_o is

$$\frac{|J| \chi_o}{N g^2 \beta^2} \simeq \frac{1}{N \Delta E} \simeq \frac{1}{2\pi^2} \qquad (5.3.15)$$

The magnetic energy gap ΔE_{even} is not obviously related to the des Cloizeaux and Pearson limiting dispersion relation: however, using the result (5.3.12) we are able to deduce that

$$\Delta E_{odd} = 2 \Delta E_{even} \qquad (5.3.16)$$

We conclude, therefore, that ΔE_{even} is, in fact, half the first excitation of the limiting dispersion spectrum. Hence

$$\chi_o \simeq \frac{1}{2N\Delta E_{even}} \simeq \frac{1}{2\pi^2} \qquad \text{as in (5.3.15).}$$

The apparent disagreement between the value for χ_o predicted by extrapolation, $\chi_o \sim 0.0555 \pm 0.0010$ and Griffiths' analytic value of $1/2\pi^2$ (a disagreement well outside cur quite generous estimates of extrapolation uncertainty) stimulated Griffiths to examine in detail the behaviour of M(H) near H=0. Let us consider again Fig. (5.18), in particular the finite N extrapolation points for $\Delta E_{1,0}$. Since for small M and H, $\chi_o \sim \frac{\Delta M}{\Delta H} \sim \frac{M}{H}$, these four points constitute a finite N approximation to the limiting values for M/H. If the horizontal axis scale is considered to be enlarged by a factor of 2, it is equivalent to an axis of magnetisation (normalised per spin). (The point for N=10 at 1/N = 0.1 corresponds to a magnetisation value of 0.5 (ignoring units)). For the $\Delta E_{1,0}$ points only, therefore, we have essentially a finite N plot of M/H versus M. Griffiths plotted the corresponding limiting values of M/H versus M (Griffiths, 1963, private communication) which are shown as a series of crosses on Fig. (5.18). We observe that over the range M = 0.3 to 1.2 (or 1/N = 0.6 to 2.4) Griffiths' points lie very close to a straight line, since Griffiths' curve, in fact, has a point of inflection in this region. This line lies very close to our 'best straight line' for $\Delta E_{1,0}$ (which intersects the M/H axis at 0.0556) and intersects the M/H axis at a value 0.0553. Below M/H = 0.3, Griffiths' points start to bend downwards suddenly, and the M/H curve eventually intersects the M/H axis at $1/2\pi^2 \sim 0.0507$ (shown by the arrow). It can be estimated that it would be necessary to go out to a ring length of about 20 to 30 spins, corresponding to M ~ 0.0250 to 0.0167, before traces of this asymptotic limiting behaviour became apparent. In fact, Fig. (5.18) well illustrates the strengths and weaknesses of our finite cluster extrapolation techniques. If the M/H curve had continued in to the limit with the same trend as is shown in the region above M = 0.03, our 'best straight extrapolation line' would have predicted a limiting value within 1/2% of the

"true" value of 0.0553. This situation is equivalent to the analyticity of M/H as M and H → 0. However, Griffiths' results showed conclusively that M/H was not analytic at H=0. In fact, $\frac{\partial^2 M}{\partial H^2}$ diverges sharply to + ∞ at this point (or $\frac{\partial^2 H}{\partial M^2}$ diverges to - ∞). This divergence accounts for why extrapolation of the gradients g_{jN} linearly with 1/N leads to an overestimate of about 10% for χ_o. $\chi(H)$ i.e. M/H for small H, of order 1/N, is well approximated by the g_{jN}, but does not itself approximate χ_o well unless H is exponentially small. We must conclude that our extrapolation methods appear to lead to excellent agreement with analytic results where the properties extrapolated are analytic. At non-analytic points however, the method may run into error, in this example of the order of 10%.

3.5) Anisotropic Magnetisation Curves

Magnetisation Curves Near Saturation

The zero-temperature magnetisation curve for other values of γ may be studied as for γ = 1. The critical field H_s is determined by the intersection of the energy level for total $S^z = N/2$ (a component of the zero-field ferromagnetic ground state) with the lowest level for $S^z = N/2-1$ (single ferromagnetic spin wave), both of which are known exactly. Thus

$$H_s(\gamma) = 2(1+\gamma)|J|/g\beta \qquad (5.3.17)$$

In order to study the form of the magnetisation wave near saturation, it is necessary to consider the width of the first magnetisation step away from saturation (see Fig. (5.16)). The position $H=H_1$ of this step is given by the intersection of the lowest level for $S^z = N/2-1$ with the lowest level for $S^z = N/2-2$, which in the limiting case, N → ∞, is given by $-4|J|(1+\gamma)$. It is seen, however, that use of the limiting curve again yields H_s; it appears, therefore, that the width of this step is directly determined by the energy discrepancy, ΔE_1, between the lowest-lying level for $S^z = N/2-2$ (finite N) and its limiting value. The situation is shown

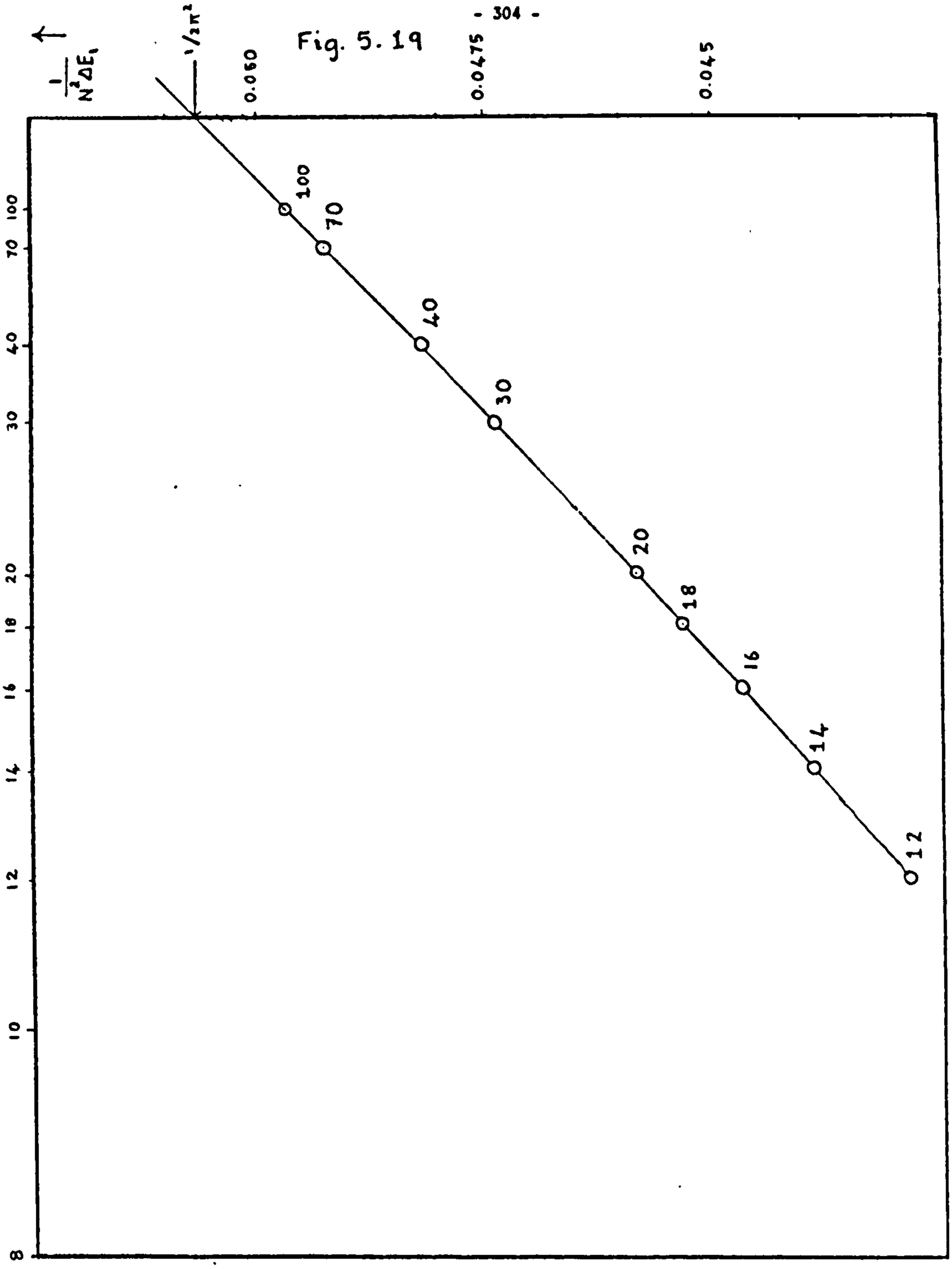

Fig. 5.19

Energy Gap Extrapolations for Magnetisation Behaviour Near Saturation

in the following sketch, fig. (5.2). Since the matrices corresponding to the blocks $S^z = N/2-2$ are only of order N(N-1)/2, effectively just (N-1)/2 when translational symmetry is taken into account. [The lowest-lying state for $|S^z| = N/2-2$ is always a k=0 state. Hence the full translational symmetry of N may be used to reduce the Hamiltonian matrices to obtain this state.] It was a simple matter,

fig. (5.2)

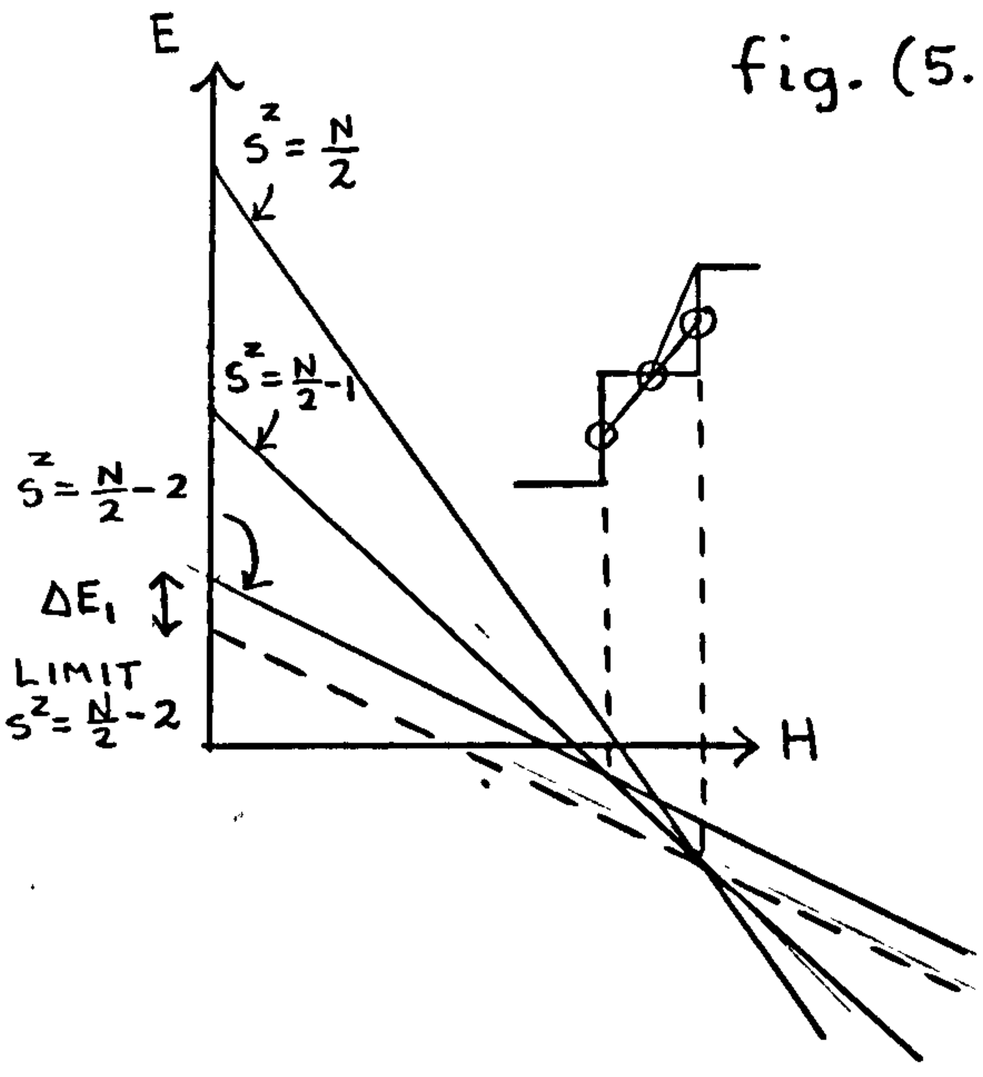

therefore, to solve the Hamiltonian block matrices numerically on a computer for N as high as 100, for various values of γ. The results are shown in Fig. (5.19), where we plot $1/N^2\Delta E_1$ versus $1/N$ for $\gamma = 1$. The N values of the various points are listed beside them. We see that the extrapolation curve is smooth and very nearly linear, a straight line extrapolation through the points for N=40, 70 and 100 yielding a limiting value of ~ 0.0506 to 0.0507. This value looks suggestively like

$$0.050661\cdots = 1/2\pi^2 \quad . \tag{5.3.18}$$

However, wary of possible non-analytic behaviour, we look for an alternative method of estimating this number.

Perturbation Studies

The matrix of fig. (5.3) is the matrix of order (N-1)/2, belonging, for convenience of calculation, to N odd.

fig. (5.3)

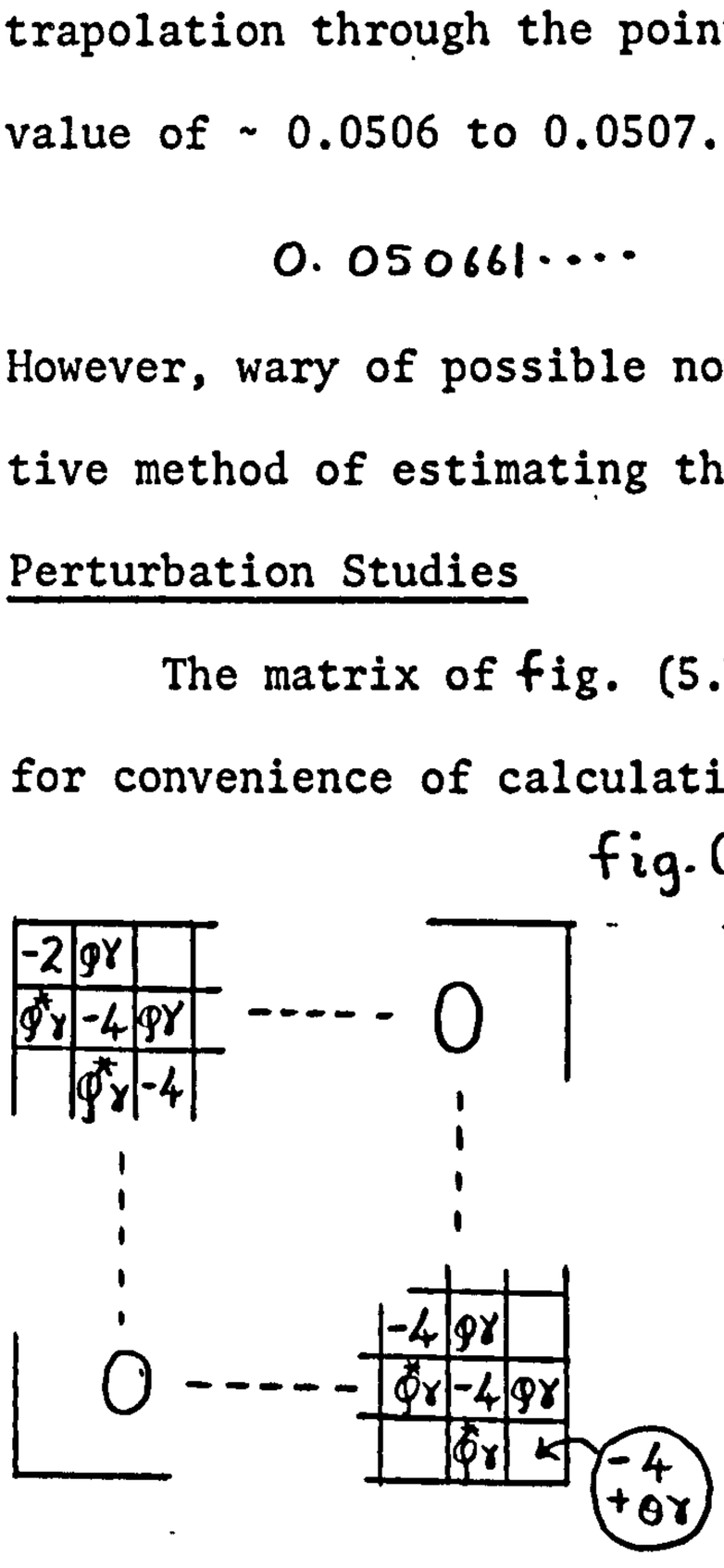

(It is a more exact form of the matrix in fig. (3.2) in Chapter III, sub-section (2.4). It differs from fig. (3.2) in that the lowest diagonal element is here given as $-4 + \theta\gamma$, appropriate to small finite N. In fig. (3.2), appropriate

to N large, the factor $\theta\gamma$ is ignored).

In fig. (5.3),

φ denotes $(1+\omega)$

and φ^* " $(1+\omega^{N-1})$ } where $\omega^N \equiv 1$

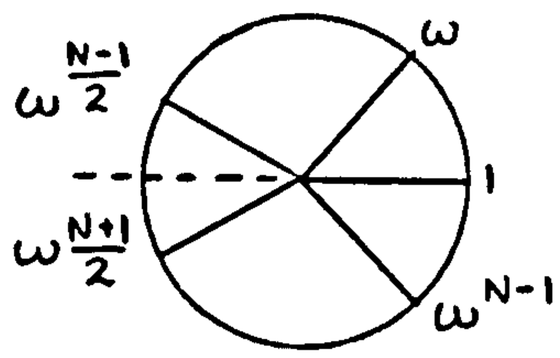

and

$$\Theta = \omega^{\frac{N-1}{2}} + \omega^{\frac{N+1}{2}} = -2\cos\frac{\pi}{N} \tag{5.3.19}$$

$$\varphi\varphi^* \doteq 2 + 2\cos 2\pi/N = 4\cos^2\pi/N = \Theta^2 . \tag{5.3.20}$$

Applying second order perturbation theory to the lowest diagonal element we have, for the minimum eigenvalue of this matrix

$$\frac{E_{min}}{|J|} = -4 + \Theta\gamma + \frac{\varphi\varphi^*\gamma^2}{\Theta\gamma}$$

$$= -4 + 2\Theta\gamma$$

$$= -4 - 4\gamma\cos\pi/N \tag{5.3.21}$$

The matrix in fig. (5.3) corresponds to q=1, N odd. By referring to the detailed ferromagnetic spectrum shown in Fig. (3.10) we observe that the lowest-lying state for two overturned spins, q=1, is, in fact, the lowest-lying finite N state, for all q, for $S^z = N/2-2$, the state we have been seeking. Expanding the curve in equation (5.3.21), we have

$$E_{min}/|J| \simeq -4(1+\gamma) + 2\gamma\pi^2/N^2 \tag{5.3.22}$$

The term $-4(1+\gamma)$ measures the low-energy limit of the two-spin-wave continuum for all γ, and the second term then represents the energy discrepancy between the lowest-lying finite N state and the limit that we are seeking.

$$\text{i.e.} \quad \Delta E_1 = 2\gamma\pi^2/N^2 , \quad \text{all } \gamma \text{ and large } N . \tag{5.3.23}$$

This result is consistent with equation (5.3.18) for $\gamma = 1$ and also with numerical extrapolations for other values of γ. This encourages us to believe that there is no non-analytical behaviour in this particular case, and that equation (5.3.23) is probably the exact limiting analytical result.

It is perhaps worth noting that linear extrapolations of points for N=4 and N=6 are in 10% agreement with the limit, for 6 and 8 in 4% agreement, for 8 and 10 in 2.5% agreement, and for 10 and 12 within 1.5% agreement with the limit. Corresponding to a magnetisation step of

$$\Delta M = g\beta \qquad \text{or } \Delta M / M_{max} = 2/N \tag{5.3.24}$$

we thus find a magnetic field step

$$\Delta H = \tfrac{1}{2}(H_s - H_1) = \frac{\Delta E_1}{2g\beta} \simeq \frac{\gamma \pi^2 |J|}{g\beta N^2} \; . \tag{5.3.25}$$

On eliminating N between (5.3.24) and (5.3.25) we have

$$\frac{\Delta M}{M_{max}} \simeq \frac{2}{\pi\sqrt{\gamma}} \left(\frac{g\beta \Delta H}{|J|} \right)^{1/2} \tag{5.3.26}$$

or

$$\frac{\Delta M}{M_{max}} \simeq \left[\frac{8(1+\gamma)}{\pi^2 \gamma} \right]^{1/2} \left(\frac{\Delta H}{H_s} \right)^{1/2} \tag{5.3.27}$$

which suggests that when $N \to \infty$ we may write more generally as $H \to H_s$

$$M / M_{max} = 1 - A(\gamma) \left[1 - (H/H_s) \right]^{1/2}$$

$$\text{with} \quad A(\gamma) = (4/\pi) \left[(1+\gamma)/2\gamma \right]^{1/2} \tag{5.3.28}$$

in agreement with equations (5.3.4) and (5.3.5) for $\gamma = 1$. Alternatively, we have, essentially, for the curvature of the H versus M curve near $M \to M$ max.

$$\left(\frac{g^3 \beta^3}{|J|} \right) \frac{\partial^2 H}{\partial M^2} \longrightarrow -2\gamma\pi^2 \tag{5.3.29}$$

Fig. 5.20

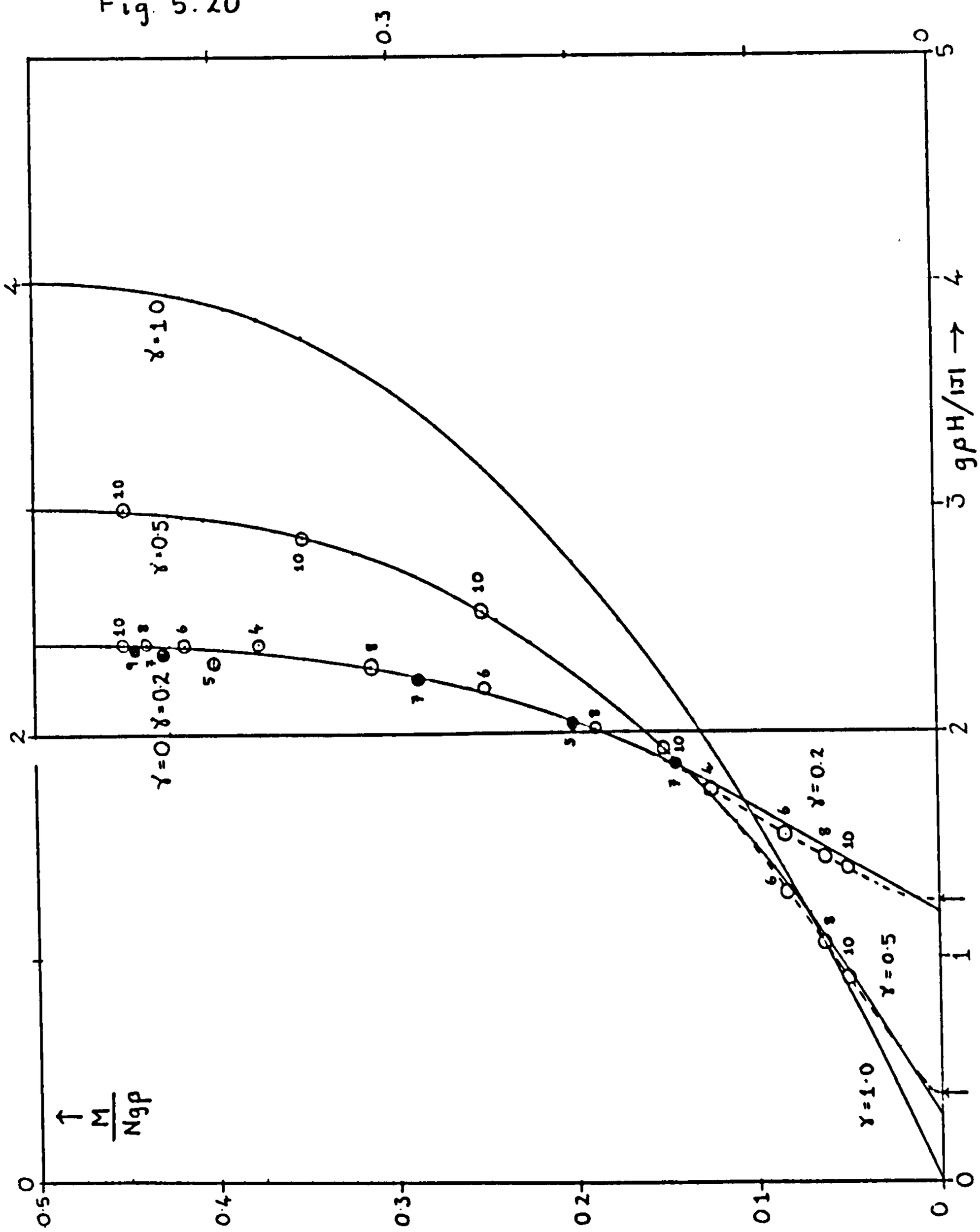

Dependence of Zero-Temperature Magnetisation Curves on Anisotropy

and, of course $$\left(\frac{q^2\beta^2}{|J|}\right)\frac{\partial H}{\partial M} \longrightarrow 0 \quad . \qquad (5.3.30)$$

Fig. (5.20) shows the complete, estimated limiting magnetisation curve for the Ising limit $\gamma = 0$, where it is a simple step function, and for intermediate values of γ .

3.6) Rigorous Zero-Temperature Results

Very recently Yang and Yang (1967) have produced a completely rigorous analytic solution for the infinite Heisenberg and anisotropic chains, for the magnetisation curve as a function of field in the limit of zero temperature. Their results confirm rigorously a) Griffiths' limiting value of $1/2\pi^2$ for the zero-point zero-field antiferromagnetic susceptibility b) Griffiths' form for the $\gamma = 1$ magnetisation curve as a whole (which, of course, agrees with our extrapolations) c) the conclusion inherent in Griffiths' work that M(H) is a non-analytic function of H near H=0, in particular that $\frac{\partial^2 M}{\partial H^2}$ tends to $+\infty$ $\left(\frac{\partial^2 H}{\partial M^2} \to -\infty\right)$ as $H \to 0$ and d) that the form of the magnetisation curve near saturation (see, for example, our equation (5.3.28)) predicted by our numerical approach is the correct answer.

Magnetisation Curves Near M=0

However, the Yang and Yang rigorous solution differs from our numerical work in one important respect, namely the form of the $0 < \gamma < 1$ magnetisation curves near M=0. Let us consider the extrapolated curve for γ=0.2 in Fig. (5.20) for $M/q\beta N < 0.13$. Our information for predicting the limiting form of the curve in this region comes from the set of four points for N=4, 6, 8 and 10 shown in Fig. (5.20) (the points for N odd are less informative). The plot for the magnetisation curve in this region is essentially our extrapolation plot described in Chapter III, sub-section (3.2) for determining the limiting anisotropy gap for $\gamma = 0.2$, turned on its side (the field axis is essentially the same as an energy axis and the magnetisation axis as a 1/N axis). Our assumption in

extrapolating the limiting anisotropy gap was that this set of points (which is clearly approximately linear) could be continued, as a smooth linear plot into the axis 1/N (i.e. M) = 0. The "best straight line" obtained by plotting these four points versus 1/(N+j), where j is a small integer suitable for straightening the plot, is shown on Fig. (5.20) as the $M \to 0$ extrapolated limit of the $\gamma = 0.2$ magnetisation curve (solid curve). The point at which the limiting magnetisation curve cuts the H axis (H~1.20) is essentially our estimate for the limiting anisotropy gap. In the case of $\gamma=1$ the corresponding plot gives rise to a smooth extrapolation which cuts the H axis at the correct point, namely H=0. If, however, at $\gamma=1$, we plot not ΔE versus 1/N or, equivalently, H versus M but the derivative H/M versus M, we know from sub-section (3.4) of this chapter that the points do not show a linear trend right into M=0, but for very small M suddenly turn up and go into the H/M axis with infinite slope. As we have said, this feature is a consequence of the non-analyticity of M(H) at M=0. At the time these magnetisation extrapolations for $1 > \gamma > 0$ were performed, we did not know whether there were corresponding singularities of M(H) as $M \to 0$ for the case of anisotropy, or any peculiar behaviour of M(H) in the region $M \to 0$ which would presage the singularity at $\gamma=1$. It was hoped that any such peculiar behaviour would not "show up" in the H versus M curves, but only in the higher derivatives, as in the case of $\gamma=1$. This assumption is, of course, the assumption on which our confidence in the reliability of the anisotropy energy gap calculations is based. However, Yang and Yang have shown rigorously that in the small M region the $\gamma > 0$ magnetisation curve "turns down at the last minute" and goes into the H axis with vertical slope, i.e. $\partial M/\partial H \to \infty$, and very large curvature. The results of Yang and Yang converted into our notation tell us that for $\gamma = 1 - \lambda^2/2$, where λ is a small positive number, the curvature

$$\frac{\partial^2 H^*}{\partial M^{*2}} \simeq 4\gamma\pi^3 \exp\left(\frac{\pi^2}{2\lambda}\right) \qquad (5.3.31)$$

(where H^* and M^* represent the reduced variables $H^* = g\beta H/|J|$ and $M^* = M/g\beta$). For the Ising limit, $\gamma=0$, the Yang and Yang results predict that

$$\lim_{\gamma \to 0} \left\{\frac{H^* - 2}{\gamma}\right\} = -\frac{d}{dM^*}\left[\frac{(1+2M^*)}{\pi} \sin \frac{\pi(1-2M^*)}{(1+2M^*)}\right] \qquad (5.3.32)$$

The function on the R.H.S. of equation (5.3.32) is such that when multiplied by γ and the limit taken, we regain the familar step function at

$$g\beta H/|J| = 2\cdot 0 \,. \qquad (5.3.33)$$

The analytic structure shown on the R.H.S. of equation (5.3.32) is therefore not revealed by our particular choice of Hamiltonian.

Rings and Chains

Let us compare the zero-temperature magnetisation curves for finite rings and chains. In the Ising limit the ring curve is the same function for both finite and infinite N. The chain curve, however, is rather anomalous in that the magnetic energy gap $\Delta E = |J|$, which determines the crossing of the two magnetic levels for $S^z = 0$ and $S^z = 1$, is only half all the other gaps (and all the ring gaps) which are given by $\Delta E = 2|J|$. A similar effect occurs for other values of γ, and distorts the finite N magnetisation curves for chains near $M = 0$ so that the curves vanish at a magnetic field value which is roughly half the corresponding value for rings. Since only a single magnetic gap is affected, it is obvious in the Ising limit that this is a 'small number effect' which will disappear in the limit. Presumably a similar result also holds for $\gamma > 0$. It is interesting that the limiting thermal properties appear to be determined by the chain energy gaps whereas the limiting magnetic properties are determined by the ring gaps.

Fig. 5.21

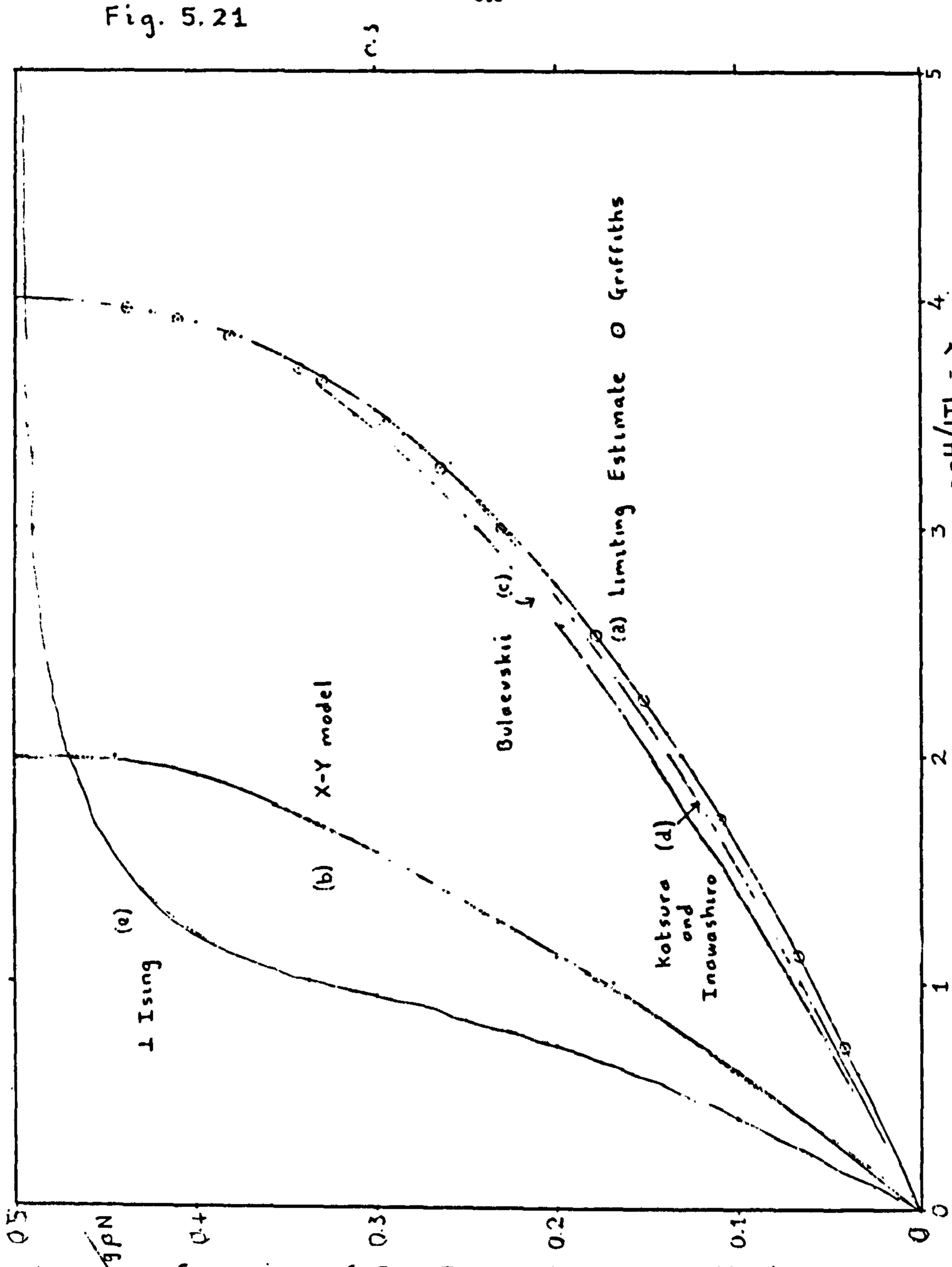

Comparison of Zero-Temperature Magnetisation Curves.

The points at which the magnetisation curves (M versus H) go to zero are non-analytic points, and it is interesting that small finite rings and chains naively might be said to predict different limiting magnetic behaviour. For the thermal properties, in zero field, T=0 is a non-analytic point, and again we might naively suppose that small finite rings and chains predict different low-temperature limiting behaviour. (But see, for example, the discussion in Chapter III, sub-section (2.6).) It is tempting to speculate generally whether apparent differences in the behaviour of rings and chains indicate a region near a non-analytic point, i.e. that in some cases the finite N thermodynamic properties in such a region are very sensitive to a change of boundary conditions.

3.7) Comparison with Other Models and Approximations

Let us now compare our zero-temperature magnetisation curve for $\gamma=1$ with the zero-temperature antiferromagnetic magnetisation curve for the X-Y model obtained by Katsura (1962), and the corresponding curve of Bulaevskii (1963). The Katsura curve has the analytic form

$$H^* = 2 \sin (\pi M^*) \qquad (5.3.34)$$

The curve is shown as curve (b) on Fig. (5.21) and has a similar form to the Heisenberg curve, (curve (a)). However, the critical field is given by $H_s = 2|J|/g\beta$ instead of $4|J|/g\beta$ for the Heisenberg model. In the region near saturation, the curve has the asymptotic form

$$M / M_{max} = 1 - A \left[1 - (H/H_s)\right]^{1/2}$$

where $$A = 2\sqrt{2}\,\pi = 0.9003 \qquad (5.3.35)$$

(c.f. the Heisenberg case, where $A = 4/\pi = 1.2732$). Near M = 0, the curve is approximately linear, and gives a finite value for χ_o of $1/2\pi$; i.e. $H \sim 2\pi M$ as $M \to 0$. The curvature near M=0 is given by

$$\partial^2 H / \partial M^2 = -2\pi^3 M \qquad (5.3.36)$$

and vanishes at M=0: this point is an analytic point for the X-Y model.

The Bulaevskii curve has the analytic form

$$H^* = 4M^* + 2\sin\pi M^* + \frac{2}{\pi}\sin 2\pi M^* \qquad (5.3.37)$$

The curve is shown on Fig. (5.21) as curve (c) and has a closely similar form to the Heisenberg curve: both curves have the same critical field $g\beta H/|J| = 4$. Near M=0, the curve is approximately linear, and gives a finite value for

$$\chi_o = \frac{1}{2(4+\pi)} = 0.0700 \qquad (5.3.38)$$

The curvature near M=0 is given by

$$\frac{\partial^2 H}{\partial M^2} \simeq -2\pi^3 M - 16\pi^2 M \qquad (5.3.39)$$

and vanishes at M=0. In Bulaevskii's treatment, in fact, M(H) is analytic at H=0 and this is the only feature in which the Bulaevskii approximation differs significantly from the exact result. For example, in the region near saturation, the curve has the asymptotic form

$$M/M_{max} = 1 - A\left[1 - (H/H_s)\right]^{1/2} \qquad (5.3.40)$$

where

$$A = 4/\pi \sim 1.2732$$

just as for the exact result. Katsura and Inawashiro (1965) have calculated a first order correction to the Bulaevskii curve (regarded as zero$^{\underline{th}}$ order), which represents a slight improvement over the range of the magnetisation curve away from saturation. The curve appears as curve (d) in Fig. (5.21), taken from the paper of Katsura and Inawashiro (1965). This treatment gives a magnetisation slope near H=0 of

$$\left(\frac{|J|}{Nq^2\beta^2}\right)\frac{M}{H} = 0.06475 \; ; \qquad (5.3.41)$$

which is 28% in error as compared with 40% in the case of the Bulaevskii first order result. However, as has already been discussed in Chapter IV, sub-section (3.5), this approach of Katsura and Inawashiro predicts a mean-field-type phase transition for the ferromagnetic linear chain,

which is well-known to be incorrect.

Finally, for interest, on Fig. (5.21) we show a magnetisation curve (curve (e)) for the Ising model in a perpendicular field. This curve is the same for both ferro- and antiferromagnets. The magnetisation curves for this model have the form Katsura (1962)

$$\frac{M}{g\beta N} = \frac{1}{2\pi}\int_0^{\pi} \frac{(C - K\cos k)\,\tanh\left[K^2 + C^2 - 2KC\cos k\right]^{1/2}}{\left[K^2 + C^2 - 2KC\cos k\right]^{1/2}}\,dk \qquad (5.3.42)$$

where $K = J/2kT$ and $C = g\beta H/2kT$.

When the temperature tends to zero, the magnetisation is expressed by complete elliptic integrals of the first and second kinds.

This curve is quite different in form from the curve for the antiferromagnetic Ising model in a parallel field (a simple step function at $g\beta H/|J| = 2.0$) and also from the curve for the ferromagnetic Ising model in a parallel field which is a simple step function like the antiferromagnet, except that the step is located at H=0. The same step function describes also the Heisenberg and general anisotropic linear chains for all N, finite and infinite. As soon as a magnetic field is applied, the (N+1)-fold degeneracy of the ferromagnetic ground state is broken, and the ferromagnetic ground state in a field is the component with maximum $S^z = N/2$ and corresponding magnetisation

$$\frac{M}{g\beta N} = \frac{1}{N} \times \frac{N}{2} = 0.5\,. \qquad (5.3.43)$$

The encircled points lying very close to our extrapolated curve (a) on Fig. (5.21) are a selection of points from the numerical calculations of Griffiths (1964) of the exact limiting curve.

The behaviour as a function of temperature of the X-Y model magnetisation curve, the Ising model in a perpendicular field, and the ferromagnetic and antiferromagnetic Ising model curves in a parallel field

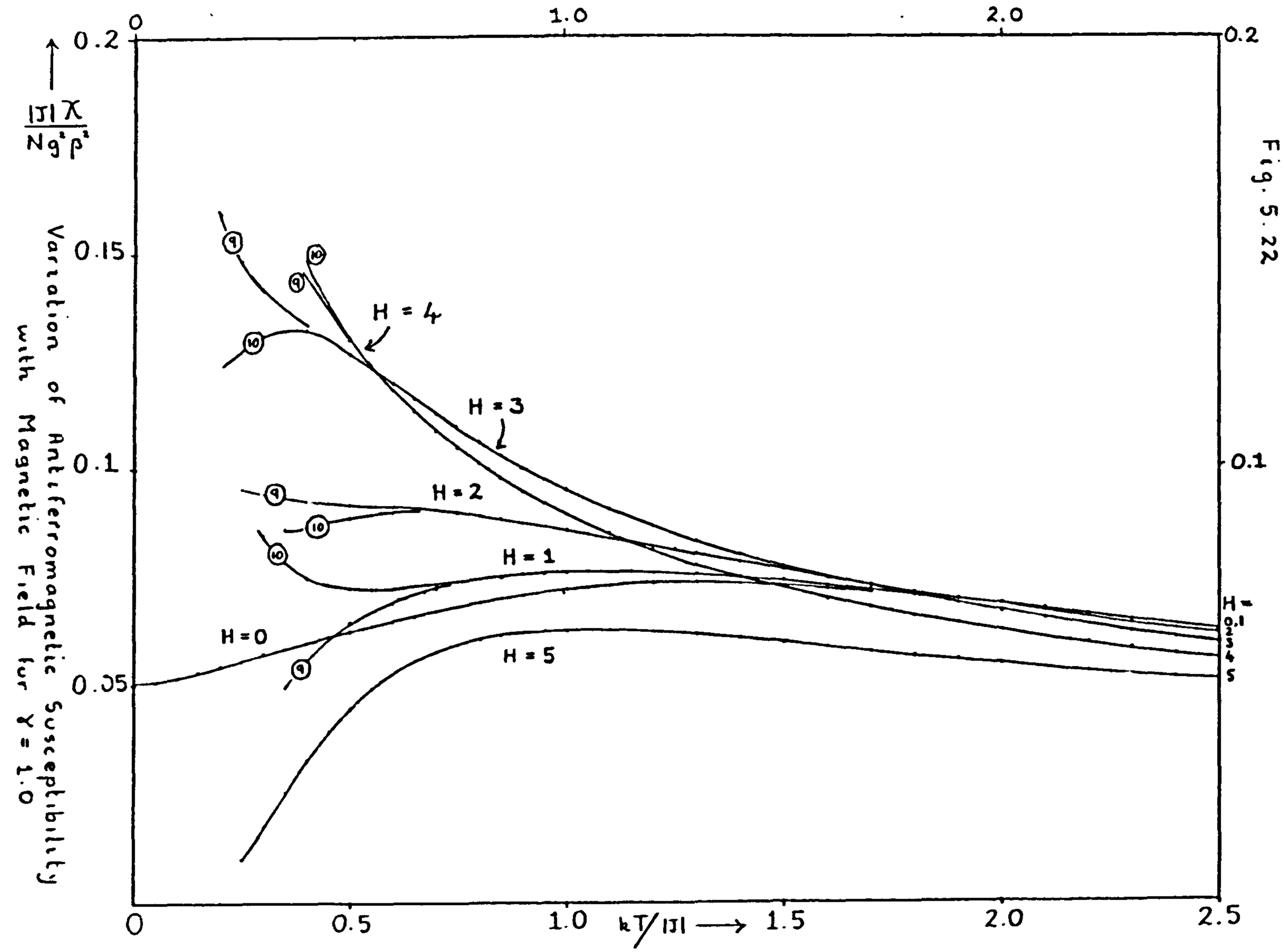
0
1.0
2.0
0.2
0.15
0.1
0.05
$\frac{|J|\chi}{Ng^2\beta^2}$
H = 4
H = 3
H = 2
H = 1
H = 0
H = 5
H = 0.1 onwards
0.5
1.0
1.5
2.0
2.5
kT/|J| ⟶
Variation of Antiferromagnetic Susceptibility with Magnetic Field for γ = 1.0

Fig. 5.22

are shown as Figs. (4a), (4b), (4c) and (4d) respectively in the paper of Katsura (1962).

3.8) Antiferromagnetic and Ferromagnetic Susceptibilities

In Fig. (5.22) the antiferromagnetic parallel susceptibility for $\gamma=1$ is shown for a variety of fields below, at and above the critical field. In general, the improved convergence in the presence of a field is shown by the fact that the curves for N=9 and N=10 do not start to deviate from each other until the temperature is decreased to the region of $kT/|J| \approx 0.5$. The temperature at which the two curves are distinguishable decreases with increasing field until, at $g\beta H/|J| = 5$, convergence is complete down to about $kT/|J| = 0.2$. The manner in which the curves finally separate is rather erratic, depending on accidental energy level confluences and is not important. We see that as the field increases from zero (for which the limiting curve is shown for comparison) the height of the maximum rises and moves to lower temperatures. In the special case of the critical field, $g\beta H/|J| = 4$, the behaviour is paramagnetic, at least down to temperatures $kT/|J| \approx 0.1$, owing to the large confluence of low-lying levels. Above the critical field the height of the maximum starts to fall below that of the zero-field curve and the position of the maximum increases in temperature steadily with field. A finite energy gap exists for all fields greater than the critical field, between the lowest and first excited states, and the susceptibility curves rise from zero exponentially, at a rate determined by the energy gap. At high temperatures, represented on Fig. (5.22) by $kT/|J| = 2.5$, the curves for all field values decrease steadily as H increases. The intermediate behaviour is rather complicated, with curves crossing. The behaviour is very similar for all anisotropy values, and we do not show any further figures.

In Fig. (5.23) we show the ferromagnetic parallel susceptibility for the ring of 8 spins in the Heisenberg limit, for various magnetic fields. The convergence with N is appreciably more rapid in a field than for

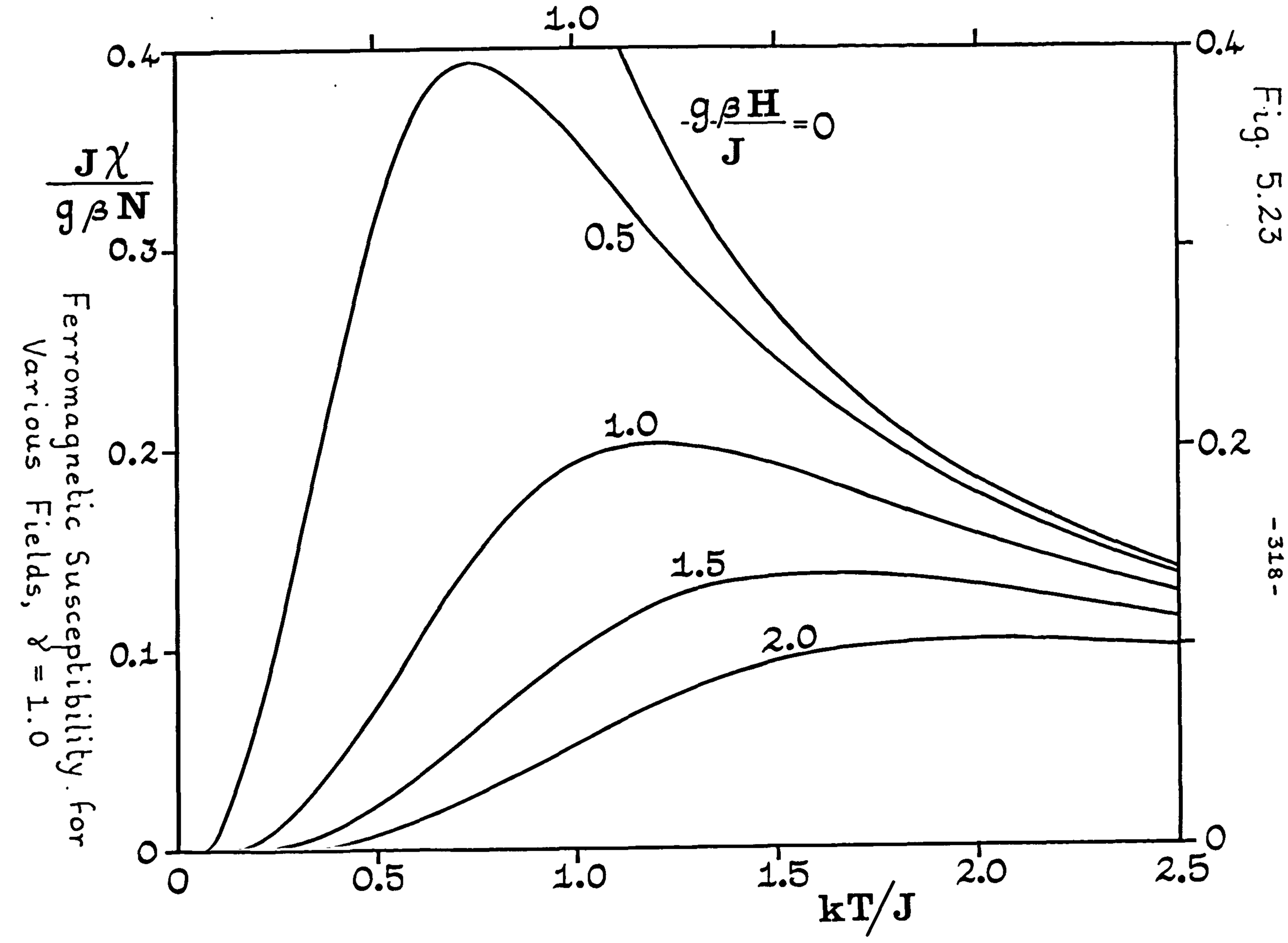

Ferromagnetic Susceptibility for Various Fields, $\gamma = 1.0$

Fig. 5.23

H=0, and the 8=ring results should be very close to the limiting results. We observe that for finite fields, the paramagnetic curve for zero-field becomes a curve with a maximum and which vanishes as $T \to 0$. The height of the maximum falls and its position in temperature increases as the field increases.

CHAPTER VI

PAIR CORRELATION FUNCTIONS

Introduction

The thermodynamic properties of greatest interest for physical systems, e.g. magnetic systems, ferro- and antiferroelectric systems, fluids and superfluids, can all be related to pair correlation functions. The pair correlations essentially essentially express the influence of one spin (or its analogue) in a lattice upon a second spin an arbitrary number of lattice sites away. They are thus of fundamental importance in the study of cooperative phenomena. In this chapter our greatest interest will lie in the evaluation of zero-temperature, antiferromagnetic, spin-pair correlation functions, which are related to the degree of order of the antiferromagnetic ground state.

In particular we are interested in the behaviour of the long-range order parameter as a function of anisotropy γ . (The long-range order as a function of γ is intimately related to the spontaneous staggered polarisation of the antiferroelectric F-model as a function of temperature (Nagle, private communication)). Earlier work has suggested that the long-range order vanishes for γ greater than some critical value γ_c , and an estimate for γ_c as low as 0.483 has been given (Kasteleijn, 1952). In the abs ence of an exact solution this point cannot be settled with a high degree of certainty. However, by combining the series of Walker (1959) as extended by Nagle with our own extrapolations we are able to present a plausible conclusion that the long-range order vanishes only in the limit $\gamma = 1$ for the spin-1/2 infinite linear chain.

1. DEFINITION AND CALCULATION OF ORDER PARAMETERS

1.1 Ising, Heisenberg and Anisotropic Correlations.

For the Ising model, the pair correlation functions are conveniently defined as

$$\omega_\ell(N) = 4/N \sum_{i=1}^{N} \langle S_i^z S_{i+\ell}^z \rangle \qquad (6.1.1)$$

where the angular brackets denote thermodynamic average. If we adopt periodic boundary conditions, then all sites on the ring are equivalent and hence

$$N^{-1} \left\langle \sum_{i=1}^{N} S_i^z S_{i+\ell}^z \right\rangle = \langle S_o^z S_\ell^z \rangle \qquad . \quad (6.1.2)$$

Thus $$\omega_\ell(N) = 4 \langle S_o^z S_\ell^z \rangle \qquad (6.1.3)$$

In this chapter our primary interest will be in zero-temperature pair correlation functions, and the thermal average will reduce to the expectation value of the appropriate correlation operator $S_o^z S_\ell^z$ for the ground state.

Let us illustrate the properties of the correlation functions (6.1.3) by means of some simple examples. Let us consider the ordering properties of the ferromagnetic ground state of a four-spin Ising ring, the ground state (actually two-fold degenerate) may be taken as $|0000\rangle$. Then $\omega_\ell = 1$ for all ℓ (and all N), which, of course indicates maximum ordering.

Let us consider also the N=4 antiferromagnetic ground state (also actually two-fold degerate) which we may take as $|1010\rangle$. We see that $\omega_1 = -1$; $\omega_2 = +1$, etc. We have the general result that $|\omega_\ell| = 1$ for all ℓ (and all N), which again shows complete ordering. However we see that an important feature of antiferromagnetic correlation functions is an alternating sign effect, i.e., $\omega_\ell = -1$ for $\ell = 2n + 1$ and $\omega_\ell = +1$ for $\ell = 2n$. We shall see that this alternating effect persists in the case of partial ordering when we consider a general anisotropic or Heisenberg model.

Heisenberg Model

In the case of the Heisenberg limit, where spin coupling exists in three dimensions, x, y and z, the most convenient choice of correlation function is not immediately apparent. We may consider either the same correlation function as in the Ising case or the full correlafunction $\langle \underline{S}_o \cdot \underline{S}_\ell \rangle$. However, the isotropy of the Heisenberg model implies that the two definitions are identical provided we choose suitable normalization. In fact,

$$4 \langle S_o^z S_\ell^z \rangle \equiv 4/3 \langle \underline{S}_o \cdot \underline{S}_\ell \rangle \qquad (6.1.4)$$

the factor 4/3 arises from the fact that if $\underline{S}_o$ and $\underline{S}_\ell$ show full anti-parallel coupling, the corresponding eigenvalue of $\underline{S}_o \cdot \underline{S}_\ell$ is -3/4. If, on the other hand, $\underline{S}_o$ and $\underline{S}_\ell$ are coupled so as to be fully parallel, the eigenvalue of $\underline{S}_o \cdot \underline{S}_\ell$ is +1/4. Hence the corresponding order parameter for ferromagnets will be

$$\omega_\ell = 4 \langle \underline{S}_o \cdot \underline{S}_\ell \rangle \qquad (6.1.5)$$

Let us investigate the ordering properties of the ferromagnetic ground state. It is convenient to introduce the permutation operator (see Chapter II, subsection (1.2)) defined as

$$P_{ij} = \frac{1}{2} (1 + 4 \underline{S}_i \cdot \underline{S}_j) \qquad (6.1.6)$$

then

$$\omega_{\ell}^{\text{ferro}} = 2 \langle P_{o\ell} \rangle - 1 \qquad (6.1.7)$$

The (N+1) fold degenerate ferromagnetic ground state is completely symmetric with respect to the interchange of any two spins. Hence

$$\langle \text{F.G.S.} | P_{o\ell} | \text{F.G.S} \rangle = 1 \text{ for all } \ell \text{ and } N, \text{ and } \omega_{\ell}^{\text{ferro}} = 1 \qquad (6.1.8)$$

Hence, with this definition of order parameter, all (N+1) components of the ferromagnetic ground state are seen to be fully ordered for all finite N and hence also for infinite N. If, instead, we consider the Ising order parameter, $\omega_\ell = 4 \langle S_o^z S_\ell^z \rangle$, only the ground state components having maximum and minimum total $S^z = \sum S_i^z$ are fully ordered.

Anisotropic Order Parameters

For the order parameter definitions in the case of general anisotropy we have a variety of choices. We may choose the Ising order parameter $\omega_\ell = 4\langle S_o^z S_\ell^z\rangle$ which is our primary interest in this chapter. We may also consider the off-diagonal order parameter defined as

$$\omega_\ell^{x+y} = 2\langle S_o^x S_\ell^x + S_o^y S_\ell^y\rangle = 4\langle S_o^x S_\ell^x\rangle . \quad (6.1.9)$$

A convenient combination which reduces to the Ising parameter for $\gamma=0$ and both the equivalent Heisenberg antiferromagnetic parameters for $\gamma=1$ is

$$\omega_\ell(\gamma) = \frac{4}{(1+2\gamma)}\langle S_o^z S_\ell^z + \gamma\left(S_o^x S_\ell^x + S_o^y S_\ell^y\right)\rangle . \quad (6.1.10)$$

1.2 Short-Range Order Parameters

When the two spins, o and ℓ, are nearest-neighbours, the corresponding order parameter, ω_1, is called the short-range order (conveniently abbreviated to S.R.O.) and is very closely related to the energy. If the Hamiltonian is $\mathcal{H} = 2|J|\sum_{i=1}^{N} \underline{S}_i\cdot\underline{S}_{i+1}$, then the energy expectation of the antiferromagnetic ground state is given by

$$\langle\mathcal{H}\rangle = 2|J|\langle\sum \underline{S}_i\cdot\underline{S}_{i+1}\rangle = 2N|J|\langle\underline{S}_o\cdot\underline{S}_1\rangle, \quad (6.1.11)$$

Hence

$$\omega_1 = \frac{4}{3}\frac{E_o}{2N|J|} = \frac{4}{3}\varepsilon(\infty,N) \quad (6.1.12)$$

In the limit $N=\infty$, ε_o is known exactly (Hulthén, 1938) to be

$$\varepsilon_o(\infty) = -0.88629\cdots \quad (6.1.13)$$

Hence

$$\omega_1(\infty) = -0.59086\cdots \quad (6.1.14)$$

The diagonal and off-diagonal short-range order parameters can be simply related to each other. If the Hamiltonian is

$$\mathcal{H} = 2|J|\sum_{i=1}^{N}\left\{S_i^z S_{i+1}^z + \gamma\left(S_i^x S_{i+1}^x + S_i^y S_{i+1}^y\right)\right\} \quad (6.1.15)$$

then

$$\frac{\partial H}{\partial \gamma} = 2|J| \sum_{i=1}^{N} \left\{ S_i^x S_{i+1}^x + S_i^y S_{i+1}^y \right\} \quad . (6.1.16)$$

By Feynman's theorem (1939) the expectation value of (6.1.16) at T=0 is

$$\frac{\partial E_o}{\partial \gamma} = 2|J| N \left\langle S_o^x S_1^x + S_o^y S_1^y \right\rangle \quad (6.1.17a)$$

or

$$\partial \mathcal{E}_o / \partial \gamma = \omega_1^{x+y} \quad . (6.1.17b)$$

Orbach (1958) calculated the antiferromagnetic ground state for linear chains numerically as a function of γ for the limit $N \to \infty$. By numerical differentiation of these values we may obtain $\omega_1^{x+y}(\infty)$ numerically. Since we also have, by considering the expectation value of the Hamiltonian (6.1.15)

$$E_o = 2|J| N \left\langle S_o^z S_1^z \right\rangle + 2\gamma |J| N \left\langle S_o^x S_1^x + S_o^y S_1^y \right\rangle \quad (6.1.18)$$

or $$\mathcal{E}_o = \tfrac{1}{2} \omega_1^z + \gamma \omega_1^{x+y} \quad . (6.1.19)$$

Hence $$\omega_1^{x+y} = \mathcal{E}_o(\gamma)/\gamma - \omega_1^z / 2\gamma \quad (6.1.20)$$

which relates the Ising and off-diagonal order parameters for finite and infinite N. Also

$$\omega_1^z = 2\mathcal{E}_o - 2\gamma \partial \mathcal{E}_o / \partial \gamma \quad (6.1.21)$$

and hence $\omega_1^z(\infty)$ may also be found numerically, as a function of γ (Orbach, 1958).

1.3 Longer-Range Order Parameters

There are two main methods for calculating the order parameters for $\ell > 1$. The Ising order parameters are diagonal in any representation involving linear combinations of basic Ising wave functions. They may therefore be calculated directly from the ground state (finite N) eigenfunction of (6.1.15) expanded in this manner. The off-diagonal order parameters $\omega_{\ell(N)}^{x+y}$ are quantum-mechanical operators with properties analogous to the properties of the operator 0^{x+y} of Chapter II,

subsection (1.1). Again, however, they may be calculated directly from the expansion of the ground state eigenfunction in terms of basic Ising wavefunctions (since the operators ω_ℓ^{x+y} are diagonal in the representation which completely diagonalises the Hamiltonian (6.1.15)).

This method is the simplest when zero-temperature results only are required, and has been used to obtain the majority of the results described in this chapter. If, however, we require the full temperature dependence of the correlation functions, we have to compute the sum of the contributions to the particular order parameter from <u>all</u> the eigenfunctions of the Hamiltonian. This process is rather tedious, and is not applicable in cases where only the eigenvalues of the Hamiltonian can be obtained (for example, because of the large size of the Hamiltonian matrix.) Alternatively, we may set up a representation of the particular order parameter, considered as a quantum-mechanical operator, and then diagonalise it directly. This approach is particularly simple if we express the order parameters in terms of the permutation operator P_{ij}, described earlier in this section.

1.4 <u>Numerical Results for Rings</u>

Numerical results for the antiferromagnetic correlations $\omega_\ell^z(N) = 4\langle S_o^z S_\ell^z \rangle$ for N = 4, 6, 8 and 10, and values of γ from $\gamma = 0$ by intervals of 0.1 through $\gamma = 1.0$ are given in Table (6.1). The antiferromagnetic sign alternation effect mentioned in sub-section (1.1) of this chapter is evident.

The accuracy of the results was checked from the finite N relation

$$\sum_{\ell=0}^{N-1} \omega_\ell^z(\gamma) = 0 \qquad (6.1.22)$$

For fixed ℓ the convergence for the case of N even is not regular: for $\gamma < 0.3$ it is monotone increasing and for $\gamma > 0.8$ monotone decreasing, the curves for different N crossing in the intermediate region. This behaviour is illustrated in Fig. (6.1), which shows the short-range

Table (6.1)

Antiferromagnetic Ground State Correlation Functions $\omega_\ell(N,\gamma)$

N	ℓ	γ = 0	γ = 0.1	γ = 0.2	γ = 0.3	γ = 0.4	γ = 0.5
10	1	-1.00000	-0.99001	-0.95954	-0.90791	-0.84189	-0.77658
	2	1.00000	0.98005	0.91949	0.81790	0.68996	0.56583
	3	-1.00000	-0.97998	-0.91826	-0.81203	-0.67581	-0.54351
	4	1.00000	0.97988	0.91664	0.80441	0.65685	0.51181
	5	-1.00000	-0.97989	-0.91668	-0.80475	-0.65823	-0.51510
8	1	-1.00000	-0.98972	-0.95673	-0.90139	-0.83547	-0.77381
	2	1.00000	0.97948	0.91389	0.80498	0.67703	0.55947
	3	-1.00000	-0.97936	-0.91228	-0.79910	-0.66548	-0.54364
	4	1.00000	0.97921	0.91023	0.79102	0.64783	0.51598
6	1	-1.00000	-0.98821	-0.94954	-0.89102	-0.82871	-0.77359
	2	1.00000	0.97645	0.89954	0.78410	0.66252	0.55640
	3	-1.00000	-0.97648	-0.90001	-0.78616	-0.66762	-0.56561
4	1	-1.00000	-0.98113	-0.93519	-0.88125	-0.83113	-0.78868
	2	1.00000	0.96225	0.87039	0.76249	0.66227	0.57735

N	ℓ	γ = 0.6	γ = 0.7	γ = 0.8	γ = 0.9	γ = 1.0
10	1	-0.72216	-0.67994	-0.64751	-0.62221	-0.60206
	2	0.46480	0.38839	0.33124	0.28782	0.25407
	3	-0.43751	-0.35953	-0.30320	-0.26199	-0.23117
	4	0.39546	0.31041	0.24956	0.20558	0.17307
	5	-0.40118	-0.31865	-0.26020	-0.21839	-0.18781
8	1	-0.72319	-0.68355	-0.65263	-0.62819	-0.60852
	2	0.46491	0.39250	0.33730	0.29464	0.26104
	3	-0.44740	-0.37551	-0.32338	-0.28238	-0.25194
	4	0.41136	0.33311	0.27520	0.23186	0.19893
6	1	-0.72865	-0.69291	-0.66446	-0.64155	-0.62284
	2	0.47114	0.40440	0.35212	0.31068	0.27735
	3	-0.49498	-0.42298	-0.37532	-0.33826	-0.30902
4	1	-0.75384	-0.72542	-0.70211	-0.68282	-0.66667
	2	0.50767	0.45084	0.40423	0.36564	0.33333

Table (6.2)

Table of Limiting Correlations $\omega_\ell(\gamma)$

γ \ accuracy (est.)	ω_1 exact	ω_2 extrap. (3%)	ω_3 extrap. (5%)	ω_4 extrap. (7%)	ω_∞ extrap.	error
1.0	-0.591	0.250	-0.192	0.150	0.000	± 0.01
0.9	-0.612	0.278	-0.221	0.180	0.036	± 0.01
0.8	-0.641	0.327	-0.267	0.225	0.112	± 0.01
0.7	-0.682	0.394	-0.336	0.297	0.227	+ 0.01 − 0.02
0.6	-0.735	0.478	-0.432	0.405	0.372	+ 0.01 − 0.02
0.5	-0.796	0.584	-0.556	0.545	0.537	+ 0.01 − 0.02
0.4	-0.859	0.710	-0.700	0.695	0.694	± 0.01
0.3	-0.916	0.831	-0.827	0.825	0.824	± 0.005
0.2	-0.961	0.921	-0.921	0.921	0.921	± 0.001
0.1	-0.990	0.980	-0.980	0.980	0.980	± 0.0001
0	-1	+1	-1	+1	1	

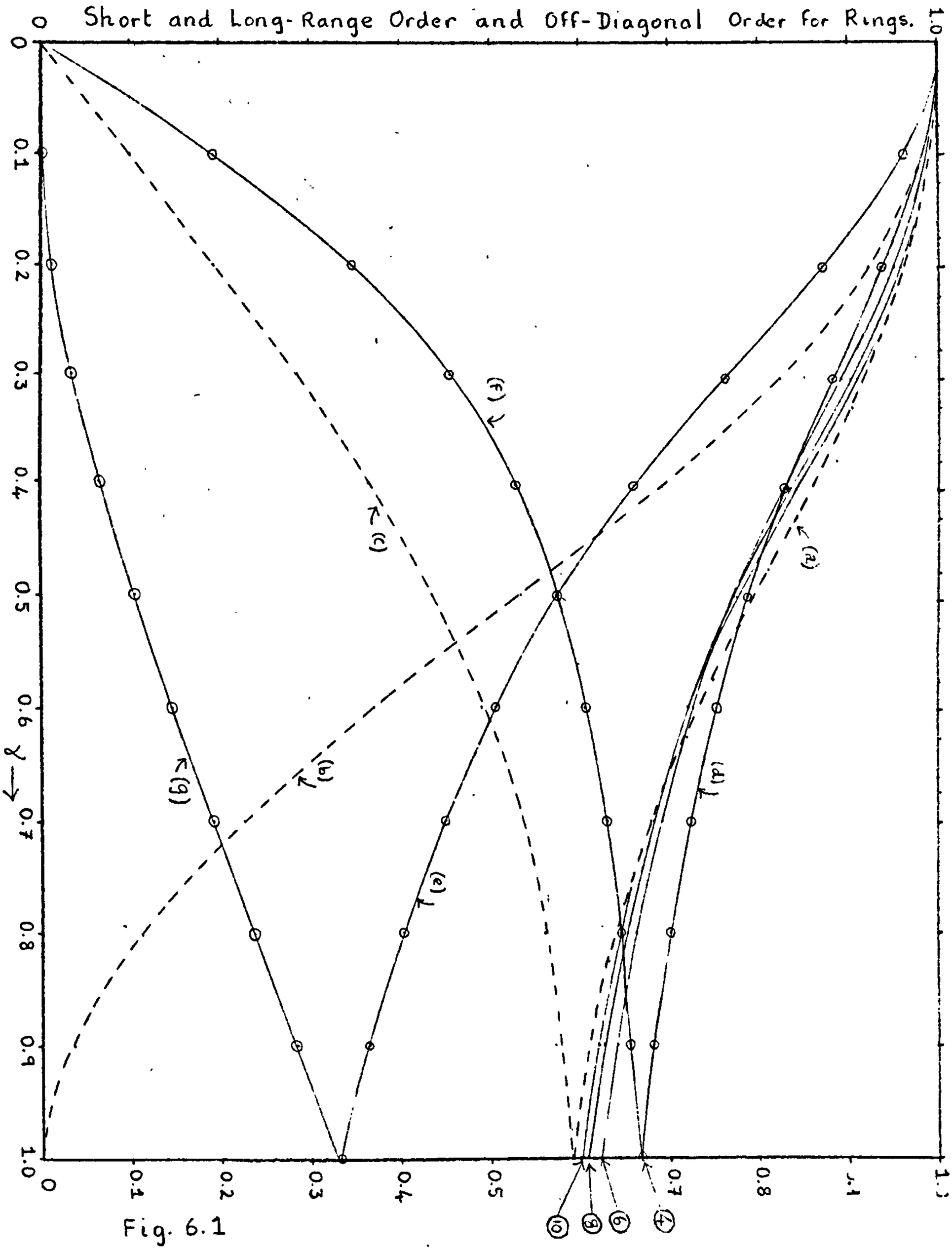
Short and Long-Range Order and Off-Diagonal Order for Rings.
ρ
0
0.1
0.2
0.3
0.4
0.5
0.6
0.7
0.8
0.9
1.0
(a)
(b)
(c)
(d)
(e)
(f)
(g)
(h)
(i)
(j)
(k)
(l)

Fig. 6.1

Fig. 6.1

short-range order for N = 4, 6, 8 and 10 and also the limiting curve (curve (a)), obtained numerically from the work of Orbach (1958). We observe, however, that the convergence is quite rapid for $\gamma < 0.3$ for $\ell = 1$, and, in fact, this is true for all ℓ. For $\gamma > 0.8$, the convergence is also rapid for $\ell \lesssim N/4$. In the case of N odd, the convergence for $\ell < N/2$ is monotone increasing for all γ, but rather slow. The convergence properties for $\ell < N/2$ are generally improved by considering sets of means of odd and even correlation functions. The set 10/9; 8/7; 6/5; for ω_1 and ω_2 are shown in Fig. (6.2). The complicated convergence of the even N curves has disappeared and the curves appear to converge smoothly and monotonically from below. The limiting result for ω_1 (dashed curve) is shown for comparison. The convergence remains quite rapid for $\gamma > 0.8$ but is rather slow near the Ising limit. However, the sets of means appear to extrapolate quite smoothly with 1/N, and the extrapolated points are shown as dark circles, for ω_1 in Fig. (6.2). Clearly the agreement is very good (to within 1%) and gives us encouragement to attempt to extrapolate the limiting curves for the cases $|\omega_2(\gamma)|$, $|\omega_3(\gamma)|$ and $|\omega_4(\gamma)|$. (See Fig. (6.3)). We see that there is a difference between the limiting short-range order and the other order parameters, all of which have almost the same values for $\gamma \lesssim 0.5$ and only for $\gamma > 0.5$ tend to deviate from the limiting curve for large ℓ labelled $\omega_\infty(\gamma)$. The curves for $|\omega_3(\gamma)|$ and $|\omega_4(\gamma)|$ cannot be expected to have the same accuracy as the other three curves, since there are fewer available points to extrapolate on account of the small size of the ring systems.

An appreciation of the decay of the correlations with distance (as well as of the convergence in N) can be gained from Fig. (6.4) which shows the finite ring correlations for $\gamma = 0.3$, 0.5 and 1.0. An alternating effect (to be distinguished from the antiferromagnetic sign alternation) is evident, the values of $|\omega_\ell|$ for even ℓ being lower relative to those for odd ℓ than might be expected. For $\ell > \frac{1}{2}N$, the correlations

Fig. 6.2

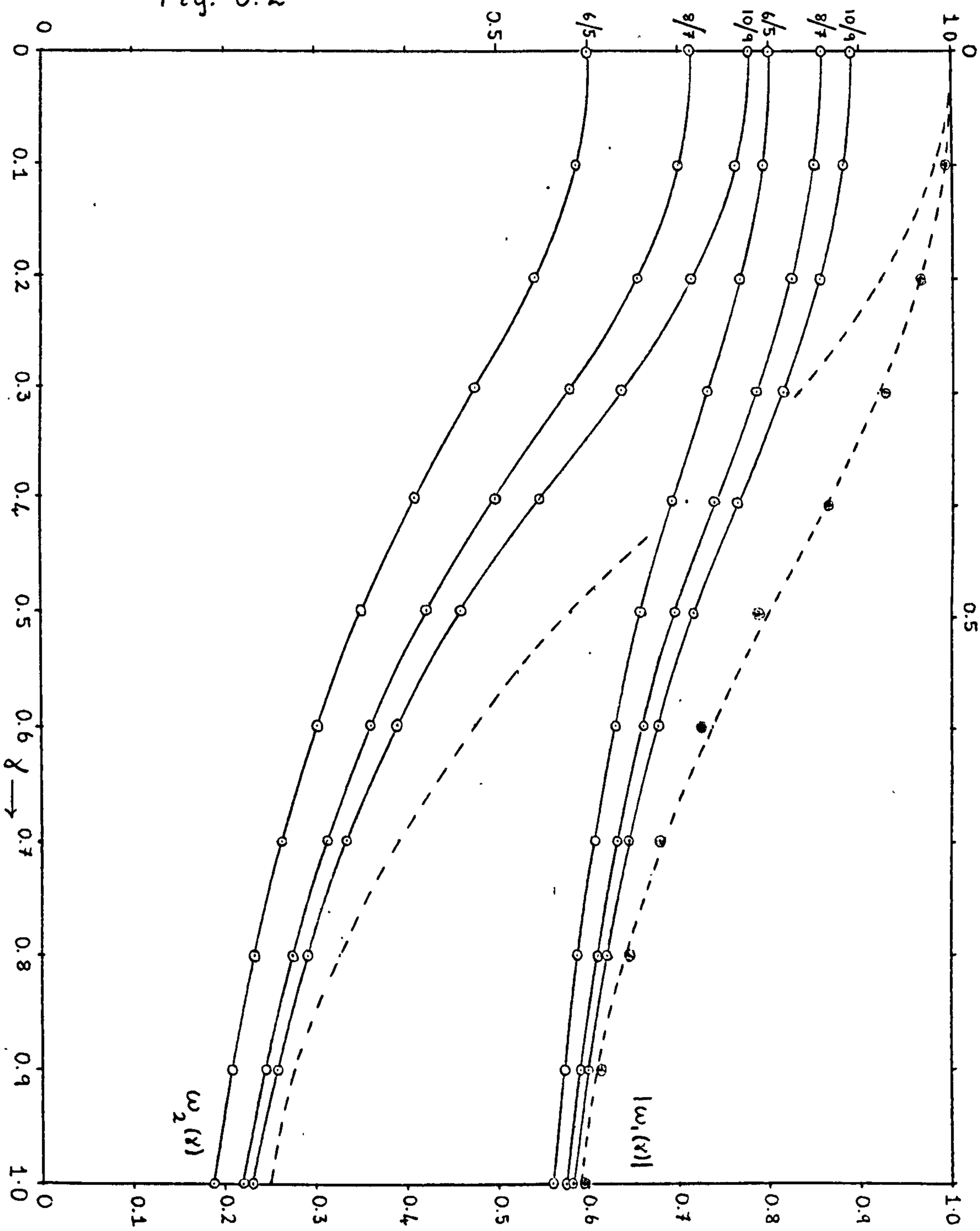

Pair Correlation Functions: Convergence of Even/Odd Means

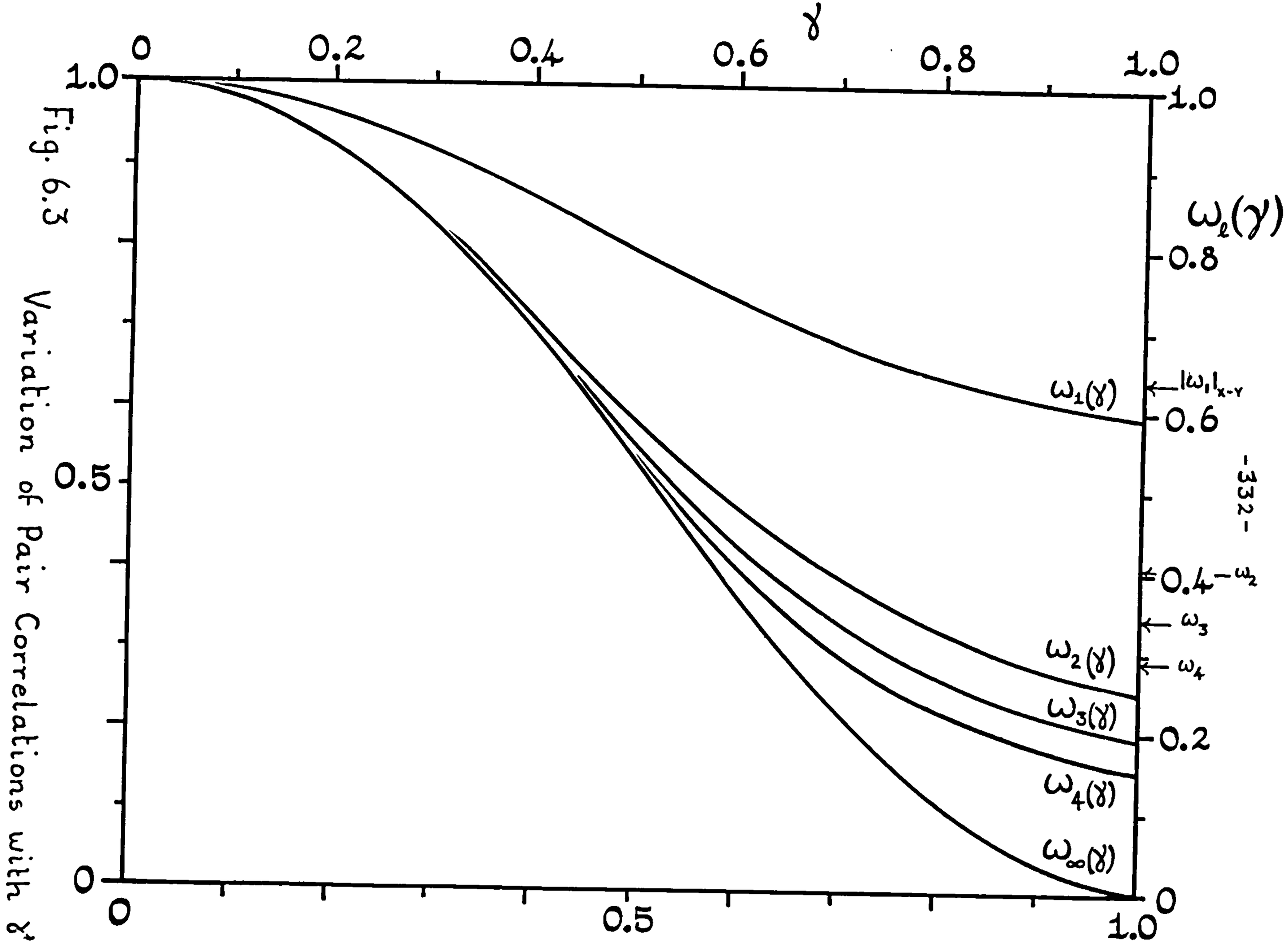

Fig. 6.3 Variation of Pair Correlations with γ

Fig. 6.4

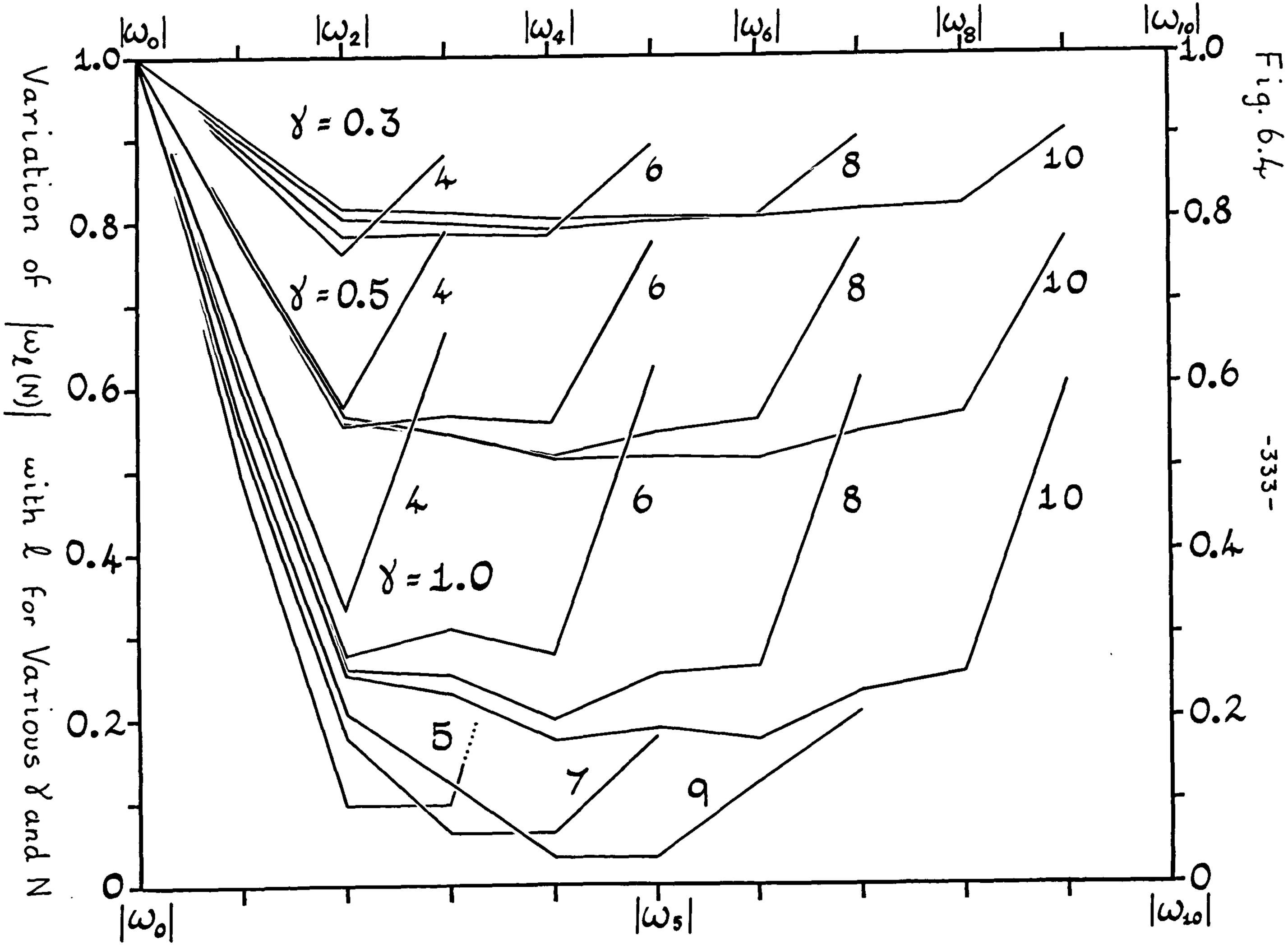
Variation of $|\omega_{l(N)}|$ with l for Various γ and N
$|\omega_0|$
$|\omega_2|$
$|\omega_4|$
$|\omega_6|$
$|\omega_8|$
$|\omega_{10}|$
$|\omega_5|$
1.0
0.8
0.6
0.4
0.2
0
$\gamma = 0.3$
$\gamma = 0.5$
$\gamma = 1.0$
4
6
8
10
5
7
9

of course, start increasing as the points 0 and ℓ approach one another around the closed ring. Nevertheless, it is clear for $\gamma = 0.3$, and reasonably so for $\gamma = 0.5$, that the correlations for $\ell < \frac{1}{2}N$ are decaying to a constant level of about 0.8 and 0.5, respectively. These values may be identified with the long-range order $\omega_\infty(\gamma)$ defined by

$$\omega_\infty(\gamma) = \lim_{\ell\to\infty} \left| \lim_{N\to\infty} \omega_\ell(N,\gamma) \right| . \qquad (6.1.23)$$

To estimate $\omega_\infty(\gamma)$ we have formed the minimum means for N even

$$\omega_{min}(\gamma,N) = \tfrac{1}{2}\left[\omega_{\frac{1}{2}N}(\gamma,N) - \omega_{\frac{1}{2}N-1}(\gamma,N)\right] \qquad (6.1.24)$$

and attempted to extrapolate to the limit $N = \infty$. These means are taken to reduce the alternation effects.

In this case we felt it was not advisable to use the results for odd N in forming the estimate because, with the above definition of long-range order, interference effects around the chain occur near the Ising limit. Note that for N odd and $\gamma = 0$,

$$\omega_\ell(N) = 1 - 2\ell/N, \quad 0 \le \ell < \tfrac{1}{2}N \qquad (6.1.25)$$

For this reason we do not expect the limiting result for ω_∞ to have accuracy comparable with our estimate for ω_1. (An estimate for ω_1 using results for even N only gives a result accurate to about 2.5%). Fig. (6.5) shows a plot of $\omega_{min}(N)$ versus 1/N. The points for $N > 4$ appear reasonably collinear, but care must be taken in extrapolation since curvature is to be expected for $\gamma < 0.7$. (A similar, though less marked, effect occurs in the case of the short-range order.) For $\gamma < 0.3$, the over-all range of variation is slight and an estimate can be made with some confidence: the limiting values here must, in fact, lie very close to the values for N = 10. For $\gamma > 0.7$ a linear extrapolation would seem to be reliable. For intermediate γ some attempt has been made to allow for curvature effects but we would not claim very high accuracy for our results in this range. We feel justified in concluding,

Fig. 6.5

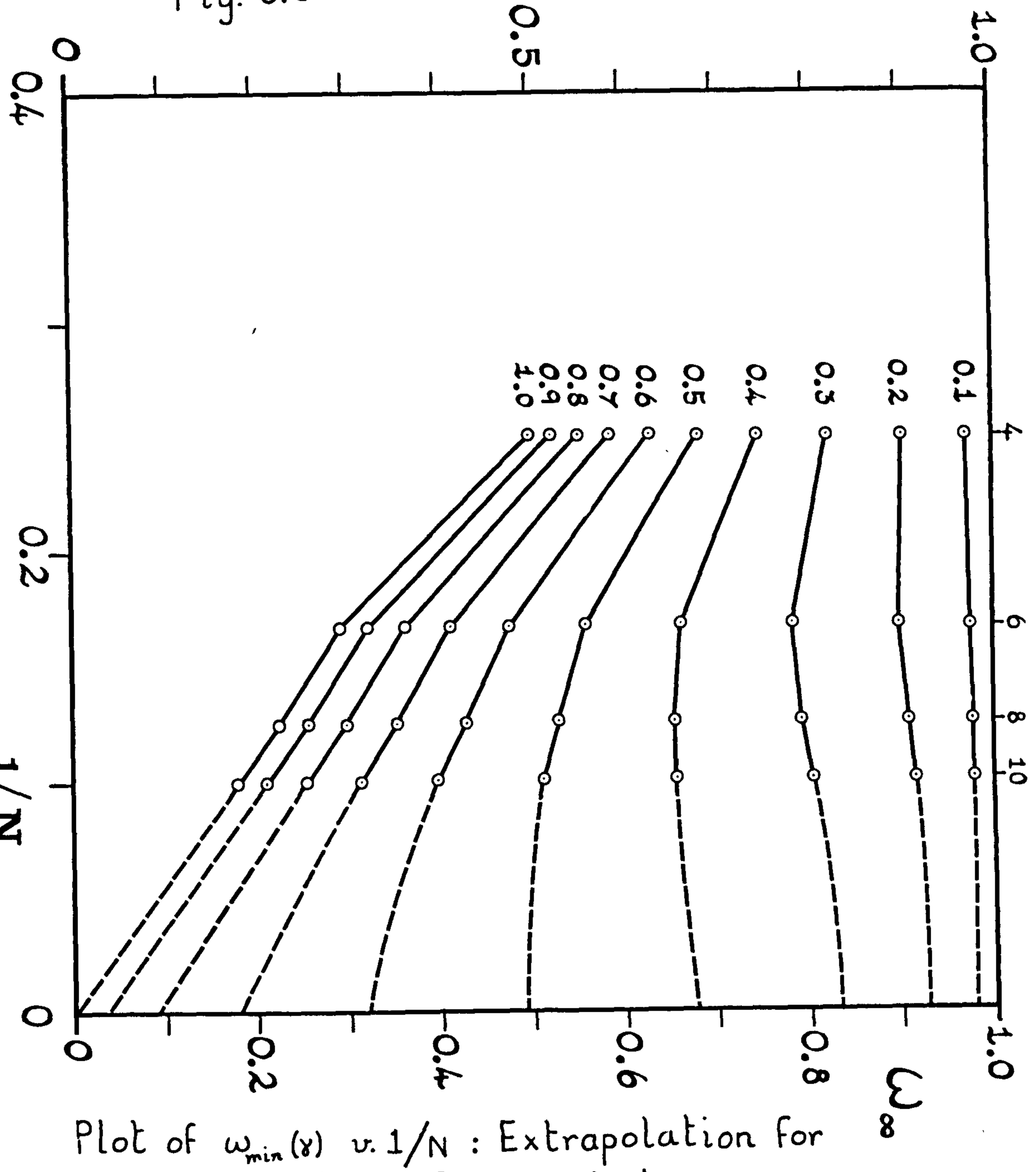

Plot of $\omega_{min}(\gamma)$ v. $1/N$: Extrapolation for Long-Range Order.

however, that the long-range order vanishes only at the Heisenberg limit, $\gamma = 1$. It is well-known that the condition for the presence of long-range order in a system is that the dominant eigenvalue of the corresponding matrix should be degenerate. The long-range order is determined by the largest eigenvectors. In the case of the infinite Ising chain we know that the antiferromagnetic ground state is two-fold degenerate, and we expect long-range order to occur at $T = 0$. In Chapter III, sub-section (3.1) we have discussed our reasons for expecting that in the limit $N = \infty$ the antiferromagnetic ground state remains two-fold degenerate for $\gamma < 1.0$. Hence again we expect long-range order at $T = 0$. In the Heisenberg limit, although the energy gap to the first excited state vanishes as $1/N$, we have decided that the antiferromagnetic ground state should still be regarded as non-degenerate. Hence the vanishing of the long-range order in the Heisenberg limit is quite plausible.

2. COMPARISON WITH OTHER MODELS AND APPROXIMATIONS

2.1 Short Range Order Comparisons

In Fig. (6.6) we make a comparison of curve (a), the exact value of $\omega_1(\gamma)$ (Orbach, 1958) with (b) our present extrapolations. Also shown are curve (c) Walker's perturbation series to γ^{14}, curve (d) Walker's perturbation series truncated to γ^6 (Walker, 1959) and (e) Davis's perturbation series (Davis, 1960). Walker's perturbation series is given by

$$\omega_1 = 1 - \gamma^2 + \tfrac{3}{4}\gamma^4 - (7/2^6)\gamma^8 - (9/2^7)\gamma^{10} - (11/2^9)\gamma^{12} + (13/2^{11})\gamma^{14} + \cdots \quad (6.2.1)$$

To obtain this series, Walker solved the integral equation of (Orbach, 1958) analytically to obtain the antiferromagnetic ground state energy as a function of γ (See Chapter III, sub-section (1.2)). He expanded this solution in powers of γ and obtained the short-range order from the relation (6.1.21). The form of the expansion was that of a perturbation series in γ about the Ising limit, with the transverse terms of

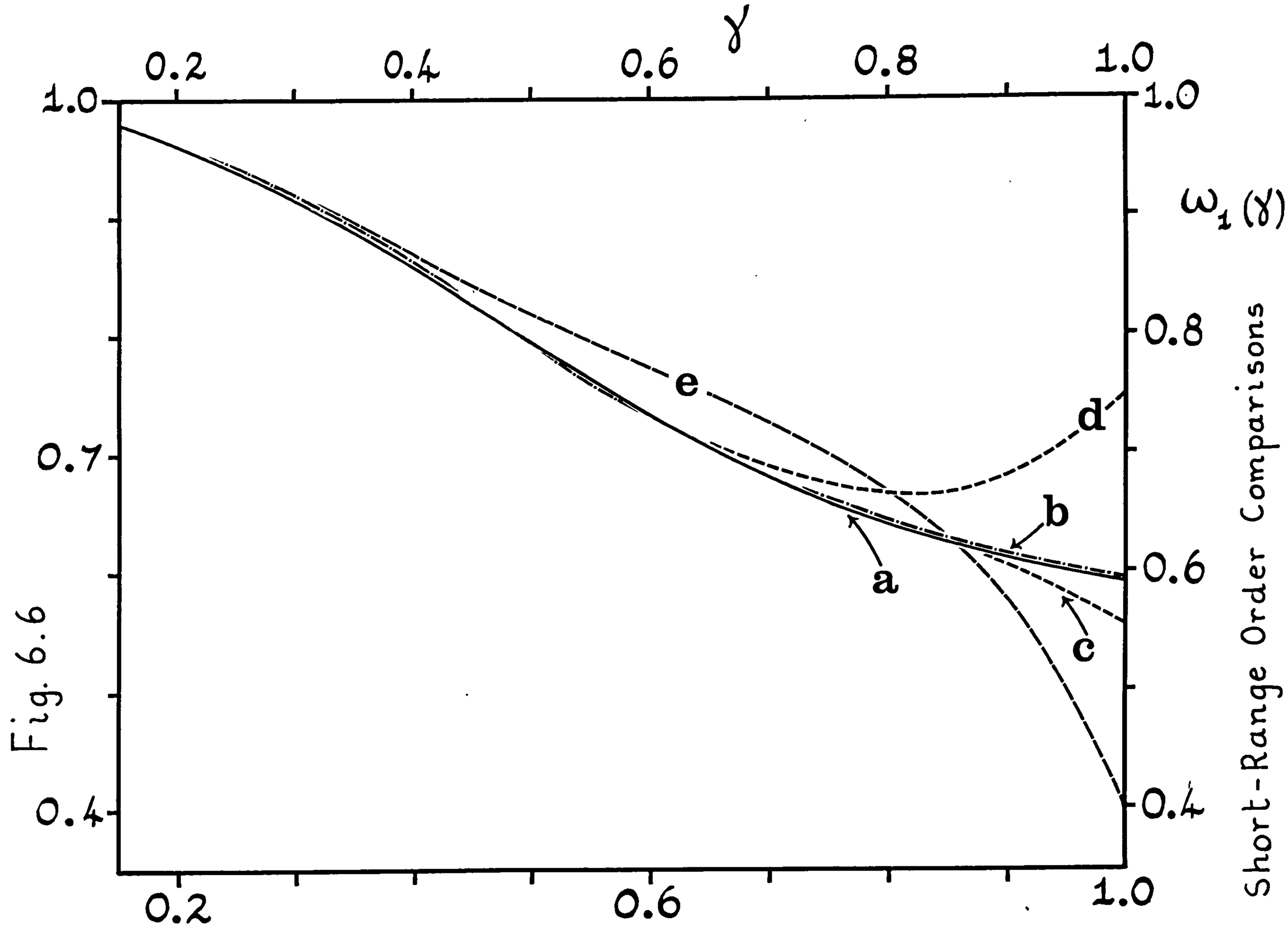
γ
0.2
0.4
0.6
0.8
1.0
1.0
0.8
0.6
0.4
0.7
$\omega_1(\gamma)$
Short-Range Order Comparisons
a
b
c
d
e

Fig. 6.6

the Hamiltonian as the perturbation. If the series up to γ^{14} is considered (curve (c)), the error is detectable only for $\gamma > 0.85$ and reaches a maximum of only 6% at $\gamma = 1$. The truncated series (curve (d)) corresponds in number of terms to an analogous perturbation series obtained by Walker for the long-range order. We see that for the shorter series, deviations from the limiting curve are significant for $\gamma \geq 0.7$. An alternative perturbation procedure was presented by Davis (1960) in which an expansion for the ground-state energy of an antiferromagnetic spin system was obtained in terms of a linked-spin-cluster expansion for an interacting bose-type system. The results (curve (e)) which are based on the series expansion

$$\omega_1 = 1 - \gamma^2 + 1.3770\gamma^4 - 0.9765\gamma^6 \cdots \qquad (6.2.2)$$

c.f. the Walker series

$$\omega_1 = 1 - \gamma^2 + 0.75\gamma^4 - O(\gamma^8) \qquad (6.2.3)$$

2.2 Long-Range Order Comparisons

To compare our estimate of the long-range order with other approximations, we must recognize that most authors have used as an order parameter the so-called "sub-lattice magnetisation" (Walker, 1959; Kastelijn, 1952; Davis, 1960; and Marshall, 1955)

$$\sigma = 4/N \left\langle \sum_{i\,\mathrm{even}} S_i^z \right\rangle = 2\langle S_o^z \rangle \qquad (6.2.4)$$

where angular brackets denote the canonical average. If this formula is interpreted literally, it is easily shown (on the grounds of spin-inversion symmetry) that σ always vanishes identically. This has given rise to considerable confusion in the literature (Pratt, Jr., 1961; and Karayianis, Morrison and Wortman, 1962). The situation really parallels that in the ferromagnetic case, which is quite well understood (Newell and Montroll, 1953). If the (reduced) spontaneous magnetisation of a ferromagnet is defined simply by $M_o = (2/N)\left\langle \sum_i S_i^z \right\rangle$, it also vanishes identically. The correct definition is made with the aid of

a non-zero magnetic field, namely

$$M_o(T) = \lim_{H \to 0+} \lim_{N \to \infty} (1/N)\, M_N(T,H) \qquad (6.2.5)$$

where

$$M_N(T,H) = 2\sum_{i=1}^{N} \langle S_i^z \rangle_N = 2N \langle S_o^z \rangle_N \qquad (6.2.6)$$

For an <u>antiferromagnet</u> one must introduce a staggered magnetic field H* by adding to the Hamiltonian a term

$$\mathcal{H}^* = H^* \sum_{i=0}^{N-1} (-1)^i S_i^z \qquad (6.2.7)$$

With the aid of the corresponding "staggered magnetisation", the sublattice magnetisation may be defined properly by

$$\begin{aligned} \sigma &= \lim_{H^* \to 0+} \lim_{N \to \infty} (1/N)\, M_N^*(H^*) \\ &= \lim_{H^* \to 0+} \left[\langle S_o^2 \rangle^* - \langle S_1^z \rangle_\infty^* \right] \end{aligned} \qquad (6.2.8)$$

An important relation exists between the spontaneous magnetisation (or the sublattice magnetisation) and the long-range order. We have

$$\begin{aligned} M_o^2(T) &= \lim_{N \to \infty} 4(1/N)^2 \left\langle \left(\sum_{i=1}^{N} S_i^z \right)^2 \right\rangle \\ &= \lim_{N \to \infty} 4(1/N)^2 \sum_{i,j=1}^{N} \langle S_i^z S_j^z \rangle \\ &= \lim_{\ell \to \infty} \lim_{N \to \infty} 4 \langle S_o^z S_\ell^z \rangle = \omega_\infty \end{aligned} \qquad (6.2.9)$$

Hence the long-range order is just equal to the square of the spontaneous magnetisation. In a similar way one concludes for antiferromagnets that the long-range order parameter is related to the sublattice magnetisation, σ , by

$$\omega_\infty = \sigma^2 \qquad (6.2.10)$$

The two order parameters are thus equivalent. The long-range order may be computed directly from its correlation function definition or, as is sometimes easier, from σ or M_o .

Let us compare our numerical results with other treatments which discuss the long-range order as a function of anisotropy. In Fig. (6.7) we display our extrapolation estimate of $\omega_\infty(\gamma)$ (curve (a)) with Walker's exact perturbation expansion (curve (b)) (Walker, 1959), with Kasteleijn's

variational formula (curve (c) (Kasteleijn, 1952), with Davis's perturbation formula (curve (d)) (Davis, 1960). It may also be noted that (Nagle, 1968) (private communication) has derived an extra term in Walker's series; Padé approximants to the series have been formed with results much like curve(b). Also shown in Fig. (6.7) are the values $\omega_{min}(10)$, (curve (e)). The Walker expansion for the sublattice magnetisation is

$$\sigma(\gamma) = 1 - \gamma^2 - \tfrac{1}{4}\gamma^4 - \tfrac{1}{16}\gamma^6 + \cdots$$

$$= 1 - \gamma^2 - 0.25\gamma^4 - 0.0625\gamma^6 + \cdots \quad (6.2.11)$$

(The series of Nagle is $\sigma(\gamma) = 1 - \gamma^2 - \frac{1}{4}\gamma^4 - \frac{1}{16}\gamma^6 + \frac{1}{64}\gamma^8 \cdots$ (6.2.12)

The series due to Davis is

$$\sigma(\gamma) = 1 - \gamma^2 + 1.1260\gamma^4 - 0.6445\gamma^6 \cdots \quad (6.2.13)$$

The squares of these two series are plotted on Fig. (6.7).

Up to $\gamma = 0.3$, all approximation (except that of Kasteleijn) agree well with the exact series but at this point Davis's approximation (d) starts deviating seriously, and predicts a relatively large non-zero value for $\omega_\infty(1)$. Kasteleijn's approximation (c) falls away sharply to zero at $\gamma_c = 0.483$, which is surely incorrect. Kasteleijn's formula also predicts a value for the coefficient of γ^2 which is half that of Walker and Davis. Our estimated curve falls some 10% below the series value in the region $\gamma = 0.45$ to 0.65, although the trend is still very similar. In this region the series is probably still converging rapidly, as suggested both by the numerical magnitude of the terms, and by the agreement of the exact short-range order with the corresponding series up to γ^6 (see Fig. (6.6)). Above $\gamma = 0.7$ we must expect the Walker series to deviate from the true value and indeed the series for $\omega(\gamma)$ (rather than for $[\sigma(\gamma)]^2$) then yields lower values, and has its zero at $\gamma = 0.817$ rather than at $\gamma = 0.897$. Our extrapolated $\omega_\infty(\gamma)$, on the other hand, does not vanish until $\gamma = 1.0$. On this evidence it seems fair to conclude that the exact series expansion provides the best approximation up to $\gamma = 0.75$ and that the true long-range

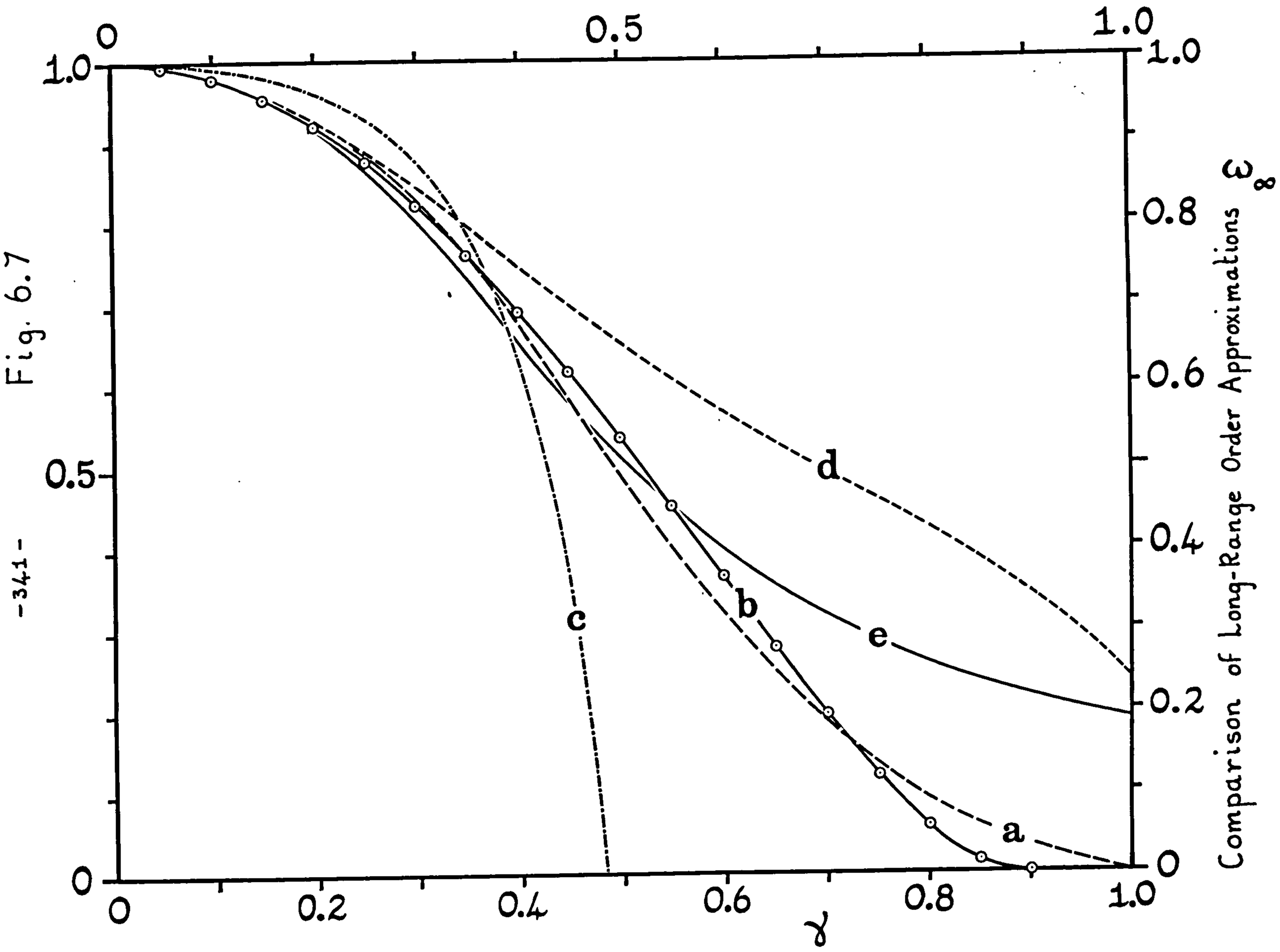
0
0.5
1.0
1.0
0.5
0
0
0.2
0.4
0.6
0.8
1.0
γ
a
b
c
d
e
Comparison of Long-Range Order Approximations ω_∞

Fig. 6.7

order is unlikely to vanish for $\gamma < 0.85$ and probably vanishes at $\gamma = 1.0$, In Fig. (6.3), therefore, we have plotted together with $\omega_1(\gamma)$ (exact) and our results for $|\omega_2|, |\omega_3|$ and $|\omega_4|$, what we think is the best estimate so far for $\omega_\infty(\gamma)$. This curve follows the series expansion up to $\gamma = 0.6$, and thereafter has the same form as our extrapolation curve (a) in Fig. (6.7), approaching the latter from above, and in close agreement for $\gamma > 0.8$.

Recently an attempt has been made (Edelstein, 1966) to describe the general ordering of antiferromagnetic anisotropic and Heisenberg linear chains in terms of some assumptions concerning the infinite N, finite temperature pair correlation functions. This approach involves the zero-temperature long-range order parameter $\omega_\infty(\gamma)$ in a fundamental way and was apparently inspired (Edelstein, 1965, private communication) by a study of our extrapolation results for $|\omega_\ell(\gamma)|$ where $\ell = 1$, 2, 3, 4 and ∞. Edelstein suggests that the following ordering relation should hold in the limit:

$$S_1 < S_3 \cdots < 0 < \cdots S_4 < S_2$$

where $$S_n = 1 - (-1)^n \omega_\infty(\gamma) + 2\sum_{\ell=1}^{n} \omega_\ell \quad . \qquad (6.2.14)$$

Plots of the behaviour of the $S_n(\gamma)$ using our estimated results show fairly smooth curves bracketing the result zero. This gives us some confidence in the general consistency and plausibility of our extrapolations. Table (6.2) contains our limiting values for $|\omega_\ell(\gamma)|$ for values of γ between 0 and 1.0, together with estimates of the probable error in compiling these values.

2.3 Survey of Approximate Results for $\gamma = 1$

p.353

In Table (6.3)A which is based on Tables due to Katsura and Inawashiro (1964) and Ruijgrok and Rodriguez (1960), we have assembled a list of the important approximate methods which have been used over the past thirty or so years to treat the antiferromagnetic ground state. For

each approach we list the ground-state energy, and also the short-range order and long-range order, where these quantities are available. An examination of the Table reveals the fact that an approximate wave function which gives a value for the ground-state energy in good agreement with the Bethe-Hulthén exact result does not necessarily give a good prediction for the short-range and particularly for the long-range order. We come to the conclusion that 'one-shot' approximations are not reliable when it comes to predicting a quantity which depends very sensitively on the structure of the ground-state eigenfunction, such as the long-range order.

2.4) X-Y Model Correlations

The X-Y model has the Hamiltonian

$$\mathcal{H} = 2|J| \sum_{i=1}^{N} \left(S_i^x S_{i+1}^x + S_i^y S_{i+1}^y \right) . \qquad (6.2.15)$$

The short-range order was found exactly by Katsura (1962) and Lieb, Schultz and Mattis (1961) to be

$$\omega_1^z = 4/N \sum_{i=1}^{N} \langle S_i^z S_{i+1}^z \rangle = -4/\pi^2 = -0.4053. \qquad (6.2.16)$$

In addition, Lieb, Schultz and Mattis investigated the x and y order parameters and obtained the exact result

$$\omega_1^x = 4/N \sum_{i=1}^{N} \langle S_i^x S_{i+1}^x \rangle = \omega_1^y = -2/\pi = -0.6366. \qquad (6.2.17)$$

By taking expectation values we have

$$\frac{E_o}{|J|} = 2N \langle S_o^x S_1^x + S_o^y S_1^y \rangle = 4N \langle S_o^x S_1^x \rangle = \omega_1^x$$

Hence,

$$E_o/|J| = -2/\pi = \omega_1^x = \omega_1^y . \qquad (6.2.18)$$

Lieb, Schultz and Mattis also investigated the intermediate range order and the results are shown in Table (6.4). Lieb, Schultz and Mattis were able to prove that for the X-Y model, $\lim_{\ell \to \infty} \omega_\ell^z = \omega_\infty^z = \omega_\infty^x = \omega_\infty^y = 0$ i.e. that the long-range order in any direction is zero. The values of $|\omega_\ell^x|$ in Table (6.4) are seen to decay monotonically and rather slowly, eventually to zero. The values for $|\omega_\ell^x|$, $\ell = 1, 2, 3,$ and 4 are

Table (6.4)

ℓ	1	2	3	4	5	6
$\frac{1}{4}\omega_\ell$	-0.1592	0.1013	-0.0860	0.0730	-0.0661	0.0597

shown on Fig. (6.3) by the labelled arrows for comparison with our extrapolated values for $|\omega_\ell^z|$ (or $|\omega_\ell^x|$) for the Heisenberg model. It is seen that in every case, the X-Y value for the magnitude of a particular correlation function is larger than its Heisenberg counterpart by an amount lying well outside the estimated errors on the extrapola tions. This is persuasive evidence for believing that if the X-Y order parameters converge to zero as $\ell \to \infty$, then so do the Heisenberg order parameters. Further, Lieb, Schultz and Mattis have considered a modified X-Y model with unequal contributions of x and y terms. In the limit of maximum anisotropy, this model becomes the Ising model and the modified X-Y model is then seen to be the two-dimensional analogue of our anisotropic Hamiltonian. Lieb, Schultz and Mattis have been able to show that the long-range order is no longer zero for non-zero anisotropy, (eventually rising to the Ising value).

2.5 Order Parameters for Chains

We shall here investigate the effect of the loss of periodic boundary conditions. First of all, this implies that the expectation value of the correlation parameter $\underline{S}_i \cdot \underline{S}_{i+\ell}$ depends on the position in the system of the site i. In particular, this result will apply to free-ended chains, for finite systems. (In the limit $N \to \infty$, of course, we expect the values of the same correlation parameter at all sites along the chain to become equivalent.) However, if we consider correlations between all the other spins on the chain and a spin at one end, it would seem that we would obtain more ℓ values, i.e. more distinct correlations for a given number of spins than if we considered a ring of spins. Let us investigate this point further using the examples of the 4-spin

and 6-spin free-ended chains. For the 4-spin chain we have the following available ground-state expectation values, say

$$\omega_1: \quad 4\langle S_1^z S_2^z\rangle ; \; 4\langle S_2^z S_3^z\rangle ; \; 4\langle S_3^z S_4^z\rangle$$
$$\omega_2: \quad 4\langle S_1^z S_3^z\rangle ; \; 4\langle S_2^z S_4^z\rangle$$
$$\omega_3: \quad 4\langle S_1^z S_4^z\rangle . \qquad (6.2.19)$$

By symmetry it is clear that $\langle S_3^z S_4^z\rangle = \langle S_1^z S_2^z\rangle$ and $\langle S_2^z S_4^z\rangle = \langle S_1^z S_3^z\rangle$.

The ground state eigenvalue for this system is $E_0 = -1 - \sqrt{3} = -4.732$

and the ground-state eigenvector is

$$|1100\rangle + (1+\sqrt{3})|0110\rangle + |0011\rangle + (1+\sqrt{3})|1001\rangle - (2+\sqrt{3})|1010\rangle - (2+\sqrt{3})|0101\rangle \qquad (6.2.20)$$

Hence

$$4\langle S_1^z S_2^z\rangle = -\tfrac{1}{3}(1+\sqrt{3}) = -0.911$$
$$4\langle S_2^z S_3^z\rangle = -1/3 = -0.333$$
$$4\langle S_1^z S_3^z\rangle = 1/3(\sqrt{3}-1) = 0.244$$
$$4\langle S_1^z S_4^z\rangle = -1/3 = -0.333 \qquad (6.2.21)$$

We see that for the short-range order we have two distinct contributions, -0.911 and -0.333. It seems reasonable to choose the average value

$$\omega_1 = \frac{4}{3}\sum_{i=1}^{3}\langle S_i^z S_{i+1}^z\rangle = \frac{1}{3}(2\times -0.911 - 0.333) = -0.718. \qquad (6.2.22)$$

and hence we have for N = 4 (chain) the values

$$\omega_1 = -0.718 \; ; \; \omega_2 = 0.244 \text{ and } \omega_3(\omega_\infty) = -0.333.$$

Lieb, Schultz and Mattis have performed exact calculations for the 6-spin chain, and from their results we present the following Table (6.5) .

ℓ	1	2	3	4	5 (∞)
ω_ℓ Heis. (6-spin)	-0.664	0.256	-0.308	0.128	-0.188
ω_ℓ x-y (6-spin)	-0.698	0.424	-0.420	0.260	-0.300
ω_ℓ Heis (Extrap. Lim)	-0.591	0.250	-0.192	0.150	-
ω_ℓ x-y (Limit)	-0.637	0.405	-0.344	0.292	-0.264

Table (6.5)

Table (6.5) contains values of ω_1 to ω_5 (inclusive) for the 6-spin Heisenberg chain and also, for comparison, corresponding estimates for the 6-spin X-Y chain. We also include in Table (6.5) our extrapolated limiting values for the Heisenberg model, and the exact limiting values for the X-Y model (taken from Tables (6.2) and (6.4) for ease of comparison).

From a careful study of this table we may draw some interesting, albeit somewhat tentative conclusions. First of all we observe that the short-range order for the Heisenberg model appears to be converging rather slowly from above to the limiting value $\omega_1(\infty) = -0.591$. For this case the chain values for N = 4 and N = 6 are, respectively, about 8% and 6-1/2% above the corresponding values for rings (see Table (6.1)). The long-range order, on the other hand, converges much faster than in the case of rings, the value for the 6-chain being 40% lower than the corresponding value for the 6-ring. In fact we see from Table (6.5) and Table (6.1) that the long-range order for the 6-chain, $\omega_5 = -0.188$ is actually equal to the long-range order for a ring of 10 spins, $\omega_5\,(\omega_\infty) = -0.188$. In general, therefore, we can say roughly, that as far as the long-range order is concerned, a chain of N spins is equivalent to a ring of about 2N spins (more exactly (2N-2) spins).

It is unfortunate that lack of time has prevented the calculation of the ground state eigenvector for a chain of 8 spins, in addition to the eigenvalues. However the author understands (Richards, 1967, private communication) that such work is now in progress as part of a more general investigation of time-dependent correlation functions.

For ω_2, we see that the value given by N = 4, $\omega_2 = 0.244$ is actually slightly lower than our limiting extrapolation estimate of 0.250 (though within our quoted errors - see Table (6.2)) and also lower than the value of $\omega_4 = 0.256$ for N = 6. In the corresponding entry in Table (6.5) for the X-Y 6-spin and infinite chains we see that the 6-spin value

is both an upper bound on, and very close to the limiting value for ω_2. If, in Table (6.5), we observe the order parameter (in this case ω_4) which occurs immediately prior to the long-range order, we see that the X-Y 6-spin value lies <u>below</u> the limiting value for this special case. This case corresponds to ω_2 for N = 4, and we therefore tentatively conclude that ω_2 (6) = 0.256 and ω_2(4) = 0.244 are upper and <u>lower</u> bounds, respectively, for the Heisenberg $\omega_2(\infty)$. This result, if correct, is in excellent agreement with our ring extrapolations. Further investigations on chains of 6 and 8 (or more) spins are really needed to verify this point. Again we observe that the value of ω_2 for the 6-spin chain agrees with the corresponding value for the 10-spin ring.

It seems that the chains, which appear to display a much more marked alternation effect of the $|\omega_\ell|$ than do rings, do not give a very good value for ω_3. The result for the 6-chain is 50% (in magnitude) above our extrapolation estimate. The value of ω_3 for chains in general could, however, probably be improved by taking other contributions along the chain (instead of just $\langle S_1^z S_4^z \rangle$) into account. This value of ω_3 for the 6-chain, in fact, is equal to the value for ω_3 for the 6-ring. We observe again that the 6-chain value for ω_4 is likely to lie below the limiting value, as does the corresponding value for the X-Y model. This is consistent with our higher limiting extrapolation value of 0.150.

2.6 Off-Diagonal Order

The off-diagonal order, particularly the off-diagonal long-range order, is a parameter of interest in connection with the quantum lattice gas model of a superfluid. The quantum lattice gas analogy with an anisotropic antiferromagnet has been reviewed in sub-section (1.2) of Chapter I.

In Fig. (6.1) we show the O.D. S.R.O. ω_1^{x+y} for a ring of four spins as a function of anisotropy (curve (f)) which may be compared with the S.R.O. (curve (d)) for N = 4. We also show (dashed curves (c)

and (a)) the corresponding curves for $N = \infty$. For the case of the L.R.O. ω_∞^z we show the finite N LRO curve for N = 4 (curve (e)) together with the O.D. L.R.O ω_∞^{x+y} for N = 4, (curve (g)). The corresponding L.R.O. curve for $N = \infty$ is shown dashed. The O.D. L.R.O. ω_∞^{x+y} curve for N = 4 rises from zero at the Ising limit very slowly as γ increases. Since the limiting O.D. L.R.O. must be zero at the Heisenberg limit as well as at the Ising limit, it is plausible from Fig. (6.1) that the O.D. L.R.O. is zero for all γ in the limit.

2.7 Higher Spin and Higher Dimensions

The excellent convergence of Walker's perturbation series in γ suggests that this approach should be developed farther for two- and three-dimensional lattices. Unpublished calculations to this effect have been supplied by Walker (Walker, 1964, private communication). The results are in the form of series in powers of γ^2 as far as γ^6 for the ground-state antiferromagnetic energy, E_o, and sublattice magnetisation σ. The series are

$$\frac{E_o}{|J| N q S^2} = -1 - \varepsilon_2 \gamma^2 - \varepsilon_4 \gamma^4 - \varepsilon_6 \gamma^6 \cdots \quad (6.2.23)$$

and

$$\frac{\sigma}{q \beta S} = 1 - \delta_2 \gamma^2 - \delta_4 \gamma^4 - \delta_6 \gamma^6 \cdots \quad (6.2.24)$$

where q is the coordination number of the lattice. The coefficients ε_i and δ_i are displayed in the following Table (6.6) for the linear chain (L.C), simple quadratic (S.Q), simple cubic (S.C) and body-centered cubic (B.C.C.) lattices for three spin values, S = 1/2, 3/2 and 5/2. We have compared the work of Walker with series of Boon (1961) for the ground-state energy only, and series of Davis (1960) for the ground-state energy and sublattice magnetisation. All methods agree on ε_2, the coefficient of γ^2 in the series for E_o. From Boon's work we obtain the general result

$$\varepsilon_2 = \frac{1}{(2Sq-1)} \quad (6.2.25)$$

Table (6.6)

Lattice	q	S	ε_2	ε_4	ε_6	δ_2	δ_4	δ_6
L.C.	2	1/2	1.0	-0.250	0	1.0	0.25	0.0625
		3/2	0.2	0.03	0.0104	0.12	0.06867	0.0224
		5/2	0.111$\dot{1}$	0.0185	0.007119	0.0617	0.03442	0.0169
S.Q.	4	1/2	0.333$\dot{3}$	-0.00185	.000941	0.222$\dot{2}$	0.03555	-0.007
		3/2	0.090$\dot{9}$	.00988	.002808	0.0496	0.01812	0.0084
		5/2	0.05263	.006456	.001978	0.0277	0.0108	0.0054
S.C.	6	1/2	0.2	-0.000$\dot{6}$	.001429	0.12	0.008	.00264
		3/2	0.05882	.004527	.001091	0.0311	.00786	0.00308
		5/2	0.03448	.003055	.000773	0.0178	0.00496	0.00215
B.C.C.	8	1/2	0.14286	.004878	.001243	0.08163	0.01286	0.00269
		3/2	0.04348	.003732	.000931	0.02268	0.0062	0.0025
		5/2	0.02564	.002412	.000626	0.01315	0.00383	0.00164

where S is the spin, and q is the coordination number of the lattice. Boon's work is only carried as far as ε_4 and a general expression of very complicated form is quoted. This coefficient is to be regarded as suspect, since values quoted by Boon for the numbers of spin clusters of the types [•—•], [•—•—•], [square] and [•—•—•—•] for the various lattices, required in the calculation of ε_2, appear to be incorrect. Further, even when these errors are corrected, Boon's prediction for ε_4 for the spin-1/2 linear chain, which is known exactly from the work of Walker (1959) is wrong (too large). Hence Boon's

conclusion that his method gives lower values for E_o than other current methods is likely to be invalid.

The comparison with Davis's results is interesting. Davis calculates the same coefficients as Walker, and to the same order in γ^2, but includes spin 1 and spin 2 as well. The coefficients δ_2 are the same for both methods (except that there appears to be a slight numerical error in Walker's value for δ_2 for the spin 5/2 BCC lattice, which has been corrected.) The general expression for all spin values and lattices may be obtained from the work of Davis as

$$\delta_2 = \frac{qS}{(2qS-1)^2} \qquad (6.2.26)$$

If, however, we compare the higher coefficients ε_4 and ε_6 and δ_4 and δ_6 for the linear chain, we see that in the case of spin-1/2 there is considerable disagreement. However, as we move to progressively higher spin values, the agreement between the two sets of values improves considerably. In general, the agreement improves both as the spin value increases and as the coordination number of the lattice increases. For the three-dimensional lattices, S.C. and B.C.C., for spin > 1/2, the agreement is virtually complete. We expect the Davis results to be more reliable in the high S and high q limits. The agreement with Walker in these cases supports the general reliability of the Walker values for lower spin and lower q cases, where the Walker method is expected to be more reliable than the Davis method.

Results in agreement with the work of Walker have recently been published by Arai and Goodman (1967) which include values for spin-1 and spin-2, but are carried out to lower order, i.e. the coefficients ε_6 and δ_6 have not been obtained.

Pade´ approximant evaluations using the Walker long-range order series are shown on Fig. (6.8) for the linear chain with spin-1/2, spin-3/2 and spin-5/2, the simple quadratic lattice for spin-1/2 and spin 3/2, the simple cubic lattice for spin-1/2 and the body-centered

Fig. 6.8

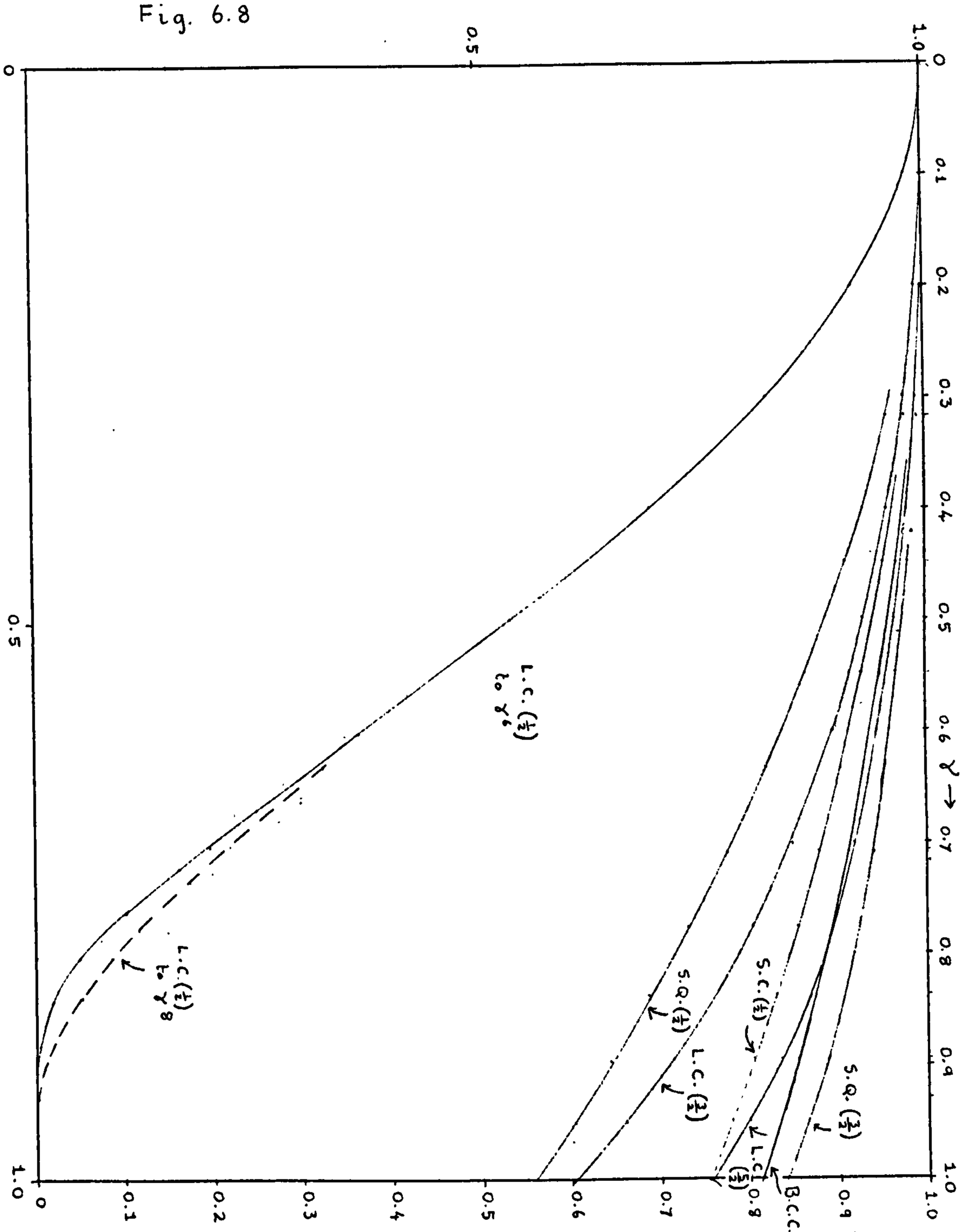

Padé Approximant Evaluations of Walker Series for the Long-Range order of Various Lattices

cubic lattice for spin-1/2. It is hard to conclude from these results that the linear chain series for higher spin definitely indicate that the long-range order vanishes at $\gamma = 1.0$ in these cases also, although the series do display signs of turning down near $\gamma = 1.0$. Indications of vanishing long-range order for two-dimensional lattices are even less marked. Clearly, longer series are required to give information on this point. On the other hand, the higher spin linear chain Padé evaluations do appear to support the conclusion that if the long-range order vanishes at all, it vanishes only at $\gamma = 1.0$ and not for $\gamma < 1.0$.

Recently Nagle (private communication, 1968) has obtained the coefficient (+1/64) of γ^8 for the Walker expansion by a suitable transformation of the spontaneous staggered polarization series for the two-dimensional antiferroelectric F-model (Lieb, 1967; Nagle, 1966). The evaluated result is shown dashed for the region $\gamma > 0.6$ and is encouragingly consistent with our final, limiting estimate (see Fig. (6.3)) for $\omega_\infty(\gamma)$.

Table (6.3)

Comparison of Approximate Methods for the Anti-ferromagnetic Ground State and Order Parameters.

Author	Classification	Year	Num. $-\mathcal{E}_0$	Analytic	ω_1	$2/3\,\mathcal{E}_0$	ω_∞
Néel	Ising model	1932	0.5000	1/2	-1.0000	-0.3333	1.0000
Kubo	Variatl-Spin Wave	1953	0.698	$1/2\,(1+0.396)$			finite
Syozi	Simple Fermion Spin Wave	1951	0.7160	$-\frac{1}{2}+2\sqrt{2}\pi\times E\left(\frac{1}{\sqrt{2}}\right)$			
Oguchi		1963					
Anderson	Singlet Pairs	1951	0.7500	3/4	-0.5000	-0.5000	0
Hulthén	Variational-	1938	0.8156	$\frac{1}{54}(7+7\sqrt{7})$	-0.5484	-0.5438	0
Kasteleijn	Constant Coupling	1952	"	"	"	"	0
Meyer	Fermions with Interactions	1956	0.8393	$2/\pi + 2/\pi^2$	-0.4052	-0.5596	0
Rodriguez		1959					
Bulaevskii		1963					
Kubo	Spin-wave	1952	0.9294	$2-4/\pi+2/\pi^2$			0
Oguchi		1960					
Hulthén	2nd Approx.n	1938	0.846				
Oguchi		1963					0.325*
Anderson	Classical Spin-wave	1952	0.8634	$3/2-2/\pi$			0
Ruijgrok-Rodriguez	Interacting Fermions.	1960	0.8646	$-1/2+(2/\pi^2)\,K^2(k)$ where $K(k)-E(k)=k\pi/2$	-0.59	-0.5764	0.2633
Oguchi		1963					
Davis	Pert.n on N-I bosons	1960	0.8682		-0.4005	-0.5788	0.232
Inawashiro-Katsura	Pert.n on X-Y model	1965	0.8702	See paper			
Walker	Perturb.n series to γ^6	1959	0.875		0.74		0
Katsura-Inawashiro	Pert.n on Bulaevskii	1964	0.8899	See paper			
Bethe	Exact Analytic	1931	0.8863	$2\ln 2-1/2$	-0.591	-0.591	?
Hulthén		1938					

* sub-lattice magnetisation

REPRESENTATIONS OF THE SYMMETRIC GROUP --- THE HEISENBERG MODEL

A.1.1) INTRODUCTION

In Chapter II we have been primarily concerned with representing the Heisenberg and anisotropic spin Hamiltonians in terms of a complete set of basis functions which are eigenfunctions of the operator S^z. However we have seen (sub-section (1.2) of Chapter II) that, in the Heisenberg limit only, the Heisenberg spin operator may be expressed in terms of operators which permute spins on the various atomic sites, and the problem of representing the Hamiltonian is therefore equivalent to finding representations of various sub-groups of the complete symmetric group (the permutation group on N spins). The Hamiltonian representation in terms of Ising eigenfunctions is, in the Heisenberg limit, a particular representation of the symmetric group. It is not, however, an irreducible representation. We have seen in sub-section (3.2) of Chapter II that a representation is possible in terms of basis functions which are simultaneous eigenstates of both S^z, and S^2, the operator standing for the square of the total spin, and, further, that the matrices obtained in this representation are of lower order than those obtained from the Ising representation. This representation is, in fact, an irreducible representation of the symmetric group for a spin cluster with no geometric symmetry axes, and further matrix reduction is not possible for this case.

Since, throughout the bulk of this thesis, our interest lies primarily in the anisotropic linear chain, we have not significantly exploited the method of irreducible representations of the symmetric group. However, its importance is such as to justify the inclusion of an account of this method in this appendix. Historically, the first to

employ an approach essentially equivalent was Hulthén (1938). Hulthen, who did not have access to electronic digital computers at that time, devised a method for finding the antiferromagnetic ground state of clusters (rings) of 4-10 spins which involved the solution of a matrix no larger than 6 x 6 for the case of N = 10. Hulthén was able to write down a set of spin functions, linear combinations of Ising eigenfunctions, of rather simple form, which he was able to show were eigenfunctions of S^2 (and also, of course, S^z). He then evaluated the Hamiltonian matrix representatives in this basis, adopted a simplification applicable to the special case of this particular eigenvalue, the largest eigenvalue of the final Hamiltonian, and finally solved by hand the resultant low order matrix. Later workers (Ledinegg and Urban, 1952) pointed out the group theoretical foundation of Hulthén's approach and extended the method to the case of N = 12.

Our interest in the Hulthén method lies in the total spin eigenfunctions, for we have not, previously, discussed the nature of the eigenfunctions of the spin problem in any detail. It is convenient to calculate eigenfunctions in order to obtain pair correlation functions. The structure of these functions throws some additional light on the basic quantum mechanics of the problem, discussed in Chapter II.

In addition to presenting a rather brief account of the main features of the Hulthén approach in section 2 of this appendix, we shall consider, in section 3, a straight group theoretical approach due to Corson (1952). For completeness it should be mentioned that Corson (ibid) gives a second method which is suitable for treating the Heisenberg spin cluster problem. This method has been extensively exploited to obtain high temperature cluster expansions (Domb and Wood, 1965) and a detailed account is presented in Wood's thesis (1965). The essence of the method is a matrix representation of the permutation operators comprising the Hamiltonian for a

given total spin S. The method has been extended to include all spin clusters with 11 or fewer spins.

A.1.2) THE HULTHÉN APPROACH: EIGENFUNCTIONS OF THE TOTAL SPIN S

Basic Quantum-Mechanical Operators

The Hamiltonian operator $\mathcal{H} = -2J\sum_{i<j=1}^{N} (\underline{S}_i \cdot \underline{S}_j - \frac{1}{4})$ is written by Hulthén as

$$\mathcal{H} = J\sum_{i<j=1}^{N} \frac{1 - \underline{\sigma}_i \cdot \underline{\sigma}_j}{2} \quad . \tag{A.1.2.1}$$

(Hulthén uses a ferromagnetic choice of J, i.e. the lowest states of the problem are ferromagnetic and the highest are antiferromagnetic.)

For the nearest-neighbour coupled linear chain with periodic boundary conditions (A.1.2.1) may be written (defining a Hamiltonian operator O_H)

$$J O_H = J\sum_{i=1}^{N} \frac{1 - \underline{\sigma}_i \cdot \underline{\sigma}_{i+1}}{2} \quad ; \quad N + i = i \; . \tag{A.1.2.2}$$

Consider the single particle wavefunctions α 'spin-up', and β 'spin-down'. Consider also the operator $O_{ij} = \frac{1 - \underline{\sigma} \cdot \underline{\sigma}_j}{2}$ (We have $O_H = \sum_{i=1}^{N} O_{i,i+1}$ (A.1.2.3)). O_{ij} has the following effect on the single particle spin functions:

$$\begin{aligned} O_{ij}\,\alpha_i\alpha_j &= O_{ij}\,\beta_i\beta_j = 0 \\ O_{ij}\,\alpha_i\beta_j &= \alpha_i\beta_j - \beta_i\alpha_j \end{aligned} \tag{A.1.2.4}$$

For the purpose of simplification, let us introduce, following Hulthén, the following notations:

$$\begin{aligned} [i\,j] &= \alpha_i\beta_j - \beta_i\alpha_j \\ \{i\,j\} &= \alpha_i\beta_j + \beta_i\alpha_j \end{aligned} \tag{A.1.2.5}$$

The expression $\{\{ i, j, \cdots\cdots, S\}\}$ signifies a set of products symmetric in α and β over all indices $i, j, \cdots, S$. e.g. $\{\{ij\}\} = \begin{matrix} \alpha_i\alpha_j \\ \alpha_i\beta_j + \beta_i\alpha_j \\ \beta_i\beta_j \end{matrix}$

Explicitly, for N=3,

$$\begin{aligned} \{\{123\}\} \quad & \alpha_1\alpha_2\alpha_3 \\ & \beta_1\alpha_2\alpha_3 + \alpha_1\beta_2\alpha_3 + \alpha_1\alpha_2\beta_3 \\ & \beta_1\beta_2\alpha_3 + \alpha_1\beta_2\beta_3 + \beta_1\alpha_2\beta_3 \\ & \beta_1\beta_2\beta_3 \end{aligned} \tag{A.1.2.6}$$

Products of terms like (A.3.2.5) are, in general, not independent of one another. The following dependency relations hold:

$$[ij][kl] + [ik][lj] + [il][jk] \equiv 0 \qquad \text{(A.1.2.7)}$$

$$[ij]\{kl\} + [jk]\{il\} + [kl]\{ij\} + [li]\{jk\} \equiv 0 \,. \qquad \text{(A.1.2.8)}$$

From equations (A.1.2.3) one may easily obtain the effect of the operator O_{ij} on the different products of [i,j], $\{kl\}$ etc.

$$O_{ij}[ij] = 2[ij] \;; \quad O_{jk}[ij][kl] = [jk][li] \qquad \text{(A.1.2.9)}$$

$$O_{ij}\{\{i,j,\cdots\cdots,s\}\} = 0 \qquad \text{(A.1.2.10)}$$

$$O_{ij}[ij]\{\{k,l,\cdots\cdots,s\}\} = -[jk]\{\{i,l,\cdots\cdots,s\}\} \,. \qquad \text{(A.1.2.11)}$$

Let us define the operator $$O = \sum_{1\le i<j}^{N} \frac{1-\sigma_i\cdot\sigma_j}{2} = \sum_{(ij)} O_{ij} \qquad \text{(A.1.2.12)}$$

It is easy to show that this operator is related to the square of the total spin by the eigenvalue expression

$$S^2 = S(S+1) = \frac{N}{2}\left(\frac{N}{2}+1\right) - O \,. \qquad \text{(A.1.2.13)}$$

Ferromagnetic Ground State Functions (S=N/2)

From equations (A.1.2.3), (A.1.2.10), (A.1.2.12) it follows that the symmetric expression $\{\{123\cdots N\}\}$, for an N-spin system, must be an eigenfunction of O_H corresponding to eigenvalue zero and spin quantum number N/2. In fact, we recognise this expression as the (N+1)-fold degenerate ferromagnetic ground state, the only state with spin quantum number N/2.

Antiferromagnetic Ground State Function (S=0)

Now consider a function $\varphi = [k_1 k_2][k_3 k_4]\cdots[k_{N-1} k_N]$ (N even).

It is easy to show (see equations (A.1.2.9)) that φ is transformed

by the operator O_H into a linear combination of functions of the same kind with suitably permuted k's. By applying the identities (A.1.2.8), one can easily show that all functions of the type φ are eigenfunctions of S^2 belonging to the same eigenvalue zero. As an example of the general result, we give a proof for N=6.

TABLE (A.1)

$O_{12}\varphi = 2\varphi$	$O_{12}\varphi_4$	$2\varphi_4$
$O_{13}\varphi = [13][24][56]$	etc.	$[13][24]\{56\}$
$O_{14}\varphi = -[14][23][56]$		$-[14][23]\{56\}$
$O_{15}\varphi = [15][26][34]$		$[15][34]\{26\}$
$O_{16}\varphi = -[16][25][34]$		$[16][34]\{25\}$
$O_{23}\varphi = -[14][23][56]$		$-[14][23]\{56\}$
$O_{24}\varphi = [13][24][56]$		$[13][24]\{56\}$
$O_{25}\varphi = -[16][25][34]$		$-[25][34]\{16\}$
$O_{26}\varphi = [15][26][34]$		$-[26][34]\{15\}$
$O_{34}\varphi = 2\varphi$		$2\varphi_4$
$O_{35}\varphi = [12][35][46]$		$[12][35]\{46\}$
$O_{36}\varphi = -[12][36][45]$		$[12][36]\{45\}$
$O_{45}\varphi = -[12][36][45]$		$-[12][45]\{36\}$
$O_{46}\varphi = [12][35][46]$		$-[12][46]\{35\}$
$O_{56}\varphi = 2\varphi$		0
Total : $O\varphi = 6\varphi + 6\varphi = 12\varphi$		$4\varphi_4 + 6\varphi_4 = 10\varphi_4$

In the left-hand column of Table (A.1) we show the constituents O_{ij} of the operator O operating on the function $\varphi = [12][34][56]$, appropriate to the case N=6. From equations (A.1.2.7) we may derive the following dependency relations:

$$\begin{aligned}[12][34][56] &= [13][24][56] - [14][23][56] \\ &= [12][35][46] - [12][36][45] \\ &= [15][26][34] - [16][25][34]\end{aligned} \qquad \text{(A.1.2.14)}$$

Table (A.2)

1	2	3	4	5	6
S	Type	Eiva.	Eigenvector	Explicit Form	S^2
0	$^5A_1$	0	$\{\{1234\}\}$	$\|0000\rangle$	+2
				$\|1000\rangle + \|0100\rangle + \|0010\rangle + \|0001\rangle$	+1
				$\|1100\rangle + \|0110\rangle + \|0011\rangle + \|1001\rangle + \|1010\rangle + \|0101\rangle$	0
				$\|0111\rangle + \|1011\rangle + \|1101\rangle + \|1110\rangle$	-1
				$\|1111\rangle$	-2
1	^3E	-2J	$[12]\{\{34\}\} + [23]\{\{41\}\}$	$\|1000\rangle - \|0010\rangle$	+1
				$\|1100\rangle - \|0110\rangle - \|0011\rangle + \|1001\rangle$	0
				$\|0111\rangle - \|1101\rangle$	-1
	^3E	-2J	$[23]\{\{41\}\} + [34]\{\{12\}\}$	$\|0100\rangle - \|0001\rangle$	+1
				$\|1100\rangle + \|0110\rangle - \|0011\rangle - \|1001\rangle$	0
				$\|1011\rangle - \|1110\rangle$	-1
	$^3B_2$	-4J	$[12]\{\{34\}\} + [34]\{\{12\}\}$	$\|1000\rangle - \|0100\rangle + \|0010\rangle - \|0001\rangle$	+1
				$2\|1010\rangle - 2\|0101\rangle$	0
				$\|0111\rangle - \|1011\rangle + \|1101\rangle - \|1110\rangle$	-1
0	$^1B_1$	-2J	$[12][34] - [23][41]$	$\|1100\rangle - \|0110\rangle + \|0011\rangle - \|1001\rangle$	0
	$^1A_1$	-6J	$[12][34] + [23][41]$	$\|1100\rangle + \|0110\rangle + \|0011\rangle + \|1001\rangle - 2\|1010\rangle - 2\|0101\rangle$	0

We observe that the operators may be combined in pairs, in accordance with(A.1.2.16), as indicated by the joining lines in Table (A.1). Hence for example, $(O_{13} + O_{14})\varphi = \varphi$ and hence $O\varphi = \sum_{(ij)} O_{ij}\varphi = 12\varphi$. Similarly, all functions of the type φ are also eigenfunctions of 0 with the same eigenvalue. From equation (A.1.2.13) we have

$$S(S+1) = 3.4 - 12 = 0 \quad \therefore S = 0 .$$

Hence a set of independent functions of the type φ comprise the singlet states of the problem. We expect that the largest eigenvalue of O_H(the antiferromagnetic ground state) will be a linear combination of these singlet functions.

Intermediate Functions (S=N/2-L/2, L=2,4....,N-2)

Now consider a function φ_L which contains L/2 antisymmetric factors and is otherwise symmetric

$$\text{e.g.} \quad \varphi_L = [k_1 k_2][k_3 k_4]\cdots\cdots[k_{L-1} k_L]\{\{ k_{L+1} \cdots\cdots k_N \}\} .$$

It is easy to show that functions of the type φ_L are transformed by O_H into linear combinations of functions of the same kind, i.e. with the same number of antisymmetric elements, and that all φ_L are eigenfunctions of S^2 with spin quantum number(N/2-L/2). As an example we consider the function $\varphi_4 = [12][34]\{\{ 56 \}\}$. In the right-hand column of Table (A.1) we see the effect of operating on φ_4 with 0. In this case the dependence relations analogous to (A.1.2.14) are somewhat more complicated:

$$\begin{aligned} 2\,[12][34]\{56\} &= 2\,[13][24]\{56\} - 2\,[14][23]\{56\} \\ &= [12][35]\{46\} + [12][36]\{45\} - [12][46]\{35\} - [12][45]\{36\} \\ &= [15][34]\{26\} + [16][34]\{25\} - [26][34]\{15\} - [25][34]\{16\} . \end{aligned} \quad (A.1.2.15)$$

Linking operators as shown in Table (A.1), we observe that and further that S(S+1) = 3.4-10. Hence S=1. We can generalise this result to conclude that all such functions φ_4 are states of spin 1, i.e. triplet states.

Relation to S^z

It is easy to show that all functions of the type φ_L, $N/2 \geq L/2 \geq 0$, are eigenfunctions of S^z. All antisymmetric factors [ij] make a zero contribution to S^z. Hence the S^z quantum number of a given state φ_L arises from the symmetric component (if any). For example, for N=6, the triplet functions φ_4, with total spin 1, can be classified as follows:

$$\begin{aligned}
&(\alpha_1\beta_2 - \beta_1\alpha_2)(\alpha_3\beta_4 - \beta_3\alpha_4)\alpha_5\alpha_6 && \text{with } S^z = +1 \\
&(\alpha_1\beta_2 - \beta_1\alpha_2)(\alpha_3\beta_4 - \beta_3\alpha_4)(\alpha_5\beta_6 - \beta_5\alpha_6) && \text{with } S^z = 0 \qquad \text{(A.1.2.16)} \\
&(\alpha_1\beta_2 - \beta_1\alpha_2)(\alpha_3\beta_4 - \beta_3\alpha_4)\beta_5\beta_6 && \text{with } S^z = -1.
\end{aligned}$$

Representation of the Hamiltonian

We see that the Hulthén approach enables us to write down easily functions which have a specified value of S and S^z (S^z = S, S-1, ...,-S). The next problem is to generate a complete set of such functions as a basis for representing the Hamiltonian. (The number of independent functions belonging to a given S is, of course, given by the branching rule of Fig. (A.1) or see Chapter II, sub-section (3.2)). The linear dependence relation s for S=0, (A.1.2.14), and for general S, (A.1.2.15), complicate the process of writing down a complete set of basis functions. In the case S=0, (Ledinegg and Urban, 1952) have described a simple graphical approach which produces, systematically, a set of independent functions. For S>0, the problem is more complicated.

Matrix Reduction

Since the square of the total spin S^2 commutes with the translation operator T and the reflection operator R (see sub-section (3.2) of Chapter II), as does the z-component of the total spin, S^z, the Hulthén matrices may be reduced in the same way as the S^z block matrices of sub-section (5.2) of Chapter II; except that we cannot further reduce the S=0 block by additional use of spin inversion symmetry as we can the S^z=0 block.

Complete Set of Eigenfunctions for N = 4

To illustrate our comments on the nature of the Hulthén eigenfunctions of the total spin operator we show, in Table(A.2) the complete set of orthogonal (but not normalised) eigenvectors of the N=4 problem, expressed in column 4 as linear combinations of the Hulthen eigenfunctions of S and in column 5 in terms of the eigenfunctions of S^z. Each eigenvector is shown with its associated eigenvalue of the Hamiltonian; the total spin S and the z-component of total spin, S^z. In addition; in column 2, its basic molecular type A, B, or E is given. The significance of this will be discussed in the following section on the Corson group theory method.

Spin Inversion Symmetry

By reference to Fig.(2.2) it is now possible to see why the singlet states of N=6 occur in the spin inversion I=-1 sub-block. Each factor [ij] in the Hulthén S=0 functions is an eigenfunction of I with eigenvalue -1. Each Hulthén spin function is a product of three such brackets and is thus also an eigenfunction of I with eigenvalue -1. The eigenvectors of the Hamiltonian are linear combinations of the Hulthén functions and thus have the same property. The pair brackets {ij} are symmetric with respect to I and therefore we have the more general result that the states of spin S=0 and S=2 (in the S^z=0 block) have inversion eigenvalues -1, since they contain an odd number of [ ]-bracket factors and an even number of { }-brackets. It follows directly that the states of spin S=1 and S=3 in the same block, which have an even number of [ ]-brackets will have inversion eigenvalues +1. Hence we can explain the result quoted in sub-section (3.2) of Chapter II.

A.1.3.) THE CORSON GROUP CHARACTER METHOD

This method is not a matrix method, i.e. it does not depend on particular matrix representations of the symmetric group. The method

requires only a knowledge of the primitive group characters of the representations of the symmetric group π_N and such sub-groups as are appropriate to the symmetry of the spin clusters under consideration; together with the group character orthogonality relations.

Corson (1952) illustrates his account by detailed calculation on the ring of six spins with first, second and third neighbour interactions (also on an 8-spin cube with face and body diagonals). Our intention is to highlight portions of the Corson account and show how this group theory method relates to the matrix techniques described in Chapter II. We will then proceed to extend the group theory approach to toroidal clusters in two-dimensions and estimate how much progress on the analogous two-dimensional problem we could reasonably hope to make.

Group Character Tables

The first step is to draw up the character table of the group of interest. For example, for rings of spins it is easily verified that the appropriate group is the dihedral group D_N, which is, of course, a subgroup of the symmetric group π_N. In Table (A.3) we present the character table for a ring of eight spins. The dihedral group on 8 spins, D_8, contains seven symmetry classes $C_1 \rightarrow C_7$ which can be represented in the standard manner in terms of products of permutation cycles, as listed beside Table (A.3). The classes C_2, C_3, C_4 and C_5 represent, respectively, one-step, two-step, etc., translations around the ring. The reflection axes appropriate to the operators R_A and R_B discussed in sub-section (2.5) of Chapter II give rise to the reflection classes C_6 and C_7 respectively. Table (A.3) contains the group characters of the irreducible representations of D_8 corresponding to these seven classes which comprise 16 (in general 2N) permutation operations. For N even there will be, in general, three types of representation called,

following customary usage in molecular chemistry, A, B and E. In the case of N odd, the group character table differs in two important respects: a) there are no B representations and b) there is only one reflection symmetry axis (of order N) corresponding to the single reflection operator R_θ of sub-section (2.5) of Chapter II.

Class	Order of class	A_1	A_2	B_1	B_2	E_1	E_2	E_3
$C_1 = E$	1	1	1	1	1	2	2	2
C_2	2	1	1	-1	-1	$\omega + \omega^7$	0	$\omega^3 + \omega^5$
C_3	2	1	1	1	1	0	-2	0
C_4	2	1	1	-1	-1	$\omega^3 + \omega^5$	0	$\omega + \omega^7$
C_5	1	1	1	1	1	-2	2	-2
C_6	4	1	-1	1	-1	0	0	0
C_7	4	1	-1	-1	1	0	0	0
Total	16							

Class Elements

$C_1 = E$

$C_2 = (12345678)^{\pm 1}$

$C_3 = [(1357)(2468)]^{\pm 1}$

$C_4 = (1472 5836)^{\pm 1}$

$C_5 = (15)(26)(37)(48)$

$C_6 = (18)(27)(36)(45)$
+ 3 others

$C_7 = (28)(37)(46)$
+ 3 others

Table (A.3)

The presence of reflection symmetry implies that we have always two A-type representations, and also two B-type representations for N even, with symmetric and antisymmetric reflection properties. All other representations must be E-type. A- and B- type representations are always one-dimensional, E-type always two-dimensional. The total number of representations is determined by the fact that the sum of the dimensions squared must equal the order of the group, 2N. Hence fór N=8, we will have 4 one-dimensional representations A_1, A_2, B_1 and B_2 and 3 two-dimensional representations E_1, E_2 and E_3, since $4(1^2) + 3(2^2) = 16$.

Relationship of Corson Method to Chapter II Matrix Method

We may now proceed further to identify the A, B and E states with known eigenfunctions of the corresponding matrix problem as discussed

in Chapter II. We realise that the nomenclature A, B or E relates to the symmetry properties of the state under the translation operators of the group. First of all we surmise that the E-type states are related to the $\ell^{\frac{2\pi i}{N}k} = \omega, \omega^2, \cdots, \omega^{N-2}, \omega^{N-1}$ states (excluding the $\omega^{N/2}$ state for N even) of the matrix problem. The fact that the two-dimensional E states are doubly degenerate indicates that the E representation contains both the ω^r and complex conjugate ω^{r*} states ($r \neq 0, N/2$), which we know from previous theory are always degenerate. It is then very tempting to infer that the A-type states are $k=0$ states and the B-type states are $k=N/2$ states. However, Corson's account implies that under the general requirement of anti-symmetry it would be necessary to replace the permutations $P_{12345678}$ characteristic of class C_2; $P_{14725836}$ of C_4; and $P_{28}P_{37}P_{46}$ of C_7 by the signed permutations $\delta_P P$ where δ_P is a signature function which depends on the parity of the class. These three classes all have $\delta_P = -1$ (whereas the remainder all have $\delta_P = +1$ and would remain unchanged). This procedure effectively changes the sign of the group characters of these classes. Under this prescription our character tables will look the same as Corson's, but we must bear in mind that his A states are now our B states and vice-versa.

We have now completed our analysis of the eigenstates and shown explicitly how the group character method and the reduced matrix method are equivalent. There are two further comments we would like to make before passing on to outline briefly how eigenvalues are finally extracted. Firstly we notice how reflection symmetry is effective in splitting the $k=0$, A classes and the $k=N/2$, B classes into groups 1 and 2, but does not affect the E states. Secondly, we observe that since it is no more difficult to find a E state eigenvalue than say an A state eigenvalue, we have effectively circumvented the difficulty of complex matrices

discussed in sub-section(5.2) of Chapter II. The group theory method therefore gives us an overall reduction factor of N rather than N/2 (assuming the initial S breakdown). The approximate size of the largest ring which may conveniently be handled by this method would be 16 spins with present day computers.

Obtaining Eigenvalues

Since the dihedral group D_N is a subgroup of the symmetric group π_N, the irreducible representations of π_8 for the allowed total spin values S=0, S=1, S=2 and S=3 will be reducible representations of D_8. (The dihedral and symmetric group representations of the state of highest total spin, in this case S=4, are identical and therefore irreducible.) The number of times each irreducible representation of D_8 occurs in the 14th order (S=0); 28th order (S=1); etc; represen tation of π_8 may be found by standard techniques involving group charcter orthogonality relations, described in Corson. The results are set out in Table(A.4) which will shortly be discussed. The states may be explicitly evaluated by an elimination technique described in Corson involving traces of powers of permutation operators. The trace of a particular class of permutation operators for a representation of π_N corresponding to

Table (A.4)

	SINGLETS S = 0					TRIPLETS S = 1					
STATE	$^1A_1$	$^1B_1$	$^1E_1$	$^1E_2$	$^1E_3$	$^3A_1$	$^3A_2$	$^3B_2$	$^3E_1$	$^3E_2$	$^3E_3$
No. of irreduc. represenlns.	3	3	1	2	1	1	2	3	4	3	4
	QUINTETS S = 2						SEPTETS S = 3				S=4
STATE	$^5A_1$	$^5B_1$	$^5B_2$	$^5E_1$	$^5E_2$	$^5E_3$	$^7B_2$	$^7E_1$	$^7E_2$	$^7E_3$	$^9A_1$
No. of irreduc. represenlns.	3	2	1	2	3	2	1	1	1	1	1

a given total spin S is given by formula 13.15a of(Wigner, 1959). This formula states that the trace of the class of permutations of ρ cycles with cycle lengths λ_1, λ_2, ..., λ_ρ is the coefficient of x^k, (k=N/2-S) in

$$(-1)^{\rho}(1-x)(1+x^{\lambda_1})(1+x^{\lambda_2})\cdots\cdots(1+x^{\lambda_\rho}) \qquad . (A.1.3.1)$$

For example, consider the permutation (28)(37)(46) representative of C_7 in Table (A.3). In full, this operator appears as(1) (28) (37) (46) (5) i.e. a product of two unary cycles and three binary cycles. Hence the trace of this permutation in the S=1 representation of π_8 is given by the coefficient of x^3 in the algebraic product $(-1)^5(1-x)(1+x)(1+x)(1+x^2)(1+x^2)(1+x^2)$, which is -2. In this way a set of traces for the given symmetry classes $C_1 \rightarrow C_7$ of D_8 in π_8 for all allowed values of total spin S is shown in Table (A.5).

Table (A.5)

Class	Permutation	S=0	S=1	S=2	S=3	S=4
C_1	E	14	28	20	7	1
C_2	(12345678)	0	0	0	1	-1
C_3	(1357)(2468)	2	0	0	-1	1
C_4	(14725836)	0	0	0	1	-1
C_5	(15)(26)(37)(48)	6	-4	4	-1	1
C_6	(12)(38)(47)(56)	6	-4	4	-1	1
C_7	(1)(28)(37)(46)(5)	0	-2	-2	-1	-1

Traces of Powers of the Hamiltonian

It is worth remarking that Wigner's formula, in conjunction with the fact that the Hamiltonian itself is expressible in terms of permutation operators, can be used as the basis of a very simple and direct high temperature cluster series expansion. The type of expansion described

in section (2.1) of Chapter II depends on computing traces of powers of the Hamiltonian matrix $\mathcal{H}$, i.e. the partition function may be expanded as

$$Z_N(\beta, H) = \langle e^{-\beta \mathcal{H}} \rangle = 1 - \beta \langle \mathcal{H} \rangle + \frac{\beta^2}{2!} \langle \mathcal{H}^2 \rangle - \frac{\beta^3}{3!} \langle \mathcal{H}^3 \rangle + \cdots \quad (A.1.3.2)$$

where Z_N is the N-spin partition function as a function of $\beta = 1/kT$ and applied magnetic field H.

Let us consider the simple example of a cluster of 4 (spin 1/2) spins on a ring 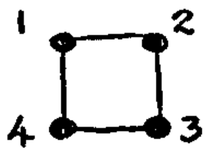

. The Heisenberg Hamiltonian for this cluster is essentially given by

$$V = P_{12} + P_{23} + P_{34} + P_{41} \quad (A.1.3.3)$$

These four permutation operators are equivalent and therefore have the same trace. Thus Tr V = 4 Tr P_{12}. By direct multiplication we have also

$$V^2 = 4E + 2P_{12}P_{34} + 2P_{23}P_{14} + P_{123}^{\pm 1} + P_{124}^{\pm 1} + P_{134}^{\pm 1} + P_{234}^{\pm 1} \quad (A.1.3.4)$$

and $$V^3 = 7P_{12} + 7P_{23} + 7P_{34} + 7P_{41} + 8P_{13} + 8P_{24} + 4P_{1234}^{\pm 1} + 3P_{1243}^{\pm 1} + 3P_{1324}^{\pm 1} \quad (A.1.3.5)$$

symmetry result that all permutation operators having the same number of binary, ternary etc. cycles will have the same trace. Hence

$$\begin{aligned} \mathrm{Tr}\, V &= 4\,[2] \\ \mathrm{Tr}\, V^2 &= 4\,[1] + 4\,[2^2] + 8\,[3] \quad (A.1.3.6) \\ \mathrm{Tr}\, V^3 &= 44\,[2] + 20\,[4]. \end{aligned}$$

The numbers in the brackets list the order of cycles in the permutation and the corresponding indices give the number of occurrences of each type of cycle. Hence by successively obtaining higher powers of the Hamiltonian and taking the appropriate traces at each stage by Wigner's formula (A.1.3.1), a high temperature expansion may be developed.

From Table (A.4) we may observe that the problem of finding the eigenvalues reduces essentially to separating say the 3 $^1A_1$ states, the 3 $^1B_1$ states, the $4\,^3E_1$ states, etc. (In the corresponding matrix approach, the matrices to be diagonalised are of order 3 for the $^1A_1$, and $^1B_1$ states and of order 4 for the $^3E_1$ states, etc..) States of different molecular types A, B or E are relatively easy to separate. The Corson approach we are describing requires the computation of V; V^2; V^3 and V^4 to evaluate the $^3E_1$ states. (In general, to separate N states of the same molecular type we require to compute all powers of V up to, and including V^N.)

Unfortunately for the Corson method, the computation of higher powers of the Hamiltonian in terms of permutation operators becomes very complicated (as we might suspect from inspection of equations (A.1.3.4) and (A.1.3.5) -- for example, these operators do not generally commute. It would thus seem that a matrix approach would be more profitable. The same comment would apply to the high temperature series expansion we have just described.

Group Theory Applied to Two-Dimensional Clusters

The final sub-sections of this appendix concern the possibility of extending the method of solving small finite clusters in the hope of extrapolation to the entire lattice limit to higher dimensions. We shall employ the powerful group theory approach to discover how far we could reasonably hope to go in solving small two-dimensional toroidal spin-1/2 clusters. There is a significant increase in complexity, in addition to the increased sizes of clusters required for an extrapolation set, in two-dimensions. This additional complexity will be reflected in the structure of the group character tables for toroidally bounded clusters of 9 and 25 spins. First of all let us consider the 3 x 3 cluster

of fig. (A.1) whose character is shown in Table (A.6).

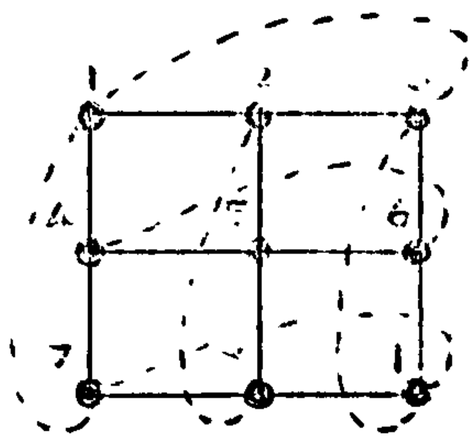

fig. (A.1)

Table (A.6)

Class	Type	Order	χ_1	χ_2	χ_3	χ_4	χ_5	χ_6	χ_7	χ_8	χ_9
C_1	E	1	1	1	1	1	2	4	4	4	4
C_2	T_1	4	1	1	1	1	2	1	1	-2	-2
C_3	T_1T_2	4	1	1	1	1	2	-2	-2	1	1
C_4	R_1R_2	9	1	1	1	1	-2	0	0	0	0
C_5	R_2	6	1	-1	1	-1	0	-2	2	0	0
C_6	T_2R_2	12	1	-1	1	-1	0	1	-1	0	0
C_7	R_D	6	1	-1	-1	1	0	0	0	-2	2
C_8	T_2R_D	12	1	-1	-1	1	0	0	0	1	-1
C_9	R_DR_2	18	1	-1	-1	-1	0	0	0	0	0

We see there are 9 symmetry classes, $C_1 \rightarrow C_9$, and corresponding irreducible representations $\chi_1 \rightarrow \chi_9$. We choose the five basic symmetry operators T_1, T_2, R_1, R_2, R_D, where T_1 and R_1 refer, respectively, to translation and reflection about a vertical axis, as shown in fig. (A.2), and T_2 and R_2 to translation and reflection about a horizontal axis. R_D is a cluster-diagonal reflection operator, a new type of operator not encountered in linear systems. The principal commutation properties of these operators will be briefly summarised:

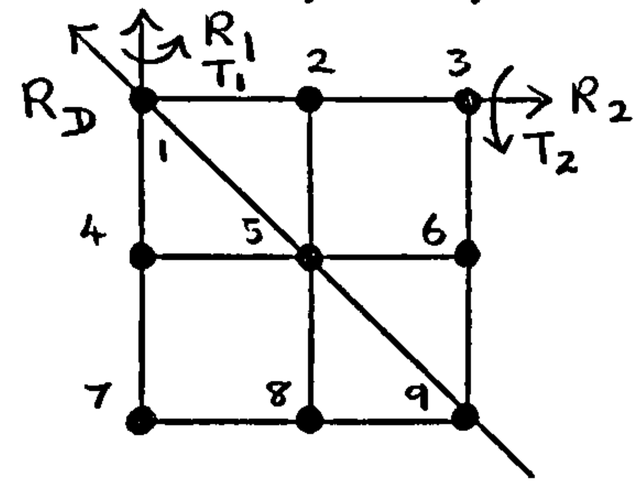

fig. (A.2)

$$[T_1, T_2] = 0 \; ; \; [R_1, R_2] = 0 \; ; \; [T_1T_2, R_D] = 0 ;$$

$$[R_1R_2, R_D] = 0 \quad \text{and} \quad R_1R_2\,T_1T_2 = (T_1T_2)^{-1} R_1R_2 \,. \qquad (A.1.3.7)$$

The symmetry elements of the group are combinations of these basic operators and the order of the corresponding subgroup is shown beside the

particular element. (The permutation operator representation of the symmetry elements which has been used is not convenient here.) Some of the symmetry elements have a particularly simple physical interpretation: for example, $C_4 = 9R_1R_2$ represents a centrosymmetric inversion and $C_9 = 18R_DR_2$ represents a rotation of $\pi/2$ about a particular spin. The order of the complete group equals

$$\tau_1 \times \tau_2 \times R_1 \times R_2 \times R_D = 3 \times 3 \times 2 \times 2 \times 2 = 72 \quad (8N) \qquad (A.1.3.8)$$

where τ_1 is the order of the translation subgroup T_1, etc.. Let us now consider the physical significance of the states Γ_1 to Γ_9. The four non-degenerate states $\Gamma_1, \Gamma_2, \Gamma_3, \Gamma_4$ are analogous to the A states of the linear problem; they are invariant under translation and centrosymmetric inversion but vary in their reflection properties. Note that since we have two principal axes to consider, horizontal and vertical, there are now four A type states, not two. Also the analogous E states of the problem are the four-fold degenerate states $\Gamma_6, \Gamma_7, \Gamma_8, \Gamma_9$. However we observe the appearance of a new type of state, two-fold degenerate, Γ_5. This state is antisymmetric under R_1R_2 and has ano analogue in the case of a linear ring. If we go on to larger clusters, yet another type of state appears which is eight-fold degenerate and again has no analogue in the linear case. This is the state Γ_{10} of Table (A.7), which is the group character table for a 5x5 toroid.

Estimate of Current Upper Limit on Cluster Size

We are now in a position to make an estimate of maximal, soluble, two-dimensional cluster size by two different methods. The first is a very rough order-of-magnitude calculation based on the group character table. We shall illustrate it by referring to the 3x3 cluster. The first reduction which occurs is reduction by total spin S. A rapid calculation based on Fig.(A.1) suggests that spin degeneracy yields a

Table (A.7)

Class	Order	χ_1	χ_2	χ_3	χ_4	χ_5	χ_6	χ_7	χ_8	χ_9	χ_{10}	χ_{11}	χ_{12}	χ_{13}	χ_{14}
E	1	1	1	1	1	2	4	4	4	4	4	4	4	4	8
T_1	4	1	1	1	1	2	$2+\tilde{\omega}$	$2+\tilde{\omega}$	$2+\tilde{\omega}^2$	$2+\tilde{\omega}^2$	$2\tilde{\omega}$	$2\tilde{\omega}$	$2\tilde{\omega}^2$	$2\tilde{\omega}^2$	-2
T_1^2	4	1	1	1	1	2	$2+\tilde{\omega}^2$	$2+\tilde{\omega}^2$	$2+\tilde{\omega}$	$2+\tilde{\omega}$	$2\tilde{\omega}^2$	$2\tilde{\omega}^2$	$2\tilde{\omega}$	$2\tilde{\omega}$	-2
T_1T_2	4	1	1	1	1	2	$2\tilde{\omega}$	$2\tilde{\omega}$	$2\tilde{\omega}^2$	$2\tilde{\omega}^2$	$2+\tilde{\omega}$	$2+\tilde{\omega}$	$2+\tilde{\omega}^2$	$2+\tilde{\omega}^2$	-2
$T_1^2T_2^2$	4	1	1	1	1	2	$2\tilde{\omega}^2$	$2\tilde{\omega}^2$	$2\tilde{\omega}$	$2\tilde{\omega}$	$2+\tilde{\omega}^2$	$2+\tilde{\omega}^2$	$2+\tilde{\omega}$	$2+\tilde{\omega}$	-2
$T_1^2T_2$	8	1	1	1	1	2	-1	-1	-1	-1	-1	-1	-1	-1	3
R_1R_2	25	1	1	1	1	-2	0	0	0	0	0	0	0	0	0
R_2	10	1	-1	1	-1	0	2	-2	2	-2	0	0	0	0	0
T_2R_2	20	1	-1	1	-1	0	$\tilde{\omega}$	$-\tilde{\omega}$	$\tilde{\omega}^2$	$-\tilde{\omega}^2$	0	0	0	0	0
$T_2^2R_2$	20	1	-1	1	-1	0	$\tilde{\omega}^2$	$-\tilde{\omega}^2$	$\tilde{\omega}$	$-\tilde{\omega}$	0	0	0	0	0
R_3	10	1	-1	-1	1	0	0	0	0	0	2	-2	2	-2	0
T_2R_3	20	1	-1	-1	1	0	0	0	0	0	$\tilde{\omega}$	$-\tilde{\omega}$	$\tilde{\omega}^2$	$-\tilde{\omega}^2$	0
$T_1^2R_3$	20	1	-1	-1	1	0	0	0	0	0	$\tilde{\omega}^2$	$-\tilde{\omega}^2$	$\tilde{\omega}$	$-\tilde{\omega}$	0
R_3R_2	50	1	1	-1	-1	0	0	0	0	0	[illegible]	[illegible]	[illegible]	[illegible]	[illegible]

where $\tilde{\omega} = \omega + \omega^4$ and $\tilde{\omega}^2 = \omega^2 + \omega^3$; $\omega^5 \equiv 1$.

reduction factor which goes as N. However, consideration of the exact formula (equation (2.3.5) of Chapter II) for the size of a matrix block of given total spin S $A(S) = \frac{2S+1}{(N/2+S+1)} \binom{N}{N/2+S}$ indicates that A(S) is a maximum for S = O(1), when $A(S) \sim 2^N / N^{\frac{3}{2}}$ (9.1.3.9) Hence the spin degeneracy reduction factor is more accurately $N^{3/2}$. It is interesting to note that in this factor $N^{3/2}$, $N^{1/2}$ arises from conservation of S^z, whereas additional total spin conservation yields a further factor N. Each set of states of a given total spin is then divided into the irreducible representations χ_i shown in the group character table. It is a standard group theory result that the number of irreducible representations is equal to the number of symmetry

classes. There are nine symmetry classes for the 3x3 cluster, 14 for the 5x5 cluster(see Tables (A.6) and (A.7) and there are 20 symmetry classes for the 7x7 cluster. These are

$$E;\ T_1;\ T_1^2;\ T_1^3;\ T_1T_2;\ T_1^2T_2;\ T_1^3T_2;\ T_1^2T_2^2;\ T_1^3T_2^2,\ T_1T_2^2;\ R_1R_2;$$

$$R_1R_2;\ R_2;\ R_2;\ T_1R_2;\ T_1^2R_2;\ T_1^3R_2;\ T_1R_2;\ T_1^2R_2;\ T_1R_2. \qquad (A.1.3.10)$$

The 20 η_i have the following degeneracies 1,1,1,1,2,4,4,4,4,4,4, 4,4,4,4,4,4,8,8,8. We must also divide by the average degeneracy of each representation, which is easily found to be $\frac{4\times1+2\cdot4\times4}{1} = \frac{22}{1}$ for 3x 3; $\frac{46}{14}$ for 5x5 and $\frac{78}{20}$ for 7x7. For the case of 3x3 we therefore obtain as an estimate for the size of the largest matrix to be solved

$$\frac{512}{9\times4\times22/9} \simeq 2.5 \qquad (A.1.3.11)$$

Let us compare this figure with an ex act calculation, the results of which are set out in Table (A.8). We see that the largest matrix has, in fact, order 3, in agreement with our order-of-magnitude result (A.1.3.11). For 5x5 we similarly estimate $\sim 3 \times 10^4$ and for 7x7 we have $\sim 2 \times 10^{10}$ (A.1.3.12)

Table (A.8)

	χ_1	χ_2	χ_3	χ_4	χ_5	χ_6	χ_7	χ_8	χ_9
$S = 1/2$	1	1	0	0	0	3	2	3	2
$S = 3/2$	0	2	1	1	2	3	2	3	2
$S = 5/2$	0	1	1	1	0	2	1	2	1
$S = 7/2$	0	0	0	0	0	1	0	1	0
$S = 1/2$	0	1	0	0	0	2	1	2	1

We must therefore conclude that this method is not capable of extension to even the simplest sequence of two-dimensional clusters, namely 3x3, 5x5, and 7x7. In fact, 5x5 seems completely out of the

question. We could have expected this result by observing that, whereas the total number of states increases as 2^N (N= nxn), the number of symmetry classes and hence the number of irreducible representations (see Tables (A.6 and (A.7) increases only as N, and the mean spin degeneracy as $N^{3/2}$. Hence the maximum matrix size increases asymptotically as $2^N/N^{5/2}$. This is the same as for linear systems, in which case N is the number of spins on the ring. We have already observed in this appendix that the largest linear system we could hope to solve at present consists of a ring of 16 spins. We infer that the largest two-dimensional square cluster would be the 4x4 spin array with periodic boundary conditions.

These results are supported by an alternative approach which considers matrix reduction in terms of the operators T_1T_2, R_D and R_1R_2. Conservation of T_1T_2 gives a reduction factor of N = nxn, and conserfation of R_D an additional reduction factor of 2, since $[T_1T_2,R_D]=0$. R_1R_2 commutes with R_D, and also with T_1T_2 in certain special cases, analogous to the cases where T and R commute in one-dimension (see sub-section (3.2) of Chapter ID . Hence R_1R_2 does not, in general, give any further reduction for toroids. We have, therefore, an overall reduction factor of 2N for square clusters. (If we consider rectangular clusters we lose the reduction factor of 2 corresponding to R_D). Let us now refer to the 16-spin cluster of Fig.(A.1). The largest matrix occurs for total spin S=2, and has order 3640. A reduction factor of 2 x 16 reduces the matrix order to approximately 114, comfortably soluble on a reasonably large computer. An inspection of Fig. (A.1) allows a rough order-of magnitude estimate of the size of the largest matrix for N=25 to be $\sim 1.6 \times 10^6$. A reduction factor of 50 yields an irreducible matrix size of 3×10^4, in agreement with our earlier result.

FIGURE (A.1)

Branching Rule Diagram for Dimensions of Spin Representations

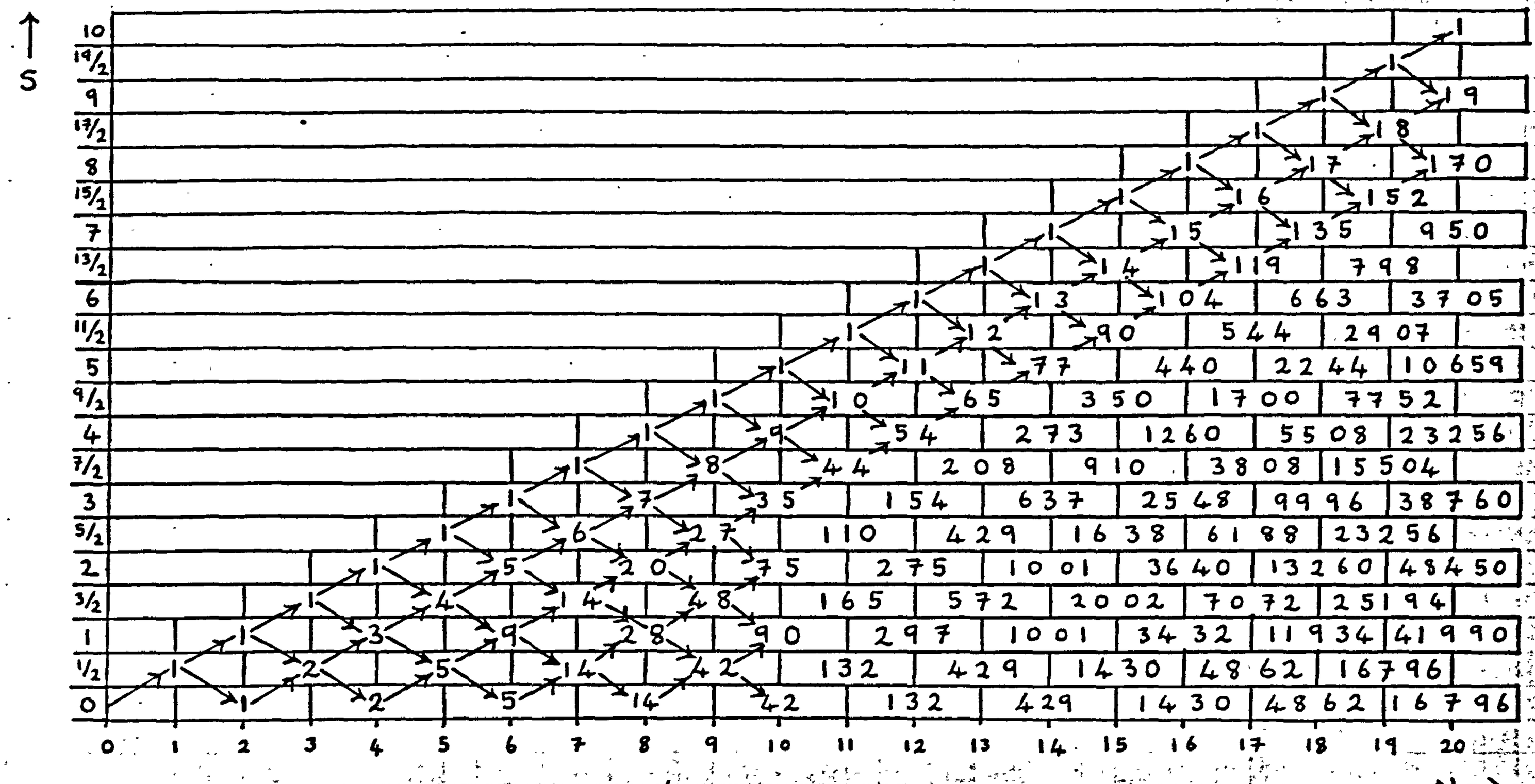

APPENDIX 2

EIGENVALUES OF RINGS AND CHAINS

TABLE I : Ring Eigenvalues: γ =1.0

RING

N= 2 γ=1.0

0 S^2=1.0

0.000000, 0

1 S^2=0.0

0.000000, 0

-4.000000, 0

RING

N= 3 γ=1.00

0 S^2=1.5

0

1 S^2=0.5

0

-3.000000, 0

-3.000000, 0

RING

N= 4 γ=1.00

0 S^2=2

2.000000, 0

1 S^2=1

2.000000, 0

0

0

-2.000000, 0

2 S^2=0

2.000000, 0

-4.000000, 0

0

0

0

-2.000000, 0

RING

N= 5 γ=1.00

0 S^2=2.5

0

1 S^2=1.5

0

-1.381966, 0

-3.618034, 0

-3.618034, 0

-1.381966, 0

2 S^2=0.5

0

-4.000000, 0

-1.381966, 0

-6.236068, 0

-1.763932, 0

-3.618034, 0

-1.763932, 0

-3.618034, 0

-1.381966, 0

-6.236068, 0

RING

N= 6 γ=1.00

0 S^2=3

3.000000, 0

1 S^2=2

3.000000, 0

2.000000, 0

0

-1.000000, 0

0

2.000000, 0

2 S^2=1

2.360680, -1

3.000000, 0

-4.236068, 0

2.000000, 0

-2.000000, 0

0

1.561553, 0

-2.561553, 0

-1.000000, 0

0

1.561553, 0

-2.561553, 0

2.000000, 0

-2.000000, 0

3 S^2=0

2.360680, -1

-3.000000, 0

3.000000, 0

-4.236068, 0

-1.000000, 0

2.000000, 0

-2.000000, 0

-1.000000, 0

2.000000, 0

-2.000000, 0

0

1.561553, 0

-2.561553, 0

0

1.561553, 0

-2.561553, 0

2.000000, 0

-2.000000, 0

1.000000, 0

-1.000000, 0

1.605551, 0

-5.605551, 0

TABLE I (cont.).

RING

N = 7. γ = 1.00

0 S^2 = 3.5

0

1 S^2 = 2.5

0

−7.530204, −1
−2.445042, 0
−3.801938, 0
−3.801938, 0
−2.445042, 0
−7.530204, −1

2 S^2 = 1.5

0

−2.000000, 0
−6.000000, 0
−7.530204, −1
−3.936364, 0
−7.112555, 0
−2.445044, 0
−1.163333, 0
−5.144643, 0
−3.801958, 0
−1.901956, 0
−4.741126, 0
−3.801958, 0
−1.901956, 0
−4.741126, 0
−2.445044, 0
−1.163333, 0
−5.144643, 0
−7.530204, −1
−3.936364, 0
−7.112555, 0

3.0 S^2 = 0.5

1.862645, −9
−2.000000, 0
−5.000000, 0
−5.000000, 0
−6.000000, 0

−7.530204, −1
−7.530205, −1
−2.919292, 0
−2.919292, 0
−3.936367, 0
−3.936367, 0
−5.723812, 0
−5.723812, 0
−7.112555, 0
−7.112551, 0

−1.163333, 0
−1.163333, 0
−2.445042, 0
−2.445042, 0
−3.838559, 0
−3.838559, 0
−5.144646, 0
−5.144646, 0
−9.210358, 0
−9.210359, 0

−1.269616, 0
−1.269616, 0
−1.901957, 0
−1.901957, 0
−3.801938, 0
−3.801938, 0
−4.741147, 0
−4.741147, 0
−7.038363, 0
−7.038363, 0

RING

N = 8 γ = 1.00

0 S^2 = 4

4.000000, 0

1 S^2 = 3

4.000000, 0
3.414214, 0
2.000000, 0
5.857864, −1

0

5.857864, −1
2.000000, 0
3.414214, 0

2.0 S^2 = 2.0

4.000000, 0
2.493959, 0
−8.900837, −1
−3.603875, 0

3.414214, 0
3.414213, 0
8.740320, −1
8.740320, −1
−2.288246, 0
−2.288246, 0

3.051374, 0
3.051374, 0
2.000000, 0
2.000000, 0
−5.173040, −1
−5.173041, −1
−2.534070, 0
−2.534070, 0

2.288246, 0
2.288246, 0
5.857865, −1
5.857864, −1
−8.740320, −1
−8.740321, −1

2.000000, 0
1.053671, −8
−1.387779, −17
−1.053671, −8

TABLE I (cont.)

N=8 Y=1.0 (cont.)

z

3.0 S=1.0

4.000000, 0
2.493959, 0
1.862645, -8
-1.862645, -9
-8.900838, -1
-2.000000, 0
-3.603875, 0

3.414214, 0
3.414214, 0
1.785387, 0
1.785387, 0
8.740321, -1
8.740321, -1
-1.025366, 0
-1.025366, 0
-1.256757, 0
-1.256757, 0
-2.288246, 0
-2.288246, 0
-4.917477, 0
-4.917477, 0

3.051374, 0
3.051374, 0
2.000000, 0
2.000000, 0
9.032120, -1
9.032119, -1
-5.173040, -1
-5.173041, -1
-1.193936, 0
-1.193937, 0
-2.534079, 0
-2.534070, 0
-3.709275, 0
-3.709275, 0

2.891452, 0
2.891452, 0
2.288246, 0
2.288246, 0
5.857865, -1
5.857865, -1
5.309055, -1
5.309055, -1
-8.740320, -1
-8.740320, -1
-1.717847, 0
-1.717847, 0
-4.290297, 0
-4.290297, 0

2.660117, 0
2.000000, 0
7.823110, -8
9.794719, -9
-4.842877, -8
-2.403279, 0
-6.256838, 0

z

4.0 S=0.0

4.000000, 0
2.493959, 0
7.544057, -1
2.770685, -8
1.968435, -8
-8.900837, -1
-1.452219, 0
-2.000000, 0
-3.603875, 0
-7.302187, 0

3.414214, 0
3.414214, 0
1.785387, 0
1.785387, 0
8.740321, -1
8.740320, -1
-5.857864, -1
-5.857864, -1
-1.025366, 0
-1.025366, 0
-1.256757, 0
-1.256757, 0
-2.288246, 0
-2.288246, 0
-4.917477, 0
-4.917477, 0

3.051374, 0
3.051374, 0
2.000000, 0
2.000000, 0
9.032120, -1
9.032119, -1
-5.173040, -1
-5.173041, -1
-1.193936, 0
-1.193937, 0
-2.534070, 0
-2.534070, 0
-3.709275, 0
-3.709275, 0

2.891452, 0
2.891452, 0
2.288246, 0
2.288246, 0
5.857865, -1
5.857864, -1
5.309054, -1
5.309054, -1
-8.740320, -1
-8.740321, -1
-1.717847, 0
-1.717847, 0
-3.414214, 0
-3.414214, 0
-4.290297, 0
-4.290297, 0

2.921010, 0
2.660118, 0
2.000000, 0
2.971774, -8
0.000000, -128
-4.590934, -8
-1.521753, 0
-2.403279, 0
-5.399256, 0
-6.256838, 0

TABLE I (cont.)

N = 0 γ = 1.00

0.0 S^2 = 4.5

0

1.0 S^2 = 3.5

-7.450581,	-9
-4.679111,	-1
-4.679111;	-1
-1.652704,	0
-1.652704;	0
-3.000000,	0
-3.000000;	0
-3.879385,	0
-3.879385;	0

2.0 S^2 = 2.5

-2.235174,	-8
-1.171573;	0
-4.000000,	0
-6.828427,	0
-4.679111,	-1
-4.679112;	-1
-2.520796,	0
-2.520796;	0
-5.420264,	0
-5.420265,	0
-7.470414,	0
-7.470414;	0
-7.833249,	-1
-7.833249;	-1
-1.652704;	0
-1.652704;	0
-3.895673;	0
-3.895673,	0
-6.136209;	0
-6.136210,	0
-1.509136,	0
-1.509136;	0
-3.000000;	0
-3.000000,	0
-4.656620;	0
-4.656620;	0
-5.834243;	0
-5.834243;	0
-1.939684,	0
-1.939684;	0
-3.382489;	0
-3.382489;	0
-3.879385;	0
-3.879385,	0
-4.451146,	0
-4.451146,	0

3.0 S^2 = 1.5

-6.705523,	-8
-1.171573;	0
-3.228613,	0
-3.228613;	0
-4.000000;	0
-5.519969;	0
-5.519969,	0
-6.828427,	0
-8.253418;	0
-8.253418;	0
-4.679111,	-1
-4.679112,	-1
-1.731272,	0
-1.731272,	0
-2.520796;	0
-2.520796;	0
-4.180682;	0
-4.180682;	0
-4.577711,	0
-4.577711,	0
-5.420265,	0
-5.420265;	0
-5.838732,	0
-5.838732,	0
-7.470414,	0
-7.470414;	0
-7.792219,	0
-7.792219,	0
-7.833249,	-1
-7.833249;	-1
-1.652704;	0
-1.652704;	0
-3.895673;	0
-3.895673,	0
-6.136209;	0
-6.136210,	0
-9.573172,	-1
-9.573173;	-1
-1.509136;	0
-1.509136,	0
-3.000000;	0
-3.000000;	0
-3.000000,	0
-3.000000,	0
-4.627719;	0
-4.627719;	0
-4.656620;	0
-4.656621;	0
-4.685220,	0
-4.685220,	0
-5.834243,	0
-5.834243,	0
-7.357463,	0
-7.357463;	0
-1.037228;	1
-1.037228,	1
-1.091940,	0
-1.091940;	0
-1.939684;	0
-1.939684;	0
-3.069014;	0
-3.069014;	0
-3.382489;	0
-3.382489;	0
-3.879385;	0
-3.879385;	0
-4.451146;	0
-4.451146;	0
-5.674357;	0
-5.674357,	0
-7.259512,	0
-7.259512;	0
-9.052473;	0
-9.052473;	0

TABLE I (cont.)

N = 9 γ = 1·0
(cont.)

4·0 S^2 = 0·5

−4·470348,	−8
−1·171573;	0
−2·535898,	0
−3·226613,	0
−3·726613;	0
−4·000000,	0
−5·000000,	0
−5·519969,	0
−5·519969;	0
−6·828427;	0
−8·253418;	0
−8·253418;	0
−9·464102,	0
−4·679111,	−1
−4·679113;	−1
−1·731272,	0
−1·731272,	0
−2·520796;	0
−2·520796,	0
−3·379435,	0
−3·379435,	0
−3·777010;	0
−3·777010,	0
−4·180682;	0
−4·180682;	0
−4·577711;	0
−4·577711;	0
−5·234170;	0
−5·234171;	0
−5·420265,	0
−5·420265;	0
−5·838732;	0
−5·838732,	0
−7·054094;	0
−7·054094;	0
−7·470414;	0
−7·470414;	0
−7·792219;	0
−7·792219,	0
−1·020800;	1
−1·020800;	1
−7·833349,	−1
−7·833349;	−1
−1·652704,	0
−1·652704,	0
−2·171074,	0
−2·171074;	0
−2·562021;	0
−2·562021,	0
−3·895673;	0
−3·895673,	0
−4·249325;	0
−4·249325;	0
−4·753630;	0
−4·753630;	0
−5·141083;	0
−5·141083;	0
−5·852275,	0
−5·852275;	0
−6·136210;	0
−6·136210;	0
−6·397330;	0
−6·397330,	0
−7·512112,	0
−7·512112;	0
−8·678026;	0
−8·678026;	0
−1·209460,	1
−1·209460;	1
−9·573173,	−1
−9·573173;	−1
−1·509136,	0
−1·509137;	0
−2·619053;	0
−2·619053;	0
−3·000000;	0
−3·000000;	0
−3·000000,	0
−3·000000;	0
−4·627719;	0
−4·627719,	0
−4·656621;	0
−4·656621;	0
−4·685220;	0
−4·685220,	0
−5·834243,	0
−5·834244;	0
−6·399464,	0
−6·399464,	0
−6·670984,	0
−6·670985;	0
−7·357463,	0
−7·357463,	0
−9·310500;	0
−9·310500,	0
−1·037228;	1
−1·037228,	1
−9·983435,	−1
−9·983435;	−1
−1·291940,	0
−1·291940;	0
−1·939684;	0
−1·939684,	0
−3·069014,	0
−3·069014,	0
−3·382489,	0
−3·382489,	0
−3·879385,	0
−3·879386;	0
−4·451146;	0
−4·451146,	0
−4·593645,	0
−4·593645,	0
−5·674358,	0
−5·674358,	0
−6·297294,	0
−6·297294,	0
−7·259512,	0
−7·259512,	0
−8·141983,	0
−8·141983,	0
−8·436648;	0
−8·436648,	0
−9·052474;	0
−9·052474;	0

TABLE I (cont.)

N=10 γ=1.0

S^2=1.0

-7.415058I,	-0
-3.819660,	-I
-3.819660;	-I
-I.38I966,	0
-I.38I966;	0
-2.618034,	0
-2.618034;	0
-3.618034,	0
-3.618034;	0
-4.000000,	0

2.0 S^2=3.0

-4.470348,	-8
-9.358223;	-I
-3.305407;	0
-6.000000;	0
-7.758771;	0

-3.819660,	-I
-3.819661;	-I
-2.065827;	0
-2.065827;	0
-4.642984;	0
-4.642984;	0
-5.909223;	0
-6.909223;	0
-6.553442,	-I
-6.553442;	-I
-I.38I966;	0
-I.38I966;	0
-3.347075;	0
-3.347075;	0
-5.579367;	0
-5.579367;	0
-7.036248;	0
-7.036249;	0

-I.322III,	0
-I.322III;	0
-2.618034;	0
-2.618034;	0
-4.291900;	0
-4.291900;	0
-5.767956;	0
-5.767956;	0

-I.80888I,	0
-I.80888I;	0
-2.880445;	0
-2.880446;	0
-3.618034;	0
-3.618034;	0
-4.540670;	0
-4.540671;	0
-5.I51969;	0
-5.I51969;	0
-2.000000,	0
-4.000000,	0
-4.000000;	0
-4.000000;	0

3.0 S^2=2.0

-4.470348,	-8
-9.358223;	-I
-2.638531;	0
-2.638531;	0
-3.305407;	0
-4.832551;	0
-4.832551;	0
-6.000000;	0
-6.000000;	0
-7.528918;	0
-7.528918;	0
-7.758771;	0

-3.819660,	-I
-3.819662;	-I
-I.387500;	0
-I.387501;	0
-2.065827;	0
-2.065827;	0
-3.409372;	0
-3.409372;	0
-3.938562;	0
-3.938562;	0
-4.642984;	0
-4.642984;	0
-5.438585;	0
-5.438585;	0

-5.600525,	0
-5.600525;	0
-6.715760;	0
-6.715760,	0
-6.909223;	0
-6.909223;	0
-7.483055;	0
-7.483055;	0
-8.545673;	0
-8.545674;	0
-6.553442,	-I
-6.553443;	-I
-I.38I966;	0
-I.38I966;	0
-3.144977;	0
-3.144977,	0
-3.347075;	0
-3.347075;	0
-4.097790;	0
-4.097790;	0
-4.787385;	0
-4.787385;	0
-5.333796;	0
-5.333796;	0
-5.486459;	0
-5.486460;	0
-5.579367;	0
-5.579367;	0
-7.036249;	0
-7.036249;	0
-7.722403;	0
-7.722403;	0
-9.075326;	0
-9.075326;	0
-8.266249,	-I
-8.266250;	-I
-I.322III;	0
-I.322III;	0
-2.618034;	0
-2.618034;	0
-2.653755;	0
-2.653755,	0
-3.887924;	0
-3.887924;	0
-4.291899;	0
-4.291900;	0
-4.373107;	0
-4.373107;	0
-4.854546;	0
-4.854546;	0
-5.767956;	0
-5.767956;	0
-6.434244;	0
-6.434245;	0

TABLE I (cont.)

N=10 γ=1.0
(cont.)

-8.096159;	0
-8.096159;	0
-9.255609,	0
-9.255609;	0
-1.200419,	0
-1.200419;	0
-1.808881;	0
-1.808881;	0
-2.793727;	0
-2.793727;	0
-2.880446;	0
-2.880446;	0
-3.612034;	0
-3.612034;	0
-4.100855,	0
-4.100855;	0
-4.540670;	0
-4.540671;	0
-4.982060,	0
-4.982061;	0
-5.151969;	0
-5.151969;	0
-6.801283;	0
-6.801283;	0
-7.862953;	0
-7.862953;	0
-9.640569;	0
-9.640569;	0
-1.334057,	0
-2.000000;	0
-2.697224;	0
-2.697224;	0
-4.000000;	0
-4.000000;	0
-4.000000;	0
-5.401102;	0
-6.302776;	0
-6.302776;	0
-8.312887;	0
-1.095186;	1

α=0 S^2=1.0

-1.341105,	-7
-9.358223;	-1
-2.022118;	0
-2.638537;	0
-2.638537;	0
-3.030408;	0
-3.659375;	0
-4.381966;	0
-4.381966;	0
-7.832551;	0
-7.832551;	0
-5.552155;	0
-6.000000;	0
-6.000001;	0
-6.618034;	0
-6.618035;	0
-7.529019;	0
-7.529019;	0
-7.758771;	0
-7.904308;	0
-9.877631;	0
-1.318442;	1
-3.819660,	-1
-3.819661;	-1
-1.387500;	0
-1.387501;	0
-2.065827;	0
-2.065827;	0
-2.831061;	0
-2.831061;	0
-3.107284;	0
-3.107284;	0
-3.499372;	0
-3.499372;	0
-3.938562;	0
-3.938563;	0
-4.642984;	0
-4.642984;	0
-4.868085;	0
-4.868085;	0
-5.070977;	0
-5.070978;	0
-5.438585;	0
-5.438585;	0
-5.609525;	0
-5.609525;	0
-5.837044;	0
-5.837044;	0
-6.715762;	0
-6.715763;	0
-6.909233;	0
-6.909234;	0
-7.253493;	0
-7.253493;	0
-7.483055;	0
-7.483055;	0
-8.545673;	0
-8.545673;	0
-8.921703;	0
-8.921703;	0
-1.149233;	1
-1.149233;	1
-6.553443,	-1
-6.553443;	-1
-1.381966;	0
-1.381966;	0
-1.743645;	0
-1.743655;	0
-2.144977;	0
-2.144977;	0
-3.270429;	0
-3.270429;	0
-3.347075;	0
-3.347075;	0
-3.652655;	0
-3.652655;	0
-4.097790;	0
-4.097790;	0
-4.787295;	0
-4.787295;	0
-4.802083;	0
-4.802083;	0
-4.892625;	0
-4.892625;	0
-5.333796;	0
-5.333796;	0
-5.486460;	0
-5.486460;	0
-5.579367;	0
-5.579367;	0
-6.725094;	0
-6.725095;	0
-6.810936,	0
-6.810937;	0
-7.036249;	0
-7.036249;	0
-7.722403;	0
-7.722403;	0
-8.859706;	0
-8.859706;	0
-9.057827;	0
-9.057828;	0
-9.975326,	0
-9.975326;	0
-1.056098,	1
-1.056098;	1
-8.266249,	-1
-8.266249;	-1
-1.322111;	0
-1.322111;	0
-2.200389;	0
-2.200389,	0
-2.618034;	0
-2.618034;	0
-2.653755;	0
-2.653755;	0
-3.859455;	0
-3.859455;	0
-3.887934;	0
-3.887934;	0

TABLE I (cont.)

N = 10 Y = 1.0
(cont.)

-4.291900;	0
-4.291900,	0
-4.373107;	0
-4.373107;	0
-4.854546;	0
-4.854546;	0
-5.409259,	0
-5.409259;	0
-5.767956;	0
-5.767956;	0
-5.828983;	0
-5.828983;	0
-6.434245,	0
-6.434245;	0
-6.798021;	0
-6.798021;	0
-8.096158;	0
-8.096158;	0
-8.304150;	0
-8.304150;	0
-8.435307,	0
-8.435307;	0
-9.255608,	0
-9.255609;	0
-1.078247;	1
-1.078247;	1
-9.010971,	-1
-9.010972;	-1
-1.200419;	0
-1.200419;	0
-1.808881;	0
-1.808881;	0
-2.406141;	0
-2.406141;	0
-2.793728;	0
-2.793728;	0
-2.880446;	0
-2.880446;	0
-3.618034;	0
-3.618034;	0
-3.868566;	0
-3.868566;	0
-4.100855;	0
-4.100855;	0
-4.540671;	0
-4.540671;	0
-4.982060;	0
-4.982061;	0
-5.151969;	0
-5.151969;	0
-5.644155;	0
-5.644155;	0

-6.061359;	0
-6.061359;	0
-6.801383;	0
-6.801383;	0
-6.973176;	0
-6.973176;	0
-7.305876;	0
-7.305876;	0
-7.862953;	0
-7.862953;	0
-8.477235;	0
-8.477235;	0
-8.893973;	0
-8.893974;	0
-9.640670;	0
-9.640670;	0
-1.208656;	1
-1.208656;	1
-1.018270,	0
-1.334057;	0
-2.000000;	0
-2.697224;	0
-2.697224;	0
-4.000000;	0
-4.000000;	0
-4.000000;	0
-4.000000;	0
-5.381966;	0
-5.381966;	0
-5.401192;	0
-6.302776;	0
-6.302776;	0
-7.313241;	0
-7.618034;	0
-7.618034;	0
-8.312887;	0
-9.668487;	0
-1.095186;	1

N = 10 Y = 1.0 S^2 = 0.0

-1.937151,	-7
-9.358323;	-1
-2.022117;	0
-2.638531;	0
-2.638531;	0
-3.305408;	0
-3.322678;	0
-3.659275;	0
-4.381966;	0
-4.381966;	0
-4.832551;	0
-4.832551;	0
-5.097886;	0
-5.352155;	0

-6.000000;	0
-6.000000;	0
-6.618034;	0
-6.618034;	0
-7.523918;	0
-7.523918;	0
-7.758771;	0
-7.904308;	0
-9.033242;	0
-9.877631;	0
-1.254120;	1
-1.318442;	1
-3.819661,	-1
-3.819661;	-1
-1.387500;	0
-1.387501;	0
-2.065827;	0
-2.065827;	0
-2.578692;	0
-2.578692;	0
-2.831062;	0
-2.831062;	0
-3.107284;	0
-3.107284;	0
-3.499372;	0
-3.499372;	0
-3.938563;	0
-3.938563;	0
-4.636140;	0
-4.636140;	0
-4.642985;	0
-4.642985;	0
-4.868085;	0
-4.868085;	0
-5.070978;	0
-5.070978;	0
-5.438535;	0
-5.738586;	0
-5.609526;	0
-5.609526;	0
-5.658744;	0
-5.658744;	0
-5.837044;	0
-5.837044;	0
-6.715763;	0
-6.715763;	0
-6.909224;	0
-6.909224;	0
-7.353485;	0
-7.353484;	0
-7.483055;	0
-7.483055;	0
-8.353852;	0
-8.353852;	0
-8.545673;	0

TABLE I (cont.)

N = 10 γ = 1.0

(cont.)

-8.545674;	0
-8.921703,	0
-8.921704;	0
-1.077257;	1
-1.077257;	1
-1.149233;	1
-1.149233;	1
-6.553443,	-1
-6.553444;	-1
-1.381966;	0
-1.381966;	0
-1.749634;	0
-1.749635;	0
-2.144977;	0
-2.144977;	0
-3.270428;	0
-3.270428;	0
-3.347075;	0
-3.347075;	0
-3.459749;	0
-3.459750;	0
-3.632655,	0
-3.632655;	0
-4.097790;	0
-4.097790;	0
-4.787285;	0
-4.787285;	0
-4.802083;	0
-4.802083;	0
-4.892624;	0
-4.892625;	0
-5.333796;	0
-5.333796;	0
-5.486460;	0
-5.486460;	0
-5.579367;	0
-5.579367;	0
-6.511653;	0
-6.511653;	0
-6.725094;	0
-6.725095;	0
-6.810936;	0
-6.810937;	0
-7.036249;	0
-7.036249;	0
-7.792403;	0
-7.792403;	0
-8.039705,	0
-8.039706;	0
-9.057827;	0
-9.057828;	0
-9.075326;	0
-9.075327;	0
-1.002860;	1
-1.002860,	1
-1.056098,	1
-1.056098;	1

-8.266249,	-1
-8.266250,	-1
-1.322111;	0
-1.322111;	0
-2.037166;	0
-2.037167;	0
-2.200389;	0
-2.200389;	0
-2.618034;	0
-2.618034;	0
-2.653755;	0
-2.653755;	0
-3.859455;	0
-3.859455;	0
-3.887924;	0
-3.887924;	0
-4.291900;	0
-4.291900;	0
-4.373107;	0
-4.373107;	0
-4.854546;	0
-4.854546;	0
-4.906926;	0
-4.906926;	0
-5.409259;	0
-5.409259;	0
-5.767957;	0
-5.767957;	0
-5.828993;	0
-5.828993;	0
-6.434245;	0
-6.434245;	0
-6.437016;	0
-6.437017;	0
-6.798021;	0
-6.798021;	0
-8.083623;	0
-8.083623;	0
-8.096158;	0
-8.096158;	0
-8.304150;	0
-8.304150;	0
-8.435307;	0
-8.435308;	0
-9.255608;	0
-9.255609;	0
-1.053527;	1
-1.053527;	1
-1.078247;	1
-1.078247;	1
-9.610971,	-1
-9.610972;	-1
-1.200419;	0
-1.200419;	0
-1.808881;	0
-1.808881;	0

-2.406141;	0
-2.406141;	0
-2.793729;	0
-2.793729;	0
-2.880446;	0
-2.880446;	0
-3.618034;	0
-3.618034;	0
-3.868566;	0
-3.868566;	0
-4.100855;	0
-4.100855;	0
-4.540671;	0
-4.540671;	0
-4.982061;	0
-4.982061;	0
-5.151969;	0
-5.151969;	0
-5.353785;	0
-5.353785;	0
-5.644155;	0
-5.644155;	0
-6.061259;	0
-6.061259;	0
-6.569151;	0
-6.569151;	0
-6.801293;	0
-6.801294;	0
-6.973175;	0
-6.973176;	0
-7.305876;	0
-7.305876;	0
-7.862953;	0
-7.862953;	0
-8.077066;	0
-8.077066;	0
-8.477235;	0
-8.477235;	0
-8.893973;	0
-8.893974;	0
-9.640670;	0
-9.640670;	0
-1.208656;	1
-1.208656;	1
-8.821637,	-1
-1.018273;	0
-1.334057;	0
-2.000000;	0
-2.697224;	0
-2.697225;	0
-3.788453;	0
-4.000000;	0
-4.000000;	0
-4.000000;	0
-4.000000;	0
-5.381966;	0
-5.381966;	0

TABLE I (cont.)

N = 10 Y = 1.0
(cont.)

-5.401193; 0
-6.302776; 0
-6.302776; 0
-6.974839; 0
-7.131227; 0
-7.313241; 0
-7.618034; 0
-7.618035; 0
-8.312888; 0
-9.192426; 0
-9.668487; 0
-1.095186; 1
-1.403089; 1

RING

N = 11 Y = 1.0

0.0 S^2 = 5.5

0

1.0 S^2 = 4.5

-7.450581, -9

-3.174930, -1
-3.174930; -1

-1.169170, 0
-1.169170; 0

-2.284630, 0
-2.284630; 0

-3.309721, 0
-3.309721; 0

-3.918986, 0
-3.918986; 0

2.0 S^2 = 3.5

-4.470348, -8
-7.639321; -1
-2.763932; 0
-5.236068; 0
-7.236068; 0

-3.174929, -1
-3.174930; -1
-1.718735; 0
-1.718735; 0
-3.984069; 0
-3.984069; 0
-6.249341; 0
-6.249341; 0
-7.649349; 0
-7.649349; 0

-5.550846, -1
-5.550847; -1
-1.169170; 0
-1.169170; 0
-2.882926; 0
-2.882926; 0
-4.999188; 0
-4.999188; 0
-6.711125; 0
-6.711125; 0

-1.158401, 0
-1.158401; 0
-2.284630; 0
-2.284630; 0
-3.887736; 0
-3.887736; 0
-5.493235; 0
-5.493235; 0
-6.485719; 0
-6.485719; 0

-1.654358, 0
-1.654358; 0
-2.473937; 0
-2.473937; 0
-3.309721; 0
-3.309722; 0
-4.414650; 0
-4.414650; 0
-5.316504; 0
-5.316504; 0

-1.959493, 0
-1.959493; 0
-3.572566; 0
-3.572566; 0
-3.918986; 0
-3.918986; 0
-4.296871; 0
-4.296871; 0
-4.536714; 0
-4.536714; 0

3.0 S^2 = 2.5

-1.117587, -7
-7.639321; -1
-2.188575; 0
-2.188575; 0
-2.763932; 0
-4.196791; 0
-4.196791; 0
-5.236068; 0
-5.726648; 0
-5.726648; 0
-6.745235; 0
-6.745235; 0
-7.236068; 0
-8.142752; 0
-8.142752; 0

-3.174929, -1
-3.174932; -1
-1.135293; 0
-1.135293; 0
-1.718735; 0
-1.718735; 0
-2.954334; 0
-2.954334; 0
-3.386952; 0
-3.386953; 0
-3.984069; 0
-3.984069; 0
-4.831293; 0
-4.831294; 0
-5.139461; 0
-5.139461; 0
-5.778472; 0
-5.778472; 0
-5.889532; 0
-5.889532; 0
-6.249341; 0
-6.249341; 0
-7.093307; 0
-7.093308; 0
-7.649349; 0
-7.649349; 0
-7.842725; 0
-7.842725; 0
-9.339368; 0
-9.339368; 0

TABLE I (cont.)

N = 11 γ = 1.0

(cont.)

-5.550847,	-1
-5.550848;	-1
-1.169170;	0
-1.169170;	0
-1.815439;	0
-1.815439;	0
-1.815439;	0
-2.882926;	0
-2.882926;	0
-3.553935;	0
-3.553935;	0
-4.348403;	0
-4.348403;	0
-4.488102;	0
-4.488102;	0
-4.999188;	0
-4.999188;	0
-5.183598;	0
-5.183598;	0
-5.471819;	0
-5.471819;	0
-6.711125;	0
-6.711125;	0
-6.725767;	0
-6.725767;	0
-6.901796;	0
-6.901796;	0
-8.394972;	0
-8.394973;	0
-9.083309;	0
-9.083309;	0

-7.167693,	-1
-7.167694;	-1
-1.158401;	0
-1.158401;	0
-2.284630;	0
-2.284630;	0
-2.343700;	0
-2.343700;	0
-3.268762;	0
-3.268762;	0
-3.887737;	0
-3.887737;	0
-3.889234;	0
-3.889234;	0
-4.765508;	0
-4.765508;	0
-5.065912;	0
-5.065913;	0
-5.493235;	0
-5.493236;	0
-5.609453;	0
-5.609453;	0

-6.485719;	0
-6.485720;	0
-7.503069;	0
-7.503070;	0
-8.146597;	0
-8.146597;	0
-9.698767;	0
-9.698768;	0

-1.096697,	0
-1.096697;	0
-1.654358;	0
-1.654358;	0
-2.473937;	0
-2.473937;	0
-2.614195;	0
-2.614195;	0
-3.309722;	0
-3.309722;	0
-3.969657;	0
-3.969657;	0
-4.368400;	0
-4.368400;	0
-4.414650;	0
-4.414650;	0
-4.502452;	0
-4.502452;	0
-5.316504;	0
-5.316507;	0
-6.241020;	0
-6.241020;	0
-6.807678;	0
-6.807678;	0
-7.396774;	0
-7.396774;	0
-8.812735;	0
-8.812736;	0
-1.094021;	1
-1.094021;	1

-1.306101,	0
-1.306101;	0
-1.959493;	0
-1.959493;	0
-2.370427;	0
-2.370427;	0
-2.551300;	0
-2.551300;	0
-3.572566;	0
-3.572566;	0
-3.634502;	0
-3.634502;	0
-3.918986;	0
-3.918986;	0
-4.296871;	0
-4.296871;	0

-4.536714;	0
-4.536714;	0
-5.023545;	0
-5.023545;	0
-5.470593;	0
-5.470593;	0
-6.185718;	0
-6.185718;	0
-7.503589;	0
-7.503589;	0
-8.759366;	0
-8.759366;	0
-1.007940;	1
-1.007940;	1

4.0 S^2 = 1.5

-2.533197,	-7
-7.639321;	-1
-1.645181;	0
-2.188575;	0
-2.188575;	0
-2.763932;	0
-3.171573;	0
-3.794604;	0
-3.794604;	0
-4.196791;	0
-4.196792;	0
-5.134646;	0
-5.134646;	0
-5.236068;	0
-5.594927;	0
-5.594927;	0
-5.726648;	0
-5.726648;	0
-6.643275;	0
-6.745235;	0
-6.745235;	0
-6.836468;	0
-6.836468;	0
-7.236068;	0
-8.142752;	0
-8.142752;	0
-8.828428;	0
-1.063936;	1
-1.063936;	1
-1.171155;	1

-3.174930,	-1
-3.174932;	-1
-1.135293;	0
-1.135293;	0
-1.718735;	0
-1.718735;	0
-2.382497;	0
-2.382498;	0
-2.583783;	0
-2.583784;	0

TABLE I (cont.)

N = 11 γ = 1.0

(cont.)

-2.954334,	0
-2.954334,	0
-3.386953,	0
-3.386953,	0
-3.674267,	0
-3.674268,	0
-3.984069,	0
-3.984069,	0
-4.332464,	0
-4.332464,	0
-4.680063,	0
-4.680063,	0
-4.831294,	0
-4.831297,	0
-4.908023,	0
-4.908023,	0
-5.139461,	0
-5.139461,	0
-5.345187,	0
-5.345187,	0
-5.778472,	0
-5.778472,	0
-5.889532,	0
-5.889532,	0
-6.094276,	0
-6.094276,	0
-6.249341,	0
-6.249341,	0
-6.638839,	0
-6.638840,	0
-6.723511,	0
-6.723511,	0
-7.093308,	0
-7.093308,	0
-7.649350,	0
-7.649350,	0
-7.748381,	0
-7.748381,	0
-7.842726,	0
-7.842726,	0
-8.262716,	0
-8.262717,	0
-9.279299,	0
-9.279300,	0
-9.339368,	0
-9.339368,	0
-1.022780,	1
-1.022780,	1
-1.219381,	1
-1.219381,	1
-5.550847,	-1
-5.550847,	-1
-1.169170,	0
-1.169170,	0
-1.438830,	0
-1.438830,	0
-1.815439,	0
-1.815439,	0
-2.882926,	0
-2.882926,	0
-2.898653,	0
-2.898653,	0
-3.109621,	0
-3.109621,	0
-3.553935,	0
-3.553935,	0
-3.996471,	0
-3.996471,	0
-4.348403,	0
-4.348403,	0
-4.488102,	0
-4.488102,	0
-4.603665,	0
-4.603665,	0
-4.951957,	0
-4.951957,	0
-4.999189,	0
-4.999189,	0
-5.183598,	0
-5.183598,	0
-5.471819,	0
-5.471819,	0
-5.878118,	0
-5.878118,	0
-5.985096,	0
-5.985096,	0
-6.711125,	0
-6.711126,	0
-6.725767,	0
-6.725767,	0
-6.884071,	0
-6.884072,	0
-6.901796,	0
-6.901797,	0
-8.122639,	0
-8.122639,	0
-8.142891,	0
-8.142891,	0
-8.248988,	0
-8.248988,	0
-8.394973,	0
-8.394973,	0
-9.083309,	0
-9.083310,	0
-9.142302,	0
-9.142303,	0
-1.074703,	1
-1.074703,	1
-1.348404,	1
-1.348404,	1
-7.116769,	-1
-7.116769,	-1
-1.158402,	0
-1.158402,	0
-1.188017,	0
-1.188017,	0
-2.284630,	0
-2.284630,	0
-2.543706,	0
-2.543706,	0
-3.063394,	0
-3.063394,	0
-3.268762,	0
-3.268762,	0
-3.432792,	0
-3.432792,	0
-3.887737,	0
-3.887737,	0
-3.889234,	0
-3.889234,	0
-4.513866,	0
-4.513866,	0
-4.594448,	0
-4.594448,	0
-4.765508,	0
-4.765508,	0
-5.065913,	0
-5.065913,	0
-5.075033,	0
-5.075033,	0
-5.403236,	0
-5.403236,	0
-5.609453,	0
-5.609454,	0
-6.193256,	0
-6.193256,	0
-6.454734,	0
-6.454734,	0
-6.485426,	0
-6.485426,	0
-7.295826,	0
-7.295826,	0
-7.326187,	0
-7.326187,	0
-7.563076,	0
-7.503076,	0
-7.994721,	0
-7.994721,	0
-8.146508,	0
-8.146508,	0
-8.461621,	0
-8.461621,	0
-8.898269,	0
-8.898270,	0
-9.698768,	0
-9.698768,	0
-9.712769,	0
-9.712770,	0
-1.804467,	1
-1.804467,	1

TABLE I (cont.)

N = 11 Y = 1.0

(cont.)

-8.05931,	-1
-8.05931,	-1
-1.09697,	.0
-1.09697,	0
-1.65435,	0
-1.65435,	0
-2.12425,	0
-2.12425,	0
-4.73937,	0
-4.47393,	0
-4.61495,	0
-4.61495,	0
-3.09820,	0
-3.09820,	0
-3.50976,	0
-3.30976,	0
-3.47765,	0
-3.47765,	0
-3.96954,	0
-3.96954,	0
-4.36840,	0
-4.36840,	0
-4.41465,	0
-4.41465,	0
-4.50845,	0
-4.50845,	0
-4.89689,	0
-4.89689,	0
-5.31650,	0
-5.31650,	0
-5.62755,	0
-5.62755,	0
-5.97597,	0
-5.97597,	0
-5.99116,	0
-6.12405,	0
-6.12405,	0
-6.24105,	0
-6.24105,	0
-6.50837,	0
-6.30837,	0
-6.80767,	0
-6.80767,	0
-7.39677,	0
-7.39677,	0
-7.71468,	0
-7.71468,	0
-8.63176,	0
-8.63176,	0
-8.09446,	0
-8.09446,	0
-8.81873,	0
-8.81873,	0
-9.50732,	0
-9.50732,	0
-9.56828,	0
-9.56828,	0
-1.09402,	1
-1.09402,	1
-1.00939,	1
-1.00939,	1
-9.85863,	-1
-9.85863,	-1
-1.20610,	.0
-1.30610,	0
-9.59493,	0
-9.59493,	0
-1.81555,	0
-1.81556,	0
-3.70427,	0
-3.70427,	0
-5.51306,	0
-5.51306,	0
-3.51664,	0
-3.51664,	0
-3.57256,	0
-3.57256,	0
-3.63450,	0
-3.63450,	0
-3.91898,	0
-3.91898,	0
-4.29687,	0
-4.29687,	0
-4.53675,	0
-4.53675,	0
-4.63743,	0
-4.63743,	0
-4.99064,	0
-4.99064,	0
-5.02345,	0
-5.02345,	0
-5.46944,	0
-5.46944,	0
-5.47059,	0
-5.47059,	0
-6.18571,	0
-6.18571,	0
-6.41628,	0
-6.41628,	0
-6.81403,	0
-6.81403,	0
-6.92395,	0
-6.92395,	0
-7.50358,	0
-7.50358,	0
-7.56712,	0
-7.56712,	0
-8.15344,	0
-8.15344,	0
-8.75936,	0
-8.75936,	0
-8.87034,	0
-8.87034,	0
-9.18655,	0
-9.18655,	0
-1.00791,	1
-1.00791,	1
-1.08540,	1
-1.08540,	1
-1.16367,	1
-1.16367,	1
-1.17115,	1

5.0 0.5

-1.93715,	-7
-7.63932,	-2
-1.64518,	.0
-2.18857,	0
-2.18857,	0
-7.63932,	0
-2.85269,	0
-2.85270,	0
-3.17257,	0
-3.79460,	0
-3.79460,	0
-4.29679,	0
-4.29679,	0
-4.86068,	0
-4.86068,	0
-5.13647,	0
-5.13647,	0
-5.23068,	0
-5.37888,	0
-5.37889,	0
-5.59427,	0
-5.59427,	0
-5.72664,	0
-5.72664,	0
-6.64327,	0
-6.74523,	0
-6.74523,	0
-6.83648,	0
-6.83648,	0
-7.23668,	0
-8.02127,	0
-8.02127,	0
-8.14275,	0
-8.14275,	0
-8.82842,	0
-9.79537,	0
-9.79537,	0
-1.06393,	1
-1.06393,	1
-1.10911,	1
-1.10911,	1
-1.17115,	1

TABLE I (cont.)

N = 11 Y = 1.0

(cont.)

-3.17403,	-1
-3.17493,	-1
-1.13529,	0
-1.13593,	0
-1.71873,	0
-1.71873,	0
-.09576,	0
-.09576,	0
-.08249,	0
-.38649,	0
-.58573,	0
-.58748,	0
-.95433,	0
-.95433,	0
-.25613,	0
-.25613,	0
-.38653,	0
-.38653,	0
-.67428,	0
-.67428,	0
-.96469,	0
-.98409,	0
-.09242,	0
-.09242,	0
-.33246,	0
-.33246,	0
-.67457,	0
-.67457,	0
-.68006,	0
-.68006,	0
-.83129,	0
-.83129,	0
-.90826,	0
-.90826,	0
-.95588,	0
-.95588,	0
-1.13946,	0
-1.13946,	0
-1.24587,	0
-1.24587,	0
-1.45184,	0
-1.77847,	0
-1.77847,	0
-1.88953,	0
-1.88953,	0
-2.09427,	0
-2.09427,	0
-2.40341,	0
-2.40341,	0
-2.82259,	0
-2.82259,	0
-3.09884,	0
-3.09884,	0
-3.72356,	0
-3.72356,	0
-4.09243,	0
-4.09243,	0
-4.33246,	0
-4.33246,	0
-4.67457,	0
-4.67457,	0
-4.68006,	0
-4.68006,	0
-4.83129,	0
-4.83129,	0
-4.90826,	0
-4.90826,	0
-4.95588,	0
-4.95588,	0
-5.13946,	0
-5.13946,	0
-5.24587,	0
-5.24587,	0
-5.45184,	0
-5.77847,	0
-5.77847,	0
-5.88953,	0
-5.88953,	0
-6.09427,	0
-6.09427,	0
-6.24034,	0
-6.24034,	0
-6.28259,	0
-6.28259,	0
-6.62884,	0
-6.62884,	0
-6.72355,	0
-6.72355,	0

-4.03643,	0
-4.01846,	0
-4.09336,	0
-4.09336,	0
-4.64250,	0
-4.64250,	0
-4.74838,	0
-4.74838,	0
-4.84638,	0
-4.84638,	0
-4.87272,	0
-4.87272,	0
-4.88908,	0
-4.88908,	0
-4.89722,	0
-4.89722,	0
-4.89865,	0
-4.89865,	0
-4.90462,	0
-4.90462,	0
-4.90463,	0
-4.90463,	0
-4.90962,	0
-4.90962,	0
-4.91539,	0
-4.91539,	0
-4.99647,	0
-4.99647,	0
-5.00000,	0
-5.00000,	0
-5.00000

TABLE I (cont.)

N = 11 Y = 1.0

(cont.)

-7.167695,	-1
-7.167695,	-1
-1.158401,	0
-1.158401,	0
-1.682653,	0
-1.682653,	0
-1.681178,	0
-1.680178,	0
-2.284630,	0
-2.284630,	0
-3.543701,	0
-3.343701,	0
-3.063947,	0
-3.063947,	0
-3.203027,	0
-3.203027,	0
-3.768763,	0
-3.768763,	0
-3.432521,	0
-3.432521,	0
-3.432521,	0
-3.432521,	0
-3.889343,	0
-3.889343,	0
-3.889343,	0
-4.133371,	0
-4.133371,	0
-4.513866,	0
-4.513866,	0
-4.504448,	0
-4.504448,	0
-4.765508,	0
-4.765509,	0
-5.065913,	0
-5.065913,	0
-5.075033,	0
-5.075034,	0
-5.493226,	0
-5.493226,	0
-5.609453,	0
-5.609454,	0
-5.831891,	0
-5.831891,	0
-6.034233,	0
-6.034233,	0
-6.084233,	0
-6.193250,	0
-6.193250,	0
-6.454734,	0
-6.454734,	0
-6.485420,	0
-6.485720,	0
-6.559624,	0
-6.559624,	0
-7.040383,	0
-7.040383,	0
-7.295836,	0
-7.295836,	0
-7.326183,	0
-7.326183,	0
-7.399471,	0
-7.399471,	0
-8.146597,	1
-8.146597,	1
-8.201455,	1
-8.201455,	1
-8.493407,	1
-8.059301,	-1
-8.059301,	-1
-1.096697,	0
-1.096697,	0
-1.654359,	0
-1.654358,	0
-1.930967,	0
-1.930967,	0
-1.205459,	0
-1.205459,	0
-1.275278,	0
-1.425483,	0
-1.678768,	0
-1.698668,	0
-1.727706,	0
-1.727706,	0
-1.826535,	1
-1.826535,	1
-1.846593,	1
-1.846593,	1
-1.846593,	1
-1.846593,	1
-2.208353,	1
-2.208353,	1
-2.290821,	0
-2.290821,	0
-2.290821,	0
-2.509753,	0
-2.509753,	0
-3.177584,	0
-3.475685,	0
-3.596585,	0
-3.596585,	0
-4.323026,	0
-4.323026,	0
-4.363068,	0
-4.363068,	0
-4.368402,	0
-4.368402,	0
-4.464659,	0
-4.464659,	0
-4.465421,	0
-4.465421,	0
-4.465421,	0
-4.465421,	0
-4.599601,	0
-4.599601,	0
-4.699601,	0
-4.699601,	0
-5.021659,	0
-5.021659,	0
-5.021659,	0
-5.058402,	0
-5.058402,	0
-5.062459,	0
-5.062459,	0
-5.068459,	0
-5.068459,	0
-5.099402,	0
-5.099402,	0
-6.124045,	0
-6.124045,	0
-6.124045

TABLE I (cont.)

$N = 11 \quad \gamma = 1.0$

(cont.)

-8.250652	-1
-8.250656	-1
-9.858633	-1
-9.858634	-1
-1.306101	0
-1.306101	0
-1.059493	0
-1.059493	0
-2.181556	0
-2.181556	0
-2.370427	0
-2.370427	0
-2.551306	0
-2.551306	0
-3.049229	0
-3.049229	0
-3.516648	0
-3.516648	0
-3.572566	0
-3.572566	0
-3.634502	0
-3.634503	0
-5.091886	0
-5.091887	0
-4.296872	0
-4.296872	0
-4.536734	0
-4.536734	0
-4.637433	0
-4.637434	0
-4.637234	0
-4.637234	0
-4.990642	0
-4.990642	0
-5.023546	0
-5.023546	0
-5.469449	0
-5.469449	0
-5.470594	0
-5.470594	0
-5.861639	0
-5.861639	0
-6.060142	0
-6.060144	0
-6.185736	0
-6.185736	0
-6.352771	0
-6.352772	0
-6.418622	0
-6.418622	0
-6.814028	0
-6.814028	0

-6.923954	0
-6.923954	0
-7.032875	0
-7.032874	0
-4.151389	0
-4.151389	0
-4.503589	0
-4.503590	0
-4.567126	0
-4.567127	0
-8.153456	0
-8.153456	0
-8.385702	0
-8.385702	0
-8.683294	0
-8.683294	0
-8.759366	0
-8.759367	0
-8.870345	0
-8.870346	0
-9.126575	0
-9.126575	0
-1.000740	1
-1.000740	1
-1.042226	1
-1.042226	1
-1.085469	1
-1.085469	1
-1.163679	1
-1.163679	1
-1.234755	1
-1.234755	1

TABLE II : Ring Eigenvalues: $\gamma = 0.5$.

RING

N = 2 γ = 0.5

0 S^2 = 1.0

0.000000, 0

1 S^2 = 0.0

-1.000000, 0
-3.000000, 0

RING

N = 3 γ = 0.5

0 S^2 = 1.5

0.000000, 0

1 S^2 = 0.5

-1.000000, 0
-2.500000, 0
-2.500000, 0

RING

N = 4 γ = 0.5

0 S^2 = 2.0

2.000000, 0

1 S^2 = 1.0

1.000000, 0
0.000000, 0
0.000000, 0
-1.000000, 0

2 S^2 = 0.0

7.320508, -1
-2.732051, 0
0.000000, 0
0.000000, 0
0.000000, 0
-2.000000, 0

RING

N = 5 S^2 = 0.5

0 S^2 = 2.5

0.000000, 0

1 S^2 = 1.5

-1.000000, 0
-1.690983, 0
-2.809017, 0
-2.809017, 0
-1.690983, 0

2 S^2 = 0.5

-1.381966, 0
-3.618034, 0

-1.783659, 0
-5.025358, 0

-1.945299, 0
-3.745684, 0

-1.945299, 0
-3.745684, 0

-1.783659, 0
-5.025358, 0

RING

N = 6 γ = 0.50

0 S^2 = 3

3.000000, 0

1 S^2 = 2

2.000000, 0
1.500000, 0
5.000000, -1
0.000000, 0
5.000000, -1
1.500000, 0

2 S^2 = 1

0.000000, 0
1.561553, 0
-2.561553, 0
1.322876, 0
-1.322876, 0
-3.778200, -1
1.131771, 0
-1.753951, 0
1.000000, 0
-1.000000, 0
-3.778200, -1
1.131771, 0
-1.753951, 0
1.322876, 0
-1.322876, 0

3 S^2 = 0

0.000000, 0
-2.000000, 0
1.449490, 0
-3.449490, 0
-7.807764, -1
1.280776, 0
-1.500000, 0
-7.807764, -1
1.280776, 0
-1.500000, 0
-5.000000, -1
1.186141, 0
-1.686141, 0
-5.000000, -1
1.186141, 0
-1.686141, 0
0.000000, 0
-1.321637, 0
1.177410, 0
-3.855773, 0

TABLE II (cont.)

RING

N = 7. γ = 0.50

0 S^2 = 3.5

0.000000, 0

1 S^2 = 2.5

-1.000000, 0
-1.376510; 0
-2.222521; 0
-2.900969; 0
-2.900969; 0
-2.222521; 0
-1.376510; 0

.2 S^2 = 1.5

-2.652704, 0
-1.467911; 0
-4.879385; 0
-3.754560; 0
-1.619465; 0
-5.526945; 0
-3.074517; 0
-1.800891; 0
-4.501101; 0
-3.881229; 0
-1.975277; 0
-4.366014; 0
-3.881229; 0
-1.975277; 0
-4.366014; 0
-3.074517; 0
-1.800891; 0
-4.501101; 0
-3.754560; 0
-1.619465; 0
-5.526945; 0

3.0-S^2 = 0.5

-1.622797, 0
-2.726109, 0
-4.500000, 0
-4.500000, 0
-5.651093; 0

-1.696767, 0
-1.696767; 0
-3.254305; 0
-3.254305; 0
-3.945745, 0
-3.945745; 0
-4.906350; 0
-4.906350; 0
-6.419354; 0
-6.419354; 0

-1.764077, 0
-1.764078, 0
-3.257695, 0
-3.257695; 0
-3.794426; 0
-3.794426, 0
-4.700034, 0
-4.700034; 0
-7.384736, 0
-7.384736; 0

-1.798689, 0
-1.798689; 0
-2.970432; 0
-2.970432; 0
-4.266100; 0
-4.266101; 0
-4.317750; 0
-4.317751; 0
-6.023538; 0
-6.023538; 0

RING

N = 8 γ = 0.50

0.0 S^2 = 4.0

4.000000, 0

1.0 S^2 = 3.0

3.000000, 0

2.707107, 0
2.707107, 0

2.000000, 0
2.000000, 0

1.292893, 0
1.292893, 0

1.000000, 0

2.0 S^2 = 2.0

2.516580, 0
1.552409, 0
-2.873358, -1
-1.781653, 0

2.414214, 0
2.414214, 0
6.589186, -1
6.589186, -1
-1.073132, 0
-1.073132, 0

N = 8 γ = 0.5 (cont.)

2.252962,	0
2.252962,	0
1.153548,	0
1.153548,	0
-1.535475,	-1
-1.535475,	-1
-1.252962,	0
-1.252962,	0

2.073132,	0
2.073132,	0
3.410814,	-1
3.410814,	-1
-4.142136,	-1
-4.142136,	-1
2.000000,	0
0.000000,	0
0.000000,	0
0.000000,	0

3.0 $S^2 = 1.0$

2.348894,	0
1.395932,	0
1.862645,	-9
-2.222805,	-9
-1.000000,	0
-1.000000,	0
-2.744826,	0
2.312602,	0
2.312602,	0
1.025796,	0
1.025796,	0
4.489752,	-1
4.489752,	-1
-4.569070,	-1
-4.569070,	-1
-7.676647,	-1
-7.676647,	-1
-1.913007,	0
-1.913007,	0
-3.356902,	0
-3.356902,	0

2.261097,	0
2.261097,	0
9.252571,	-1
9.252570,	-1
6.029699,	-1
6.029698,	-1
-4.173907,	-1
-4.173908,	-1
-7.039294,	-1
-7.039294,	-1
-2.107169,	0
-2.107169,	0
-2.560835,	0
-2.560835,	0
2.217989,	0
2.217989,	0
1.086758,	0
1.086758,	0
3.102177,	-1
3.102177,	-1
-5.554979,	-2
-5.554980,	-2
-6.227553,	-1
-6.227554,	-1
-2.176887,	0
-2.176887,	0
-2.321676,	0
-2.321676,	0
-2.593783,	0
-2.593783,	0
2.243037,	0
2.243037,	0
1.073132,	0
1.073132,	0
3.452610,	-1
3.452610,	-1
-1.438521,	-1
-1.438521,	-1
-6.589186,	-1
-6.589186,	-1
-1.345261,	0
-1.345261,	0
-2.414214,	0
-2.414214,	0
-3.099185,	0
-3.099185,	0
2.237757,	0
1.193743,	0
6.064811,	-1
3.602892,	-9
-1.373701,	-8
-5.706347,	-1
-1.219766,	0
-1.842443,	0
-3.624472,	0
-4.780665,	0

-1.360006,	0
-1.360006,	0
-2.869546,	0
-2.869546,	0
2.199114,	0
1.000000,	0
7.450580,	-9
5.397605,	-78
-4.527204,	-1
-1.766757,	0
-3.979637,	0

4.0 $S^2 = 0.0$

2.312706,	0
1.346496,	0
3.676806,	-1
5.415075,	-25
-1.396984,	-9
-8.421197,	-1
-1.071106,	0
-2.000000,	0
-3.074228,	0
-5.039429,	0
2.290257,	0
2.290257,	0
1.042874,	0
1.042874,	0
4.142136,	-1
4.142135,	-1
-3.410814,	-1
-3.410814,	-1
-7.308419,	-1
-7.308420,	-1
-1.312032,	0
-1.312032,	0
-2.073132,	0
-2.073132,	0
-3.290257,	0
-3.290257,	0
2.261626,	0
2.261626,	0
8.677206,	-1
8.677206,	-1
7.217769,	-1
7.217769,	-1
3.538627,	-1
3.538627,	-1
-4.848404,	-1
-4.848404,	-1
-6.278006,	-1
-6.278006,	-1

RING

N = 9; γ = 0.50

0.0 S^2 = 4.5

0.000000, 0

1.0 S^2 = 3.5

-1.000000, 0

-1.233956, 0
-1.233956, 0

-1.826352, 0
-1.826352, 0

-2.500000, 0
-2.500000, 0

-2.939693, 0
-2.939693, 0

2.0 S^2 = 2.5

-1.491519, 0
-3.320357, 0
-3.825785, 0
-5.362340, 0

-1.564790, 0
-1.564790, 0
-3.044069, 0
-3.044069, 0
-4.608323, 0
-4.608323, 0
-5.722511, 0
-5.722511, 0

-1.704839, 0
-1.704839, 0
-2.677439, 0
-2.677439, 0
-3.822450, 0
-3.822450, 0
-5.029228, 0
-5.029228, 0

-1.875107, 0
-1.875107, 0
-3.430409, 0
-3.430409, 0

3.0 S^2 = 1.5

-1.661339, 0
-2.548943, 0
-3.636245, 0
-3.636245, 0
-4.519120, 0
-4.780058, 0
-4.780058, 0
-6.270597, 0
-7.083698, 0

-1.602519, 0
-1.602519, 0
-2.813186, 0
-2.813186, 0
-3.279059, 0
-3.279059, 0
-4.025008, 0
-4.025008, 0
-4.442880, 0
-4.442880, 0
-4.937078, 0
-4.937078, 0
-5.409562, 0
-5.409562, 0
-6.679222, 0
-6.679222, 0
-6.731488, 0
-6.731488, 0

-1.723726, 0
-1.723726, 0
-2.942852, 0
-2.942852, 0
-3.158315, 0
-3.158315, 0
-4.113805, 0
-4.113805, 0
-4.324211, 0
-4.324211, 0

-4.283393, 0
-4.283393, 0
-4.911091, 0
-4.911091, 0

-1.984923, 0
-1.984923, 0
-3.688920, 0
-3.688920, 0
-3.931093, 0
-3.931098, 0
-4.221411, 0
-4.221411, 0

-4.723376, 0
-4.723377, 0
-5.861949, 0
-5.861949, 0
-5.882839, 0
-5.882839, 0
-7.198927, 0
-7.198928, 0

-1.767158, 0
-1.767158, 0
-2.855409, 0
-2.855409, 0
-3.409093, 0
-3.409098, 0
-3.827420, 0
-3.827420, 0
-4.470997, 0
-4.470998, 0
-4.580054, 0
-4.580054, 0
-4.863637, 0
-4.863637, 0
-5.734544, 0
-5.734544, 0
-6.396846, 0
-6.396846, 0
-8.094838, 0
-8.094838, 0

-1.796172, 0
-1.796172, 0
-2.980264, 0
-2.980264, 0
-3.557028, 0
-3.557028, 0
-3.742351, 0
-3.742351, 0
-4.397375, 0
-4.397375, 0
-4.443127, 0
-4.443127, 0
-5.442253, 0
-5.442253, 0
-6.324007, 0
-6.324008, 0
-7.317424, 0
-7.317424, 0

4.0 S^2 = 0.5

-1.706653, 0
-2.646357, 0
-3.368772, 0
-3.641084, 0
-3.641084, 0

TABLE (cont.)

N = 9 γ = 0.5
(cont.)

-1.744194, 0
-1.744194, 0
-2.886851, 0
-2.886851, 0
-3.273795, 0
-3.273795, 0
-3.663759, 0
-3.663759, 0
-3.941032, 0
-3.941032, 0
-4.398402, 0
-4.398402, 0
-4.672265, 0
-4.672265, 0
-4.889041, 0
-4.889041, 0
-5.836883, 0
-5.836883, 0
-5.894803, 0
-5.894804, 0
-6.118723, 0
-6.118723, 0
-6.595398, 0
-6.595398, 0
-7.645168, 0
-7.645168, 0
-8.939689, 0
-8.939689, 0

-1.751988, 0
-1.751988, 0
-2.805242, 0
-2.805242, 0
-3.407907, 0
-3.407907, 0
-3.523443, 0
-3.523443, 0
-3.762142, 0
-3.762142, 0
-4.497373, 0
-4.497373, 0
-4.548105, 0
-4.548105, 0
-4.797179, 0
-4.797179, 0
-5.567591, 0
-5.567592, 0
-5.858279, 0
-5.858279, 0
-6.559555, 0
-6.559555, 0
-6.946508, 0
-6.946508, 0
-7.167770, 0
-7.167770, 0
-8.040876, 0
-8.040876, 0

-4.628823, 0
-4.644136, 0
-4.644136, 0
-5.708664, 0
-5.708664, 0
-6.615078, 0
-7.006116, 0
-7.006117, 0
-8.034317, 0

-1.715036, 0
-1.715036, 0
-2.820570, 0
-2.820570, 0
-3.336177, 0
-3.336177, 0
-3.775926, 0
-3.775926, 0
-3.929871, 0
-3.929871, 0
-4.449773, 0
-4.449773, 0
-4.762061, 0
-4.762061, 0
-4.810621, 0
-4.810621, 0
-5.614681, 0
-5.614681, 0
-5.934419, 0
-5.934419, 0
-6.325795, 0
-6.325795, 0
-6.778496, 0
-6.778496, 0
-7.058323, 0
-7.058323, 0
-8.514607, 0
-8.514607, 0

-1.730367, 0
-1.730367, 0
-3.034355, 0
-3.034355, 0
-3.035145, 0
-3.035145, 0
-3.444300, 0
-3.444300, 0
-4.190236, 0
-4.190287, 0
-4.205021, 0
-4.205021, 0
-4.757759, 0
-4.757760, 0
-5.222763, 0
-5.222763, 0
-5.610301, 0
-5.610301, 0
-5.901958, 0
-5.901959, 0
-6.091105, 0
-6.091106, 0
-6.590203, 0
-6.590203, 0
-7.439212, 0
-7.439212, 0
-9.686919, 0
-9.686919, 0

RING

N = 10 γ=0.50

0.0 S^2 = 5.0

0.000000, 0

1.0 S^2 = 4.0

-1.000000, 0

-1.190983, 0
-1.190983, 0

-1.690983, 0
-1.690983, 0

-2.309017, 0
-2.309017, 0

-2.809017, 0
-2.809017, 0

-3.000000, 0

TABLE I (cont.)

N = 10 γ = 0.5

(cont.)

δ^2 = 3.0 S^2 = 2.0

-1.495697,	0
-2.237866,	0
-3.474344,	0
-4.922159,	0
-5.869935,	0
-1.550926,	0
-1.550926,	0
-2.828381,	0
-2.828381,	0
-4.200809,	0
-4.200809,	0
-5.419884,	0
-5.419884,	0
-1.671747,	0
-1.671747,	0
-2.551244,	0
-2.551244,	0
-3.538200,	0
-3.538200,	0
-4.728228,	0
-4.728228,	0
-5.510581,	0
-5.510581,	0
-1.827347,	0
-1.827347,	0
-3.226203,	0
-3.226203,	0
-4.082147,	0
-4.082147,	0
-4.864303,	0
-4.864303,	0
-1.952254,	0
-1.952254,	0
-3.433344,	0
-3.433344,	0
-3.785341,	0
-3.785341,	0
-4.255155,	0
-4.255155,	0
-4.573906,	0
-4.573906,	0
-2.000000,	0
-4.000000,	0
-4.000000,	0
-4.000000,	0

δ^2 = 3.0 S^2 = 2.0

-1.664872,	0
-2.523475,	0
-3.375551,	0
-3.375551,	0
-4.170582,	0
-4.448902,	0
-4.448902,	0
-5.000000,	0
-5.737535,	0
-6.675547,	0
-6.675547,	0
-6.953537,	0
-1.679440,	0
-1.679440,	0
-2.715690,	0
-2.715690,	0
-3.090125,	0
-3.090125,	0
-3.701911,	0
-3.701911,	0
-4.132070,	0
-4.132070,	0
-4.698135,	0
-4.698135,	0
-4.887370,	0
-4.887371,	0
-4.981671,	0
-4.981672,	0
-6.144257,	0
-6.144257,	0
-6.345456,	0
-6.345456,	0
-6.724775,	0
-6.724775,	0
-7.208119,	0
-7.208119,	0
-1.713428,	0
-1.713423,	0
-2.847899,	0
-2.847899,	0
-2.998394,	0
-2.998394,	0
-3.847478,	0
-3.847478,	0
-3.974902,	0
-3.974902,	0
-4.645880,	0
-4.645880,	0
-4.794344,	0
-4.794344,	0

-5.311342,	0
-5.311342,	0
-5.570763,	0
-5.570763,	0
-6.441704,	0
-6.441704,	0
-6.728248,	0
-6.728248,	0
-7.934137,	0
-7.934137,	0
-1.754100,	0
-1.754100,	0
-2.804761,	0
-2.804761,	0
-3.232315,	0
-3.232315,	0
-3.622264,	0
-3.622265,	0
-4.160341,	0
-4.160341,	0
-4.417569,	0
-4.417569,	0
-4.494541,	0
-4.494542,	0
-4.698950,	0
-4.698950,	0
-5.716212,	0
-5.716212,	0
-5.926376,	0
-5.926376,	0
-6.876924,	0
-6.876924,	0
-7.486631,	0
-7.486632,	0
-1.787312,	0
-1.787312,	0
-2.939329,	0
-2.939330,	0
-3.365892,	0
-3.365892,	0
-3.536992,	0
-3.536992	0
-4.244154,	0
-4.244154,	0
-4.248087,	0
-4.248087,	0
-4.569412,	0
-4.569413,	0
-5.125759,	0
-5.125759,	0
-5.380033,	0
-5.380033,	0
-6.126853,	0
-6.126853,	0
-6.683543,	0
-6.683543,	0
-7.684560,	0
-7.684560,	0

TABLE (cont.)

N = 10 γ = 0.5
(cont.)

-1.800035,	0
-3.000000,	0
-3.427449,	0
-3.427449,	0
-4.238012,	0
-4.238012,	0
-4.487413,	0
-5.369982,	0
-5.834540,	0
-5.834540,	0
-6.933359,	0
-8.400211,	0

4.0 S^2 = 1.0

-1.712137,	0
-2.653300,	0
-3.223324,	0
-3.392738,	0
-3.392738,	0
-3.875069,	0
-4.314947,	0
-4.363884,	0
-4.363884,	0
-4.802545,	0
-5.328719,	0
-5.328720,	0
-6.000001,	0
-6.125592,	0
-6.177699,	0
-6.177699,	0
-6.736961,	0
-6.736962,	0
-7.218569,	0
-7.302440,	0
-8.440598,	0
-1.033148,	1
-1.716583,	0
-1.716583,	0
-2.754398,	0
-2.754398,	0
-3.166313,	0
-3.166313,	0
-3.572586,	0
-3.572586,	0
-3.622761,	0
-3.622761,	0
-4.161937,	0
-4.161937,	0
-4.466223,	0
-4.466229,	0
-4.531769,	0
-4.531769,	0
-4.761334,	0
-4.761334,	0
-5.209403,	0
-5.209403,	0
-5.646001,	0
-5.646001,	0
-5.679157,	0
-5.679157,	0
-5.848445,	0
-5.848445,	0
-6.234893,	0
-6.234893,	0
-6.560311,	0
-6.560311,	0
-6.665702,	0
-6.665702,	0
-6.734037,	0
-6.734037,	0
-7.437550,	0
-7.437550,	0
-7.856641,	0
-7.856641,	0
-9.373907,	0
-9.373907,	0
-1.726883,	0
-1.726883,	0
-2.903998,	0
-2.903998,	0
-2.960585,	0
-2.960585,	0
-3.311436,	0
-3.311436,	0
-3.796106,	0
-3.796106,	0
-3.843987,	0
-3.843987,	0
-3.948732,	0
-3.948732,	0
-4.639326,	0
-4.639327,	0
-4.662203,	0
-4.662203,	0
-4.811260,	0
-4.811260,	0
-5.114710,	0
-5.114710,	0
-5.373189,	0
-5.373189,	0
-5.781756,	0
-5.781756,	0
-5.830797,	0
-5.830798,	0
-6.227340,	0
-6.227340,	0
-6.236634,	0
-6.236634,	0
-6.813814,	0
-6.813815,	0
-6.965975,	0
-6.965975,	0
-7.483290,	0
-7.483290,	0
-7.963497,	0
-7.963498,	0
-8.768419,	0
-8.768420,	0
-8.826069,	0
-8.826070,	0
-1.738480,	0
-1.738480,	0
-2.854108,	0
-2.854108,	0
-3.073724,	0
-3.073724,	0
-3.549463,	0
-3.549463,	0
-3.742043,	0
-3.742043,	0
-4.036808,	0
-4.036808,	0
-4.533024,	0
-4.533024,	0
-4.575534,	0
-4.575534,	0
-4.677388,	0
-4.677388,	0
-5.071402,	0
-5.071402,	0
-5.405466,	0
-5.405466,	0
-5.748157,	0
-5.748157,	0
-5.946996,	0
-5.946996,	0
-6.116159,	0
-6.116160,	0
-6.195805,	0
-6.195805,	0
-7.126085,	0
-7.126085,	0
-7.160652,	0
-7.160653,	0
-7.173281,	0
-7.173281,	0
-8.270493,	0
-8.270493,	0
-8.999836,	0
-8.999836,	0

TABLE II (cont.)

N = 10 γ = 0·5

(cont.)

-1.747394,	0
-1.747394,	0
-2.803615,	0
-2.803615,	0
-3.239036,	0
-3.239036,	0
-3.372622,	0
-3.372622,	0
-3.573878,	0
-3.573878,	0
-3.622759,	0
-3.622759,	0
-4.194473,	0
-4.194473,	0
-4.401159,	0
-4.401159,	0
-4.509845,	0
-4.509845,	0
-4.671712,	0
-4.671712,	0
-5.300054,	0
-5.300055,	0
-5.489896,	0
-5.489896,	0
-5.509359,	0
-5.509359,	0
-5.889999,	0
-5.889999,	0
-6.349353,	0
-6.349353,	0
-6.370702,	0
-6.370702,	0
-6.583693,	0
-6.583693,	0
-7.118729,	0
-7.118729,	0
-7.356877,	0
-7.356877,	0
-7.552803,	0
-7.552803,	0
-8.499585,	0
-8.499585,	0
-9.838465,	0
-9.838465,	0
-1.750752,	0
-2.800248,	0
-3.407489,	0
-3.407489,	0
-3.471549,	0
-4.305101,	0
-4.305101,	0
-4.546885,	0
-4.654418,	0
-5.448013,	0
-5.448013,	0
-5.575109,	0
-6.066697,	0
-6.066697,	0
-6.425836,	0
-6.772700,	0
-6.772701,	0
-7.642825,	0
-7.804979,	0
-9.327400,	0

5.0 S^2 = 0.0

-1.721724,	0
-2.685386,	0
-3.227163,	0
-3.396335,	0
-3.396336,	0
-3.796664,	0
-4.348612,	0
-4.348612,	0
-4.351421,	0
-4.755006,	0
-4.764419,	0
-5.357009,	0
-5.357009,	0
-5.816375,	0
-6.151388,	0
-6.151388,	0
-6.194992,	0
-6.418385,	0
-6.746656,	0
-6.746656,	0
-7.203964,	0
-7.420007,	0
-7.933184,	0
-3.556369,	0
-1.008735,	1
-1.106760,	1
-1.724193,	0
-1.724193,	0
-2.764700,	0
-2.764701,	0
-3.183042,	0
-3.183042,	0
-3.489183,	0
-3.489183,	0
-3.610122,	0
-3.610122,	0
-3.610594,	0
-3.610594,	0
-4.169452,	0
-4.169452,	0
-4.476942,	0
-4.476942,	0
-4.498621,	0
-4.498621,	0
-4.738153,	0
-4.738154,	0
-5.262900,	0
-5.262901,	0
-5.491007,	0
-5.491007,	0
-5.617043,	0
-5.617043,	0
-5.768058,	0
-5.768058,	0
-5.857616,	0
-5.857616,	0
-6.010957,	0
-6.010957,	0
-6.259979,	0
-6.259979,	0
-6.511530,	0
-6.511530,	0
-6.650144,	0
-6.650144,	0
-6.822052,	0
-6.822053,	0
-7.468688,	0
-7.468688,	0
-7.495426,	0
-7.495427,	0
-7.888975,	0
-7.888976,	0
-9.017061,	0
-9.017061,	0
-9.613571,	0
-9.613572,	0
-1.729711,	0
-1.729711,	0
-2.890286,	0
-2.890286,	0
-2.986578,	0
-2.986578,	0
-3.333191,	0
-3.333191,	0
-3.754668,	0
-3.754668,	0
-3.818057,	0
-3.818057,	0
-3.970072,	0
-3.970072,	0
-4.611426,	0
-4.611427,	0
-4.665832,	0
-4.665832,	0
-4.688809,	0
-4.688810,	0
-5.025131,	0
-5.025131,	0
-5.103485,	0
-5.103485,	0
-5.382299,	0
-5.382299,	0

TABLE II (cont.)

N = 10 γ = 0.5 (cont.)

-5.771300, o	-7.111434, o	-8.680260, o
-5.771300, o	-7.111434, o	-8.680260, o
-5.903765, o	-7.256981, o	-9.781049, o
-5.903765, o	-7.256981, o	-9.781049, o
-6.135474, o	-7.913111, o	
-6.135474, o	-7.913111, o	-1.741032, o
-6.200251, o	-8.363659, o	-2.758462, o
-6.200251, o	-8.363659, o	-3.257114, o
-6.484595, o	-8.897937, o	-3.403709, o
-6.484595, o	-8.897938, o	-3.403709, o
-6.891393, o	-8.986882, o	-3.612001, o
-6.891393, o	-8.986882, o	-4.319266, o
-7.014484, o		-4.319266, o
-7.014484, o		-4.446764, o
-7.411506, o	-1.739598, o	-4.685961, o
-7.411506, o	-1.739598, o	-4.690303, o
-7.947458, o	-2.789038, o	-5.416276, o
-7.947458, o	-2.789038, o	-5.416276, o
-8.555379, o	-3.218744, o	-5.637247, o
-8.555379, o	-3.218745, o	-6.096291, o
-8.812280, o	-3.409676, o	-6.096291, o
-8.812280, o	-3.409676, o	-6.343316, o
-8.917581, o	-3.588756, o	-6.584232, o
-8.917581, o	-3.588756, o	-6.764459, o
	-3.623382, o	-6.764460, o
-1.735508, o	-3.623382, o	-7.169509, o
-1.735509, o	-4.185712, o	-7.671908, o
-2.865469, o	-4.185712, o	-7.735940, o
-2.865469, o	-4.433252, o	-8.774067, o
-3.043059, o	-4.433252, o	-9.647563, o
-3.043059, o	-4.498705, o	-1.124458, 1
-3.393583, o	-4.498705, o	
-3.393583, o	-4.693381, o	
-3.647777, o	-4.693381, o	
-3.647777, o	-5.349232, o	
-3.767053, o	-5.349232, o	
-3.767053, o	-5.392596, o	
-4.014069, o	-5.392597, o	
-4.014069, o	-5.540448, o	
-4.558319, o	-5.540448, o	
-4.558319, o	-5.738213, o	
-4.602586, o	-5.738213, o	
-4.602587, o	-5.878291, o	
-4.673426, o	-5.878291, o	
-4.673426, o	-6.213062, o	
-5.081934, o	-6.213063, o	
-5.081934, o	-6.316686, o	
-5.172502, o	-6.316687, o	
-5.172502, o	-6.417137, o	
-5.398545, o	-6.417137, o	
-5.398546, o	-6.611013, o	
-5.754581, o	-6.611013, o	
-5.754581, o	-7.013230, o	
-6.001831, o	-7.013230, o	
-6.001831, o	-7.403104, o	
-6.069140, o	-7.403104, o	
-6.069140, o	-7.525892, o	
-6.145016, o	-7.525892, o	
-6.145016, o	-7.959551, o	
-6.502181, o	-7.959552, o	
-6.502181, o		
-7.043428, o		
-7.043428, o		

Table III : Chain Eigenvalues: $\gamma = 1$

CHAIN

N = 4 γ = 1.00

0 $S^z = 2$

0.000000, 0

1 $S^z = 1$

0.000000, 0
-2.000000, 0
-3.357864, -1
-3.414214, 0

2 $S^z = 0$

0.000000, 0
-1.267949, 0
-4.732051, 0
-2.000000, 0
-5.857864, -1
-3.414214, 0

CHAIN

N = 6 γ = 1.0

0 $S^z = 3$

0.000000, 0

1 $S^z = 2$

-5.820766, -11
-2.679492, -1
-1.000000
-2.000000
-3.000000
-3.732051

2 $S^z = 1$

6.402843, -9
-2.679492, -1
-5.727298, -1
-1.000000
-1.186303
-1.735286
-2.000000
-2.414002
-3.000000
-3.470683
-3.732051
-4.245578
-4.528414
-5.342923
-6.503991

3 $S^z = 0$

-6.984919, -10
-2.679492, -1
-5.727298, -1
-9.302159, -1
-1.000000
-1.186303
-1.735286
-2.000000
-2.414002
-2.712176
-3.000000
-3.470683
-3.732051
-4.000000
-4.245573
-4.528414
-4.870454
-5.342923
-6.503991
-7.487154

CHAIN

N = 8 γ = 1.0

0 $S^z = 4$

0.000000, 0

1 $S^z = 3$

0.000000, 0
-1.522409, -1
-5.857864, -1
-1.234633
-2.000000
-2.765367
-3.414214
-3.847759

2 $S^z = 2$

7.581548, -2
-1.522409, -1
-3.212040, -1
-5.857863, -1
-7.133182, -1
-1.127361
-1.234633
-1.421348
-1.547427
-1.870982
-2.000000
-2.206419
-2.765367
-2.780368
-2.991539
-3.414214
-3.595995
-3.657132
-3.847759
-4.101866
-4.283406
-4.402134
-4.743536

N = 8 Y = 1·0 (cont.)

-5.104340
-5.576228
-5.951266
-6.431333
-7.163227

3 $S^2 = 1$

7.450521, -9
-1.522409, -1
-3.212940, -1
-5.126023, -1
-5.957429, -1
-7.133100, -1
-8.531426, -1
-1.127362
-1.159064
-1.234633
-1.421343
-1.547427
-1.598160
-1.870932
-1.945750
-2.000000
-2.206419
-2.301007
-2.429298
-2.765367
-2.789368
-2.858353
-2.991539
-3.163890
-3.244613
-3.414214
-3.595995
-3.657132
-3.740516
-3.847759
-3.934070
-4.101866
-4.133507
-4.283406
-4.394407
-4.402134
-4.471988
-4.733282
-4.743536
-4.954900
-4.958371
-5.104340
-5.465525
-5.493333
-5.576203
-5.951266
-5.956542
-6.348830
-6.431332
-7.849413
-7.163227
-7.197667
-7.611525
-7.716258
-8.507503
-9.464421

4 $S^2 = 0$

-5.268725, -6
-1.522507, -1
-3.212954, -1
-5.126065, -1
-5.957364, -1
-7.133180, -1
-7.349781, -1
-8.531426, -1
-1.127366
-1.159078
-1.234635
-1.421354
-1.547427
-1.598164
-1.792308
-1.870984
-1.945698
-2.000000
-2.206419
-2.301009
-2.429352
-2.665586
-2.765367
-2.789368
-2.804318
-2.858353
-2.991541
-3.163890
-3.244613
-3.414214
-3.531078
-3.595995
-3.657132
-3.740515
-3.847764
-3.934070
-4.101869
-4.133507
-4.258036
-4.283428
-4.394405
-4.402134
-4.471988
-4.733282
-4.742546
-4.743536
-4.896846
-4.954900
-4.958371
-5.104840
-5.465525
-5.493378
-5.576207
-5.741964

-5.951270
-5.956543
-6.290021
-6.348830
-6.431333
-6.790404
-6.849413
-7.163223
-7.197667
-7.334414
-7.611502
-7.716257
-8.167606
-8.507458
-9.464452
-1.024986, 1

Table IV : Chain Eigenvalues: $\gamma = 0.5$

CHAIN

N = 4 γ = 0.50

$\Sigma S^z = 2$

0.000000, 0

$\Sigma S^z = 1$

-6.909830, -1
-1.809017, 0
-8.486122, -1
-2.651388, 0

$\Sigma S^z = 0$

-1.500000, 0
-8.138594, -1
-3.686141, 0
-2.000000, 0
-8.819660, -1
-3.118034, 0

CHAIN

N = 6 γ = 0.5

$\Sigma S^z = 3$

0.000000, 0

$\Sigma S^z = 2$

-7.339556, -1
-7.697476, -1
-1.326352
-1.880438
-2.439693
-2.849814

$\Sigma S^z = 1$

-8.562909, -1
-8.577972, -1
-1.442180
-1.625718
-1.672305
-1.895698
-2.383575
-2.497181
-3.045630
-3.156519
-3.528071
-3.640479
-3.900893
-4.401733
-5.095920

$\Sigma S^z = 0$

-3.644943, -1
-8.649178, -1
-1.509866
-1.613087
-1.674453
-1.715575
-2.400679
-2.151973
-2.500000
-2.761402
-3.136945
-3.182224
-3.640195
-3.686308
-3.683601
-4.018366
-4.273996
-4.602201
-5.520286
-5.894429

CHAIN

N = 8 γ = 0.5

$\Sigma S^z = 4$

0.000000, 0

$\Sigma S^z = 3$

-7.457594, -1
-7.545682, -1
-1.160178
-1.500000
-1.912892
-2.328310
-2.681170
-2.917122

$\Sigma S^z = 2$

-3.571269, -1
-3.571575, -1
-1.475529
-1.533816
-1.565901
-1.701062
-1.845438
-1.957038
-2.053221
-2.083944
-2.514829
-2.542239
-2.981532
-3.008130
-3.019521
-3.373679
-3.405193
-3.490246
-3.644392
-3.671001
-3.894370
-3.938786
-4.165714

N = 8 γ = 0.5 (cont.)

-4.346214
-4.520437
-4.525539
-5.102703
-5.520141

2 $S^2 = 1$

-8.653806, -1
-8.653815, -1
-1.587179
-1.595959
-1.623324
-1.623660
-1.706181
-1.767784
-2.137071
-2.138542
-2.252197
-2.408820
-2.474899
-2.552418
-2.598377
-2.599494
-2.651668
-2.717714
-3.053634
-3.076073
-3.077102
-3.193221
-3.202593
-3.336274
-3.485368
-3.486377
-3.592426
-3.728173
-3.759932
-3.760939
-3.764395
-3.911045
-4.045153
-4.130015
-4.233049
-4.346945
-4.356296
-4.419557
-4.442410
-4.483268
-4.544456
-4.759066
-4.819518
-4.905679
-5.129837
-5.216677
-5.374769
-5.456349
-5.689628
-5.771759
-6.072620
-6.168019
-6.249815
-6.396129
-6.834780
-7.454696

4 $S^2 = 0$

-8.659330, -1
-8.659333, -1
-1.598025
-1.600842
-1.632018
-1.633754
-1.714054
-1.719003
-2.143026
-2.143449
-2.239761
-2.362363
-2.441808
-2.502897
-2.534733
-2.567833
-2.603809
-2.604126
-2.752451
-2.773749
-3.082156
-3.082446
-3.092492
-3.157593
-3.217664
-3.236167
-3.320749
-3.492382
-3.492665
-3.562687
-3.642402
-3.718139
-3.762654
-3.767727
-3.768009
-3.792634
-4.106295
-4.191222
-4.226374
-4.265284
-4.330888
-4.400606
-4.415971
-4.436435
-4.507095
-4.536783
-4.581398
-4.587239
-4.877725
-4.896042
-4.913538
-5.152238
-5.198058
-5.234357
-5.260977
-5.446164
-5.477948
-5.517016
-5.771690
-5.803780
-5.922132
-6.157024
-6.266099
-6.284818

-6.297654
-6.519130
-6.844364
-7.079059
-7.345186
-8.111274

TABLE V ANTIFERROMAGNETIC GROUND STATE ENERGIES OF RINGS AND CHAINS.

N ↓ \ γ →	1.0	0.9	0.8	0.7	0.6	0.5	0.4	0.3	0.2	0.1	0.0
	LIMITING CURVE (ORBACH, 1958)										
∞	0.88629	0.82774	0.77056	0.71556	0.66396	0.61722	0.57681	0.54399	0.51980	0.50499	0.50000
	EVEN RINGS										
2	1.50000	1.40000	1.30000	1.20000	1.10000	1.00000	0.90000	0.80000	0.70000	0.60000	0.50000
4	1.00000	0.93374	0.86847	0.80453	0.74244	0.68301	0.62749	0.57787	0.53723	0.50981	0.50000
6	0.93425	0.87244	0.81179	0.75274	0.69599	0.64263	0.59434	0.55358	0.52325	0.50547	0.50000
8	0.91277	0.85241	0.79328	0.73588	0.68101	0.62993	0.58456	0.54739	0.52065	0.50505	0.50000
10	0.90309	0.84339	0.78495	0.72831	0.67435	0.62446	0.58067	0.54534	0.52003	0.50500	0.50000
12	0.8979	* (Ledinegg and Urban, 1952)									
	ODD RINGS										
3	0.50000	0.46667	0.43333	0.40000	0.36667	0.33333	0.30000	0.26667	0.23333	0.20000	0.16667
5	0.74721	0.69760	0.64843	0.59985	0.55199	0.50507	0.45940	0.41537	0.37357	0.33477	0.30000
7	0.81577	0.76168	0.70831	0.65586	0.60461	0.55496	0.50746	0.46285	0.42211	0.38646	0.35714
9	0.84384	0.78795	0.73292	0.67903	0.62665	0.57632	0.52879	0.48504	0.44628	0.41383	0.38889
11	0.85799		0.74535		0.63799		0.54041		0.46073		0.40909
	EVEN CHAINS										
2	0.75000	0.70000	0.65000	0.60000	0.55000	0.50000	0.45000	0.40000	0.35000	0.30000	0.25000
4	0.80801	0.75434	0.70113	0.64856	0.59689	0.54654	0.49822	0.45327	0.41421	0.38581	0.37500
6	0.83119	0.77606	0.72160	0.66809	0.61591	0.56574	0.51873	0.47692	0.44370	0.42311	0.41667
8	0.84373	0.78781	0.73270	0.67870	0.62632	0.57641	0.53042	0.49080	0.46093	0.44320	0.43750

TABLE VI. THERMODYNAMIC PROPERTIES FOR ANTIFERROMAGNETIC

RINGS FOR THE HEISENBERG LIMIT ($\gamma = 1$).

$kT/\|J\|$	$u / N\|J\|$	S / Nk	C / Nk	$\|J\|\chi / Ng^2\beta^2$
5.0	-0.16180	0.67663	0.03396	0.04015
4.4	-0.18501	0.67167	0.04404	0.044151
3.8	-0.21564	0.66416	0.05911	0.048922
3.2	-0.25763	0.65208	0.08273	0.054603
2.6	-0.31797	0.63106	0.12178	0.061222
2.2	-0.37429	0.60744	0.16228	0.065959
2.0	-0.40931	0.59074	0.18866	0.068271
1.8	-0.45007	0.56923	0.21976	0.070398
1.7	-0.47290	0.55618	0.23706	0.071336
1.6	-0.49751	0.54125	0.2554	0.072151
	-0.52396	0.52418	0.27416	0.072808
1.5	-0.52399	0.52415	0.2743	0.072806
	-0.52403	0.52413	0.27453	0.072803
	-0.53790	0.51472	0.28372	0.073063
1.45	-0.53795	0.51469	0.2840	0.073059
	-0.53800	0.51466	0.28419	0.073056
	-0.55233	0.50460	0.29322	0.073261
1.4	-0.55239	0.50456	0.2935	0.073256
	-0.55245	0.50452	0.29385	0.073251
	-0.56722	0.49376	0.30255	0.073396
1.35	-0.56730	0.49371	0.3030	0.073390
	-0.56738	0.49366	0.3o338	0.073383
	-0.58258	0.48217	0.31158	0.073463
1.3	-0.58268	0.48210	0.3121	0.073454
	-0.58278	0.48203	0.31266	0.073445
	-0.59837	0.46978	0.32012	0.073454
1.25	-0.5985	0.4697	0.321	0.07344
	-0.59864	0.46959	0.32156	0.073429
	-0.61458	0.45655	0.32796	0.073364
1.2	-0.6148	0.4564	0.329	0.07335
	-0.61493	0.45629	0.32987	0.073333
	-0.63115	0.44244	0.33488	0.073186
1.15	-0.6314	0.4423	0.336	0.07316
	-0.63161	0.44209	0.33742	0.073135
	-0.64805	0.42742	0.34058	0.072916
1.1	-0.6484	0.4272	0.342	0.07288
	-0.64865	0.42694	0.34395	0.072843
	-0.66518	0.41147	0.34473	0.072549
1.05	-0.6656	0.4112	0.347	0.07250
	-0.66599	0.41081	0.34922	0.072445
	-0.68249	0.39459	0.34698	0.072084
1.0	-0.6830	0.3942	0.350	0.07201
	-0.68355	0.39367	0.35294	0.071933

$kT/\lvert J\rvert$	$U/N\lvert J\rvert$	S/Nk	C/Nk	$\lvert J\rvert\chi/Ng^2\beta^2$
	-0.69984	0.37678	0.34692	0.071521
0.95	-0.700	0.3762	0.350	0.0714
	-0.70125	0.37551	0.35482	0.071301
	-0.71713	0.35809	0.34412	0.070863
0.9	-0.718	0.3575	0.34(8)	0.0707
	-0.71900	0.35632	0.35457	0.070542
	-0.73420	0.33857	0.33816	0.070121
0.85	-0.735	0.337	0.34(3)	0.0700
	-0.73667	0.33612	0.35190	0.069649
	-0.75089	0.31835	0.32861	0.069310
0.8	-0.752	0.317	0.33(5)	0.069(0)
	-0.75414	0.31494	0.34655	0.068611
	-0.76700	0.29756	0.31512	0.068457
0.75	-0.768	0.296	0.32(4)	0.068(0)
	-0.77128	0.29282	0.33834	0.067415
	-0.78233	0.27641	0.29742	0.067602
0.7	-0.784	0.274	0.31(0)	0.067(0)
	-0.78793	0.26985	0.32714	0.066040
	-0.79667	0.25517	0.27541	0.066806
0.65	-0.799	0.252	0.29(2)	0.065(9)
	-0.80394	0.24612	0.31294	0.064451
	-0.80980	0.23416	0.24924	0.066159
0.6	-0.813	0.229	0.27(1)	0.064(9)
	-0.81917	0.22175	0.29587	0.062589
	-0.82153	0.21377	0.21930	0.065793
0.55	-0.826	0.207	0.24(6)	0.063(7)
	-0.83348	0.19686	0.27618	0.060357
	-0.83168	0.19444	0.18636	0.065909
0.5	-0.838	0.185	0.22(1)	0.062(4)
	-0.84675	0.17158	0.25427	0.057602
	-0.84013	0.17666	0.15149	0.066815
0.45	-0.84(8)	0.16(4)	0.19(6)	0.061(2)
	-0.85888	0.14604	0.23062	0.054086
	-0.84682	0.16095	0.11610	0.068984
0.4	-0.85(6)	0.14(4)	0.17(0)	0.059(9)
	-0.86979	0.12037	0.20568	0.049473
	-0.85176	0.14780	0.08188	0.073163
0.35	-0.86(3)	0.12(5)	0.14(6)	0.05(85)
	-0.87943	0.09467	0.17948	0.043332
	-0.85506	0.13769	0.05086	0.080543
0.3	-0.87(0)	0.10(6)	0.12(0)	0.05(73)
	-0.88771	0.06921	0.15114	0.035247
	-0.85694	0.13090	0.02554	0.093082
0.25	-0.87(4)	0.08(7)	0.09(6)	0.05(58)
	-0.89447	0.04465	0.11823	0.025147
	-0.85776	0.12734	0.00865	0.114270
0.2	-0.87(8)	0.07(0)	0.07(4)	0.05(44)
	-0.89940	0.02278	0.07798	0.014021

$kT/\|J\|$	$U/N\|J\|$	S/Nk	C/Nk	$\|J\|\chi/Ng^2\beta^2$
	-0.85797	0.12617	0.00127	0.151590
0.15	-0.88(1)	0.05(3)	0.05(5)	0.05(30)
	-0.90219	0.00706	0.03384	0.004679
	-0.85799	0.12603	0.00002	0.227274
0.1	-0.885	0.035	0.035	0.05(16)
	-0.90304	0.00060	0.00453	0.000421
	-0.85799	0.12603	0.0	0.454545
0.05	-0.886	0.018	0.018	0.050(8)
	-0.90309	0.0	0.0	0.0
	-0.85799	0.12603		$+\infty$
0.0	-0.88629	0	0	0.050661
	-0.90309	0		0

For $kT/|J| \leq 1.5$ three values are listed: the top value corresponds to N =11, the lowest to N =10, and our extrapolation estimate for $N\to\infty$ is shown in between. The accuracy we expect for the limiting result is indicated by the number of figures quoted in the estimate. Brackets round the last figure signify an uncertainty of $\gtrsim \pm 3$, and brackets round the last two figures a possible error of $\gtrsim \pm 10$.

TABLE VII THERMODYNAMIC PROPERTIES FOR FERROMAGNETIC RINGS FOR THE HEISENBERG LIMIT ($\gamma = 1$).

kT/J	U/NJ	S/Nk	C/Nk	$\xi(T)/4$
5.0	-0.13324	0.68040	0.02309	0.29943
4.4	-0.14865	0.67711	0.02854	0.30600
3.8	-0.16790	0.67240	0.03604	0.31455
3.2	-0.19251	0.66532	0.04663	0.42615
2.6	-0.22479	0.65410	0.06192	0.34271
2.2	-0.25221	0.64261	0.07571	0.35834
2.0	-0.26815	0.63501	0.08388	0.36826
1.8	-0.28581	0.62570	0.09286	0.38014
1.7	-0.29534	0.62025	0.09762	0.38702
1.6	-0.30534	0.61418	0.10250	0.39465
	-0.31584	0.60741	0.1074	0.40317
1.5	-0.31584	0.60741	0.10745	0.40317
	-0.31585	0.60740	0.10748	0.40316

kT/J	U/NJ	S/Nk	C/Nk	$\xi(T)/4$
	-0.32683	0.59982	0.1124	0.41275
1.4	-0.32683	0.59982	0.11238	0.41275
	-0.32684	0.59982	0.11243	0.41274
	-0.33831	0.59131	0.1172	0.42361
1.3	-0.33831	0.59131	0.11719	0.42361
⋮	-0.33833	0.59130	0.11726	0.42360
	-0.35025	0.58176	0.1217	0.43602
1.2	-0.35026	0.58175	0.12174	0.43602
	-0.35029	0.58173	0.12185	0.43601
	-0.36264	0.5710	0.1258	0.45039
1.1	-0.36265	0.57097	0.12586	0.45038
	-0.36268	0.57094	0.12604	0.45036
	-0.36897	0.5651	0.1276	0.45845
1.05	-0.36899	0.56507	0.12771	0.45844
	-0.36903	0.56503	0.12794	0.45841
	-0.3753	0.5588	0.1292	0.4672
1.0	-0.37541	0.55880	0.12939	0.46720
	-0.37548	0.55874	0.12969	0.46715
	-0.3819	0.5522	0.1306	0.4768
0.95	-0.38192	0.55212	0.13090	0.47675
	-0.38200	0.55205	0.13128	0.47668
	-0.3884	0.5451	0.1318	0.4873
0.9	-0.38850	0.54501	0.13221	0.48721
	-0.38860	0.54491	0.13270	0.48712
	-0.3950	0.5375	0.1327	0.4988
0.85	-0.39514	0.53742	0.13332	0.49872
	-0.39527	0.53729	0.13397	0.49859
	-0.4017	0.5295	0.1334	0.5116
0.8	-0.40183	0.52930	0.13426	0.51147
	-0.40200	0.52913	0.13510	0.51128
	-0.4083	0.5208	0.134(0)	0.5258
0.75	-0.40856	0.52061	0.13505	0.52567
	-0.40878	0.52038	0.13613	0.52540
	-0.4151	0.5116	0.134(4)	0.5420
0.7	-0.41533	0.51127	0.13574	0.54159
	-0.41561	0.51095	0.13713	0.54119
	-0.4218	0.501(6)	0.134(0)	0.5601
0.65	-0.42214	0.50118	0.13642	0.55958
	-0.42249	0.50075	0.13820	0.55899
	-0.4285	0.490(9)	0.133(8)	0.581(1)
0.6	-0.42898	0.49024	0.13718	0.58008
	-0.42943	0.48964	0.13946	0.57919
	-0.4354	0.480	0.133(4)	0.605(3)
0.55	-0.43586	0.47826	0.13813	0.60365
	-0.43644	0.47744	0.14104	0.60228
	-0.4420	0.468	0.133	0.633(5)
0.5	-0.44280	0.46502	0.13955	0.63099
	-0.44354	0.46390	0.14306	0.62887

kT/J	U/NJ	S/Nk	C/Nk	$\xi(T)/4$
	-0.448(8)	0.454	0.13(2)	0.667
0.45	-0.44982	0.45023	0.14143	0.66301
	-0.45076	0.44870	0.14559	0.65968
	-0.455(3)	0.43(9)	0.13(1)	0.708
0.4	-0.45695	0.43343	0.14384	0.70083
	-0.45811	0.43138	0.14847	0.69554
	-0.462(1)	0.42(1)	0.13(0)	0.76(0)
0.35	-0.46421	0.41404	0.14654	0.74574
	-0.46560	0.41136	0.15116	0.73724
	-0.468(6)	0.40(1)	0.12(8)	0.82(7)
0.3	-0.47160	0.39126	0.14865	0.79900
	-0.47320	0.38794	0.15229	0.78527
	-0.47(48)	0.37(7)	0.12(6)	0.9(18)
0.25	-0.47903	0.36415	0.14801	0.86119
	-0.48076	0.36037	0.14918	0.83914
	-0.48(08)	0.3(50)	0.1(23)	1.05
0.2	-0.48628	0.33183	0.14028	0.93068
	-0.48797	0.32825	0.13722	0.89608
	-0.48(37)	0.3(34)	0.1(20)	1.1(4)
0.175	-0.48969	0.31364	0.13177	0.96640
	-0.49127	0.31065	0.12589	0.92377
	-0.48(65)	0.3(15)	0.1(18)	1.2(6)
0.15	-0.49283	0.29429	0.11886	1.00093
	-0.49422	0.29246	0.10959	0.94928
	-0.48(92)	0.2(91)	0.1(15)	1.4(1)
0.125	-0.49559	0.27426	0.10038	1.03221
	-0.49670	0.27448	0.08726	0.97096
	-0.49(19)	0.2(64)	0.1(11)	1.6(4)
0.1	-0.49779	0.25466	0.07495	1.05773
	-0.49853	0.25821	0.05870	0.98713
	-0.49(46)	0.2(32)	0.1(04)	1.(75)
0.075	-0.49927	0.23787	0.04239	1.07490
	-0.49961	0.24608	0.02735	0.99655
	-0.497(0)	0.1(89)	0.0(95)	2.(67)
0.05	-0.49992	0.22786	0.01085	1.08235
	-0.49997	0.24047	0.00463	0.99974
	-0.498(9)	0.1(34)	0.0(67)	3.(57)
0.025	-0.50000	0.22591	0.00007	1.08333
	-0.50000	0.23979	0.00001	1.00000
0		0		∞
	-0.50000	0.22590	0	1.08333
		0.23979		1.00000

For $kT/J \leq 1.5$ three values are listed as in the antiferromagnetic case. The topmost value, however, is the estimated limit (with uncertainties indicated as in Table VI), then follow in order the results for N =11 and N =10.

TABLE VIII THERMODYNAMIC PROPERTIES FOR ANTIFERROMAGNETIC RINGS FOR $\gamma = 0.5$.

$kT/\|J\|$	$u/N\|J\|$	S/Nk	C/Nk	$\|J\|\chi/Ng^2\beta^2$
5.0	-0.07810	0.68525	0.01609	0.040736
4.2	-0.09348	0.68188	0.02295	0.046589
3.4	-0.11622	0.67582	0.03518	0.054226
2.6	-0.15300	0.66334	0.05994	0.064330
2.0	-0.19925	0.64290	0.09877	0.073735
	-0.24748	0.61580	0.14650	0.080313
1.6	-0.248	0.616	0.146	0.0803
	-0.24743	0.61582	0.14630	0.080318
	-0.26293	0.60582	0.16294	0.081816
1.5	-0.263	0.606	0.163	0.o818
	-0.26286	0.60586	0.16261	0.081825
	-0.28014	0.59394	0.18170	0.083174
1.4	-0.280	0.594	0.182	0.o832
	-0.28003	0.59401	0.18113	0.083191
	-0.29935	0.57969	0.20301	0.084315
1.3	-0.300	0.580	0.201	0.0843
	-0.29917	0.57981	0.20202	0.084346
	-0.32083	0.56248	0.22703	0.085143
1.2	-0.321	0.563	0.226	0.0852
	-0.32051	0.56272	0.22526	0.085203
	-0.34485	0.54157	0.25370	0.085531
1.1	-0.344	0.542	0.252	0.0856
	-0.34428	0.54202	0.25046	0.085651
	-0.37165	0.51601	0.28260	0.085311
1.0	-0.371	0.516	0.280	0.0855
	-0.37064	0.51688	0.27658	0.085561
	-0.40141	0.48462	0.31265	0.084258
0.9	-0.400	0.485	0.309	0.0844
	-0.39956	0.48639	0.30134	0.084800
	-0.43415	0.44603	0.34171	0.082071
0.8	-0.432	0.448	0.335	0.0826
	-0.43072	0.44966	0.32057	0.083278
	-0.45157	0.42354	0.35477	0.080423
0.75	-0.449	0.426	0.345	0.0814
	-0.44690	0.42877	0.32611	0.082244
	-0.46959	0.39866	0.36595	0.078310
0.7	-0.466	0.403	0.353	0.0800
	-0.46326	0.40619	0.32753	0.081074
	-0.48811	0.37121	0.37430	0.075636
0.65	-0.484	0.377	0.358	0.0783
	-0.47957	0.38203	0.32367	0.079845
	-0.50695	0.34104	0.37851	0.072276
0.6	-0.501	0.349	0.356	0.0764
	-0.49552	0.35649	0.31343	0.078696
	-0.52587	0.30813	0.37675	0.068066
0.55	-0.518	0.320	0.339	0.0742
	-0.51079	0.32993	0.29599	0.077843

$kT/\|J\|$	$U / N\|J\|$	S / Nk	C / Nk	$\|J\|\chi / Ng^2\beta^2$
	-0.54449	0.27264	0.36655	0.062805
0.5	-0.535	0.288	0.337	0.0714
	-0.52500	0.30287	0.27113	0.077622
	-0.56233	0.23507	0.34487	0.056274
0.45	-0.550	0.255	0.314	0.0683
	-0.53779	0.27594	0.23952	0.078520
	-0.57873	0.19646	0.30876	0.048301
0.4	-0.564	0.220	0.288	0.0647
	-0.54887	0.24990	0.20282	0.081236
	-0.59294	0.15860	0.25712	0.038894
0.35	-0.577	0.185	0.256	0.0603
	-0.55803	0.22549	0.16347	0.086756
	-0.60424	0.12389	0.19339	0.028434
0.3	-0.588	0.150	0.219	0.0554
	-0.56521	0.20342	0.12399	0.096503
	-0.61224	0.09491	0.12719	0.017852
0.25	-0.598	0.115	0.181	0.0488
	-0.57046	0.18439	0.08628	0.112688
	-0.61715	0.07321	0.07251	0.008641
0.2	-0.606	0.080	0.130	0.0395
	-0.57389	0.16923	0.05154	0.139282
	-0.62186	0.04169	0.04058	0.000188
0.1	-0.615	0.019	0.056	0.0112
	-0.57638	0.15458	0.00365	0.277778
	-0.62446	0	0	0
0	-0.61722	0	0	0
	-0.57632	0.15403	0	∞

For $kT/|J| \leq 1.6$ three values are listed: the top value corresponds to the ring $N = 10$, the lowest to $N = 9$, and our extrapolation estimate for $N \to \infty$ is shown in between.

TABLE IX THERMODYNAMIC PROPERTIES FOR FERROMAGNETIC RINGS AND CHAINS FOR $\gamma' = 0.5$.

kT/J	u/NJ	S/Nk	C/Nk	$\xi(T)/4$
5.0	-0.07078	0.68622	0.01324	0.30385
4.2	-0.08321	0.68349	0.01823	0.31501
3.4	-0.10084	0.67881	0.02661	0.33199
2.6	-0.12766	0.66972	0.04216	0.36086
2.0	-0.15890	0.65593	0.06422	0.40047
1.5	-0.19856	0.63288	0.09772	0.46382
	-0.19859	0.63287	0.09782	0.46380
	-0.2370	0.6401	0.0865	
		0.633	0.098	
1.2	-0.23251	0.60750	0.13089	0.53546
	-0.23260	0.60743	0.13137	0.53536
	-0.2670	0.6176	0.1158	
		0.613	0.131	
1.1	-0.24631	0.59548	0.14567	0.57112
	-0.24648	0.59535	0.14649	0.57093
	-0.2792	0.6070	0.1286	
		0.596	0.145	
1.0	-0.26173	0.58077	0.16325	0.61671
	-0.26201	0.58054	0.16471	0.61631
	-0.2928	0.5940	0.1435	
		5.582	0.161	
0.9	-0.27910	0.56245	0.18482	0.67685
	-0.27956	0.56201	0.18741	0.67597
	-0.3080	0.5780	0.1610	
		0.565	0.181	
0.8	-0.29890	0.53909	0.21265	0.75930
	-0.29972	0.53824	0.21725	0.75726
	-0.3252	0.5578	0.1819	
		0.545	0.204	
0.7	-0.32198	0.50822	0.25130	0.87770
	-0.32341	0.50654	0·25916	0.87267
	-0.3446	0.5318	0.2074	
		0.520	0.232	
0.6	-0.34981	0.46520	0.30950	1.05651
	-0.35223	0.46200	0.32128	1.04331
	-0.3668	0.4974	0.2393	
		0.485	0.271	
0.55	-0.36625	0.43657	0.34953	1.18076
	-0.36929	0.43228	0.36224	1.15898
	-0.3793	0.4758	0.2584	
		0.458	0.293	
0.5	-0.38489	0.40100	0.39713	1.33670
	-0.38854	0.39555	0.40818	1.30065
	-0.3927	0.4501	0.2798	
		0.426	0.318	

kT/J	U/NJ	S/Nk	C/Nk	$\xi(\tau)/4$
0.45	-0.40601	0.35646	0.44693	1.52961
	-0.41007	0.35014	0.45152	1.47055
	-0.4073	0.4194	0.3032	
		0.387	0.348	
0.4	-0.42935	0.30144	0.48187	1.75838
	-0.43335	0.29527	0.47409	1.66459
	-0.4231	0.3823	0.3269	
		0.340	0.377	
0.375	-0.44145	0.27019	0.48394	1.88187
	-0.44517	0.26477	0.46873	1.76618
	-0.4314	0.3608	0.3374	
		0.311	0.389	
0.35	-0.45340	0.23721	0.46923	2.00632
	-0.45665	0.23308	0.44725	1.86649
	-0.4399	0.3372	0.3458	
		0.283	0.393	
0.3	-0.47493	0.17104	0.37763	2.23474
	-0.47688	0.17092	0.35017	2.04574
	-0.4574	0.2834	0.3492	
		0.217	0.382	
0.25	-0.49009	0.11619	0.22370	2.39698
	-0.49084	0.12043	0.20498	2.17020
	-0.4743	0.2219	0.3184	
		0.143	0.336	
0.2	-0.49754	0.08349	0.08390	2.47556
	-0.49769	0.09038	0.07773	2.23052
	-0.4883	0.1595	0.2345	
		0.070	0.250	
0.15	-0.49972	0.07145	0.01546	2.49738
	-0.49972	0.07909	0.01482	2.24780
	-0.4970	0.1105	0.1095	
		0.020	0.114	
0.1	-0.49999	0.06939	0.00069	2.49994
	-0.49999	0.07709	0.00069	2.24995
	-0.4998	0.0089	0.0163	
		0.001	0.012	
0	-0.50000	0.06931	0	2.50000
	-0.50000	0.07702	0	2.25000
	-0.50000	0.08864	0	
	-0.5	0	0	∞

For $kT/J \leq 1.5$, up to four values may be listed: the top two correspond to the N =10 Ring and the N=9 Ring, the third is a value for the N =8 Chain, and the fourth is a limiting $N \to \infty$ value, where available.

REFERENCES.

Anderson, P.W., 1951, Phys. Rev., 83, 1260.

Anderson, P.W., 1963, Magnetism, Vol. 1, Academic Press, p. 25.

Arai, T., and Goodman, B., 1967, Phys. Rev., 155, 514.

Baker, G.A.Jr., Rushbrooke, G.S., and Gilbert, H.E., 1964, Phys. Rev., 135, A1273.

Barraclough, C.G., and Ng, C.F., 1964, Trans. Faraday Soc. (GB) 60, 836.

Berger, L., Friedberg, S.A., and Schriempf, J.T., 1963, Phys. Rev., 132, 1057.

Bethe, H.A., 1931, Z. Physik, 71, 205.

Bleaney, B., and Bowers, K.D., 1952, Proc. Roy. Soc., A214, 451.

Bloch, F., 1929, Z. Physik, 57, 545.

Bloch, F., 1930, Z. Physik, 61, 206; 1932, 74, 295.

Bonner, J.C., and Fisher, M.E., 1964, Phys. Rev., 135, A640.

Boon, M.H., 1961, Nuovo Cimento, 21, 885.

Brooks, J.E., and Domb, C., 1951, Proc. Roy. Soc., A207, 343.

Bulaevskii, L.N., 1963, Soviet Phys.—JETP., 16, 685. (Translation of Zh. Eksperim. i Teor. Fiz., 43, 968, 1962.)

Carboni, F., 1966, Thesis, University of Kansas.

Carboni, F., and Richards, P.M., 1968, J. Appl. Phys., 39, 967.

Des Cloizeaux, J., and Pearson, J.J., 1962, Phys. Rev., 128, 2131.

Des Cloizeaux, J., and Gaudin, M., 1966, J. Math. Phys., 7, 1384.

Corson, E.M., 1951, Perturbation Methods in the Quantum Mechanics of n-Electron Systems, Blackie and Son, Chapter X.

Davis, H.L., 1960, Phys. Rev., 120, 789.

Domb, C., 1960, Advan. Phys., 9, 149.

Domb, C., and Miedema., A.R., 1964, Progress in Low Temperature Physics, Vol IV, p. 296.

Domb, C., and Wood, D.W., 1965, Proc. Phys. Soc., 86, 1.

Duffy, W.Jr., Lubbers, J., van Kempen, H., Haseda, T., and Miedema, A.r 1962, Proc. 8th Int. Conf. Low Temp. Phys. (London).

Duffy, W. Jr., and Barr, K.P., 1968, Phys, Rev., 165, 647.

Duffy, W. Jr., and Strandburg, D., 1967, J. Chem. Phys., 46, 456.

Dyson, F.J., 1956, Phys. Rev., 102, 1217, 1230.

Edelstein, A.S., 1966, Phys. Rev., 142, 259.

Edelstein, A.S., 1965, Private Communication.

Falk, H., 1965, Private Communication.

Falk, H., and Ruijgrok, T.W., 1961, Physica, 27, 710.

Falk, H., and Ruijgrok, T.W., 1965, Phys. Rev., 139, A1203.

Feynman, R.P., 1939, Phys. Rev., 56, 340.

Fisher, M.E., 1960, Proc. Roy, Soc., A256, 502.

Fisher, M.E., 1960a, Physica, 26, 618.

Fisher, M.E., 1963, J.Math. Phys., 4, 124.

Fisher, M.E., 1964, Am. J. Phys., 32, 343.

Fisher, M.E., 1965, Lectures in Theoretical Physics, Vol. VIIC, University of Colorado Press.

Fisher, M.E., 1966, Phys. Rev. Letters, 16, 11.

Fisher, M.E., 1967, Repts. Prog. Phys., 30, Part II , 615.

Frank, D., 1956, Z. Physik, 146, 615.

Friedberg, S.A., and Raquet, C.A., 1968, J. Appl. Phys., 39, no.2 (part II), 1132.

Fritz, J.J., and Pinch, H.L., 1959, J. Am. Chem. Soc., 79, 3644.

Geballe, T.H., and Giauque, W.F., 1962, J. Am. Chem. Soc., 74, 3513.

Ginzburg, V.L., and Fain, V.M., 1962, Soviet Phys.—JETP., 15, 131 (Translation of Zh. Eksperim. i Teor. Fiz., 42, 180, 1962.)

Goodenough, J.B., 1963, Magnetism and the Chemical Bond, N.Y. Inter-Science.

Gorter et al., 1955: see van der Marel, van den Broek, Wasscher and Gorter, 1955.

Griffiths, R.B., 1961, Mimeographed Report, Stanford University, (unpublished).

Griffiths, R.B., 1963, Mimeographed Report, University of California, La Jolla, (unpublished).

Griffiths, R.B., 1963, Private Communication.

Griffiths, R.B., 1964, Phys. Rev., 133, A768.

Griffiths, R.B., 1964a, Phys. Rev., 135, A659.

Griffiths, R.B., 1964b, Phys. Rev., 136, A751.

Haas, C.W., and Jarrett, H.S., 1964, Phys. Rev., 135, A1089.

Haseda, T., and Kobayashi, H., 1964, J. Phys, Soc. Japan, 19, 1260.

Haseda, T., and Miedema, A.R., 1961, Physica, 27, 1102.

Haseda, T., Miedema, A.R., Kobayashi, H., and Kanda, E., 1962, J. Phys. Soc. Japan, Supp. B-I, 518.

Hulthén, L., 1938, Arkiv. Mat. Astron. Fysik, 26A, No. 11, 1.

Hunt, J.T., and Girardeau, M.D., 1967, Phys. Rev., 160, 455.

Ising, E., 1925, Z. Physik, 31, 253.

Joyce, G.S., 1967, Phys. Rev., 155, 478.

Kadota, S., Yamada, I., Yoneyama, S., Hirakawa, K., 1967, J. Phys. Soc. Japan, 23, 751.

Kanamori, J., 1963, Magnetism, Vol. 1, Academic Press, p. 127.

Kanda, S., Ito, K., and Nogaito, T., 1967, J. Polymer Science, Part C, No. 17, 151.

Karayianis, N., Morrison, C.A., and Wortman, D.E., 1962, Phys. Rev., 126, 1443.

Kasteleijn, P.W., 1952, Physica, 18, 104.

Kasteleijn, P.W., 1960, Private Communication.

Katsura, S., 1962, Phys. Rev., 127, 1508.

Katsura, S., 1965, Ann. Phys. (N.Y.), 31, 325.

Katsura, S., and Inawashiro, S., 1964, J.Math. Phys., 5, 1091.

Katsura, S., and Inawashiro, S., 1965: should read Inawashiro, S., and Katsura, S., 1965, Phys. Rev, 140, A892.

Katsura, S., and Inawashiro, S., 1965a, J. Math. Phys., 6, 1916.

Kawasaki, K., 1966, Ann. Phys. (N.Y.), 37, 142.

Van Kempen, H., 1965, Thesis, University of Leiden.

Kittel, C., and Shore, H., 1965, Phys. Rev., 138, A1165.

Kobayashi, N., Haseda, T., Kanda, E., and Kanda, S., 1963, J. Phys. Soc. Japan, 18, 349.

Kobayashi, H., and Haseda, T., 1964, J. Phys. Soc. Japan, 19, 765.

Van Kranendonk, J., and van Vleck, J.H., 1958, Rev. Mod. Phys., 30, 1.

Kubo, R., 1952, Phys. Rev., 87, 568.

Kubo, R., Rev. Mod. Phys., 25, 344.

Ledinegg, E., and Urban, P., 1952, Acta Physica Austriaca, 6, No. 1, 7.

Lieb, E.H., 1967, Phys, Rev. Letters, 18, 692, 1046; 19, 108.

Lieb, E., Schultz, T., and Mattis, D., 1961, Ann. Phys.(N.Y.), 16, 407.

Mannari, I., 1958, Prog. Theor. Phys. (Kyoto), 19, 201.

Van der Marel, L.C., van den Broek, J., Wasscher, J.D., Gorter, C.J., 1955, Physica, 21, 685.

Marshall, W., 1955, Proc. Roy. Soc., A232, 48.

Matsubara, T., and Matsuda, H., 1956, Prog. Theor. Phys. (Kyoto), 16, 416, 569.

Matsubara, T., and Matsuda, H., 1957, Prog. Theor. Phys. (Kyoto), 17, 19.

Mattheiss, L.F., 1961, Phys. Rev., 123, 1209, 1219.

Mattis, D.C., 1965, The Theory of Magnetism, Harper and Row.

Mazzi, F., 1955, Acta. Cryst., 8, 137.

Mermin, N.D., and Wagner, H., 1966, Phys. Rev.Letters, 17, 1133.

Meyer, K., 1956, Z. Naturforsh. 11A, 865.

Miedema, A.R., van Kempen, H., Haseda, T., and Huiskamp, W.J., 1962, Physica, 28, 119.

Muir, T., 1960, A Treatise on the Theory of Determinants, Dover Publications Inc., p. 485.

Nagle, J.F., 1966, J. Math. Phys., 7, 1492.

Nagle, J.F., 1968, Private Communication.

Nambu, Y., 1950, Prog. Theor. Phys. (Kyoto), 5, 1.

Néel, L., 1932, Ann. Phys. (Paris), 17, 64.

Newell, G.F., and Montroll, E.W., 1953, Rev. Mod. Phys., 25, 353.

Nordio, P.L., Soos, Z.G., and McConnell, H.M., 1966, Ann. Rev. Physical Chem., 17, 237.

Oguchi, T., 1960, Phys. Rev., 117, 117.

Oguchi, T., 1963, Phys. Rev. Letters, 11, 266.

Oguchi, T., 1963a, J. Phys. Chem. Solids, 24, 1049.

Oguchi, T., 1964, Phys. Rev., 133, A1098.

Oguchi, T., and Takano, F., 1964, J. Phys. Soc. Japan, 19, 1265.

Ohtsuka, T.J., 1961, J. Phys, Soc. Japan, 16, 1549.

Onsager, L., 1944, Phys. Rev., 65, 117.

Orbach, R.L., 1958, Phys. Rev., 112, 309.

Orbach, R.L., 1959, Phys. Rev., 115, 1181; Ph.D. Dissertation, University of California,(unpublished).

Pólya, G., 1937, Acta Math., 68, 145.

Poulis, N.J., and Hardeman, G.E.G., 1952, Physica, 18, 201.

Pratt, G.W.Jr., 1961, Phys. Rev., 122, 489.

Rado, G.T., and Suhl, H., 1963, Magnetism, Vols. 1 and 3; 1965, Vol 2A; 1966, Vol. 2B; Academic Press.

Richards, P.M., 1967, Private Communication.

Rodriguez, S., 1959, Phys. Rev., 116, 1474.

Rogers, R.N., Carboni, F., and Richards, P.M., 1967, Phys. Rev. Letters 19, 1016.

Rogers, R.N., and Dempesy, C.W., 1967, Phys. Rev., 162, 333.

Ruijgrok, T.W., and Rodriguez, S., 1960, Phys. Rev., 119, 596.

Runnels, L.K., and Combs, L.L., 1966, J.Chem. Phys., 45, 2482.

Slater, J.C., 1936, Phys. Rev., 49, 537, 931.

Smart, J.S., 1963, Magnetism, Vol. 3, Academic Press, p. 63.

Stevens, K.W.H., 1963, Magnetism, Vol. 1, Academic Press, p. 1.

Stoner, E.C., 1938, Proc. Roy. Soc., A165, 372.

Stout, J.W., and Chisholm, R.C., 1962, J. Chem. Phys., 36 , 979.

Syozi, I., 1951, Busseiron-Kenkyu No. 39, 55.

Thompson, C.J., To be published.

Uhlenbeck, G.E., and Ford, G.W., 1962, Studies in Statistical Mechanics Vol. I , North-Holland, p. 167.

Ukei, K., Unpublished specific heat measurements.

Walker, L.R., 1959, Phys. Rev., 116, 1089.

Walker, L.R., 1964, Private Communication; 1965, Proc. Int. Mag. Conf. (I.P.P.S.), p. 21.

Watanabe, T., and Haseda, T., 1958, J.Chem. Phys., 28, 323.

Weng, C-Y., and Griffiths, R.B., Private Communication.

Wilks, J., 1961, The Third Law of Thermodynamics, Oxford: Clarendon Press, Chapter X.

Wigner, E.P., 1959, Group Theory and its Application to the Quantum Mechanics of Atomic Spectra (Translation), Academic Press, p. 138.

Wilkinson, J.H., 1958, Computer Journal, 1, No. 2, 90 : 1960, Computer Journal, 3, No. 1, 23.

Wittekoek, S., 1967, Thesis, University of Leiden.

Wittekoek, S., Poulis, N.J., and Miedema, A.R., 1964, Physica, 30, 1051

Wood, D.W., 1965, Ph.D. Thesis, University of London.

Wortis, M., 1963, Phys. Rev., 132, 85.

Yang, C.N., and Lee, T.D., 1952, Phys. Rev., 87, 404, 410.

Yang, C.N., and Yang, C.P., 1966, Phys. Rev., 150, 321, 327; 151, 258.

Yang, C.P., 1963, Proc. Symp. Appl. Math., XV, 351.

The Entropy of an Antiferromagnet in a Magnetic Field

By JILL C. BONNER and MICHAEL E. FISHER

Reprinted from
Proceedings of the Physical Society, Vol. 80, Part 2, No. 514, pp 508–515
1962
Printed in Great Britain by J. W. Arrowsmith Ltd., Bristol 3

PROC. PHYS. SOC., 1962, VOL. 80

The Entropy of an Antiferromagnet in a Magnetic Field

BY JILL C. BONNER AND MICHAEL E. FISHER

Wheatstone Physics Laboratory, King's College, London

MS. received 19*th March* 1962

Abstract. The Ising model of an antiferromagnet exhibits an anomalous entropy peak at a critical magnetic field which remains even at the absolute zero of temperature, in violation of the third law of thermodynamics. By investigating numerically the behaviour of finite chains of spins interacting through the more general anisotropic Heisenberg coupling, described by the Hamiltonian

$$\mathscr{H} = 2|J| \sum_{i=1}^{N} \{S_i^z S_{i+1}^z + \gamma(S_i^x S_{i+1}^x + S_i^y S_{i+1}^y)\} - g\beta H \sum_{i=1}^{N} S_i^z$$

it is shown that the zero point anomalous entropy is peculiar to the Ising model ($\gamma = 0$). If the anisotropy is sufficiently great, however, an appreciable entropy peak does persist down to low temperatures although in the anisotropic (pure Heisenberg) limit the entropy has only a broad maximum which falls steadily in height as T approaches zero.

§ 1. INTRODUCTION

THE third law of thermodynamics implies that the entropy of a physical system in equilibrium must vanish as the absolute zero of temperature is approached. More precisely for a macroscopic system consisting of N subsystems (e.g. 'spins') interacting with one another the third law implies that the entropy per subsystem should vanish in the limits $N \to \infty$ and $T \to 0$. A magnetic material in thermodynamic equilibrium which did not obey the law could be used in an adiabatic demagnetization process to reach the absolute zero in a finite number of steps (Wilks 1961).

It was noted by Brooks and Domb (1951) that the plane square Ising model of an antiferromagnet is anomalous in this respect since the entropy displays a maximum as a function of magnetic field which persists down to absolute zero. The point has been discussed more recently by Fisher (1960) and Domb (1960).

In an antiferromagnetically ordered system at low temperatures a small magnetic field tends to reduce the order (by reversing spins aligned against the field) so that the entropy rises as the field is increased. In a strong field on the other hand all the spins become ferromagnetically aligned and the entropy falls to zero. Consequently at an intermediate field (and low enough temperature) the entropy displays a maximum, (see, for example, figure 1). It is a characteristic feature of the Ising model, however, that this entropy maximum persists as a sharp peak right down to $T = 0$ where it occurs at a field $H = H_c$ (see figure 1). The critical field H_c is simply the field at which the gain in magnetic energy on reversing a single spin coupled antiferromagnetically to q neighbouring spins is balanced by the loss of coupling energy due to the change over to ferromagnetic alignment. Explicitly if the Hamiltonian is

$$\mathscr{H} = 2|J| \sum_{(ij)} S_i^z S_j^z - g\beta H \sum_i S_i^z \tag{1}$$

the critical field is

$$H_c = q|J|/g\beta. \tag{2}$$

The height of the anomalous peak is found to be an appreciable fraction of the maximum possible entropy change ($k \ln 2$ per spin). Thus for the linear Ising chain (Domb 1960)

$$\frac{S}{S_{\max}} = \frac{\ln \frac{1}{2}(1+\sqrt{5})}{\ln 2} = 0{\cdot}69424 \tag{3}$$

while for the plane square 'superexchange' model (Fisher 1960)

$$\frac{S}{S_{\max}} = 0{\cdot}51481. \tag{4}$$

For the standard two-dimensional Ising lattices the anomalous entropy is not known exactly but is approximately 50% of the maximum.

It was suggested (Fisher 1960) that the anomalous zero point entropy was a direct consequence of the simplicity of the Ising form of coupling which would not arise with a more realistic form of interaction. To establish this point and to investigate the probable behaviour of the entropy of real antiferromagnets we have considered the generalized anisotropic Heisenberg Hamiltonian

$$\mathscr{H} = 2|J| \sum_{(ij)} \{S_i^z S_j^z + \gamma(S_i^x S_j^x + S_i^y S_j^y)\} - g\beta H \sum_{i=1}^{N} S_i^z. \tag{5}$$

Here the spin operators S_i^x, S_i^y and S_i^z obey the usual commutation relations while the isotropy parameter γ varies between the value zero, corresponding to the pure Ising interaction, and the value unity corresponding to the pure (isotropic) Heisenberg coupling $\mathbf{S}_i \cdot \mathbf{S}_j$.

The Hamiltonian (5) is essentially the same as that discussed by Kasteleijn (1952), by Orbach (1958) and by various other authors. Although some exact results are available for the ground state energy and related properties of the model in the limit $N \to \infty$ (Orbach 1958) the thermodynamic functions and the behaviour in a magnetic field are unfortunately not known even for a one-dimensional chain of spins. Accordingly we have undertaken a numerical study of the general properties of the model for finite chains and rings of spins.

Our calculations have so far been extended up to rings of 11 spins with nearest neighbour coupling, and cover the dependence of the energy, entropy, specific heat and susceptibility on the temperature, the field, the anisotropy and the number of spins. One of our main conclusions is that many features of the behaviour of long chains are already displayed by chains of seven to ten spins. The detailed evidence for this and the majority of our results will be presented in another paper. Here we confine ourselves to the question of the anomalous entropy and show that it can be settled by examining the results for short rings.

When our calculations were under way we learned that Dr. R. B. Griffiths at Stanford University, California, was making similar calculations for the isotropic Heisenberg Hamiltonian ($\gamma = 1$). His computations covered the zero field behaviour of energy, entropy, specific heat and susceptibility for rings of up to ten spins. We are very grateful to Dr. Griffiths for sending us details of his work which incidentally provided us with a useful check on some of our numerical results.

§ 2. NUMERICAL CALCULATIONS

The calculations of the eigenvalues of the Hamiltonian (5) and thence of the thermodynamic functions by the standard formulae of statistical mechanics, were performed

on the University of London 'Mercury' computer. The basic task is the diagonalization of a $2^N \times 2^N$ matrix. However by using the eigenfunctions of the operator ΣS_i^z which commutes with $\mathscr{H}$ the characteristic determinant factorizes into blocks, the largest being of order $N!/[(\frac{1}{2}N)!]^2$ (for N even). An appreciable further reduction can be achieved by using the translational symmetry of a ring of similar spins.

§ 3. PROPERTIES OF THE EIGENVALUES

In figure 1 we have plotted the entropy per spin for an Ising ring of eight spins ($\gamma = 0$) as a function of the field for various temperatures. The anomalous entropy

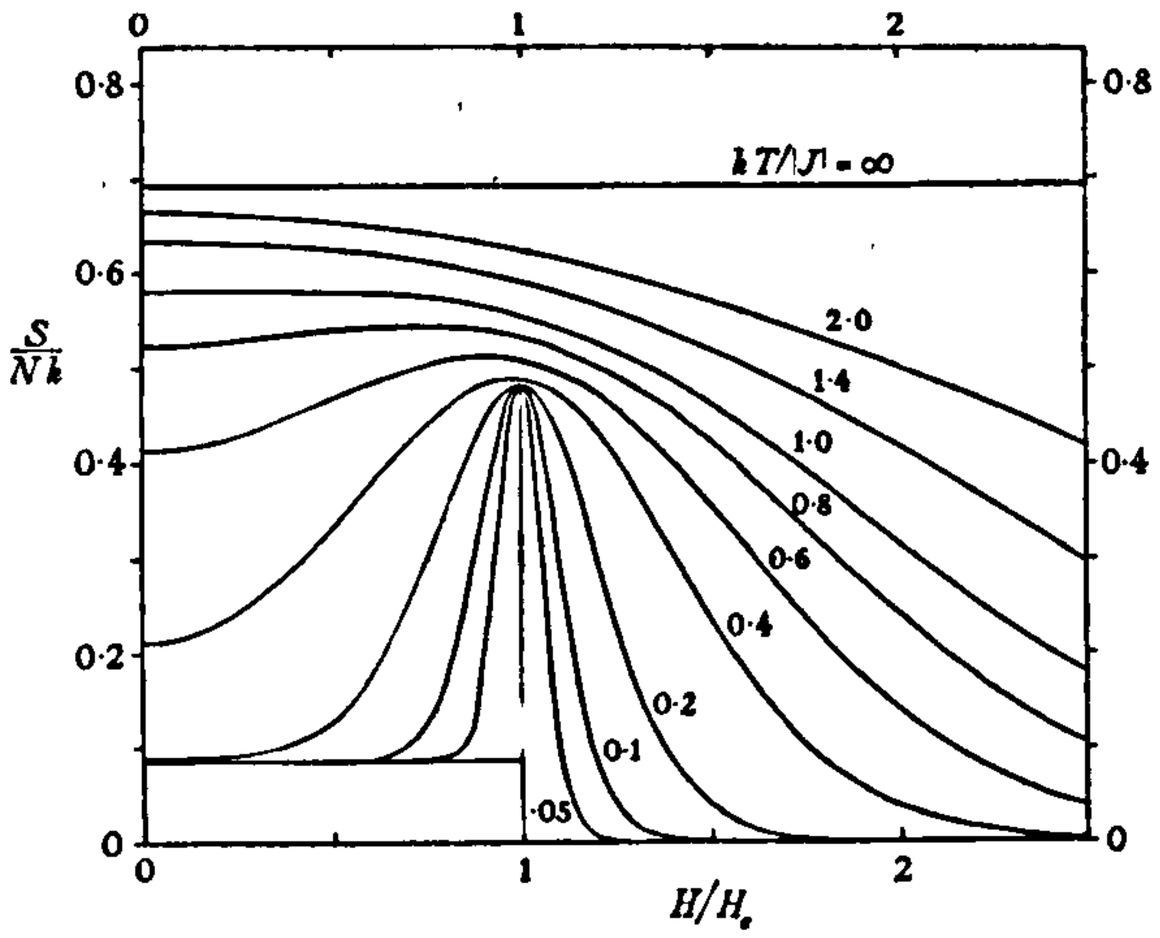

Figure 1. Variation of the entropy with magnetic field and temperature for a ring of 8 spins coupled with the Ising interaction ($\gamma = 0$).

peak is evident. Its height is given by $S/Nk = \frac{1}{8} \ln 47 = 0{\cdot}4813$ which differs from the limiting ($N = \infty$) result 0·4812 by less than 0·03%. For fields less than H_c, however, the entropy does not fall to zero as might be expected, but to the value $(k/N) \ln 2 = 0{\cdot}0866k$ ($N = 8$). This is a 'small number' effect arising from the twofold degeneracy of the antiferromagnetic ground state of the Ising model. In the limit $N \to \infty$, of course, this contribution vanishes.

Examination of the spectrum of eigenvalues of the Ising ring as a function of magnetic field (see figure 2) reveals that the anomalous entropy peak is due to a confluence of a large fraction of the energy levels at the critical field $H = H_c$. The multiplicity of this degeneracy for rings of $N = 2, 3, 4, \ldots$ spins is given by the Fibonacci series 3, 4, 7, 11, 18, 29, 47, ... the Nth term of which varies as $(\frac{1}{2}+\frac{1}{2}\sqrt{5})^N$. From this the limiting result (3) follows immediately. It is clear that any perturbation of the pure Ising Hamiltonian which splits this high degeneracy should result in the disappearance of the anomalous entropy at a sufficiently low temperature. When $\gamma > 0$ in (5) the transverse part of the Hamiltonian represents such a perturbation and calculation shows that the degeneracy is indeed appreciably split. Figure 3 shows the relevant part of the spectrum when $\gamma = 0{\cdot}1$ which still corresponds to a rather anisotropic antiferromagnet. Although the multiple degeneracy is split there is still a considerable density of low-lying levels near the critical field. The doubly degenerate zero-field antiferromagnetic ground

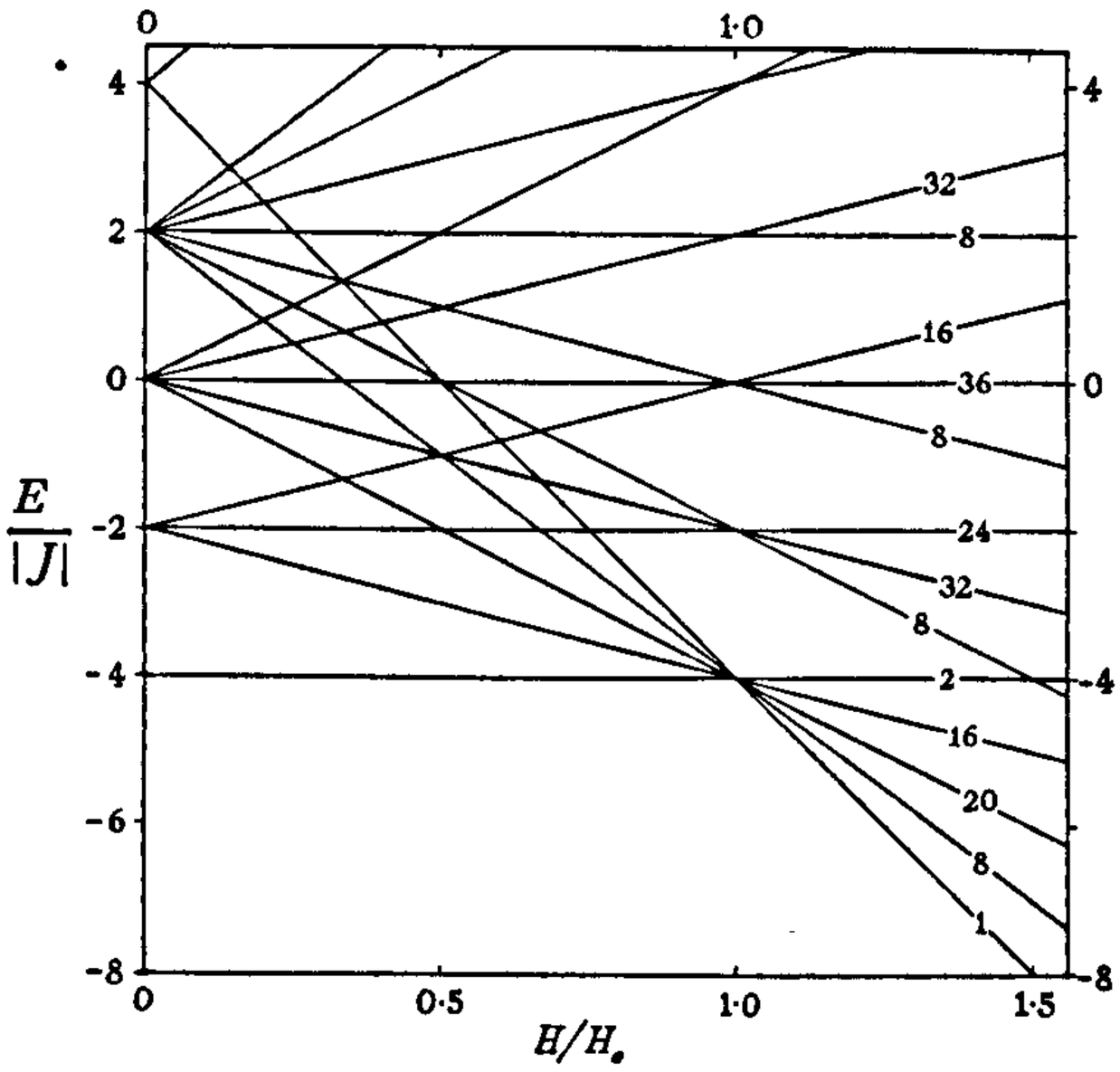

Figure 2. Spectrum of eigenvalues for an Ising ring of 8 spins as a function of magnetic field ($\gamma = 0$). The numbers indicate the degeneracy of the corresponding levels.

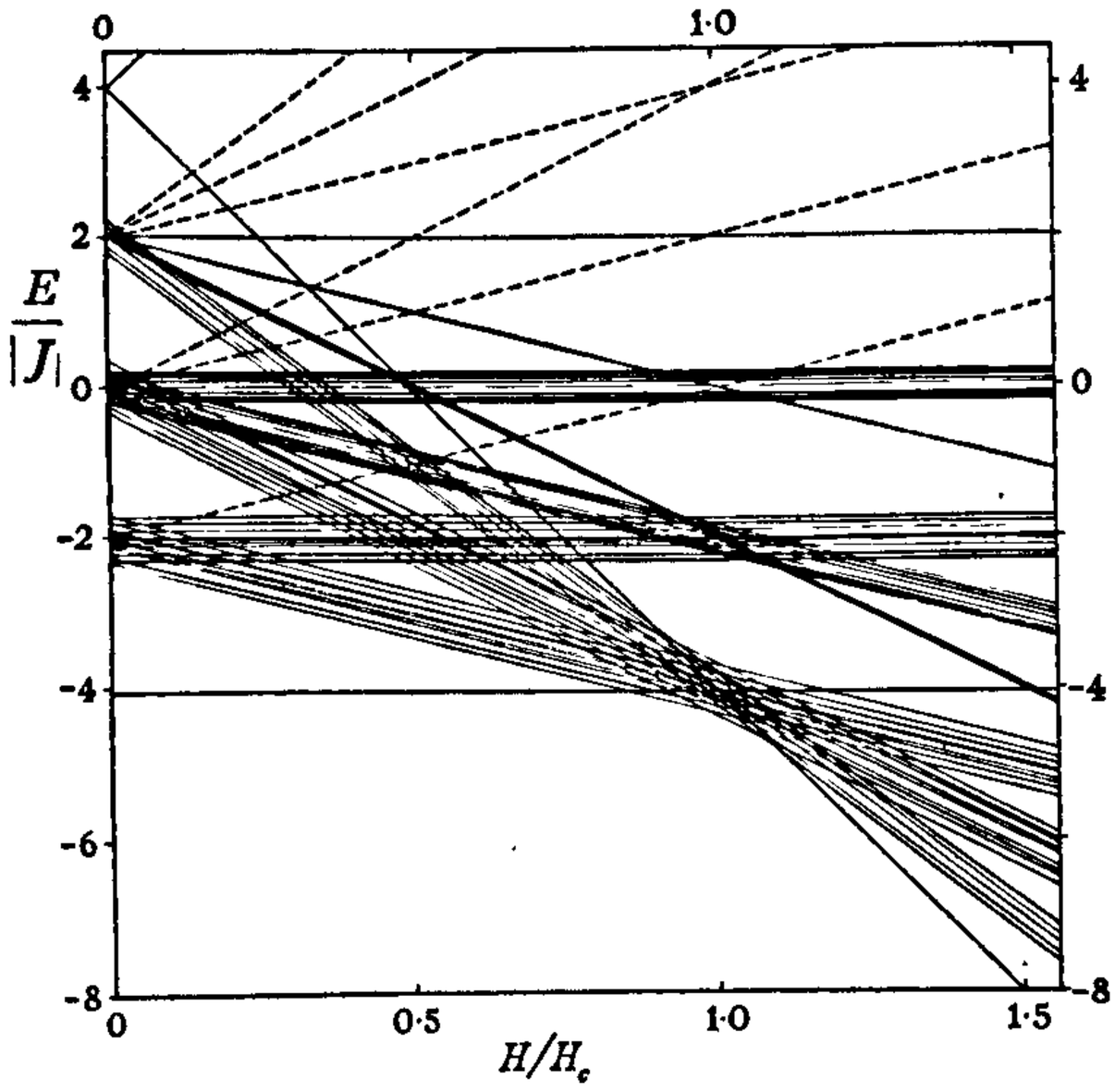

Figure 3. Spectrum of eigenvalues for $\gamma = 0{\cdot}1$. Note that the groups of levels of negative S^z are merely indicated by broken lines.

state is actually split but by such a small amount (0·024%) that the two levels cannot be distinguished on the scale of the figure.

The situation is quite different at the Heisenberg extreme ($\gamma = 1$, complete isotropy) as shown in figure 4. The level density is rather uniform and only slowly changing. The only degeneracies in the ground state are twofold and arise in a field from the crossing of one level by a level of higher total S^z. In the general case there will be $\frac{1}{2}N$ of these intersections ($H > 0$). It will be noticed that they are spread out between $H = 0$ and $H = 2H_c$ although they tend to cluster more closely towards $H = 2H_c$ (see below).

These general features of the energy level spectra are quite typical of longer chains and examination of more complicated spin clusters indicates that they will be equally typical of two- and three-dimensional lattices.

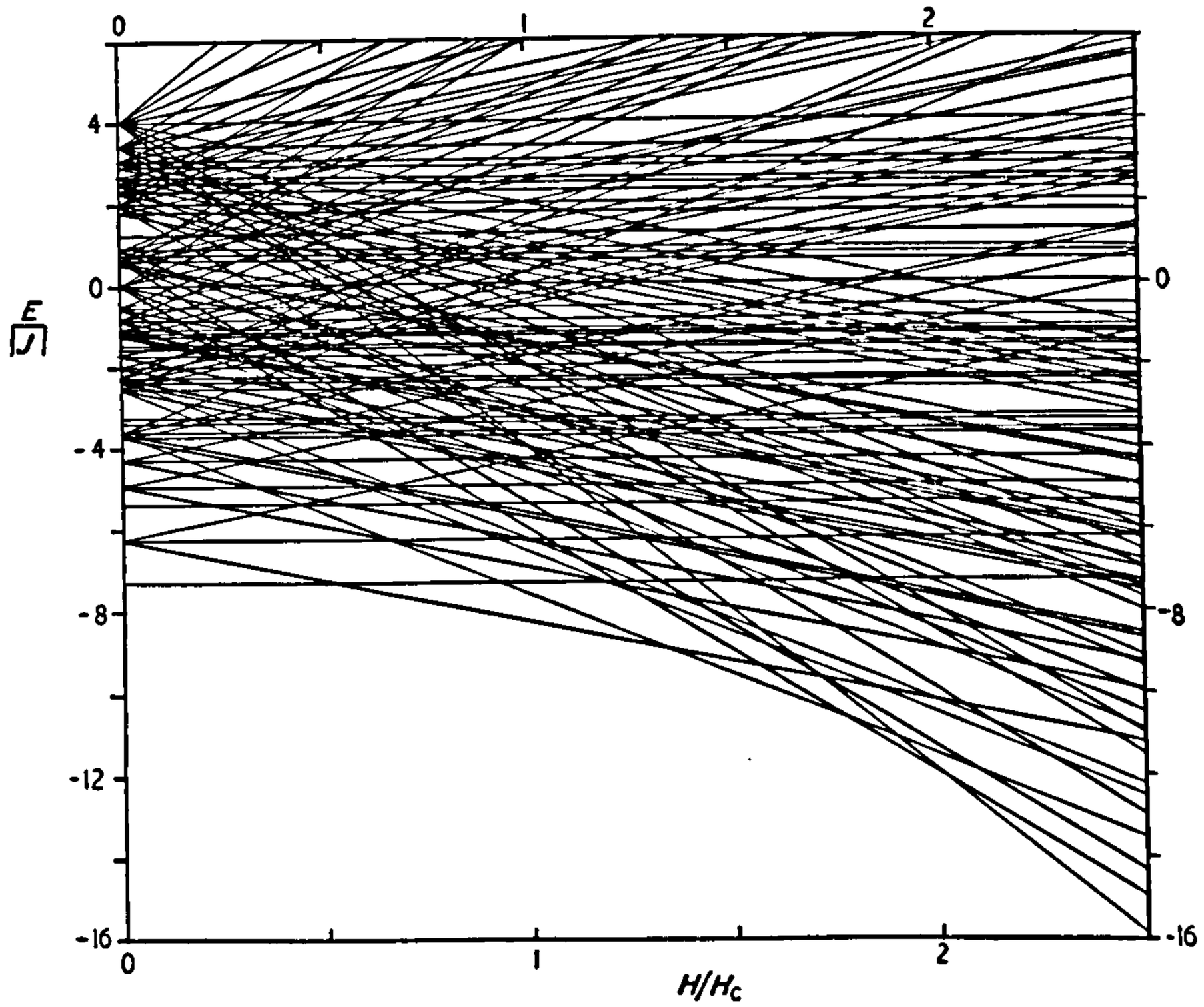

Figure 4. Spectrum of eigenvalues for a Heisenberg ring of 8 spins ($\gamma = 1$). (Note that the scales are not the same as in figures 2 and 3.)

§ 3. ENTROPY VARIATION

In figures 5, 6 and 7 we have plotted the entropies as derived from the calculated spectra for the cases $\gamma = 0{\cdot}1, 0{\cdot}5$ and 1 respectively. In figure 5 with $\gamma = 0{\cdot}1$ we are

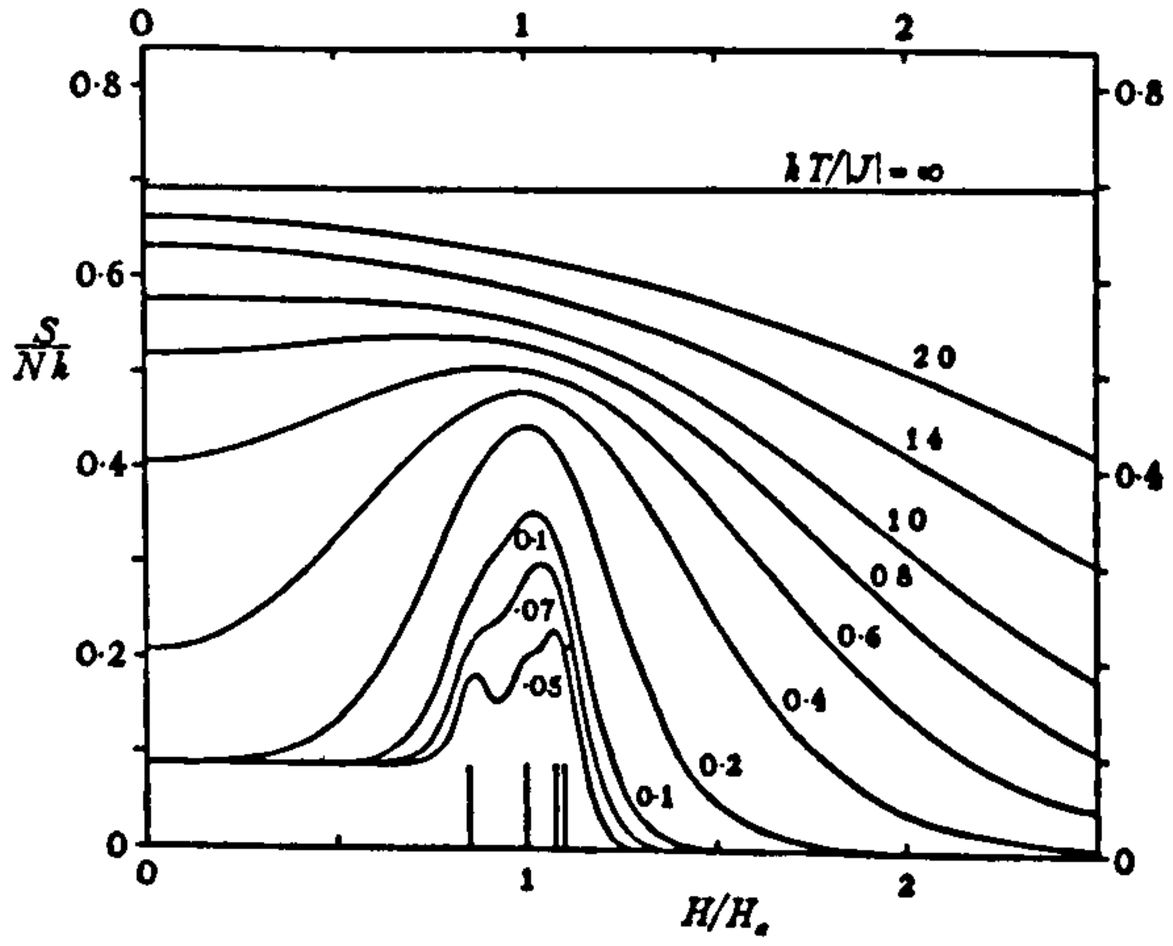

Figure 5. Variation of the entropy for an anisotropic ring when $\gamma = 0{\cdot}1$.

still close to the pure Ising model (figure 1) and the entropy isotherms are almost unchanged down to temperatures for which $kT/|J| = 0{\cdot}2$. Below this temperature, however, the height of the entropy peak begins to fall rapidly and eventually the peak splits into separate components. This again is a small number effect (see below) and we must presume that in the limit $N \to \infty$ the peak will fall smoothly to zero. (Owing to the very small splitting of the zero-field antiferromagnet ground state, noted above, the entropy below H_c still appears to fall to the value $(k \ln 2/N)$ rather than to zero. At very low temperatures, however, it will now fall to zero.)

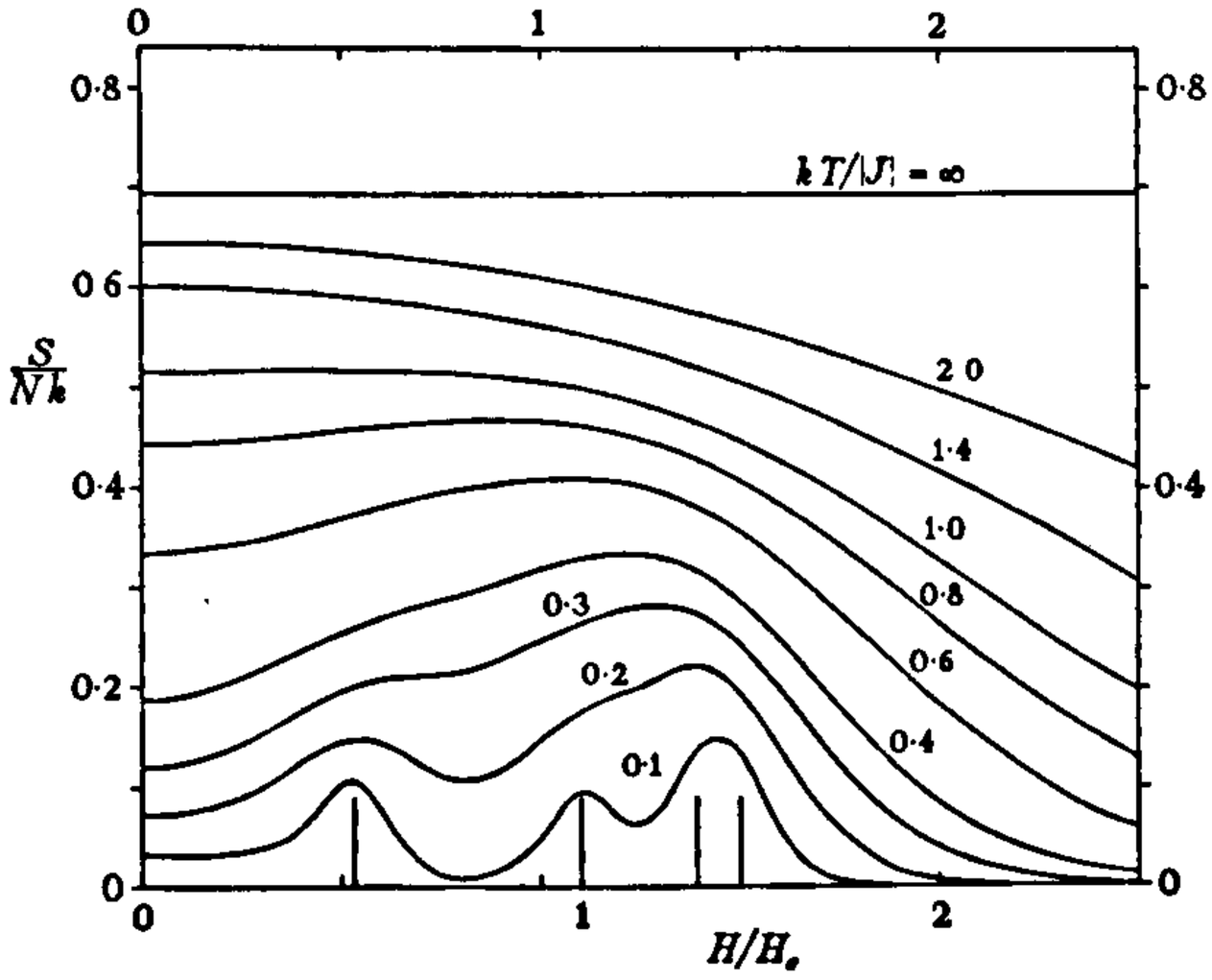

Figure 6. Variation of the entropy when $\gamma = 0{\cdot}5$.

In the case of moderate anisotropy ($\gamma = 0{\cdot}5$) shown in figure 6, the entropy maximum is much broader and has shifted to a higher value of the field. The height of the maximum falls steadily even at higher temperatures but at a temperature below $kT/|J| = 0{\cdot}3$ the maximum again splits into a series of smaller separated peaks. The same phenomenon occurs in the pure Heisenberg case (figure 7) where the maximum is so spread out and

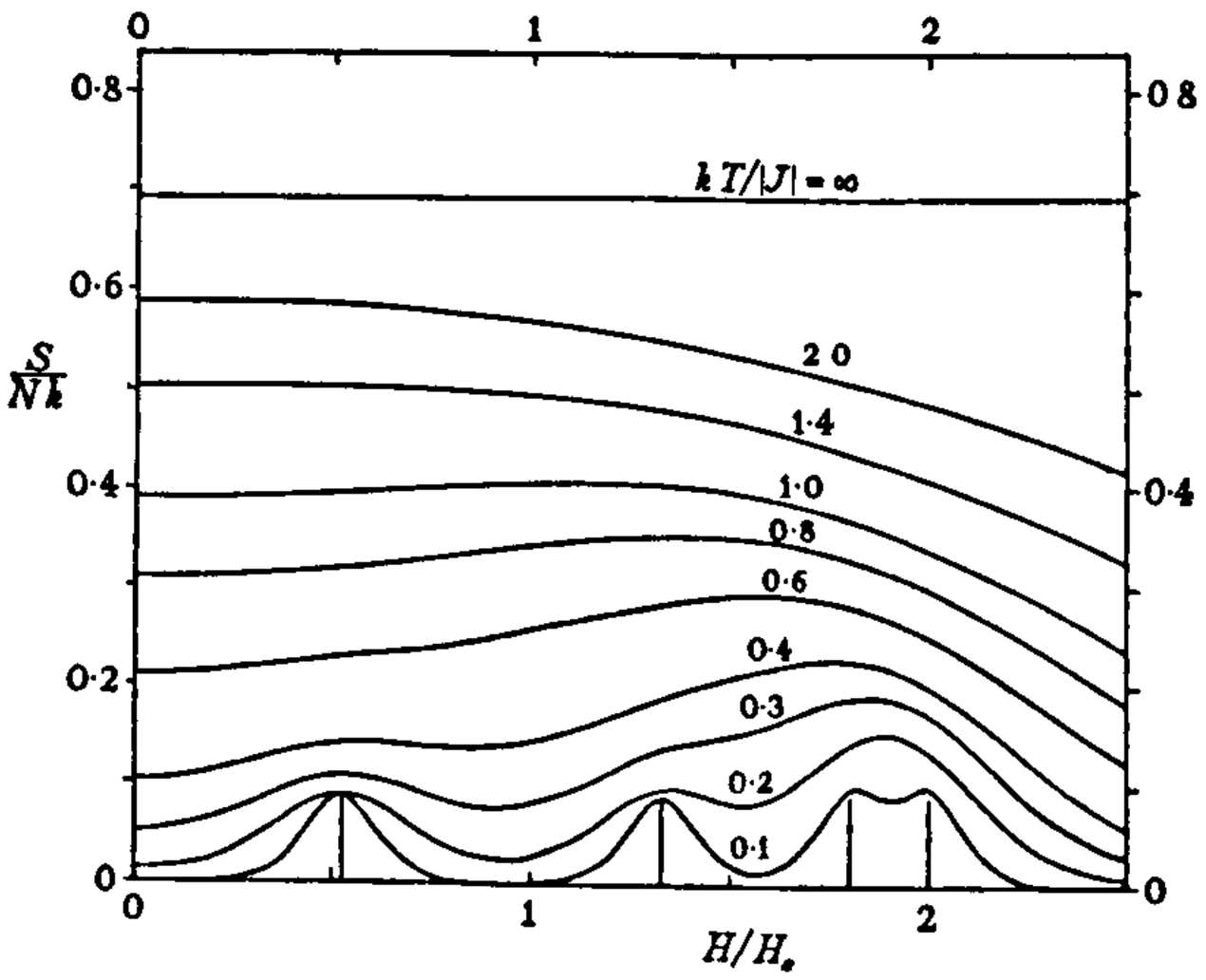

Figure 7. Variation of the entropy for the Heisenberg case ($\gamma = 1$).

so low in height as to be scarcely identified as a feature of interest. The small peaks in all these cases are of height $k \ln 2 /N$ and correspond simply to the twofold degeneracy that occurs when levels of adjacent S^z cross in a field as mentioned above. In the limit

$N \to \infty$ these peaks will be absent and the entropy must fall smoothly to zero in all fields.

The main features of the dependence on anisotropy are summarized in figures 8 and 9 which show the loci of the entropy maxima in the (H, T) plane and the variation of the height of the maximum with temperature for different values of γ. As the anisotropy decreases the maximum becomes lower and broader and shifts to higher fields.

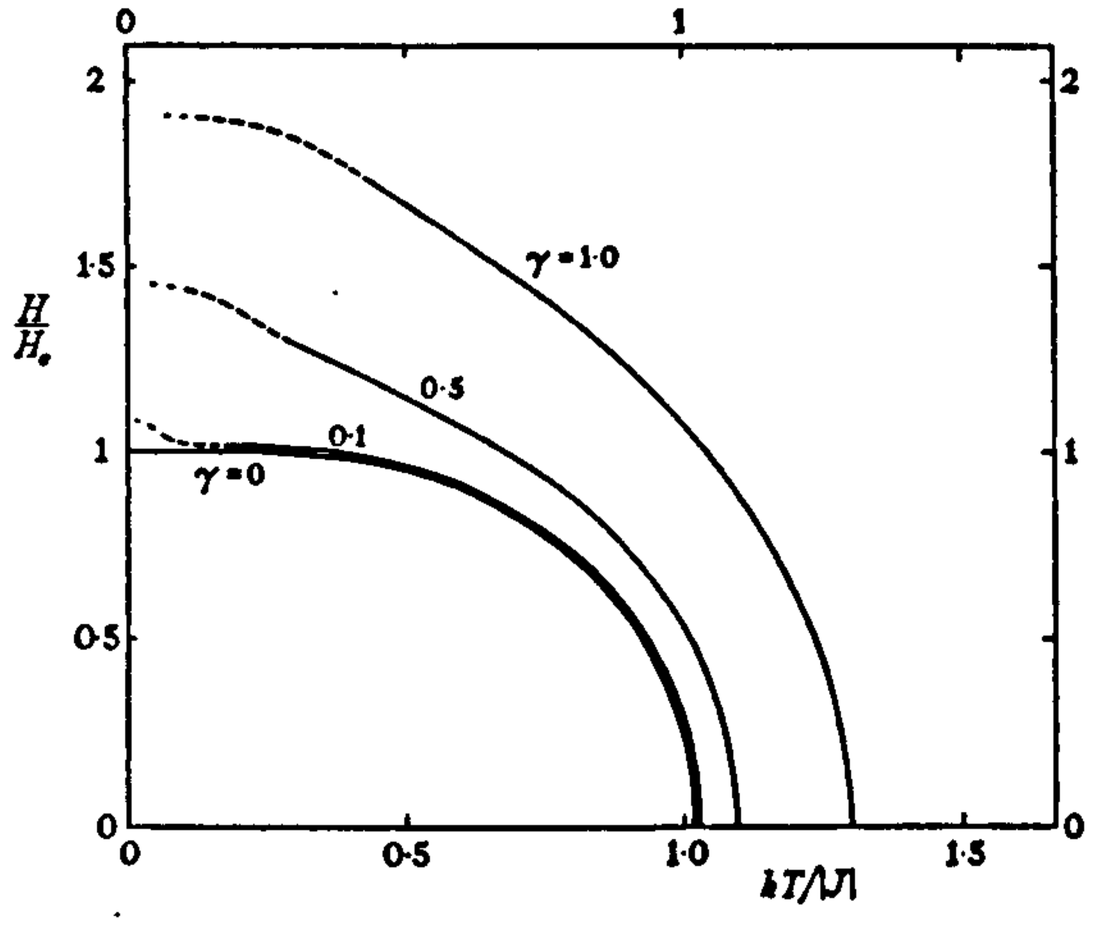

Figure 8. Loci of entropy maxima as a function of temperature and field for different degrees of anisotropy.

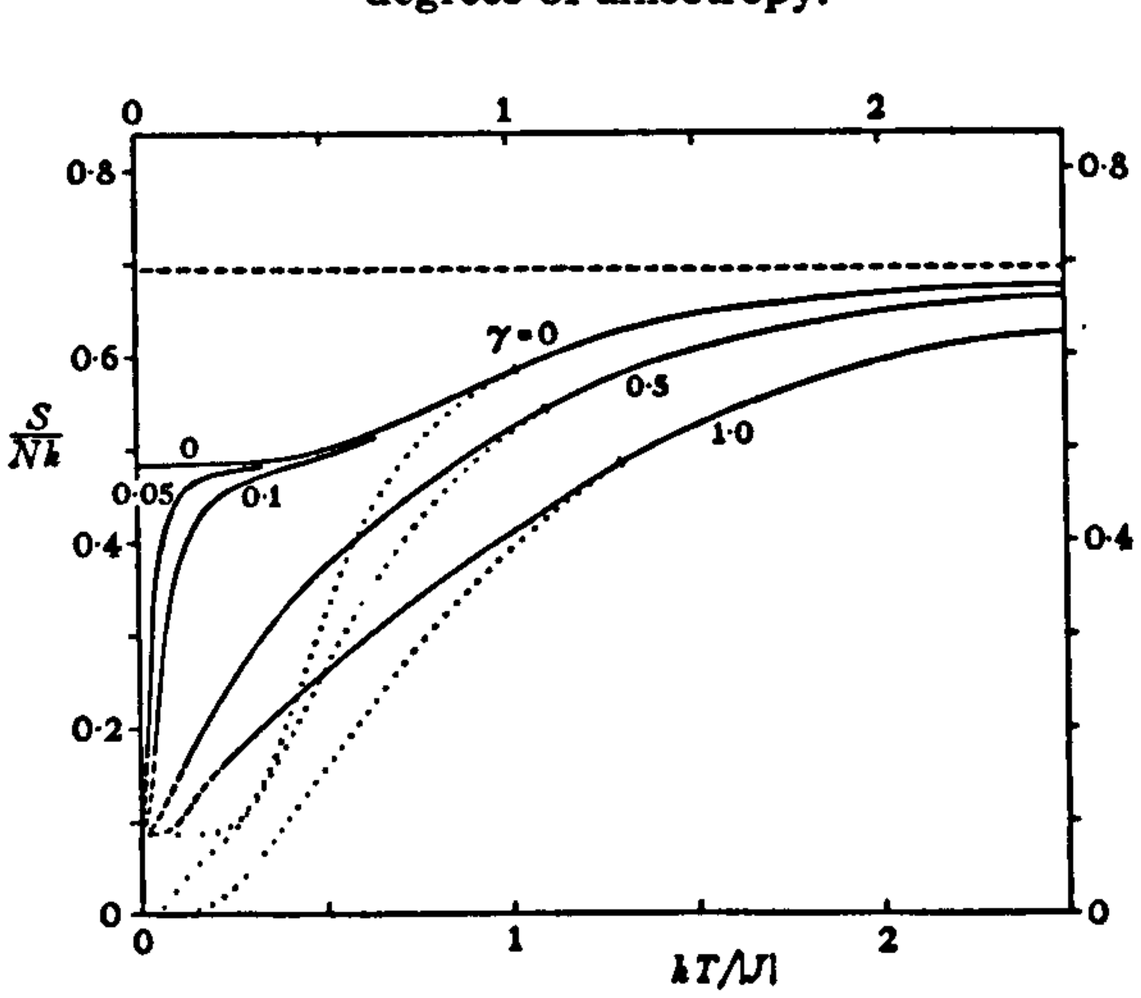

Figure 9. Variation of the height of the entropy maxima with temperature for different degrees of anisotropy. Note that the dotted curves represent the zero-field entropy minima.

Quite clearly the anomalous zero point entropy occurs only at the Ising limit although, if there is sufficient anisotropy, an appreciable entropy peak remains to quite low temperatures even when $\gamma > 0$. These curves are plotted for the case $N = 8$ but except at the lowest temperatures, where the curves are shown by broken lines, they will differ by no more than a few per cent from the limiting results (for $N = \infty$).

A linear chain of coupled spins does not, of course, show a phase transition although we may loosely distinguish a predominantly antiferromagnetic region (lying below the

locus in figure 8) from a predominantly paramagnetic region, at high fields and temperatures. Two- and three-dimensional models (except for the Heisenberg limit in two dimensions) must be expected to show a proper transition with an associated specific heat anomaly, as do real antiferromagnets. The effect of a transition on the entropy variation, however, should not be very marked as is demonstrated, for example, by the exactly soluble two-dimensional super-exchange Ising model (Fisher 1960). The main change will be merely a steepening up of the rate of increase of entropy with field on the low field side of the entropy maximum. (It is probable that $\partial S/\partial H$ becomes infinite at the transition but it seems unlikely, in view of experimental and theoretical knowledge of the specific heat anomaly, that this infinity is much sharper than logarithmic.) Consequently the general features of the entropy variation and its dependence on anisotropy which we have discussed should be valid for two- and three-dimensional Heisenberg-type models and for real antiferromagnets of simple structure.

ACKNOWLEDGMENTS

We are indebted to Professor C. Domb for stimulating our interest in this problem and for discussing its significance with us.

One of us (J.C.B.) is grateful to the Department of Scientific and Industrial Research for the award of a grant.

REFERENCES

Brooks, J. E., and Domb, C., 1951, *Proc. Roy. Soc.* A, **207**, 343.
Domb, C., 1960, *Advanc. Phys.*, **9**, 165.
Fisher, M. E., 1960, *Proc. Roy. Soc.* A, **256**, 502.
Kasteleijn, P. W., 1952, *Physica*, **18**, 104.
Orbach, R., 1958, *Phys, Rev.*, **112**, 309.
Wilks, J., 1961, *The Third Law of Thermodynamics*, Ch. X (Oxford: Clarendon Press).

Reprinted from THE PHYSICAL REVIEW, Vol. 135, No. 3A, A640–A658, 3 August 1964
Printed in U. S. A.

Linear Magnetic Chains with Anisotropic Coupling

JILL C. BONNER
Department of Physics, Royal Holloway College, Englefield Green, Surrey, England

AND

MICHAEL E. FISHER
Wheatstone Physics Laboratory, King's College, London W. C. 2, England

(Received 11 February 1964; revised manuscript received 8 April 1964)

Linear chains (and rings) of $S=\frac{1}{2}$ spins with the anisotropic (Ising-Heisenberg) Hamiltonian

$$\mathcal{H}=-2J\sum_{i=1}^{N}\{S_i^xS_{i+1}^x+\gamma(S_i^xS_{i+1}^x+S_i^yS_{i+1}^y)\}-g\beta\sum_{i=1}^{N}\mathbf{H}\cdot\mathbf{S}_i$$

have been studied by exact machine calculations for $N=2$ to 11, $\gamma=0$ to 1 and for ferro- and antiferromagnetic coupling. The results reveal the dependence on finite size and anisotropy of the spectrum and dispersion laws, of the energy, entropy, and specific heat, of the magnetization and susceptibilities, and of the pair correlations. The limiting $N\to\infty$ behavior is accurately indicated, for all γ, in the region $kT/|J|\gtrsim 0.5$ which includes the maxima in the specific heat and susceptibility. The behavior of thermal and magnetic properties of infinite chains at lower temperatures is estimated by extrapolation. For infinite antiferromagnetic chains the ground-state degeneracy, the anisotropy gap, and the magnetization, perpendicular susceptibility, and pair correlations at $T=0$ are similarly studied. Estimates of the long-range order suggest that it vanishes only at the Heisenberg limit $\gamma=1$ and confirm the accuracy of Walker's perturbation series in γ.

1. INTRODUCTION

EXPERIMENTAL and theoretical studies have shown that in many magnetic materials, the magnetic part of the Hamiltonian may be quite accurately represented as a set of localized spins $\mathbf{S}_i$ with bilinear interactions. For certain highly anisotropic systems,[1] the coupling energy can be approximated by the pure Ising form $-2JS_i^zS_j^z$, but for most systems the anisotropy, although important, is not very large and the pure Heisenberg coupling $-2J\mathbf{S}_i\cdot\mathbf{S}_j$ is more realistic. Between these extremes is the anisotropic "intermediate" coupling $-2J\{\gamma\mathbf{S}_i\cdot\mathbf{S}_j+(1-\gamma)S_i^zS_j^z\}$ which reduces to the Ising case when $\gamma=0$ and the Heisenberg case when $\gamma=1$.

With pure Ising interaction the partition function of a finite or infinite chain of spins in a parallel magnetic field, and thence the thermal and magnetic properties, may be calculated exactly.[2] For simple two-dimensional Ising lattices exact solutions may be obtained in zero field.[2] For the Heisenberg, or intermediate γ spin Hamiltonians, however, exact closed formulas for the finite-temperature behavior have not been found even for the linear chain despite much theoretical effort (see below). Although, naturally, greatest interest attaches to three-dimensional lattices, the properties of linear chains with non-Ising spin coupling are of both experimental and theoretical significance.

Experimentally a number of crystals are known,[3] for example copper tetramine sulfate monohydrate,[3a,b,4] in which the magnetic ions are arranged in chains with strong interactions within each chain but rather weak interactions between chains. Except at the lowest temperatures, the chains should be almost independent and theoretical values based on a one-dimensional model may be confronted directly with experimental measurements. Furthermore, the experimental evidence on various cupric quinone complex salts[3c,d] indicates the existence of independent *finite* chains of 10 to 20 magnetic ions. A one-dimensional model is similarly valid for magnetically active polymeric molecular chains of finite or indefinitely great length.[5]

Theoretically the linear chain Heisenberg-Ising model is interesting as one of the simplest many-body systems in which quantum effects play a vital part. This is especially so for the antiferromagnetic chain where the calculation of even the ground-state energy is not easy, although it has been performed exactly.[6–9] Accurate

---

[1] A. H. Cooke, D. T. Edmonds, C. B. P. Flinn, and W. P. Wolf, Proc. Phys. Soc. (London) 74, 791 (1959); M. Ball, M. T. Hutchings, M. J. M. Leask, and W. P. Wolf, Proceedings of the Eighth International Congress on Low-Temperature Physics (to be published); M. Ball, M. J. M. Leask, W. P. Wolf, and A. F. G. Wyatt, J. Appl. Phys. 34, 1104 (1963).

[2] C. Domb, Advan. Phys. 9, 149 (1960). The perpendicular susceptibility (in zero field) may also be calculated exactly with Ising coupling in one and two dimensions. See Refs. 43 and 44.

[3] (a) T. Haseda and A. R. Miedema, Physica 27, 1102 (1961); (b) T. Watanabe and T. Haseda, J. Chem. Phys. 28, 323 (1958); (c) T. Haseda, A. R. Miedema, H. Kobayashi, and E. Kanda, J. Phys. Soc. Japan 17, Suppl. B-I, 518 (1962); (d) H. Kobayashi, T. Haseda, E. Kanda, and S. Kanda, J. Phys. Soc. Japan 18, 349 (1963); (e) L. Berger, S. A. Friedberg, and J. T. Schriempf, Phys. Rev. 132, 1057 (1963).

[4] R. B. Griffiths, Phys. Rev. following paper 135, A659 (1964).

[5] V. L. Ginsburg and V. M. Fain, Dokl. Acad. Nauk SSSR 131, 785 (1960); L. A. Blyumenfel'd, A. E. Kalmanson, and S. P'ei-Ken, *ibid.* 124, 1144 (1959); L. A. Blyumenfel'd and V. A. Benderskii, *ibid.* 133, 1451 (1960) [English transls.: Soviet Phys.—Doklady 5, 328 (1960); 4, 260 (1959); 5, 919 (1961)]; L. A. Blyumenfel'd, Biofizika 4, 515 (1959) [English transl.: Biophysics USSR 4, 3 (1959)].

[6] H. A. Bethe, Z. Physik 71, 205 (1931).

[7] L. Hulthén, Arkiv Mat. Astron. Fysik 26A, No. 11 (1938).

[8] R. L. Orbach, Phys. Rev. 112, 309 (1958).

[9] L. R. Walker, Phys. Rev. 116, 1089 (1959).

values for other properties would be valuable as an aid to judging various approximate theoretical treatments which are also applicable to more complex systems. From the viewpoint of statistical mechanics, it is also of interest to study how the limiting behavior for infinite systems is approached by finite systems. Such insight is useful since, with the advent of fast digital computers, it is feasible to perform exact or Monte Carlo calculations on finite models of many types of physical system.

With this motivation we have undertaken a numerical study of finite chains and rings of N spins with the Hamiltonian,

$$\mathcal{H}=-2J\sum_{i=1}^{N}\{S_i^zS_{i+1}^z+\gamma(S_i^xS_{i+1}^x+S_i^yS_{i+1}^y)\}-g\beta\sum_{i=1}^{N}\mathbf{H}\cdot\mathbf{S}_i \quad (1.1)$$

for spin $S=\frac{1}{2}$. We have computed the energy levels and eigenvectors and thence the thermal and magnetic properties for varying anisotropy γ and varying magnetic field H for rings of size $N=2$–11 (and for some open chains) for both ferro- and antiferromagnetic coupling ($J=+|J|$ and $J=-|J|$, respectively). (Our results for the antiferromagnetic entropy in a magnetic field for varying γ have already been reported and discussed in the light of the third law of thermodynamics.[10])

Previously, Orbach[11] had computed the energy levels and eigenvectors for $N=2$, 4, 6, 8 and (unpublished) $N=10$ for the case $\gamma=1$, and for some intermediate γ values in the case of $N=8$ (also unpublished), but he did not compute the thermal or magnetic properties. Independently of the present authors Griffiths[12] has calculated the energy levels for $N=3$, 5, 7, 9, and 10 for $\gamma=1$. He evaluated the energies, entropies, specific heats, and susceptibilities in zero field for $N=2$–10, and compared them with the series expansions. We are deeply indebted to both Dr. R. L. Orbach and Dr. R. B. Griffiths for sending us their own unpublished calculations and for helpful discussions and correspondence.

Theoretical work on the Hamiltonian (1.1) with $\gamma=1$ dates back to 1930 when Bloch[13] introduced the concept of a spin wave and gave the exact eigenstates for one overturned spin ($\sum S_i^z=NS-1$) for ferromagnetic interactions. Using a similar approach, Bethe[6] obtained the exact eigenstates corresponding to interacting spin waves for an arbitrary number of overturned spins on a linear chain ($\gamma=1$). He showed how the states may be classified as "unbound" or "bound." Hulthén, in a comprehensive paper,[7] used Bethe's solutions to obtain an integral equation from which he obtained the exact value for the antiferromagnetic ground-state energy of the infinite linear chain. He also obtained the exact ground states for rings of $N=4$, 6, 8, and 10 spins and estimated the susceptibility at $T=0$.

The arguments of Bethe and Hulthén were extended by Orbach[8] to the full anisotropic Hamiltonian (1.1), which had also been considered by Kasteleyn.[14] Kasteleyn used a variational method which indicated a critical anisotropy constant $\gamma_c=0.483$ beyond which the zero-temperature long-range order (present when $\gamma=0$) vanished identically. The variational short-range order and energy showed singularities in γ at the same point. With the aid of an exact integral equation Orbach showed that these latter singularities were spurious but he was unable to calculate the long-range order exactly. Walker,[9] in an important paper, obtained an analytic solution of Orbach's integral equation which revealed that the antiferromagnetic ground state $E_0(\gamma)$ as a function of γ was nonanalytic at $\gamma=1$. This implies that the Heisenberg limit ($\gamma=1$) is a special point perhaps analogous to a critical point.[15] Walker also gave perturbation series in powers of γ^2 for the energy and for the short-range and long-range order. His series for the long-range order seems to indicate that it does not vanish for γ less than about 0.9.

Perturbation calculations equivalent to those of Walker have been presented by Boon,[16] who also considered two- and three-dimensional lattices. Alternative perturbation procedures have been proposed by Davis, Rodriguez, Frank, Mannari, and Mills, Kenan, and Korringa.[17–19] Ruijgrok and Rodriguez[20] developed a variation method which was rather accurate for the ground state but which yielded a finite long-range order even for $\gamma=1$.

Earlier calculations based on the spin-wave approach have been reviewed by Van Kranendonk and Van Vleck.[21] One of the most striking predictions is that for a pure Heisenberg antiferromagnet the lowest energy states should obey a dispersion law of the form

---

[10] J. C. Bonner and M. E. Fisher, Proc. Phys. Soc. (London) 80, 508 (1962).

[11] R. L. Orbach, Ph.D. dissertation, University of California, 1959 (unpublished); Phys. Rev. 115, 1181 (1959).

[12] R. B. Griffiths, mimeographed reports, Stanford University, 1961, and La Jolla, California, 1963 (unpublished).

[13] F. Bloch, Z. Physik 61, 206 (1930).

[14] P. W. Kasteleyn, Physica 18, 104 (1952).

[15] The fact that $\gamma=1$ is a mathematical singularity (nonanalytic point) of $E_0(\gamma)$, follows immediately from Walker's observation that his formula exhibits a pole in any interval, however small, of the open segments $|\gamma|>1$. It should be noted, however, that the singularity at $\gamma=1$ is not visible in graphs of $E_0(\gamma)$ for $\gamma\leqslant 1$ contrary to what might be expected. One may regard Kasteleyn's variational transition point $\gamma_c=0.48$ (where the energy was nonanalytic as in any phase transition) as an approximation to the "true transition point" at $\gamma=1$.

[16] M. H. Boon, Nuovo Cimento 21, 885 (1961).

[17] H. L. Davis, Phys. Rev. 120, 789 (1960). These results are presented as a power series in $\gamma(=1-\alpha$ in Davis's notation), but the higher coefficients are inexact since the perturbation Hamiltonian is not just the transverse part of (1.1).

[18] S. Rodriguez, Phys. Rev. 116, 1474 (1959); R. L. Mills, R. P. Kenan, and J. Korringa, Physica 26, S204 (1960).

[19] D. Frank, Z. Physik 146, 615 (1956); I. Mannari, Progr. Theoret. Phys. (Kyoto) 19, 201 (1958).

[20] T. W. Ruijgrok and S. Rodriguez, Phys. Rev. 119, 596 (1960).

[21] J. Van Kranendonk and J. H. Van Vleck, Rev. Mod. Phys. 30, 1 (1958).

$\epsilon(k)=E-E_0\sim|\sin k|$.[21–24] This conclusion was tested against the numerical spectra for finite rings of $N=6$ and 8 spins by Mattheiss,[25] who found an approximately $|\sin k|$ dependence, but with a modified amplitude. More recently, des Cloizeaux and Pearson[26] extended the computation to the lowest antiferromagnetic states for rings of 16 and 48 spins. They were also able to derive the limiting dispersion law $\epsilon(k)=\pi|J||\sin k|$ for the corresponding class of states of an infinite chain.

The theoretical knowledge of the ground and lower excited states of Heisenberg-Ising chains is not matched by a corresponding knowledge of the thermodynamic behavior. For example, the positions of the maxima in the specific heat and susceptibility do not previously seem to have been estimated with any accuracy. (Although recently, Bulaevskii[27] has reported a finite temperature Hartree-Fock calculation which reproduces the general features quite well.)

It is interesting, however, that the spin-$\frac{1}{2}$ model obtained by deleting the parallel or Ising terms $S_i^zS_{i+1}^z$ from Eq. (1.1) to leave only the transverse Hamiltonian is completely soluble. Lieb, Schultz, and Mattis[28] investiagated the spectrum in detail while Katsura[29] studied the thermal and magnetic properties including the behavior in a field. Although the transverse Hamiltonian is somewhat artificial, the behavior of this model resembles in many respects the results we have found with the full Hamiltonian (1.1).[30]

It is also possible to calculate by elementary methods the zero-field free energy, correlations and susceptibility for isotropic Heisenberg chains in the limit of infinite spin.[31] The low-temperature behavior of the thermal properties in this case is somewhat unrealistic since in the classical limit $S=\infty$ the specific heat necessarily goes to a nonzero value as $T\to 0$. The susceptibility, however, correlates quite closely with the results we find for the $S=\frac{1}{2}$ Heisenberg chains (except that a nonphysical contradiction of the third law is shown again by a nonzero slope for small T).

The plan of this paper is as follows: In Sec. 2, the machine computations are outlined and the possibilities of extrapolation from finite N to the limit $N\to\infty$ are illustrated by examining the antiferromagnetic ground state as a function of γ. The thermal properties, in particular the specific heat, are discussed in Sec. 3 for antiferromagnetic and ferromagnetic rings. The magnetic properties are described in Sec. 4. Attention is given especially to the magnetization curve at $T=0$ and the corresponding parallel and perpendicular susceptibilities. In Sec. 5 details of the energy spectrum are discussed and the antiferromagnetic anisotropy gap and the asymptotic degeneracy of the ground state are estimated. The spin-wave dispersion laws for ferro- and antiferromagnetic chains are illustrated. The short-range antiferromagnetic order and further pair correlation functions $\langle S_0^zS_l^z\rangle$ are described in Sec. 6. The long-range order is estimated by extrapolation and compared with previous approximations. Our results are for the most part presented graphically but tables of the thermal and magnetic properties for $\gamma=1$ and 0.5 and $N=9$, 10, and 11 have been prepared and will be made available on request to the authors. (For reasons of economy they are not reproduced in this article.)

2. FINITE CHAIN CALCULATIONS AND THE ANTIFERROMAGNETIC GROUND STATE

For a finite system of N ($S=\frac{1}{2}$) spins the problem of calculating the energy levels reduces to the diagonalization of the $2^N\times 2^N$ matrix representing the Hamiltonian. (As basic states it is covenient to use direct products of "UP" and "DOWN" single-spin states: These are, of course, eigenstates of the Ising Hamiltonian $\gamma=0$.) By classifying the states by the value of S^z, the z component of the total spin, the matrix splits into $N+1$ blocks of order $1, N, \binom{N}{2}, \cdots\binom{N}{\frac{1}{2}N}, \cdots N, 1$ (N even). A further reduction can be obtained for closed chains (rings) of spins by using the translational invariance. Each level is then also classified by a (total) wave number $k=2\pi r/N$ with $r=0, 1, 2, \cdots, N-1$ (k is only determined up to a multiple of 2π).

The largest value of N which can be handled numerically is limited by the size of the largest block matrix in relation to the speed and capacity of the electronic computer available. Our calculations were performed on the now relatively slow University of London Ferranti "Mercury" which restricted us to $N=11$ or less. To economize on computing time many of the calculations for intermediate values of γ and magnetic field, etc., were, in fact, performed with $N=8$, or 10, once the trend with increasing N was clear.[10] The diagonalization, yielding both energy levels and eigenstates, was performed by standard subroutines and the results checked against the other available computations.[11,12,32] The calculation of the thermodynamic properties was performed by direct evaluation of the appropriately weighted partition sums.

The possibilities of estimating the properties of

[22] P. W. Anderson, Phys. Rev. 86, 694 (1952).
[23] R. Kubo, Phys. Rev. 87, 568 (1952).
[24] T. Oguchi, Phys. Rev. 117, 117 (1960).
[25] L. F. Mattheiss, Phys. Rev. 123, 1209 (1961).
[26] J. des Cloizeaux and J. J. Pearson, Phys. Rev. 128, 2131 (1962).
[27] L. N. Bulaevskii, Zh. Eksperim. i Teor. Fiz. 43, 968 (1962); see also V. L. Ginsburg and V. M. Fain, *ibid.* 39, 1323 (1960); 42, 180 (1962) [English transls.: Soviet Phys.—JETP 16, 685 (1963); 12, 923 (1961); 15, 131 (1962)].
[28] E. Lieb, T. Schultz and D. Mattis, Ann. Phys. (N. Y.) 16, 407 (1961).
[29] S. Katsura, Phys. Rev. 127, 1508 (1962).
[30] S. Katsura (preprint) has discussed the full Hamiltonian by treating the parallel terms as a perturbation.
[31] M. E. Fisher, Am. J. Phys. 32, 343 (1964).
[32] For the Heisenberg limit $\gamma=1$ one has a further check since the total spin S is also conserved so that many levels from different blocks coincide. It was not found possible to use this added invariance to reduce the calculations.

TABLE I. Energy of the antiferromagnetic ground state $\mathcal{E}_0(N)$.

N	Even	N	Odd
4	−1.00000	3	−0.50000
6	−0.93425	5	−0.74721
8	−0.91277	7	−0.81577
10	−0.90309	9	−0.84384
12	−0.8979	11	−0.85799
⋮		⋮	
∞	−0.88629	∞	−0.88629

infinite chains from those of finite chains are revealed by a study of the pure Heisenberg antiferromagnetic ground state energies. The antiferromagnetic ground state E_0 is equal to $-2N|J|\ln 2+\frac{1}{2}N|J|$ for the Hamiltonian (1.1) with $H=0$ and $\gamma=1$ in the limit $N\to\infty$. It is convenient to define normalized ground-state energies for finite N

$$\mathcal{E}_0(N)=E_0(N)/N|J|$$

and these energies are tabulated numerically in Table I. (The values for $N=4$, 6, 8, and 10 were given exactly by Hulthén,[7] that for $N=12$ by Ledinegg and Urban.[33]) In Fig. 1 the energies are plotted versus $1/N$ (circles) and versus $(1/N)^2$ (squares). The values form two sequences (N odd or even) and it is evident that the limiting energy is approached linearly with $(1/N)^2$. A relation of the form

$$\mathcal{E}_0(N)=\mathcal{E}_0(\infty)+a/N^2 \qquad (2.1)$$

holds quite accurately even down to $N=4$ or 5 with $a_{\text{odd}}\simeq -2a_{\text{even}}$.

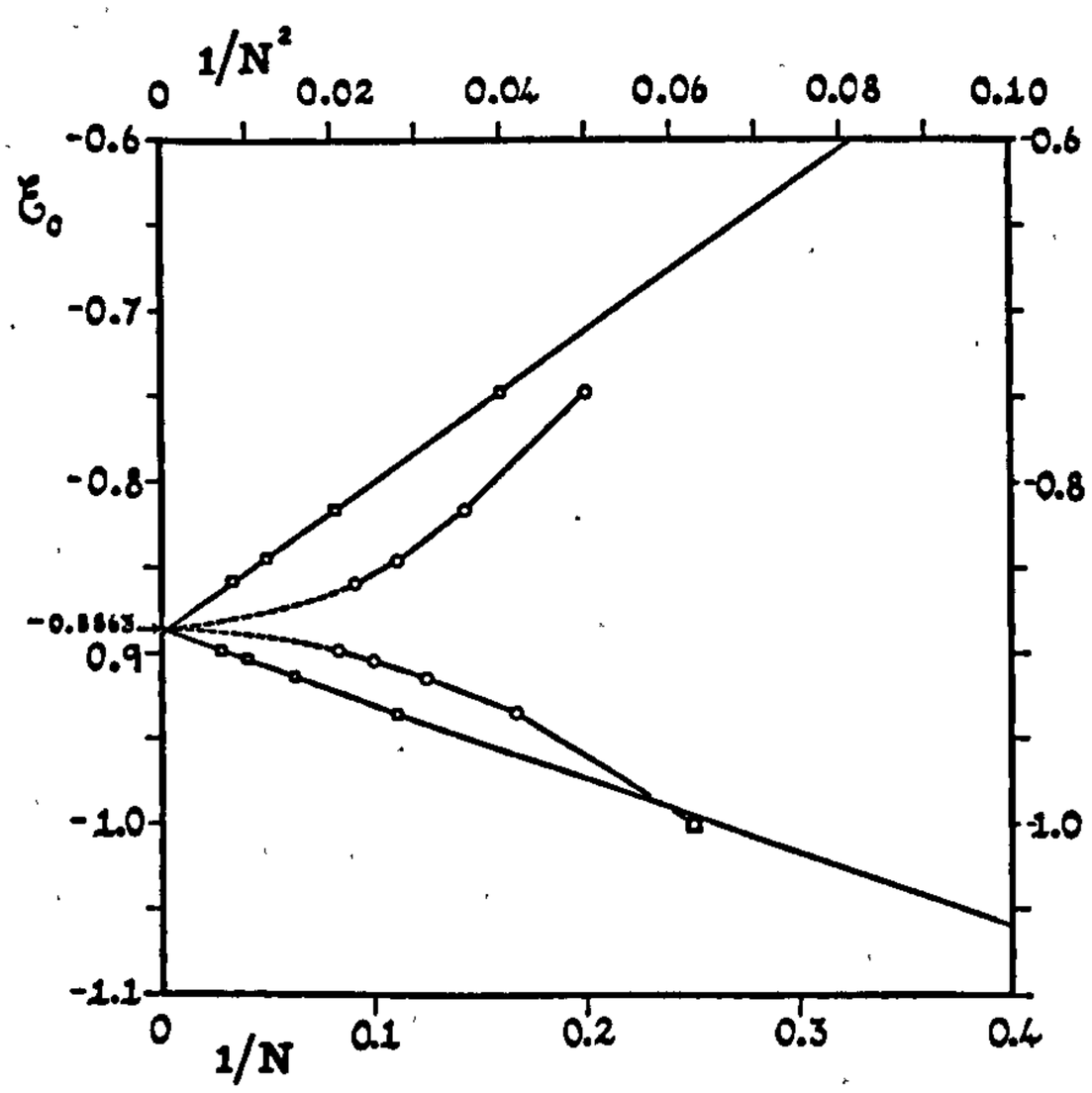

FIG. 1. Antiferromagnetic ground-state energies versus $1/N$ (circles) and versus $(1/N)^2$ (squares) for pure Heisenberg rings ($\gamma=1$).

[33] E. Ledinegg and P. Urban, Acta Phys. Austriaca 6, 257 (1953).

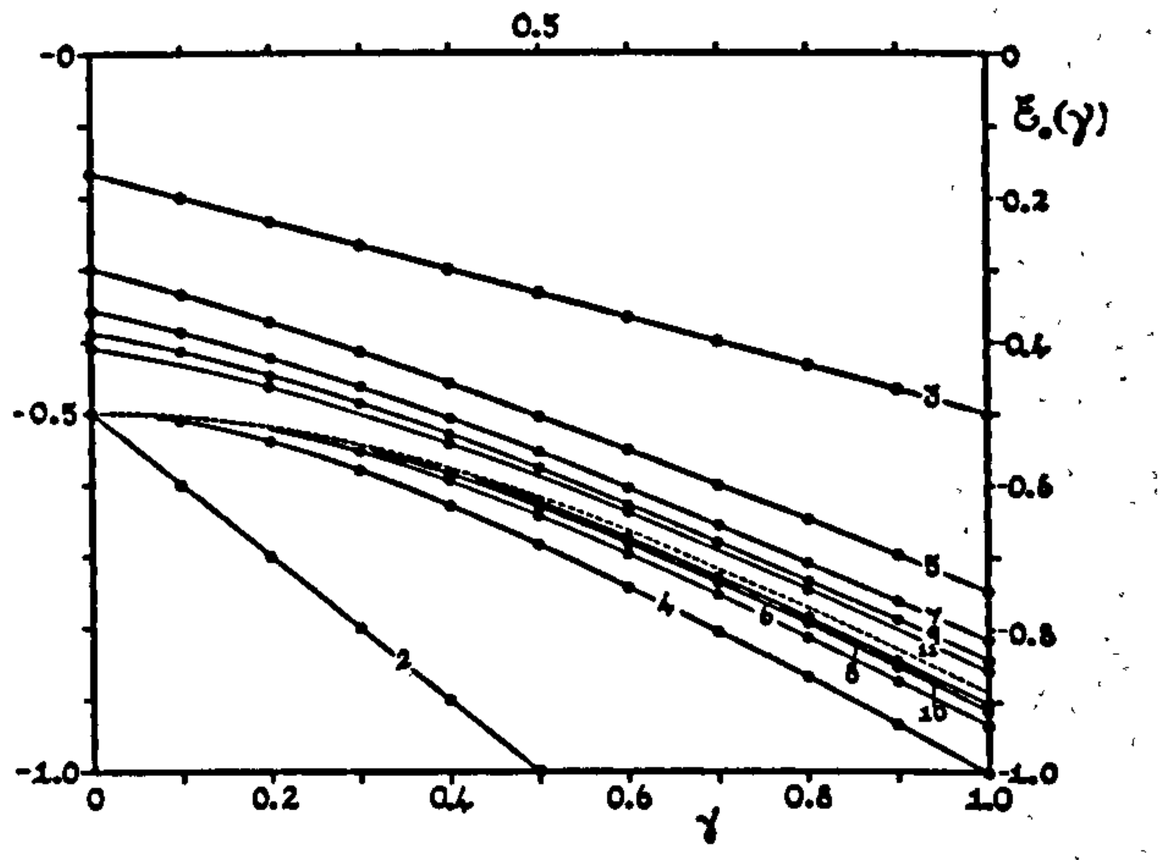

FIG. 2. Antiferromagnetic ground state as a function of γ for finite and infinite rings. The exact limiting curve due to Orbach (Ref. 8) is shown by the dashed curve.

If the limiting value had not been known, it could have been estimated to about 0.1% accuracy by linear extrapolation with $1/N^2$. Heisenberg chains with open ends show a slower convergence, apparently linear with $1/N$. For pure Ising ($\gamma=0$) rings the ground state is exact for N even but approaches the limit as $1/N$ for N odd on account of the "misfit seam." In Fig. 2 the approach of the antiferromagnetic ground state to the limit is shown as a function of γ for $N=2$–11. The limiting curve (due to Orbach[8]) is rather well defined by these results.

Encouraged by the relatively simple and regular behavior of the finite N results found here, we may go on to examine properties for which the exact $N=\infty$ limits are unknown with the reasonable expectation that careful extrapolation to large N will not be misleading.

3. THERMAL PROPERTIES

In this section we consider the thermal properties firstly of antiferromagnetic and then of ferromagnetic chains.

Antiferromagnetic Coupling

In Fig. 3 is shown the energy per spin in zero field as a function of temperature for antiferromagnetic pure Ising and Heisenberg rings of $N=2$–11 spins. As for the ground states, odd and even rings form two distinct sequences. For the Ising case ($\gamma=0$), where the exact limit is known, the two sequences approach the limiting curve monotonically from above and below. There seems no reason to doubt that the same situation prevails at $\gamma=1$. The energy of an infinite Heisenberg chain is thus defined to an accuracy of better than $\pm 0.5\%$ down to temperatures of $kT/|J|=0.5$ by the mean of the curves for $N=10$ and 11. (These two curves and the estimated limiting curve have been tabulated and are available on request.) Below this temperature the true limiting curve is less certain, but since the value for

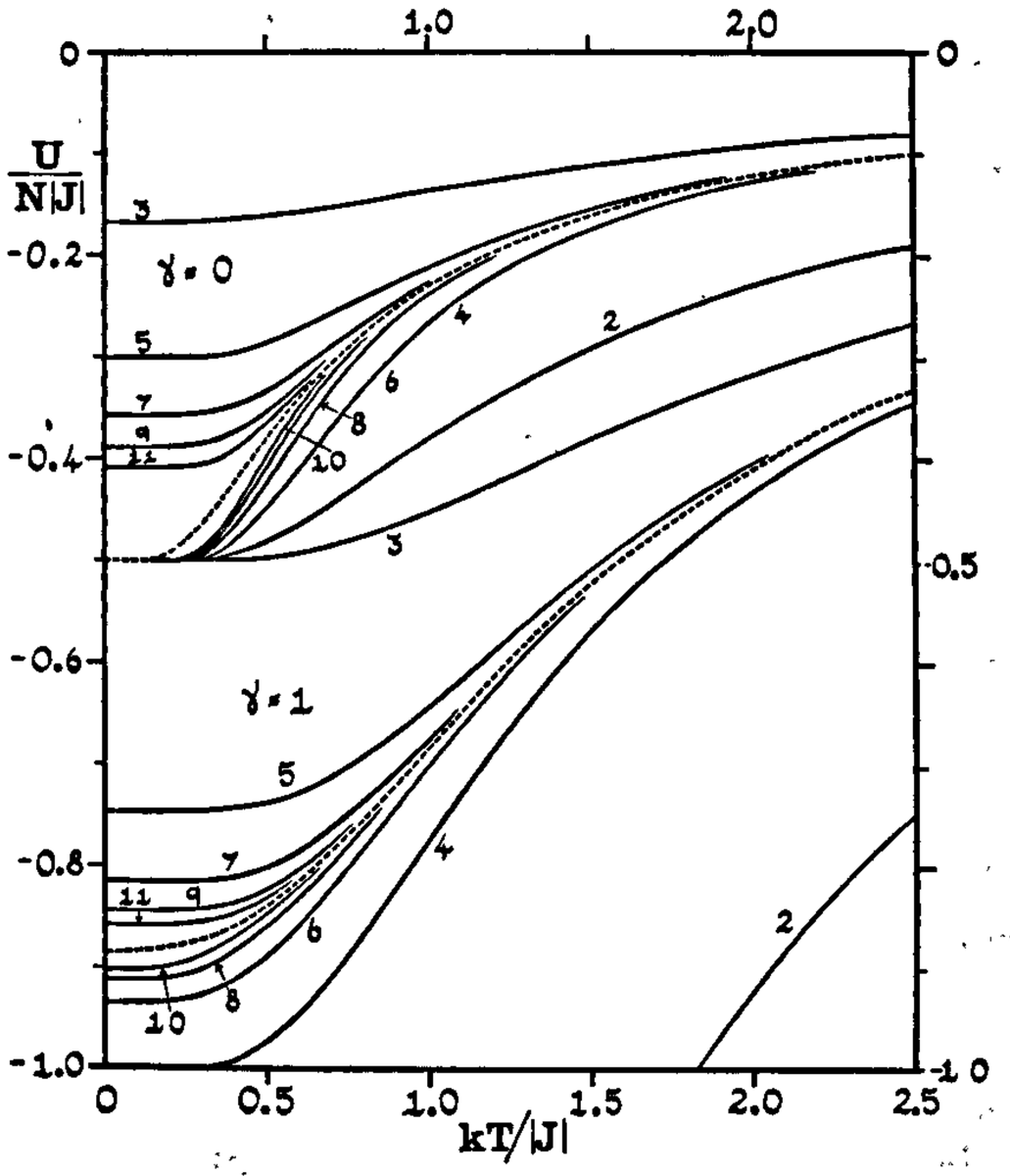

FIG. 3. Zero-field energy as a function of temperature for finite antiferromagnetic Ising and Heisenberg chains. The limiting ($N=\infty$) curve is shown dashed in each case.

$T=0$ is known exactly, even a roughly estimated limiting curve would be accurate to $\pm 1\%$. We return to this point shortly in considering the entropy.

The entropy for the pure antiferromagnetic Heisenberg chains is shown in Fig. 4. The convergence appears

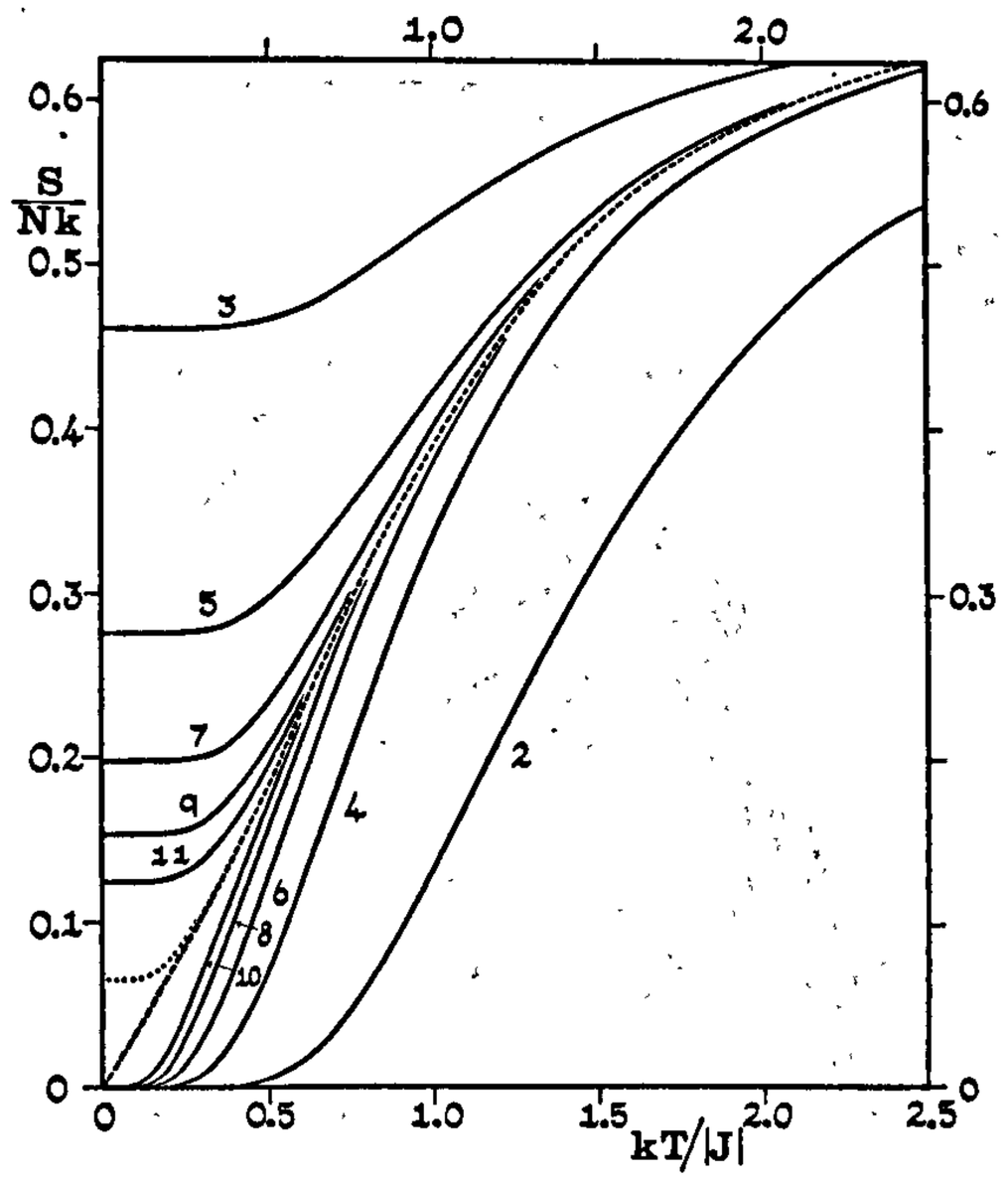

FIG. 4. Entropy versus temperature for antiferromagnetic Heisenberg chains ($\gamma=1$). The dotted curve is the mean of $N=10$ and $N=11$ weighted as in (a) (Ref. 35), and the dashed curve is the estimated limit.

to be similar to that for the energy and the limit seems well determined down to $kT/|J|=0.5$ by interpolation between the curves for odd and even N. For odd N at $T=0$ the ground state is fourfold degenerate and the entropy per spin thus goes to zero only as $2k\ln 2/N$.

To estimate the nature of the low-temperature behavior for $N\to\infty$, we may reasonably postulate a power law for the limiting free energy per spin (or, more directly, for the limiting internal energy). Thus, suppose[34]

$$U(T)-U(0)=AN|J|(kT/|J|)^{\alpha}, \qquad (3.1)$$

where A and α are fixed (as $T\to 0$). Then for the specific heat we have

$$C/Nk=A\alpha(kT/|J|)^{\alpha-1} \qquad (3.2)$$

and for the entropy

$$S(T)/Nk=A\alpha(\alpha-1)^{-1}(kT/|J|)^{\alpha-1}. \qquad (3.3)$$

By combining (3.1) and (3.3) we obtain

$$U(T)-U(0)=(1-\alpha^{-1})TS(T) \qquad (3.4)$$

so that a plot of energy $U/N|J|$ versus $TS/N|J|$ for $N\to\infty$ should be linear with slope determined by the index α. Such a plot is shown in Fig. 5 for $N=10$ and $N=11$ and supports the view that the limiting curve would indeed be linear. The solid line which is drawn from the exact ($N\to\infty$) ground state with slope 0.515 should be close to any reasonable "best" fit and yields the estimate $\alpha\simeq 2.06\pm 0.03$. This value is largely determined by the data for temperatures in the range $kT/|J|=0.30$–0.60. The dashed line, on the other hand, is of slope $\frac{1}{2}$ and corresponds to $\alpha=2$ exactly. It seems likely that this is the true limiting value which would be obtained by fitting data for larger N at lower temperatures.[35]

If we assume $\alpha=2$, the amplitude A may be estimated by various methods; for example, from the temperature variation of $U/N|J|$ and $TS/N|J|$, from plots of $U/N|J|$ versus $(S/Nk)^2$ using the weighted means,[35] and from the slope of the weighted entropy means at low temperatures. We thus obtain the approximate results

$$U(T)\approx U(0)+0.175N|J|(kT/|J|)^2, \qquad (3.5)$$

$$S(T)\approx 0.35Nk(kT/|J|), \quad (\gamma=1) \qquad (3.6)$$

valid up to $kT/|J|=0.4$ to 0.5.[36] These are shown as

[34] Our method is a slight modification of a procedure devised by Griffiths (Ref. 12) who plotted $U(T)$ versus $S(T)$ and estimated the index α by fitting B and β in the power law $U-U(0)=BS^{\beta}$.

[35] Griffiths (Ref. 12) estimated $\alpha=2.1$, but also suggested that $\alpha=2$ was probably the exact value. This conclusion is supported more closely by analyzing the trends of the weighted means (a) $[NP_N+(N-1)P_{N-1}]/(2N-1)$, (b) $\frac{1}{2}P_N+\frac{1}{2}P_{N-1}$, (c) $[(N-1)P_N+NP_{N-1}]/(2N-1)$ (where P is the thermodynamic property in question), which converge more rapidly.

[36] Our conclusions regarding the amplitude A agree closely with those of Griffiths. The spin-wave theory of the low-temperature behavior is given by R. Kubo, Phys. Rev. 87, 568 (1952); J. Van Kranendonk and J. H. Van Vleck, Rev. Mod. Phys. 30, 1 (1958).

dashed curves in Figs. 3 and 4 and seem to be the most reasonable estimates of the low-temperature behavior.

It is interesting that the functional forms of (3.5) and (3.6) agree with the predictions of simple antiferromagnetic spin-wave theory but the corresponding amplitude[36] $A_{s.w.}=\pi/6=0.52$ is too great by a factor of about three. A T^2 law for the energy is exact for the pure transverse Hamiltonian discussed by Katsura.[29]

The corresponding specific heats for pure antiferromagnetic Heisenberg chains are shown in Fig. 6. For temperatures above $kT/|J|=0.5$ the convergence again appears to be monotonic from above and below and the limiting curve (shown dashed) can be estimated quite accurately through the maximum of height

$$C_{\max}/Nk\simeq 0.350 \quad (\gamma=1) \tag{3.7}$$

at

$$kT_{\max}/|J|\simeq 0.962 \quad (\gamma=1). \tag{3.8}$$

At lower temperatures the convergence must be more complex since, for finite N, the specific heat always vanishes exponentially fast as $T\to 0$, owing to the finite energy gap between the ground and first excited states. As $N\to\infty$, however, the states close up (as $1/N$) and merge into a continuum, which runs from the ground state (see below). The probable limiting low-temperature behavior follows from (3.5) and (3.6), which yield

$$C(T)\simeq 0.35Nk(kT/|J|) \quad (\gamma=1), \tag{3.9}$$

and this has been used in deriving the estimated curve for the limit $N=\infty$ shown by the dashed line in Fig. 6.

The variation of the antiferromagnetic specific heat with anisotropy may be seen from Fig. 7 which shows the specific heats for rings of $N=8$ spins. The exact limiting curve for $\gamma=0$ and the estimated limit for $\gamma=1$ are plotted as dashed lines to indicate the degree to which the results for $N=8$ approach the limit. The effect of increasing γ from the Ising value $\gamma=0$ is to shift the specific heat maximum to higher temperatures, to reduce its height and to broaden the peak. At low temperatures ($kT/|J|\simeq 0.1$) the curves for finite N (even) and γ in the range 0.1–0.6 display anomalous small peaks and points of inflection. These are "small number effects" due to the finite splitting of the degenerate Ising ground state by the transverse terms in the Hamiltonian. For fixed γ and increasing N, this splitting diminishes and eventually goes to zero as $N\to\infty$ (see Sec. 5). Correspondingly, the anomalies move to lower temperatures and are reduced in magnitude, finally disappearing in the limit $N=\infty$.

For $\gamma\neq 1$ and large but finite N, the specific heat curves at low temperature (but above the anomalies) vanish exponentially fast, roughly as $\exp[-\Delta E_A(\gamma)/kT]$, where $\Delta E_A(\gamma)$ is the limiting anisotropy gap between the ground state and the first excited states. The value of this gap is estimated in Sec. 5; it approaches zero as $\gamma\to 1$ and the Ising value, $2|J|$, as $\gamma\to 0$.

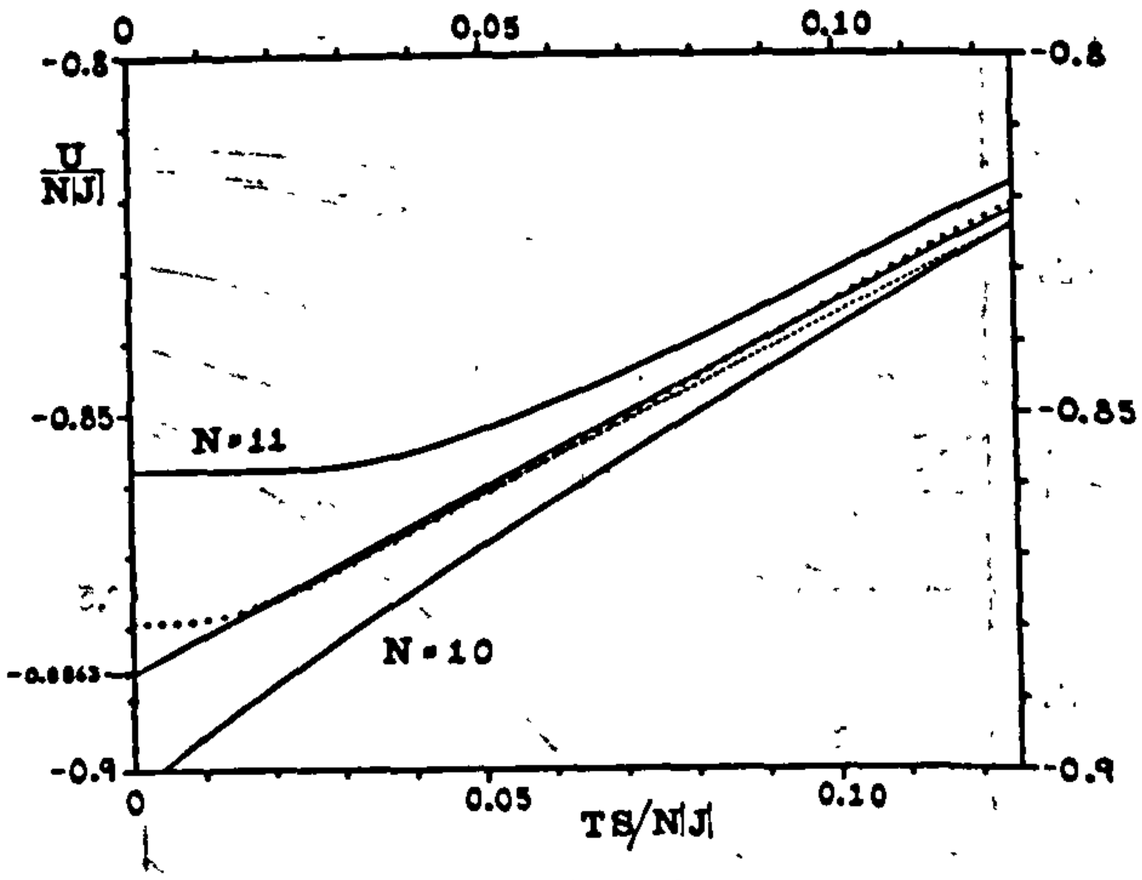

FIG. 5. Energy versus the product of temperature and entropy for $N=10$ and $N=11$ Heisenberg antiferromagnetic chains. The line of crosses is the 11/10 mean weighted as in (a) (Ref. 35).

[Owing to the existence of "bound states" of indefinitely large groupings of adjacent "overturned spins," the number of states just above the gap might be of order N^2 rather than N. Consequently, it is possible that the true limiting specific heats might rise faster than $\exp[-\Delta E_A/kT]$. If this were the case, $\Delta E_A(\gamma)$ should be replaced by an "effective gap" $\Delta E_A^*(\gamma)<\Delta E_A(\gamma)$ as happens at the Ising limit $\gamma=0$ where, in fact, one finds that $\Delta E_A^*(0)=\frac{1}{2}\Delta E_A(0)$.]

The variation of specific heat with magnetic field may be studied just as for zero field. The convergence at temperatures above $kT/|J|\simeq 0.3$ is found to be

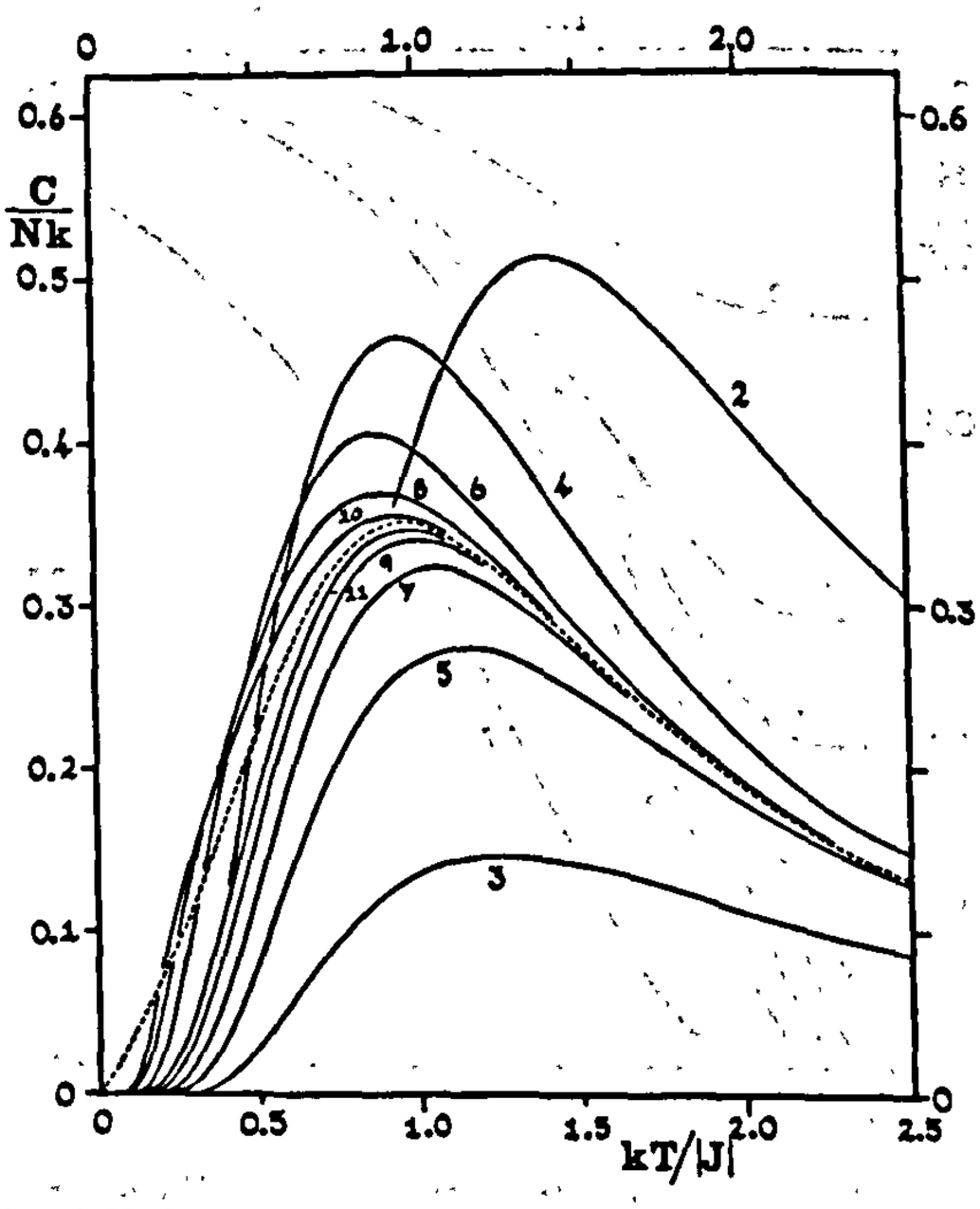

FIG. 6. Variation of specific heat with temperature for antiferromagnetic Heisenberg chains: finite N, solid lines; estimated limit $N=\infty$, dashed line.

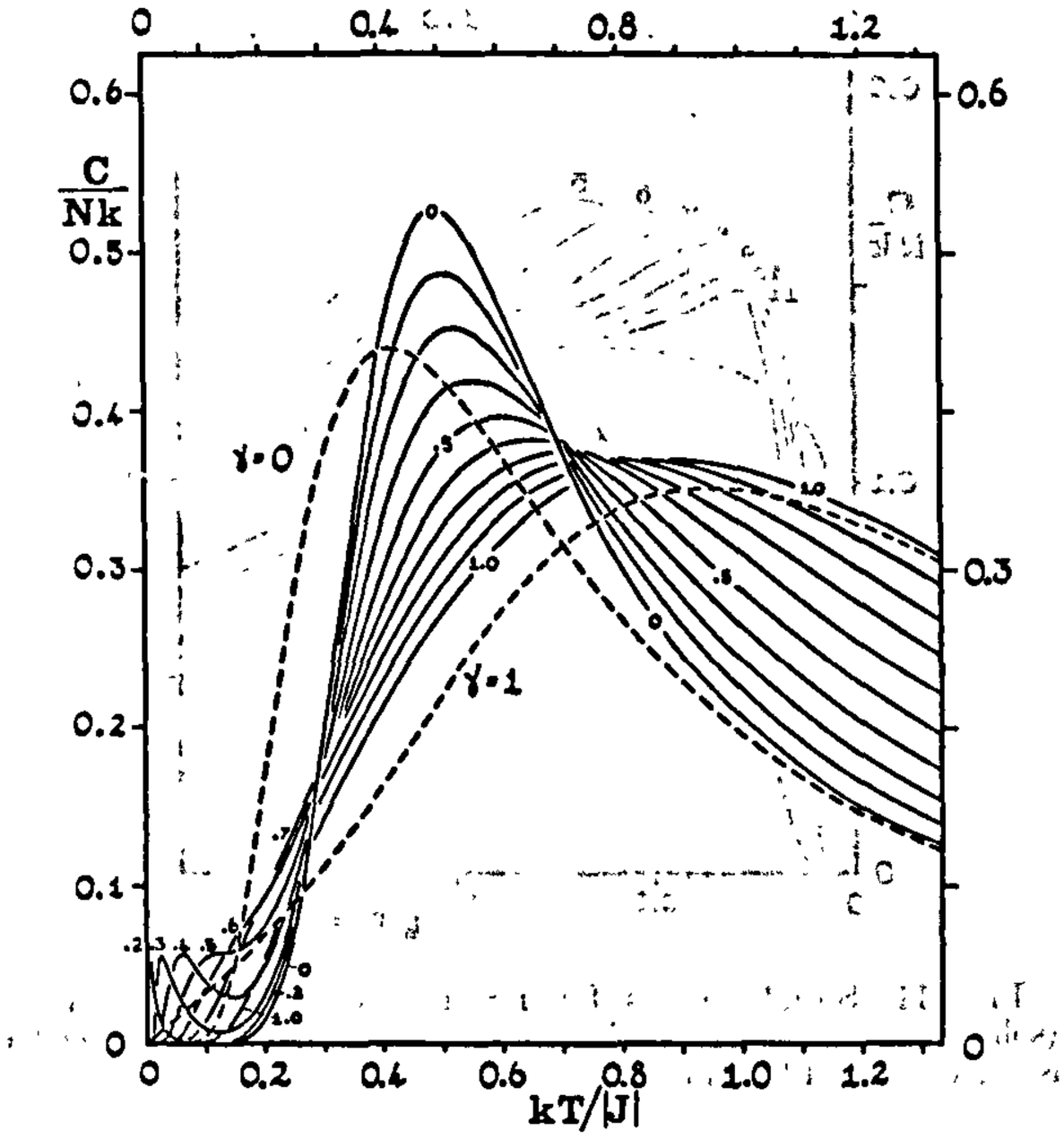

FIG. 7. Antiferromagnetic specific heat for rings of $N=8$ spins for various anisotropies γ. The dashed curves are the exact and estimated limiting curves ($N=\infty$) for $\gamma=0$ and $\gamma=1$, respectively.

quite rapid especially if the consecutive means for $N=2n$ and $N=2n-1$ are considered. Accordingly, in Fig. 8, we have plotted for the pure Heisenberg case only the mean specific heats for $N=10$ and 9 at various fields (except at $H=0$ where the estimated limit is shown). These means should represent the true limiting curves to within 1 or 2% down to temperatures of $kT/|J|\simeq 0.5$. With increasing field the maximum shifts to lower temperatures and falls in height. However, at the field $H_s(g\beta/|J|)=4$, which represents a "critical field" above which the antiferromagnet becomes fully magnetized at zero temperature (i.e., saturation occurs, see Sec. 4), there remains only a broad low maximum at a higher temperature. The behavior is similar for other values of γ as can be seen from Fig. 9, where the specific heat for $\gamma=0.5$ is plotted. The critical field in this case is $H_s=3(|J|/g\beta)$. Above the critical field the initial rise is governed by the energy gap $\Delta E_H(\gamma)=Hg\beta-2(1+\gamma)|J|$ and it may be observed that the maximum starts to increase in height again.

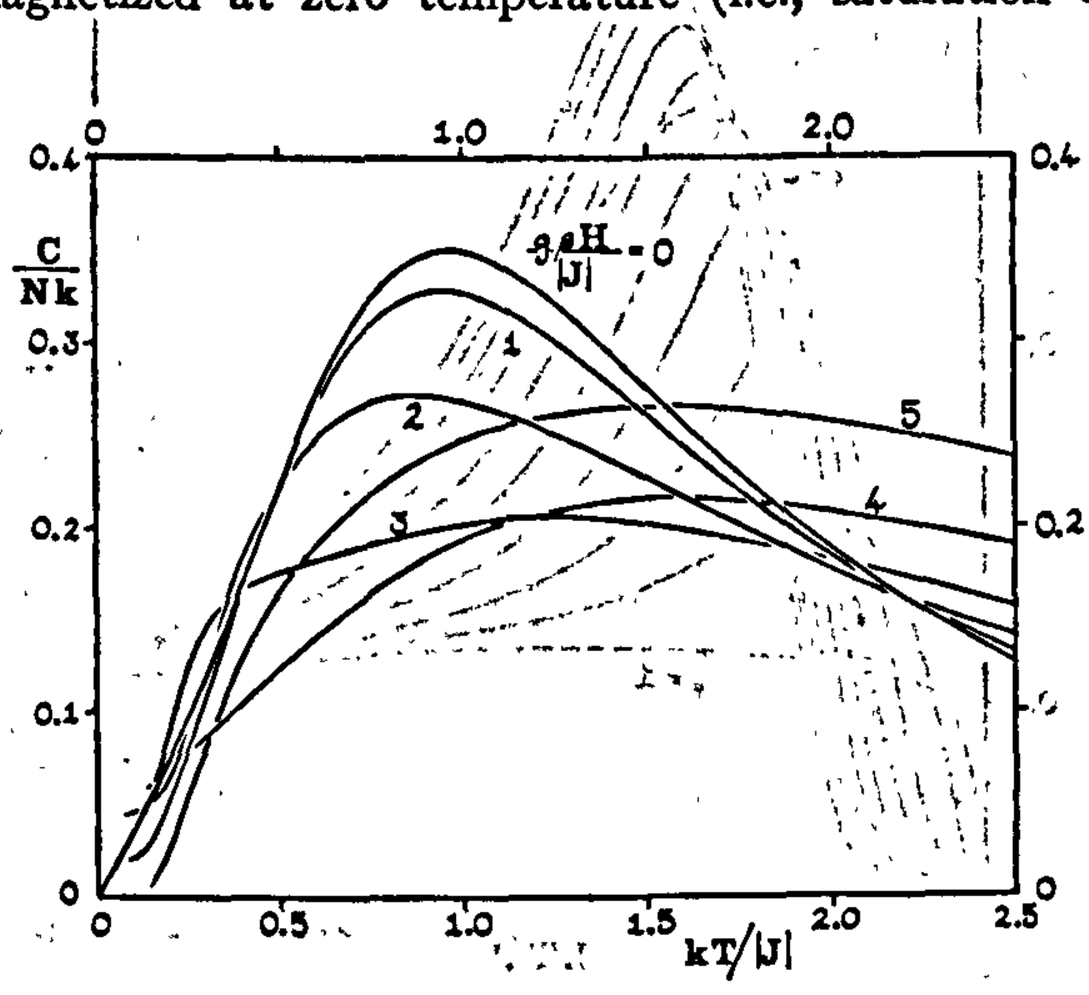

FIG. 8. Variation of the antiferromagnetic specific heat with magnetic field for $\gamma=1$. Except for $H=0$, the curves are the means of the values for $N=9$ and 10.

Ferromagnetic Coupling

We turn now to ferromagnetic chains: Values of the energy, entropy, and specific heat for the longest chains and $\gamma=1$ and 0.5 have been tabulated and are available on request. The energy (per spin) is plotted versus the temperature for Heisenberg chains of $N=3, 4, \cdots, 10, 11$ spins in Fig. 10. In contrast to the antiferromagnetic case, the curves for finite N do not appear to bracket the limiting curve, but rather increase monotonically

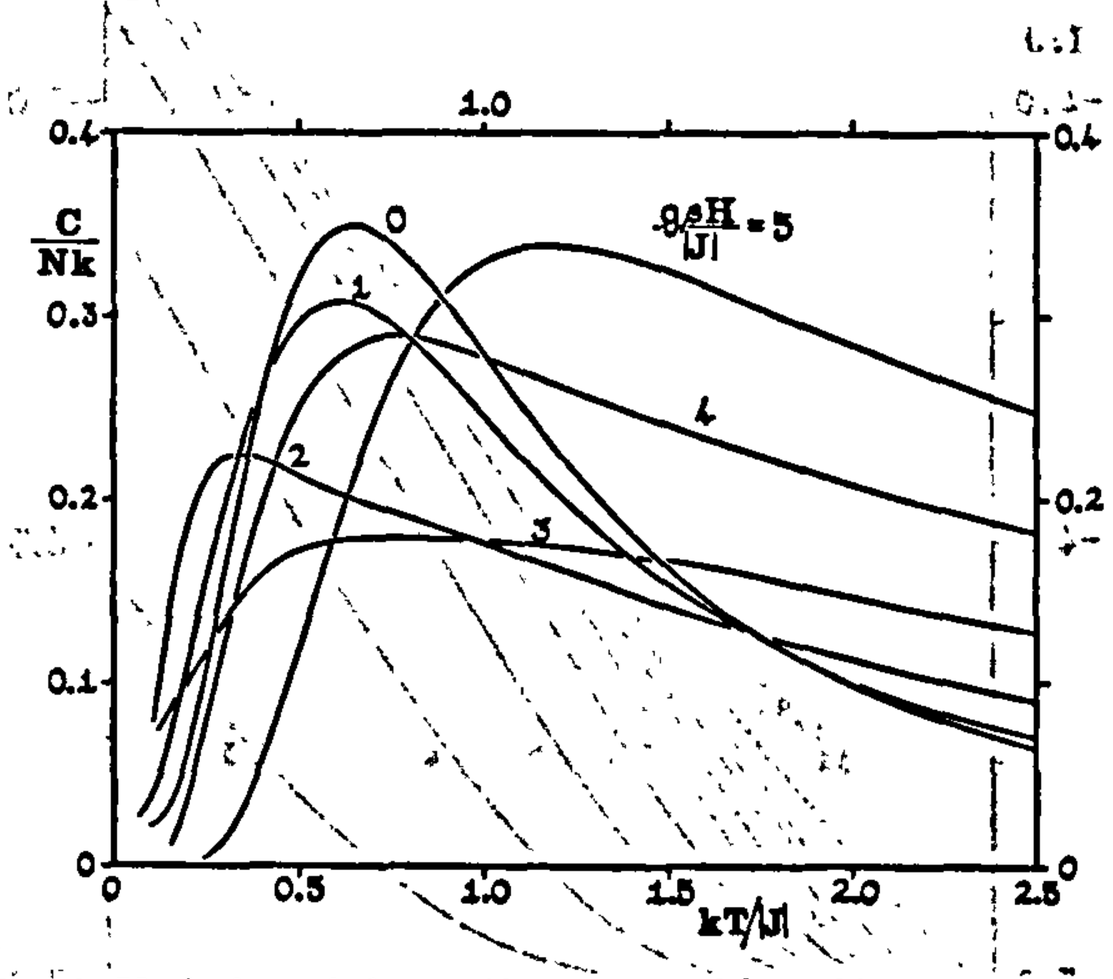

FIG. 9. Variation of the antiferromagnetic specific heat with field as in Fig. 8, but for $\gamma=0.5$.

towards it. This makes extrapolation at low temperatures more difficult although the limit seems quite accurately defined down to $kT/J=0.5$. (All curves, of course, approach the exact limiting ground state $\mathcal{E}=-\frac{1}{2}$).

The curves for the entropy display a more complicated convergence, successive curves crossing at low temperatures. The ground state of the ferromagnet when $\gamma=1$ has spin $NS=\frac{1}{2}N$, and hence degeneracy $N+1$. Consequently, the zero-point entropy is $(k/N)\ln(N+1)$, which approaches zero rather slowly. We may, nonetheless, attempt to estimate the low-temperature behavior of the energy and entropy by the power law analysis presented in Eq. (3.1) to (3.4). The corresponding $U(T)$ versus $TS(T)$ plots are not very straight and their slopes increase monotonically with N.[37] The maximum slopes for $N=9$ and 10 correspond to an index in (3.1)

[8] The curves are concave downwards except for very small values of TS/NJ (below 0.04), where an exponential decay sets in.

of $\alpha=1.42$ and 1.43, respectively, while the slopes of the tangents through the origin correspond to $\alpha=1.312$ and 1.324. Rough extrapolation linearly in $1/N$ suggests that the true index might lie in the neighborhood of $\alpha=1.45$–1.50, but the corresponding pure power laws would only be followed closely below temperatures of $kT/J\simeq 0.25$. Simple spin-wave theory predicts $\alpha=\frac{3}{2}$, and one might expect this to be accurate since the ground and first excited states are described exactly in the ferromagnetic case. However, as is known, spin-wave theory does not give any account of the lower lying "bound" states which arise for further overturned spins. Nevertheless, our results do indicate that $\alpha=\frac{3}{2}$ might be exact. Accepting this, one may estimate the amplitudes

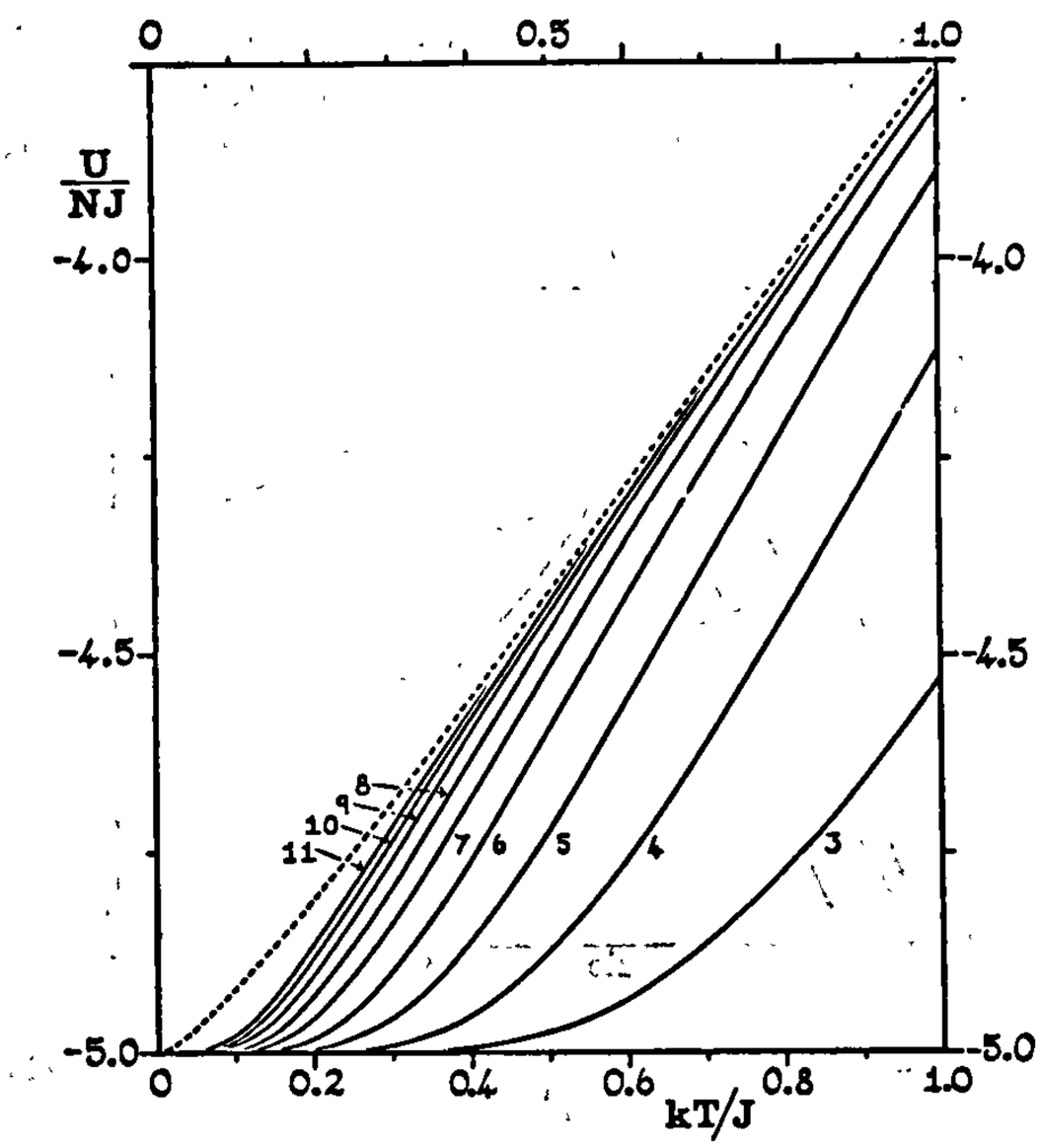

FIG. 10. Energy of ferromagnetic Heisenberg chains ($\gamma=1$) for increasing N.

roughly which yields

$$U(T)\simeq 0.28NJ(kT/J)^{3/2}, \quad (T\to 0) \qquad (3.10)$$

$$S(T)\simeq 0.85Nk(kT/J)^{1/2}. \qquad (3.11)$$

The amplitudes predicted by spin-wave theory are larger by a factor of about 1.3.

The specific heats for the Heisenberg rings are shown in Fig. 11 as solid curves. The convergence is monotonic decreasing at temperatures above $kT/J=0.3$ for $N\geqslant 8$.

It seems clear that a *double* maximum will develop when $N=13$ or 14 and that the maximum of the limiting curve will not derive from the maxima in the curves for $N\leqslant 11$. The broken curves in Fig. 11 correspond to *open* chains of 3 and 4 spins. Although they do not seem to converge very rapidly, they do approach the limit from below and seem to give a truer representa-

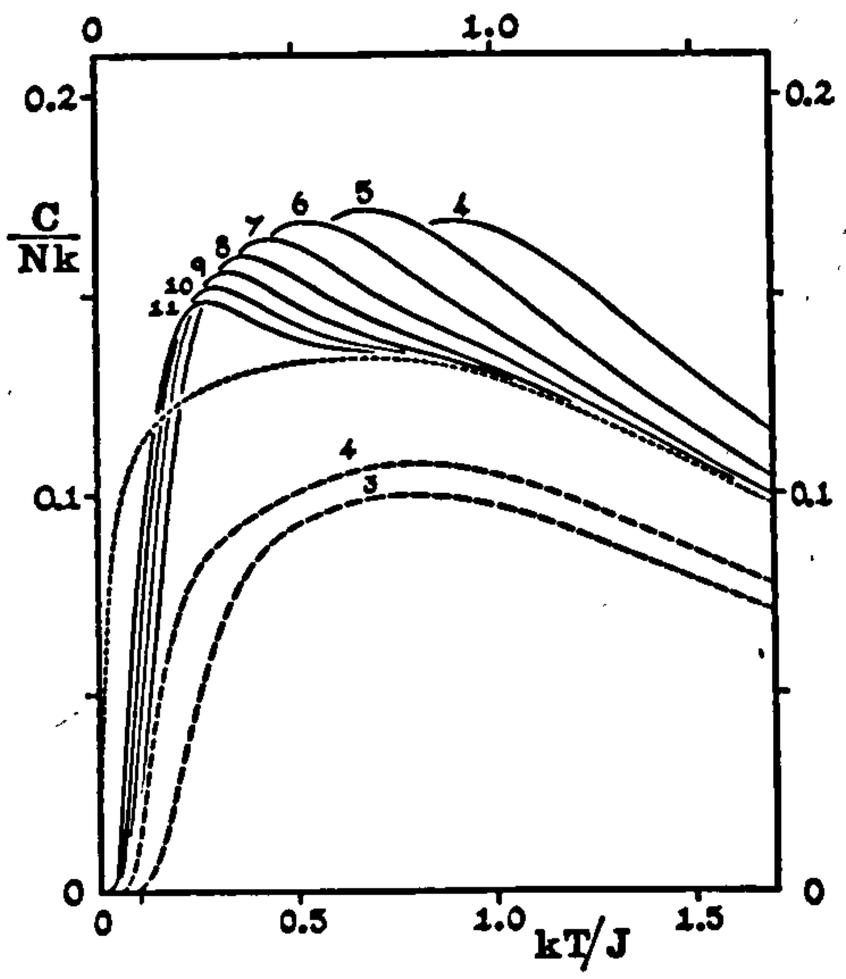

FIG. 11. Specific heats for ferromagnetic Heisenberg rings (solid curves) and open chains (broken curves). The dashed curve is the estimated limiting curve.

tion of its shape. (Calculations for longer open chains were not performed since, as translational symmetry is absent, they would have required more machine time than available.) Guided by these results and the low-temperature estimates following from (3.10) [which indicate that $C(T)\sim T^{1/2}$] and remembering that the integrated area under the specific heat curve must check with the energy one may estimate with moderate accuracy the limiting ferromagnetic specific heat curve.

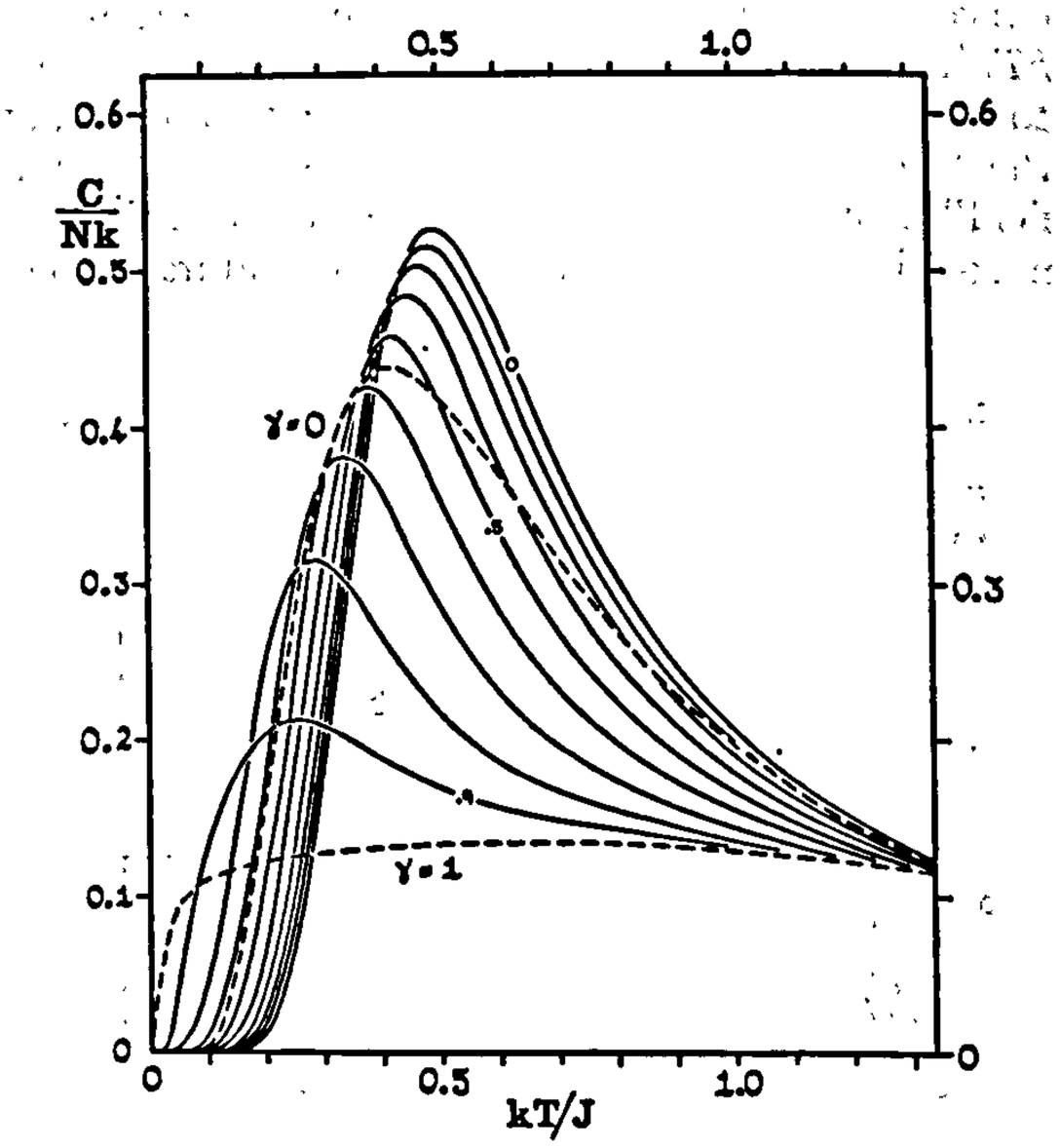

FIG. 12. Variation of ferromagnetic specific heats with anisotropy for rings of $N=8$. (For $\gamma=0$ and 1, the exact and estimated limiting curves are also plotted.)

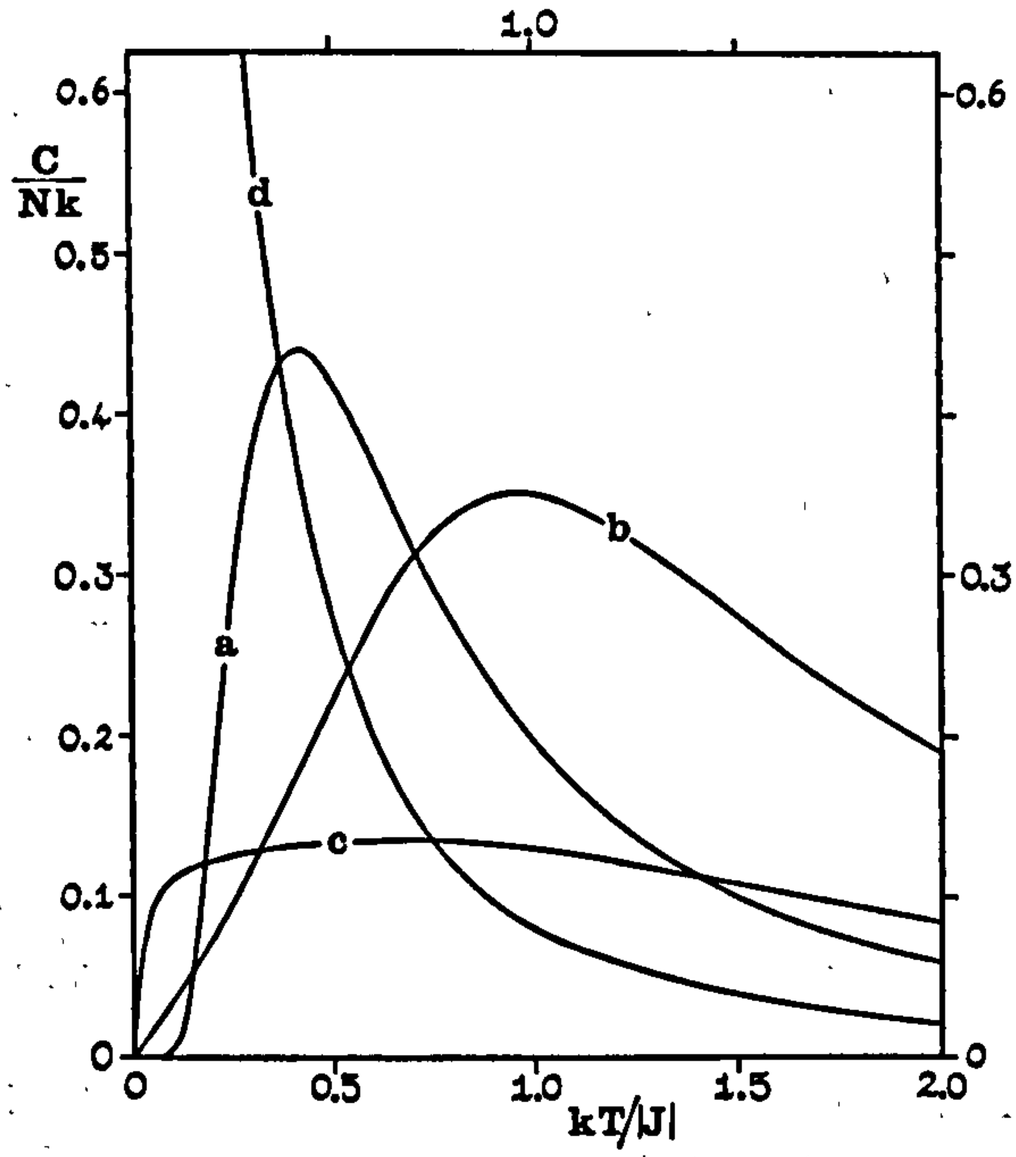

FIG. 13. Comparison of specific heats for infinite chains for (a) $S=\frac{1}{2}$ Ising coupling, (b) $S=\frac{1}{2}$ Heisenberg antiferromagnetic coupling, (c) $S=\frac{1}{2}$ Heisenberg ferromagnetic coupling, and (d) $S=\infty$ Heisenberg coupling (classical spins).

This is shown dashed in Fig. 11; the rather broad peak has a maximum height

$$C_{\max}/Nk \approx 0.134, \tag{3.12}$$

at

$$kT_{\max}/J \approx 0.70. \tag{3.13}$$

The nature of the variation of specific heat with anisotropy can be gauged from Fig. 12, which (except for $\gamma=1$ where the estimated limit is plotted) shows the results for rings of $N=8$ spins at intervals of $\Delta\gamma=0.1$. The effects of a magnetic field (for $\gamma=1$) are rather similar to those due to anisotropy so that we do not present a figure. With a field $H(g\beta/J)=0.5$, the specific heat maximum increases sharply to a height of about $C/Nk=0.37$ at $(kT/J)=0.61$. Further increase of the field to $H(g\beta/J)=1.0$ and 2.0 increases the maximum to $C/Nk=0.42$ and 0.45 and raises the corresponding temperatures to $(kT/J)=0.94$ and 1.45, respectively. These figures are derived for $N=8$ but should not differ significantly from the limiting results since convergence is faster when $H\neq 0$ or $\gamma\neq 1$, since the ferromagnetic ground state is then nondegenerate, and is separated by a finite energy gap, even in the limit $N=\infty$.

Finally, in Fig. 13 are compared on the same scale the exact and estimated specific heats for infinite chains with (a) $S=\frac{1}{2}$ Ising coupling, ferro- or antiferromagnetic, (b) $S=\frac{1}{2}$ Heisenberg antiferromagnetic coupling, (c) $S=\frac{1}{2}$ Heisenberg ferromagnetic coupling, and (d) $S=\infty$ (classical) Heisenberg ferro- or antiferromagnetic coupling.[31] The large difference between the relatively sharp antiferromagnetic $S=\frac{1}{2}$ Heisenberg specific heat and the low broad ferromagnetic specific heat is striking testimony to the lower stability of the isotropic ferromagnetic coupling. Curve (d) for $S=\infty$ continues to rise monotonically to a maximum at $T=0$ of height $C/Nk=1$.

4. MAGNETIC PROPERTIES

Antiferromagnetic Coupling

In Fig. 14 are plotted the antiferromagnetic susceptibilities for isotropic Heisenberg coupling ($\gamma=1$) in zero field for finite rings of $N=3, 4, 5, \cdots, 11$ spins. (The tabulated values for $N=10$ and 11 are available.) The limiting curve is apparently bracketed by the curves for odd N, which approach monotonically from above, and those for even N, which approach monotonically from below. The convergence is rather rapid above $kT/|J|=0.6$, at which temperature the values for $N=10$ and 11 differ by only 5%, and their mean probably differs from the true limiting curve by less than 1%. The susceptibility displays a rounded maximum of height (for $N\to\infty$)

$$\chi_{\max}/(g^2\beta^2/|J|) \simeq 0.07346, \quad (\gamma=1) \tag{4.1}$$

at

$$kT_{\max}/|J| \simeq 1.282. \quad (\gamma=1). \tag{4.2}$$

The situation at low temperatures as zero is approached is more complicated. For finite chains with N even, the antiferromagnetic ground state for all values

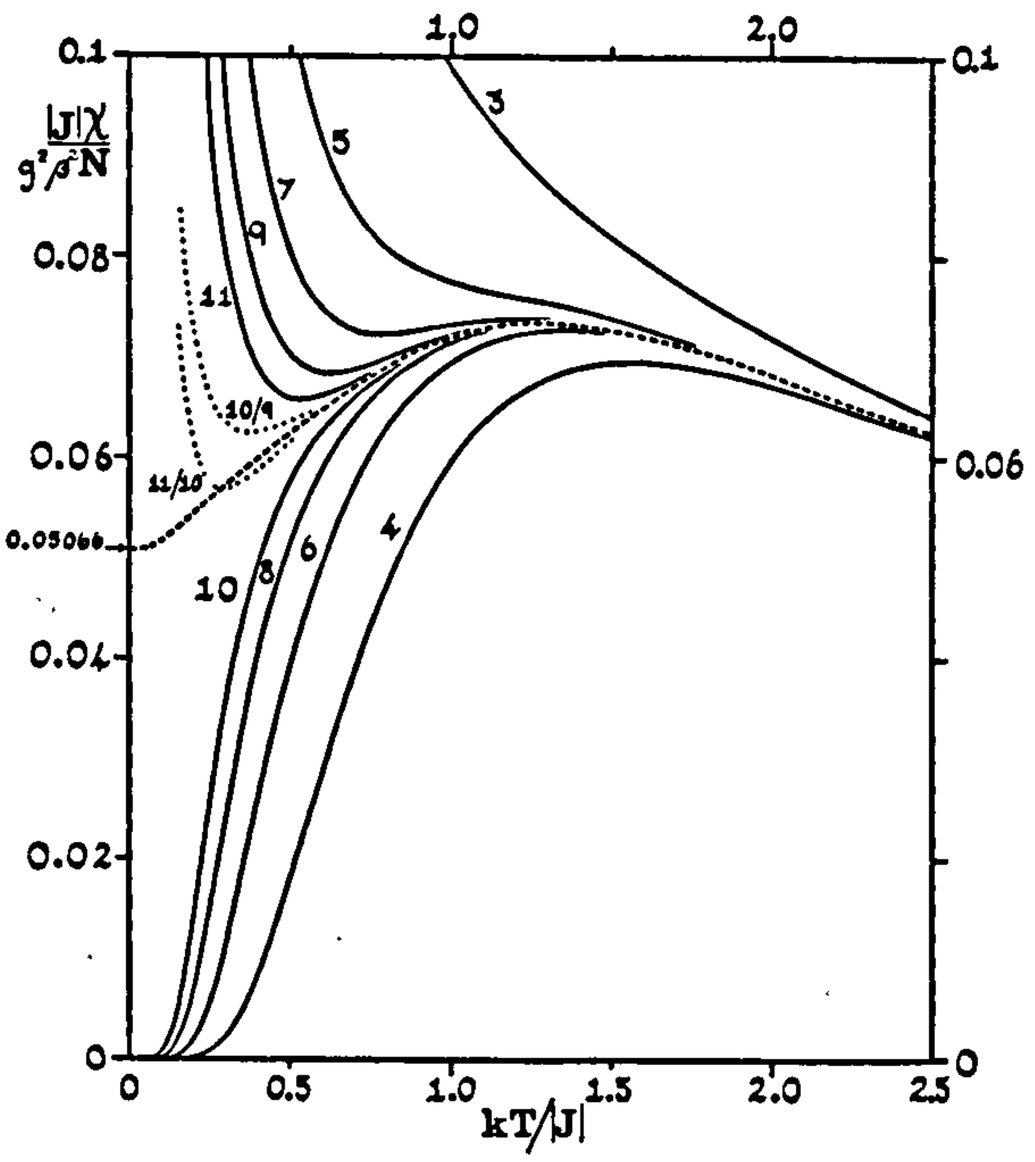

FIG. 14. Antiferromagnetic susceptibility versus temperature for finite Heisenberg rings (solid curves) and the estimated limit for infinite rings (dashed curve). The dotted curves are means of $N=9$ and 10, and $N=10$ and 11 weighted as in (a) and (c) (Ref. 35), respectively.

of γ is characterized by total spin component $S^z=0$, and there is a finite gap to the first excited state of nonzero S^z. Consequently, for all chains of even N (finite), the susceptibility parallel to the z axis approaches zero exponentially fast as $T\rightarrow 0$, at a rate governed by the energy gap. On the other hand, for finite odd N, the ground state, or rather degenerate ground states, have $S^z=\pm\frac{1}{2}$. (Clearly, $S^z=0$ is impossible.) The susceptibility for odd N thus diverges as $1/T$ as T approaches zero. However, as N increases the (relative) amplitude of the divergence falls in magnitude, and it sets in at a lower temperature. These remarks may be verified explicitly in the case $\gamma=0$ (Ising limit), where the exact

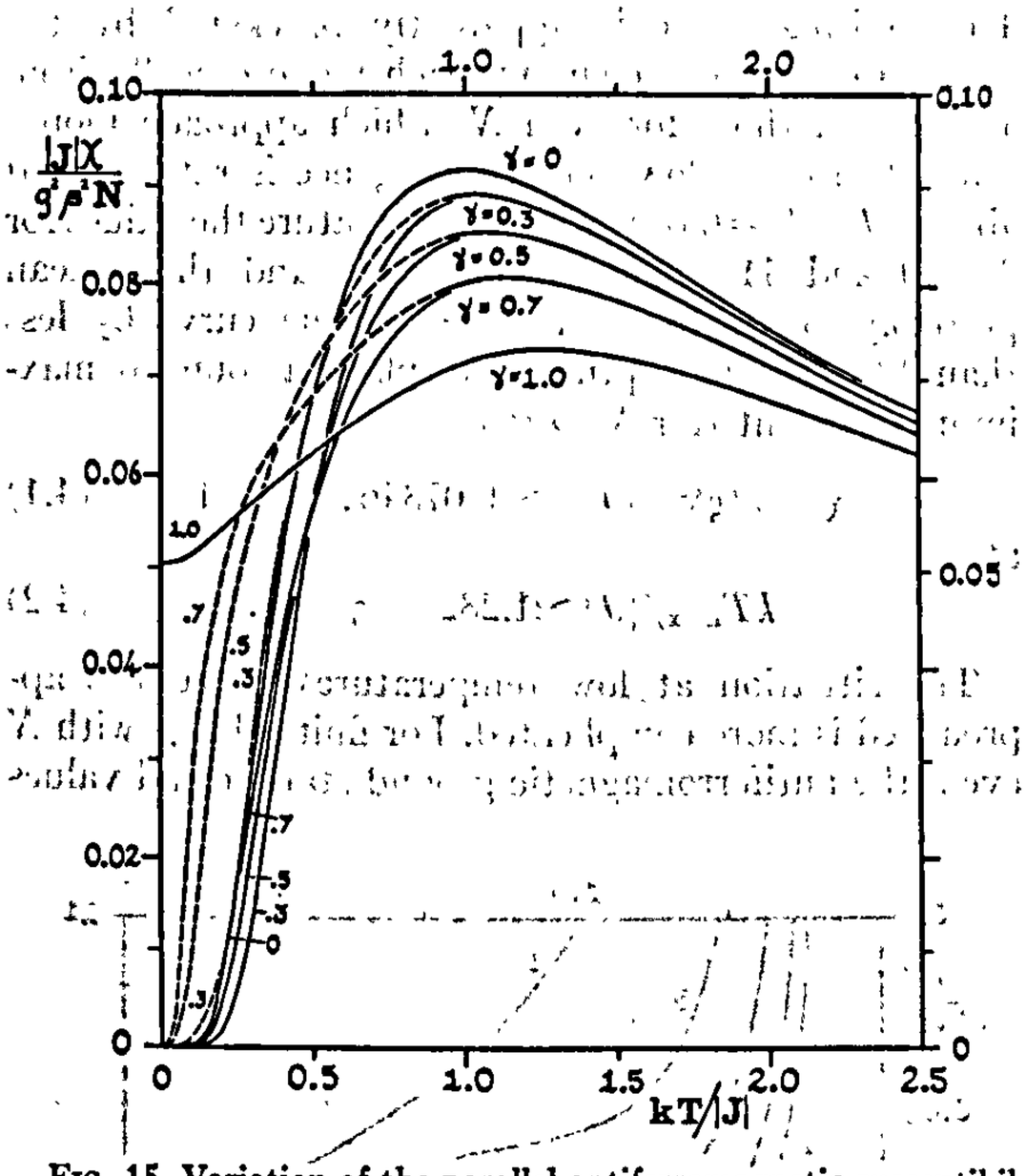

FIG. 15. Variation of the parallel antiferromagnetic susceptibility with anisotropy for rings of $N=8$ spins (solid curves). The estimated limiting values are shown by broken curves. Note that for $\gamma=0$ and $\gamma=1$ only the exact and estimated limiting curves are plotted.

result for the parallel susceptibility of a finite chain is

$$\chi_{11}(\gamma=0)=\frac{g^2\beta^2N}{4kT}e^{-|J|/kT}\left\{\frac{1-(-\tanh K)^N}{1+(-\tanh K)^N}\right\} \quad (4.3)$$

with

$$K=|J|/2kT. \quad (4.4)$$

In this case, as is well known, the limiting susceptibility, which is approached both for even N and odd N ($T>0$), goes to zero exponentially fast (see curve for $\gamma=0$ in Fig. 15).

Now for γ nonzero, but less than unity, the anisotropy gap between the ground state(s) and first excited states persists even in the limit $N\rightarrow\infty$ (see next section). Consequently, the limiting behavior should be similar to the Ising case with $\chi_{11}(T)\rightarrow 0$ as $T\rightarrow 0$. Figure 15

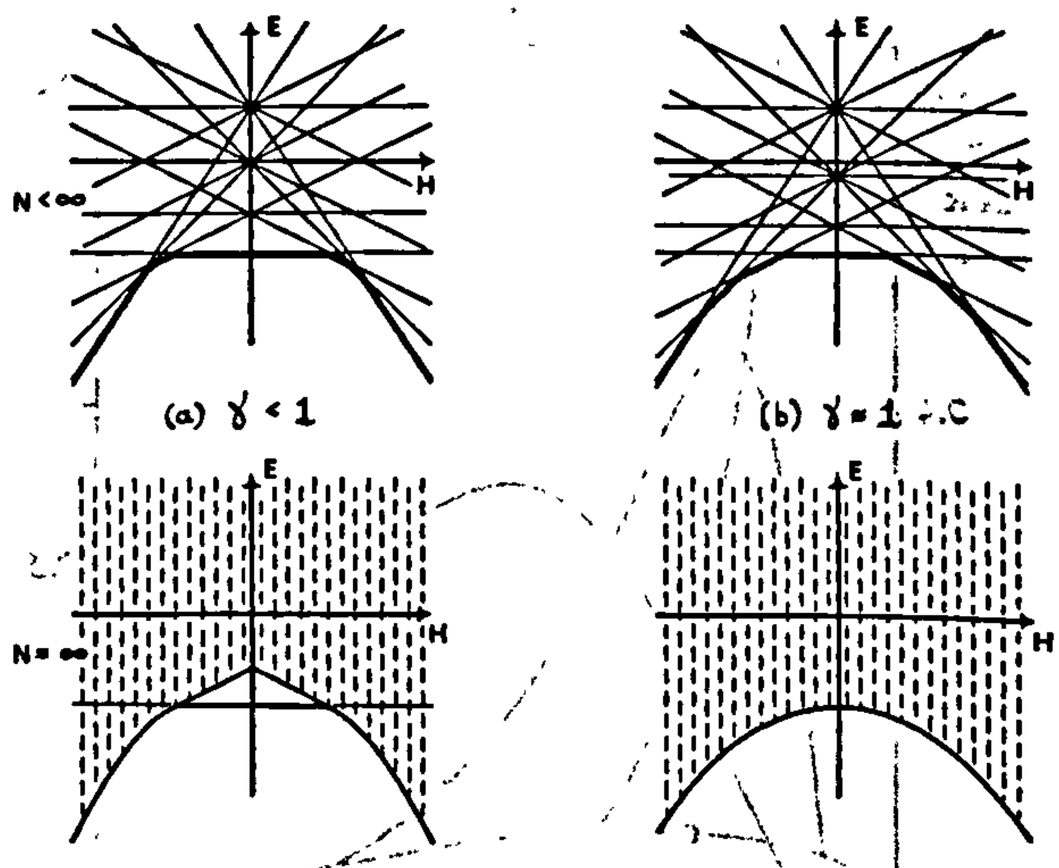

FIG. 16. Sketch of the energy levels versus magnetic field for finite and infinite isotropic ($\gamma=1$) and anisotropic ($\gamma<1$) systems (Ref. 39). The shading indicates a continuum of levels.

shows the parallel susceptibilities for rings of $N=8$ spins for $\gamma=0.3$, 0.5, and 0.7 (solid lines) and the approximate limiting curves (broken lines) roughly estimated on the basis of the limiting anisotropy gap. These curves should be accurate to within 5 or 10% down to $kT/|J|=0.3$. Evidently the effect of increasing γ is to shift the susceptibility peak to a higher temperature, to reduce its height and to increase its width. The positions of the maxima are for $\gamma=0$, $\theta_{\max}=kT_{\max}/|J|=1$; for $\gamma=0.3$, $\theta_{\max}\simeq 1.03$, for $\gamma=0.5$, $\theta_{\max}\simeq 1.07$ and for $\gamma=0.7$, $\theta_{\max}\simeq 1.14$. (For small γ the variation is quadratic in γ.)

For the isotropic pure Heisenberg case $\gamma=1$, however, the behavior as $T\rightarrow 0$ is different. As N increases, the gap between the ground state and the first excited states with $S^z\neq 0$ shrinks and approaches zero as $1/N$.[38] In the limit $N=\infty$, there is no anisotropy gap. This

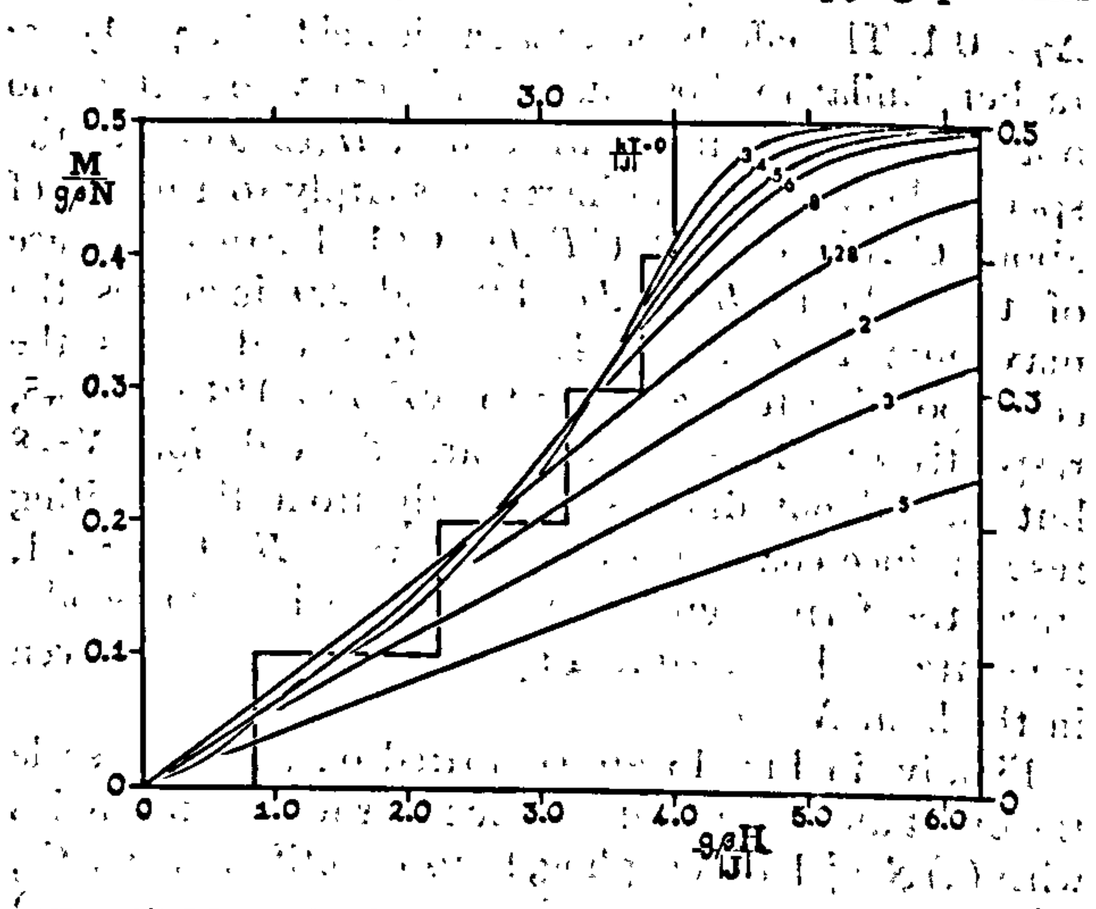

FIG. 17. Magnetization curves for an isotropic antiferromagnetic chain of $N=10$ spins. The numbers on the curves give the appropriate values of $kT/|J|$.

[38] For simplicity we describe only the case for N even.

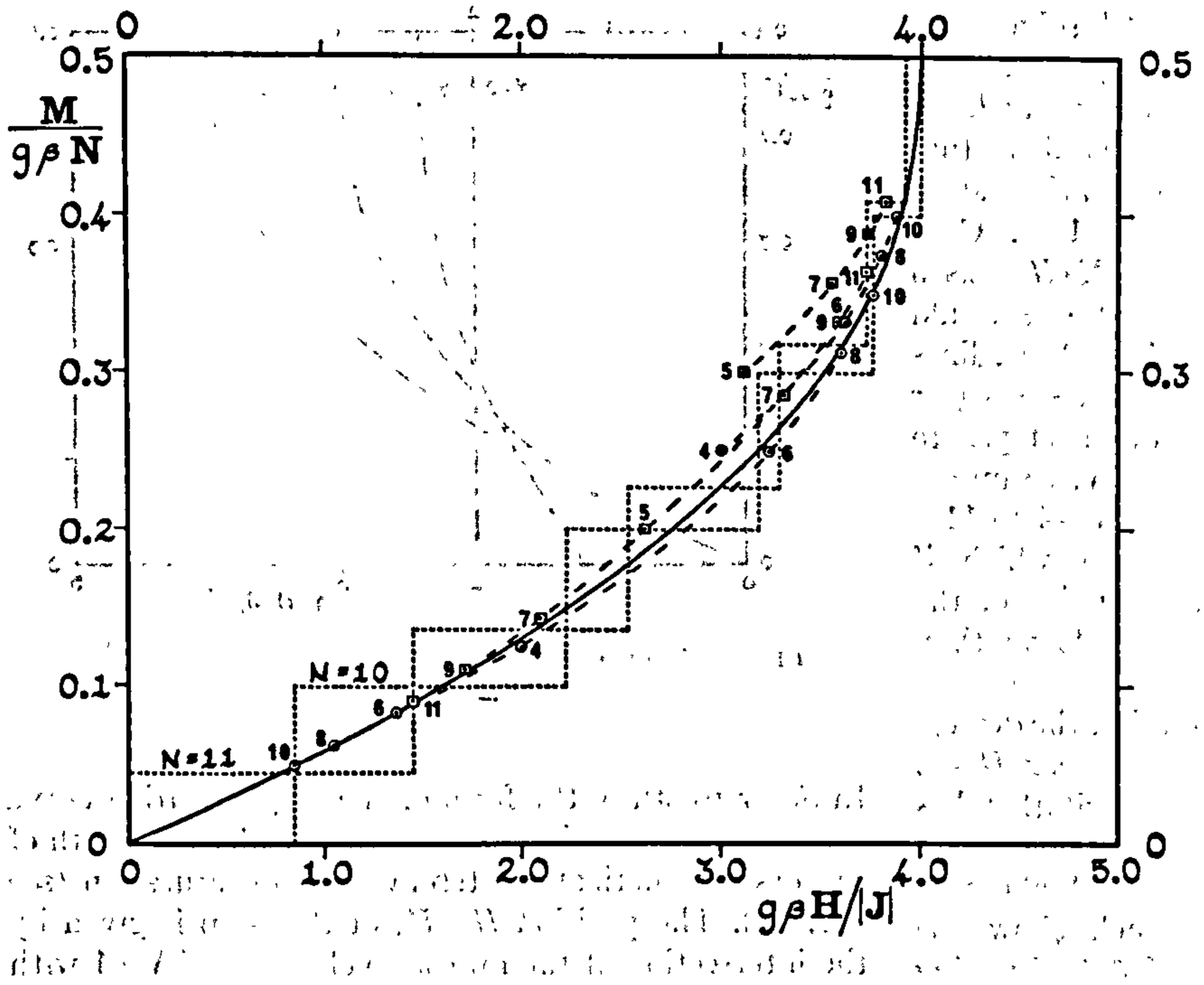

FIG. 18. Estimation of the limiting zero-temperature magnetization curve from the midpoints of the steps of the finite N curves [circles N even and squares N odd]. The zero-point step functions corresponding to $N=10$ and 11 are shown dotted.

implies that the limiting susceptibility for $\gamma=1$ can approach a finite *nonzero* value χ_0 at $T=0$.

To illustrate the detailed mechanism by which this occurs, we have sketched in Fig. 16 the relevant energy levels for (a) $\gamma<1$ and (b) $\gamma=1$ for finite systems[39] and for the corresponding infinite systems as a function of magnetic field. The susceptibility at $T=0$ is essentially the curvature of the ground state $E_0(H)$ since $\chi(H)=(\partial^2/\partial H^2)E_0(H)$. [Similarly the magnetization is just the slope of $E_0(H)$.] For finite N, the ground state (marked by a bold curve) consists of a series of straight lines and consequently (for N even) the curvature for small H is always zero, so that $\chi_N(0)\equiv 0$ for all γ. In the limit $N\to\infty$, however, the ground-state curve for $\gamma=1$ is smooth with continuous slope and definite (in general nonzero) curvature. When $\gamma<1$, on the other hand, the limiting curve consists of a horizontal straight line out to a finite field strength H_a at which the anisotropy gap vanishes. The curvature, and hence the susceptibility, near $H=0$ remains zero.

It is worth remarking that the existence of a nonzero χ_0 for isotropic coupling can be demonstrated rigorously for chains in the limiting case of infinite spin.[31]

To estimate roughly the value of the limiting zero-point susceptibility χ_0 for $S=\frac{1}{2}$, one may examine the trend of the means of $\chi_N(T)$ for $N=9$ and 10, and $N=10$ and 11 in the range $kT/|J|=0.4$ to 0.8 (see Fig. 14). These curves suggest that χ_0 lies between 0.045 and 0.06 (in units of $g^2\beta^2N/|J|$). Indeed, some time ago, Hulthén, by means of an approximate calculation, estimated that $\chi_0\simeq 0.0591 g^2\beta^2N/|J|$.[40] In an attempt to improve this estimate, we examined the magnetization curve for the finite chains, which is also of interest in its own right.

Figure 17 shows the magnetization for a chain of $N=10$ spins as a function of field for different temperatures. For temperatures above $kT/|J|=0.3$ the curves are smooth and investigation of the convergence with N suggests that the limiting curves are well approximated. For lower temperatures the magnetization displays oscillations and approaches a step function at $T=0$, the discontinuities being $\Delta M/M_{\max}=2/N$. This behavior is, of course, just what follows from our previous discussion of the ground state when N is finite.

Despite the discontinuities, one notices that the midpoints of the vertical and horizontal parts of the steps lie near a smooth curve which presumably approximates the limiting ($N=\infty$) zero-temperature magnetization curve. This is confirmed by Fig. 18 where the midpoints for a number of the longer chains are plotted. The solid line shows the estimated limiting curve which should be accurate to within about 1% of the saturation value. This is supported by the analytic calculations of Griffiths.[41]

As mentioned previously, the magnetization at $T=0$ attains its saturation value at a finite critical field $H_s=4|J|/g\beta$. Below this critical field the magnetization appears to follow a square root law

$$M/M_{\max}=1-A[1-(H/H_s)]^{1/2}, \qquad (4.5)$$

as $H\to H_s$ with $A\approx 1.2$–$1.3\approx 4/\pi=1.2732$. (For further discussion, see below.) This behavior is also a

[39] Accurate graphs of all the energy levels as a function of field are given in Ref. 10 for $N=8$.

[40] Reference 7, p. 78.

[41] R. B. Griffiths (private communication); Phys. Rev. 133 A768 (1964).

feature of the transverse ($J^{||}=0$) model solved rigorously by Katsura.[29] In that case $A=2\sqrt{2}/\pi=0.9003$.

The slope of the limiting magnetization curve at $H=0$ is the zero-point susceptibility χ_0. It seems likely that the midpoints of the finite N magnetization steps approach the limiting curve as fast as $1/N$. Consequently, if the limiting magnetization $M(H)$ has a Taylor series expansion in H about $H=0$, one would expect the gradients $g_{1,N}=\frac{1}{2}\Delta M_{1,N}/\Delta H_{1,N}$ of the lines from the origin to the midpoints of the first steps (for N even), and similar gradients to other steps, to approach the limiting slope χ_0 as fast as $1/N$. Examination of the gradients $g_{j,N}$ for small j and $N=4$ to 11 [42] does yield roughly linear plots versus $1/N$ which, if extrapolated, suggest that $\chi_0/(g^2\beta^2N/|J|)$ lies in the range 0.0555 ± 0.0020. This is significantly lower than Hulthén's estimate of 0.0591.

This estimate rests on the assumption that the derivative of $M(H)$ does not vary too rapidly near $H=0$. Since this work was performed, however, Griffiths[41] has produced strong (though not quite rigorous) theoretical arguments based on an analysis of the "unbound" antiferromagnetic spin-wave states which show (a) that $M(H)$ is nonanalytic at $H=0$ ($\partial^2M/\partial H^2$ diverging sharply to $+\infty$ as $H\rightarrow 0$) and, (b) that

$$\chi_0/(g^2\beta^2N/|J|)=0.050661\cdots\approx 1/2\pi^2. \qquad (4.6)$$

In view of Walker's results[9] mentioned in the Introduction, which show that the point $\gamma=1$, $T=0$, $H=0$ is in some ways analogous to a phase transition point,[15] one should not really be surprised that $M(H)$ is nonanalytic at $H=0$. The divergence of $\partial^2M/\partial H^2$ shows why extrapolation of the gradients $g_{j,N}$ linearly with $1/N$ leads to an overestimate of χ_0. [Essentially $\chi(H)$ for small H, of order $1/N$, is well approximated by the $g_{j,N}$ but does not itself approximate χ_0 well unless H is exponentially small.] It seems very probable that $1/2\pi^2$ is the exact constant in (4.6) so that the estimate from the gradients is 10% high.

Accepting (4.6) as correct we may complete the estimation of the antiferromagnetic susceptibility for $\gamma=1$ down to zero temperature. The result is shown in Fig. 14 (as a dashed curve) and in Fig. 15. Above $kT/|J|=0.60$ it should be accurate to within 1% but in the region $kT/|J|=0.05$ to 0.50 the error might perhaps rise to 5%.

The zero-temperature magnetization curve for other values of γ may be studied as for $\gamma=1$. The critical field H_s is determined by the intersection of the energy level for total $S^z=\frac{1}{2}N$ (a component of the zero-field ferromagnetic ground state) with the lowest level for $S^z=\frac{1}{2}N-1$ (single ferromagnetic spin wave)[39] both of which are known exactly. Thus,

$$H_s(\gamma)=2(1+\gamma)|J|/g\beta. \qquad (4.7)$$

[42] The gradients from the origin to the midpoints of the vertical parts of the steps are given by

$g_{j,N}=(j-\frac{1}{2})\Delta M_{j,N}/\Delta H_{j,N}$ for N even and
$g_{j,N}=j\Delta M_{j,N}/\Delta H_{j,N}$ for N odd.

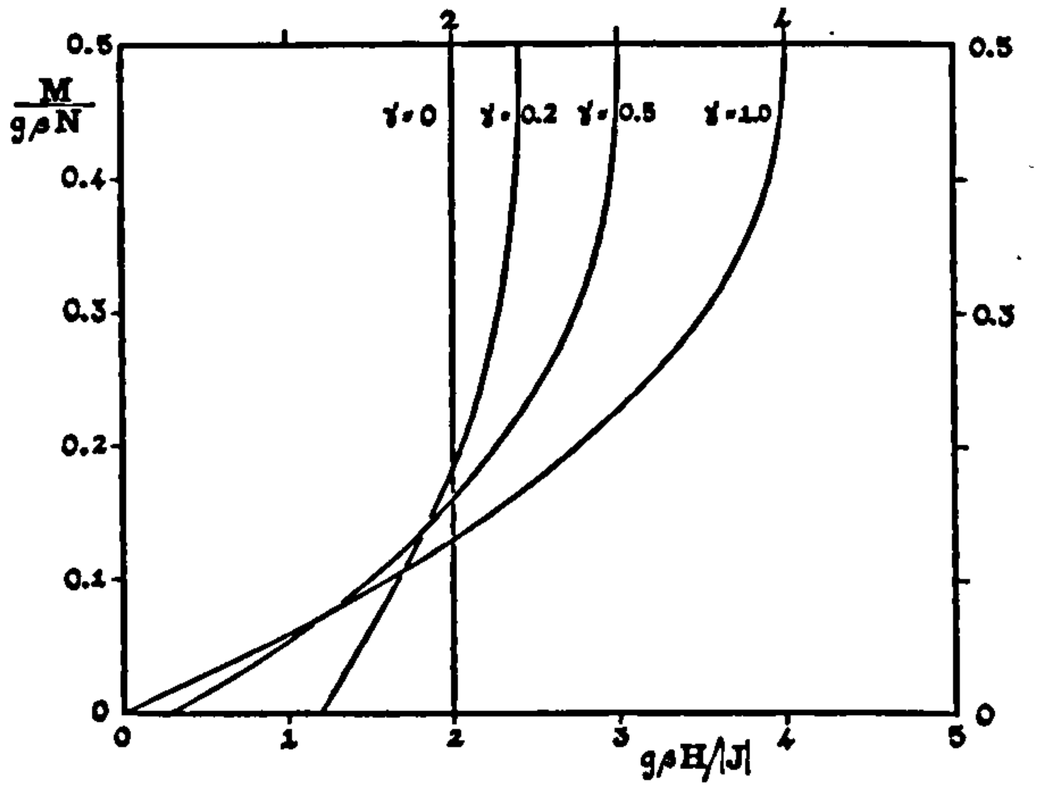

FIG. 19. Dependence of zero-temperature magnetization curves on anisotropy.

In order to study the form of the magnetization curve near saturation, it is necessary to consider the width of the first magnetization step away from saturation (see Fig. 18). The position $H=H_1$ of this step is given by the intersection of the lowest level for $S^z=\frac{1}{2}N-1$ with the lowest level for $S^z=\frac{1}{2}N-2$ which in the limiting case, $N\rightarrow\infty$, is given by $-4|J|(1+\gamma)$ [Eq. (5.4), Sec. 5, with $k=2\pi$]. It is seen, however, that use of the limiting curve again yields H_s; it appears, therefore, that the width of this step is directly determined by the energy discrepancy ΔE_1 between the lowest lying level for $S^z=\frac{1}{2}N-2$ (finite N) and its limiting value. An estimate of the lowest, finite N, energy level as a function of γ may be obtained, for example, by applying second-order perturbation theory to the appropriate submatrices of the Hamiltonian (1.1). One finds that for large N, $\Delta E_1\simeq 2\gamma\pi^2|J|/N^2$. Corresponding to a magnetization step of $\Delta M=g\beta$ or $\Delta M/M_{\max}=2/N$, we thus find a magnetic field step $\Delta H_1=\frac{1}{2}(H_s-H_1)=\Delta E_1/2g\beta\simeq\gamma\pi^2|J|/g\beta N^2$. On eliminating N we obtain

$$\frac{\Delta M}{M_{\max}}\simeq\left[\frac{8(1+\gamma)}{\pi^2\gamma}\right]^{1/2}\left(\frac{\Delta H_1}{H_s}\right)^{1/2},$$

which suggests that when $N\rightarrow\infty$ we may write more generally, as $H\rightarrow H_s$,

$$M/M_{\max}=1-A(\gamma)[1-(H/H_s)]^{1/2} \qquad (4.8)$$

with

$$A(\gamma)=(4/\pi)[(1+\gamma)/2\gamma]^{1/2}.$$

This argument is, of course, not rigorous but it should be at least qualitatively correct and its accuracy is supported by the results for finite N and by agreement with Griffiths' analysis at $\gamma=1$.[42]

Figure 19 shows the complete estimated limiting magnetization curve for the Ising limit $\gamma=0$, where it is a simple step function, and for intermediate values of γ.

When $\gamma<1$ we must, as mentioned, distinguish between a *perpendicular* and a *parallel* susceptibility.

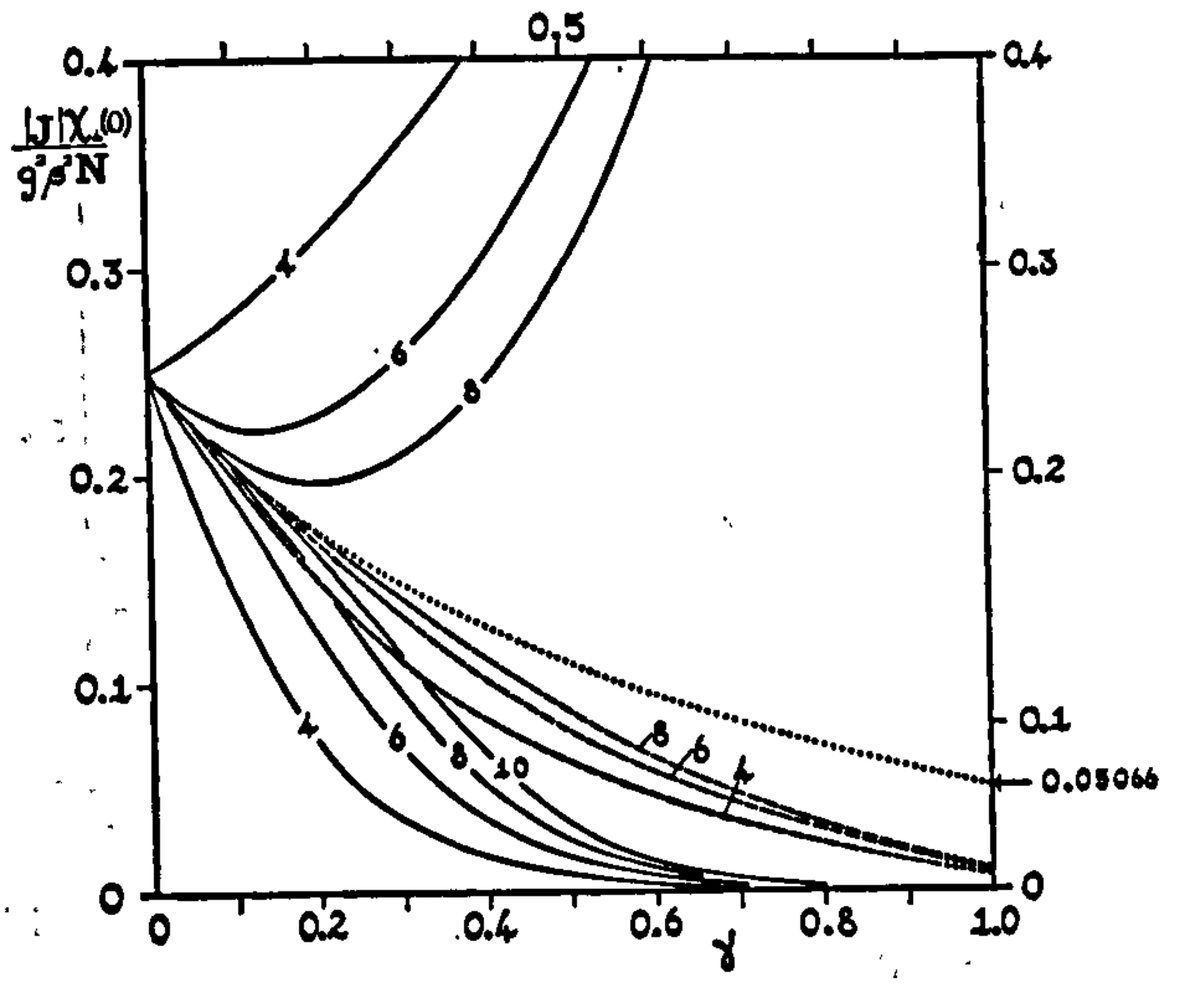

FIG. 20. Perpendicular susceptibilities for the ground and first $S^z=0$ excited states for finite rings (solid curves) and the geometric means (broken curves). The dotted curve represents the probable limit for $N\to\infty$.

For the Ising limit we have the exact result[43,44]

$$\chi_\perp(T)=\frac{g^2\beta^2N}{4|J|}[\tanh K+K\,\mathrm{sech}^2K]\quad(\gamma=0),\quad(4.9)$$

where K is defined in (4.4). From this we see that $\chi_\perp(0)$ for $\gamma=0$, is nonzero. In the limit $N\to\infty$ this will remain true for all γ and in fact as $\gamma\to1$, $\chi_\perp(0,\gamma)\to\chi_0$. For this reason the susceptibility in the isotropic case is perhaps best regarded as a *perpendicular* susceptibility.

For finite N the situation is again more complicated. The lowest set of solid curves in Fig. 20 show $\chi_{\perp N}(0,\gamma)$ for rings of $N=4$, 6, 8, and 10 spins. (The derivation requires the numerical calculation of matrix elements with the ground-state eigenvector.) As $\gamma\to1$, for N even and finite, $\chi_{\perp N}(0,\gamma)$ approaches zero as the previous arguments have shown it must. (For odd N it diverges at $\gamma=1$.) Furthermore, for $\gamma>0.2$ the convergence for N increasing is evidently very slow. The upper solid curves in Fig. 20 represent the perpendicular susceptibilities calculated for the lowest excited states. In the limit $N\to\infty$ these are expected to approach the ground-state results. The broken curves are the geometric means of these two sets of values and they seem to be converging somewhat more rapidly, at least for $\gamma<0.5$. Accepting the value (4.6) for χ_0, the limiting zero-point perpendicular susceptibility $\chi_\perp(0,\gamma)$ must resemble in general form the dotted curve in Fig. 20. The slope of the limiting curve at $\gamma=0$ is known exactly,[43] but for $0.2<\gamma<0.5$ the dotted curve is probably accurate only to within 10%.

Ferromagnetic Coupling

The susceptibility for ferromagnetic chains is conveniently discussed in terms of the deviations from Curie's law. Quite generally we can write for the parallel susceptibility

$$\chi_N(T)=[g^2\beta^2N/4kT]\xi_N(T),\quad(4.10)$$

where

$$\xi_N(T)=(4/N)\langle[\sum_{i=1}^{N}S_i^z]^2\rangle,\quad(4.11)$$

the angular brackets denoting the canonical average. At high temperatures $\xi_N(T)$ approaches unity as $1/T$. As the temperature falls $\xi_N(T)$ rises monotonically (for $J>0$) and, for finite N, levels off at a value determined by the properties of the ground state. For anisotropic chains ($\gamma<1$) the ferromagnetic ground state is twofold degenerate with $\sum S_i^z=\pm\frac{1}{2}N$ so that $\xi_N(0)=N$. In the isotropic ($\gamma=1$) case, on the other hand, the ground state has total spin $S=\frac{1}{2}N$ and hence is $(N+1)$-fold degenerate, $\sum S_i^z$ taking the values $\frac{1}{2}N$, $\frac{1}{2}N-1$, $\cdots-\frac{1}{2}N+1$, $-\frac{1}{2}N$. For finite pure Heisenberg chains, therefore, $\xi_N(T)$ rises to a maximum value $\xi_N(0)=\frac{1}{3}(N+2)$.

In the limit $N\to\infty$ we see that for all γ, $\xi(T)$ diverges as $T\to0$. For Ising chains ($\gamma=0$) this divergence is exponentially fast since we have rigorously

$$\xi(T)=\exp[J/kT],\quad(\gamma=0).\quad(4.12)$$

This rapid divergence finds its origin in the anisotropy gap which ensures that all the pair correlation functions $\langle S_i^zS_j^z\rangle$ approach their zero-point values exponentially fast. For this reason we expect the limiting divergence for other values of $\gamma<1$ will also be of the form $\exp[\alpha J/kT]$ with α depending on the limiting anisotropy gap.

For pure Heisenberg coupling, however, a power law might be expected. Indeed, in the limit $S=\infty$ ($\gamma=1$), the susceptibility diverges as $1/T^2$ so that $\xi(T)\sim1/T$ as $T\to0$.[31] Fig. 21 is a log-log plot of $[\xi_N(T)-1]$ versus the temperature for finite isotropic chains of $N=3$, 4, $\cdots$, 10, 11 spins. The curves evidently approach the

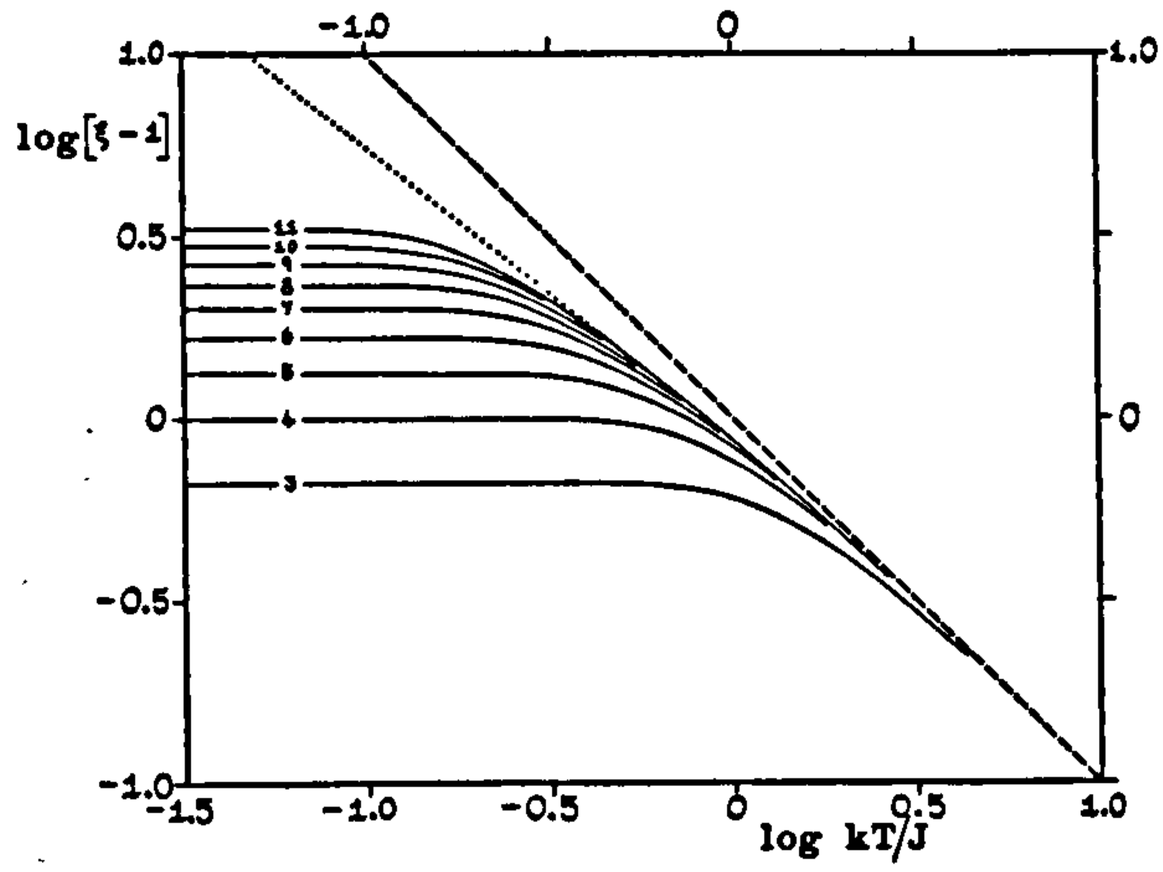

FIG. 21. Log-log plot of the reduced ferromagnetic susceptibility $\xi(T)-1$ for finite isotropic chains.

[43] M. E. Fisher, Physica 26, 618 (1960).
[44] M. E. Fisher, J. Math. Phys. 4, 124 (1963), and Ref. 29.

limit monotonically from below. The convergence is quite rapid and for $kT/J>0.3$ the limiting curve is indicated quite accurately. At high temperatures the log-log plot becomes linear with slope unity as shown by the broken line in Fig. 21. This simply confirms the $1/T$ deviations from Curie's law. At lower temperatures in the range $kT/J=0.25$–1.0, the limiting curve is again almost linear but with slope close to $\frac{4}{5}$ (see dotted line in Fig. 21). If the curves for larger N continued this trend it would imply a divergence of $\xi(T)$ like $1/T^{4/5}$ and of $\chi(T)$ like $1/T^{9/5}$ as $T\to 0$. It is quite possible, however, that the true asymptotic behavior sets in only below $kT/J=0.2$. Nevertheless, the qualitative behavior is clearly rather similar to that for $S=\infty$.

The nature of the variation of the susceptibility with magnetic field can be seen in Fig. 22 which shows the ferromagnetic susceptibility of isotropic chains of $N=8$ spins in various fields. The convergence with N is appreciably more rapid in a field than for $H=0$.

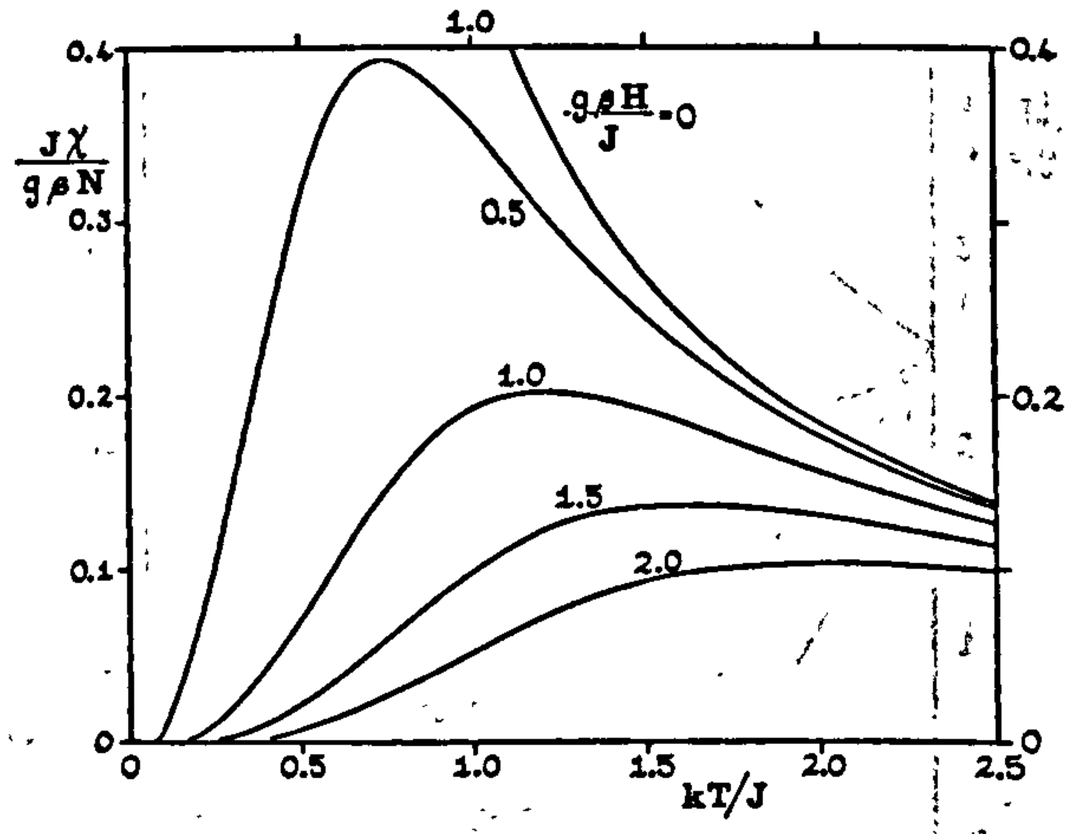

FIG. 22. Ferromagnetic susceptibility for rings of $N=8$ spins with isotropic coupling for different magnetic fields.

5. SPECTRUM

In the following account we confine our attention to a discussion of the spectrum of energy levels in the absence of an applied field, i.e., the eigenvalues of the Hamiltonian (1.1) with $H=0$.

Ferromagnetic Coupling

The ferromagnetic ground state for all γ is, of course, exactly $E_0=-\frac{1}{2}NJ$ corresponding to $\sum S_i^z=\frac{1}{2}N$ (all spins aligned). With one "overturned spin" we have a single "spin wave" of energy

$$E-E_0=\epsilon(k)=2J[1-\gamma\cos k], \tag{5.1}$$

where

$$k=2\pi r/N, \quad r=0, \pm 1, \pm 2, \cdots.$$

With two overturned spins, the simple spin-wave approximation predicts

$$E-E_0=\epsilon(k_1)+\epsilon(k_2), \tag{5.2}$$

but this is not exact owing to the spin-wave "interactions." For anisotropic linear chains the interaction of

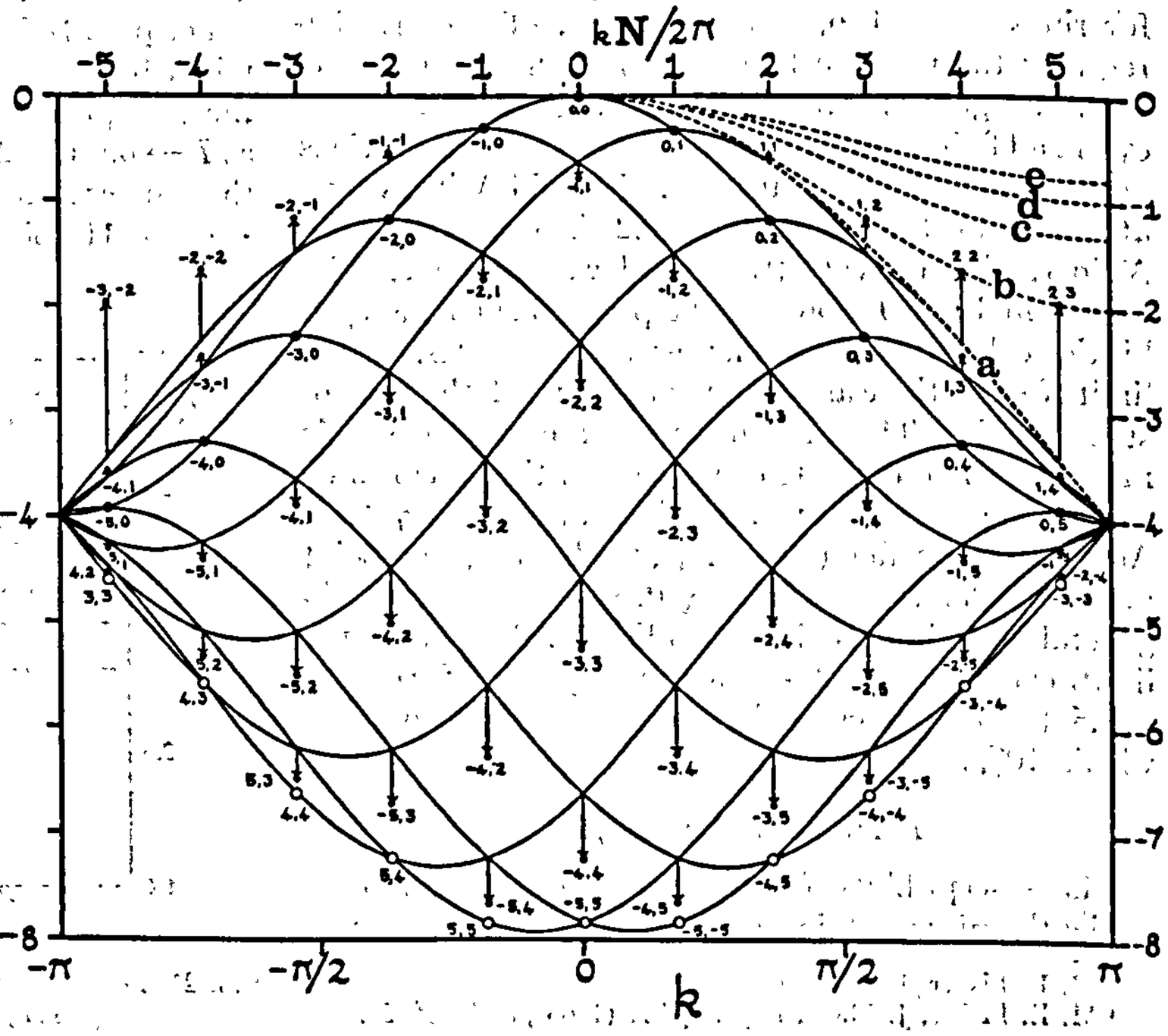

FIG. 23. Energy levels for two overturned spins (interacting spin waves) for a ring of $N=11$ spins and $\gamma=1$. The arrows indicate the deviations from the levels for two independent spin waves. Note that we are taking an "antiferromagnetic view" of the energy levels ($J=-|J|$), and each level has been normalized by subtraction of an energy $-\frac{1}{2}NJ$.

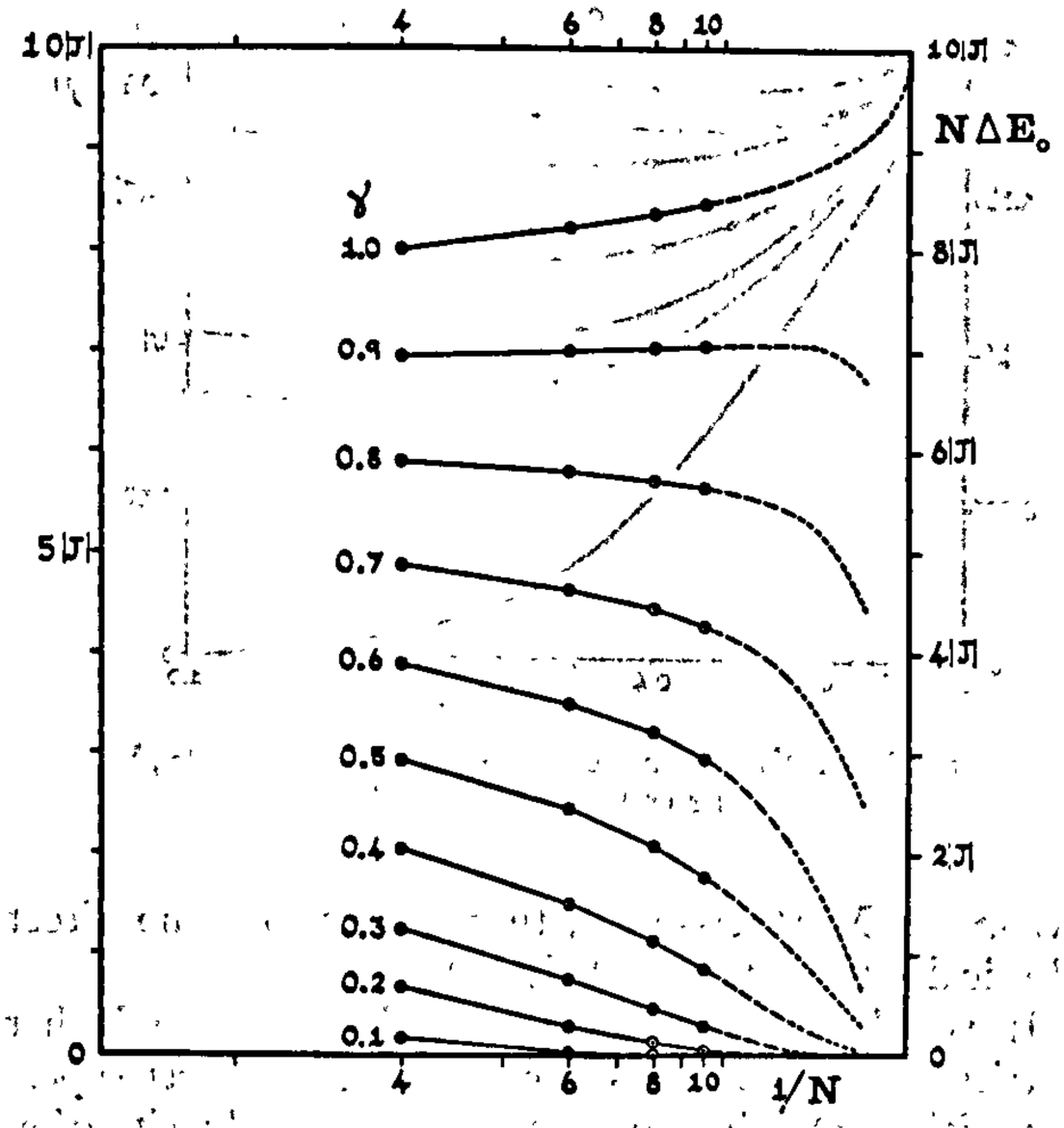

FIG. 24. Dependence of the splitting ΔE_0 of the antiferromagnetic ground state on γ and N.

two spin waves has been analyzed theoretically by Orbach,[8] who followed Bethe's analysis for $\gamma=1$.[6]

A graphic understanding of these results can be obtained from Fig. 23, which shows energy levels for a ring of $N=11$ spins for $\gamma=1$. The solid curve through the dark circles is the single spin-wave dispersion law (5.1). The other solid curves represent the superimpositions (5.2), and their intersections are thus the spin-wave approximations to the levels for two overturned spins. The arrows indicate the energy shifts due to the interactions, the exact energy levels lying at the points of the arrowheads.

The open circles represent "missing states," i.e., levels predicted by (5.2) which do not occur for the true Hamiltonian (essentially because two spins cannot be overturned at the same site). For most combinations of k_1 and k_2 the interactions are evidently repulsive and the spin waves "scatter" and remain "unbound" (category I states[8]). However, for $k_1\simeq k_2\simeq\frac{1}{2}k$, the interactions are strongly attractive and the spin waves condense into a bound state (category II) given by,[8]

$$\epsilon_{II}(k)=2J[1-\tfrac{1}{2}\gamma^2(1+\cos k)]. \tag{5.3}$$

This is indicated by the dotted line (b) in Fig. 23. As the form of this dispersion relation suggests, the corresponding eigenfunction relates to two closely associated overturned spins traveling around the ring together. The dotted line (a) in Fig. 23 is the $N=\infty$ limit of the energies of the unbound states namely,[8]

$$\epsilon_I{}^{\min}(k)=4J(1-\gamma\cos\tfrac{1}{2}k), \tag{5.4}$$

which is just the envelope of the curves (5.2).

One may in a similar way study numerically the bound states for r overturned spins. The lowest states seem to follow the relation

$$\epsilon^{(r)}(k)\simeq(2J/r)[1-\cos k] \tag{5.5}$$

when $\gamma=1$, as illustrated in curves (c), (d), and (e) of Fig. 23, corresponding to 3, 4, and 5 overturned spins, respectively. For $\gamma\neq1$ the amplitudes of the $\cos k$ term appear to decrease as γ^r or more rapidly.

Antiferromagnetic Coupling

The approach of the antiferromagnetic ground-state energies for finite chains to the limiting value was discussed in Sec. 2. The question of the degeneracy of the ground state has not, however, been considered. When N is even[45] the antiferromagnetic ground state at the Ising limit ($\gamma=0$) is twofold degenerate. This degeneracy, however, is split by the transverse terms in the Hamiltonian, although, as is well known, the splitting only arises in Nth-order perturbation theory. This suggests that in the limit $N\to\infty$, the ground state should again become degenerate, at least in some sense.

To investigate this point we may examine the ground-state splitting $\Delta E_0(N)$ as a function of N. If ΔE_0 varies as $1/N$ for N large, the levels close up, but only at a rate characteristic of a continuum of levels in the limit of $N=\infty$. Conversely, if ΔE_0 vanishes more rapidly than $1/N$, e.g., as $1/N^2$, then we may consider the levels as asymptotically degenerate even if they lie within a continuum. In Fig. 24, the product $N\Delta E_0(N)$ has been plotted versus $1/N$ for $N=4$, 6, 8, and 10, and for values of γ in the range 0 to 1. For $\gamma\leqslant0.5$, $N\Delta E_0$ is rapidly decreasing, and there seems little doubt that the limit is zero. For $\gamma=0.6$, 0.7, and 0.8, the decrease is slower, but the rate increases for larger N, and it seems probable that the limit is again zero, as suggested by the broken lines. (These lines are purely suggestive and are not to be taken as numerical extrapolations.) At $\gamma=0.9$ the values of $N\Delta E_0$ at first increase slightly with N, but for $N=8$ and 10 they are almost equal, and we believe that larger values of N would again yield a product decreasing at first slowly, but eventually rapidly. At the limit $\gamma=1$, on the other hand, $N\Delta E_0$ seems to be rising steadily and approaching a definite limit at $1/N=0$, consistent with a state lying in a continuum bounded by the ground state. (Consideration of the des Cloizeaux-Griffiths analysis[26,41] suggests that this limit should be $\pi^2|J|$).

In summary, we feel that the evidence of Fig. 24 definitely suggests that for all $\gamma<1$ (i.e., anisotropic coupling) ΔE_0 decreases more rapidly than $1/N$ ($N\Delta E_0\to0$), so that the limiting ground state may be said to be (twofold) degenerate. In the isotropic limit, however, ΔE_0 decreases only as $1/N$ and the anti-

[45] When N is odd, the Ising ground state is $2N$-fold degenerate, but for $\gamma>0$, only a fourfold degeneracy corresponding to $\Sigma S_i{}^z=\pm\frac{1}{2}$ remains. We will not consider this case further.

ferromagnetic ground state should be regarded as nondegenerate.

For an Ising chain the first excited states lie at an energy $\Delta E_A(0)=2|J|$ above the ground states, but at the Heisenberg limit the ground state is the limit of a continuum, and there is no anisotropy gap. (This may be seen explicitly from the theoretical calculation of the antiferromagnetic spin-wave states for $\gamma=1$ by des Cloizeaux and Pearson.[26]) To estimate the limiting anisotropy gap $\Delta E_A(\gamma)$ for intermediate values of γ, we have studied (a) the difference $\Delta E_A(\gamma,N)$ between the "lowest excited state" $E_s(\gamma,N)$ [actually two degenerate ($S^z=\pm 1$) states which must be distinguished from the higher component of the split ground state] and the finite N ground state $E_0(\gamma,N)$, and (b) the gap $\Delta E_A'(\gamma,N)$ between $E_s(\gamma,N)$ and the *limiting* ground state $N|J|\mathcal{E}_0(\gamma,\infty)$. At the Heisenberg limit $E_s(\gamma,N)$ becomes a continuum state and the fact that $\Delta E_A(1,N)$ and $\Delta E_A'(1,N)$ fall to zero like $1/N$ may be checked from the values for small finite N. For other values of γ also, linear extrapolation with $1/N$ seems to be appropriate in estimating the limit. The two sets of values form two distinct sequences but, as one would expect, they tend to the same limiting value. In the case $\gamma=1$, the lowest excited state $E_s(1,N)$ becomes degenerate with the continuum state ($S^z=0$) split off the degenerate ($\gamma=0$) ground state, and hence $N\Delta E_A(1,N)=N\Delta E_0$ tends to a limit [which, as mentioned, is probably $\pi^2|J|$ although $N\Delta E_A'(1,N)$ appears to tend to a slightly different value]. Figure 25 shows the variation with γ of the gap for finite N and the estimated limit $\Delta E_A(\gamma)$, which is probably accurate to within $\pm 0.05J$. The main feature of interest is the very slow increase in the gap as $(1-\gamma)$ increases from zero to 0.3 or 0.4.

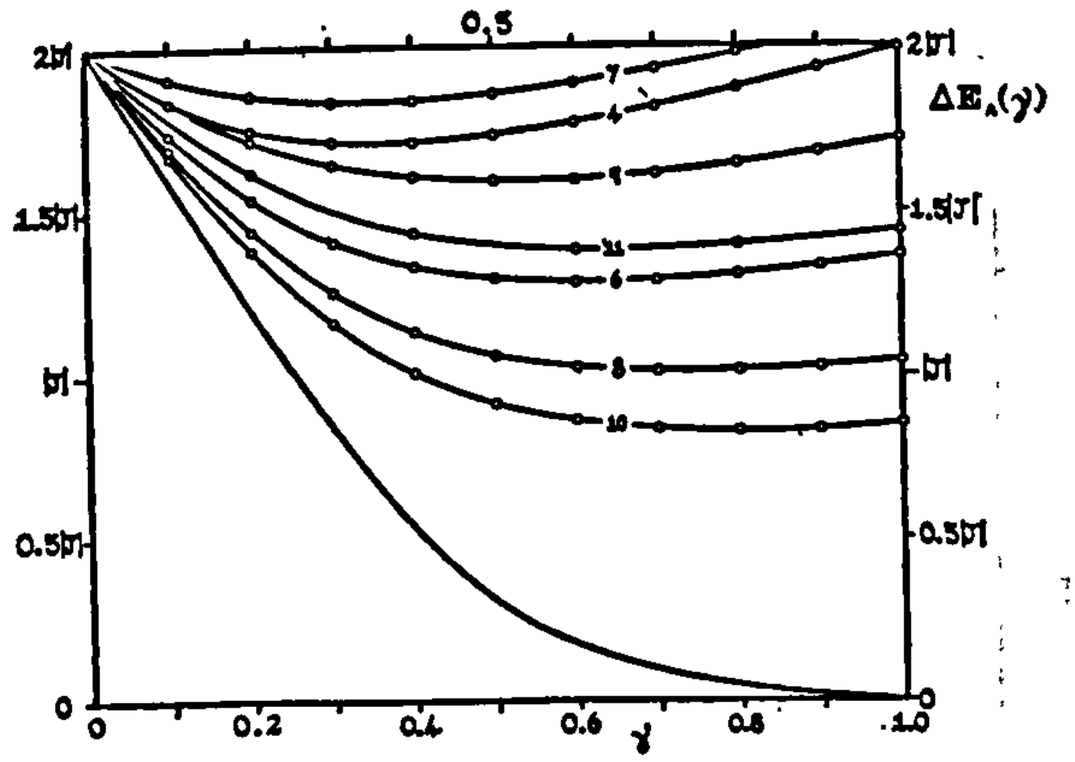

FIG. 25. Antiferromagnetic anisotropy gap $\Delta E_A(\gamma,N)$ and the estimated limit $\Delta E_A(\gamma)$.

The problem of the antiferromagnetic spin-wave spectrum has recently been studied in detail by des Cloizeaux and Pearson,[26] who computed numerically the lowest category I states for $\gamma=1$ and rings of $N=6$, 8, 16, and 48 spins. They showed analytically that the limiting dispersion law is

$$\epsilon(k)=E^{(1)}(k)-E_0=|J|\pi|\sin k|\,. \tag{5.6}$$

Extrapolation of the appropriate energy differences versus $1/N$ for N up to 11 yields the amplitude $|J|\pi$ to within 5 to 10%, which confirms the validity of extrapolating the spectral properties.

Mattheiss[25] has given a plot of all the energy levels versus k for $N=6$ and 8. The results for higher values of N are more complex since there are more levels but they do not differ much qualitatively and so we do not present a figure. Mattheiss remarked that for even $N=2m$, the antiferromagnetic ground state corresponded to $k=0$ when m was even, but to $k=\pi$ when m was odd. For odd $N=2m+1$, we have found that the two degenerate ground states are at $k\simeq\pm\frac{1}{2}\pi$, and the state at $k=0$ or π is the higher according as m is odd or even.[46] As Mattheiss says, there seems to be no direct physical interpretation of these facts.

It would be of interest to decide how well the higher antiferromagnetic states can be represented as superimpositions of spin waves obeying (5.6). The situation seems appreciably more complex than for the ferromagnetic chains, and although the exact spectra do display levels that lie roughly on curves $|J|\pi(|\sin k_1|+|\sin k_2|)$ with $k=k_1+k_2$, we have not been able to discover any simple numerical correlations, and some low-lying states (presumably "bound states") are definitely not representable in this way.

6. ANTIFERROMAGNETIC CORRELATIONS AND ORDER

For an antiferromagnetic chain at zero temperature the pair-correlation functions

$$\omega_l(N)=4\langle S_0^z S_l^z\rangle=(4/N)\sum_{j=1}^{N}\langle S_j^z S_{j+l}^z\rangle \tag{6.1}$$

can be calculated from the detailed expansion of the ground-state wave function in the basis of functions of definite "up" and "down" spins. Numerical results for $N=4$, 6, 8 and 10, and $\gamma=0.1, 0.3, \cdots, 1.0$ are given in Table II. For fixed l the convergence in the case of N even is not regular: for $\gamma<0.3$ it is monotone increasing and for $\gamma>0.8$ monotone decreasing, the curves for different N crossing in the intermediate region. However, the convergence is quite rapid for $\gamma<0.3$ for all l, and for $l<\frac{1}{4}N$ in the case of $\gamma>0.8$. In the case of N odd the convergence for $l<\frac{1}{2}N$ is monotone increasing for all γ but rather slow. (These values are not tabulated.) The case of $l=\frac{1}{2}N$ is of special interest and will be discussed later.

Despite the relatively erratic convergence, extrapolation procedures for the limit $N\to\infty$ may be attempted and their accuracy checked against Orbach's exact calculation[8] of the limiting zero-temperature short-

[46] More precisely, the ground states are at $k=\pm\pi m/N$ for m even and $k=\pm\pi(m+1)/N$ for m odd.

TABLE II. Antiferromagnetic ground state correlation functions $\omega_l(N,\gamma)$. [Note that $\omega_0=1$.]

N	l	$\gamma=0.1$	$\gamma=0.3$	$\gamma=0.5$	$\gamma=0.7$	$\gamma=0.9$	$\gamma=1.0$
10	1	−0.99001	−0.90791	−0.77658	−0.67994	−0.62221	−0.60206
	2	0.98005	0.81790	0.56583	0.38839	0.28782	0.25407
	3	−0.97998	−0.81203	−0.54351	−0.35953	−0.26199	−0.23117
	4	0.97988	0.80441	0.51181	0.31041	0.20558	0.17307
	5	−0.97989	−0.80475	−0.51510	−0.31865	−0.21839	−0.18781
8	1	−0.98972	−0.90139	−0.77381	−0.68355	−0.62819	−0.60852
	2	0.97948	0.80498	0.55947	0.39250	0.29464	0.26104
	3	−0.97936	−0.79910	−0.54364	−0.37551	−0.28238	−0.25194
	4	0.97921	0.79102	0.51598	0.33311	0.23186	0.19883
6	1	−0.98821	−0.89102	−0.77359	−0.69291	−0.64155	−0.62284
	2	0.97645	0.78410	0.55640	0.40440	0.31068	0.27735
	3	−0.97648	−0.78616	−0.56561	−0.42298	−0.33826	−0.30902
4	1	−0.98113	−0.88125	−0.78868	−0.72542	−0.68282	−0.66667
	2	0.96225	0.76249	0.57735	0.45084	0.36564	0.33333

range order $\omega_1(\gamma)$. In Fig. 26 this exact result (a) is compared with an extrapolation estimate (b) based on sequences of means, 10/9, 9/8, 8/7, etc., which show monotone increasing behavior for all γ. As may be seen, the agreement is very good (to within 1%) and a similar technique has therefore been applied to estimate the limiting curve for the cases $|\omega_2(\gamma)|$, $|\omega_3(\gamma)|$, and $|\omega_4(\gamma)|$ (see Fig. 27). However, as the value of l successively increases, the accuracy is expected to fall off somewhat, since there are fewer points to extrapolate.

Also shown in Fig. 26 are sums of Walker's perturbation series[9]

$$\omega_1=1-\gamma^2+\tfrac{3}{4}\gamma^4-(7/2^6)\gamma^8-(9/2^7)\gamma^{10}-(11/2^9)\gamma^{12}+(13/2^{11})\gamma^{14}+\cdots \quad (6.2)$$

truncated at γ^{14} [curve (c)] and at γ^6 [curve (d)]. In the former case the error is detectable only for $\gamma>0.85$ and reaches a maximum of only 6% at $\gamma=1$. In the latter case, however, the deviations are significant for $\gamma\gtrsim 0.7$. Curve (e) is derived from Davis's perturbation expansion[17] and is evidently less accurate than the extrapolations once $\gamma>0.40$ and seriously in error for $\gamma>0.85$.

An appreciation of the decay of the correlations with distance l (as well as of the convergence in N) can be gained from Fig. 28 which shows the finite ring correlations for $\gamma=0.3$, 0.5, and 1.0. An alternating effect is evident, the values of $|\omega_l|$ for even l being lower relative to those for odd l than might be expected. For $l>\frac{1}{2}N$ the correlations, of course, start increasing as the points 0 and l approach one another around the closed ring. Nevertheless, it is clear for $\gamma=0.3$, and reasonably so for $\gamma=0.5$, that the correlations for $l<\frac{1}{2}N$ are decaying to a constant level of about 0.8 and 0.5, respectively. These values may be identified with the long-range order $\omega_\infty(\gamma)$ defined by

$$\omega_\infty(\gamma)=\lim_{l\to\infty}|\lim_{N\to\infty}\omega_l(\gamma,N)|\,. \quad (6.3)$$

To estimate $\omega_\infty(\gamma)$ we have formed the minimum

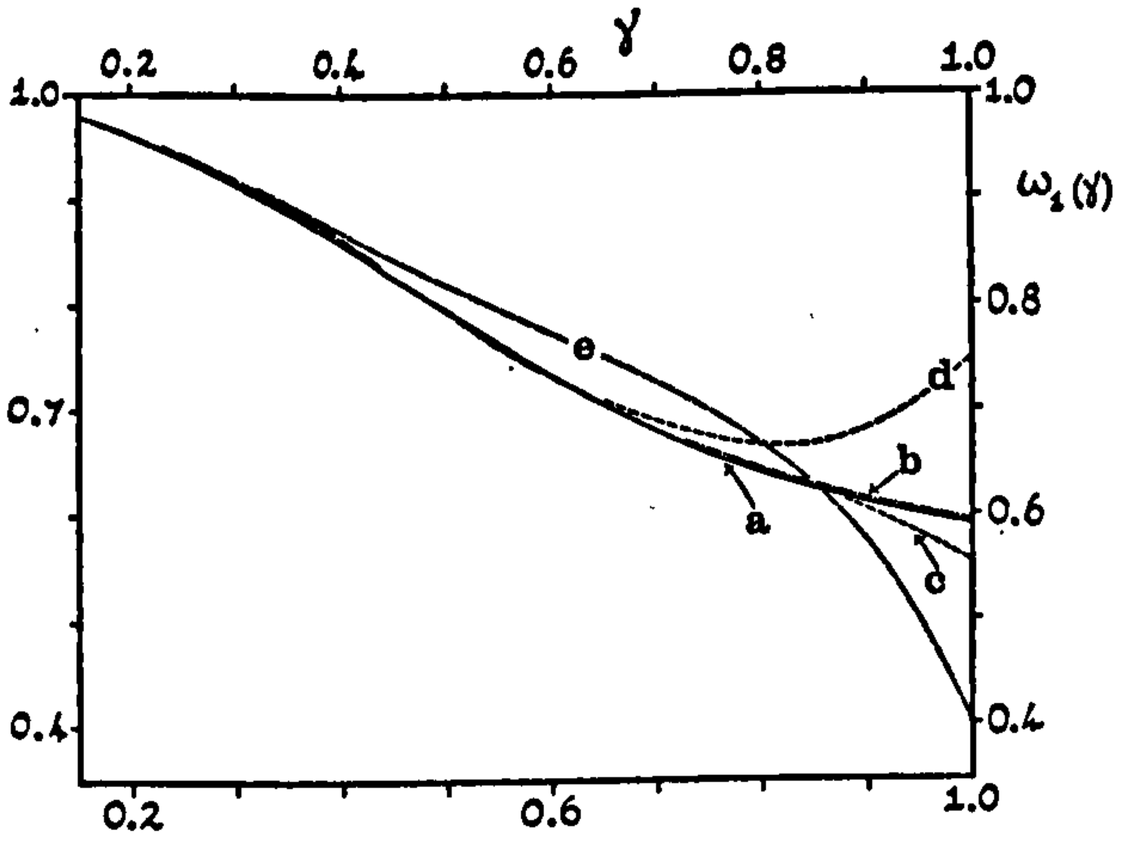

FIG. 26. Comparison of (a) the exact value of $\omega_1(\gamma)$ with (b) present extrapolations, (c) Walker's perturbation series to γ^{14}, (d) to γ^6 and (e) Davis's perturbation series.

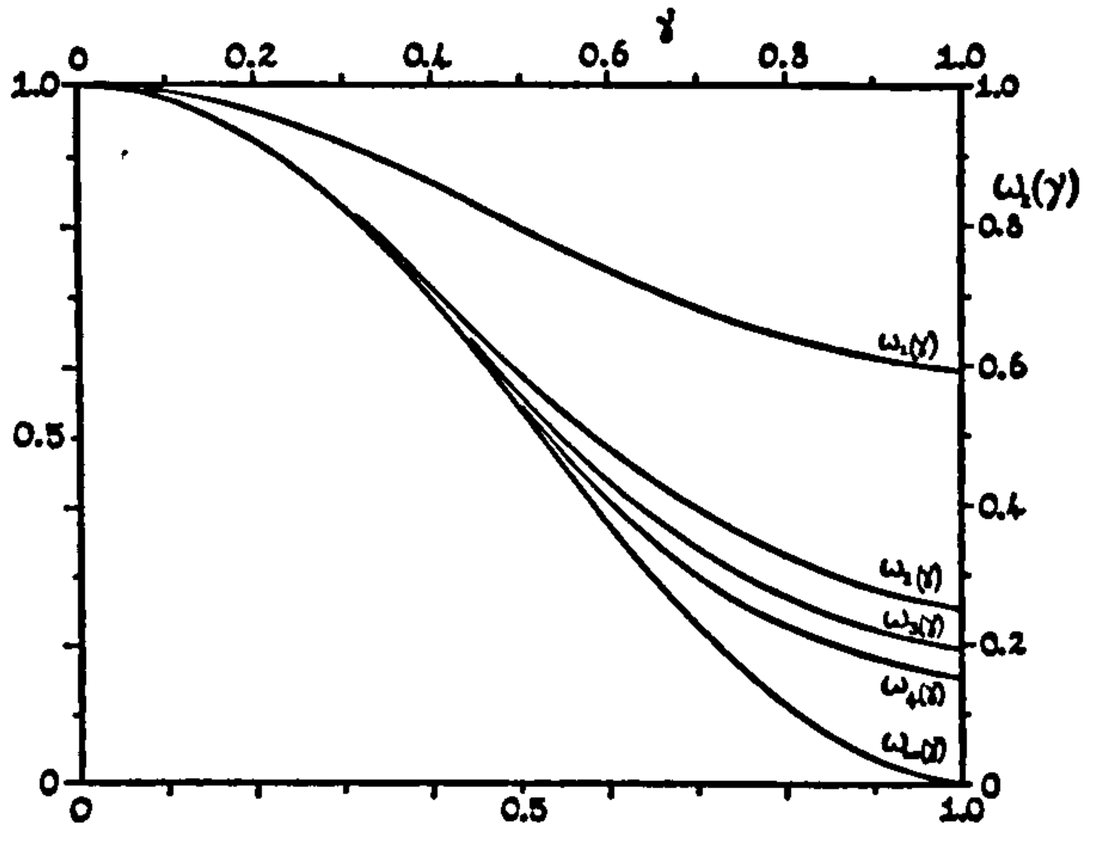

FIG. 27. Variation of the pair correlations $|\omega_l|$ with γ for $l=1$ (exact) and $l=2$, 3, 4 (estimated) and $l=\infty$, the final estimate of the long-range order.

means for N even

$$\omega_{\min}(\gamma,N)=\tfrac{1}{2}|[\omega_{\frac{1}{2}N}(\gamma,N)-\omega_{\frac{1}{2}N-1}(\gamma,N)]| \quad (6.4)$$

and attempted to extrapolate to the limit $N=\infty$, which should agree with (6.3). These means are taken to reduce the alternation effects.

In this case we felt it was not advisable to use the results for odd N in forming the estimate because, with the above definition of long-range order, interference effects around the chain occur near the Ising limit. (Note that for N odd and $\gamma=0$, $\omega_l(N)=1-2l/N$, $0\leqslant l<\frac{1}{2}N$.) For this reason we do not expect the limiting result for ω_∞ to have accuracy comparable with our estimate for ω_1. (An estimate for ω_1 using results for even N only gives a result accurate to about 2.5%.) Figure 29 shows a plot of $\omega_{\min}(N)$ versus $1/N$. The points for $N>4$ appear reasonably collinear but care must be taken in extrapolation since curvature is to be expected for $\gamma<0.7$. (A similar, though less marked, effect occurs in the case of the short-range order.) For $\gamma<0.3$, the over-all range of variation is slight and an estimate can be made with some confidence: The limiting values here must, in fact, lie very close to the values for $N=10$. For $\gamma>0.7$ a linear extrapolation would seem to be reliable. For intermediate γ some attempt has been made to allow for curvature effects but we would not claim very high accuracy for our results in this range. In fact, for $0.4<\gamma<0.6$, we have probably underestimated by several percent. We feel justified in concluding, however, that the long-range order vanishes only at the Heisenberg limit $\gamma=1$. In view of our conclusions regarding the asymptotic degeneracy of the ground state (and the vanishing of the anisotropy gap at $\gamma=1$) this is perhaps not unexpected.

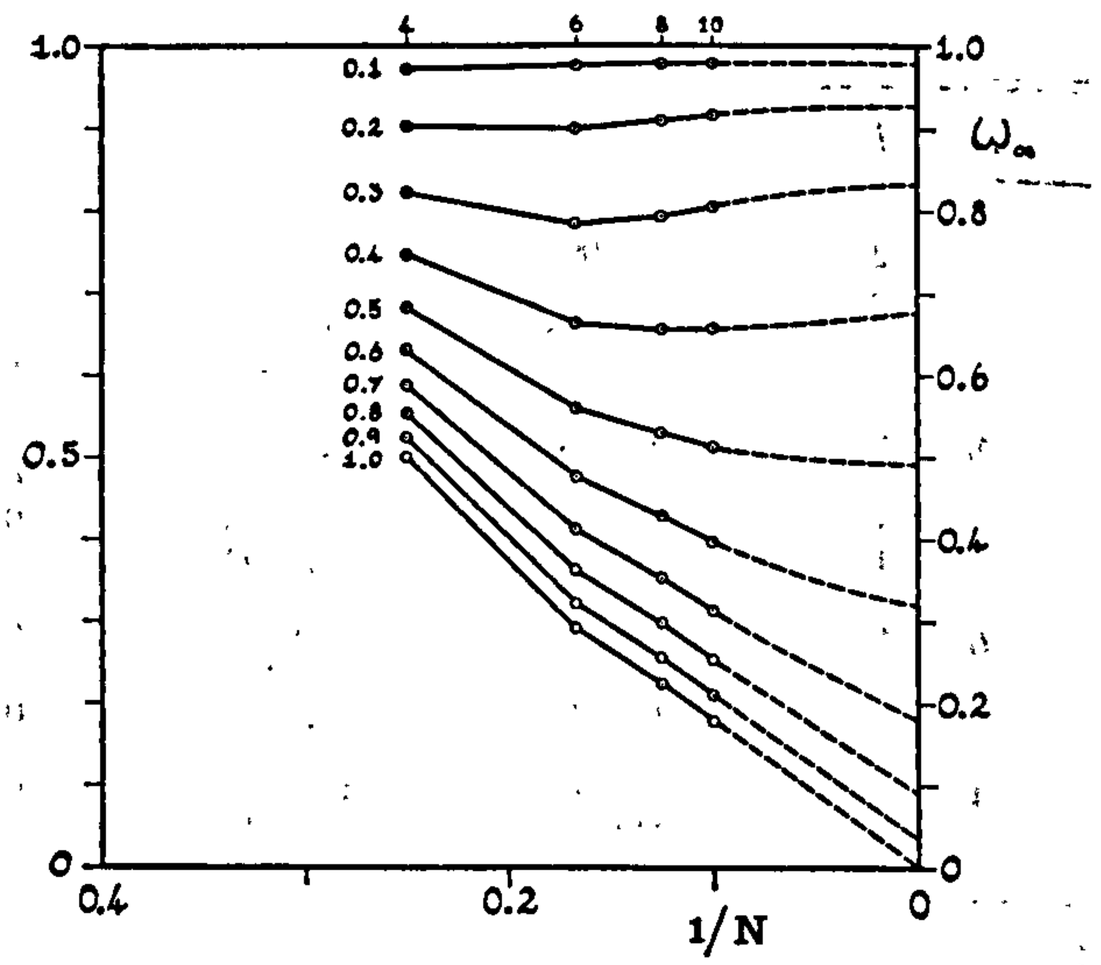

FIG. 29. Plot of $\omega_{\min}(\gamma,N)$ versus $1/N$. Extrapolation yields an estimate of the long-range order.

To compare our estimate of the long-range order with other approximations we must recognize that most authors have used as an order parameter the so-called

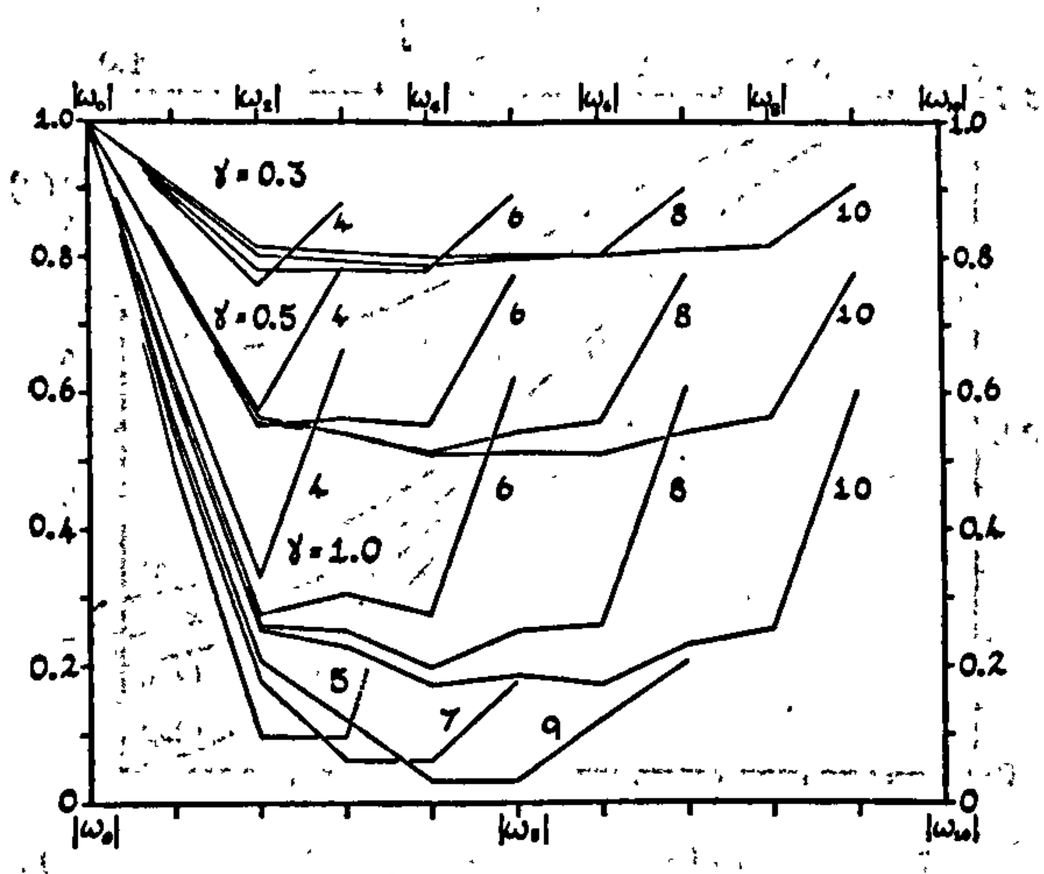

FIG. 28. Variation of $|\omega_l(N)|$ with l for $\gamma=0.3$, 0.5, and 1.0. and rings of $N=4$, 6, 8, and 10 spins.

"sublattice magnetization"[9,14,17,47]

$$\sigma=(2/\tfrac{1}{2}N)\langle\sum_{j\ \text{even}}S_j^x\rangle=2\langle S_0^x\rangle, \quad (6.5)$$

where the angular brackets denote the canonical average. If this formula is interpreted literally, it is easily shown (on the grounds of spin reversal symmetry) that σ always vanishes identically. Although this seems to have given rise to some confusion in the literature,[20,48,49] the situation really parallels that in the ferromagnetic case which is quite well understood.[50] If the (reduced) spontaneous magnetization of a ferromagnet is defined simply by $M_0=(2/N)\langle\sum_i S_i^z\rangle$, it also vanishes identically. The correct definition is made with the aid of a nonzero magnetic field, namely,

$$M_0(T)=\lim_{H\to 0+}\lim_{N\to\infty}(1/N)M_N(T,H), \quad (6.6)$$

where

$$M_N(T,H)=2\sum_{j=1}^{N}\langle S_j^z\rangle_N=2N\langle S_0^z\rangle_N. \quad (6.7)$$

By considering the finiteness of the susceptibility per spin in the limit $H\to 0$ [which implies the convergence of the sum $\sum_l(\langle S_0^xS_l^x\rangle-\langle S_0^x\rangle^2)$] one can then see that

$$M_0^2(T)=\lim_{N\to\infty}(1/N)^2\sum_{i,j=1}^{N}\langle S_i^xS_j^x\rangle,$$

$$=\lim_{l\to\infty}\lim_{N\to\infty}\langle S_0^xS_l^x\rangle=\omega_\infty(T), \quad (6.8)$$

[47] W. Marshall, Proc. Roy. Soc. (London) A232, 48 (1955).
[48] G. W. Pratt, Jr., Phys. Rev. 122, 489 (1961).
[49] N. Karayianis, C. A. Morrison, and D. E. Wortman, Phys. Rev. 126, 1443 (1962).
[50] See, for example, the discussion of the Ising model by G. F. Newell and E. W. Montroll, Rev. Mod. Phys. 25, 353 (1953).

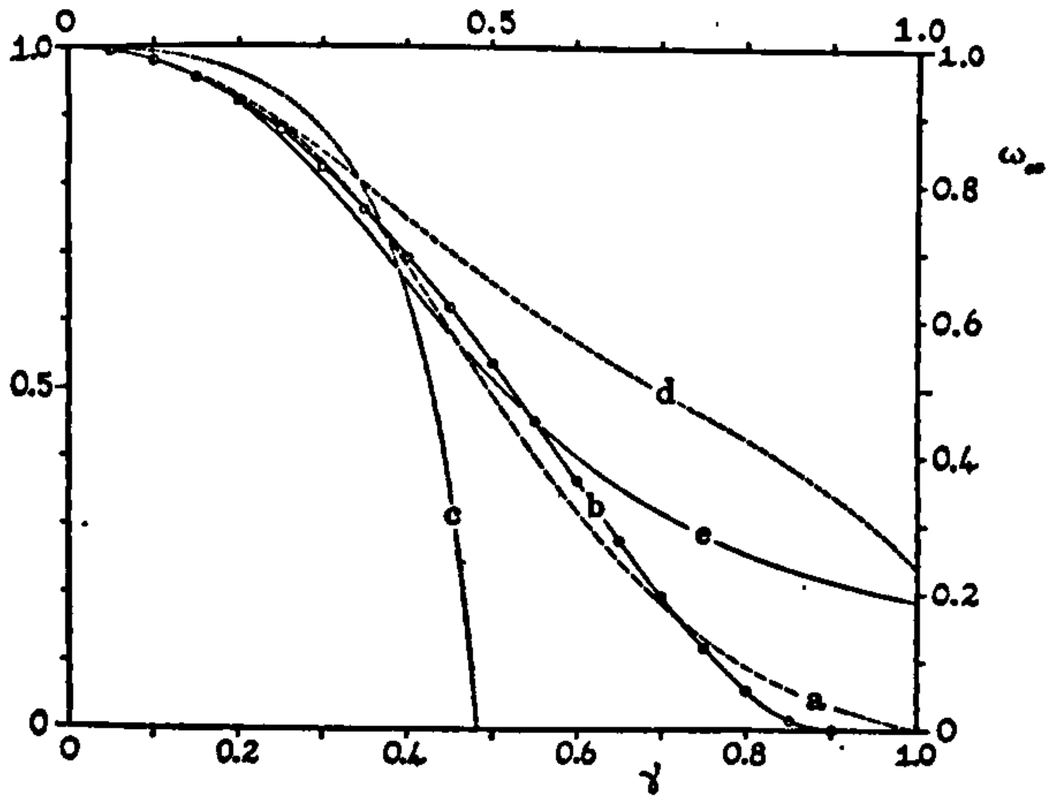

FIG. 30. Comparison of different approximations for the long-range order $\omega_\infty(\gamma)$: (a) extrapolation estimates, (b) Walker's perturbation series to γ^6, (c) Kasteleyn's variational formula, (d) Davis's perturbation series, (e) $\omega_{\min}$ for a finite chain of 10 spins.

i.e., the long-range order is just equal to the square of the spontaneous magnetization.

For an antiferromagnetic one must introduce a "staggered" magnetic field H^* by adding to the Hamiltonian a term

$$\mathcal{H}^* = H^* \sum_{j=0}^{N-1} (-)^j S_j^z. \tag{6.9}$$

With the aid of the corresponding "staggered magnetization" the sublattice magnetization may be defined properly by

$$\sigma = \lim_{H^*\to 0+} \lim_{N\to\infty} (1/N) M_N^*(H^*),$$
$$= \lim_{H^*\to 0+} [\langle S_0^z\rangle_\infty^* - \langle S_1^z\rangle_\infty^*]. \tag{6.10}$$

In a similar way one can then conclude that the long-range order defined by (6.3) is related to σ by[51]

$$\omega_\infty = \sigma^2. \tag{6.11}$$

We thus see that the two-order parameters are equivalent. One may, of course, avoid the somewhat artificial introduction of a staggered field by sticking to the definition (6.3) in terms of the correlation functions which, as argued by Ruijgrok and Rodriguez,[20] also has other features to recommend it. In practice, however, it is often easier to compute σ (or M_0) than to compute ω_∞ directly.

With these preliminaries we may compare our estimate of $\omega_\infty(\gamma)$ [curve (a) in Fig. 30] with Walker's exact perturbation expansion

$$\sigma(\gamma) = 1 - \gamma^2 - \tfrac{1}{4}\gamma^4 - \tfrac{1}{16}\gamma^6 + \cdots \tag{6.12}$$

[curve (b)],[9] with Kasteleyn's variational formula [curve (c)],[14] and with Davis's perturbation formula [curve (d)].[17] Also shown in Fig. 30 are the values $\omega_{\min}(10)$ [curve (e)]. Up to $\gamma=0.3$, all approximations agree well with the exact series but at this point Davis's approximation (d) starts deviating seriously and predicts a relatively large nonzero value for $\omega_\infty(1)$. Kasteleyn's approximation (c) falls away sharply to zero at $\gamma_c=0.483$, which is surely incorrect. Our estimated curve falls some 10% below the series value in the region $\gamma=0.45$ to 0.65, although the trend is very similar. In this region the series is probably still converging rapidly, as suggested both by the numerical magnitude of the terms, and by the agreement of the exact short-range order with the corresponding series up to γ^6 (Fig. 26). Above $\gamma=0.7$ we must expect the series to deviate from the true value and indeed the series for $\omega(\gamma)$ (rather than for $[\sigma(\gamma)]^2$) then yields lower values and has its zero at $\gamma=0.817$ rather than at $\gamma=0.897$. As already observed our extrapolated $\omega_\infty(\gamma)$ does not vanish until $\gamma=1$. Although we suspect this is the true situation it would be of great interest to have more precise information—ideally the rigorous answer—in the range above $\gamma=0.8$! At present it seems fair to conclude that the exact series expansion provides the best approximation up to $\gamma=0.75$ and that the true long-range order is unlikely to vanish for $\gamma<0.85$ and probably vanishes at $\gamma=1$.

In Fig. 27, therefore, we have plotted together with $\omega_1(\gamma)$ [exact] and our results for $|\omega_2|$, $|\omega_3|$, and $|\omega_4|$, what we think is the best estimate so far for $\omega_\infty(\gamma)$. This curve follows the series expansion up to $\gamma=0.6$, and thereafter has the same form as our extrapolation curve (a) in Fig. 30, approaching the latter from above and in close agreement for $\gamma>0.8$.

The excellent convergence of Walker's perturbation series in γ suggests that this approach should be developed further for two- and three-dimensional lattices where convergence seems to be even better. We remark in passing that it is possible to calculate exactly the γ^2 correction to the energy and specific heat for all temperatures in the case of two-dimensional lattices for which the Ising problem has been solved, by expressing the perturbation in terms of the multiple correlation functions for $\gamma=0$.[52]

ACKNOWLEDGMENTS

Weare grateful for the interest of Professor C. Domb and Dr. M. F. Sykes and for the assistance of members of the University of London Computer Unit. One of us (J.C.B.) is indebted to the Department of Scientific and Industrial Research for the award of a maintenance grant. As mentioned in the Introduction, we have greatly benefited from correspondence and discussion with Dr. R. L. Orbach and Dr. R. B. Griffiths, who also made their own computations freely available to us. We wish to apologize to Dr. Griffiths for inadvertently delaying publication of his own work.

[51] Strictly, it may be necessary to define the long-range order as an average over the two sublattices [e.g., if the limit in (6.3) differs as $l\to\infty$ through even or through odd integers].

[52] The technique is similar to that expounded in Ref. 43.